



TECHNISCHE
UNIVERSITÄT
WIEN

DISSERTATION

**PULSING HEART AT THE MICROSCALE:
GENERATION AND CHARACTERIZATION OF HUMAN ORGANOTYPIC
CARDIAC MICROTISSUES FOR TRANSLATIONAL MEDICINE**

Thema

ausgeführt zum Zwecke der Erlangung des akademischen Grades einer/eines
Doktorin/Doktors der technischen Wissenschaften/der Naturwissenschaften/
der Sozial- und Wirtschaftswissenschaften unter der Leitung von

(Betreuung)

Univ. Prof. Dipl.-Ing. Dr. Peter Ertl

Name

E163 & E164

Institutsnummer

Institute for Applied Synthetic Chemistry & Institute for Chemical Technologies and Analytics

Institutsbezeichnung

eingereicht an der Technischen Universität Wien

Faculty of Technical Chemistry

Fakultät

von

(VerfasserInn)

Ece Ergir

Name

01067709

Matrikelnummer



eigenhändige Unterschrift

Wien, am April 2023



VIENNA UNIVERSITY OF TECHNOLOGY

Faculty of Technical Chemistry

Institute for Applied Synthetic Chemistry (E163) & Institute for Chemical Technologies
and Analytics (E164)

Cell Chip Group

Conducted at International Clinical Research Center, St. Anne's University Hospital,
(FNUSA-ICRC), Center for Translational Medicine (CTM), Brno, Czech Republic

PULSING HEART AT THE MICROSCALE: GENERATION AND CHARACTERIZATION OF HUMAN ORGANOTYPIC CARDIAC MICROTISSUES FOR TRANSLATIONAL MEDICINE

Doctoral Dissertation

Submitted in partial fulfilment of the requirements for the degree of

DOCTOR OF TECHNICAL SCIENCES

In Technical Chemistry

Supervisors:

Univ. Prof. Dipl.-Ing. Dr. Peter Ertl

Giancarlo Forte, Ph.D.

Author:

Ece Ergir, M.Sc.

Matr. Nr.: 01067709

Vienna, April 2023

Affidavit

I declare in lieu of oath, that I wrote this thesis and performed the associated research myself, using only literature cited in this volume. If text passages from sources are used literally, they are marked as such. I confirm that this work is original and has not been submitted elsewhere for any examination, nor is it currently under consideration for a thesis elsewhere.

Vienna, April 2023


Signature

Acknowledgements

Dedicated to my parents Rabia and Yalçın Ergir...

“Çeni çok çeviyom çeniii....”

“If you wish to make an apple pie from scratch, you must first invent the universe.”
— Carl Sagan, Cosmos

“If you wish to make a heart from scratch, you must first know its universe!” – EE, Brno

In a journey stretching from Vienna to Brno, I would like to express my sincerest gratitude to my thesis supervisors Prof. Peter Ertl and Dr. Giancarlo Forte for welcoming me in the Cell Chip Group and Mechanobiology of Disease Group to conduct my PhD dissertation. Thank you from the bottom of my heart for your mentorship, guidance, and granting me the freedom to develop my own scientific ideas. Thank you for your patience and constant support during this journey, especially through the difficult times of the last few years of the world. Similarly, I would like to thank Prof. Heinz Redl for believing in me and helping me kick-start my PhD at the very beginning.

Deep diving into the world of tissue engineering with your support is a privilege that I will always cherish.

“Ludwig Boltzmann, who spent much of his life studying statistical mechanics, died in 1906, by his own hand. Paul Ehrenfest, carrying on the work, died similarly in 1933. Now it is our turn to study statistical mechanics. Perhaps it will be wise to approach the subject cautiously.” — **Opening lines of "States of Matter", by D.L. Goodstein**

I would like to acknowledge Center for Translational Medicine (CTM) at FNUSA-ICRC as a world-class research institution located in Brno, Czech Republic, with its state-of-the-art facilities, the multicultural environment and ambitious researchers with valuable expertise and possibility of excellent interdisciplinary science.

I would like to thank my colleagues at CTM for creating a professional and familiar atmosphere, and for many cheerful hours inside and outside the lab – particularly to all the present and past members of Mechanobiology of Disease (MBD) group: Jorge, Soraia, Marco, Francesco, Daniel, Sofia, Rubi, Fabi, Vláďa, Honzino, Stefania, Helča, Jana, Pavel... and Mia! (actually also to the dancing cactus in the later years) Especially to Jorge, Soraia, Marco and Rubi: Thank you for... basically everything - I would have been lost without your guidance and support! You are inspiring and brilliant scientists and people I am proud to work with and look up to. Special shoutout to Romana, Hanka, and Neda as well for their never-ending support!

“Cardiovascular disease is the leading cause of death worldwide” – Absolutely everyone (almost)

I would also like to thank Prof. Stjepan Uldrijan, Natália Vadovičová and Doriana Debellis for supporting the final stretches of my research with their valuable expertise.

I want to acknowledge Prof. Frank Caruso and Dr. Francesca Cavalieri from the University of Melbourne, for hosting me in their labs.

I would also like to acknowledge Dr. Veronika Hruschka for supporting me at LBI Trauma at the beginning of my PhD with the FEMTECH fellowship together with Prof. Heinz Redl.

Mario, Barbara, Sarah, Christoph, Cristian, Helene, Julie and Faheem, thank you for accompanying me during the time I spent with the Cell Chip Group.

Thanks to Michaela Purtscher for correcting the German abstract. 😊

Thanks to “Pint of Science Austria” team for allowing me to volunteer even from a distance for helping the organization of an amazing science communication festival!

To the City of Brno and my Brno family: My "Brno'lu İnsanlar" (who are slowly growing out of Brno), my "Brno Brunch [redacted]... Ladies", "Pinky and the Brains" of Clubwash Pubquiz, people I will most likely find at ~~The Immigrant~~, ~~The “Irish”~~, East Village ☑ (if I manage to finish working on time), Piano and German meetings, and countless others... With the ungodly amounts of caffeine and pivo consumed, thank you for making this unique city a new home for me.

Eda, Zeynep, Kerem: Thank you for your friendship and keeping me sane virtually and in person with our impromptu but lasting support group during this time.

Thanks to my family (including my extended international family) and friends for their continuous and loving support through my education and life.

Last but not least, special thanks to Viktor, for “staying here next to me and we'll just keep drivin'.” 😊

Abstract

As cardiovascular diseases (CVD) remain the leading cause of mortality worldwide; there is an increasing demand for developing physiologically relevant *in vitro* cardiovascular tissue models suitable for studying personalized medicine and pre-clinical tests. Although recent technologies provide some insight into how human CVDs can be modelled *in vitro*, they may not always give a comprehensive overview of the complexity of the human heart due to their limits in cellular heterogeneity, physiological complexity and maturity.

The aim of this dissertation is to provide a deeper understanding of microphysiological technologies in cardiovascular biology, and to establish a miniaturized cardiac tissue model *in vitro* that could better reflect the physiological complexity, cellular heterogeneity and maturity of a human heart, and demonstrate its functional applications for translational research.

We have developed a simple and effective protocol to generate scaffold-free multicellular beating human cardiac microtissues *in vitro* from human induced pluripotent stem cells (hiPSCs) – namely human organotypic cardiac microtissues (hOCMTs) – that show a degree of proto-self-organization and can be cultured for long term. [I]. The 3D hOCMTs contain multiple cell types of the heart, and show functional beating activity without external stimuli for more than 100 days. The 3D hOCMTs show improved cardiac specification, survival and metabolic maturation compared to standard 2D monolayer cardiac differentiation. Furthermore, we show that the 3D hOCMTs could respond to cardioactive and cardiotoxic drugs in a dose dependent manner. Due to their tendency for self-organization, cellular heterogeneity, and functionality in our 3D microtissues over extended culture time, we could confirm these constructs as human cardiac organoids (hCOs).

Finally, we reviewed *in vitro* technologies already described in the literature and proposed to enable *in-vivo-like* biomechanical cues in microphysiological tissue models [II], and further overviewed nanomedical applications for cardiac therapies [III].

This work shows the potential of 3D hCOs to enable the development of more physiologically-relevant cardiac tissue models, and represent a powerful platform that could lead to future translational research in cardiovascular biology.

Keywords: 3D cardiac organoid, induced pluripotent stem cells, organotypic cardiac microtissues, tissue engineering, cardiotoxicity

[I] **Ergir, E.**, Oliver-De La Cruz, J., Fernandes, S. *et al.* (2022). "Generation and maturation of human iPSC-derived 3D organotypic cardiac microtissues in long-term culture." *Sci Rep* **12**, 17409. <https://doi.org/10.1038/s41598-022-22225-w>

[II] **Ergir, E.**, Bachmann, B., Redl, H., Forte, G., & Ertl, P. (2018). "Small Force, Big Impact: Next Generation Organ-on-a-Chip Systems Incorporating Biomechanical Cues." *Frontiers in Physiology*, *9*, 1417. <https://doi.org/10.3389/fphys.2018.01417>

[III] Cassani M., Fernandes S., Vrbsky J., **Ergir E.**, Cavalieri F., Forte G. (2020) "Combining Nanomaterials and Developmental Pathways to Design New Treatments for Cardiac Regeneration: The Pulsing Heart of Advanced Therapies" *Frontiers in Bioengineering and Biotechnology*, *8*, 323. <https://doi.org/10.3389/fbioe.2020.00323>

Kurzfassung

Da Herz-Kreislauf-Erkrankungen (CVD) weltweit als häufigste Todesursache bestehen bleibt besteht ein zunehmender Bedarf an der Entwicklung physiologisch relevanter *in-vitro*-Modelle von kardiovaskulärem Gewebe, die für die Untersuchung personalisierter Medizin und präklinischer Tests geeignet sind. Obwohl neuere Technologien einige Einblicke in die Modellierung menschlicher CVDs *in vitro* geben, geben sie aufgrund ihrer Grenzen in zellulärer Heterogenität, physiologischer Komplexität und Reife möglicherweise nicht immer einen umfassenden Überblick über die Komplexität des menschlichen Herzens.

Ziel dieser Dissertation ist es, ein tieferes Verständnis mikrophysiologischer Technologien in der kardiovaskulären Biologie zu gewinnen und ein miniaturisiertes Herzgewebemodell *in vitro* zu etablieren, das die physiologische Komplexität, zelluläre Heterogenität und Reife eines menschlichen Herzens besser widerspiegeln und seine funktionellen Anwendungen demonstrieren könnte für translationale Forschung.

Wir haben ein einfaches und effektives Protokoll entwickelt, um gerüstfreie multizelluläre schlagende menschliche Herzmikrogewebe *in vitro* aus humanen induzierten pluripotenten Stammzellen (hiPSCs) – benannt als humane organotypische Herzmikrogewebe (hOCMTs) – zu erzeugen, die einen Grad an Proto-Selbstorganisation aufweisen und langfristig kultiviert werden können. [I]. Die 3D-hOCMTs enthalten mehrere Zelltypen des Herzens und zeigen eine funktionelle Schlagaktivität ohne der Stimulation durch äußere Reize für mehr als 100 Tage. Die 3D-hOCMTs zeigen eine verbesserte kardiale Spezifikation, Überlebensrate und metabolische Reifung im Vergleich zur standardmäßigen 2D-Monoschicht-Herzdifferenzierung. Darüber hinaus zeigen wir, dass die 3D-hOCMTs dosisabhängig auf kardioaktive und kardiotoxische Medikamente reagieren könnten. Aufgrund ihrer Tendenz zur Selbstorganisation, zellulären Heterogenität und Funktionalität in unseren 3D-Mikrogeweben über längere Kulturzeit konnten wir diese Konstrukte als menschliche Herzorganoide (hCOs) bestätigen.

Schließlich überprüften wir bereits in der Literatur beschriebene *in-vitro*-Technologien und schlugen vor, *in-vivo*-ähnliche biomechanische Hinweise in mikrophysiologischen Gewebemodellen zu ermöglichen [II], und gaben einen weiteren Überblick über nanomedizinische Anwendungen für Herztherapien [III].

Diese Arbeit zeigt das Potenzial von 3D-hCOs, die Entwicklung physiologisch relevanter Herzgewebemodelle zu ermöglichen, und stellt eine leistungsstarke Plattform dar, die zu zukünftiger translationaler Forschung in der kardiovaskulären Biologie führen könnte.

Schlüsselwörter: 3D-Herz-Organoid, induzierte pluripotente Stammzellen, organotypische Herz-Mikrogewebe, Tissue Engineering, Kardiotoxizität

- [I] **Ergir, E.**, Oliver-De La Cruz, J., Fernandes, S. *et al.* (2022). "Generation and maturation of human iPSC-derived 3D organotypic cardiac microtissues in long-term culture." *Sci Rep* **12**, 17409. <https://doi.org/10.1038/s41598-022-22225-w>
- [II] **Ergir, E.**, Bachmann, B., Redl, H., Forte, G., & Ertl, P. (2018). "Small Force, Big Impact: Next Generation Organ-on-a-Chip Systems Incorporating Biomechanical Cues." *Frontiers in Physiology*, *9*, 1417. <https://doi.org/10.3389/fphys.2018.01417>
- [III] Cassani M., Fernandes S., Vrbsky J., **Ergir E.**, Cavalieri F., Forte G. (2020) "Combining Nanomaterials and Developmental Pathways to Design New Treatments for Cardiac Regeneration: The Pulsing Heart of Advanced Therapies" *Frontiers in Bioengineering and Biotechnology*, *8*, 323. <https://doi.org/10.3389/fbioe.2020.00323>

Author Contribution Statement/Acknowledgements

Manuscript I: Parts of this dissertation, including figures and tables, have been reproduced, with or without modifications, based on my original manuscript (Ergir et al., 2022) licensed for reuse under Creative Commons Attribution 4.0 International License. To view a copy of this licence, visit <http://creativecommons.org/licenses/by/4.0/>.

Generation and Maturation of Human iPSC-derived 3D Organotypic Cardiac Microtissues in Long-Term Culture

Sci Rep 12, 17409 (2022). <https://doi.org/10.1038/s41598-022-22225-w>

Ece Ergir^{1,2}, Jorge Oliver-De La Cruz¹, Soraia Fernandes¹, Marco Cassani¹, Francesco Niro^{1,3}, Daniel Pereira-Sousa^{1,3}, Jan Vrbský¹, Vladimír Vinarský¹, Ana Rubina Perestrelo¹, Doriana Debellis⁴, Natália Vadovičová³, Stjepan Uldrijan³, Francesca Cavalieri^{5,6}, Stefania Pagliari¹, Heinz Redl^{7,8}, Peter Ertl^{2,8}, and Giancarlo Forte^{1,9}

1 Center for Translational Medicine (CTM), St. Anne's University Hospital, International Clinical Research Centre (FNUSA-ICRC), CZ-62500, Brno, Czech Republic

2 Faculty of Technical Chemistry, Institute of Applied Synthetic Chemistry & Institute of Chemical Technologies and Analytics, Vienna University of Technology, AT-1040, Vienna, Austria

3 Faculty of Medicine, Department of Biomedical Sciences, Masaryk University, CZ-62500, Brno, Czech Republic.

4 Electron Microscopy Facility, Fondazione Istituto Italiano Di Tecnologia, Via Morego 30, IT-16163, Genova, Italy

5 Department of Chemical Engineering, The University of Melbourne, Parkville, Victoria 3010, Australia;

6 Dipartimento di Scienze e Tecnologie Chimiche, Università degli Studi di Roma Tor Vergata, via della Ricerca Scientifica 1, 00133, Rome, Italy

7 Ludwig Boltzmann Institute for Experimental and Clinical Traumatology, AUVA Research Center, AT-1200, Vienna, Austria

8 Austrian Cluster for Tissue Regeneration, AT-1200, Vienna, Austria

9 Department of Biomaterials Science, Institute of Dentistry, University of Turku, FI-20014, Turku, Finland

Contribution: E.E. conceptualized the study, designed and performed the experiments, analysed the data and drafted the manuscript.

Manuscript II: Parts of this dissertation, including figures and tables, have been reproduced, with or without modifications, based on my original published mini-review article (Ergir et al., 2018) licensed for reuse under Creative Commons Attribution 4.0 International License. To view a copy of this licence, visit <http://creativecommons.org/licenses/by/4.0/>.

MINI REVIEW article
Front. Physiol., 09 October 2018
Sec. Integrative Physiology
<https://doi.org/10.3389/fphys.2018.01417>

Small Force, Big Impact: Next Generation Organ-on-a-Chip Systems Incorporating Biomechanical Cues

Ece Ergir^{1,2†}, Barbara Bachmann^{2,3,4,5†}, Heinz Redl^{3,4,5}, Giancarlo Forte^{1,6,7} and Peter Ertl^{2,4,5}

1 Center for Translational Medicine, International Clinical Research Center, St. Anne's University Hospital, Brno, Czechia,

2 Faculty of Technical Chemistry, Institute of Applied Synthetic Chemistry and Institute of Chemical Technologies and Analytics, Vienna University of Technology, Vienna, Austria

3 AUVA Research Centre, Ludwig Boltzmann Institute for Experimental and Clinical Traumatology, Vienna, Austria

4 Austrian Cluster for Tissue Regeneration, Vienna, Austria

5 Kompetenzzentrum für MechanoBiologie (INTERREG V-A Austria – Czech Republic Programme, ATCZ133), Vienna, Austria

6 Competence Center for Mechanobiology (INTERREG V-A Austria – Czech Republic Programme, ATCZ133), Brno, Czechia

7 Department of Biomaterials Science, Institute of Dentistry, University of Turku, Turku, Finland

† These authors have contributed equally to this work

Contribution: EE conceived the general structure of the review, revised the existing literature, and drafted the manuscript. Figure 1 was drawn by EE.

Manuscript III: Parts of this dissertation, including figures and tables, have been reproduced, with or without modifications, based on my contribution to the original published review article (Cassani et al., 2020) licensed for reuse under Creative Commons Attribution 4.0 International License. To view a copy of this licence, visit <http://creativecommons.org/licenses/by/4.0/>.

REVIEW article

Front. Bioeng. Biotechnol., 24 April 2020

Sec. Biomaterials

<https://doi.org/10.3389/fbioe.2020.00323>

Combining Nanomaterials and Developmental Pathways to Design New Treatments for Cardiac Regeneration: The Pulsing Heart of Advanced Therapies

Marco Cassani¹, Soraia Fernandes¹, Jan Vrbsky¹, **Ece Ergir**^{1,2}, Francesca Cavalieri^{3,4} and Giancarlo Forte¹

1 International Clinical Research Center, St Anne's University Hospital, Brno, Czechia

2 Faculty of Technical Chemistry, Institute of Applied Synthetic Chemistry and Institute of Chemical Technologies and Analytics, Vienna University of Technology, Vienna, Austria

3 School of Science, RMIT University, Melbourne, VIC, Australia

4 Dipartimento di Scienze e Tecnologie Chimiche, Università di Roma "Tor Vergata", Via Della Ricerca Scientifica, Rome, Italy

Contribution: EE revised the literature on cardiac diseases biology, and contributed to the writing, discussion and conclusions.

Table of Contents

1	INTRODUCTION	1
1.1	Problem and Motivation	1
1.2	The Complexity of (Making) the Human Heart	4
1.2.1	Heart Development in the Early Embryo	5
1.2.2	The Cellular Composition of the Adult Heart	12
1.2.2.1	Cardiomyocytes (CM) and their maturation	13
1.2.2.2	Cardiac fibroblasts (CF).....	20
1.2.2.3	Endothelial cells (EC)	22
1.2.2.4	Mural cells: Smooth muscle cells (SMC) & Pericytes	24
1.2.3	The Biology of Common Cardiomyopathies.....	26
1.3	Strategies for In Vitro Cardiac Tissue Modelling.....	29
1.3.1	Human (Induced) Pluripotent Stem Cells.....	29
1.3.2	Bioengineering Approaches	34
1.3.2.1	(Micro)physiological Systems	36
1.3.2.2	“Heart-on-a-chip” Technologies	39
1.3.2.3	Spheroids, Gastruloids and Organoids.....	47
1.4	Aim of the Dissertation	65
2	MATERIALS AND METHODS	66
2.1	Stem cell culture and maintenance.....	66
2.2	hiPSC-derived monolayer cardiac differentiation and maintenance.....	66
2.3	hiPSC-derived 3D organotypic cardiac microtissue (hOCMT) generation and maintenance	67
2.4	Cell viability with Calcein AM/EthD-1 staining	67
2.5	Terminal deoxynucleotidyl transferase (TdT) dUTP Nick-End Labeling (TUNEL) assay	67
2.6	Histology and Immunofluorescence (IF)	68
2.7	Microscopy and image analysis	70

2.8	3D hOCMT dissociation	70
2.9	Flow cytometry	70
2.10	Transmission Electron Microscopy (TEM) sample preparation and analysis ..	71
2.11	RNA isolation, bulk RNA-sequencing and differential expression (DE) analysis	71
2.11.1	RNA isolation and quality control.....	71
2.11.2	Sequencing library preparation.....	71
2.11.3	Differential expression (DE) analysis.....	72
2.11.4	Gene ontology enrichment, clustering, and comparison with other datasets	73
2.12	Metabolic flux analysis	73
2.13	Drug treatments.....	74
2.14	Live video acquisition and contraction analysis	74
2.15	Luminescence-based cell viability assay	74
2.16	Statistics	75
2.17	Data availability	75
3	RESULTS	76
3.1	2D-to-3D culture switch promotes spontaneous cardiac microtissue formation in scaffold-free conditions.....	76
3.2	2D-to-3D culture switch prompts the formation of human iPSC-derived organotypic cardiac microtissues composed of multiple heart cell types.....	84
3.3	Human iPSC-derived organotypic cardiac microtissues display ultrastructural organization and maturation in long-term culture	92
3.4	3D long-term culture induces human iPSC-derived organotypic cardiac microtissue maturation.....	95
3.5	Long-term human iPSC-derived organotypic cardiac microtissues display enhanced metabolic activity.....	104
3.6	Human iPSC-derived organotypic cardiac microtissues functionally respond to drugs in a dose dependent fashion in long-term culture	107
4	DISCUSSION.....	111
5	CONCLUSION AND SCIENTIFIC VALUE.....	116
6	BIBLIOGRAPHY.....	117
7	LIST OF ONLINE SUPPLEMENTARY MATERIALS.....	156

7.1	List of Supplementary Videos.....	156
7.2	List of Supplementary Datasets	157
8	LIST OF ABBREVIATIONS.....	158
9	LIST OF FIGURES	162
10	LIST OF TABLES.....	166
11	Curriculum Vitae as of April 2023	167
12	APPENDIX A: Additional Data and Clarifications	172
12.1	Excerpts from point-by-point responses to reviewers.....	172
13	APPENDIX B: First attempt at hCO-on-Chip.....	176
14	APPENDIX C: Original Publications During Dissertation	178
	Manuscript I.....	179
	Manuscript II	211
	Manuscript III	220

1 INTRODUCTION

1.1 Problem and Motivation

Cardiovascular diseases (CVD) still remain the leading cause of death worldwide. As of 2019, an estimated 17.9 million people died from CVDs, representing 32% of all global deaths. Of these deaths, 85% were due to coronary heart diseases (e.g. heart attacks) and cerebrovascular diseases (e.g. strokes) and they have disproportionately affected low- and middle-income countries [1], [2]. CVDs have many causes such as smoking, diabetes, obesity and high-blood pressure, or underlying congenital forms. In the era of global COVID-19 pandemics, understanding and treating CVDs has become even more crucial as these pathologies have emerged as both a risk factor and a result of acute infection and its longer-term outcomes [3]–[8].

Developing new therapies for CVD remains a major challenge, as a significant number of drug candidates fail to pass clinical trials, or are withdrawn from the market due to adverse side effects [9]–[11]. In order to approve safer and more effective therapies, there is an increasing demand to develop faithful models of human heart tissue for pre-clinical research [11]. While recent technologies provide some insight into how human CVDs can be modelled *in vitro*, a comprehensive overview of the complexity of the human heart remains elusive due to the limited cellular heterogeneity, physiological complexity, or maturity of the constructs produced [12]. Furthermore, animal models may not always faithfully reflect the unique features of human biology and disease, and could give rise to ethical concerns [13]–[15].

Induced pluripotent stem cell (iPSC) technology has been revolutionary for the differentiation and derivation of cardiomyocytes for studying developmental biology, disease modelling and drug testing [12], [16]–[24]. However, when cultured in 2D, these cardiomyocytes do not reflect the 3D complexity of the native tissue [22], [25], [26], where the topology, the cellular heterogeneity and the interactions with the extracellular matrix (ECM) play a crucial role.

The heart is the first organ to form during mammalian development. It is a very complex organ with its unique tissue composition at different levels containing many different structures (eg. Heart valves, arteries, veins, capillaries, cardiac/smooth muscles, pacemaker cells, Purkinje fibers, ...), and different cell types (cardiomyocytes, cardiac fibroblasts, endothelial cells, epicardial cells, smooth muscle cells, pacemaker cells, ...) [27] in addition to distinctive metabolic and mechanical features. While the neonatal heart tissue has an ability to regenerate, this potential is greatly reduced in the adult life of higher mammals [28]. Therefore, it is not surprising to see CVD remains as a leading cause of death worldwide.

Further elaboration on the complexity of heart tissue has revealed a need of new models to reflect relevant heart models to study cardiovascular biology, its development, make healthy/disease tissue models, or develop alternative platforms for drug screening [29]. Since the past few decades, there has been a growing interest in 3D culture and tissue engineering applications to make more realistic cardiovascular tissue models for both normal and pathological conditions. By dissecting the interplay between the different cell types, scaffolds and biophysical stimuli, many advances of tissue engineering methods have been reported that best replicate cardiac development (Figure 1.1). Thus, 3D culture methods and tissue engineering approaches could have a great potential for both basic and translational cardiovascular research.

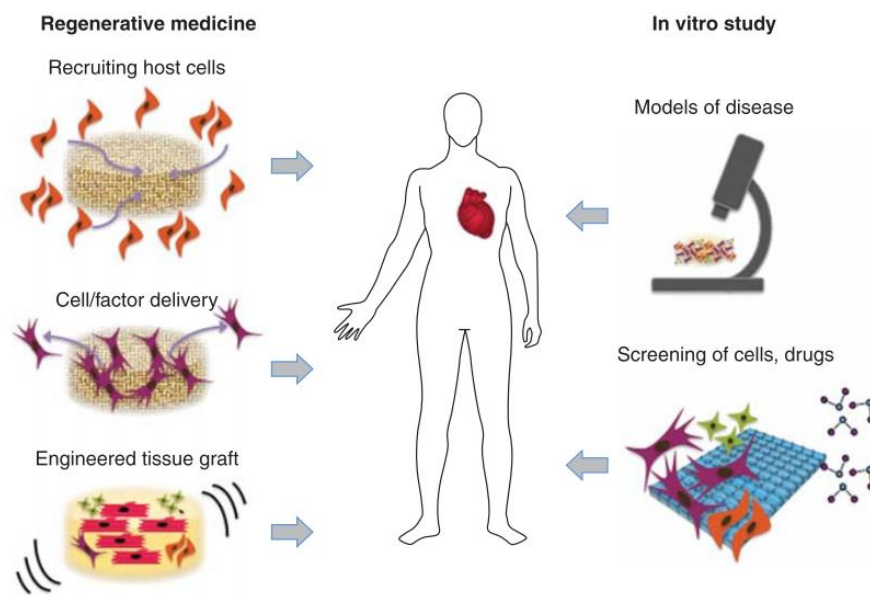


Figure 1. 1 Classical approaches in cardiovascular tissue engineering

The classical tissue engineering approach involves cultivating cells on scaffolds in presence of biochemical and mechanical stimuli (e.g. Bioreactors). An alternative approach for regenerative medicine entails the recruitment of host cells to the site of injury by implanted scaffolds and/or cells. Recently, tissue engineering approaches are also being used as a platform for (high-throughput) disease modelling or for screening for drugs and therapeutic targets. Adapted from: [30].

Early 3D cardiac tissue models were developed by culturing human heart tissue biopsies, or by mixing non-isogenic populations of cardiomyocytes, non-myocytes and biocompatible hydrogels, called “cardiospheres” or “cardiac microtissues”. [31]–[33]. However, such microtissues tend to survive limited time in culture, display poor self-organization and fail to capture the complex cellular heterogeneity of the organ they aim to model. Recently, cardiac tissue engineering technologies have emerged that develop more physiologically-

relevant tissue models with higher degree of complexity, organization and dynamics [34]–[37], such as engineered heart tissues (EHTs) [30], [35], [38], isogenic cardiac microtissues [32], [39]–[44], and lately organs-on-a-chip [45]–[55] and organoids [13], [56]–[58].

Organoids are 3D miniaturized versions of an organ, showing faithful micro-anatomy, and organ specific function compared to the organ being modelled after [13], [56]–[58]. To be considered as an "organoid", an *in vitro* model must fulfil specific requirements, including: (1) 3D cellular heterogeneity with organ-specific cell types, (2) self-organization and histology similar to the tissue of origin and (3) recapitulation of at least one specialized biological function similar to the organ being modelled [58]–[60].

To this date, well-established organoids have been already generated for many organs such as the brain, kidneys, intestines, guts, lungs and many other organs [13], [61]. On the other hand, organoid models of the heart have only started to emerge in the last couple of years [62], [63]. Of note, early mammalian cardiac organoids showing spontaneous self-organization with distinct atrium- and ventricle- like regions were generated from mouse pluripotent stem cells (PSCs) [64], [65], or as a part of gastruloids [66]. Subsequently, human PSC-derived cardiac organoid models were described [63], [67]–[72], which were developed by various approaches such as assembling different cardiac cell types [69], followed by other self-organized models more faithful to cardiac development [63], [70]–[73].

Recently published human cardiac organoids include single chamber models - i.e. "cardioids" modelling the left ventricle [63] - relying on an external ECM scaffold, such as Matrigel [68], [70], exhibit chamber-like structures [63], [71], showing the co-emergence of gut tissue together with atrial- and ventricular-like regions [70], [72]. Although extremely informative, most of these models are generated by short-term culture, whereas longer-term culture could help them acquire a more mature phenotype, which is desirable for more physiologically relevant *in vitro* tissue models [74], [75].

The main motivation/research question of this dissertation has been to focus on the development of 3D cardiac microtissues that could demonstrate improved cardiac specification and maturation and could act as an *in vitro* platform for modelling the complexity of human heart.

1.2 The Complexity of (Making) the Human Heart

In order to be able to faithfully bioengineer and replicate the characteristics of a human heart *in vitro*, we first need to understand its biology, developmental timeline, and its cellular composition.

The fully developed mammalian heart consists of four chambers and many different cell types (Figure 1.2A), where each of them is involved in specific biochemical, mechanical, structural and electrical functions. There are three main layers: Epicardium (outermost), myocardium (middle), and the endocardium (innermost) (Figure 1.2B). The first layer, epicardium, consists of cardiac fibroblasts and smooth muscle cells. Cardiac fibroblasts are the main mediators of extracellular matrix production, maintenance and healing response of the heart after injury [76]. Smooth muscle cells (SMCs) are involved in arteries' inflow and outflow properties, and vasculature (Aortic and Vascular SMCs). The muscular walls of the heart – myocardium – are composed of cardiomyocytes (CMs) – with atrial and ventricular subtypes (sino-atrial node cardiomyocytes: SA-CMs and atrio-ventricular cardiomyocytes: AV-CMs). In addition, Pacemaker cells (from SA-CMs) and Purkinje fibers are specialised CMs that generate the electrical impulse necessary to initiate the beating of the heart. The SA-CMs/Pacemaker cells are located at the sinoatrial node (SAN) near the right atrium, while the AV-CMs are found at the atrioventricular node (AV), located between atria and ventricles. AV-CMs are quiescent CMs, until they receive the electrical impulse from SA-CMs, and conduct this impulse from atria to the ventricles to complete the beating. Finally, the innermost layer – endocardium – consists of endothelial cells (ECs) that provide the innermost lining of blood vessels and heart valves [77]

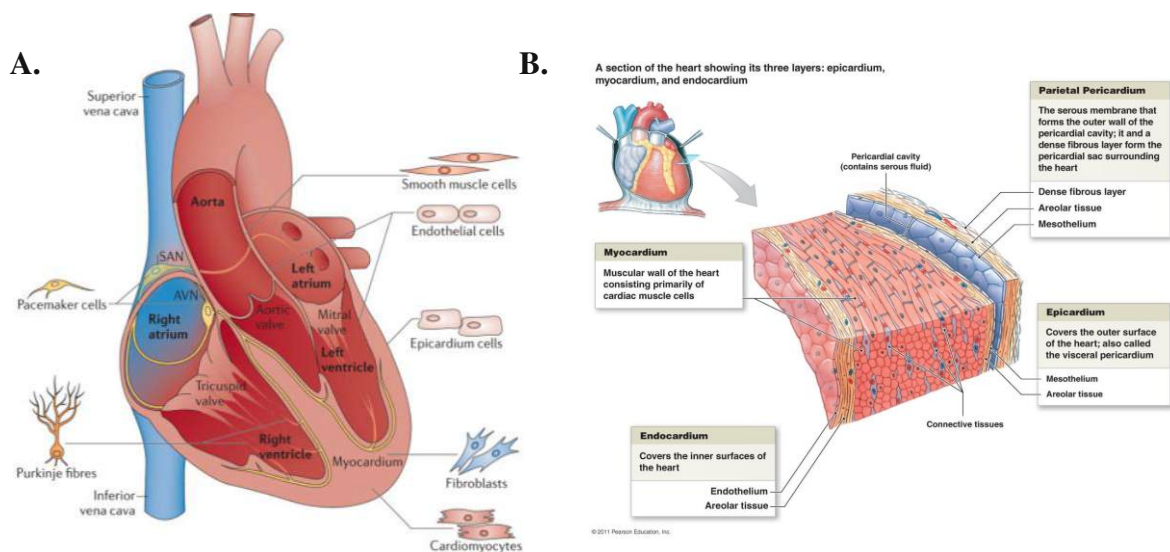


Figure 1. 2 Anatomy and cell types of the mammalian heart.

A. The four chambered mammalian heart with their anatomic locations. Epicardium: Smooth muscle cells, cardiac fibroblasts. Myocardium: Cardiomyocytes (Pacemaker cells/SA-CMs, AV-

CMs, Purkinje fibers). Endocardium: Endothelial cells. Adapted from [77] **B.** A cross-section diagram of the heart wall showing the relative positions of pericardium/epicardium, myocardium and endocardium layers (thickness not to scale as myocardium is much thicker. Adapted from [78].

1.2.1 Heart Development in the Early Embryo

The heart is the first organ to form and function during mammalian embryogenesis [79].

On week 3 of human embryonic development (equivalent to embryonic day 7.5 (E7.5) of mouse), the embryo consists of three germ layers: the ectoderm, the mesoderm, and the endoderm [80]. This stage is where the heart formation starts, where most of the cardiac tissue would be derived from the mesoderm layer. During gastrulation, the early cardiac progenitor cells could be found at bilateral regions in the midline of embryo, and when the embryo starts to fold, these two regions fuse and form the “cardiac crescent”. From this point on, two major progenitor cell types, namely the first heart field (FHF) and the second heart field (SHF) contribute to the developing heart [81]. Figure 1.3 shows a summary of the developmental timeline of mammalian cardiogenesis.

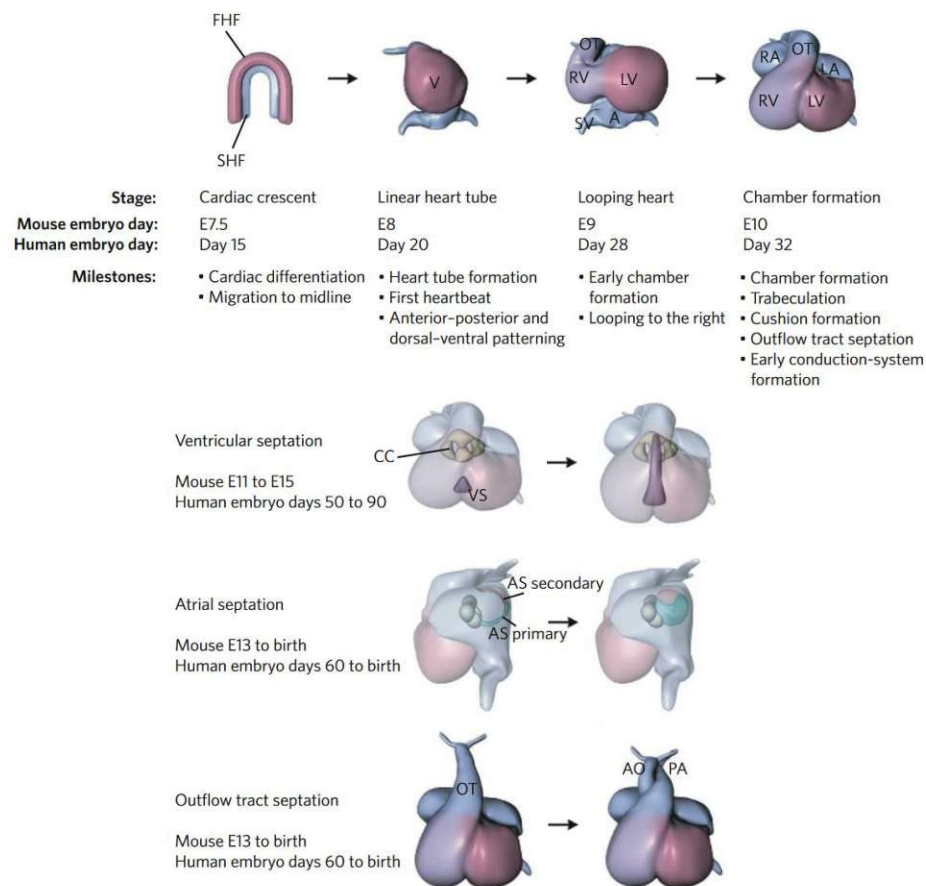


Figure 1. 3 Developmental timeline of mammalian cardiogenesis.

At the earliest stages of heart formation (cardiac crescent), two pools of cardiac precursors exist: The first (FHF) and second heart field (SHF). At intermediate stages, these pools merge to form the linear heart tube, followed by looping and chamber formation. FHF contributes to left ventricle (LV), and SHF contributes to right ventricle (RV), outflow tract (OT), sinus venosus (SV), and left and right atria (LA and RA). (V, Ventricle). At the later stages towards maturation, the cardiac cushions (CC) lead the formation of atrioventricular valves. Ventricular septum (VS) is formed from myocardium of LV and RV. Atrial septation (AS) happens via the growth of primary septum (green) and secondary septum (pink). Finally, the outflow tract septation gives rise to the aorta (AO, at left ventricle), and the pulmonary artery (PA, at right ventricle). Adapted from [82].

An interactive version of this process can be found at <http://pie.med.utoronto.ca/HTBG/index.htm>.

The cells of the cardiac crescent subsequently fuse along the midline to form the linear heart tube, serving as a scaffold for subsequent heart growth [77]. The early heart tube consists of an outer myocardial layer and an inner endocardial layer separated by cardiac jelly [83]. This stage is also where the first beating activity is observed. The linear heart tube then undergoes a rightward looping (week 4-5 in humans, E8.5 in mice) in order to enable cardiac chamber formation (week 5-6 in humans, E10.5 in mice). Cardiac trabeculation also begins after looping, where a network of luminal projections called “trabeculae” are formed – made of myocardial cells covered by the endocardial layer (Figure 1.4) [84], [85]. This enables nutrition and oxygen uptake in the embryonic myocardium before vascularization [85], [86]. Septation and valve formation marks heart maturation by week 10 in humans, and day E15 in mice. Finally, cardiac chamber maturation can be achieved by trabeculae formation, establishment of the conduction system, and thickening of the compact myocardium [85].

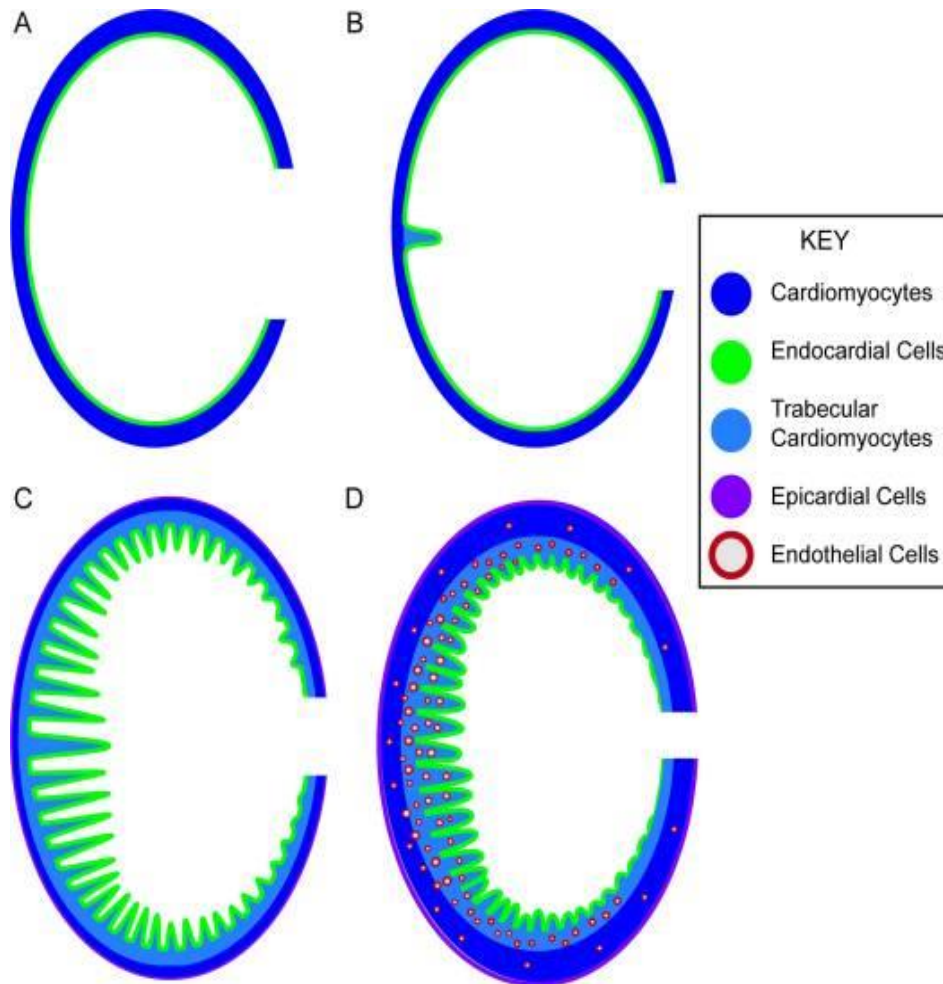


Figure 1. 4 Cardiac trabeculation and chamber maturation.

A. At early development, the cardiac chamber wall is smooth and made of endocardial cells and myocardial cells. **B. Emergence:** Myocardial projections called trabeculae start to appear in the outer curvature of the ventricle, projecting into the lumen, which are lined by a continuous layer of endocardium. **C. Trabeculation:** Trabeculae increase in length and the chamber wall becomes more complex while the myocardium does not thicken significantly. Meanwhile, the outermost layer of the heart – the epicardium – starts to surround the developing heart. **D. Compaction/Remodelling.** Trabeculae stops the luminal growth, thicken radially, and their base joins to form part of the myocardial wall. The compact myocardium increases in mass together with coronary vessel formation in the myocardial wall. The compact myocardium is shown in dark blue, trabecular cardiomyocytes in light blue, endocardial cells in green, and epicardial cells in purple. The developing cardiac vasculature is shown by gray circles outlined in green. Adapted from [85].

In mammals, the FHF cells mainly contribute to the formation of left ventricular myocardium, conductive cells of atrioventricular canal, and parts of cardiac conduction system [87], while the SHF cells contribute to various lineages such as right ventricular

myocytes, atria, sinoatrial conductive cells, vascular smooth muscle cells and endothelial cells [80], [88], [89].

Meanwhile, tissues from outside the cardiac field also contribute to cardiac development. Cardiac neural crest cells (cNCCs) originate from the dorsal neural tube, migrate from dorsal mesoderm with the help of SHF, and participate in the septation of the outflow tract. The “proepicardial organ” (PEO) at the paraxial mesoderm at the ventral region of the embryo gives rise to “proepicardial cells” that migrate to the developing heart, and contribute to the formation of the outermost layer of the heart – the epicardium – via epithelial-to-mesenchymal transition (EMT), as well as cardiac fibroblasts, smooth muscles, coronary artery and valve development (Figure 1.5) [77], [90]–[92].

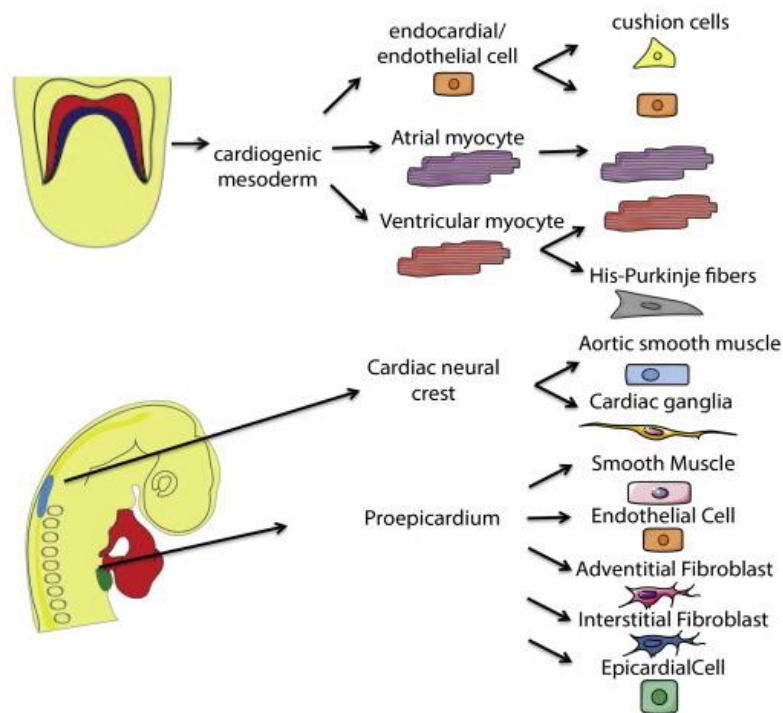


Figure 1. 5 Developmental origins of different cardiac cell types.

Multiple cardiac cell types originate from cardiac mesoderm such as multiple cardiomyocyte subtypes (top), and from extra-cardiac lineages: cardiac neural crest and pro-epicardium contribute to the heart and coronary vessel cells, epicardial cells and fibroblasts (bottom). Adapted from [93].

Cardiogenesis is precisely regulated temporally and spatially by a myriad of signalling pathways and networks of transcription factors (TFs), where excellent reviews provide detailed discussions of this topic [77], [81], [82], [88]–[95]. Briefly, some of the most important mechanisms for vertebrate cardiogenesis involve the modulation of canonical and non-canonical WNTs, transforming growth factor beta (TGF β) superfamily members

like bone morphogenic protein (BMP) and Activin/Nodal, fibroblast growth factors (FGFs), sonic hedgehog (Shh), and Notch signalling pathways that consequently activate a set of transcription factors specific for mesoderm induction (e.g. Brachyury: T or Bry) cardiac mesoderm specification (eg. mesoderm posterior 1: MESP1), cardiac growth and patterning, where committed cardiovascular progenitors can be defined by key transcription factors such as NKX2.5 (NK2 homeobox 5), GATA4, TBX5 (T-box 5), MEF2C (myocyte-specific enhancer factor 2C) and ISL1 (Islet 1). GATA4 and NKX2.5 are central for both FHF and SHF specification; however TBX5 is restricted to FHF only, while ISL1 and MEF2C mark the cardiac progenitor cells in the SHF. A summary of differentiation steps and key transcription factors related to early FHF and SHF development is shown in Figure 1.6.

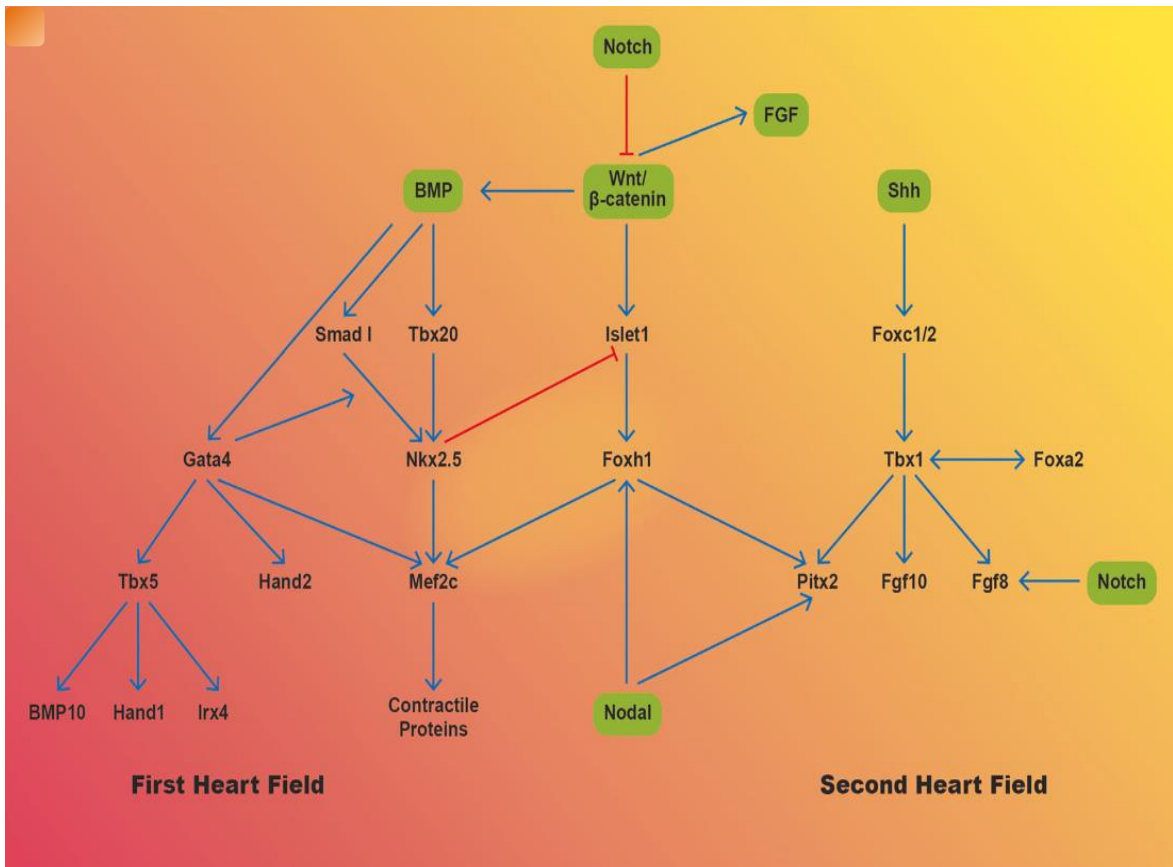


Figure 1. 6 Regulation of heart development by transcriptional networks and signalling pathways.

Summary of signalling pathways (green) and transcription factor interactions during FHF and SHF development, where some of them overlap in both fields. Adapted from [90].

Meanwhile, early endocardial cells can be distinguished by the expression of the transcription factor nuclear factor of activated T cells 1 (NFAT2 or NFATC1) [84], [96], and BMP10 signalling plays an important role in their development [97]. While

endocardial development still arises from early stages of cardiac mesoderm, the epicardium arises at later stages of development. Pro-epicardial development relies on FGF and BMP signalling [98], and pro-epicardial/epicardial cells are marked by the expression of TBX18 and WT1 (Wilms Tumor 1), as well as by FHF and SHF markers NKX2.5 and ISL1 [92], [99]–[102]. Notably, other sources of progenitors can contribute to the formation of cardiomyocyte subtype lineages, a process which is further regulated by signalling pathways such as BMP, Notch and retinoic acid (RA) (Figure 1.7) [103]. For example, HCN4+ FHF cells may contribute to the formation of SAN conduction cells. Recently, single-cell RNA sequencing (scRNA-seq) studies have been instrumental for the detection of transcriptional signatures of subtype-specific cardiomyocytes during early mouse development and mammalian PSCs at single cell level [104]–[106].

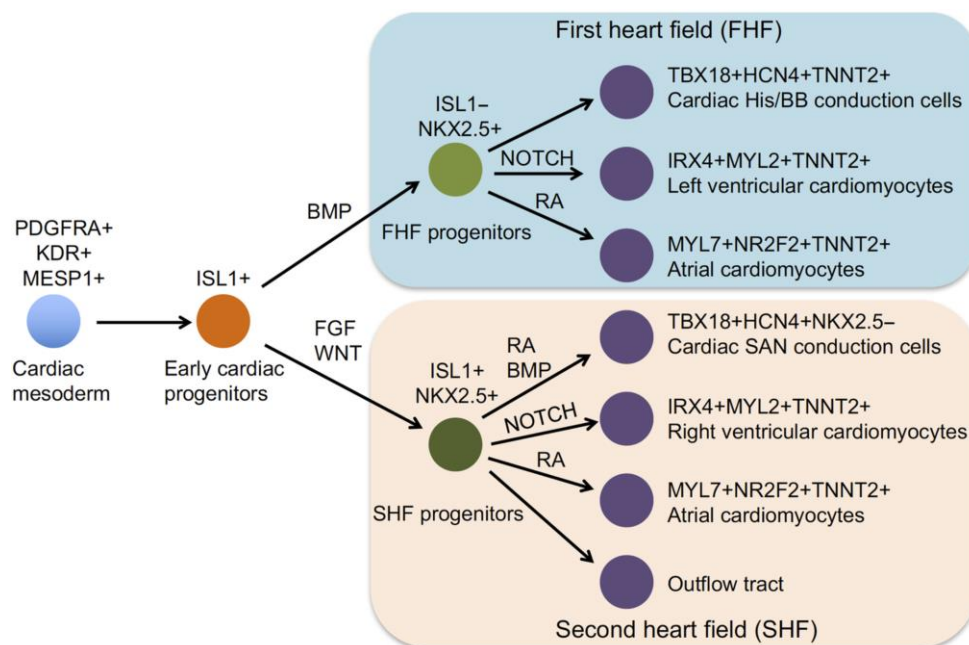


Figure 1. 7 Regulation of cardiac subtype commitment in response to signalling pathways.

The comparison of molecular markers and signalling pathways leading to final cardiomyocyte subtypes in mammalian cardiogenesis. Adapted from [103].

In addition to the biochemical cues, mechanotransduction events like stretching and shear stress were also reported to be influencing CM, SMC and EC differentiation [107]–[114]. Finally, a scheme of developmental cardiac commitment of all general cell types and distinct regions of the mammalian heart is summarized in Figure 1.8 [115].

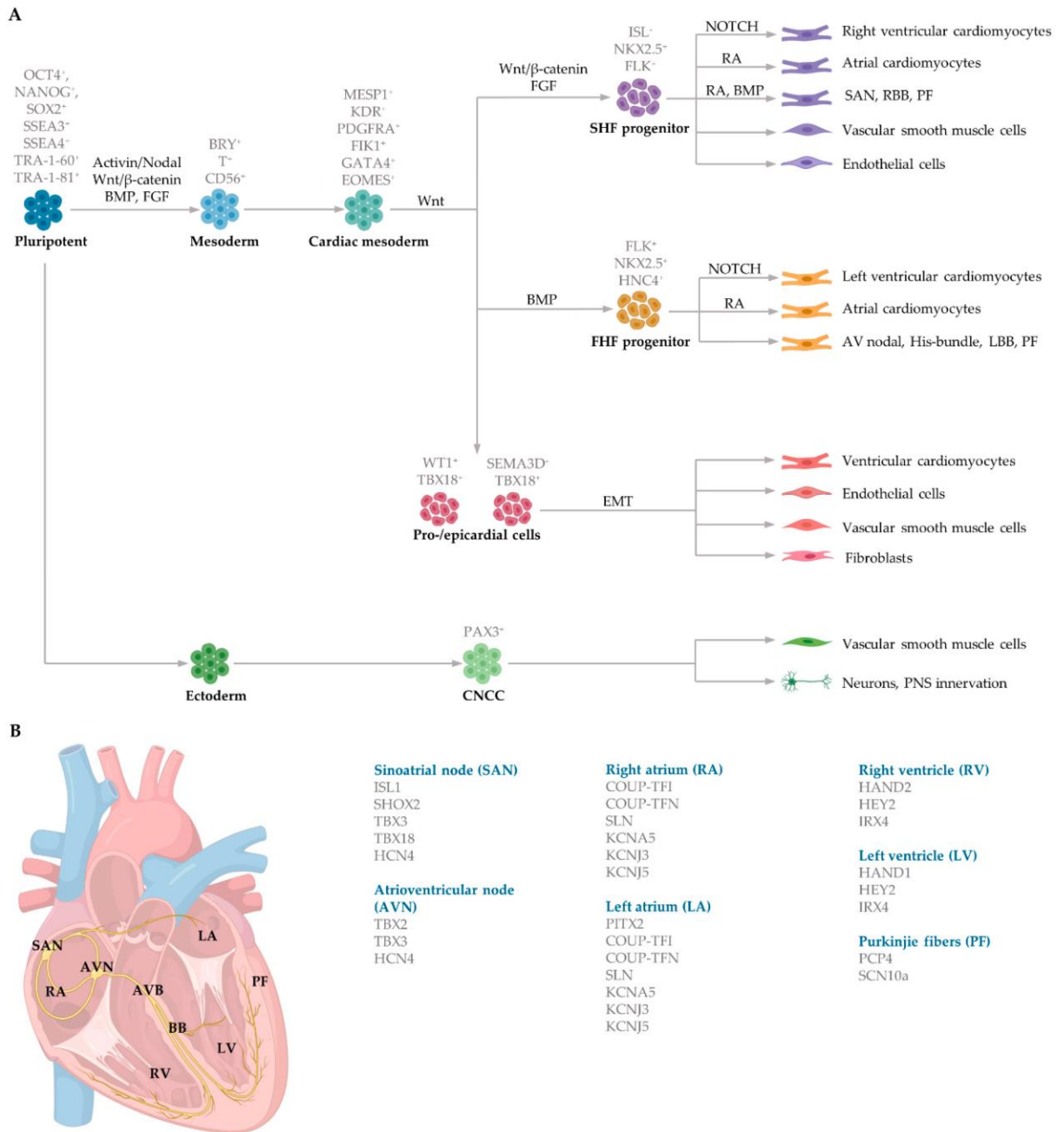


Figure 1. 8 Summary of mammalian cardiac commitment from embryonic development to mature heart.

A. Key signalling pathways and markers regulating the development of pluripotent stem cells into the different lineages of the heart. **B.** Markers for distinct compartments of the human heart. Adapted from [115].

1.2.2 The Cellular Composition of the Adult Heart

Defining the exact cellular composition and the interactions among the distinct components of the human heart is crucial for modelling the complexity and the heterogeneity of this organ *in vitro*, as this information could help predict outcomes of healthy vs. diseased states more precisely. In the scope of complex cellular heterogeneity in the mammalian heart, the four major cell types are generally defined as cardiac fibroblasts (CFs), cardiomyocytes (CMs), smooth muscle cells (SMCs), and endothelial cells (ECs) [77], while determining their exact proportions in terms of cell numbers and volume has been historically challenging.

During the last decade, techniques such as flow cytometry, fluorescence-activated cell sorting (FACS) [116], proteomics [117], and more recently single-cell technologies (e.g. scRNA-seq) have been employed to revisit and identify different cell populations of the adult heart [118]. In particular, scRNA-seq technologies have enabled the detection of novel individual cell phenotypes at higher resolution as well as rare cell populations [119].

Of note, in a recent study by Litviňuková and collaborators, single cell technologies were applied to profile the transcriptome of 486,134 cells and nuclei from six anatomical cardiac regions from a diverse cohort of adult heart donors. By integrating this data with machine learning methods, 11 major cardiac cell types and 62 different cell states were identified under the so called *Human Heart Cell Atlas* (Figure 1.9) [118], [120]. Here, not only the traditionally four-major cardiac cell types (CMs, CFs, SMCs and ECs) were characterized, but also other non-myocytes such as cardiac-resident macrophages (myeloid & lymphoid), adipocytes, pericytes, neuronal and mesothelial (~epicardial) cells were described. Furthermore, distinct populations of atrial and ventricular CM subsets with stark transcriptional and functional differences were revealed.

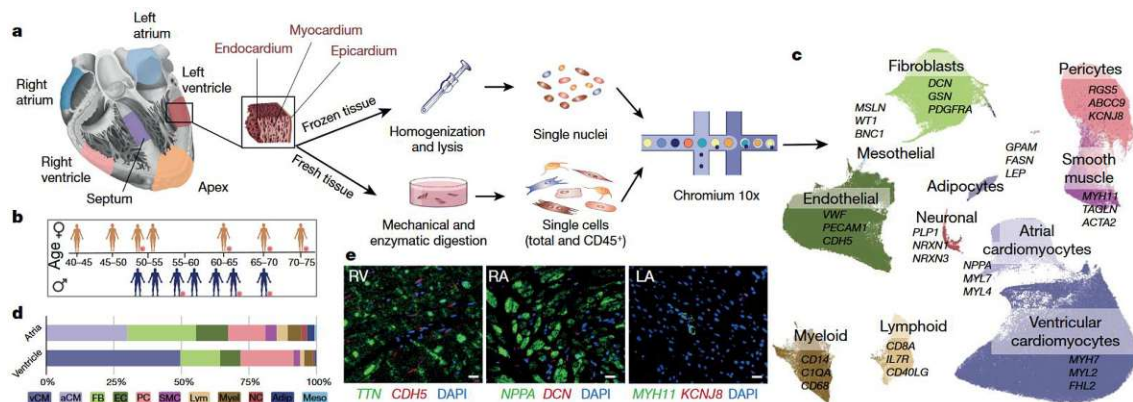


Figure 1. 9 Cells of the adult human heart.

A. Sample collection from heart-wall sections including left and right atria, left and right ventricles, apex and septum. **B.** Infographic for the cohort of adult heart donors. **C.** Uniform manifold approximation and projection (UMAP) detecting 487,106 cells and nuclei outline 11 cardiac cell

types and marker genes. **D.** Different cell populations between atria and ventricles. **E.** RNA fluorescence in situ hybridization (FISH) staining for cell type specific transcripts for right ventricle (RV): *TTN* (green, cardiomyocytes) and *CDH5* (red, EC), right atrium (RA): *NPPA* (green, aCM) and *DCN* (red, FB), and left atrium (LA): *MYH11* (green, SMCs) and *KCNJ8* (red, pericytes). Counterstaining with DAPI (blue). Adapted from [118].

Remarkably, it was also revealed that the populations of the main cell types varied between atrial and ventricular tissues in the adult heart. Atrial tissues were found to contain 30.1% cardiomyocytes, 24.3% fibroblasts 17.1% mural cells (pericytes and SMCs), 12.2% endothelial cells and 10.4% immune cells (myeloid and lymphoid). In comparison, ventricular tissues (apex, interventricular septum, left and ventricle) were found to contain 49.2% ventricular cardiomyocytes, 21.2% mural cells, 15.5% fibroblasts, 7.8% endothelial cells and 5.3% immune cells. [118] In the following sections, we will mainly focus on the four major cell types of the human heart in more detail for the scope of the dissertation.

1.2.2.1 Cardiomyocytes (CM) and their maturation

Cardiomyocytes (CM) are the powerhouse, the specialized muscle cells of the heart that make up the thick contractile “myocardium” layer. Similar to skeletal muscle cells, cardiomyocytes are also defined to compose a striated, although involuntary, muscle.

Previous rodent studies had estimated the cardiomyocyte population would cover ~75% of normal adult myocardial volume, but recent histological, flow cytometry and single cell sequencing results revealed that they account for 30-40% of total cell numbers with variations between mouse, rat and human hearts [116], [118], [121]–[124].

A typical cardiomyocyte is filled with long chains of myofibril structures known as *sarcomeres* – the major contractile units of the striated cardiac muscle deputed to ensure the beating [125], [126]. Sarcomeres are composed of structures called A, M, I and Z-lines (Figure 1.10A). The A-band contains thick filaments of myosin and their associated proteins. The M-line stands for the “middle” of A-band, I-band stands for “intermediate” filaments consisting of thin actin filaments and actin-binding proteins. The Z-line is the defining units of sarcomeric boundaries, which is found in the middle of the I-band, contains the greatest number of sarcomeric proteins and considered as the scaffold that links the contractile units among themselves [127]. Mature sarcomeres consist of thin filaments (sarcomeric actin, troponins, tropomyosin), thick filaments (myosin heavy and light chains and their associated proteins, such as myosin binding protein C), TTN (titin) filaments, Z-lines (actinin and its interacting proteins), and M-lines (myomesin, and its interacting proteins) [128]. A brief scheme of CM ultrastructure is depicted in Figure 1.10B.

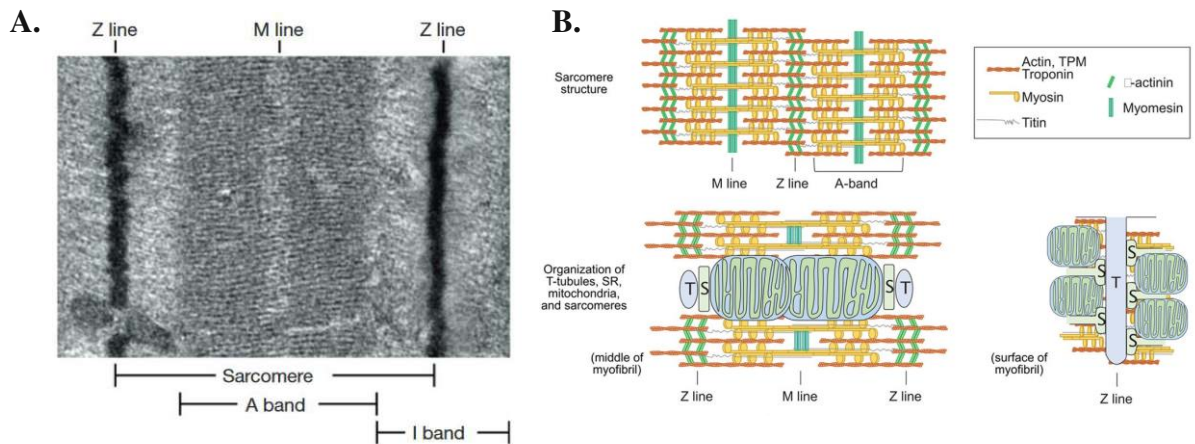


Figure 1. 10 Cardiomyocyte ultrastructure.

A. Electron microscopy image of a striated muscle sarcomere. Adapted from [127]. **B.** Scheme of sarcomere components in mature CM, and spatial relationship between sarcomeres (S), t-tubules (T), sarcoplasmic reticulum (SR) and mitochondria in mature CMs. TPM; Tropomyosin. Adapted from [128].

Specialized structural sarcomeric proteins present in all CMs include sarcomeric α -actinin (ACTN2), which localize at the sarcomeres; and Cardiac Troponin T (TNNT2), a tropomyosin binding protein regulating the thin filaments, which determine the calcium (Ca^{2+}) sensitivity required for the contraction of the CMs by regulating the structure of actin filaments [129], [130]. Cardiomyocytes show high-level expression of genes that encode for contractile force-generating sarcomere proteins (TTN, MYBPC3 and TNNT2) and calcium-mediated processes (RYR2, PLN and SLC8A1) [118].

As all the striated muscles, cardiac muscle is also characterized by the presence of highly branched invaginations of CM sarcolemma (ie. plasma membrane), called cardiac transverse tubules (t-tubules), that are rich in ion channels important for excitation-contraction coupling, maintenance of resting membrane potential, action potential initiation and regulation, and signal transduction [131]–[135]. Early ultrastructural studies of cardiac muscle have shown that t-tubules are found at the Z-line, at the end of each sarcomere (Figure 1.11) [136]. However, not all CMs have t-tubules or they may only have limited structures. For example, in vitro pluripotent stem cell-derived CMs (PSC-CMs), in vivo embryonic and neonatal CMs lack t-tubules, as these structures only start to develop during the first weeks of life through adulthood (Figure 1.11); mostly in ventricular CMs [128], [132]–[134]. Meanwhile atrial CMs and Purkinje cells also lack distinct occurrence of t-tubules [133], [134], [137]. In addition, primary adult ventricular CMs kept in culture start

to lose their t-tubules, gradually losing their maturity and showing more fetal-like features, making it difficult to maintain the characteristics of adult CMs in vitro [134], [138], [139].

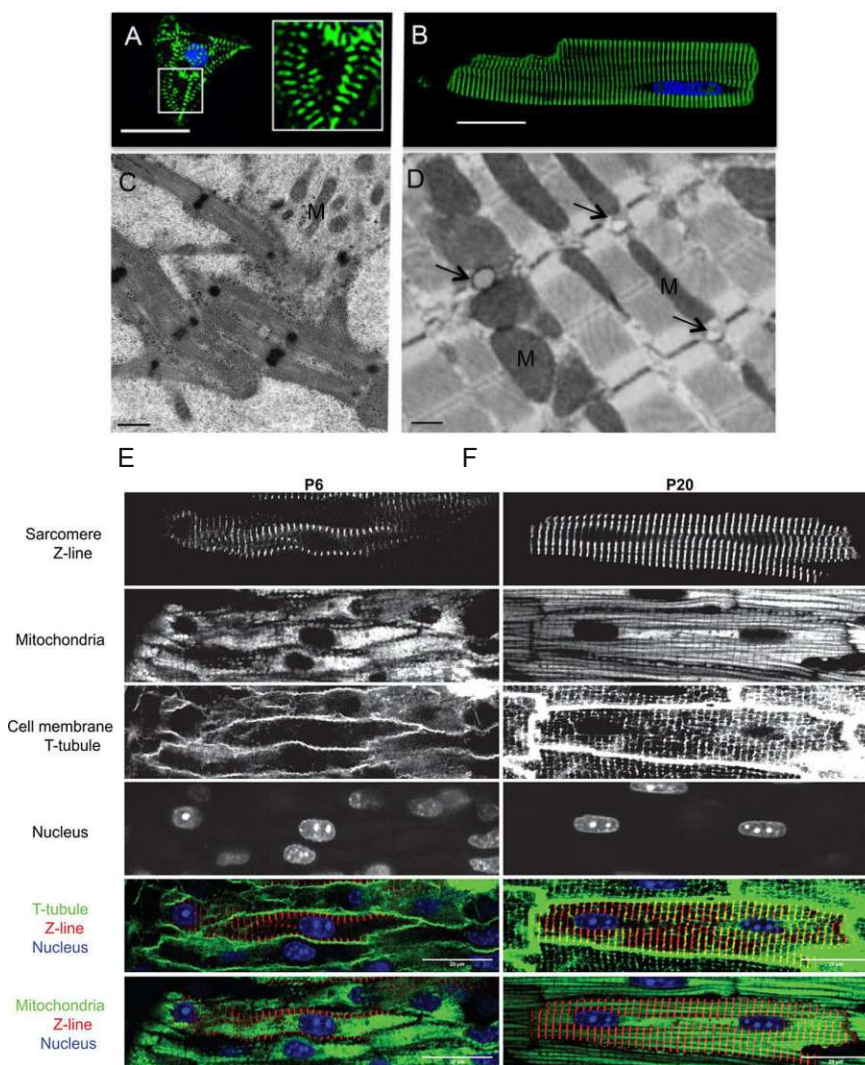


Figure 1. 11 Ultrastructural differences in immature and mature CMs.

A. (hPSC-CM) and **B.** (adult rat) cardiomyocytes with alpha-actinin immunostaining (green) and blue nuclear counterstain, with their ultrastructure by electron microscopy (**C.** hPSC-CM and **D.** adult rat): M: Mitochondria, arrows depict t-tubules cellular ultrastructure by electron microscopy (Scale bar in A and B: 25 μm , C and D: 0.2 μm) **E.** Confocal image of murine CMs at postnatal day 6 (P6) as compared to **F.** postnatal day 20 (P20).

Note the differences between cell size, length-to-width ratio, mitochondria quantity, size and morphology, appearance of t-tubules and elongated nuclei. A-D. Adapted from [140] E-F. Adapted from [128].

As for CM subtypes, according to single-cell sequencing analyses, ventricular cardiomyocytes can be distinguished by genes encoding sarcomere proteins (MYH7 and MYL2), transcription factors (IRX3, IRX5, IRX6, MASP1 and HEY2), and PRDM16, while atrial cardiomyocytes express prototypic genes (predominantly MYL7, NR2F2), and ALDH1A2 (an enzyme required for retinoic acid synthesis), ROR2, (important for Wnt modulation), and SYNPR, which is important for the mechanosensing of TRP channels by atrial volume receptors [118]. Additionally nodal cells feature the expression of [hyperpolarization-activated cyclic nucleotide-gated potassium channel 4 (HCN4) [141 and Figure 1.7].

In terms of contractility, the varying occurrence of t-tubules results in differences in calcium handling properties between immature and mature CMs. While immature CMs can rely on the calcium released at the cell periphery to initiate sarcomere contraction, mature CMs with t-tubules wrapped around the myofibrils could make calcium release and re-uptake faster and more efficient with the help of ryanodine receptors (RYR) in sarcoplasmic reticulum [142], [143].

As can be seen above, there are some major differences between immature and mature CMs, in which the latter is difficult to replicate *in vitro* (Table 1.1).

During CM maturation, sarcomeres go through further ultrastructural changes. When observed by transmission electron microscope (TEM), sarcomere bandings in mature CMs appear clearer and more aligned as compared to immature CMs, as the distance between Z-lines (sarcomere length) increases to $\sim 2.2 \mu\text{m}$ upon maturation [128], [140], [144].

A major hallmark of CM maturation is the switching of myofibril gene isoforms in the sarcomeres. In maturing adult hearts, the most well-known switch is the myosin heavy chain (MYH) switch in CMs, where the predominant gene variant switches from *MYH6* to *MYH7*, which is already established by 5 weeks of gestation [104], [145]. In *in vitro* hiPSC-derived CMs, the predominant isoform is *MYH6*, as in fetal CMs [146]. It should be noted that in rodents such as mice, unlike humans, this switch is the opposite during heart maturation, where *Myh6* becomes predominant compared to *Myh7* [128], [147].

Other sarcomeric components such as myosin light chains (MYL or MLC), cardiac troponin I (TNNI), and titin (TTN) also go through isoform switch during maturation of human CMs. During early development, the *MYL7* isoform (also known as *MLC2a* for *atrial*) is expressed on all cardiomyocytes, however, as CMs mature, *MYL7* becomes restricted to atrial myocytes, whereas the predominant isoform switches to *MYL2* (also known as *MLC2v* for *ventricular*) for ventricular myocytes [148], [149]. While fetal CMs predominantly express slow skeletal troponin I (*TNNI1*), mature CMs express cardiac troponin I isoform (*TNNI3*) [150]. Titin (*TTN*), which is responsible for the maintenance of sarcomere integrity and tissue elasticity, undergoes alternative splicing and switches from a longer N2BA isoform (i.e. including both N2B and N2A elements of titin) to a shorter and stiffer N2B isoform, excluding the N2A component [151], [152]. RBM20 and RBM24

(RNA-binding motif protein 20; 24) have been defined as key splicing regulators in the heart especially during maturation [152].

For contractility and electrophysiology, in addition to the appearance of t-tubules – as mentioned previously – genes regulating their structure and calcium handling are also differentially expressed between early and mature CMs. In mature CMs, the first polarization activates the release of calcium stored in the sarcoplasmic reticulum by RYR2, which is then pumped back to the sarcoplasmic reticulum by SERCA2 (sarco/endoplasmic reticulum Ca^{2+} -ATPase, or ATP2A2). Along with *RYR2* and *SERCA2A*, genes involved with many ion channels have increased expression in mature CMs, such as L-type calcium channels (*Cav1.2*), inwardly rectifying potassium channels (*Kir2.1* and *Kir2.2*, encoded by *KCNJ2* and *KCNJ12*), voltage-gated sodium channels (*Nav1.5*, encoded by *SCN5A*), and pacemaker channels such as hyperpolarization-activated cyclic nucleotide-gated potassium channel 4 (*HCN4*), in addition to calcium-binding proteins such as calsequestrins (*CASQ1*, *CASQ2*) [115], [128], [140], [143]. Furthermore, mature CMs can be characterized by the increased expression of the gap-junction protein Connexin 43 (*CX43* or *GJA1*), since a tight conduction of the cells is required to propagate the electrical impulse for the beating [153], [154].

CMs are known to have very active mitochondria, since they rapidly need to produce ATP required for their beating activity [155]. In accordance to this, more mature CMs feature an increased number and size of mitochondria, where they occupy up to 20-40% of the cell volume, they become more elongated, and localize closer to the sarcomeres [156], [157]. Also metabolic differences exist between fetal and mature CMs: while fetal CMs depend on glycolysis, mature CMs switch to fatty acid oxidation right after birth in order to generate the required amount of ATP [158],[159]. This transition is mediated by transcriptional regulators such as *PPARGC1A/B*, *PPARA*, *NRF1/2*, the upregulation of genes involved in fatty acid oxidation, oxidative phosphorylation and mitochondrial biogenesis, and downregulation of glycolytic genes [157], [160], [161]. Additionally, the increased number of mitochondria in mature CMs is associated with increased expression or isoform switch of genes related to ATP synthesis-coupled electron transport chain. For example, *COX* (cytochrome c oxidase) subunit 8, a component of complex IV of the electron transport chain, switches between *COX8A* and *COX8B* isoforms in cardiomyocyte maturation [128], [162].

Unlike adult CMs, immature CMs and *in vitro* hiPSC-derived CMs continue to rely on glycolysis as the primary source of energy [163]. While the healthy heart can oxidize several substrates from energy production, classic studies estimate that ATP production comes preferentially from fatty acid (FA) oxidation, accounting for around 70% of the total generation. The rest is provided by alternative substrates, such as glucose, lactate and pyruvate [164].

The viscoelastic properties of cardiac extracellular matrix (ECM) are also different in immature vs adult hearts. For example, the stiffness – or elastic modulus – of ECM

progressively increases from neonatal (<10 kPa) to adult (~25 kPa) heart, which is also modulated by the increased number in cardiac fibroblasts and their ECM secretion [165].

Another hallmark of CM maturation is the post-natal emergence of binucleated cells, as compared to mononucleated. This is linked to a transition from proliferation-to-hypertrophy during pre-natal to post-natal transition. In pre-natal development, CMs can still proliferate, but although this rate declines rapidly in post-natal life, the heart size increases by ~30-fold postnatally by volume in a process called *maturational hypertrophy* [128]. In adult humans, although ~75% of CMs are mononucleated, due to DNA replication without karyokinesis, around 25-30% of CMs are binucleated, which largely happens during the second decade of life [166]–[168].

Although the cardiac cells have an ability to regenerate during pre-natal development (in which they are in a low-oxygen environment), after birth CMs lose the ability to regenerate. After birth, the metabolic switch from a glycolytic to an oxidative metabolism results with an increase in reactive oxygen species (ROS) making the cells more prone to DNA damage response [169]. This causes the CMs to have cell-cycle arrest and mostly lose the capacity to regenerate [170]. CM turnover decreases exponentially with age and is estimated to be <1% per year in adult humans [168]. The mechanisms that force the CMs to exit cell cycle include the downregulation of mitogenic signals, such as the neuregulin-ErbB (Erb-B2 receptor tyrosine kinase) axis [171], and the inhibition of Yes-associated protein (YAP) by the mechanosensitive Hippo pathway [172], [173].

During pre-natal CM development, Hippo activity is high, and YAP activity is low, which is necessary for CM proliferation and heart development. However, during postnatal CM maturation, YAP is inhibited by the Hippo pathway, cell-to-cell and –ECM interactions by integrins and focal adhesions, resulting in the negative regulation of Wnt target genes, and thus the prohibition of CM proliferation and myocardium regeneration [173]–[177]. If Hippo is inactivated or YAP is activated, CM proliferation increases while apoptosis decreases. YAP activation also causes fetal gene expression and CMs could dedifferentiate [176], [178]–[180] (Figure 1.12).

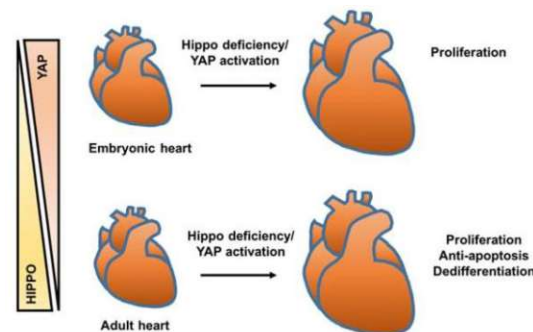


Figure 1. 12 Hippo pathway during heart development and homeostasis.

In pre-natal heart development, Hippo activity is low and YAP activity is high, while in post-natal heart this is the opposite causing the loss of heart regenerative ability. The reactivation of YAP (or Hippo inhibition) in adult cardiomyocytes occurs in injured hearts as a strategy to increase their survival and is associated with fetal gene re-expression. Adapted from [179].

A summary of major characteristics of immature and mature CMs are summarized in Table 1.1.

Table 1. 1 Major Hallmarks of CM Maturation

Parameters	Immature CM	Mature CM
Cell morphology	Circular	Rod-shaped
Sarcomeres	1.6 μm , disorganized	2.2 μm , highly organized
Predominant myofibrillar isoforms	MYH6 (human)	MYH7 (human)
	MYH7(mouse)	MYH6 (mouse)
	MYL7 (all CMs)	MYL2 (ventricular) vs. MYL7 (atrial)
	TNNI1	TNNI3
	TTN-N2BA	TTN-N2B
T-tubules	No	Yes
Mitochondria	Irregular, small, round shaped, occupies small fraction of cell volume	Regular, oval shaped, occupies ~20-40% of cell volume
Nucleation	Mononucleated	~25-30 % Binucleated
Metabolism	Glycolysis	Fatty acid oxidation Oxidative phosphorylation Increased gene expression of eg. <i>PPARGCIA</i> , <i>PPARA</i> , <i>ESRRA</i>
Ca ²⁺ handling	Immature Ca ²⁺ handling, low expression of Ca ²⁺ handling molecules	Increase of Ca ²⁺ handling molecules, such as <i>Cav1.2</i> , <i>RYR2</i> , and <i>SERCA2</i>
Cell cycle	Mitogens drive proliferation	Mitogens drive hypertrophy
ECM binding	β 1 integrin, collagen I, fibronectin	Laminin, basement membrane

Compiled with modifications from [115], [128], [140], [143]

Due to the inability of CM proliferation in post-natal life, many forms of heart disease are linked to a decrease, or irreversible damage in CMs, and their remodelling is influenced by cell-to-cell and -ECM interactions between CMs and other cell types of the heart.

1.2.2.2 Cardiac fibroblasts (CF)

Cardiac fibroblasts (CFs) are the most abundant non-myocyte cell type of the heart, dispersed as sheets and strands providing a scaffold between cardiomyocytes. They were initially believed to be making up between 27%-50% of the mammalian cardiac cell population [76], [77]. However this belief was challenged by recent histology and flow cytometry studies showing that CFs cover less than 20% of the adult murine and human heart [116].

Fibroblasts are the main mediators of extracellular matrix (ECM) production and of tissue repair in every organ [181], and CFs produce the ECM scaffold of the heart, involved in cell-to-cell communication, take part in cardiac conductivity through gap junction proteins (e.g., connexin-43), and are involved in ECM remodelling in response to heart failure (HF) [76], [182]–[188]. CFs maintain ECM homeostasis via matrix metalloproteinases and their inhibitors, thus facilitate the secretion and degradation of collagen [189].

As mentioned previously, in a healthy human heart, according to recent single-cell sequencing studies, the fibroblast population is believed to be roughly equivalent to the number of cardiomyocytes: 25-32% of the total number of cells of the heart; however, these numbers could change with development, ageing and disease [183], [191]. For example, an increase in CFs was reported in heart failure and following myocardial infarction (MI)[192]–[194].

Common markers for adult CFs include decorin (DCN), gelsolin (GSN), transgelin (TAGLN or SM22 α), regulator of G protein signalling 5 (RGS5), α -smooth muscle actin 2 (ACTA2 or α -SMA), Thy-1 cell surface antigen (THY1 or CD90), platelet derived growth factor receptor alpha (PDGFR- α), S100 calcium binding protein A4 (S100A4), discoidin domain receptor tyrosine kinase 2 (DDR2), lymphocyte antigen 6 complex, locus A (LY6A or Sca-1) 1, vimentin (VIM), and collagen type I alpha 1 chain (COL1A1) [76]. Due to their primarily epicardial origin during embryonic development, TCF21, WT1, TBX18, and PDGFR- α are well-established markers of early CFs – although only TCF21 and PDGFR- α are known to be expressed by resident mature fibroblasts of the adult heart [76], [195]–[198]. Fibroblast-specific protein 1 (FSP-1) is another reported CF marker that is also expressed on endothelial cells [199]. In addition, the mesenchymal marker Fibroblast TE-7 is also frequently used to label primary and iPSC-derived CFs [200]–[203].

In response to disease or injury, such as myocardial infarction (MI), CFs become activated, and eventually transdifferentiate into myofibroblasts (Figure 1.13). The activated myofibroblasts tend to have a spindled shape, contain actin stress fibers, highly express markers such as α -SMA, FSP-1, fibroblast activating protein (FAP), fibronectin splice variant ED-A, periostin (POSTN) [76], [204], have a contractile phenotype, increased proliferation, and increased secretion of ECM such as collagens (eg COL1 and COL3) and fibronectin (FN1) [183], [205]–[208]. This phenomenon is known as “cardiac fibrosis”.

Multiple mechanisms are involved for CF activation, such as mechanical stimuli, or paracrine factors such as transforming growth factor- β (TGF- β) and angiotensin II (Ang II) [209]–[214]. Moreover, YAP activation in activated CFs sustains ECM remodelling during cardiac fibrosis [182]. After injury or MI, because of increased ECM secretion from activated CFs, a fibrotic scar is formed on the myocardium to prevent its rupture. Due to its contractile phenotype, the fibrotic scar shrinks, produces tension, and increases the stiffness of the myocardium [205], [215]–[217]. While this initially helps to maintain the heart wall integrity and avoid further damage to the myocardium, in long term, if persistent pro-fibrotic mechanisms are triggered, this leads to the deterioration of heart function, and ultimately resulting in heart failure (HF) (Figure 1.14) [181]–[183], [214], [218].

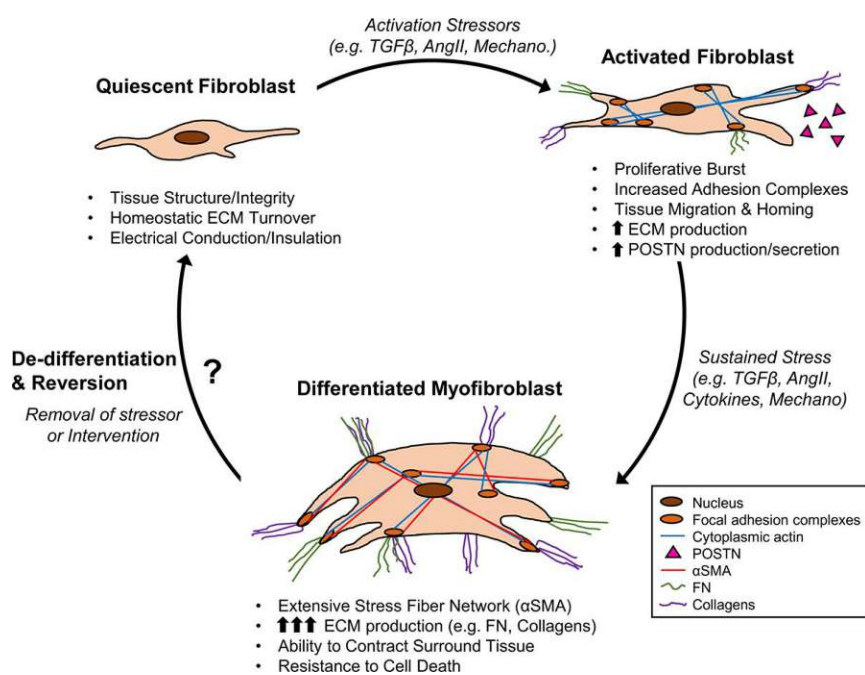
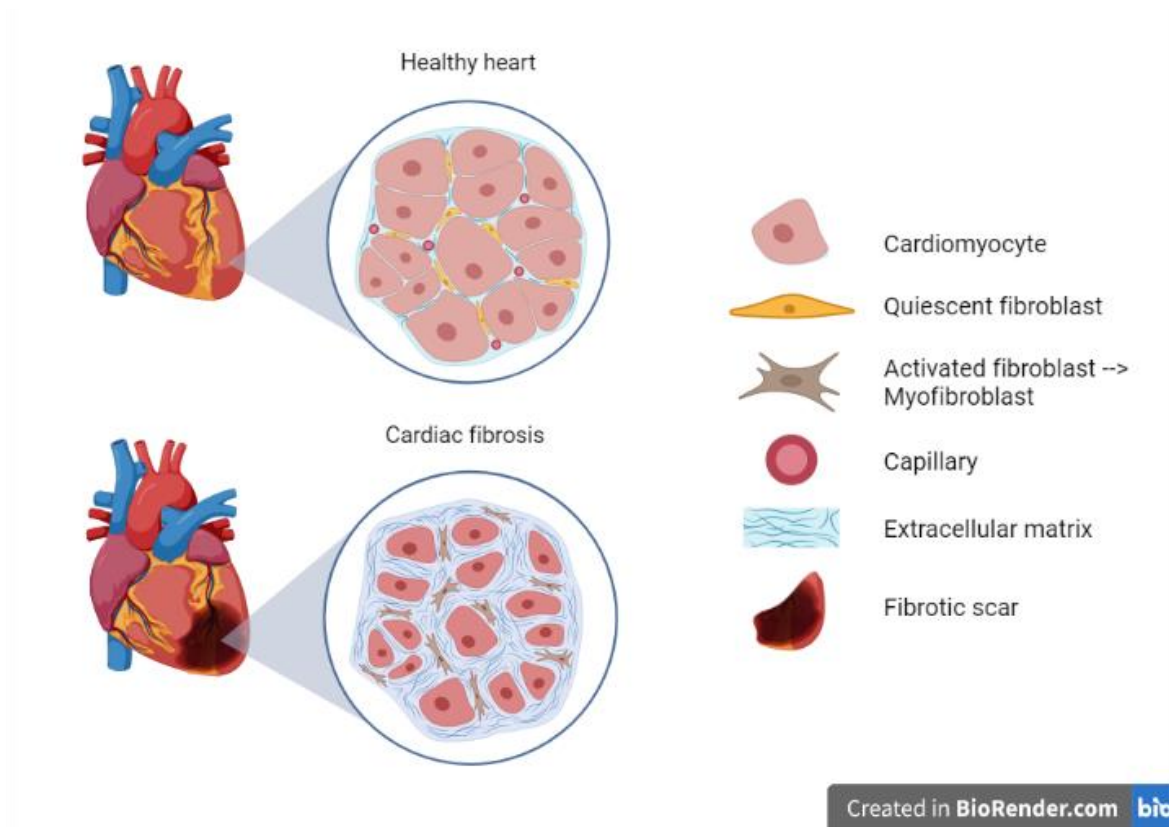


Figure 1. 13 Cardiac fibroblast to myofibroblast conversion.

Quiescent CFs are responsible for cardiac homeostasis under normal physiological conditions. In response to mechanical stress, injury, disease or pro-fibrotic mediators (eg, TGF β , AngII), resident CFs become activated, infiltrate and proliferate at the site of injury, and begin ECM remodelling. In case of sustained pro-fibrotic stressors, these fibroblasts differentiate into “myofibroblasts” characterized by the expression of α SMA and POSTN, and the excessive production of ECM proteins (FN [fibronectin], collagens). Persistent myofibroblast activation leads to maladaptive tissue remodelling, deterioration of cardiac function, and ultimately heart failure. Myofibroblasts may also de-differentiate upon removal of stress stimuli; however, these mechanisms are understudied. Adapted from [181].



Created in [BioRender.com](https://www.biorender.com/) **bio**

Figure 1. 14 Histopathology from healthy heart to cardiac fibrosis.

In the healthy heart, the ECM is a 3D network of collagen fibers embedding cardiomyocytes, capillaries and quiescent cardiac fibroblasts, while maintaining the cardiac homeostasis under normal physiological conditions. In response to mechanical stress, injury, disease or pro-fibrotic events, CFs become activated, transdifferentiate into myofibroblasts, and start remodelling the ECM at the site of the injury. Persistent injury leads to maladaptive tissue remodelling, deterioration of cardiac function, high deposition of ECM – thus stiffening of the heart tissue with a “fibrotic scar”, and ultimately heart failure. Created with [BioRender.com](https://www.biorender.com/).

1.2.2.3 Endothelial cells (EC)

Endothelial cells in the mammalian heart cover the lumen of cardiac chambers, blood and lymphatic vessels [141]. In the normal mammalian myocardium, cardiomyocytes are surrounded by a network of capillaries and are contiguous to endothelial cells [219]. As cells with high metabolic demands, cardiomyocytes depend on the network of endothelial cells not only for oxygen and nutrient supply, but also for paracrine signals that promote cardiomyocyte organization and survival (Figure 1.15) [219], [220]. It was recently shown that endothelial cells make more than 60% of non-myocytes in the adult mouse-heart, which is much higher than previously estimated [116]. Commonly known markers of ECs of the human heart include platelet and endothelial cell adhesion molecule 1 (PECAM1 or CD31), cadherin 5 (CDH5), von Willebrand factor (VWF), and vascular endothelial growth

factor receptor type 2 (VEGFR2; Flk-1; KDR), while EC subtypes such as arterial ECs could be marked by the expression of prospero homeobox 1 (PROX1), FMS related tyrosine kinase 4 (FLT4), podoplanin (PDPN), bone marrow tyrosine kinase gene in chromosome X non-receptor tyrosine kinase (BMX), and natriuretic peptide receptor 3 (NPR3) [141], [191], [221], [222].

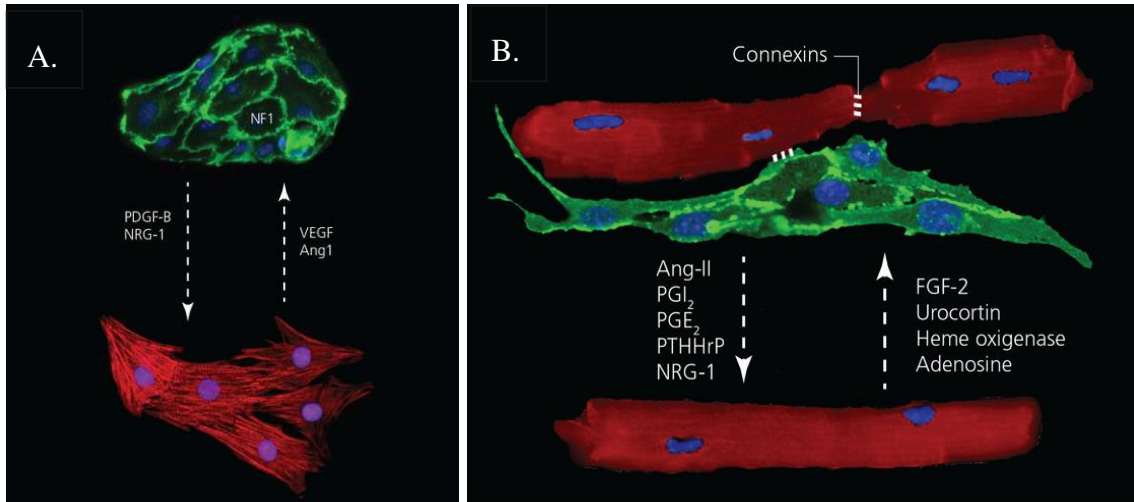


Figure 1.15 Endothelial cell – cardiomyocyte crosstalk.

EC and CM crosstalk mediated by the bidirectional signalling of secreted molecules, transcription factors and cell-cell interactions (A.) during early development and (B.) during post-natal life. Dashed arrows show the direction of signals. ECs are labelled with CD31 (green), and CMs with α -actinin (red). Nuclear counterstaining in blue by 4',6-diamidino-2-phenylindole (DAPI). [Ang-I&-II, angiotensin-I & -II; NF1, neurofibromin-1; NRG-1, neuregulin-1; PDGF, platelet-derived growth factor; VEGF, vascular endothelial growth factor; ET-1, endothelin-1; FGF2, fibroblast growth factor 2; NO, nitric oxide; NRG-1, neuregulin-1; PGE2, prostaglandin E2; PGI2, prostacyclin; PTHrP, parathyroid hormone-related peptide.]

Adapted from [220].

For regulating EC-CM crosstalk and function, in addition to the markers unique to endothelial cells, other CM-related genes like Connexin 43 (*CX43* or *GJA1*), ATPase sarcoplasmic/endoplasmic reticulum calcium transporting 2 (*SERCA2A* or *ATP2A2*); titin (*TTN*); ryanodine receptor 2 (*RYR2*), myosin heavy chain 6 (*MYH6*) are also involved [141], [223].

In response to injury or myocardial infarction, genes involved in leukocyte migration [e.g., chemokine (C-C motif) ligand 9 (*CCL9*), C-X-C motif chemokine ligand 2 (*CXCL2*)] are upregulated in endothelial cells. Interestingly, about 7 days after MI, different genes related to collagen production (*COL3A1*), ribosome assembly and protein translation [ribosomal protein L9 (*RPL9*) and S12 (*RPS12*)], and cell proliferation [tumor protein, translationally

controlled 1 (*TPT1*), could be enriched [141], [224]. In case of heart failure (HF), the most relevant genes upregulated in ECs are linked with cell adhesion, angiogenesis, and cell migration (major histocompatibility complex, class I, B, *HLA-B*; EGF like domain multiple 7, *EGFL7*; receptor activity modifying protein 1 and 2, *RAMP1*, *RAMP2*; plasmalemma vesicle associated protein, *PLVAP*; inhibitor of DNA binding 1, *ID1*; and formin like, *FMNL3*), inflammatory response (*CX3CL1*; cluster of differentiation 74, *CD74*), as well as development and maturation (*SOX17*, *SOX18*) [141], [225].

1.2.2.4 Mural cells: Smooth muscle cells (SMC) & Pericytes

Smooth muscle cells (SMCs) are important for the vascular structures of the heart together with mural cells that surround the walls of capillaries, known as **pericytes**. SMCs are found in walls of larger vessels, whereas pericytes are found within microvessels. By contracting and relaxing, they regulate the blood vessel tone in order to maintain the blood pressure. They are commonly characterized by the expression of smooth muscle protein 22-alpha (*TAGLN* or *SM22 α*), - as an actin cross-linking/gelling protein – α -smooth muscle actin 2 (*ACTA2* or α -*SMA*), the specialized actin filament unique to SMCs, myosin heavy chain 11 (*MYH11*) [118]. Additional contractile markers include vitronectin (*VTN*), *RGS5*, potassium voltage-gated channel subfamily J member 8 (*KCNJ8*) and myocardin (*MYOCD*) [118], [141], [226]. It should be noted that markers such as *SM22 α* and α -*SMA* are also common to cardiac fibroblasts. Important mediators of SMCs include serum response factor (*SRF*), and its co-activator *MYOCD* are essential transcriptional regulators to determine the smooth muscle identity [227]–[229]. Furthermore, the most important signalling pathways for smooth muscle cells include *PDGF β* , *TGF β* , activin A, retinoids, angiotensin II, tumour necrosis factor- α (*TNF- α*), *FGF*, insulin-growth factor (*IGF*), endothelin-1, and nitric oxide (*NO*) [109], [230], [231], as summarized in Figure 1.16A.

SMCs have two very different phenotypes: synthetic SMC (sSMC) and contractile SMC (cSMC), which can convert into each other according to extracellular signals. Contractile SMCs are elongated, spindle-shaped cells, with a distinct pattern of actin filaments, while synthetic SMCs are less elongated and display cobblestone morphology [109]. Due to the peculiar distribution of actin network in the cSMCs, the regions where actin and ECM converge have been historically known as “dense bodies”. Interestingly, although being considered primarily specific to CMs, the protein cardiac troponin T (*TNNT2*) can also be expressed at the dense bodies of cSMCs, as part of the Ca^{2+} turnover regulatory system operating during SMC contraction [232]. Meanwhile, sSMCs are more proliferative and migratory than cSMCs [109]. The differences between sSMCs and cSMCs are briefly summarized in Figure 1.16B.

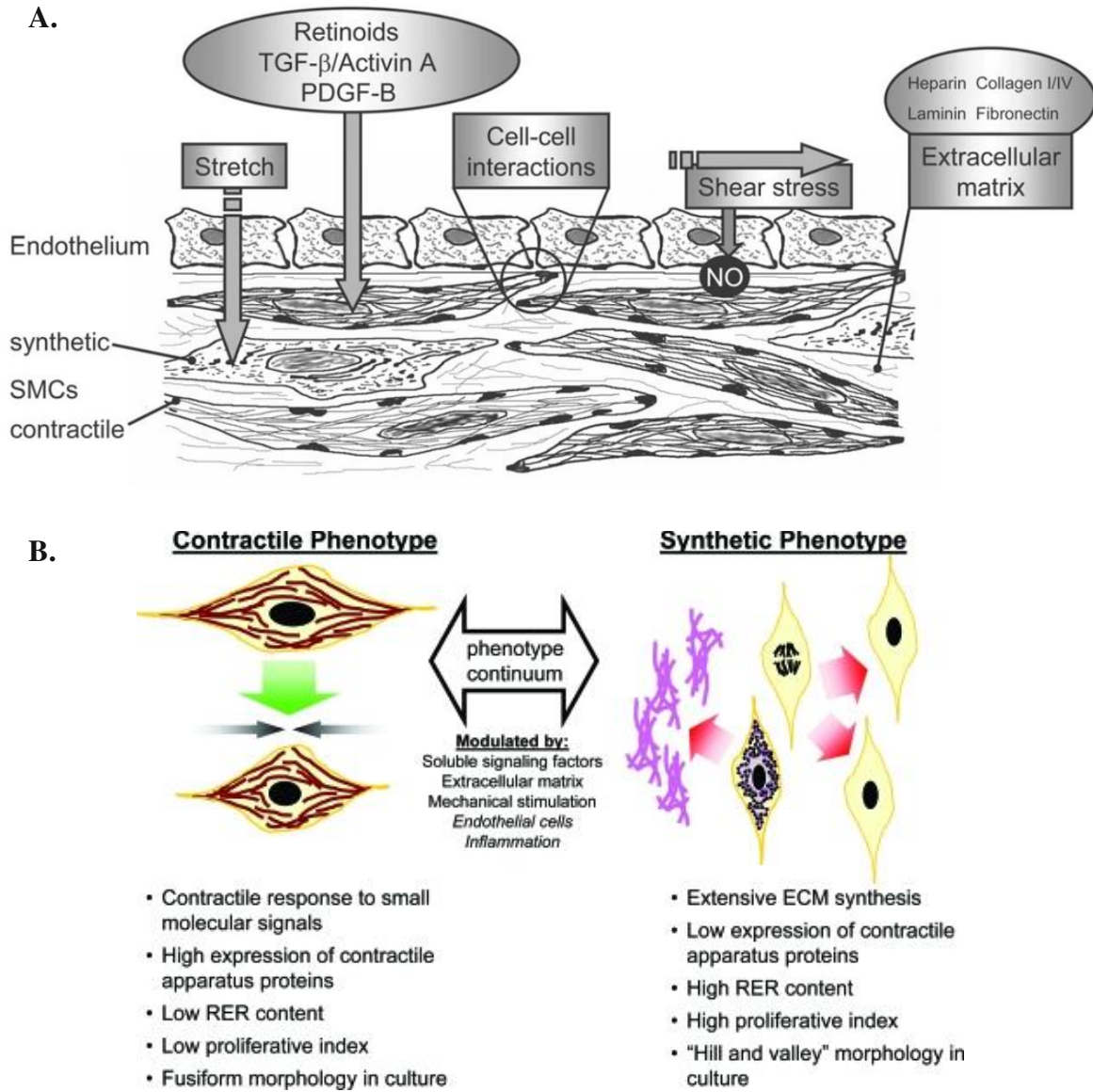


Figure 1. 16 Characteristics of the smooth muscle cells.

A. A brief summary of factors involved in SMC development, differentiation and phenotypic modulation, including PDGF, TGF β , activin A, retinoids, angiotensin II, nitric oxide (NO), and other factors, including mechanical cues like shear stress and stretch. Adapted from [109]. **B.** The differentiation/dedifferentiation of SMCs is regulated by a variety of extracellular signals. ECM, extracellular matrix; RER, rough endoplasmic reticulum; SMC, smooth muscle cell. Adapted from [233].

1.2.3 The Biology of Common Cardiomyopathies

Heart failure (HF) is a clinical condition due to the inability of the heart to provide adequate blood perfusion to meet the metabolic needs and oxygenation requirements of the tissues in the body. HF can be due to numerous causes leading either to impaired cardiac contractile function (systolic dysfunction) or ventricular filling (diastolic) dysfunction. HF is frequently associated with a decrease in heart ejection fraction (EF), which measures how much blood the left ventricle pumps out with each contraction (www.heart.org).

The main causes of HF are coronary artery disease or long-term high blood pressure, which determine cardiomyopathies either resulting from a primary cardiac event, such as in myocardial infarction (MI), or acquired over long time exposure to non-ischemic insults [234].

The treatment options for MI span from the use of anti-inflammatory, anti-coagulants and analgesic drugs to angioplasty, coronary bypass or electronic implants, up to heart transplantation in the most severe cases. When the blood flow interruption persists for an extended time, it can cause irreversible damage to the myocardial tissue and muscle cell death. Myocardial tissue substitution occurs in these cases, where the accumulation of non-compliant fibrotic tissue results in diminished cardiac function [235].

Non-ischemic cardiomyopathies refer - instead - to diseases of the heart muscle affecting heart size, shape and structure and determining diminished pumping function of the organ [236] via the remodelling of cardiac structures. These diseases can eventually lead to HF. Several types of cardiomyopathies exist, such as hypertrophic (HCM), dilated (DCM), restrictive (RC), and arrhythmogenic right ventricular (ARVC) cardiomyopathies – which are inheritable, and caused by single gene mutations [237]. These pathologies and possible treatments are discussed in **Manuscript 3** (Cassani et al, [238]).

HCM results from single gene mutations of sarcomeric proteins transmitted in a dominant fashion, meaning relatives of affected people will have 50% probability of acquiring the disease [239]. Diagnosis is usually made during adulthood [240]. HCM is characterized by a left ventricular hypertrophy (LVH) due to an absence of pressure overload or infiltration [241]. Similarly, gene mutations can result in very distinct LVH patterns in terms of myocardial fibrosis and susceptibility to arrhythmias. Several sarcomeric genes that cause pathogenic mutations causing HCM have been identified, such as combined cardiac myosin binding protein-C (MYBPC3), and-myosin heavy chain (MYH7); which account for up 50% of the clinically recognized HCM cases [242]. Histologically, HCM is defined by interstitial fibrosis, myocyte enlargement and microstructure disarray (Figure 1.17, middle panel) [238].

DCM is the most common cardiomyopathy and a leading cause of heart failure, transplantation and death [238], [243]. It results from the pathological dilation of the left ventricle, followed by progressive contractile failure. Histologically, DCM can be characterized by cardiomyocyte hypertrophy, loss of myofibrils, and interstitial fibrosis

(Figure 1.17, right panel) [244]. DCM is a progressive disease that can be caused by acquired or inherited cues such as ischemia, infection, autoimmune disease, collagen vascular disease, toxins and drugs, nutritional deficiency and genetic disease [245], [246]. While patients with DCM may be initially asymptomatic, in time, progressive heart failure or arrhythmia could cause sudden death. DCM could have many familial or sporadic genetic causes, due to sarcomeric and structural proteins of the heart [247], such as mutations in the titin (TTN) are the most common causes of the disease (~25–27.6% of familial and 11.6–18% of sporadic cases) [248]. Other frequent mutations could be found in myosin heavy chain (MYH7) [249], tropomyosin 1 chain (TPM1) [250], and cardiac troponins (eg. TNNT2) [251].

ARVC is caused by the replacement of right ventricular myocardium by fibro-fatty tissue leading to ventricular arrhythmias and sudden death [252]. Disease-causing mutations for ARVC include cardiac desmosome (causing >50% of the cases) [252], plakoglobin (JUP), plakophilin-2 (PKP2), desmoplakin (DSP), desmoglein-2 (DSG2), and desmocollin-2 (DSC2) [252].

Analogously to DCM, restrictive cardiomyopathy (RC) – a rare cardiopathy - could be caused by both acquired and inherited causes. The most significant inherited gene mutations include TNNT2, troponin I (TNNI3), α -actin (ACTC), and MYH7 [253]. In RC, myocardial stiffness increases, which eventually leads to impaired ventricular filling [253].

Other acquired disorders include stress-induced myopathies and myocarditis. According to WHO classification of cardiomyopathies, stress-induced cardiomyopathies are inflammatory diseases caused by viral infections, lately famously by COVID-19 infections as well [254]. They are clinically manifested by ventricular arrhythmias, heart failure or cardiogenic shock, linked to significant rates of morbidity and death [254].

Presently available treatments for cardiomyopathies are mostly symptomatic rather than curative, and in most cases the only solution is heart transplantation [255].

As a significant amount of causes of heart failure are inherited due to single gene mutations, thanks to the possibility to generate patient-derived CMs from hiPSCs, it is now possible to generate personalized disease models to study the pathobiology of HF, and find personalized treatments. In the next section, we will discuss strategies for generating *in vitro* cardiac models.

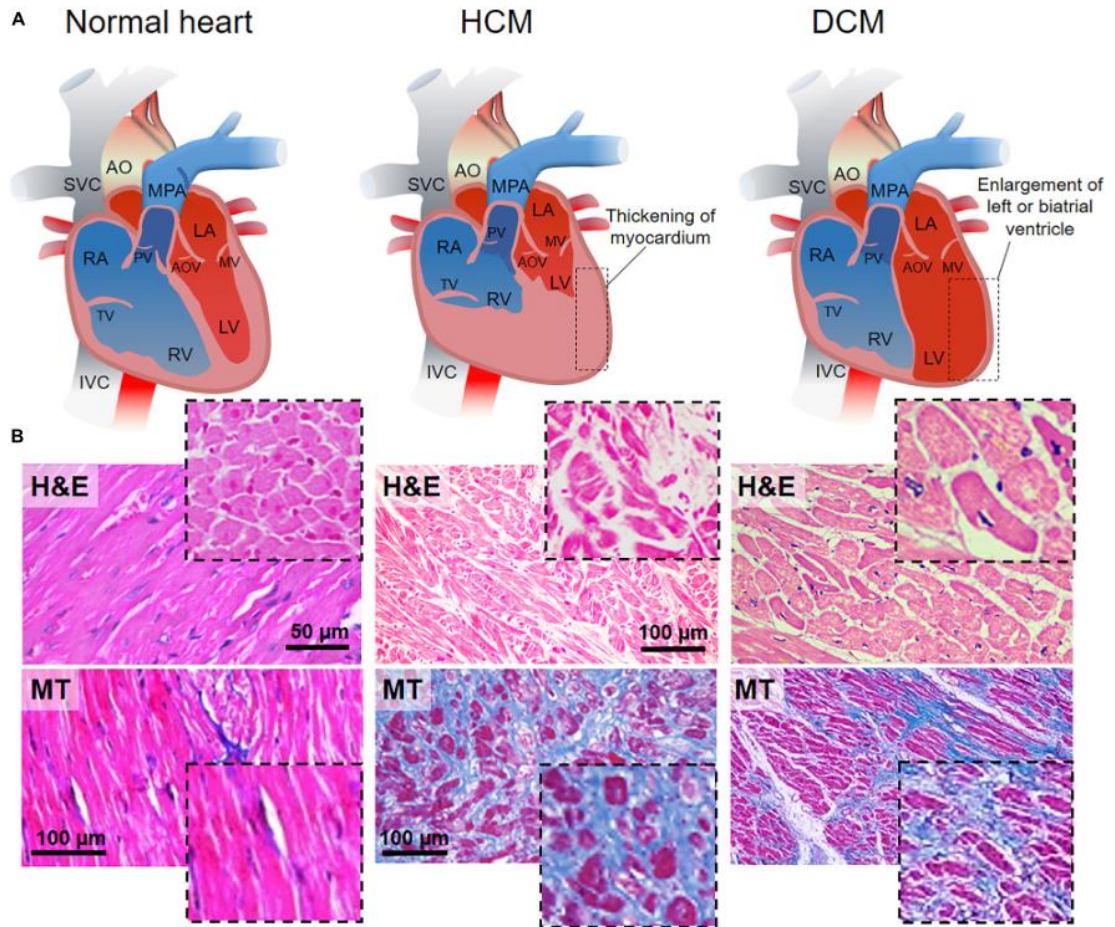


Figure 1.17 The histopathology of common cardiomyopathies: HCM and DCM

A. Anatomy of normal heart (left), HCM (middle), and DCM (right). **B.** Hematoxylin & Eosin (H & E) staining for normal heart, HCM, and DCM myocardium.

Adapted from **Manuscript 3**: Cassani et al [238].

1.3 Strategies for In Vitro Cardiac Tissue Modelling

1.3.1 Human (Induced) Pluripotent Stem Cells

Given the biological complexity of the human heart, there are major constraints for progress in studying cardiovascular diseases and developing novel therapies. There are limited resources to find donor hearts from patients to isolate native cells from, and access to healthy controls from deceased individuals is even more difficult. Furthermore, it is challenging to keep primary cardiac cells in culture for extended time, as they do not proliferate, and do not remain viable in long-term [134], [138], [139]. Therefore, alternative ways to obtain or generate *de novo* human cardiac cells are needed.

Since the last two decades, human embryonic stem cells (hESC), and later human induced pluripotent stem cells (hiPSC) have been key resources to obtain *in vitro* cardiac cells. The first iPSCs were developed in 2006 by Yamanaka et. al by expressing four pluripotency factors into mouse somatic cells (Oct 3/4, Sox2, Klf4, c-Myc: also known as “Yamanaka factors”) [256] to reprogram them into embryonic stem-like cells. The generation of human iPSCs was reported in 2007 [16]. Since then, human pluripotent stem-cell derived cardiomyocytes (hPSC-CMs) have become extremely valuable for studying developmental biology, disease modelling and drug testing. Given the possibility to obtain iPSCs from virtually any individual somatic cells, their potential for personalized medicine appears obvious [12], [16]–[24].

Usually, the stemness of PSC colonies is maintained by either culturing them on a fibroblast-feeder layer (e.g. mouse embryonic fibroblasts; MEF), or on feeder-free formats [257] such as with ECM coating with basement membrane extract (BME) derived from mouse Engelbreth-Holm-Swarm (EHS) sarcoma tumor (eg. Matrigel®, Geltrex™, Cultrex®). Alternatively, pluripotent stem cell colonies are grown on xeno-free synthetic ECM substrates (eg. Vitronectin, Synthemax ®) [258]. *(Trivia: During post-pandemic 2021-2022, a worldwide Matrigel® shortage has impacted much of iPSC/organoid research worldwide, as lots of experiments had to be re-optimized with alternative substrate, if available, or had to be delayed [259]).*

For the maintenance of hESCs and hiPSCs, it’s also common to use Y-27632 ROCK inhibitor (Rho-kinase inhibitor) after each dissociation (eg. for splitting, or for re-seeding at different formats, aggregating for making spheroids...), in order to improve the survival of PSCs [260].

Several protocols exist for the maintenance of hPSCs, and the differentiation of CMs from them. On Table 1.2, a literature summary of the evolution of the protocols designed for the differentiation of cardiomyocytes is shown, ranging from embryoid-body (EB) derived 3D differentiation to 2D monolayer differentiation with small molecules with different efficiency of resulting CM populations. 3D aggregate protocols usually rely on spontaneous differentiation of stem cells into embryoid bodies, or inducing mesoderm

formation and cardiac specification by growth factors and small molecules, followed by the dissociation and selection of desired cell types [257], [261]–[266]. In contrast, 2D monolayer differentiation exclusively relies on the utilization of growth factors and small molecules such as Activin A, FGF2 and BMP4 following developmental biology cues. The mesoderm formation is induced by transient WNT activation via either the previously mentioned recombinant molecules [267], or via chemical compounds such as CHIR99021 (an inhibitor of glycogen synthase kinase 3 β , GSK3, to activate WNT) followed by inhibitors of WNT, such as IWR-1, IWP-2 and IWP-4 (i.e. palmitoleoyltransferase PORCN inhibitors) [17], [18], [20], [268]–[270]. The first cardiac progenitor cells start to appear and spontaneously beat between day 7-10 of differentiation. Until this point, insulin-free media helps with cardiomyocyte differentiation, but after the beating starts, insulin is usually needed [271].

From this point on, the culture can continue with the same media for a long time. However, in extended culture periods in 2D, the contractile cardiomyocytes lose their ability to proliferate and tend to delaminate from the traditional tissue culture plates [272], causing non-myocyte cell populations such as fibroblasts to take over and overgrow, instead. Figure 1.18 depicts the expected molecular and phenotypical features at different timepoints of hiPSC-CM differentiation in 2D culture up to a year [90].

Cardiomyocyte subtype-specific protocols are starting to emerge which involve the addition of other small molecules such as retinoic acid (RA), which favours the formation of atrial CMs, whereas its removal from the culture medium followed by additional WNT modulation promotes ventricular or nodal CM shift, depending on media formulation [103], [115], [257].

Although extremely useful for numerous *in vitro* applications, when cultured in 2D, hPSC-derived cardiomyocytes (hPSC-CMs) do not reflect the 3D complexity of the native tissue [22], [25], [26], where the interplay of topology, the cellular heterogeneity and the interactions with the extracellular matrix (ECM) are also involved. hPSC-CMs cultured in 2D vessels continue displaying fetal-like features in terms of morphology, electrophysiology, calcium handling, metabolism and gene expression, while never fully reaching the state of adult cardiomyocytes (See Table 1.1 and Figure 1.11) despite extended culture time [115]. Furthermore, hiPSC-CM differentiation protocols suffer from batch-to-batch variations and usually do not provide 100% efficiency in CM differentiation, with non-cardiomyocyte and undifferentiated cells contaminating hiPSC-derived-CMs cultures [257].

Recently, different efforts have been documented that address the maturation issue of cultured hiPSC-CMs via biochemical, cellular, and mechanical cues (Figure 1.19). One of the proposed approaches entails long-term culture in 2D up to 120 days or 1 year [277], [278], resulting in improved sarcomeric ultrastructure and electrophysiology. As far as the cell-cell interactions are concerned, CM co-culture with cardiac fibroblasts and/or endothelial cells has been shown to determine improved maturation with enhanced

connexin 43 gap junctions compared to plain hiPSC-derived CM cultures [42], [279], [280]. Another method proposed to improve hiPSC-derived CM maturation requires modulating substrate stiffness of culture dishes: softer matrices mimicking native heart extracellular matrix elasticity (~10kPa) made of polydimethylsiloxane (PDMS) or polyacrylamide prompted enhanced CM maturation in terms of contractility, t-tubule formation, mitochondria elongation and electrophysiology, compared to standard plastic culture dishes, which are very stiff (~1GPa) [281]–[284]. Biochemical cues such as thyroid (T3), and glucocorticoid hormones were shown to initiate t-tubule formation and to improve excitation-contraction coupling in hiPSC-CMs [285]–[288]. Furthermore, fatty acid supplementation has been proposed in an attempt to help hiPSC-CM structural and metabolic maturation, because although most typical hiPSC-CM cultures are routinely based on high-glucose media (eg. Lian and collaborators’ protocols [17], [18]), physiologically maturing CMs shift from glycolysis to fatty acid oxidation as their main energy source [163], [289], [290]. Recently, culture on micropatterned surfaces was also shown to result in the derivation of structurally and functionally more mature hiPSC-CMs [283], [291], [292].

Finally, bioengineering approaches are emerging as tools suitable to mimic cardiac structure, which will be discussed in the next section.

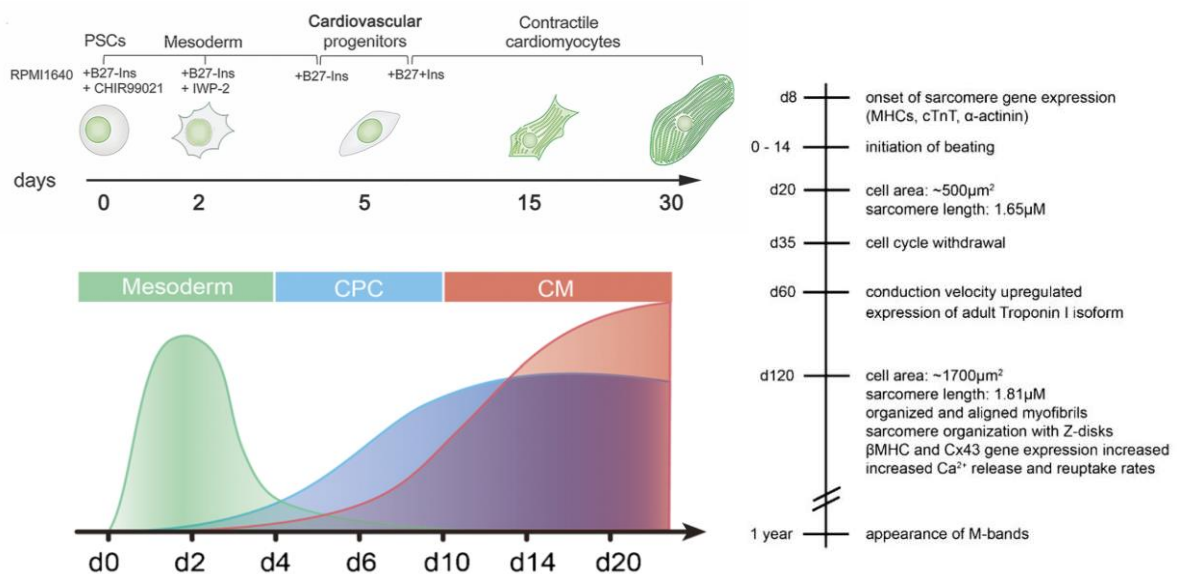


Figure 1. 18 Characteristics of 2D hiPSC-derived CMs during culture timeline

Scheme of gene expression patterns and CM characteristics during the first 20-30 days of differentiation, and structural and functional characteristics from CPC formation to CM maturation up to a year culture. Beating CMs could be observed from D7 on followed by proliferation until d30 and features of maturation in long-term culture [150], [277], [293]. CPC; Cardiovascular Progenitor Cells. CM; Cardiomyocytes. Modified from [90], [294].

Table 1. 2 Various differentiation protocols to generate hPSC-derived CMs

PSC type	Differentiation Method	Culture substrate	Pluripotency Media	Timeline, Differentiation Media, Growth Factors, Small Molecules												Differentiation Efficiency	Reference	
				Mesoderm Induction				Cardiac Progenitors						Cardiomyocytes				
				Day 0	Day 1	Day 2	Day 3	Day 4	Day 5	Day 6	Day 7	Day 8	Day 9	Day 10	Day 11			Day 12
hESC	EB	MEF	KO-DMEM, 20%FBS					20% FBS								8% of EBs contracting	Kehat et al., 2001 [261]	
				KO-DMEM														
hESC	Colonies in co-culture	MEF	DMEM, 20% FBS					20% FBS, END-2 cells								N/S	Mummery et al., 2003 [295]	
				DMEM														
hESC	EB	Matrigel®	MEF-CMM	Activin A, FGF2		20% FBS										24% of EBs contracting		Burridge et al., 2007 [262]
				CDM-PVA (IMDM/F12, Ascorbic Acid, ITG, insulin, transferrin, PVA)				DMEM										
hESC	Monolayer	Matrigel®	MEF-CMM	Activin A	BMP4				RPMI + B27™								30% MYH7+	Laflamme et al., 2007 [267]
hESC	EB	MEF	DMEM/F12, 20% KSR, FGF2	BMP4	BMP4, Activin A, FGF2				DKK1, VEGFA		DKK1, VEGFA, FGF2						50% TNNT2+	Yang et al., 2008 [263]
				StemPro™-34, ascorbic acid														
hESC	EB	MEF, then Matrigel®	DMEM/F12, 20% KSR, FGF2	BMP4	BMP4, Activin A, FGF2				DKK1, VEGFA		VEGFA, FGF2						50-70% TNNT2+	Kattman et al., 2011 [264]
hiPSC				StemPro™-34, ascorbic acid, L-Glutamine, ITG														
hiPSC	EB	Geltrex™	MEF-CMM	BMP4, FGF2		20% FBS or HSA		RPMI, insulin, lipids								94% of EBs contracting	Burridge et al., 2011 [265]	
				RPMI + PVA		RPMI + Ascorbic acid												
hESC	EB	MEF	KO-DMEM, 20% FGF2	BMP4	BMP4, Activin A, FGF2				IWR-1	IWR-1, FGF2, VEGFA				FGF2, VEGFA	2% FBS	30% MYH6+	Willems et al., 2011 [266]	
				StemPro™ -34														
hESC	Monolayer	Matrigel® or Synthemax®	mTeSR1™	CHIR99021	IWP-4				RPMI+B27™ with insulin								85% TNNT2+	Lian et al., 2012 [17]
hiPSC				RPMI+B27™ without insulin													Lian et al., 2013 [18]	
hESC	Monolayer	Synthemax® or Laminin-521	Essential 8™ (E8)	CHIR99021	Wnt-C59				CDM3 (RPMI, recombinant HSA, ascorbic acid 2-phosphate)								95% TNNT2+	Burridge et al., 2014 [20]
hiPSC																		
hESC	Monolayer	Synthemax®	E8 or mTeSR1™	CHIR99021	IWP-2				RPMI, insulin, ascorbic acid 2-phosphate								88-98% TNNT2+	Lian et al., 2015 [268]
hiPSC				RPMI, putrescine, progesterone, sodium selenite														
hESC	Monolayer	Matrigel®	E8	CHIR99021	IWP-2				RPMI, insulin, ascorbic acid 2-phosphate								94% TNNT2+	Lin et al., 2017 [269]
hiPSC				DMEM/F12, ascorbic acid, lipids, transferrin, sodium selenite, sodium bicarbonate (heparin from Day 1 – Day 7)													Lin and Zou, 2020 [270]	

Light purple cells indicate positive inducers (growth factors, sera, small molecules); light yellow cells indicate inhibitors; blue cells indicate media and additional supplements.

Acronyms: ITG, monothio glycerol; BMP4, bone morphogenetic protein 4; CDM, Chemically defined medium; CHIR99021, GSK3(glycogen synthase kinase 3) inhibitor; DKK1, Dickkopf-related protein-1; DMEM, Dulbecco's Modified Eagle's Medium; DMEM/F12, DMEM/ Nutrient Mixture F-12; E8, Essential 8™ Medium; EB, embryoid body; END-2, endoderm-like cell line; FBS, fetal bovine serum; FGF2, basic fibroblast growth factor; HSA, human serum albumin; IMDM, Iscove's Modified Dulbecco's Medium; ITS, insulin, transferrin, selenium supplement; IWR-1, inhibitor of Wnt response-1; IWP-2, inhibitor of Wnt production 2; IWP-4, inhibitor of Wnt production 4; KO-DMEM, KnockOut DMEM; KSR, KnockOut Serum Replacement; MEF, mouse embryonic fibroblasts; MEF-CMM, MEF conditioned medium; N/S, not stated; PVA, polyvinyl alcohol; RPMI, Roswell Park Memorial Institute Medium; VEGFA, vascular endothelial growth factor. Modified from [257].

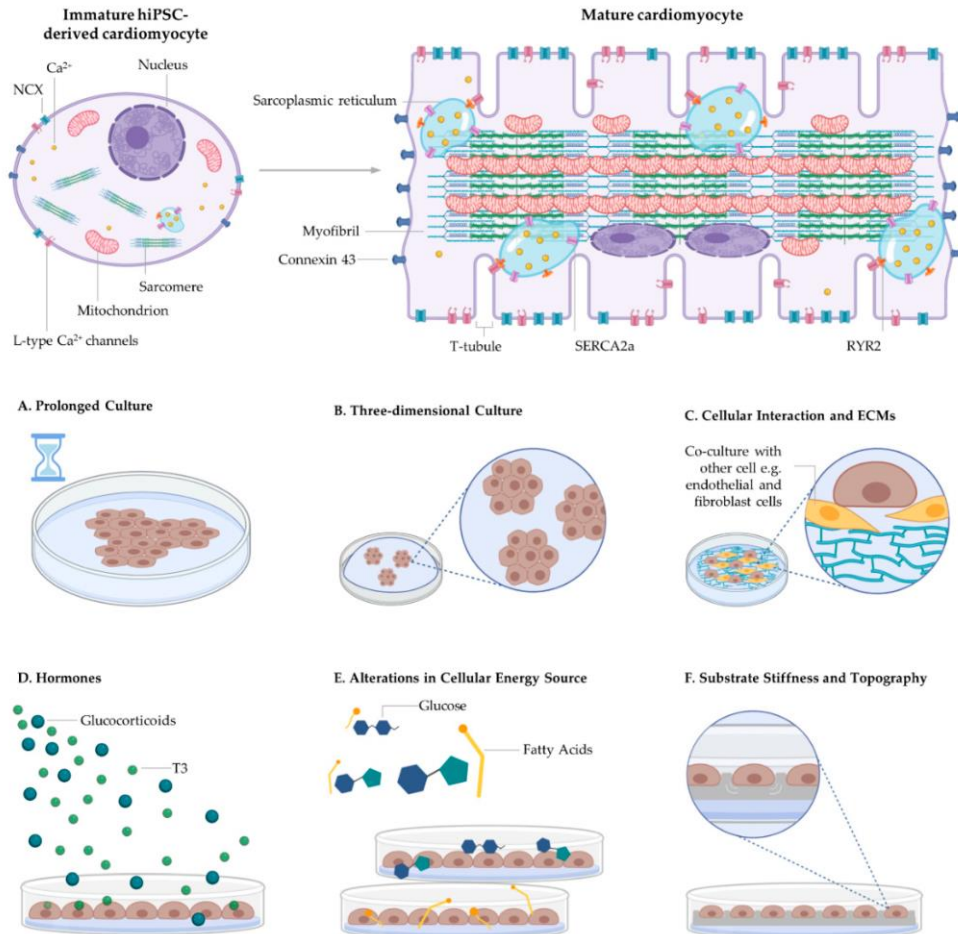


Figure 1. 19 Different maturation approaches for hiPSC-CM cultures

TOP: Comparison of immature vs. mature CMs. *BOTTOM:* Current approaches. **A.** Long- term culture **B.** 3D culture **C.** Co-culture with non-myocytes **D.** Biochemical hormones **E.** Fatty acid supplementation **F.** Substrate stiffness and topology. Adapted with modifications from [115].

1.3.2 Bioengineering Approaches

By providing a more dynamic and physiological environment, similar to the native heart tissue, bioengineering approaches recently became the gold standard to improve the function and maturation of hiPSC-derived *in vitro* heart models. These strategies allow for the generation of models with higher degree of complexity, organization and dynamics combining different cell types, biomaterials, soluble factors and engineered devices [34]–[37].

Examples of scaffolds and biomaterials used to mimic cardiac ECM include collagen, Matrigel™, fibrin, alginate, and gelatin which were all shown to improve the attachment of cardiac cells *in vitro* and their engraftment in *in vivo* models [89], [296], [297]. Bioreactors have also been proposed in bioengineered cardiac models to stimulate the cells electrically and mechanically, or to provide dynamic culture conditions via perfusion systems [298]. As an example, in a study where cardiac tissue constructs derived from ESCs were encapsulated in gelatin or collagen-based matrices, and exposed to cyclic strain, the tissue constructs showed improved signs of maturation, with more aligned cellular architecture, and increased its spontaneous beating rate [154], [299]. Similarly, several studies showed that fluid shear stress could also improve cardiomyogenic differentiation in PSCs [107], [108], [110].

Well-established examples of bioengineered heart models include the so called engineered heart tissues (EHTs) [30], [35], [38], isogenic cardiac (micro)tissues [32], [39]–[44], and more recently heart-on-a-chip [45]–[55] and organoids [13], [56]–[58]. Some examples are listed in Figure 1.20.

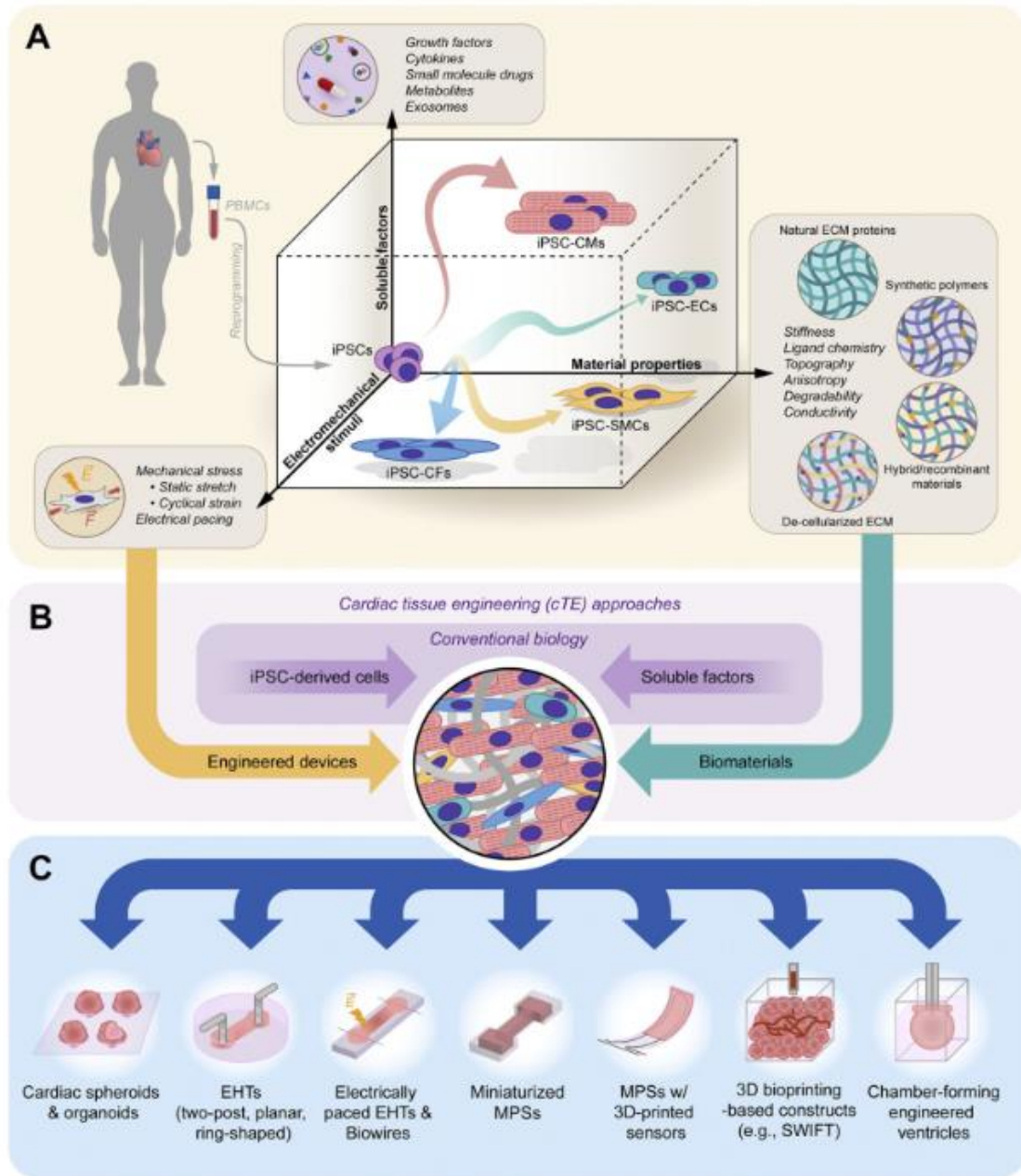


Figure 1.20 Bioengineering approaches for cardiovascular tissue modelling

A. Different cardiac cell types can be derived from hiPSC such as cardiomyocytes (CMs), cardiac fibroblasts (CFs), endothelial cells (ECs), etc. **B.** Their maturation could be improved by chemical and biophysical cues, such as by combining different cell types, biomaterials, soluble factors and other engineered devices. **C.** Examples of bioengineered cardiac tissue models including EHTs, heart-on-a chip technologies and spheroids/organoids. Adapted from [300].

1.3.2.1 (Micro)physiological Systems

Engineered Heart tissues (EHTs) are made by mixing hydrogels with cardiomyocytes or multiple types of cardiac cells in casting molds, followed by their attachment to two elastomeric poles to allow contraction analysis under stretch conditions. The first EHTs were developed by using neonatal or embryonic CMs from rat or chicken hearts [301]–[308], but nowadays they are widely available made of hiPSC-derived CMs and hydrogels such as Matrigel-collagen mix, and fibrin. The presence of multiple cell types and biophysical stimuli coming from the hydrogel and the contraction motion allowed the microtissue construct to show more mature features as compared to standard 2D hiPSC-CM cultures, by structural and metabolic maturation [35], [309]. EHTs were shown to contain a higher number of mitochondria, and displayed increased oxidative phosphorylation instead of glycolysis. Lately, electrical pacing and inclusion of fatty acids to the culture media were also shown to improve the maturation. [163], [310]–[312]

A variant of EHTs are **biowires**, where, hPSC-derived cardiomyocytes and supporting cells were used to generate 3D, self-assembled cardiac wires by cell seeding into a template polydimethylsiloxane (PDMS) channel, around a sterile surgical suture in type I collagen gels [313]–[316]. In a week, seeded cells remodelled and contracted the collagen gel and the biowire construct could be removed from the PDMS template, followed by electrical stimulation to improve the structural and functional maturation. In this platform, it was also possible to perfuse cell culture media for further mechanical stimulation by flow [313]–[316].

Another variant of EHTs include the “**ring**”-type, which similarly involves pipetting cell/hydrogel mixtures into ring-shaped casting molds [67], [309], [317], [318]. The difference between the ring-type EHT to the classical “strip” type EHT is by a hole in the EHT, thus reducing the risk of necrosis in the middle of the construct. Similarly, the ring-type EHTs can be hooked around silicon posts for active/passive mechanical stimulation, for force measurements, and electrical pacing [311], [312]. The ring-shaped EHTs have been used for drug testing, disease modelling (eg. cryoinjury), and cardiac regeneration studies. In an example study, chamber-specific ring-EHTs were generated by differentiating hPSCs into atrial and ventricular cardiomyocytes, followed by their embedding into a collagen hydrogel, which was later transferred to a passive stretcher for further culture [317]. While this model was shown to be promising for improving microtissue physiology, disease modelling and drug testing, and despite some degree of CMs maturity could be achieved that was better than classical 2D cultures, the EHT phenotype was still distant from adult human CMs [140], [144].

An interesting variant of EHTs are “**chamber-forming engineered ventricles**”, with an aim to generate a 3D hollow fluid ejecting EHTs mimicking the native human heart [319], [320]. This hollow-chambered model could be achieved by “catheter-type” or “nanofibrous scaffolds-type” methods. In the catheter type, a mixture of hPSC-derived CM and collagen mix was polymerized on a silicon Foley catheter, followed by incubation in a bioreactor

containing cell culture medium [319]. In the nanofibrous scaffold type, tissue-engineered ventricles were created by nanofiber spinning and nanofibrous scaffolds [320]. These scaffolds were then incubated with fibronectin and rat ventricular or hiPSC-derived CMs, Such engineered cardiac tissue models allowed multiscale cardiac assays *in vitro* such as tissue coverage and alignment, calcium-transient propagation, and pressure-volume loops in the presence or absence of test compounds.

Because of challenges in obtaining high cell numbers, the purity required for the cell types, cost-intensiveness, culture time and mixed maturation outcomes, engineered heart tissues are usually not preferable for high-throughput screening applications [321].

To enable high-throughput screening applications and minimize the amount of material needed for classical EHTs, there is a growing interest in miniaturization of such systems into so-called “**microtissues**” or “**microphysiological systems**”. An early example of such microtissues were composed by PEG-patterned substrates suited to confine hiPSC colonies, and spatially differentiate them into self-organized cardiac microchambers by culturing with Wnt signalling modulation media while in geometric confinement [40]. Another early example is 3D micro-heart muscle (μ HM) arrays which was obtained by seeding a mixture of hPSC-derived CMs and CFs without any ECM hydrogel into miniature “dogbone” shaped microchambers (stencils), thus forcing microtissue-strip formation with uniaxial contraction by geometric confinement [322].

A remarkable study by Mills et al. has shown a microtissue example (**Heart-Dyno**) reminiscent of a miniaturized version of the classical EHT model with two elastomeric posts, where hiPSC-CMs and fibroblasts were seeded with a Matrigel-collagen mix, and allowed to polymerize in an array of PDMS microchambers with two elastomeric posts (Figure 1.21) [68]. Remarkably, it was shown that under optimized maturation conditions (eg. cell concentration, ECM formula and culture medium optimization), functional and molecular characterization revealed that a switch to fatty acid metabolism was a central driver of cardiac maturation and cell cycle arrest. A follow-up study by the same authors describe a functional screening of 105 pro-regenerative potential on the Heart-Dyno system, revealing that mevalonate pathway is essential for cardiomyocyte cell cycle re-entry [323].

Interestingly, although the Heart-Dyno model is referred to as “cardiac organoid” in published literature, whether it should be termed as “organoid” or “microtissue” is open to discussion, since specific requirements were recently established as a consensus to be fulfilled by a given *in vitro* model in order to be considered as an organoid. While this model utilizes the co-culture of only two differentiated cardiac cell types mixed in a hydrogel (hiPSC-derived CMs and CFs mixed with Matrigel-collagen), a *bona fide* organoid should essentially contain multiple organ-specific cell types, and show self-organization, histology and functionality similar to the tissue of origin [58]–[60] (See section 1.3.2.3).

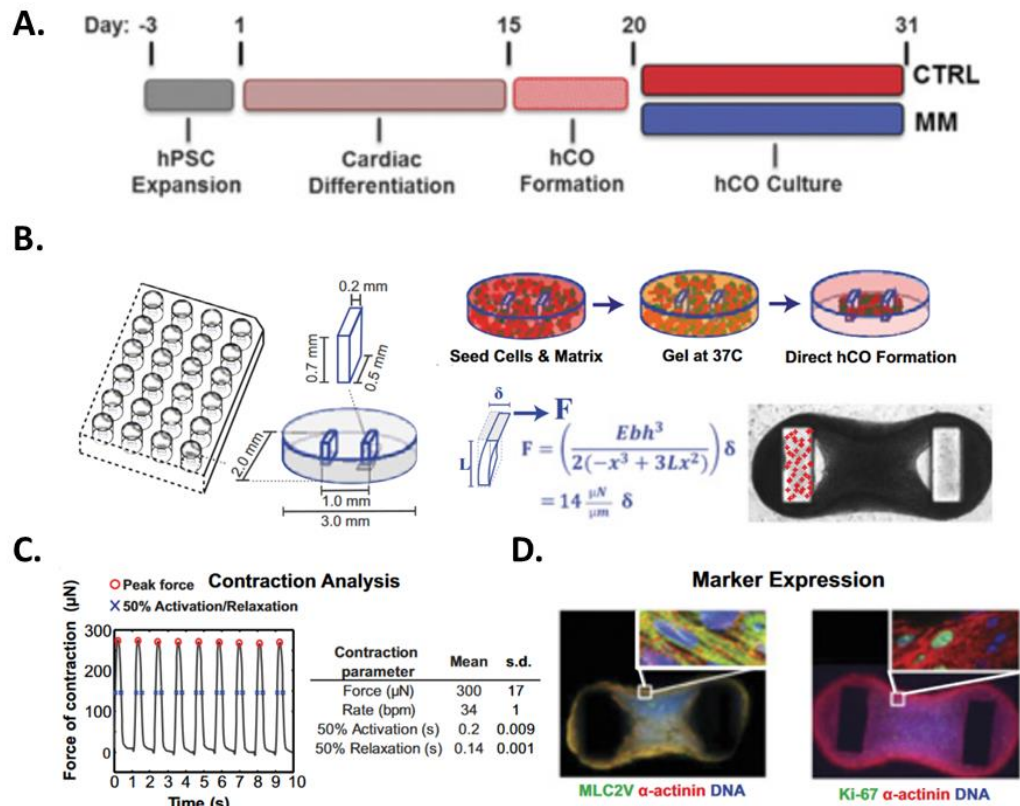


Figure 1.21 Heart-Dyno platform as a miniaturized EHT model.

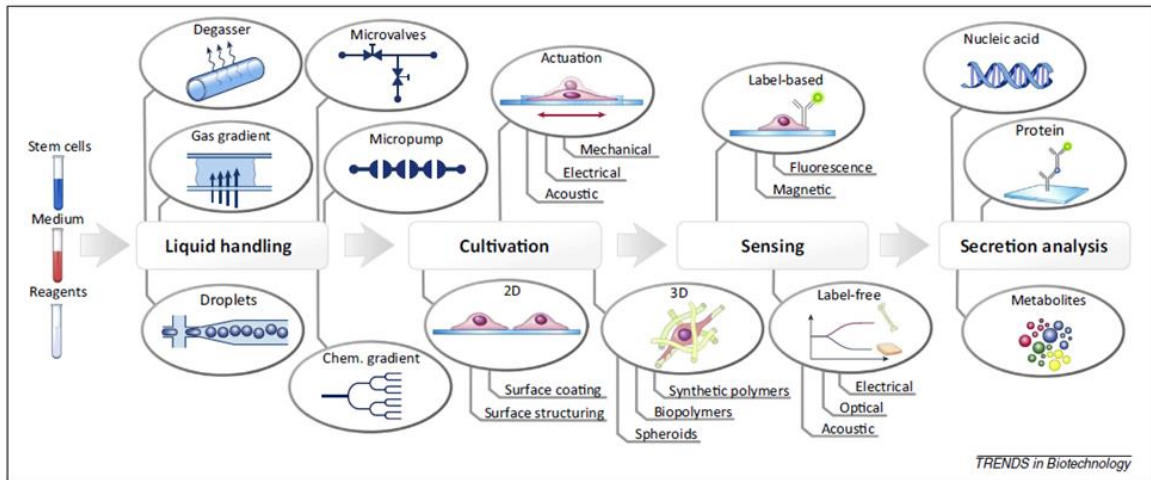
A. Culture timeline of cardiac maturation protocol indicating timing and duration of hPSC expansion, cardiac differentiation, microtissue (hCO) formation and culture in CTRL (control) medium or MM (Maturation Medium). **B.** Microfabrication of the Heart-Dyno platform by seeding hiPSC-CMs and fibroblasts in a Matrigel-collagen mix and allowing to polymerize in an array of PDMS microchambers with two elastomeric posts. **C.** and **D.** indicate functional and structural analyses such as contraction (C), and histology of cardiac specific (MLC2v, α -actinin) and proliferative (Ki-67) markers. Modified from [68].

More specialized forms of such miniaturized EHTs are described under the “heart-on-a-chip” technologies section.

1.3.2.2 “Heart-on-a-chip” Technologies

Recently, *in vitro* heart models based on microfluidics - collectively defined as **heart-on-a-chip** (HoC) - were generated that provide new opportunities in organ modelling [324]. An “organ-on-a-chip” (OoC), “lab-on-a-chip” (LOC), or to be more advanced, a “body-on-a-chip” (multiple microfluidic organ models connected together) may allow for the generation of a relevant miniaturized *in vitro* tissue/organ models, fostering the growth and maintenance of the cells in an environment comparable to *in vivo* conditions. Such models allow for deeper insight into cellular behaviour, cell-cell communications and regulatory mechanisms, thereby providing the conditions for the creation of highly complex devices. Not only do they emerge as an alternative to traditional 2D or 3D models, but are also suitable for non-invasive monitoring and real-time data acquisition with the help of live-imaging and sensing technologies. The advantages of these systems lie in the possibility to tightly control the conditions, such as flow regime, oxygen saturation, drug distribution or mechanical forces, thanks to the incorporation of micro-pumps and micro-valves. Another advantage of microfluidics is the ability to use small cell numbers, which is particularly advantageous for developing patient-specific *in vitro* models. Furthermore, since the volume of reagents is reduced, the costs of diagnosis and screening are limited [324]–[329]. Therefore, microfluidics could be a time and cost-effective approach for *in vitro* cardiovascular models as well. Such dynamic models could improve the reproducibility of many experiments, and reduce the number of human errors by automatization, adding even more benefits to the cost-effectiveness. Figure 1.22 summarizes design principles and the readily available components for cell-analysis on microfluidic chip platforms: automated liquid handling, cultivation of stem cells, sensing and performing biomarker analysis (e.g., surface receptors, and release of cytokines) [330].

A.



B.

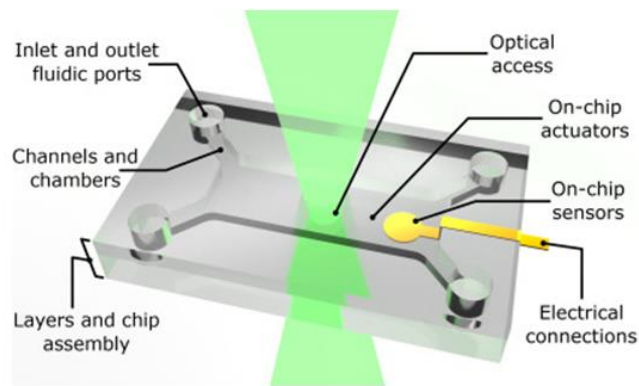


Figure 1. 22 Basic design and operating steps of an exemplary organ-on-a-chip model

A. Liquid handling can be obtained through various microfluidic strategies, and cell cultivation can be done in 2D and 3D. Furthermore, cell culture could be coupled with non-invasive detection methods involving mechanical, electrical or acoustic means. Detection systems can be added by fluorescent or magnetic labels, or label-free by electrical/optical/acoustic means (eg. impedance assays; glucose, lactate, oxygen, pH sensing... etc). End point analyses can be performed by cell lysis on chip, and analysing the nucleic acids, proteome, or the secretome. As a summary, with a combination of these methods, cellular analyses could be fully automated in “lab-on-a-chip” devices. Adapted from [330]. **B.** Design considerations for the components of a microfluidic “organ-on-a-chip” device. Adapted from [331].

While being exposed to continuous biological stimuli, cells in the human body are subjected to either constant or temporary mechanical stimuli. This means that the application of mechanobiological forces represents a vital step towards the establishment of physiological microenvironments *in vitro* [332], [333]. Therefore, recently the concept of “mechanobiology-on-a-chip” emerged (**Manuscript 2** [334]) in order to overcome the drawbacks associated with 2D monocultures, where 3D culture systems of cells in hydrogels, scaffolds or aggregates could be miniaturized [335]–[338]. 3D cell culture by itself allows for indirect mechanical stimulation by controlling the rigidity and stiffness of the extracellular matrix that could result in modulation of cellular responses [339], [340]. Additionally, 3D tissue models can be further subjected to dynamic mechanical stimuli including fluid flow, stretch/strain and compression. To date a variety of mechanobiological forces, shown in Figure 1.23A [334]), has been employed in 2D and 3D *in vitro* cultures including (a) matrix stiffness that mimic the respective Young’s moduli of native tissue, (b) fluid flow in vascular systems and interstitial tissue, (c) stretch/strain mechanisms in the lung, heart and gastrointestinal tract as well as (d) compression in the musculoskeletal system [341]–[344]. These mechanobiological systems demonstrated improved cell-to-cell and cell-to-matrix interactions resulting in significant progress in recapitulating physiological microenvironments *in vitro*.

Figure 1.23B shows ways of bridging the *in vitro* vs *in vivo* gap on miniaturized systems via introducing mechanical cues [334]).

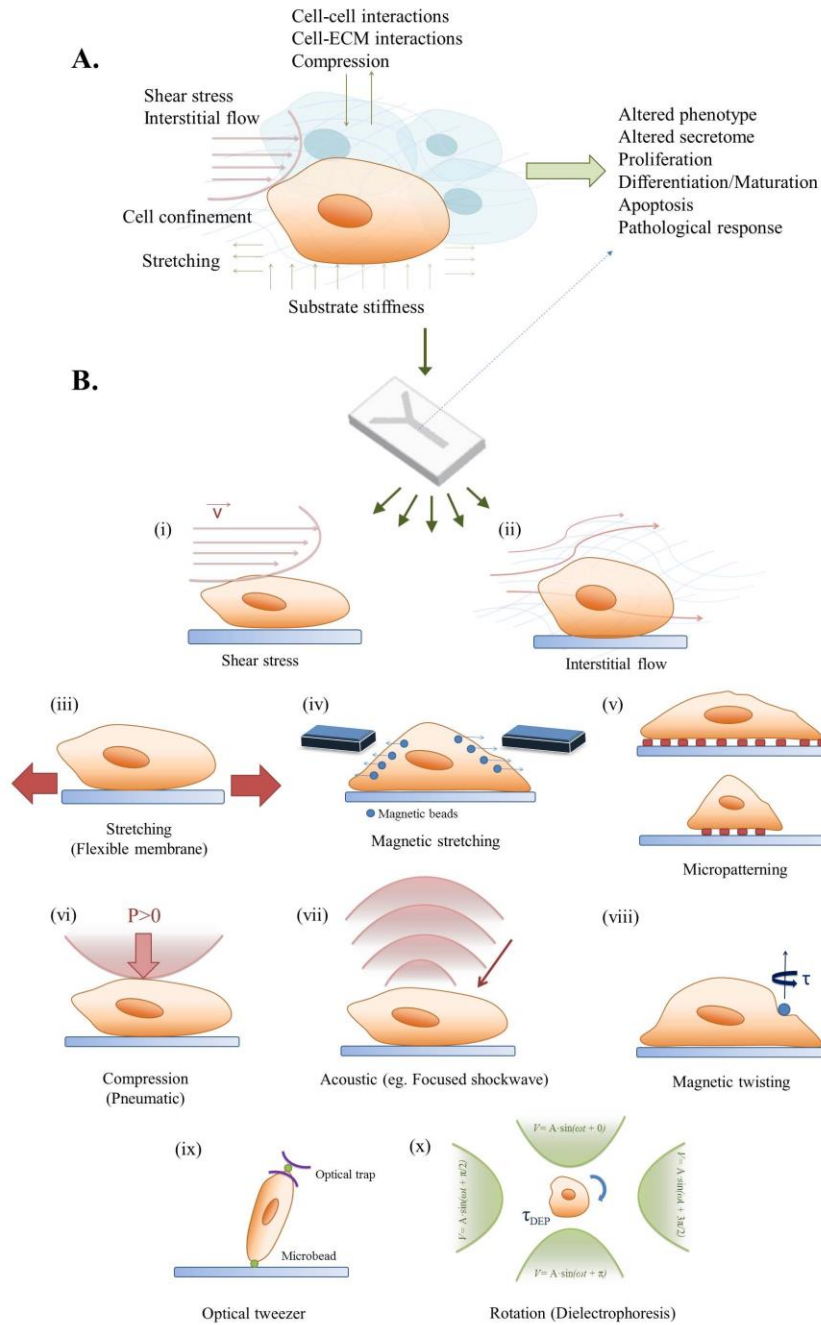


Figure 1.23 Bridging the *in vitro* vs. *in vivo* gap on a "mechanobiology-on-chip" system

A. A combination of mechanobiological cues in the microenvironment can regulate cell signalling and phenotype in physiological or pathological ways. **B.** A simplified example of a mechanobiology-on-a-chip with potential on-chip stimulation strategies for microfluidic 2D/3D cell cultures, namely: (i) Shear stress, (ii) Interstitial flow, (iii) Stretching, (iv) Magnetic stimulation, (v) Micropatterning, (vi) Compression, (vii) Acoustic stimulation, (viii) Magnetic twisting, (ix) Optical tweezers, and (x) Rotation (dielectrophoresis). Adapted from **Manuscript 2** Ergir et al. [334].

Several examples of “heart-on-a-chip” models are already being generated that provide the possibility to measure cardiomyocyte beating and contractility on-chip [345]. For instance, Grosberg *et al.* have proposed a biohybrid construct of an engineered ventricular myocardium on an elastomeric thin-film - “muscular thin film” (MTF) - to measure contractility, action potential, and cytoskeletal architecture on the same experiment [345]. For patient-specific “heart-on-a-chip” models using this technology, a good example is a model of mitochondrial cardiomyopathy of Barth syndrome produced by using patient specific iPSCs, and performing a cardiotoxicity drug test, utilizing this strategy [346].

A remarkable example of “mechanobiology-on-a-chip” application for cardiac models is by exposing 3D cardiac cell constructs to cyclic mechanical strain to develop a “beating-heart-on-a-chip” (Figure 1.24) [347]. In this study, hiPSC-CMs were embedded in a fibrin gel prior to injection into the microdevice, and subsequently exposed to mechanical stimulation using a deformable PDMS membrane (10% uniaxial strain, 1 Hz frequency). Although the mechanically stimulated constructs showed similar gene expression levels of non-actuated controls, the expression of Myosin Heavy Chain 6 (MYH6) the fetal isoform of myosin heavy chain, showed decreased expression, potentially indicating superior maturity compared to static controls. The same group employed a similar microdevice to develop a model of cardiac fibrosis by applying cyclic mechanical stretch to cardiac fibroblasts in a 3D fibrin hydrogel. Thanks to this platform, it was possible to model some key steps of cardiac fibrosis onset in a timely fashion: early fibroblast proliferation, their phenotype switch into myofibroblasts, and ECM stiffening [348].

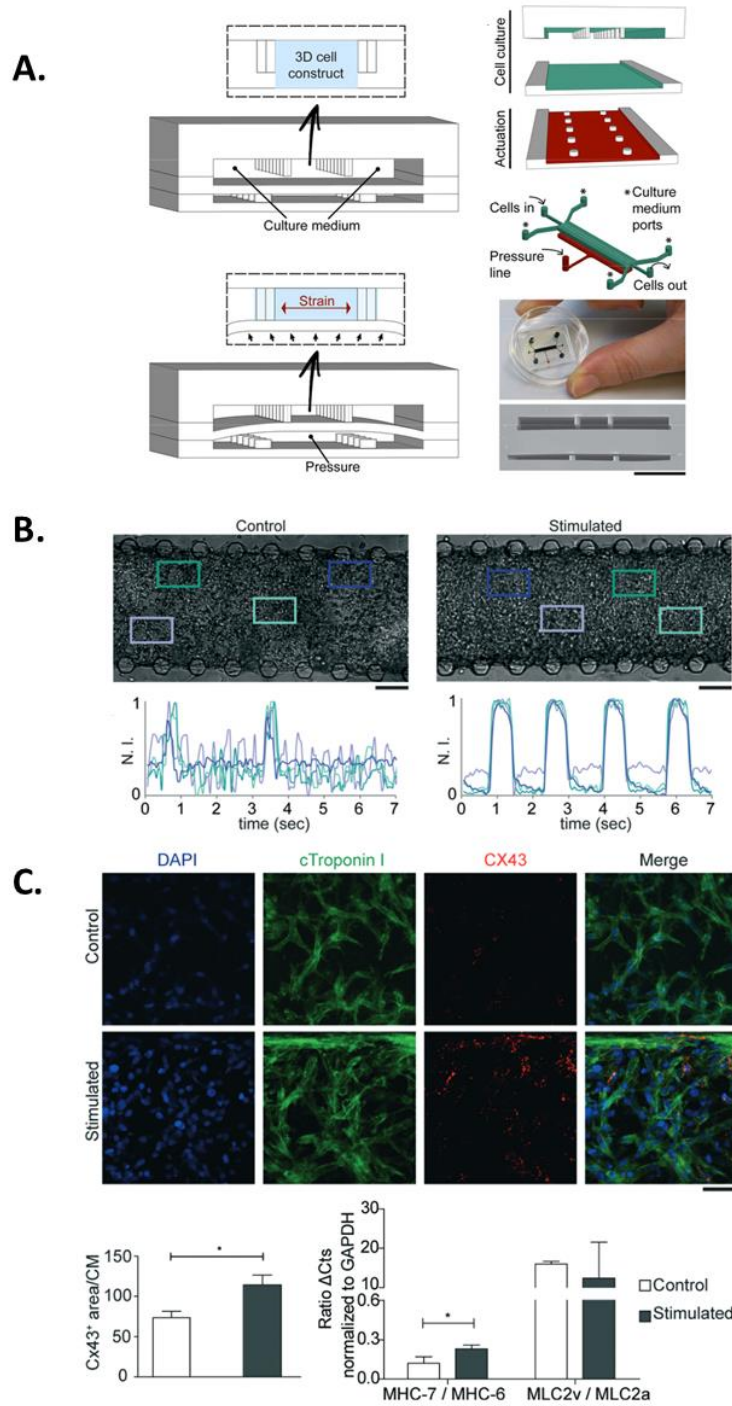


Figure 1. 24 Beating 3D “heart-on-a-chip” device featuring mechanical actuation.

A. Design principles of the 3D “heart-on-a-chip” (HoC) microdevice, which utilizes two PDMS microchambers separated by a flexible PDMS membrane that could be actuated by applying air compression. The middle channel is aimed to accommodate the 3D cell construct made of hiPSC-CMs and fibrin clot, which could be actuated. The side channels feature culture medium posts. Scale bar: 500 μm . **B.** Uniaxial cyclic mechanical strain results in synchronized beating of the cardiac microtissue, calculated by average pixel intensity (N.I.) during contraction period. **C.** Effect

of uniaxial cyclic mechanical strain resulting in more advanced maturation than static culture. TOP: Representative immunofluorescence staining for specific cardiac markers (Cardiac troponin I in green and gap junction protein as Connexin 43 in red). BOTTOM LEFT: Quantification of Cx43+ areas in control vs stimulated microtissues. BOTTOM RIGHT: Quantification of gene expression levels for myosin heavy and light chain ratios: MHC7/MHC6 ratio, and MLC2v/MLC2a ratio. Modified from [347].

In addition to mechanical cues, introducing metabolic cues were also shown to improve the maturation of cardiomyocytes in microfluidic devices. A recent study by Huebsch et al. shows the usage of microfluidic chips that enhanced the alignment and ECM production of miniaturized cardiac microtissues from various distinct sources of hiPSC-CMs, and their advanced maturation when cultured with a fatty-acid-rich media (Figure 1.25) [349]. Specifically, these microtissues showed improved mitochondrial structure, calcium handling, and cell-source dependent action-potential duration, and thus proposed to provide a better prediction platform for response to cardioactive drugs.

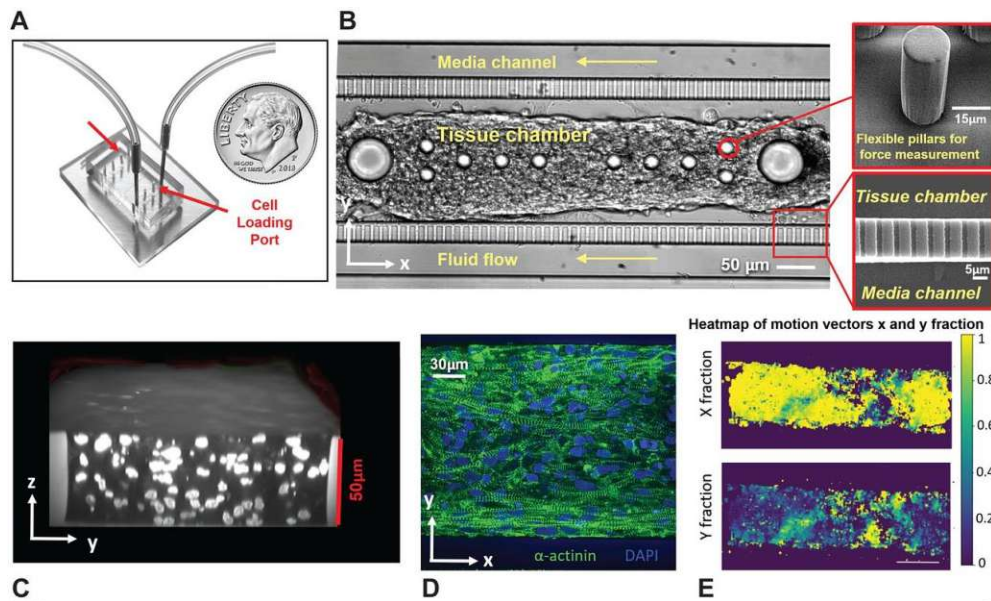


Figure 1. 25 Cardiac microtissue-chip used for metabolic maturation

A. Representative cardiac chips with fluidic inlet & outlet coupled via tubing, plus cell loading ports. **B.** Brightfield image of the cardiac chip, showing cell loading chamber surrounded by media channels, with SEM* images of flexible pillars for contraction force measurements (top), and fenestrations to enable diffusive transport of nutrients (bottom). **C.** Confocal side view to depict device thickness (nuclei stained with DRAQ5). **D.** Confocal image of cardiac microtissue showing sarcomere alignment (sarcomeric α -Actinin, green) and **E.** Heatmap motion vectors obtained by motion tracking. Adapted from [350], [349].

Additionally, heart-on-a-chip models also provide good platforms for drug screening and toxicology. As an example, it could be possible to make a perfused model of tumor cells and cardiac cells in a microfluidic co-culture to evaluate the cardiotoxicity of several chemotherapeutic agents (Figure 1.26) [351]–[353].

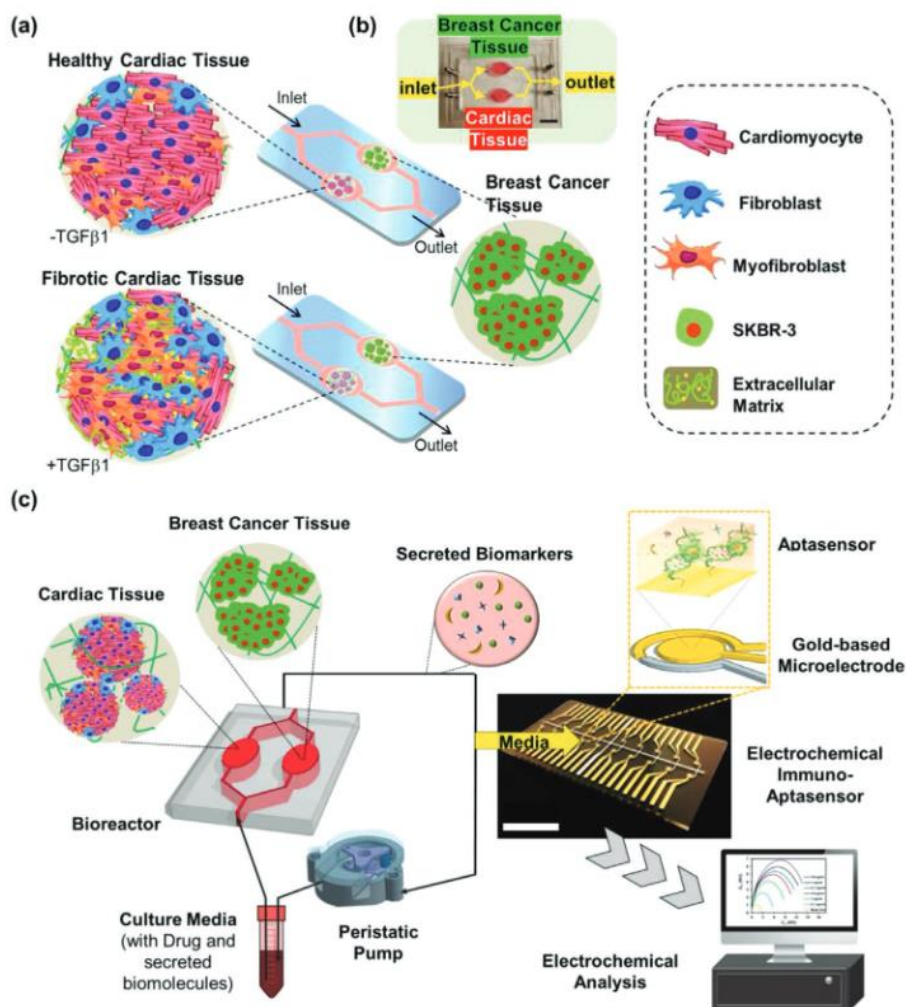


Figure 1. 26 An example of cardio-breast cancer on-a-chip platform with integrated sensors.

A. Scheme of the co-culture chip featuring healthy and fibrotic cardiac microtissues for studying chemotherapy-induced cardiotoxicity because of breast cancer treatment. **B.** An example of the fabricated microdevice. **C.** Integration of immuno-chemical aptasensors for monitoring multiple secreted biomarkers. Adapted from [354].

While HoC technologies are very promising tools to develop more physiologically-relevant cardiac models, they still only use limited types and numbers of cells and lack self-organization; hence they fail at reproducing the complex cellular heterogeneity of the native heart. Furthermore, cells in “heart-on-a-chip” devices are usually cultured for short culture times, thus only achieving limited cardiac maturity.

1.3.2.3 Spheroids, Gastruloids and Organoids

Other efforts to reproduce organ like tissues include spheroids, and scaffold-free microtissues.

Few groups have generated isogenic cardiac microtissues by combining purified hiPSC-derived CMs, CFs and ECs at defined ratios, and induced them to aggregate in low-attachment plates [32], [39]–[44] (Figure 1.27). The resulting constructs displayed spontaneous self-organization and beating activity, and showed structural, functional and metabolic signs of maturation. Although being very simple and effective, these models are limited by the presence of two or three pre-differentiated cell types not reflecting the true cellular heterogeneity of the native human heart.

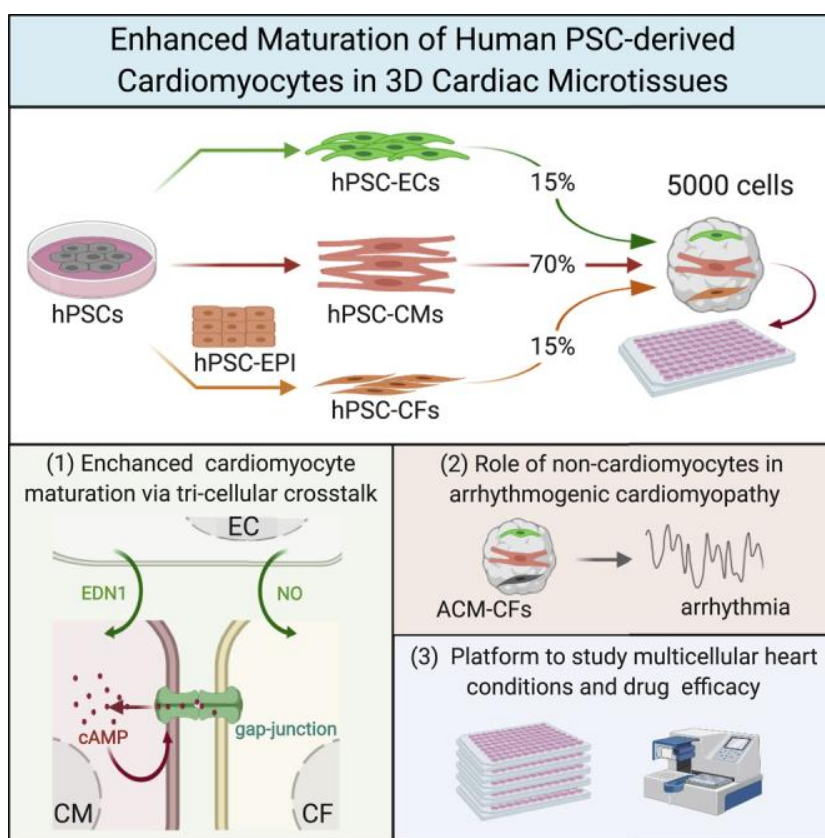


Figure 1. 27 Tri-cellular cardiac microtissues derived from pre-differentiated hiPSC-derived cell types

Purified hiPSC-derived CMs, CFs and ECs at controlled ratios, and aggregated resulting in enhanced maturation with disease modelling and drug-screening applications. Adapted from [42].

Despite the term “organoid” has been widely used in literature for some time, *bona fide* **cardiac organoid** models have only started to emerge in the last couple of years [13], [56]–[58], [62], [63]. As illustrated in Figure 1.28, after tremendous efforts towards establishing organoid models of different body parts, examples of cardiac organoid models, are still limited in addition to other bioengineered cardiac tissue models in the literature.

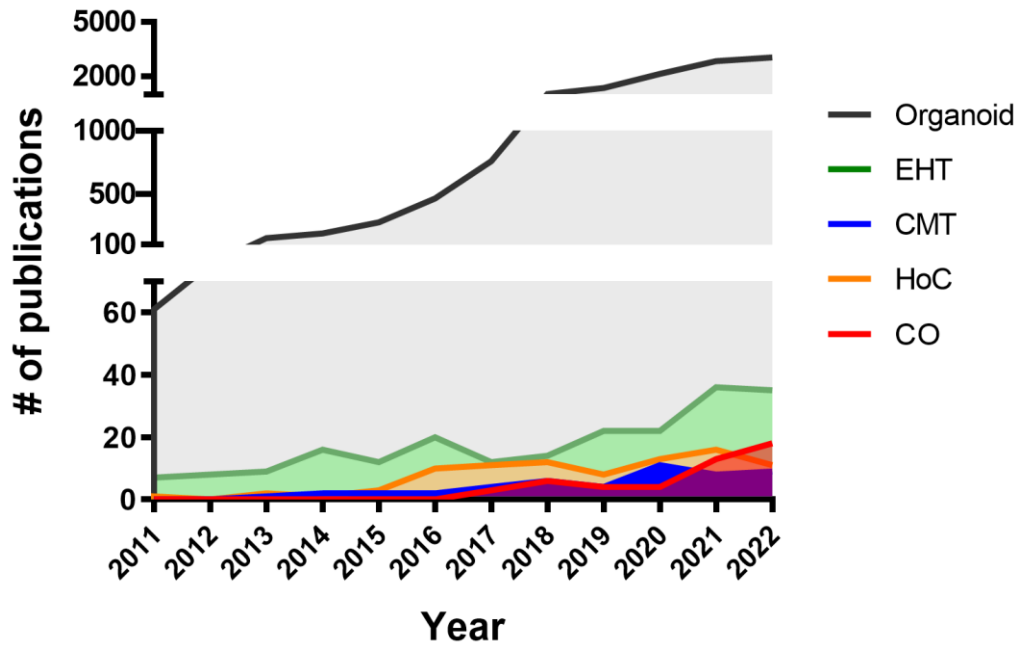


Figure 1. 28 Number of publications with keywords related to organoids and other cardiac tissue models on Pubmed between years 2011-2022.

Keywords used: “Organoid” (gray); “Engineered Heart Tissue (EHT, Green); “Cardiac microtissue” (CMT, blue); “Heart-on-a-chip” (HoC, Orange); “Cardiac organoid” (CO; red).

Organoids are defined as 3D miniaturized versions of an organ, showing faithful micro-anatomy, and organ-specific function compared to the organ they are being modelled after [13], [56]–[58]. Recently, a consensus among researchers has been reached that specific requirements must be fulfilled by an *in vitro* model in order to be considered as an organoid. These criteria include: (1) 3D cellular heterogeneity with organ-specific cell types, (2) self-organization and histology similar to the tissue of origin and (3) recapitulation of at least one specialized biological function similar to the organ being modelled [58]–[60] (Figure 1.29).

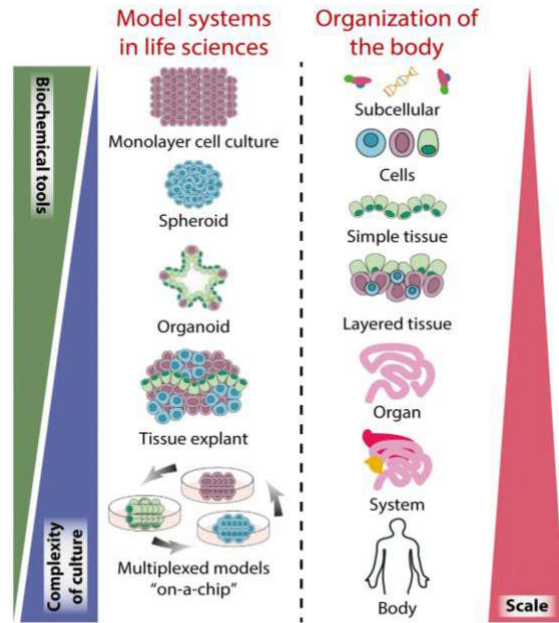


Figure 1. 29 Spheroids vs Organoids

Varying cellular complexity of spheroids vs organoids with respect to native tissues and organs. Adapted from [355].

To this date, well-established organoids have been already generated for many organs such as the brain, kidneys, intestines, guts, lungs and many other organs [13], [61] (Figure 1.30).

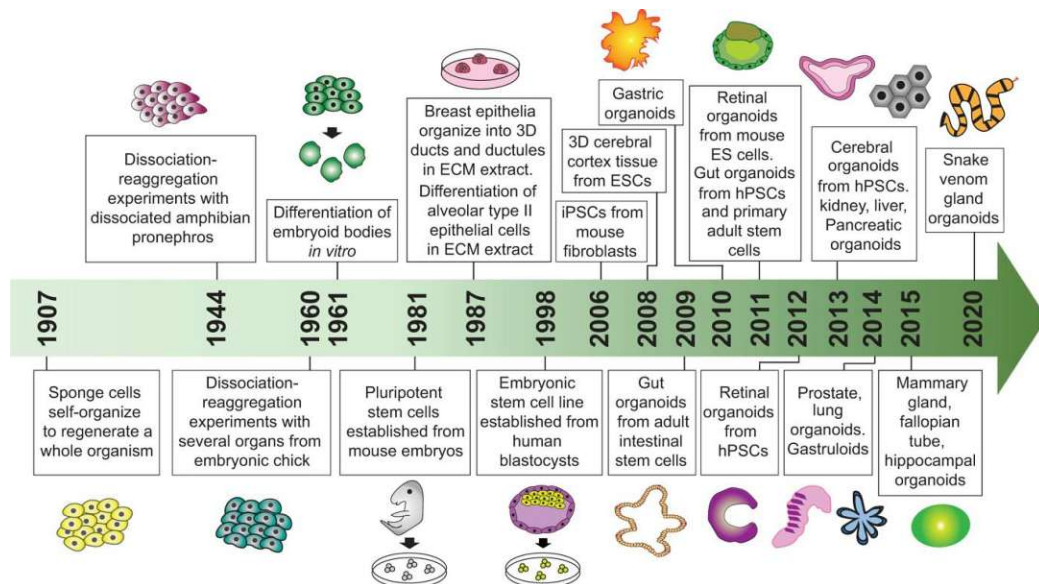


Figure 1. 30 A brief history of human organoid models

Although organoid models of almost every human organ were developed, the first attempts at generating cardiac organoids only occurred very recently. Adapted from [62].

Of note, early mammalian cardiac organoids showing spontaneous self-organization with distinct atrium- and ventricle- like regions were generated from mouse pluripotent stem cells (PSCs) [64], [65], or as a part of **gastruloids** (Figure 1.31) [66], which are defined as 3D aggregates derived from pluripotent stem cells that recapitulate the axial organization of post-implantation embryos *in vitro* [356].

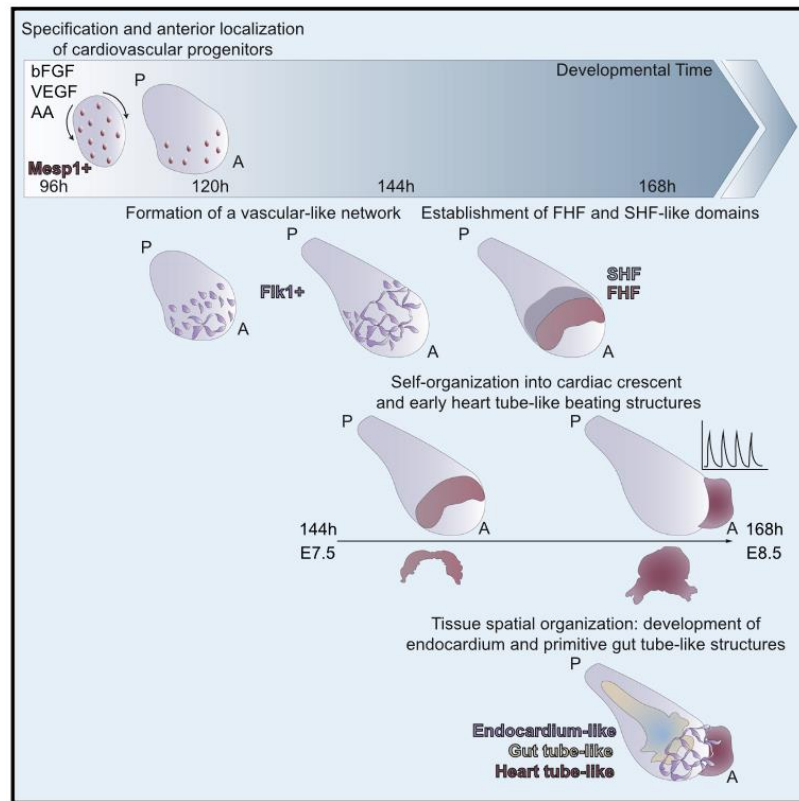


Figure 1. 31 Capturing cardiogenesis in mammalian gastruloids

Gastruloids are 3D aggregates of PSCs that recapitulate post-implantation embryos under defined differentiation conditions. In this study, gastruloids derived from mouse ESCs were shown to generate cardiovascular progenitors that can self-organize into FHF, SHF, crescent and heart-tube-like beating structures, in addition to vascular-like structures. Adapted from [66].

Subsequently, human PSC-derived cardiac organoid models started to emerge [63], [67]–[72], which were developed by various approaches such as assembling different cardiac cell types at certain ratios (hiPSC-CMs, CFs, ECs) to generate a 3D construct [69], or by direct differentiation from 3D embryoid bodies with chemically defined media for Wnt-modulation in order to mimic the embryonic heart development, and thus to generate intrinsically self-organized models that resemble some features of cardiac development [63], [70]–[73] (Figure 1.32, 1.33).

EMBRYOID BODY-LIKE CARDIAC MODELS

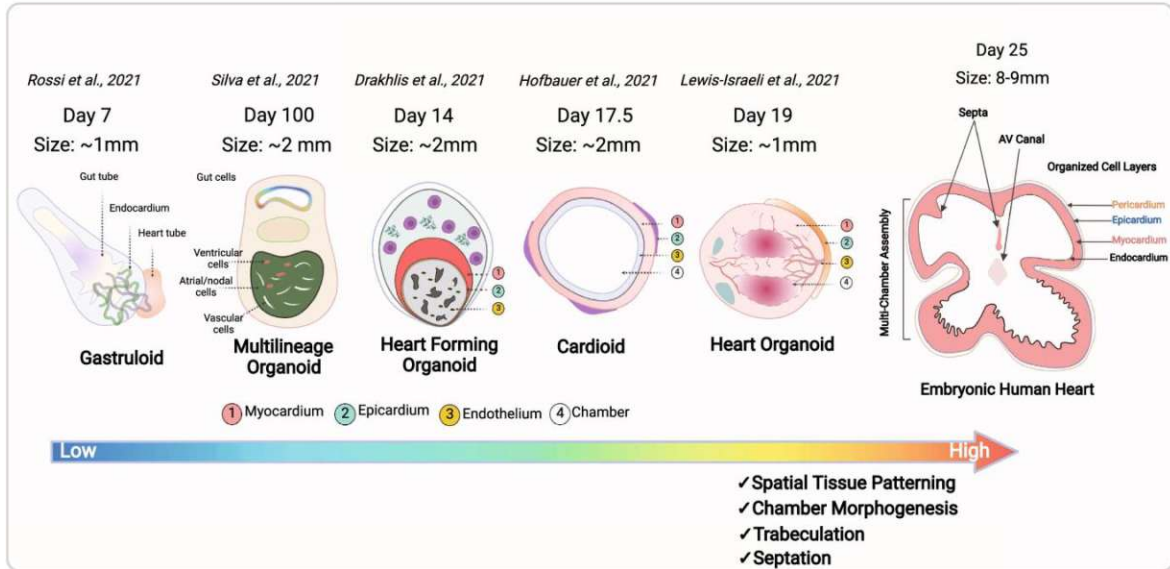
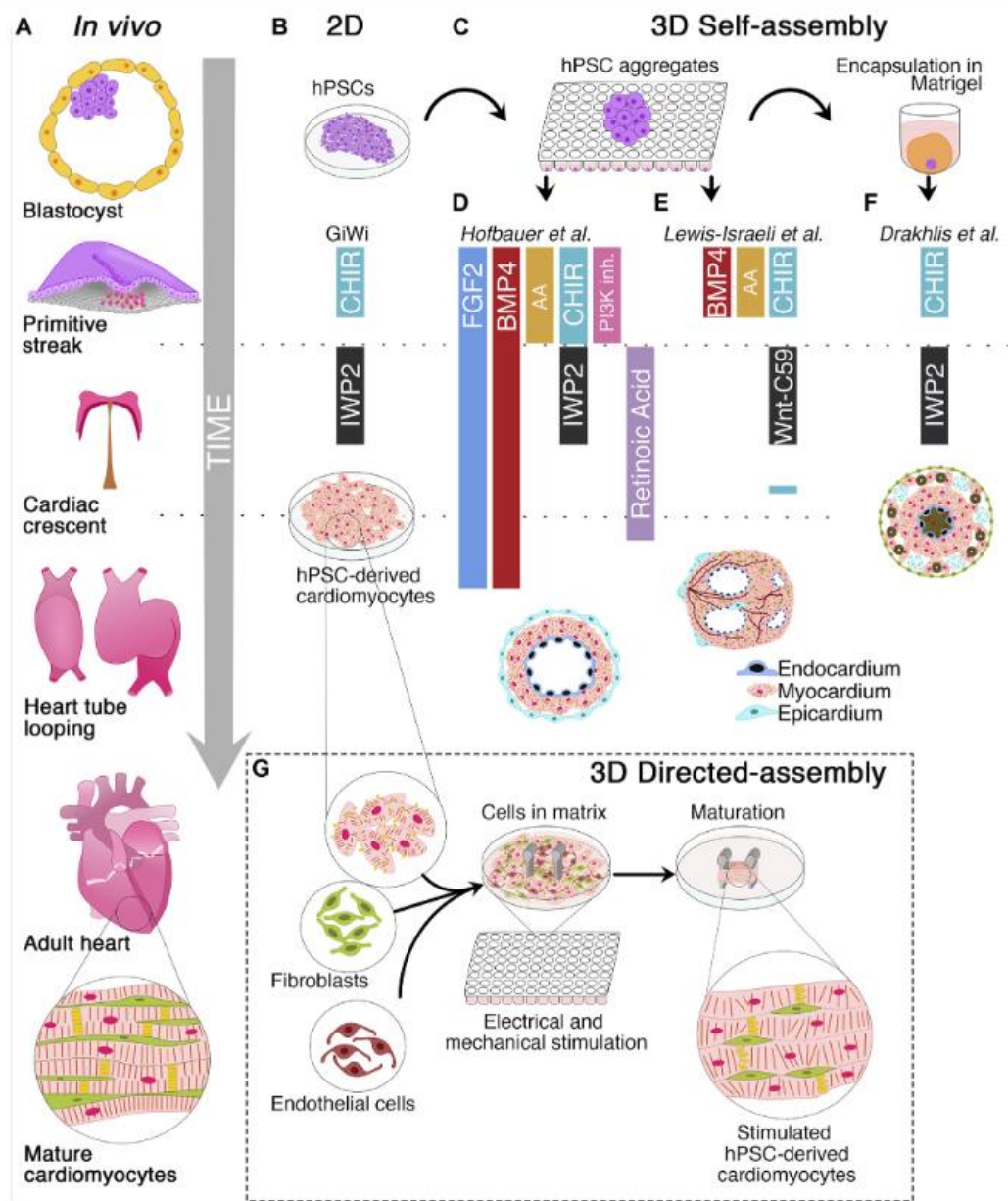


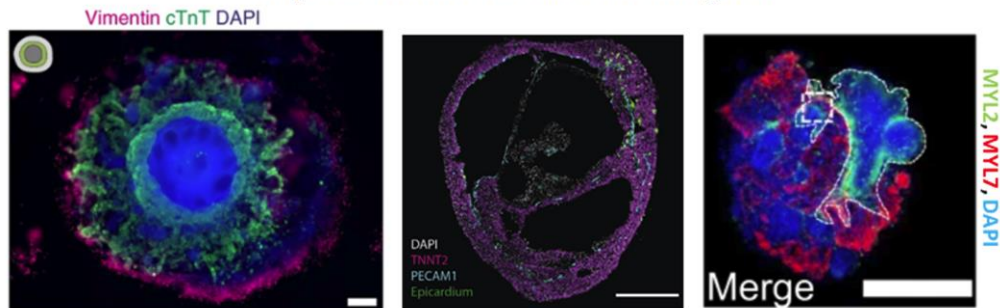
Figure 1. 32 Embryo-like Cardiac (Organoid) models vs native embryonic heart.

A summary of embryonic-heart like models from gastruloids, heart-gut co-forming organoids, and heart forming organoids as compared to features of a native embryonic heart. Adapted from [357].

Recently published human cardiac organoids include single chamber models - i.e. “cardioids” modelling the left ventricle [63] - relying on an external ECM scaffold, such as Matrigel [68], [70], exhibit chamber-like structures [63], [71], showing the co-emergence of gut tissue together with atrial- and ventricular-like regions [70], [72]. A summary of recently published “cardiac organoid” models and the protocols adopted to derive them are summarized in Figure 1.33.



Representative confocal images:



Drakhlis et al., 2021
Scale bar: 200µm

Hofbauer et al., 2021
Scale bar: 200µm

Lewis-Israeli et al., 2021
Scale bar: 500µm

Figure 1. 33 A schematic summary of 2D/3D methodologies to derive human cardiac organoids

TOP: **A.** Timeline of human cardiac development **B.** 2D hiPSC-CM differentiation protocol by Wnt signalling modulation by small molecules. **C.** hiPSC-CM differentiation by “embryoid body” formation in 3D. **D.** Cardioid formation in 3D by a scaffold-free aggregation method by Hofbauer et al, resulting in a model of left ventricle with a cavity [63]. **E.** Self-assembling cardiac organoids by Lewis-Israeli and colleagues with a modified Wnt-modulation protocol forming chamber-like structures [71]. **F.** Heart forming organoid (HFO) by Drakhlis et al by 3D aggregation and Matrigel embedding, resulting in the concomitant formation of cardiac and foregut tissues [70]. **BOTTOM:** Representative confocal images for studies depicted in D, E, F, with relevant cardiac markers. Adapted from [63], [70], [71], [358].

One of the first *bona fide* cardiac organoid studies were published by Drakhlis et al., in which heart forming organoids (HFO) were generated via hPSC aggregates embedded in Matrigel followed by Wnt- signalling modulation (Figure 1.33F) [70], [73]. The resulting HFOs are composed of a myocardial layer lined by endocardial-like cells, and by septum-transversum-like anlagen. Furthermore, they include distinct foregut endoderm tissues and a vascular network. The HFO architecture structurally recapitulates early cardiogenesis which involves on interplay between cardiac mesoderm and foregut endoderm. The HFOs were used to study a developmental disease model with a NKX2.5-knockout (KO) hESC reporter line, where the KO-HFOs displayed a similar phenotype of cardiac malformations previously observed in transgenic mice (ie. less organized microstructure, larger cardiomyocytes, and decreased cell adhesion).

In a resource paper by Hofbauer et al, hPSC-derived self-organizing structures called “cardioids” were described, with a remarkable cavity formation, the presence of major cell types (cardiomyocytes, endothelial cells, epicardial cells) of the heart resembling the left ventricular chamber of the human heart (Figure 1.33D) [63]. From day 2.5 of differentiation, the aggregates started to resemble cardiac mesoderm and merged into a bigger structure with a large cavity inside, whose formation required HAND1 expression. The average diameter of the beating cardioids reached to ~2mm after day 5.5~7.5, where cardiac specification occurs, reminiscent of the early human left ventricular heart chamber where the cavity also displayed markers of endothelial and endocardial cells. Furthermore, in order to mimic the presence of the epicardium, the authors have added hPSC-derived epicardial cells from day 8 and let them re-organize within the microstructures in a co-culture setting. The cardioids were further used for developmental disease modelling by performing localized cryoinjuries, which induced ECM accumulation by endothelial cells and fibroblast-like cells. While the study explores the potential for generating a human cardiac organoid model with a cavity, it only models early developmental stages, where the later stages such as the compaction of the myocardium, or the maturity of cardiac cells. Furthermore, introducing epicardial cells externally as a co-culture setting may not mimic an intrinsic organogenesis process.

Lewis-Israeli et al. have developed human heart organoids (hHOs) with a two-step canonical Wnt signalling modulation strategy using growth factors and chemical inhibitors on hPSC aggregates (Figure 1.33E) [71]. The resulting hHOs have developed internal chamber-like structures, contained cells of multiple cardiac lineages, with an intrinsic organization reminiscent of the heart field with atrio-ventricular-like specification. The hHOs were used to mimic congenital heart disease caused by pregestational diabetes, highlighting their potential application as an *in vitro* model for early embryonic heart development. On the other hand, the hHOs displayed limited maturity levels, where their structural and functional characteristic resemble embryonic fetal hearts, and the authors report that the long-term culture of hHOs resulted in a deviation from their normal developmental pathway, causing them to become a less relevant model over time.

In another recent study by Silva et al., hiPSCs were used to co-develop multi-lineage organoids that recapitulate cooperative cardiac and gut development and maturation (Figure 1.34) [72]. 3D mesodermal progenitor aggregates were differentiated in a cardiac-specific medium with Wnt-signalling modulation and were supplemented with ascorbic acid in dynamic shaking culture. The resulting multi-lineage organoid showed structural and functional co-development of cardiac and gut tissues. The cardio-gut organoids could be maintained in long-term culture (>1 year) up to ~1mm in diameter, and displayed improved physiological and functional maturation of the cardiomyocytes. However, there were limitations in imaging the large-size organoids at later stages of culture due to significant light scattering during microscopy imaging, and it is not known if the presence of gut tissue might have any effects in studies addressing cardiovascular diseases.

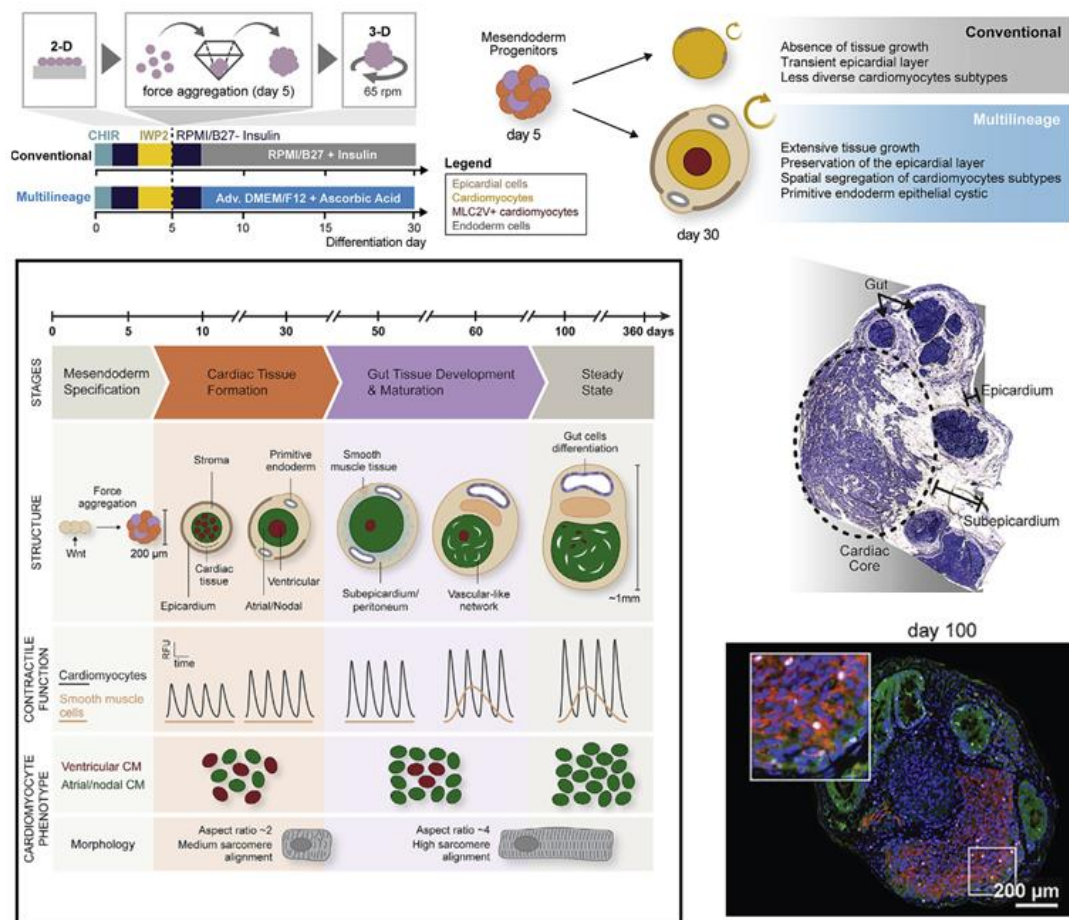


Figure 1.34 A schematic summary of developmental co-emergence of cardiac and gut tissues in long-term multilineage organoids.

hPSC-derived 3D mesodermal progenitor aggregates are differentiated in a cardiac-specific medium with Wnt-signalling modulation in dynamic culture setting, with ascorbic acid supplementation, resulting in co-emergence of cardiac and gut tissues. The resulting cardio-gut microtissues show advanced structural and functional co-development of cardiac and gut tissues, and could be maintained in long-term culture (>1 year). Modified from [72].

Studies on novel human cardiac organoid models are now rapidly growing, and in Table 1.3, a comprehensive overview of recently published cardiac microtissue, gastruloid and organoid works are summarized.

Table 1. 3 Comprehensive overview of cardiac microtissue, gastruloid and organoid models

Model	Cell source	Formation	Scaffold?	Stimulation	Readout		Application notes	Reference
					Morphological	Functional		
Human cardiac microchamber	hiPSC-CM or hESC-CM	Self-formation of 3D microchamber when seeded on 400um-patterned PEG-based substrate Beating on day 15, culture up to 20 days	PEG-Matrigel based coating for hiPSC stage, scaffold-free for spontaneous 3D-MT formation	no	Brightfield microscopy Confocal - IF	Gene expression (qRT-PCR) Cell proliferation (EdU) Single-cell migration tracking	Cardiac specification Drug testing	Ma et al, 2015 [40]
3D Cardiac Microtissue	hiPSC-CM (iCell™ Cardiomyocytes) Primary human CFs Primary human cardiac ECs	Assembly of cell mixture in 4:2:1 ratio on ULA plates Min 14 days of culture	Scaffold-free	no	Histology Confocal - IF	Gene expression (qRT-PCR) Cell viability (ATP content)	Drug testing Cardiotoxicity	Archer et al. , 2018 [359]
3D Cardiac Microtissue	hiPSC-CM (iCell2™ Cardiomyocytes) Human embryonic CFs	Assembly of cell mixture with 4:1 ratio via hanging drop system Culture up to 30 days	Scaffold-free	no	Histology Confocal - IF SEM* TEM	Gene expression (qRT-PCR) Cell viability (Live/Dead staining) Beating analysis (Ca ²⁺ imaging, video motion analysis, patch-clamp) Western Blot	Cardiac specification	Beauchamp et al., 2015 [360] Beauchamp et al., 2020 [361]

3D Cardiac Microtissue	hiPSC-CM or hESC-CM Primary human CFs or hiPSC-CFs hiPSC or hESC-cardiac EC	Assembly of cell mixture (70% CM, 15% CF,15%EC) on V-bottomed plates Culture for 21 days after MT-assembly	Scaffold-free	no	Brightfield microscopy Confocal - IF TEM	Gene expression (qRT-PCR, bulk RNA-seq, scRNA-seq) Flow cytometry Beating analysis (Ca ²⁺ imaging, video motion analysis, patch-clamp, MEA) Western Blot Metabolic flux (Seahorse)	Cardiac specification Maturation Disease modelling: arrhythmogenic cardiomyopathy	Giacomelli et al, 2017 [41] Giacomelli et al, 2018 [362] Giacomelli et al, 2020 [42]
3D MT/Human cardiac organoid	hiPSC-CM (iCell™ Cardiomyocytes) Primary human cardiac ventricular fibroblasts HUVEC hADCS	Assembly of cell mixture with 50% hiPSC-CMs + 50% non-myocytes(4:2:1 ratio of FBs, HUVECs, hADSCs) on low-attachment agarose molds 10 days of culture after MT-assembly	Scaffold-free	no	Brightfield microscopy Confocal - IF Two-photon laser scanning microscopy (2PLSM) imaging for Ca ²⁺ transients	Gene expression (qRT-PCR) Cell death (TUNEL) Mechanical testing (Micropipette aspiration) Hypoxia imaging Oxygen diffusion mathematical modelling Beating analysis (video motion analysis, Ca ²⁺ transients) Metabolic flux (Seahorse) L-lactate Assay	Disease modelling: myocardial infarction (hypoxia & drug induced) Cardiotoxicity	Richards et al., 2017 [33] Richards et al., 2020 [69]

Table continued on next page

Gastruloids	<p>mESCs aggregates</p> <p>hiPSCs aggregates</p>	mESC or hiPSC aggregates on ULA plates exposed to a cocktail of cardiogenic factors, followed by shaking culture for more than 7 days	Scaffold-free	Yes - shaking culture	<p>Brightfield microscopy</p> <p>Confocal - IF</p> <p>Light-sheet microscopy</p>	<p>Gene expression (qRT-PCR, scRNA-seq, RNAscope)</p> <p>Flow cytometry and FACS</p> <p>Angiogenesis assay</p> <p>Beating analysis (Ca²⁺ imaging, video motion analysis)</p>	<p>Modelling embryonic cardiogenesis</p> <p>Co-emergence of cardiogenesis-neurogenesis for the human model</p>	<p>Rossi et al., 2021 [66]</p> <p>Olmsted et al, 2022 [363], [364]</p>
Human heart-forming organoids (HFO)	hPSC-aggregates	<p>hPSC-aggregate formation on ULA plates, Matrigel embedding, differentiation by Wnt- modulation</p> <p>Culture for 10 days</p>	Matrigel embedded	no	<p>Brightfield microscopy</p> <p>Confocal - IF</p> <p>Multiphoton microscopy</p> <p>TEM</p>	<p>Gene expression (mRNA-microarray, scRNA-seq)</p> <p>Flow cytometry</p> <p>Beating analysis (Ca²⁺ imaging, video motion analysis, patch-clamp)</p>	<p>Modelling embryonic cardiogenesis (control vs NKX2.5-KO)</p> <p>Co-emergence of embryonic heart and foregut</p> <p>Distinctly organized layers of myocardium, endocardium, foregut, vessel-like structures</p>	Drakhlis et al., 2021 [70], [73]

Table continued on next page

Cardioids	hiPSC-CM and hESC-CM hPSC-derived epicardial cells	hPSC-aggregates on ULA plates exposed to chemically defined medium (CM specification up to d7.5, maintenance up to d27) Aligned differentiation and co-culture of hPSC-derived epicardium and cardioids (up to d20.5)	Scaffold-free	no	Brightfield microscopy Confocal - IF Histology TEM	Gene expression (qRT-PCR, bulk RNA-seq, scRNA-seq) Reporter cell lines Flow cytometry Beating analysis (Ca ²⁺ imaging, video motion analysis) Proteomics (Mass spectrometry)	Cardiac development Modelling left ventricular chamber with a cavity Cryo-injury modelling	Hofbauer et al., 2021 [63]
Human heart organoids	hESC and hiPSC aggregates	hPSC-aggregates on ULA plates exposed to chemically defined medium (3-step Wnt modulation) Culture for 15 days	Scaffold-free	no	Brightfield microscopy Confocal - IF TEM Optical coherence tomography	Gene expression (bulk RNAseq) Reporter cell lines Beating analysis (Ca ²⁺ imaging, MEA) Metabolic flux (Seahorse)	Cardiac development Distinct multi-lineage cardiac cell types with atrioventricular specification Disease modelling: pregestational diabetes-induced congenital heart defects	Lewis-Israeli et al., 2021 [71]

Table continued on next page

Spatial-organized cardiac organoid	hiPSC-CMs	<p>Self-formation of 3D microchamber when seeded on patterned PEG-based substrates (200-1000 um) under chemically defined media (Wnt modulation)</p> <p>Culture up to 20 days</p>	Scaffold-free	no	<p>Brightfield microscopy</p> <p>Confocal - IF</p>	<p>Gene expression/cell type classification (bulk RNAseq)</p> <p>Reporter cell lines</p> <p>Flow cytometry</p> <p>Beating analysis (Ca²⁺ imaging, video motion analysis)</p>	<p>Drug screening</p> <p>Cardiotoxicity</p>	<p>Hoang et al., 2018 [365]</p> <p>Hoang et al., 2021 [366]</p>
Multilineage organoid: cardio-gut	hiPSC-derived mesoderm aggregates	<p>hiPSC-derived mesoderm aggregation in chemically defined media on day 5, followed by dynamic 3D culture and addition of ascorbic acid</p> <p>Persists >1 year in culture</p>	Scaffold-free	Yes - shaking culture	<p>Brightfield microscopy</p> <p>Confocal - IF</p> <p>TEM</p> <p>Light-sheet microscopy</p> <p>Histology</p>	<p>Gene expression/cell type classification (bulk RNAseq, scRNA-seq)</p> <p>Reporter cell lines</p> <p>Beating analysis (Ca²⁺ imaging, patch-clamp)</p>	<p>Co-emergence of multilineage cardiac and gut tissues</p> <p>Advanced structural and functional properties</p> <p>Maturation</p> <p>Gut tissue supports atrial/nodal CM maturation</p> <p>Long term culture >1 year</p>	<p>Silva et al., 2021 [72]</p>

Table continued on next page

Human Organotypic Cardiac Microtissue (hOCMT)	hiPSC-derived CM differentiation aggregates	hiPSC-derived CM differentiation in 2D in chemically defined media 2D to 3D switch by aggregation on Day 15 Persists >100 days in culture	Scaffold-free	No	Brightfield microscopy Confocal - IF TEM Histology	Gene expression (bulk RNA-seq) Flow cytometry Beating analysis (video motion analysis) Cell death (TUNEL) Cell Viability (ATP content, Live/Dead staining) Metabolic flux (Seahorse)	Cardiac specification Distinct cardiac cell types without gut Maturation Advanced structural, functional, metabolic properties Long term culture Drug testing	Ergir et al., 2022 [367] (Manuscript I)
Human cardiac organoid	hiPSC aggregates	hiPSC-aggregates (EBs) in agarose mold exposed to chemically defined media and hypoxia Transfer to ULA plates on Day 5 followed by normoxia and dynamic culture Long term culture (93 days)	Scaffold-free	Yes - shaking culture after day 5	Brightfield microscopy Confocal - IF Histology	Gene expression (qRT-PCR, bulk RNA-seq) Flow cytometry Beating analysis (video motion analysis, Ca ²⁺ transients)	Cardiac specification Long term culture Disease modelling: Duchenne muscular dystrophy	Marini et al., 2022 [368]
Multi-chamber cardioids	hiPSC-CM and hESC-CM hPSC-derived ECs	Differentiation from hPSC aggregates or 2D-3D switch after 36 hrs mesoderm induction under chemically defined media (Depends on cardioid subtype) Co-culture and fusion of cardioid subtypes Culture for specification 7.5 days, max maintenance length n/a	Scaffold-free	n/a	Brightfield microscopy Spinning Disk Confocal - IF Histology	Gene expression (qRT-PCR, bulk RNA-seq, RNAscope) Flow cytometry Beating analysis (video motion analysis, Ca ²⁺ transients, patch-clamp, voltage-sensitive dye) Reporter cell lines	Cardiac development Distinct cardioids representing all major embryonic heart compartments Developmental disease modelling: control vs KO models Teratogen screening	Schmidt et al., 2022 [369] <i>(preprint)</i>

Table continued on next page

Human heart organoids (HO)	hiPSC aggregates	hiPSC-aggregates (EBs) exposed to chemically defined media in dynamic culture Culture up to 21 days	Suspension in media + 10% Matrigel	Yes - shaking culture since day 0	Brightfield microscopy Confocal - IF Histology	Gene expression (qRT-PCR, bulk RNA-seq, scRNA-seq) Flow cytometry Cell viability (Live/Dead staining) Sprouting assay In vivo vascularization on nude mice Beating analysis (Ca ²⁺ transients, video motion analysis, MEA)	Cardiac specification Drug testing	Lee et al., 2022 [370]
Multilineage heart organoids	hPSC aggregates	Distinct chemical protocols to generate multilineage organoids from hPSC aggregates Co-culture of proepicardium/foregut organoids with ventricular CM aggregates result in an epicardium/myocardium organoid	Scaffold-free	no	Brightfield microscopy Confocal - IF TEM	Gene expression (qRT-PCR, bulk RNA-seq) Flow cytometry Beating analysis (Ca ²⁺ transients)	Cardiac specification Modelling embryonic cardiogenesis Drug testing	Branco et al., 2022 [371]

Note: Studies under the pink box (Manuscript I) were published during or after the revision of our manuscript.

At the structural level, the recent cardiac organoid approaches could better represent the structure of the native human heart than EHTs and HoC platforms due to their self-organization capacity, and containing multiple cell types of the heart. On the other hand, like many *in vitro* heart tissue models, despite their structural closeness to the native heart, the maturity of CMs in the current organoid models is still limited to resembling the fetal heart at histological, transcriptional and functional levels. Furthermore, although extremely informative, most of these early cardiac organoid models are generated by short-term culture only, whereas longer-term culture, and in the future, bioengineering technologies could help them acquire a more mature phenotype, which is desirable for more physiologically relevant *in vitro* tissue models [74], [75].

Meanwhile, the demand for using *in vitro* cardiac models for translational medicine and pharmaceutical applications could be already noted by an increasing number of start-ups and companies with a focus on standardization and commercialization of hiPSC-derived EHT, HoC and cardiac microtissue/organoid platforms. Table 1.4 summarizes a non-exhaustive list of such companies focusing on bioengineered cardiac models with a goal to speed up the translation of research from bench to bedside, and to reduce the number of animals experiments required for pre-clinical studies.

Further efforts are still warranted to generate more mature and organotypic cardiac microtissues/organoids that could replicate the native heart physiology and function more precisely.

Table 1. 4 Non-exhaustive list of start-ups and companies focusing on *in vitro* cardiac models

Company	Location	Model	Proposed Applications	Reference
Ncardia	Netherlands	iPSC-CMs / Microtissues	Disease modelling, safety/efficacy screening, cardiotoxicity	[372]
Valo Health (acquired by TARA Biosystems)	USA	Biowire	Cardiac modelling, drug discovery	[373]
Myriamed	Germany	EHT	Drug screening	[374]
Evotec	Germany	iPSC-CMs / Microtissues	Personalized drug screening	[375]
Heartbeat.bio	Austria	Cardioids	Early disease modelling, drug screening, automation	[376]
Bio/nd	Netherlands	Heart-on-a-chip	Cardiac tissue modelling	[377]
Biomimx	Italy	Heart-on-a-chip (uHeart)	Cardiac modelling, maturation, disease modelling, drug discovery and screening	[378]

4D Cell	France	“SmartHeart” / ring-shaped microtissue	Cardiotoxicity/drug screening	[379]
Medera (Novoheart)	USA	Chamber-forming EHT	Cardiotoxicity and drug efficacy screening, AI-based drug discovery	[380]
Propria	USA	EHT	Predictive cardiac drug screening	[381]
EHT Technologies (acquired by Dinaqor)	Germany	EHT	Safety & potency assesment, disease modelling, gene therapy	[382]
Cellartis (acquired by Takara)	Sweden/UK	EHT	Pharmacology, toxicology, viral infection modelling	[383]
Curibio	USA	EHT	Toxicology/Safety screening, disease modelling	[384]
River Biomedics	Netherlands	3D Cardiac strip (EHT), Heart-on-a-chip, "mini heart" (chamber-formed EHT)	Compound validation, compound screening, personalized disease modelling	[385]

1.4 Aim of the Dissertation

This dissertation aims to provide a deeper understanding of microphysiological technologies in cardiovascular biology, and demonstrates the establishment of a protocol to generate induced pluripotent stem cell (iPSC)-based human 3D cardiac microtissues that could be generated in scaffold-free conditions, cultured for extended periods, featuring multiple cell types of the human heart with spontaneous proto-tissue organization, preserve coordinated contractile activity for several months, and functionally responsive to cardioactive drugs – which are hereby referred to as 3D human organotypic cardiac microtissues (hOCMTs). By combining RNA-sequencing, ultrastructural and metabolic analyses, we demonstrated that the dimensionality and the time in culture are crucial mediators of survival, differentiation, collective organization and maturation of hOCMTs. Finally, we confirmed our human organotypic cardiac microtissues (hOCMTs) qualify as 3D human cardiac organoids (hCOs), hence as an *in vitro* heart model, by proving their response to cardioactive and cardiotoxic drugs in long-term culture.

2 MATERIALS AND METHODS

Acknowledgement

This chapter, including figures and tables, has been reproduced, with or without modifications, based on my published Manuscript 1 (Ergir et al., 2022) [367], licensed for reuse under Creative Commons Attribution 4.0 International License. To view a copy of this licence, visit <http://creativecommons.org/licenses/by/4.0/>.

2.1 Stem cell culture and maintenance

The human iPSC cell line DF 19–9-7 T (iPS, karyotype: 46, XY) was purchased from WiCell (Madison, WI, USA), and the Troponin I1 reporter iPSC line (TNNI1-iPS) was purchased from Coriell Institute (Cat.no. AICS-0037- 172, Camden, New Jersey, USA). All iPSC cells were cultured and maintained in feeder-free conditions as previously described [294],[386] on Growth Factor Reduced Matrigel®-coated plates, (1:100 in DMEM/F12, Corning) in complete Essential 8™ Medium (E8, Thermo Fisher Scientific) containing penicillin/streptomycin (P/S) (0.5%, VWR), incubated at 37°C, 5% CO₂.

2.2 hiPSC-derived monolayer cardiac differentiation and maintenance

Cardiac differentiation from hiPSCs was performed following the Wnt signalling modulation protocol by Lian et.al. [17], [18], with slight modifications as previously described [294]. Briefly, prior to cardiovascular differentiation, hiPSCs were dissociated into single cells (TrypLE Select, Thermo Fisher Scientific) and re-seeded onto 12-well Matrigel-coated plates with 2.0×10^5 cells/cm², with complete Essential 8 medium including Y27632 Rock Inhibitor (RI) (1:4000 dilution from 10 μM stock, 2.5 μM final, Selleck chemicals, Houston, TX, USA). The next day, the medium was replaced with complete Essential 8 medium without RI, and the medium exchange was performed daily until the cells reached 100% confluency. On day 0, to start mesoderm differentiation, the medium was changed with RPMI 1640 with L-Glutamine (Biosera) media supplemented with P/S, B-27™ supplement minus insulin (1×, Thermo Fisher Scientific) and CHIR99021 (8 μM, Sigma-Aldrich). On day 2, the medium was exchanged with RPMI 1640+B-27 minus insulin (RPMI+B27-Ins), supplemented with IWP-2 (5 μM, Selleck chemicals). On day 4, the medium was replaced with RPMI+B27-Ins, and medium exchange was performed every 2 days until the cells started beating (usually on day 7, but may depend on the iPSC line). Once beating clusters started to emerge, the medium was replaced with RPMI 1640+B-27™ supplement (RPMI+B27+Ins) (1×, Thermo Fisher Scientific), and medium exchange was performed every 2-3 days until day 15 of

differentiation. From day 15 on, the cells were used either for generation of 3D hOCMTs or were continued to be cultured as 2D monolayers as controls, with medium exchange every 3-4 days until the end of experiments. For initial optimization steps, we have also included a day 7 timepoint for the generation of 3D hOCMTs.

2.3 hiPSC-derived 3D organotypic cardiac microtissue (hOCMT) generation and maintenance

On day 15 of monolayer cardiac differentiation, cells were dissociated by putting 0.5 mL StemPro™ Accutase™ (Gibco) per well, and incubating in room temperature or in 37°C incubator for 10-20 minutes with occasional mechanical pipetting, until the cells were visually dissociated. After sufficient dissociation, Accutase™ was stopped by putting 3mL RPMI 1640 with 20% Knockout Serum Replacement (Gibco) per well, and the cells were pelleted by centrifugation at 150xg for 3 minutes. The resulting pellet was resuspended with RPMI/B27+Ins + P/S + RI (1:2000 dilution from 10 µM stock, 5 µM final), counted by LUNA™ cell counter (Logos), and seeded 150,000 cells/well in 96-well round bottom ultra-low attachment plates (Corning Costar 7007) at a volume of 150 µL/well. The plates were then centrifuged at 200xg for 5 minutes and incubated at 37°C, 5% CO₂. As 2D control, either 200,000 cells per well were seeded in Matrigel-coated 96-well tissue culture plates at a volume of 200 µL/well, or 1.5×10^6 cells were seeded on Matrigel-coated 24-well tissue culture plates in 1 mL volume per well, or left undetached in 12-well plates. After 48 hours, medium was replaced with RPMI/B27+Ins without RI from hOCMTs and 2D-controls that were re-seeded. From this point on, medium was changed partially every 2-3 days with RPMI/B27+ Ins +P/S until day 30, then every 3-4 days at least until day 50, or longer. For initial optimization steps, we have also included a Day 7 timepoint for the generation of 3D hOCMTs, and both for day 7 and day 15 timepoints, we seeded increasing numbers of cells: 90,000 cells/well, 150,000 cells/well and 300,000 cells/well on the 96-well ultra-low attachment plates.

2.4 Cell viability with Calcein AM/EthD-1 staining

3D hOCMT viability was assessed with LIVE/DEAD™ Viability/Cytotoxicity Kit, for mammalian cells (Thermo Fisher Scientific), according to manufacturer's instructions, and confocal imaging was performed with Zeiss LSM 780 confocal microscope.

2.5 Terminal deoxynucleotidyl transferase (TdT) dUTP Nick-End Labeling (TUNEL) assay

The presence of 3D hOCMT apoptotic/necrotic core was assessed on hOCMT cryosections with Click-iT Plus TUNEL Assay Kit with Alexa Fluor 647 fluorophore (Thermo Fisher

Scientific) according to manufacturer's instructions. Positive control of cell death was performed by DNase I treatment according to manufacturer's instructions (Thermo Fisher Scientific, Cat.no. 18068015). Confocal imaging was performed with Zeiss LSM 780 confocal microscope.

2.6 Histology and Immunofluorescence (IF)

3D hOCMT fixation, cryosectioning, and immunostaining was modified from Perestrelo et al[182]. Briefly, 3D hOCMT s were collected with low binding pipette tips, and fixed in 4% PFA (Santa Cruz Biotechnology) supplemented with 0.03% eosin (Sigma Aldrich) for 2 hours at room temperature, followed by washing with 1xPBS (Lonza), and embedding in 30% sucrose solution at 4°C until they sink at the bottom (~2 days). The hOCMTs were then embedded in OCT solution (Leica), frozen in cassettes embedded in isopentane (VWR) cooled with dry ice, and were stored in -80°C until further processing. The frozen hOCMTs were cryosectioned by cryotome (Leica CM1950) onto Menzel Gläser, SuperFrost® Plus slides (Thermo Fisher Scientific) at 10µM thickness.

After organoid fixation and cryosectioning, to assess the overall histology, the sections were stained with hematoxylin and eosin (H&E) (Sigma Aldrich), and imaged under slide scanner Zeiss Axio Scan Z1 microscope using the bright-field mode.

In addition to 3D hCO cryosections, 2D monolayer cultures were used as controls. As 2D monolayer controls were grown adherently on Matrigel-coated plates, for the IF procedure, the samples were fixed with 4% PFA for 15 minutes, and rest of the IF procedures were performed as previously described in the main text. The resulting samples were stored in PBS with 0.01% Sodium Azide (VWR) at 4°C, and protected from light until confocal dimage analysis.

For IF analysis, the hOCMT sections were washed with PBS for 2x5 min at RT, followed by permeabilization with 0.2% Triton X-100 (Sigma Aldrich) for 5 min. Blocking was done by 2.5% bovine serum albumin (BSA) (Biowest) in PBS for our at room temperature. Primary antibodies were incubated overnight at 4°C (Table 2.1). The next day, the samples were washed with PBS, followed by appropriate Alexa-conjugated secondary antibodies (Table 2.1). Counterstaining was done by DAPI (Roche), and hOCMT slides were mounted with Mowiol®4-88 (Sigma Aldrich). Confocal imaging was performed with Zeiss LSM 780 confocal microscope.

Table 2. 1 List of antibodies used for immunofluorescence experiments

IMMUNOFLUORESCENCE				
<i>IF- Primary Antibodies</i>				
Name	Host species	Dilution	Company	Catalog no
Anti- α -SMA (ACTA2)	Rabbit	1:500	Abcam	ab5694
Anti-ACTN2 (sarcomeric α -actinin)	Mouse	1:800	Sigma Aldrich	A7811
Anti-ASCL2	Sheep	1:50	Thermo Fisher Scientific	PA5-47852
Anti-Brachyury (T)	Goat	1:50	R&D Systems	967332
Anti-CD31 (PECAM-1)	Mouse	1:100	Biolegend	303102
Anti-CX43 (Connexin 43, GJA1)	Rabbit	1:400	Sigma Aldrich	C6219-100UL
Anti-GATA4	Rabbit	1:400	Cell signalling	36966S
Anti-MESP1	Rabbit	1:200	Abcam	ab129387
Anti-MYL2 (α -MLC2, MLC2v)	Rabbit	1:200	Abcam	ab79935
Anti-MYL7 (MLC2a)	Mouse	1:200	Santa Cruz	sc-365255
Anti-NFAT2 (NFATc1)	Rabbit	1:100	Cell Signalling	8032S
Anti-SERCA2 (ATP2A2)	Mouse	1:100	Novus Biologicals	NB300-581
Anti-SM22a (Transgelin, TAGLN)	Rabbit	1:500	Abcam	ab14106
Anti-SOX2	Rabbit	1:400	Cell Signalling	3579
Anti-TE - 7	Mouse	1:100	Sigma Aldrich	CBL271
Anti-TBX18	Rabbit	1:200	Thermo Fisher Scientific	PA5-101921
Anti-TNNT2	Mouse	1:200	Thermo Fisher Scientific	MA5-12960
Anti-TNNT2	Rabbit	1:3000	Sigma Aldrich	HPA015774
Anti-WT1	Rabbit	1:200	Cell Signalling	83535
<i>IF- Secondary Antibodies</i>				
Name		Dilution	Company	Catalog no
Alexa Fluor 488 Donkey anti-Rabbit IgG (H+L)		1:500	Thermo Fisher Scientific	A-21206
Alexa Fluor 488 Donkey anti-Mouse IgG (H+L)		1:500	Thermo Fisher Scientific	A-21202
Alexa Fluor 555 Donkey anti-Rabbit IgG (H+L)		1:500	Thermo Fisher Scientific	A-31572
Alexa Fluor 555 Donkey anti- Mouse IgG (H+L)		1:500	Thermo Fisher Scientific	A-31570
Alexa Fluor 546 Donkey anti-Sheep IgG (H+L)		1:500	Thermo Fisher Scientific	A-21098
Alexa Fluor 647 Donkey anti-Goat IgG (H+L)		1:500	Thermo Fisher Scientific	A-21447
Alexa Fluor 647 Goat anti-Mouse IgG (H+L)		1:500	Thermo Fisher Scientific	A-21235

2.7 Microscopy and image analysis

Confocal imaging was performed with Zeiss LSM 780 confocal microscope. Light microscopy imaging was performed with Leica DM IL LED inverted microscope, and fluorescence images were collected with Leica DMI4000 B inverted fluorescence microscope. Image analysis was performed with ImageJ (v1.53o).

2.8 3D hOCMT dissociation

For flow cytometry and RNA isolation, hOCMTs were collected in Eppendorf tubes with low binding pipettes on day 30 and 50, and dissociated with MACS Multi Tissue Dissociation Kit 3 (Miltenyi Biotec, Cat.no.130–110-204) according to manufacturer’s instructions. As controls, 2D monolayer cultures were directly dissociated on the plates with the same kit.

2.9 Flow cytometry

Flow cytometry analyses on 3D hOCMTs and 2D controls were performed on day 15 (for 2D) , day 30 (for 2D and 3D) and day 50 (for 2D and 3D) timepoints as described previously [182], [386] with modifications. Briefly, on each timepoint, samples were dissociated with MACS Multi Tissue Dissociation Kit 3, washed with FACS buffer (99.4% PBS + 0.1% UltraPure™ 0.5M EDTA pH 8.0 by Invitrogen™ + 0.5% FBS by Sigma Aldrich [Cat.no.F9665-500ML]) and surface marker staining with CD90-APC (Exbio; 1:10 dilution in FACS buffer) and CD31-BV421 (Biolegend; 1:10 dilution in FACS buffer) antibodies was performed together with corresponding unstained controls for 30 minutes on ice. Afterwards, sample fixation and permeabilization was performed with Intracellular Fixation and Permeabilization Buffer Set (eBiosciences) per manufacturer’s instructions, followed by intracellular marker staining with TNNT2-FITC (Miltenyi Biotec; 1:50 dilution in 1 x Permeabilization Buffer) antibody together with corresponding unstained controls for 30 minutes in room temperature. Sample acquisition was performed by using BD FACSCanto II (Becton, Dickinson and Company, Franklin Lakes, NJ, USA), and cell populations were analysed with FlowJo v.10 (Tree Star) (Table 2.2).

Table 2. 2 List of antibodies used for flow cytometry experiments.

FLOW CYTOMETRY			
Name	Dilution	Company	Catalog no
Anti-Cardiac Troponin T-FITC Clone REA400 (REAffinity™)	1:50	Miltenyi Biotec	130-119-575
Anti-Hu CD90 APC	1:10	Exbio	1A-652-T100
Anti-Hu CD31 BV421	1:10	Biolegend	303123

2.10 Transmission Electron Microscopy (TEM) sample preparation and analysis

3D hOCMTs were transferred to new well-plates with low binding pipettes, and washed 2 x with PBS. Fixation was done by 1.5% PFA+ 1.5% glutaraldehyde (Sigma Aldrich) diluted in RPMI 1640 culture media for 1 hour, then washed with 0.1 M cacodylate buffer (pH 7.4) (Sigma Aldrich) for 3 times 5 minutes each, and incubated overnight at 4°C in cacodylate with glutaraldehyde. The next day, samples were rewashed 3 times with cacodylate buffer, and incubated at 4°C in cacodylate buffer until sending the samples, protected from light. The 3D hOCMTs were post-fixed for 1.5 hours with 1% osmium tetroxide in 0.1 M cacodylate buffer and washed for 3 times with 0.1 M cacodylate buffer, 10 minutes each, then stained with 1% uranyl acetate in milli-Q water overnight at 4°C, followed by washing in milli-Q water. The samples were then dehydrated in an ascending EtOH series using solutions of 70%, 90%, 96% and 3 times 100% for 10 minutes each, incubated in propylene oxide (PO) 3 times for 20 minutes before incubation in a mixture of PO and Epon resin overnight, and incubated in pure Epon for 2 hours and embedded by polymerizing Epon at 68°C for 48 hours. Ultra-thin sections of 70 nm were cut using a Leica Ultracut EM UC 6 Cryo-ultramicrotome. TEM images were collected with a JEOL JEM 1011 electron microscope and recorded with a 2 Mp charge coupled device camera (Gatan Orius).

2.11 RNA isolation, bulk RNA-sequencing and differential expression (DE) analysis

2.11.1 RNA isolation and quality control

For RNA isolation, 3D hOCMTs and 2D controls were dissociated by using MACS Multi Tissue Dissociation Kit 3 on day 30 and day 50. After cell dissociation, RNA was extracted with High Pure RNA Isolation Kit (Roche) according to manufacturer's instructions, and quantified with Nanodrop 2000 Spectrophotometer (Thermo Fisher Scientific). Quality control for RNA integrity number (RIN) was also determined with Agilent 2100 Bioanalyzer.

2.11.2 Sequencing library preparation

500 nanograms of total RNA per sample was used as an input for library preparation using QuantSeq FWD 3'mRNA Library Prep Kit (Lexogen). Briefly, RNA was transcribed into cDNA using oligodT primer (FS1) at half volume compared to the manufacturer's

instructions to minimize the off-target products. Following the first strand synthesis, RNA removal and second strand synthesis were performed using the UMI Second Strand Synthesis Mix (USS) containing Unique Molecular Identifiers (UMIs) that allow detection and removal of PCR duplicates. Finally, sequencing libraries were created by PCR with i5 Unique Dual Indexing Add-on Kit for Illumina (Lexogen). The quality and quantity of libraries was determined using Fragment Analyzer by DNF-474 High Sensitivity NGS Fragment Analysis Kit (Agilent Technologies) and QuantiFluor dsDNA System (Promega). Final library pool was sequenced on Illumina NextSeq 500 with 75 bp single-ends, producing about 10 million reads per library.

2.11.3 Differential expression (DE) analysis

High-throughput RNA-Seq data were prepared using Lexogen QuantSeq 3' mRNA-Seq Library Prep Kit FWD for Illumina with polyA selection and sequenced on Illumina NextSeq 500 sequencer (run length 1x75 nt). Bcl files were converted to Fastq format using bcl2fastq v. 2.20.0.422 Illumina software for basecalling. 6-nt long UMIs were extracted and subsequently used for deduplication of aligned reads by UMI-tools v. 1.1.1 [387]. As a next step 6-nt long barcode sequence related to Lexogen QuantSeq Library Prep Kit were trimmed using seqtk 1.3-r106 [388]. Quality check of raw single-end fastq reads was carried out by FastQC v0.11.9 [389]. The adapters and quality trimming of raw fastq reads was performed using Trimmomatic v0.36 [390] with settings CROP:250 LEADING:3 TRAILING:3 SLIDINGWINDOW:4:5 MINLEN:35 and adaptor sequence ILLUMINACLIP:AGATCGGAAGAGCACACGTC. Trimmed RNA-Seq reads were mapped against the human genome (hg38) and Ensembl GRCh38 v.94 annotation using STAR v2.7.3a [391] as splice-aware short read aligner and default parameters except --outFilterMismatchNoverLmax 0.1 and --twopassMode Basic. Quality control after alignment concerning the number and percentage of uniquely and multi-mapped reads, rRNA contamination, mapped regions, read coverage distribution, strand specificity, gene biotypes and PCR duplication was performed using several tools namely RSeQC v2.6.2 [392], Picard toolkit v2.18.27 [393] and Qualimap v.2.2.2 [394] and BioBloom tools v 2.3.4-6-g433f [395].

The differential gene expression analysis was calculated based on the gene counts produced using featureCounts tool v1.6.3 [396] with settings -s 2 -T 10 -F GTF -Q 0 -d 1 -D 25000 and using Bioconductor package DESeq2 v1.20.0 [397]. Data generated by DESeq2 with independent filtering were selected for the differential gene expression analysis to avoid potential false positive results. Genes were considered as differentially expressed based on a cut-off of adjusted p-value ≤ 0.05 and $\log_2(\text{fold-change}) \geq 1$ or ≤ -1 . Clustered heatmaps were generated from selected top differentially regulated genes using R package pheatmap v1.0.10 [398]. Volcano plots were produced using ggplot v3.3.3 package [399] and MA plots were generated using ggpubr v0.4.0 package [400]. The data generated were

deposited in the NCBI Gene Expression Omnibus repository with the GEO ID [GSE209997](https://www.ncbi.nlm.nih.gov/geo/query/acc.cgi?acc=GSE209997).

2.11.4 Gene ontology enrichment, clustering, and comparison with other datasets

Gene ontology (GO) enrichment analysis for biological processes was performed with EnrichR web-tool [401]–[403]. Clustering analysis of upregulated genes was done with Cytoscape [404].

RNA-seq data from this study were also compared to adult human heart RNA-seq data (from BioProjects PRJNA667310 [405] and PRJNA628736 [406]), and EHT RNA-seq data (from BioProject PRJNA831794 [407], [408]) obtained from the NCBI BioProject database (<https://www.ncbi.nlm.nih.gov/bioproject/>) (Accession numbers: SRR12771050, SRR12771052, SRR11620685, SRR11620686, SRR18911472, SRR18911473, SRR18911476, SRR18911477) by using Biojupies web-tool [409].

2.12 Metabolic flux analysis

Mitochondrial respiration of 3D hOCMTs and 2D controls was assessed using Seahorse XFp Analyzer (Agilent) with Seahorse XFp Cell Mito Stress Test Kit (Agilent). On the Day 50 timepoint, 8-well XFp Cell Culture Miniplates (Agilent) were coated with Matrigel (1:20 dilution), and both 3D hOCMTs (one centered 3D hOCMT per well) and 2D controls (dissociated with MACS Multi-tissue dissociation kit 3 and seeded at 200,000 cells/well) were plated. The miniplates were cultured for 48 hours in RPMI/B27+Ins + P/S + RI (1:2000 dilution from 10 μ M stock, 5 μ M final) media to allow stabilization, and for the next 24 hours in RPMI/B27+Ins + P/S media. For 3D hOCMTs, only beating samples located at the center of the well were included in the subsequent statistical analysis.

One hour before measurement, RPMI/B27+Ins + P/S media was replaced with Seahorse XF RPMI Medium pH 7.4 (Agilent) supplemented with 10 mM glucose, 2 mM glutamine, and 1 mM pyruvate (Agilent). Metabolic inhibitors were diluted in the supplemented XF Medium, loaded into the injection ports of the hydrated Seahorse XFp Sensor Cartridge (Agilent), and injected at specified time points to the wells as follows: Oligomycin (3 μ M), FCCP (4 μ M), and Rotenone/Antimycin A (2 μ M). The Mito Stress Test was performed according to the manufacturer's instructions and included five measurements for basal consumption and five measurements after every drug injection. An extra five-minute waiting step was included after the Oligomycin injection.

After the measurement, both 3D hOCMTs and 2D controls were dissociated with MACS MultiTissue Dissociation Kit 3 (Miltenyi Biotec), and lysed for 2 hours at 60°C (10 mM

Tris, 1mM EDTA, 50 mM KCl, 2 mM MgCl₂, 200 µg/mL Proteinase K as described previously by Giacomelli et al[42]. Metabolic data were normalized by measuring the DNA content of each sample with a Quant-iT™ PicoGreen™ dsDNA Assay Kit (Thermo Fisher Scientific) according to the manufacturer's protocol. Wave software (Agilent), Microsoft Excel, and Prism 9 (GraphPad Software) were used for data analysis.

2.13 Drug treatments

Isoproterenol hydrochloride (Sigma Aldrich) was dissolved in dimethyl sulfoxide (DMSO) (Sigma Aldrich), and Verapamil hydrochloride (Sigma Aldrich) in methanol (VWR) to prepare 1 M stock solutions. Each drug solution was 10- fold serially diluted in RPMI/B27+Ins media to make final concentrations between 0.0001-1 µM. As untreated controls, complete RPMI/B27+Ins media supplemented with DMSO or methanol were used. For data collection, the 3D hOCMTs with drug-supplemented media were incubated for 10 minutes at 37°C, 5% CO₂ each time the drug concentration changed, followed by live imaging with video acquisition per condition with Zeiss LSM 780 confocal microscope. Chemotherapy-induced cardiotoxicity was evaluated in 3D hOCMTs treated with RPMI/B27+Ins supplemented with doxorubicin (Doxo) (Sigma Aldrich), at 0.1 µg/mL and 1 µg/mL concentrations, or plain RPMI/B27+Ins as control for 6 days. Growth medium was exchanged every 3 days, and 3D hOCMT morphology and beating were monitored daily by live video recording with Zeiss LSM 780 confocal microscope for 6 days. On day 6 of drug treatment, the 3D hOCMTs were collected for evaluating viability.

2.14 Live video acquisition and contraction analysis

To evaluate the contractile function of 3D hOCMTs, live image sequences were acquired with Zeiss LSM 780 Confocal microscope using transmitted light mode (37°C, 5% CO₂), as equivalent to 60 fps for 15 seconds; where the image sequences were later turned into .avi files with ImageJ. The beating rates were counted and calculated manually from the video analysis, and representative contraction graphs were derived with the open-source video analysis software MUSCLEMOTION [362], [410] per providers' instructions.

2.15 Luminescence-based cell viability assay

3D hOCMTs viability after 6 days of Doxo treatment was assessed by CellTiter-Glo® Luminescent Cell Viability Assay Kit (Promega) according to manufacturer's instructions. After the 3D hOCMTs were dissociated by the assay treatment, the samples were transferred to a clear-bottom 96-well white assay plate (Corning Costar 3610) and cell viability was quantified with Centro LB 960 Microplate Luminometer (Berthold Technologies).

2.16 Statistics

Data are expressed as mean \pm SD or mean \pm SEM where applicable, unless otherwise stated. Statistical analyses were performed using Microsoft Excel 2010 and GraphPad Prism 8.0.2 unless otherwise stated, using one-way ANOVA (with Tukey's multiple comparisons test), two-way ANOVA (with Dunnett's multiple comparisons test), or unpaired Student's t-test (two-tailed) where $p < 0.05$ was considered to be significantly different as denoted with asterisks [(*) $p \leq 0.05$, (**) $p \leq 0.01$, (***) $p \leq 0.001$, (****) $p \leq 0.0001$]. Sample sizes of independent experiments, statistical methods used and the significance were described in the figure legends wherever applicable.

2.17 Data availability

The RNA-sequencing data obtained and presented in this study were generated at CF Genomics of CEITEC, and is available in the NCBI GEO public repository with accession no. GSE209997 (<https://www.ncbi.nlm.nih.gov/geo/query/acc.cgi?acc=GSE209997>).

3 RESULTS

Acknowledgement

This chapter, including figures and tables, has been reproduced, with or without modifications, based on my published Manuscript 1 (Ergir et al., 2022)[367], licensed for reuse under Creative Commons Attribution 4.0 International License. To view a copy of this licence, visit <http://creativecommons.org/licenses/by/4.0/>.

3.1 2D-to-3D culture switch promotes spontaneous cardiac microtissue formation in scaffold-free conditions

Since the 2D monolayer differentiation of induced pluripotent stem cell (iPSC)-derived cardiomyocytes is well established in the literature, and long-term cultures of iPSC-derived cardiomyocyte monolayers naturally tend to delaminate into beating clusters [272], we first performed human iPSC (hereafter hiPSC) differentiation in a 2D system and tested whether they could be used to generate 3D cardiac aggregates in the absence of any external ECM scaffold.

Cardiac differentiation was induced in confluent 2D hiPSC monolayers by sequential modulation of the WNT pathway with small molecules, in the absence of insulin [271] as previously described by Lian et al [17], [18]: Firstly, mesoderm specification was achieved by transient WNT activation through chemical inhibition of GSK3, followed by cardiac mesoderm differentiation through the inhibition of the WNT palmitoleoyltransferase PORCN [17], [18] (Figure 3.1). When beating cell clusters were observed (day 7), insulin supplement was added to the media, since it was needed for cell survival after early contractile cardiomyocytes emerged during differentiation [271].

On day 7 or day 15 of differentiation, the monolayer was dissociated into single cells that were seeded on round-bottom ultra-low attachment plates. Different cell numbers (90,000 cells/well, 150,000 cells/well, 300,000 cells/well for 96-well plates) were tested in order to evaluate the spontaneous formation of aggregates in the presence of ROCK inhibitor. Throughout the study, we used 2D monolayer cultures as control. A graphical representation of the protocol used in the study is shown in Figure 3.1.

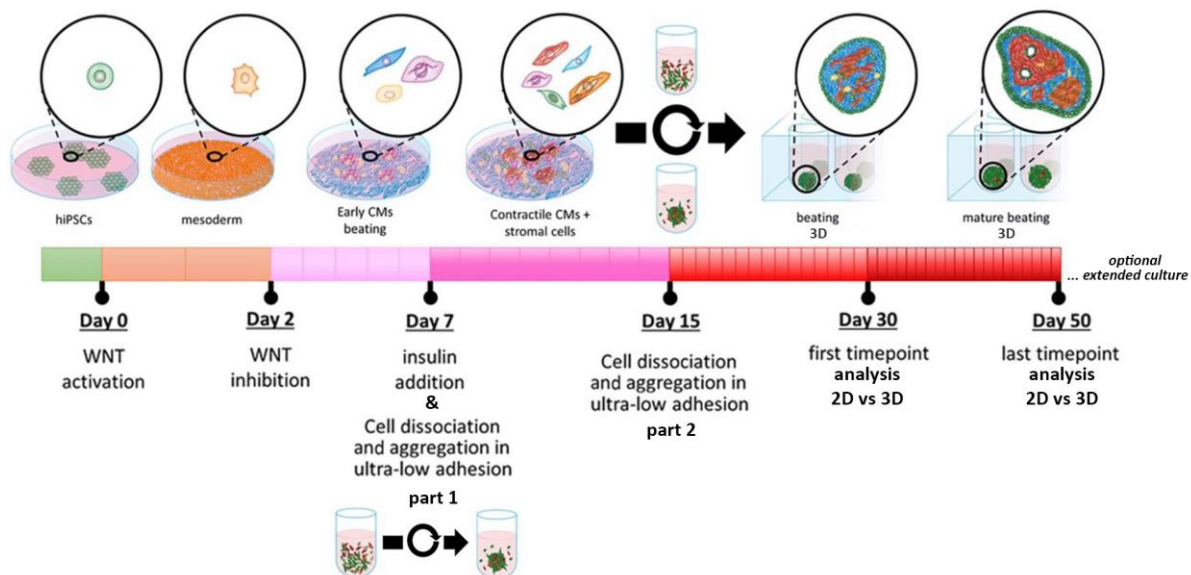


Figure 3. 1 Schematic workflow for the generation and long-term culture of hiPSC derived cardiac microtissues.

Warm colours represent cardiomyocyte lineages, while the rest of the colours represent non-myocytes.

One day after switching the culture from 2D to 3D, we observed under the light microscope a tendency for the spontaneous formation of 3D microtissues without the need for any ECM scaffold, which started to show spontaneous beating behaviour upon removing the ROCK inhibitor after 48 hours. We set out at assessing the cellular heterogeneity of the preparation and their tendency to self-organise in microtissues. For this purpose, samples aggregated on day 7 (“D7-induced”; or “D7i”) and day 15 (“D15-induced”; or “D15i”) were cultured until day 30 and day 50 timepoints, and histological analyses with haematoxylin and eosin (H&E) and IF staining were performed on microtissue cryosections.

While H&E staining for day 30 endpoint samples did not show a major difference between D7i and D15i microtissues in terms of histological complexity (Figure 3.2), this has shifted towards extended culture times up to the day 50 endpoint. Regardless of cell seeding numbers, the D7i microtissues appeared more compact on day 50 endpoint (Figure 3.3). On the other hand, D15i microtissues displayed more complex histological structures at higher seeding numbers as compared to D7i microtissues at this timepoint. Unlike D7i microtissues, chamber-like formations were observed only on D15i microtissues at the core of the microtissues at higher initial seeding numbers on day 50 (Figure 3.4).

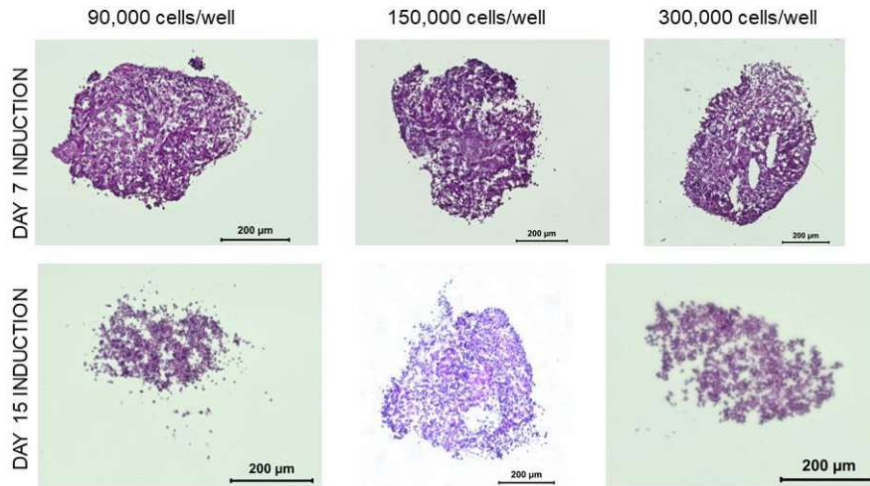


Figure 3. 2 H&E staining on day 30 endpoint for microtissues made on day 7 vs. day 15 of differentiation.

H&E staining showing the histological complexity of D7i- vs D15i-3D microtissue sections on day 30 endpoint (middle sections). Scale bars = 200μm.

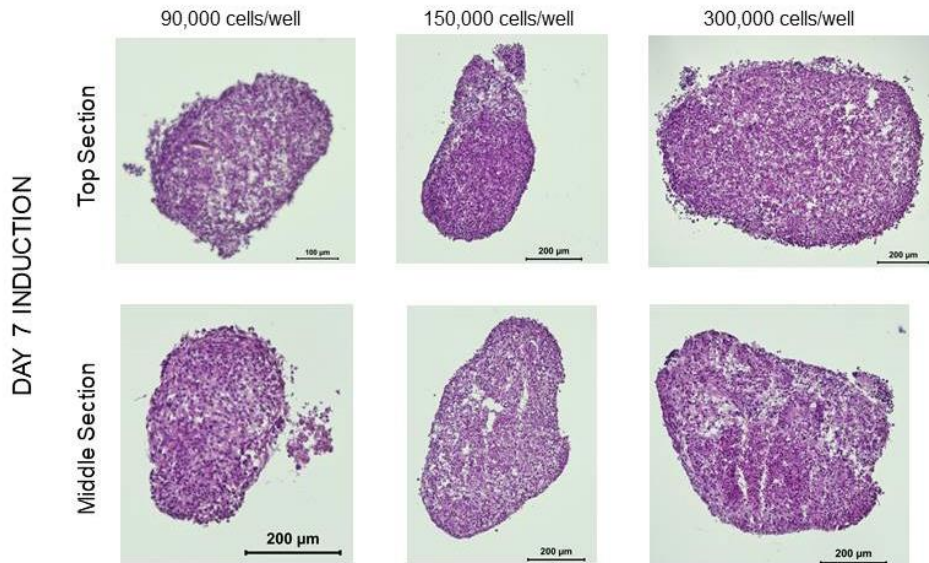


Figure 3. 3 H&E staining on day 50 endpoint for microtissues made on day 7 of differentiation (D7i).

H&E staining showing the histological complexity of D7i-3D microtissue top & middle sections on day 50 endpoint. Scale bars = 100μm for 90,000cells/well sample at top section; = 200μm for the rest.

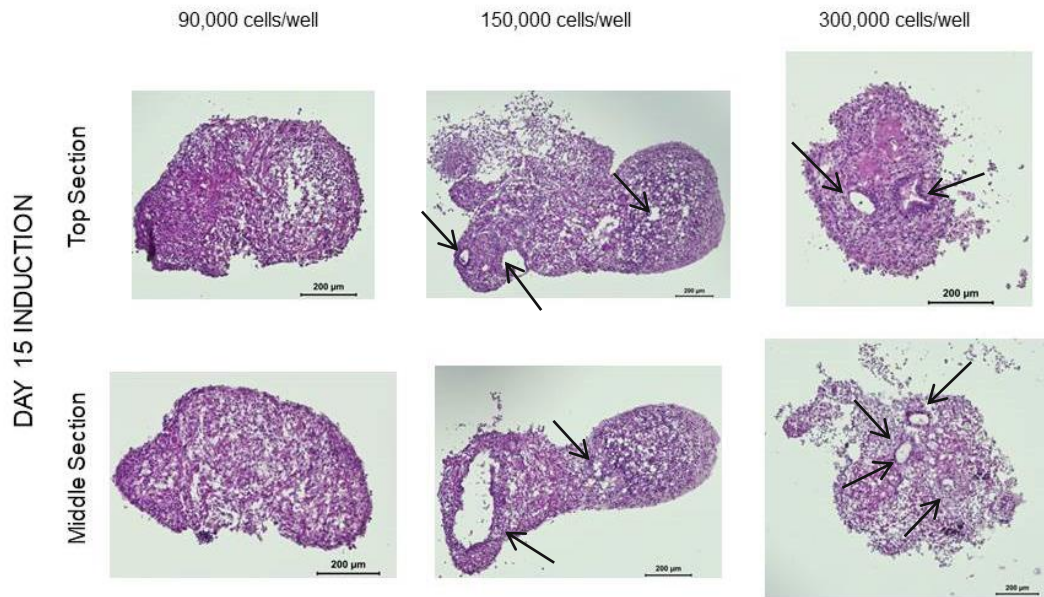


Figure 3. 4 H&E staining on day 50 endpoint for microtissues made on day 15 of differentiation (D15i).

H&E staining showing the histological complexity of D15i-3D microtissue top & middle sections on day 50 endpoint. Chamber-like structures are indicated by black arrows. Scale bars = 200µm.

With time in culture from day 30 to day 50, immunofluorescence (IF) analysis showed that contractile cardiomyocytes stained with sarcomeric α -actinin (ACTN2) and other cells stained with α -smooth muscle actin (α -SMA) were arranged in discrete regions within the microtissues. However, this phenomenon was more pronounced in D15i microtissues than in D7i microtissues (Figure 3.5). On the other hand, while the higher seeding number of 300,000 cells/well seemed to yield a reduced percentage of cardiomyocytes at day 50 timepoint, the seeding number of 90,000 cells/well displayed reduced histological complexity, as seen from the H&E stainings (Figure 3.3 - 3.5).

In light of these observations, we used the microtissues generated on day 15 of differentiation by seeding 150,000 cells/well for the following experiments.

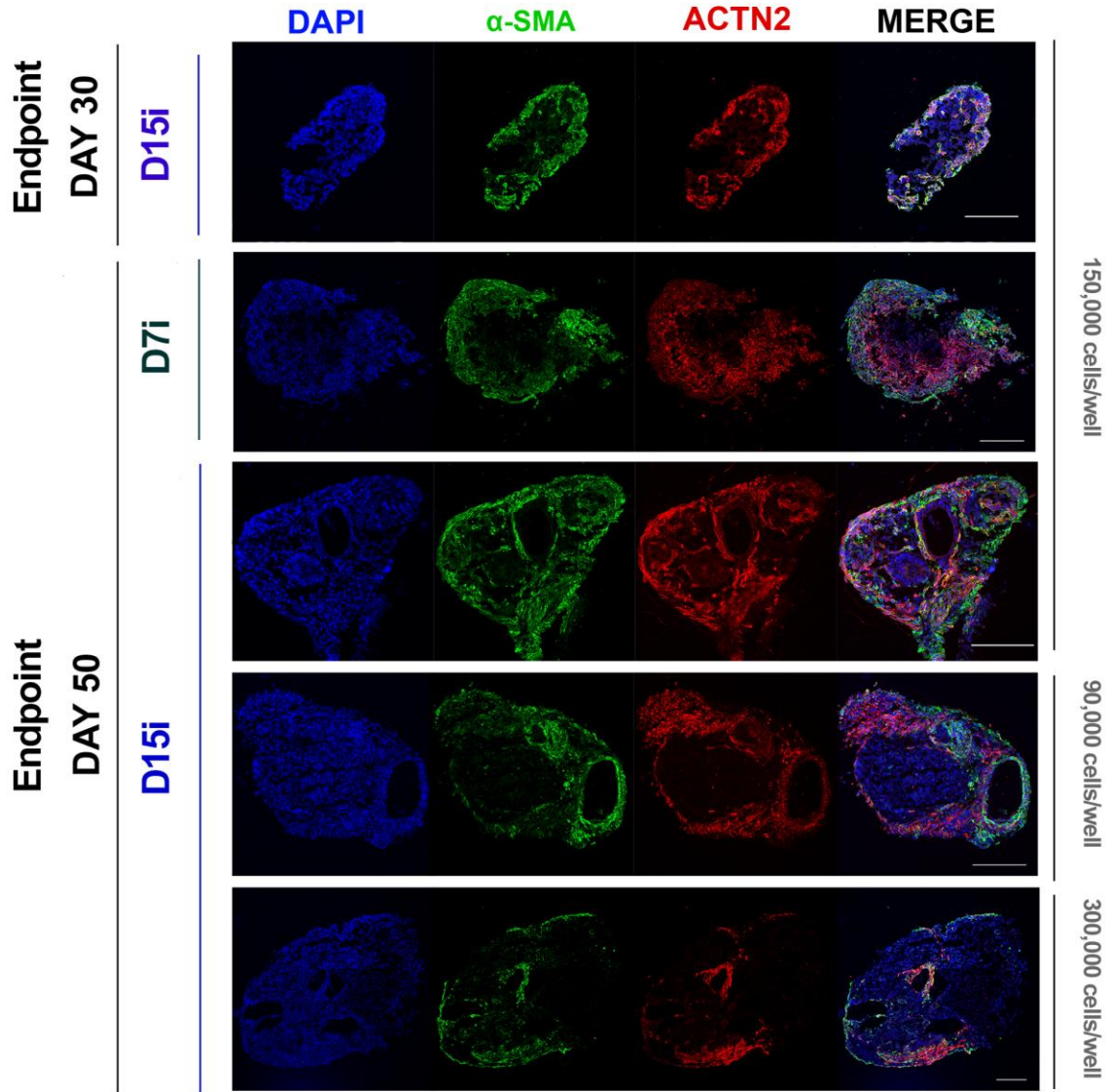


Figure 3. 5 Representative confocal images on day 30 and day 50 endpoints for D7i and D15i microtissue sections.

Immunofluorescence analysis showing the increasing histological complexity of D7i and D15i 3D microtissue sections generated by seeding the indicated cell numbers on day 30 vs day 50 endpoints (middle sections). Stainings for cardiomyocytes (alpha actinin 2, ACTN2, red), smooth muscle/fibroblastic cells (α -SMA, green) are shown. The nuclei were counterstained with DAPI (blue). Scale bars = 200 μ m.

To monitor this spontaneous cellular organization, we repeated the experiment to generate microtissues by using hiPSCs constitutively expressing GFP-tagged cardiac troponin I (TNNI1) reporter. As expected, with time in culture we observed the emergence of GFP-

expressing contractile cardiomyocytes together with non-GFP-tagged non-myocyte cells within the microtissues. From day 21 to day 42, the GFP-tagged contractile cardiomyocytes and non-myocytes gradually and spontaneously rearranged within the microtissues from a random distribution to more discrete regions (Figure 3.6). The diameter of the microtissues reached up to 0.9 ± 0.04 mm on day 21 and 1 ± 0.09 mm on day 42, in the absence of any external ECM supplementation (Figure 3.7, Online Supplementary Video 1 for day 53). The microtissues went on displaying spontaneous contractile activity in long-term culture and until at least day 100 (Online Supplementary Video 2 for day 107).

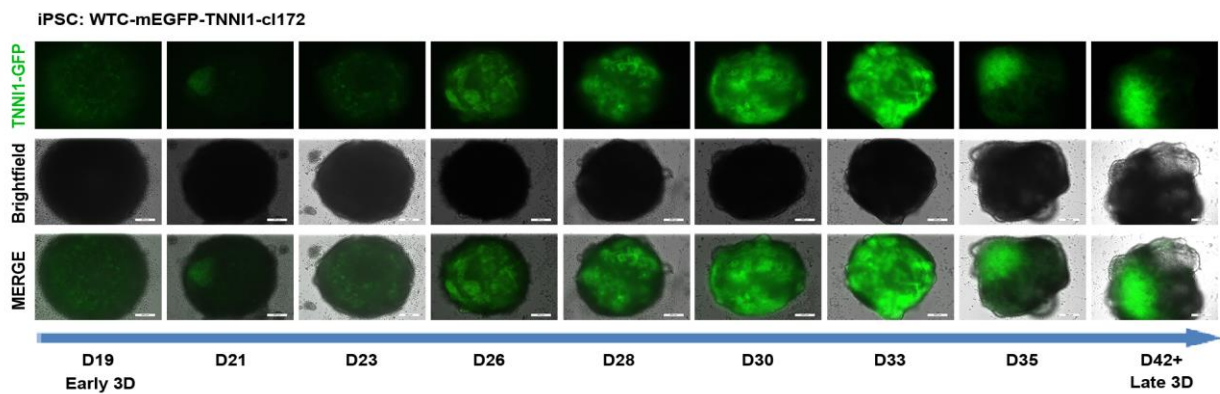


Figure 3. 6 Monitoring the spontaneous self-organization of hiPSC-derived cardiomyocytes within 3D microtissues over culture time

From day 21 to day 42, contractile cardiomyocytes expressing GFP-tagged cardiac troponin I (TNNI, green) and non-myocytes gradually and spontaneously rearranged within the microtissues from a random distribution to more discrete regions. Scale bars = $200\mu\text{m}$.

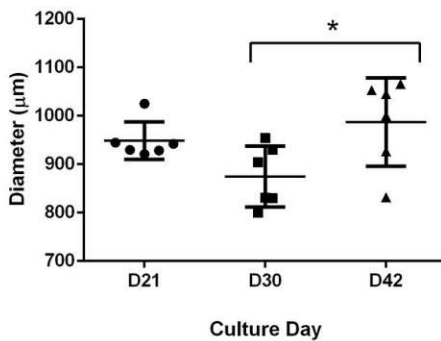


Figure 3. 7 Average diameter of 3D long-term cultured cardiac microtissues.

From day 21 to day 42, the diameter of the microtissues reached up to 0.9 ± 0.04 mm on day 21 and 1 ± 0.09 mm on day 42 in scaffold-free conditions. ($n=6$, Mean \pm SD, Tukey's multiple comparisons test)

This observation suggested that modifying a well-established 2D protocol [17], [18] into our 3D differentiation protocol could give rise to scaffold-free contractile cardiac microtissues that contain not only cardiomyocytes (GFP-tagged), but also other non-myocyte cell populations (non-GFP tagged), which collectively showed a tendency to be spontaneously redistributed in extended culture times.

A common drawback of 3D cultures is the possibility of apoptotic/necrotic core formation due to poor oxygen and nutrient diffusion towards the core of the construct [411]. In order to rule out that this occurs in our extended 3D cultures (day 50), we performed whole mount cell viability assay on the microtissues and - despite some physiological levels of dead cells throughout the structure - we demonstrated no accumulation of non-viable cells was visible at the core of the constructs (Figure 3.8).

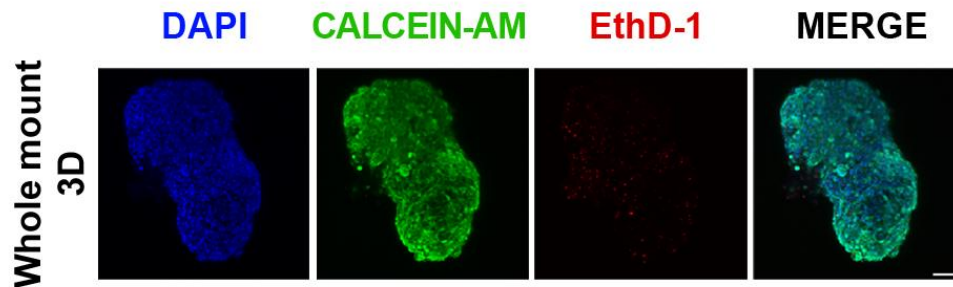


Figure 3. 8 Cell viability of 3D long-term cultured microtissues with Calcein/AM staining on day 50.

Whole mount analysis of cell viability performed on microtissues at day ... Green = live cells, red = dead cells, blue = nuclear DAPI counterstain (Scale bar = 200 μ m).

Moreover, we complemented this analysis by performing Terminal deoxynucleotidyl transferase (TdT) dUTP Nick-End Labeling (TUNEL) assay, which detects the presence of apoptotic cells, on cryosections obtained from the edge and the core of the 3D tissues. Here we noticed no accumulation of apoptotic cells at either position in the 3D microtissues (Figure 3.9). Finally, we confirmed the absence of a necrotic/apoptotic core by ultrastructural analysis of the core of the microtissue by transmission electron microscopy (TEM) (Figure 3.10).

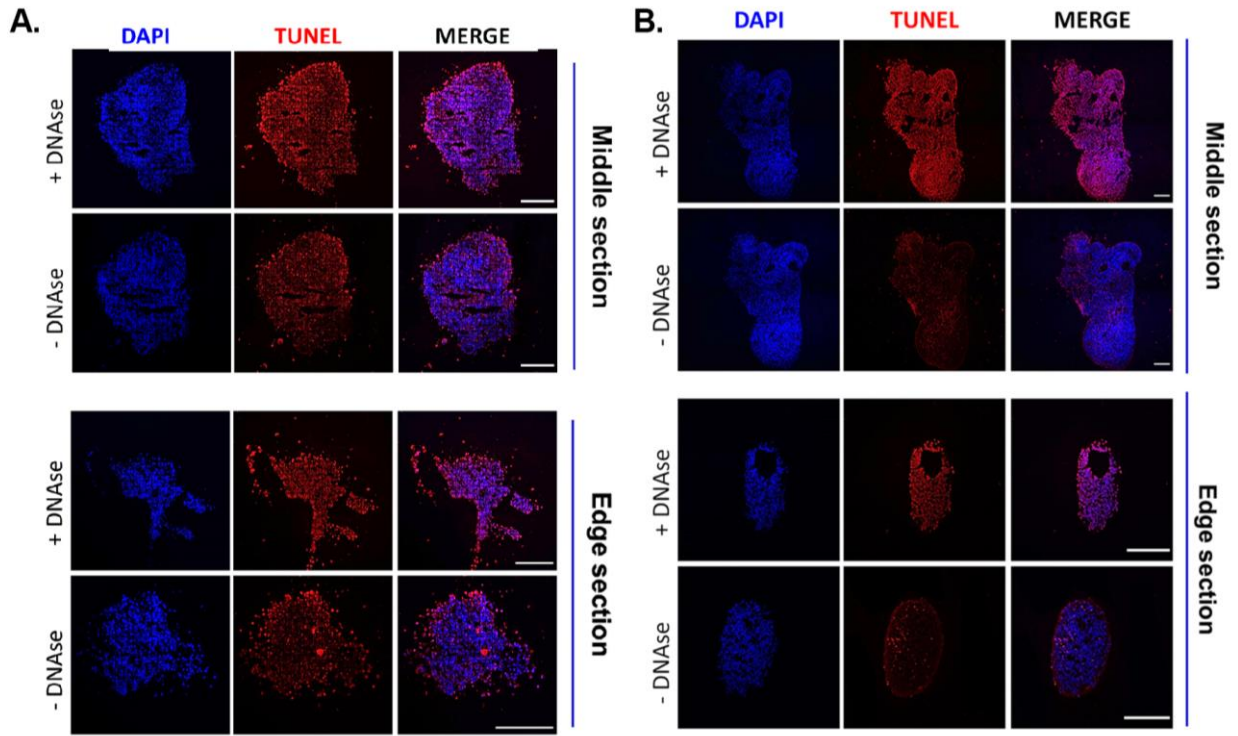


Figure 3. 9 TUNEL staining of human iPSC-derived microtissue (hOCMTs) cryosections.

(A.) TUNEL analysis performed to identify apoptotic cells (red) on 3D long-term cultured microtissue cryosections on day 30 (A) and day 50 (B). Positive controls were treated with DNase I (edge and center). Nuclei were counterstained with DAPI (blue). (Scale bar = 200 μ m).

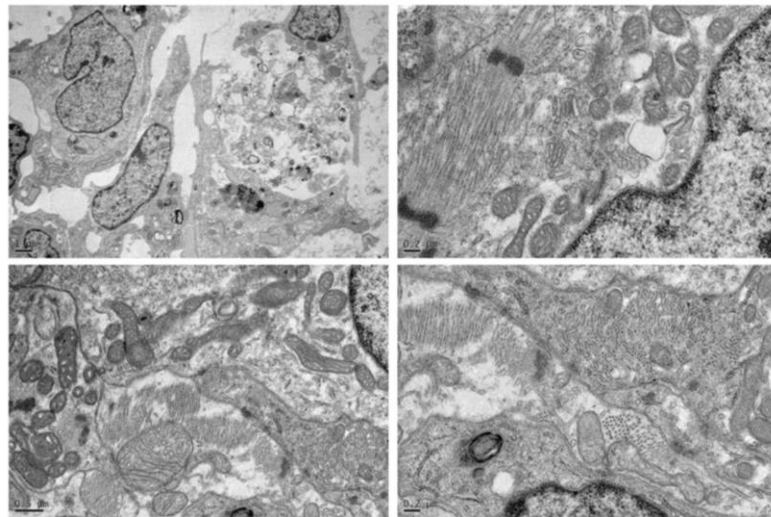


Figure 3. 10 Ultrastructural analysis of the core of the microtissues.

Transmission Electron Microscopy (TEM) images obtained from the core sections of day 50 iPSC-derived microtissue ultrastructural organization, performed to identify viable and necrotic areas. Scale bars: top left = 1 μm , top right = 0.2 μm , bottom left = 0.5 μm , bottom right = 0.2 μm .

Due to the presence of intrinsic and spontaneous signs of proto-self-organization, cellular heterogeneity, and functional beating in our 3D microtissues over extended culture time, we will hereafter refer to these constructs as human organotypic cardiac microtissues (hOCMTs).

3.2 2D-to-3D culture switch prompts the formation of human iPSC-derived organotypic cardiac microtissues composed of multiple heart cell types

As previously stated, one of the key features of *bona fide* organoids is the presence of different cell types typical of the given organ, as well as their ability to self-organize in microstructures similar to the organ being modelled [58]–[60].

To assess the cellular heterogeneity of our 3D hOCMTs, we quantified by flow cytometry the presence of the three most represented cell populations in the human heart [118], [412] – cardiomyocytes, fibroblasts and endothelial cells - at given time-points (day 15, day 30 and day 50, Figure 3.11, 3.12). We used 2D cultures as control throughout the experiment. On day 15 of differentiation (i.e. the first time-point of microtissue aggregation), the flow cytometry analysis of cardiac troponin T2 (TNNT2)-positive population indicated the protocol yielded the differentiation into cardiomyocytes in 2D ($54.14 \pm 9.08\%$), while also producing a distinct population of CD90-positive non-myocytes ($28.87 \pm 13.04\%$). The same analysis proved that 3D extended culture was associated with a significant increase in the percentage of TNNT2-positive cardiomyocytes as compared to 2D culture (3D day 50: $83.27 \pm 9.45\%$ vs 2D day 50: $27.23 \pm 15.86\%$, $p < 0.0001$) (Figure 3.12). On the contrary, 2D culture was shown to favour the overgrowth of CD90-positive cells (2D day 50: $52.97 \pm 13.44\%$ vs 3D day 50: $23.38 \pm 7.35\%$, $p < 0.001$) (Figure 3.12). While a very limited number of CD31-positive cells was observed in any of the 2D culture timepoints, a significant increase in cells expressing the endothelial marker CD31 occurred during 3D culture (3D day 50: $12.78 \pm 2.71\%$ vs 2D day 50: $4.07 \pm 2.76\%$ in, $p < 0.001$) (Figure 3.12).

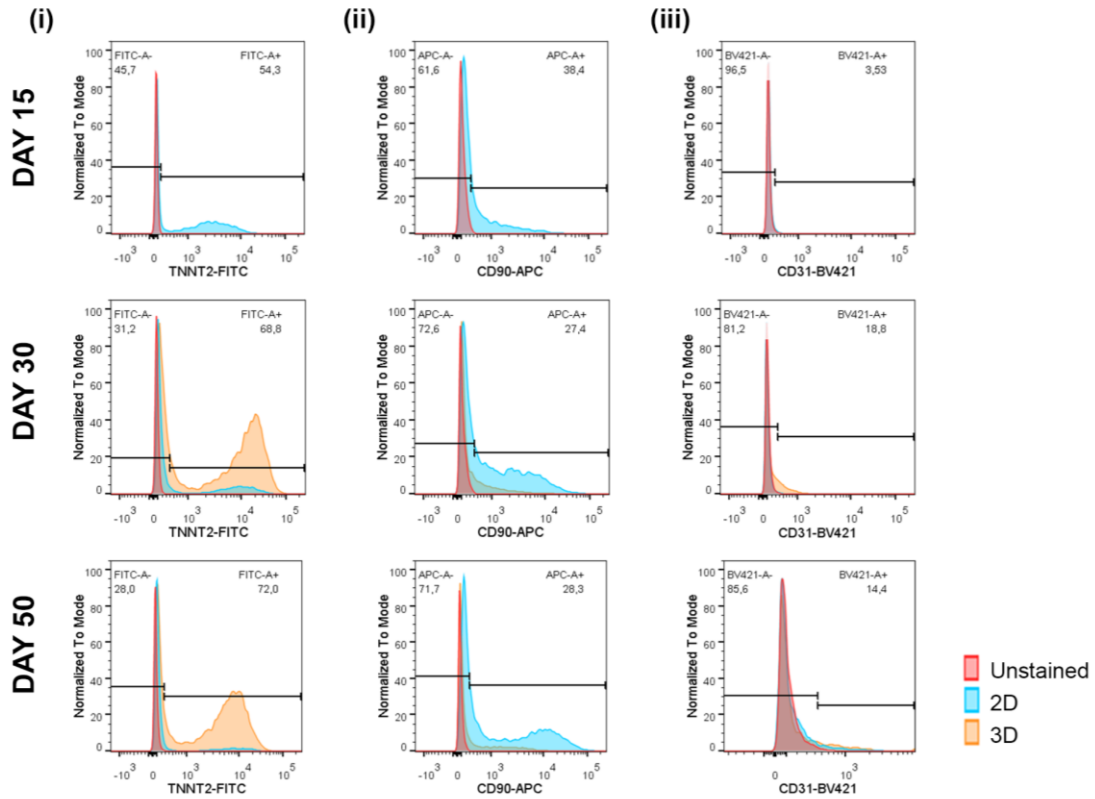


Figure 3. 11 Long-term 3D cultures of hOCMTs results in the enrichment of the contractile cell population.

Representative flow cytometry histograms depicting the expression of markers typical of cardiac cell types in 2D or 3D cultures on day 15, day 30 and day 50. (i) Cardiomyocytes were stained with TNNT2-FITC, (ii) Fibroblasts with CD90-APC, (iii) Endothelial cells with CD31-BV421. The images are representative of 3 independent experiments.

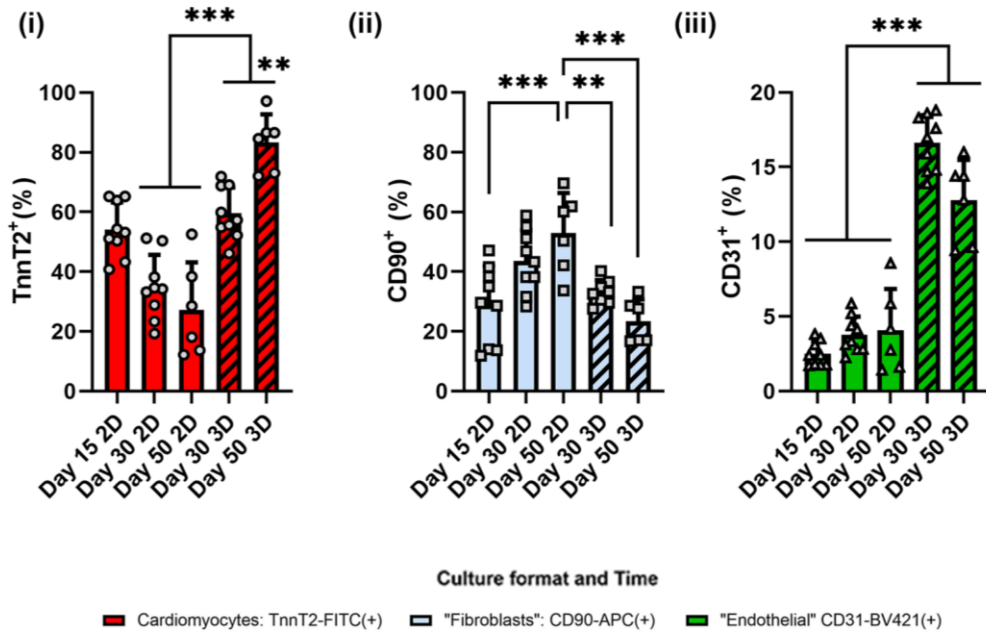


Figure 3.12 Long-term 3D cultures favour the enrichment of troponin T-positive cells.

Barplot representation of the expression of the given markers in 2D and 3D cultures at the indicated culture times. (i) Cardiomyocytes (TNNT2-FITC⁺ %), (ii) “Fibroblasts” (CD90-APC⁺ %), (iii) Endothelial cells (CD31-BV421⁺ %). The percentage indicates the positive cells versus total cells (Mean ± SD obtained in three independent analyses, n=9 per condition, Tukey's multiple comparisons test).

These results indicate that 2D-to-3D culture switch promotes the generation of heterogeneous microtissues and favours the survival of the cardiomyocyte population in extended culture.

To explore the cellular heterogeneity and the spatial distribution of different cell subsets in our 3D hOCMTs in more detail, cryosections were performed at day 50 of culture and stained to detect the presence of cells expressing markers specific of the different populations in the human heart [118] (Figure 3.13, 3.14).

Confocal imaging showed that cells located at the periphery of the construct stained positive for markers of epicardial cells Wilms tumor protein 1 (WT1) and TBX18, in addition to epicardial/fibroblast markers TE-7 and SM22a (Tagln), which suggested the presence of these cells primarily forming an outermost layer (Figure 3.13A-D). The center of the construct - instead - stained positive for cardiac troponin T2 (TNNT2) and sarcomeric α -actinin (ACTN2), thus describing the formation of a discrete cluster of cardiomyocytes. This result further confirmed the tendency of contractile cells to re-locate to the core of the construct within time in 3D culture, a phenomenon that we noticed by using GFP-tagged cardiac troponin I (TNNI1) reporter hiPSC line (see Figure 3.6).

Discrete areas could also be stained with endocardial cell markers NFAT2 and endothelial cell marker CD31 (Figure 3.14A, B).

Next, we stained for ventricular (MYL2) or atrial (MYL7) Myosin Light Chain isoforms, as specific markers of atrial and ventricular cardiomyocytes or contractile cells at different stages of maturation [158]. Here we could identify two distinct pools of cardiomyocytes that stained either positive for MYL7 only, or co-stained positive MYL2 and MYL7 (Figure 3.14C). This result hinted at the possibility that either differentially specified cardiomyocytes or contractile cells at different stages of maturation co-existed within the contractile core of the 3D constructs. In recent reports, the formation of 3D cardiac organoids was associated with the developmental co-emergence of elements of endoderm and mesoderm tissues resembling the development of the heart and gut in the embryo [70], [72]. We thus stained for markers of embryonic (SOX2) or adult gut tissue (ASCL2) together with markers of undifferentiated cells (MESP1, Brachyury) and detected no such cells in day 50 3D constructs (Figure 3.15A, B). Furthermore, for cardiac morphogenesis (GATA4), Sarcoplasmic/Endoplasmic Reticulum Calcium ATPase 2 (SERCA2), smooth muscle/fibroblastic cells (α -SMA), and gap junction proteins (Connexin 43, or Cx43) were also observed within the microstructures (Figure 3.15C).

Altogether, these results confirmed that iPSC-derived 3D hOCMTs favours the survival of cardiomyocytes and contain multiple cell types of the human heart organized in distinct domains.

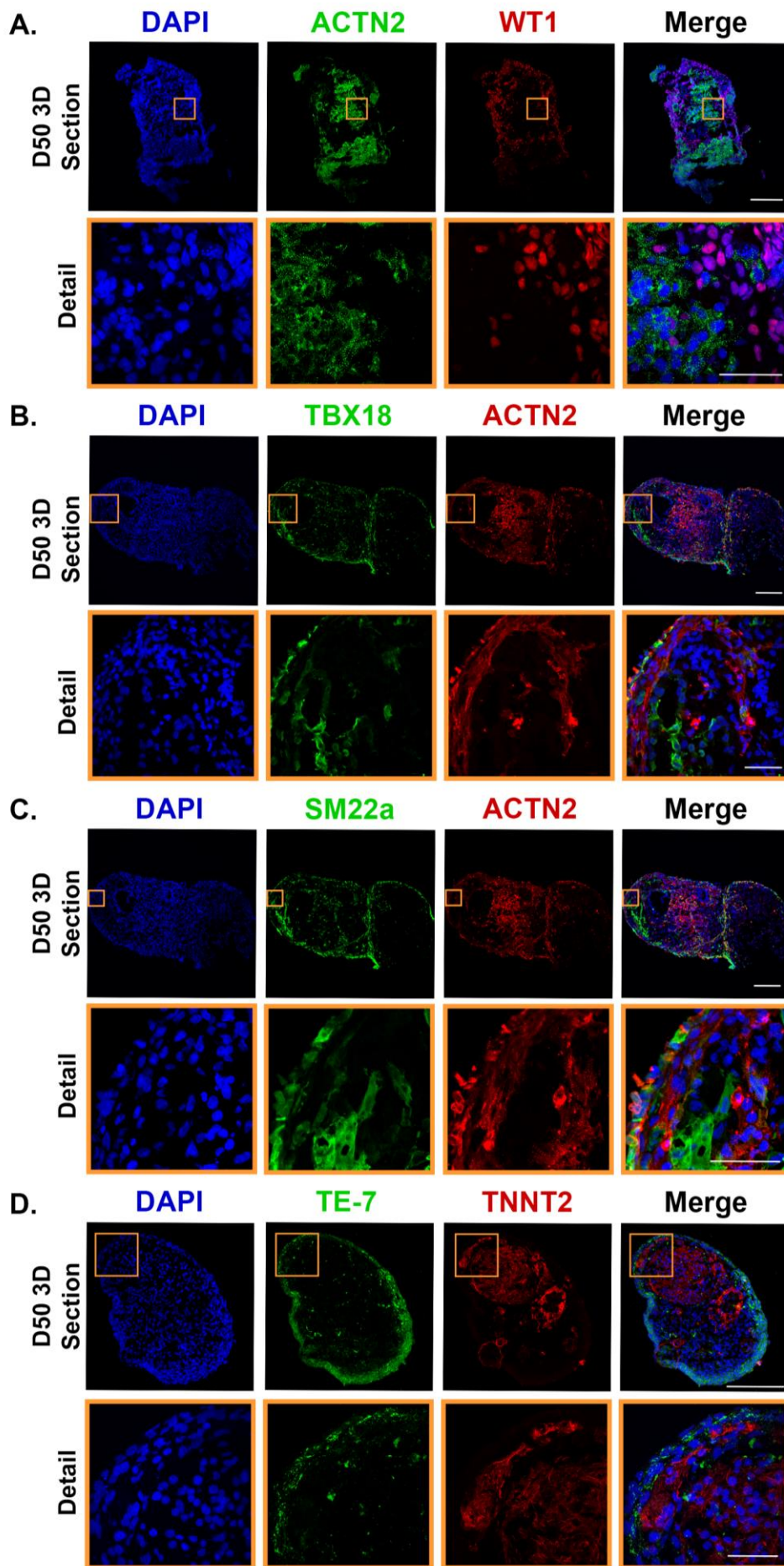


Figure 3. 13 Long-term 3D culture of hOCMTs recapitulate es advanced cardiac morphology and cellular heterogeneity in vitro showing markers for cardiomyocyte, epicardial and fibroblast cell types.

Representative immunofluorescence pictures showing the concomitant expression of the indicated markers of different cardiac cell types in 3D long-term cultured hOCMT sections on day 50. Cardiomyocytes: ACTN2 in green or red, TNNT2 in red, epicardial cells: WT1 TBX18 SM22a, epicardial/fibroblastic and smooth muscle cells: SM22a, fibroblasts TE-7. Nuclei were counterstained with DAPI (blue). Full 3D hOCMTs scale bar = 200µm, Detail scale bar = 50 µm.

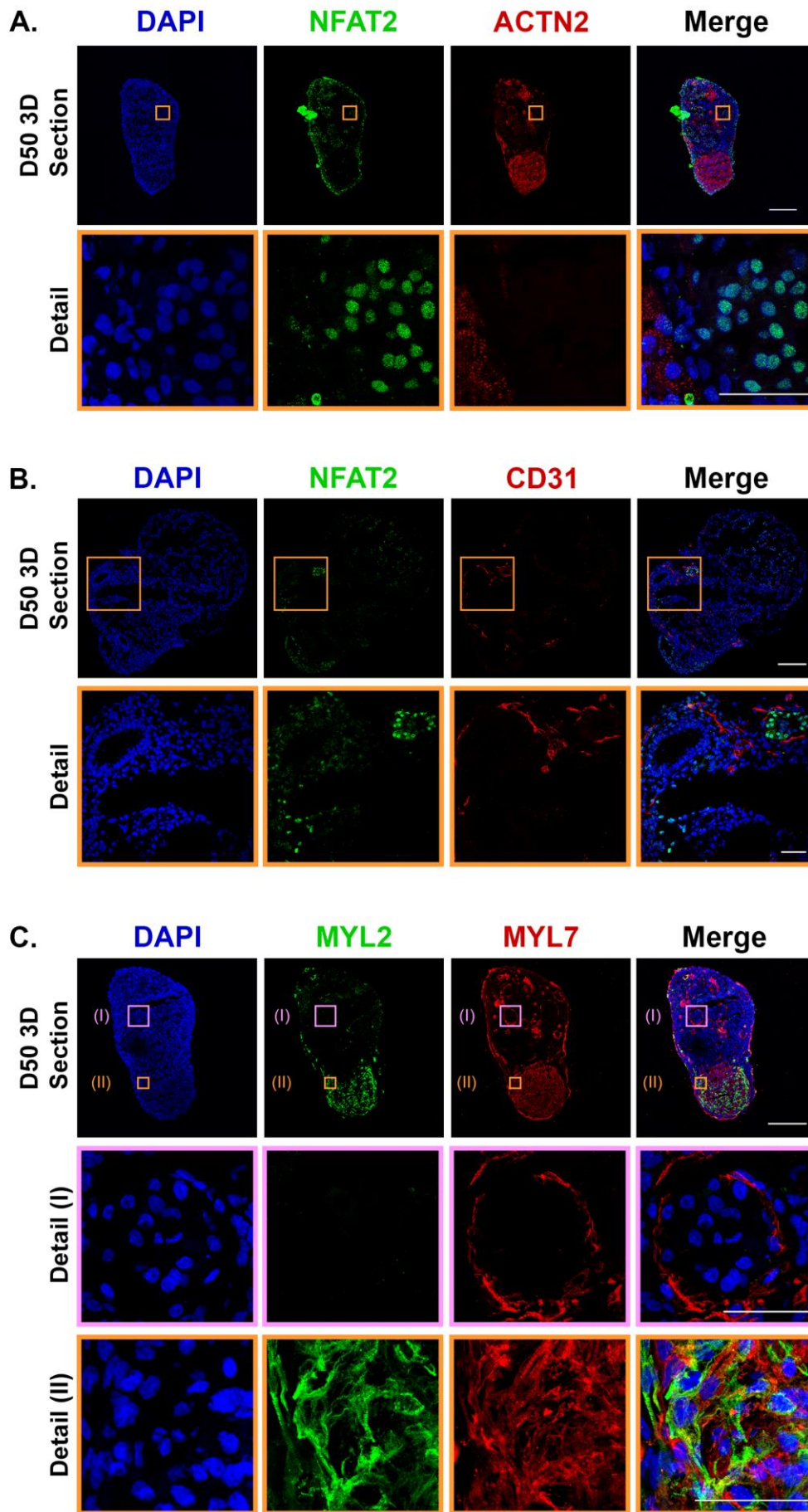


Figure 3. 14 Long-term 3D culture of hOCMTs recapitulates advanced cardiac morphology and cellular heterogeneity in vitro showing markers for endocardial, endothelial, and cardiomyocyte subtypes.

Representative immunofluorescence pictures showing the concomitant expression of the indicated markers of different cardiac cell types in 3D long-term cultured hOCMT sections on day 50. Cardiomyocytes: ACTN2, atrial cardiomyocytes: MYL7 in green), ventricular cardiomyocytes: MYL2, endocardial cells: NFAT2, endothelial cells: CD31. Nuclei were counterstained with DAPI (blue). Full 3D hOCMTs scale bar = 200µm, Close-up scale bar = 50 µm.

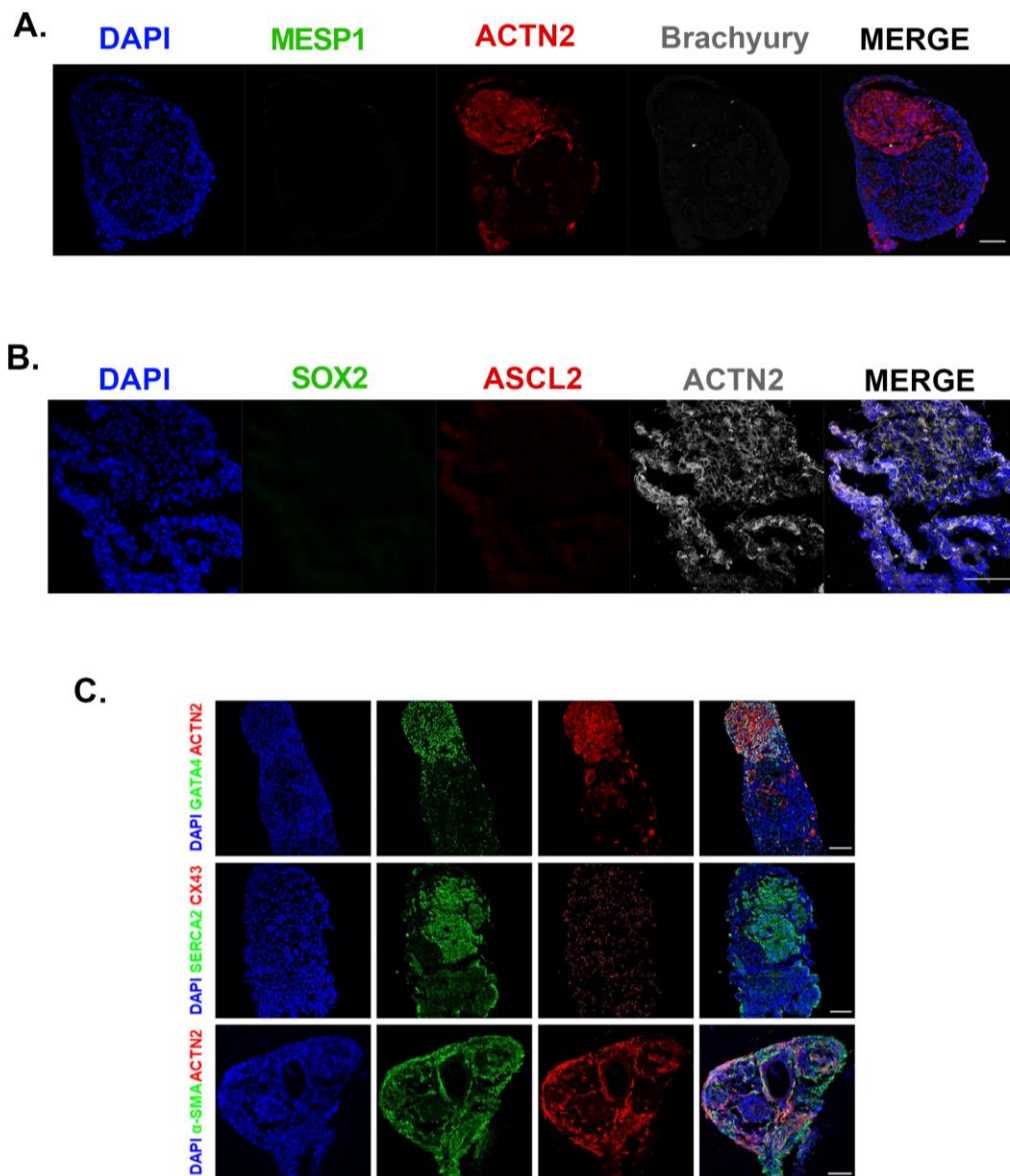


Figure 3. 15 Long-term hOCMTs show no evidence of gut tissue emergence.

A. Representative confocal image showing the staining of day 50 hOCMT sections for early mesoderm cell markers including MESP1 (green) and Brachyury (grey). Differentiated cardiomyocytes are stained alpha actinin 2 (ACTN2, grey). Nuclei were counterstained with DAPI (blue). Scale bar = 100µm.

B. Representative confocal image showing the staining of day 50 hOCMT sections for undifferentiated embryonic and early gut marker SOX2 (green), together with the marker of adult gut ASCL2 (red) Differentiated cardiomyocytes are stained alpha actinin 2 (ACTN2, grey). Nuclei were counterstained with DAPI (blue). Scale bar = 100µm.

C. Representative confocal image showing the staining of day 50 hOCMT sections with markers of cardiac morphogenesis (GATA4, green), calcium ATPase (SERCA2, green), gap junction protein 1 (CX43, red), and smooth muscle/fibroblastic cells (α -SMA, green) in combination with cardiomyocyte marker ACTN2 (red). Nuclei were counterstained with DAPI (blue). Scale bar = 100µm.

3.3 Human iPSC-derived organotypic cardiac microtissues display ultrastructural organization and maturation in long-term culture

A key feature of the adult heart is the existence of a highly recognizable three-dimensional ultrastructure due to the periodical repetition of the functional units of the contractile apparatus, the sarcomere. The length and the alignment of the sarcomeres, together with the interspacing of myosin-actin myofilaments and the abundance and shape of mitochondria, are considered representative of the maturity of the contractile tissue.

We analysed the ultrastructure of the contractile core of hOCMTs and assessed how it developed with time in culture by transmission electron microscopy (TEM). TEM analysis clarified that the prototypical contractile apparatus was hardly recognizable in hOCMTs cultured for 21 days, while highly organized sarcomeres with distinct z-disks and evenly distributed myofilaments could be detected in those cultured for 50 days (Figure 3.16A, B).

The same analysis also demonstrated that longer culture times (day 85) led to the assembly of t-tubules close to the regularly spaced myofibrils, together with the appearance of packed and elongated mitochondria (Figure 3.16C, F and 3.17). The presence of t-tubules, extensions of the sarcolemma interspersed around the contractile apparatus to maximize the efficiency of calcium exchange, is only found in mature cardiac muscle and was not reported in standard 2D monolayer cultures [196]. We found the sarcomere length under these experimental conditions to be approximately 1.5 µm (Figure 3.16C, D). This value did not change at later time-points (day 85) and is consistent with the values described for young mammalian cardiomyocytes [74]. Meanwhile, Z-band was found to increase slightly in width, but not significantly, with time in culture (700 ± 250 nm on day 85 vs. 450 ± 100

nm on day 50, $p < 0.0001$) as to get closer to the values typical of adult heart [140] (Figure 3.16E,G).

Furthermore, TEM also demonstrated a higher amount of mitochondria and glycogen accumulation at later time-points (day 50 and 85) compared to day 21 (Figure 3.17), which suggests a metabolic shift to advanced maturation of cardiomyocytes [140]. All these features indicate hOCMTs undergo structural and metabolic maturation [74] when cultured for long time in 3D.

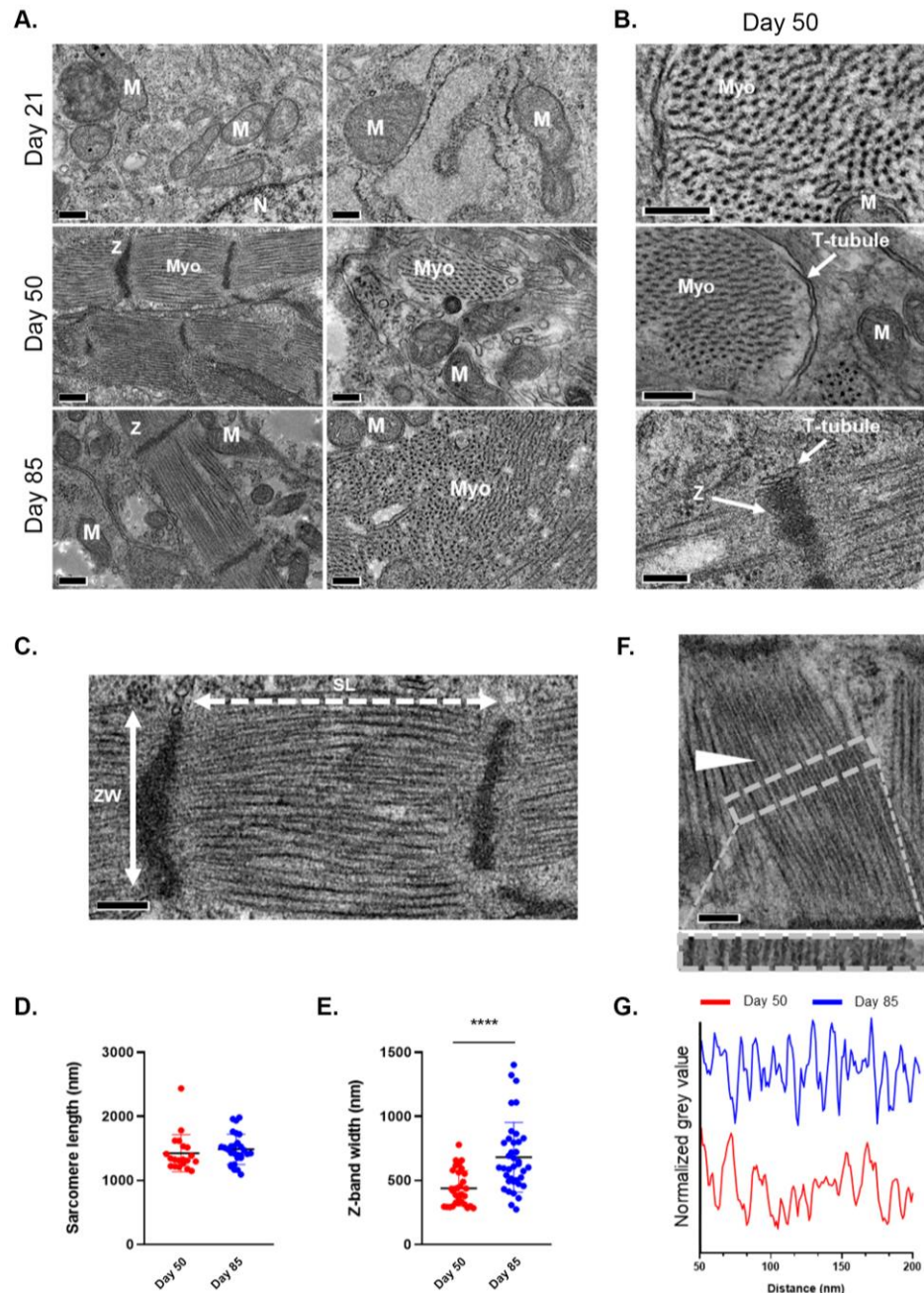


Figure 3. 16 Ultrastructural analysis of 3D hOCMTs indicates enhanced maturation in 3D environment over time.

A. TEM images of 3D hOCMTs showing increasing ultrastructural organization over time, from day 21 to day 85. Cardiomyocyte myofibers (Myo), Mitochondria (M) Z-band (Z), T-tubules are indicated. Scale bars = 200 nm. **B.** Close-up images on day 50. Scale bars = 200 nm **C.** Representative micrograph showing sarcomere length (SL; white dotted two-headed arrow) and z-band width (ZW; cross sectional length; white solid two-headed arrow) with the corresponding sarcomere length (**D**; day 50, 1400 ± 300 ; day 85, 1500 ± 200 ; $N > 20$, Mean \pm SD) and z-band width (**E**; day 50, 450 ± 100 nm; day 85 700 ± 250 nm; $N > 30$, Mean \pm SD). Scale bar = 200 nm. **F.** Micrograph showing myofiber organization (white arrow) with their relative organization as defined by the plot profile intensity on day 50 vs day 85 (**G**) of the area indicated by the grey dashed box of “figure 3.16F”. Scale bar = 200 nm.

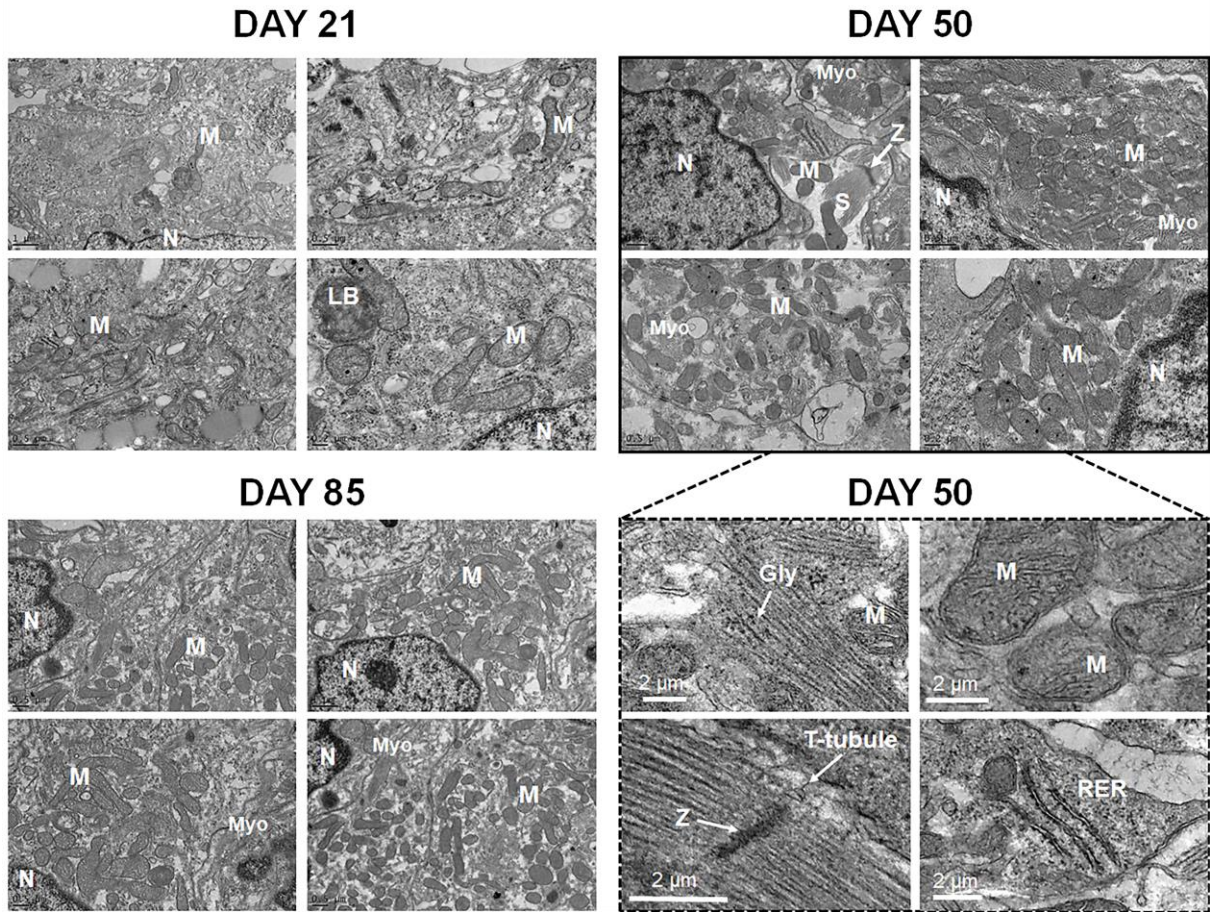


Figure 3. 17 Ultrastructural analysis of long-term hOCMTs indicates enhanced cardiomyocyte and metabolic maturation in 3D environment over time.

Transmission Electron Microscopy (TEM) images of hOCMTs increasing ultrastructural organization and structural and metabolic maturity over time, from day 21 to day 85. Cardiomyocyte myofibers (Myo), Sarcomeres (S), Mitochondria (M) Z-band (Z), T-tubules, Nuclei (N), Rough endoplasmic reticulum (RER), Glycogen granules (Gly), Lamellar bodies (LB) are

indicated. Scale bars are 1 μm and 0.5 μm for day 21, 0.5 μm for day 85, 0.5 μm for day 50 and 2 μm for magnified images of day 50.

3.4 3D long-term culture induces human iPSC-derived organotypic cardiac microtissue maturation

Contractile cell maturation can be monitored by tracking the evolution of the expression of specific genes encoding for contractile proteins. Hence, we set at investigating the transcriptional landscape of hOCMTs in order to assess the impact of time and dimensionality on the maturation of the contractile cells.

To this end, we performed bulk RNA-sequencing and differential expression analysis (DE analysis) on day 30 and 50 of the 3D culture and compared them to 2D monolayer cultures harvested at the same time-points (GEO: GSE209997), adult heart tissues and Engineered Heart Tissues (EHTs) [408] obtained from previously published datasets (NCBI Bioproject accession numbers: PRJNA667310 [405] and PRJNA628736 [406] for adult heart, and PRJNA831794 [407] for EHTs [alias GEO: GSE201437]).

A total of 2975 genes were found to be significantly and differentially regulated in 3D microtissues compared to monolayer cultures at day 30. This number increased to 6437 at day 50 (Figure 3.18 and Online Supplementary Datasets 1, 2), possibly indicating a bigger divergence between 2D and 3D cultures over time.

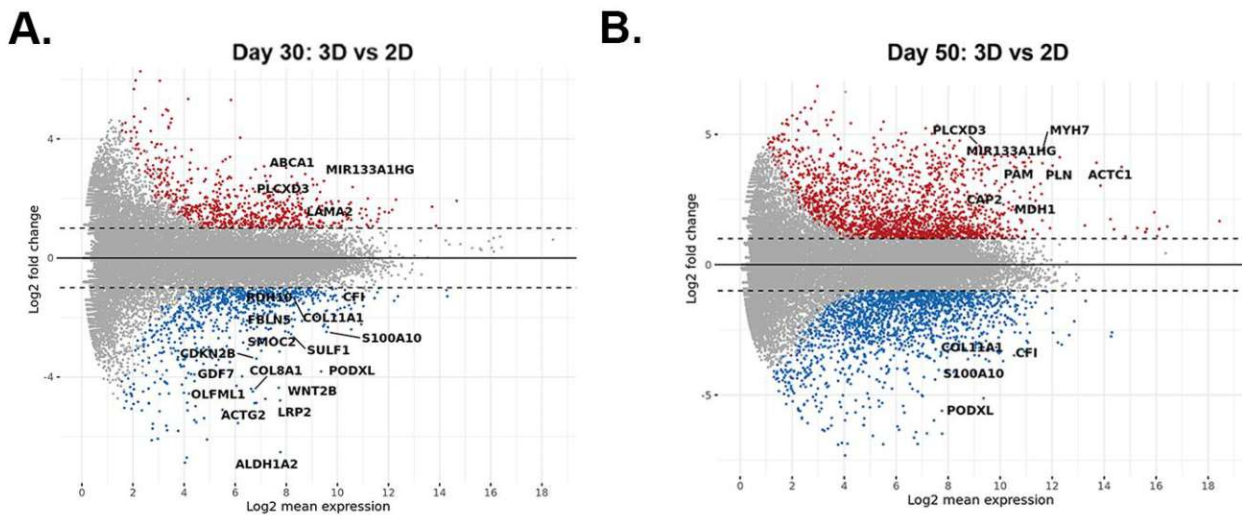


Figure 3. 18 DE analysis for 3D long-term cultures vs standard 2D monolayer cultures on day 30 and 50 timepoints

- A.** MA plot of the differentially regulated genes between 2D monolayer and 3D on day 30.
B. MA plot of the differentially regulated genes between 2D monolayer and 3D on day 50.
(log₂ mean, p_{adj} < 0.05).

The functional gene ontology (GO) annotations at both time-points revealed that the genes differentially regulated 3D hOCMTs had a fingerprint for cardiogenesis, which included the categories of myofibril assembly and sarcomeric organization, muscle contraction and cardiac tissue morphogenesis (Figure 3.19). As an example, the top 20 deregulated genes at day 50 between 3D and 2D monolayer cultures included genes which are well known to be involved in cardiac muscle maturation and function, namely cardiac muscle α -actinin (*ACTC1*), sarcomeric α -actinin (*ACTN2*), phospholamban (*PLN*) and myosin heavy chain 7 (*MYH7*) (Figure 3.20). On the contrary, 2D cultures showed an increased expression in ECM-related genes, most likely as a result of the predominance of cardiac fibroblast population over time in monolayer culture, for both day 30 and day 50 timepoints (Figures 3.19, 3.20, 3.21).

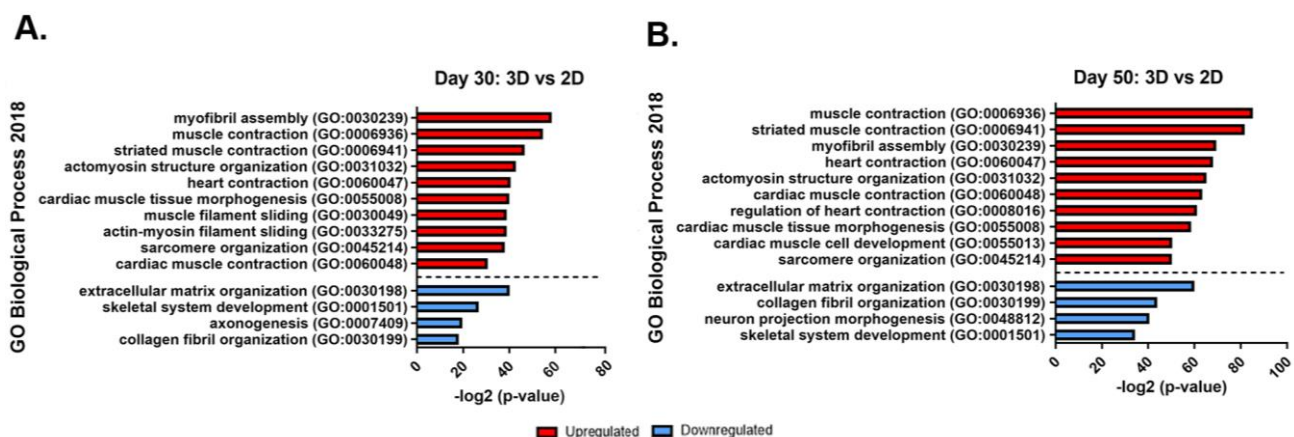


Figure 3. 19 GO biological process categories for the top 20 differentially regulated genes between 3D hOCMTs vs standard 2D monolayer cultures.

Barplot representation of significantly upregulated (red) or downregulated (blue) GO Biological process categories obtained when comparing 3D hOCMTs and 2D monolayers at day 30 (A) and day 50 (B). The values are expressed as -log₂ of p-value. (p_{adj} < 0.05)

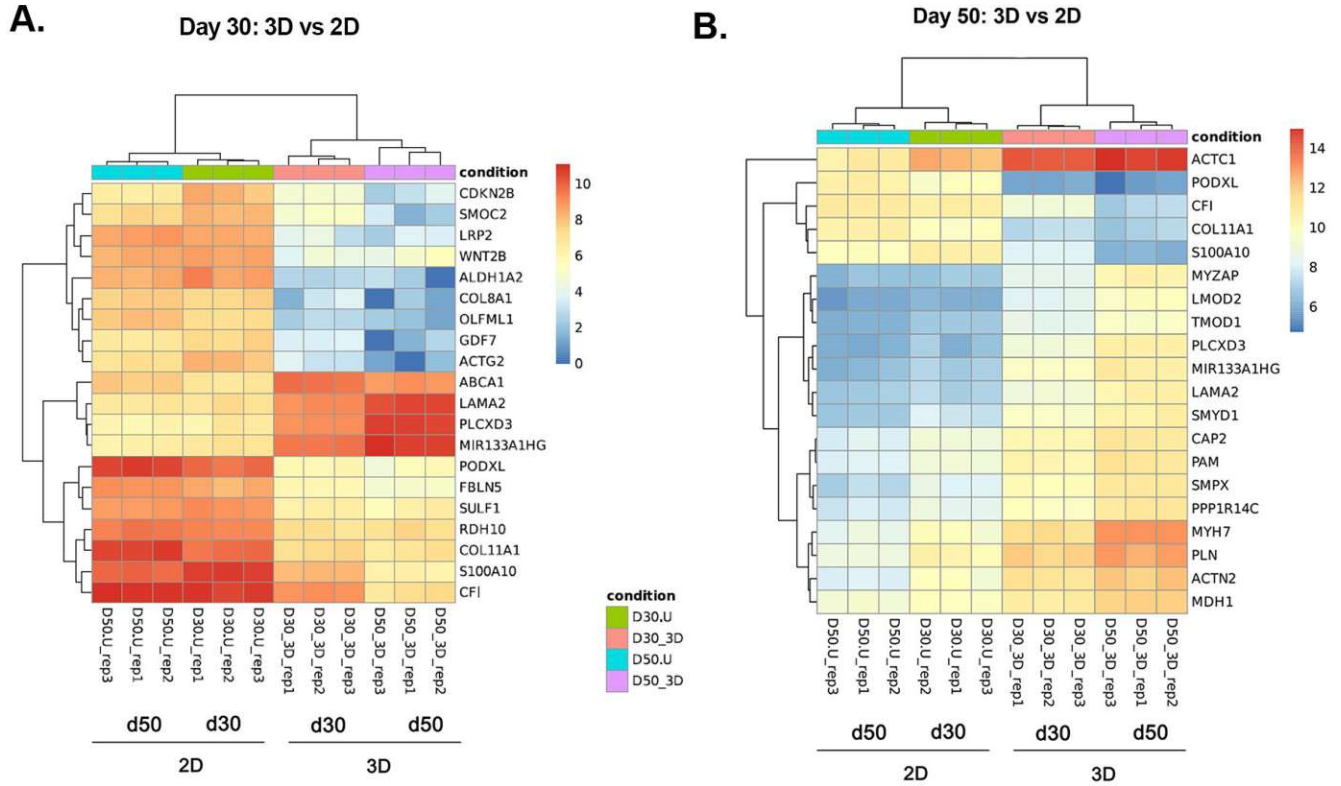


Figure 3. 2D 3D long term culture determines an enrichment in the expression of cardiomyocyte-specific genes.

Heatmap representation of top 20 differentially regulated genes between 2D monolayer and 3D hOCMTs on day 30 (A) or day 50 (B) (\log_2 mean, $p_{\text{adj}} < 0.05$). Warm colours represent upregulated, and cold colours represent downregulated genes.

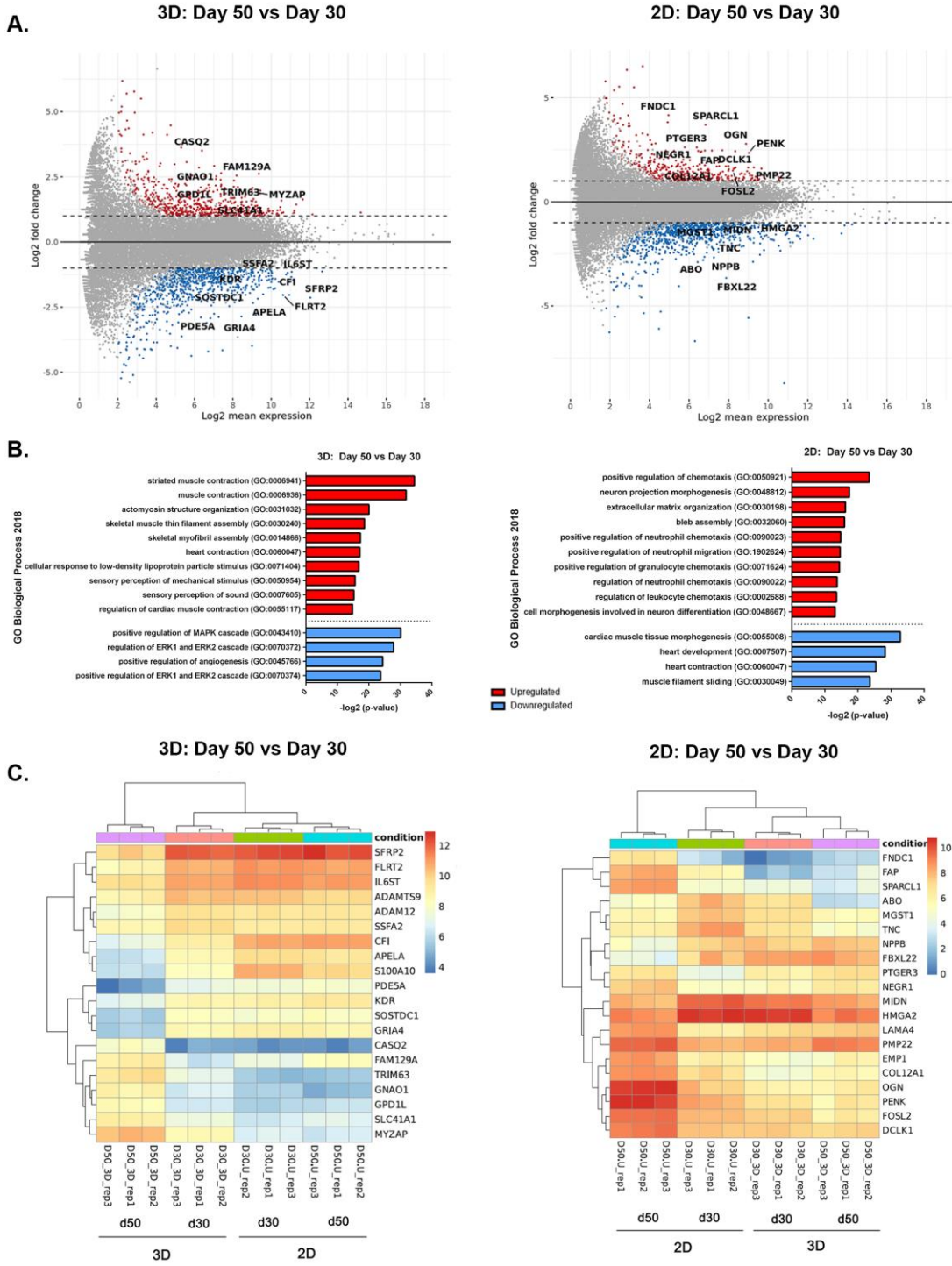


Figure 3. 21 3D culture induces improved cardiac specification and cardiomyocyte maturation.

A. MA plot of the differentially regulated genes between day 30 and day 50 for 3D hOCMTs (left) and 2D monolayer culture (right) (\log_2 mean, $p_{adj} < 0.05$).

B. Graph representing the $-\log_2$ value adjusted p-value of significantly upregulated (red) or downregulated (blue) GO Biological process categories when comparing between day 30 and day 50 of culture for 3D hOCMTs (left) and 2D monolayer culture (right) ($p_{adj} < 0.05$)

C. Heatmap representing the \log_2 fold change for the top 20 differentially regulated genes between day 30 and day 50 of culture for 3D hOCMTs (left) and 2D monolayer culture (right) ($p_{adj} < 0.05$). Warm colours represented upregulated, and cold colours represent downregulated genes.

Clustering analysis of the genes upregulated in 3D hOCMTs compared to 2D monolayer cultures at day 50 showed a highly interconnected network of genes involved in heart contraction and sarcomeric organization, which included important structural proteins of the contractile apparatus such as *ACTC1*, *ACTN2*, troponins (*TNNT2*, *TNNC1*, *TNNI1*, *TNNI3*), myosin heavy (*MYH6*, *MYH7*) and light (*MYL2*, *MYL3*) chains, dystrophin (*DMD*), titin (*TTN*), obscurin (*OBSCN*) and myozenin 2 (*MYOZ2*), among many others (Figure 3.22).

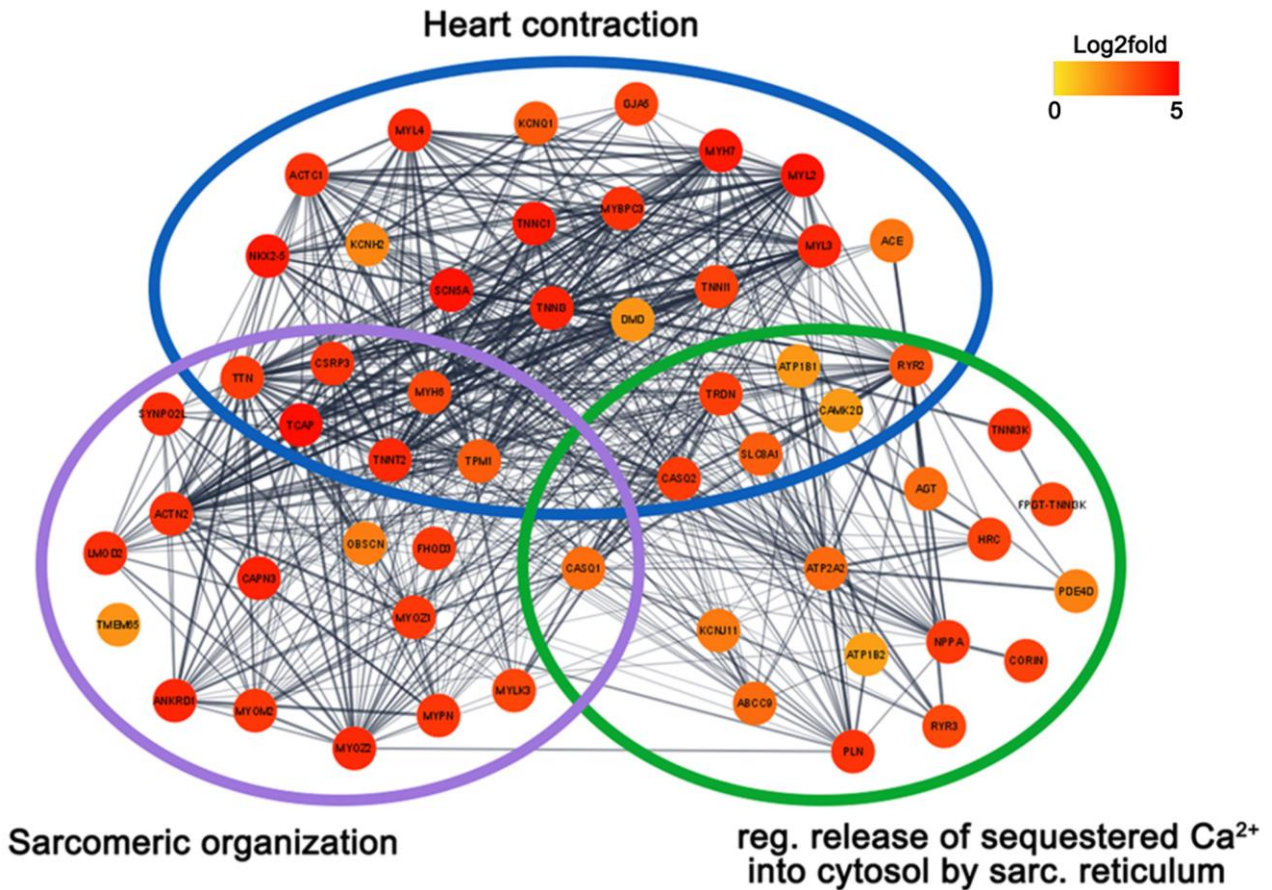
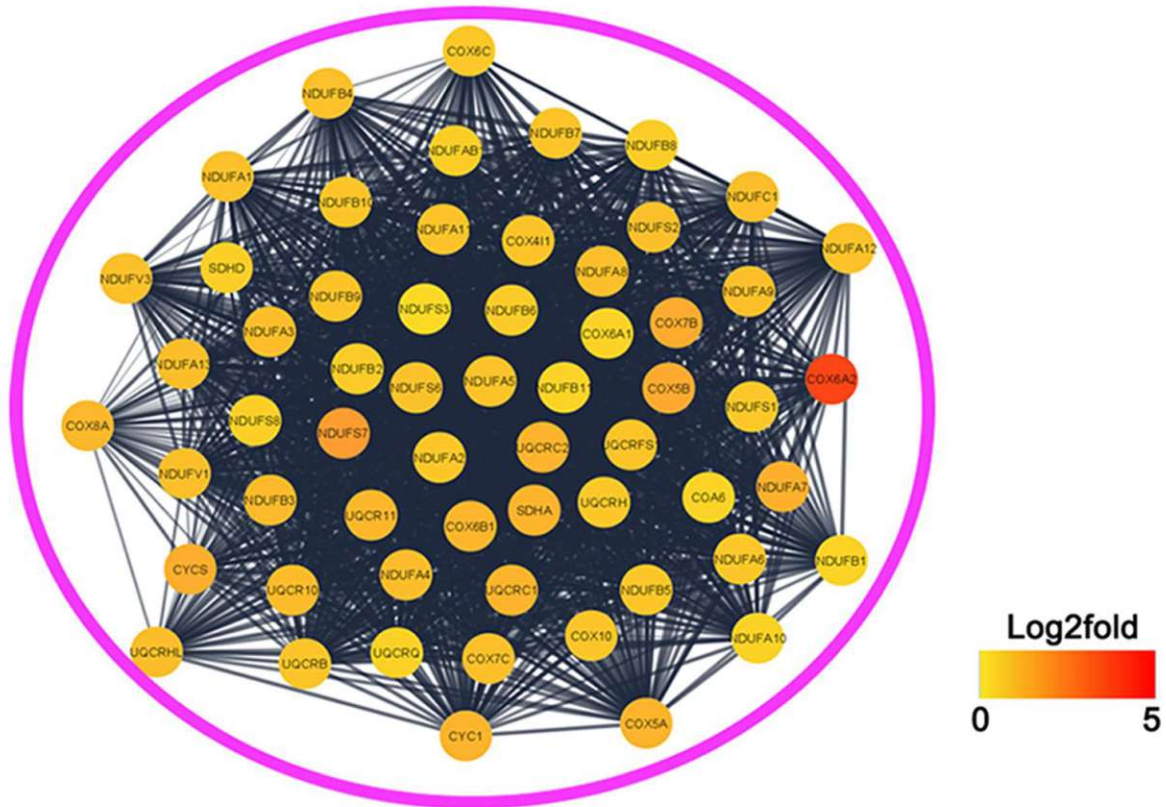


Figure 3. 22 Cluster analysis of the upregulated genes reveals an interconnected network of genes involved in heart contraction and sarcomeric organization.

STRING network representation of the upregulated genes at day 50 hOCMTs as compared to monolayer cultures for the indicated GO biological processes categories by Cytoscape. (Kappa score = 0.3). Log₂fold change for the nodes (genes) is represented using a color-coded scale.

In good agreement with the presence of t-tubules in 3D hOCMTs and their drift towards a more mature intracellular Ca²⁺-dependent contraction, we detected the enhanced expression of the SERCA Ca-ATPase 2 (*ATP2A2*) and its inhibitor phospholamban (*PLN*), triadin (*TRDN*), ryanodine receptors (*RYR2* and the Purkinje's cell specific *RYR3*), calsequestrins (*CASQ1*, *CASQ2*), as well as genes related to cardio-renal homeostasis angiotensinogen (*AGT*), atrial natriuretic peptide (*NPPA*) and corin (*CORIN*). Interestingly, in accordance with the marked increase in the number of mitochondria observed in the TEM images (see Figures 3.17A, 3.18), day 50 3D hOCMTs showed an upregulation in the network of genes associated with mitochondrial ATP synthesis coupled electron transport, including several NADH:ubiquinone oxidoreductase and Cytochrome c oxidase subunits.(Figure 3.23).



Mitochondrial ATP synthesis coupled electron transport

Figure 3. 23 Cluster analysis of the upregulated genes hints at a network of genes involved in cardiomyocyte metabolism.

STRING network representation of the upregulated genes at day 50 hOCMTs as compared to monolayer cultures for the indicated GO biological processes categories by Cytoscape. (Kappa score = 0.3). Log₂fold change for the nodes (genes) is represented using a color-coded scale.

Since long-term 3D cultures seemed to be able to promote the maturation of hOCMTs, we set at comparing the transcriptomic landscape of our *in vitro* constructs with available datasets obtained from adult atrial and ventricular heart tissues [405], [406] (Figure 3.24).

Sample clustering showed that day 50 3D hOCMTs were closer to adult heart at transcriptional level, with the most similar levels being associated with the expression of several sarcomere-associated genes, including *TTN*, *ACTN2*, troponins (*TNNT2*, *TNNI3K*, *TNNC1*, *TNNI3*) and Myosin heavy chains (*MYH6*, *MYH7*, *MYH7B*), as well as important components of the calcium handling apparatus (*RYR2*, *ATP2A2*, *PLN*). Consistent with our immunostaining results, day 50 3D microtissues displayed both atrial (*MYL4*, *MYL7*,

MYBHL) and ventricular (*MYL2*, *MYL3*, *FHL2*) chamber markers (Figure 3.24). In accordance with the increased number of mitochondria (see Figures 3.16A, 3.17), and the upregulation of mitochondrial ATP-synthesis related transcript (Figure 3.23), the comparison of day 50 hOCMTs also showed similar clusters on metabolic genes to adult heart, such as oxidative phosphorylation (*PPARGC1A*, *MT-ATP6*), fatty acid metabolism (*FABP3*, *GPAT3*, *PAM*), lipid metabolism (*FITM1*, *PRKAA2*, *INPP4B*), and glycogen metabolism (*PPP1R3A*).

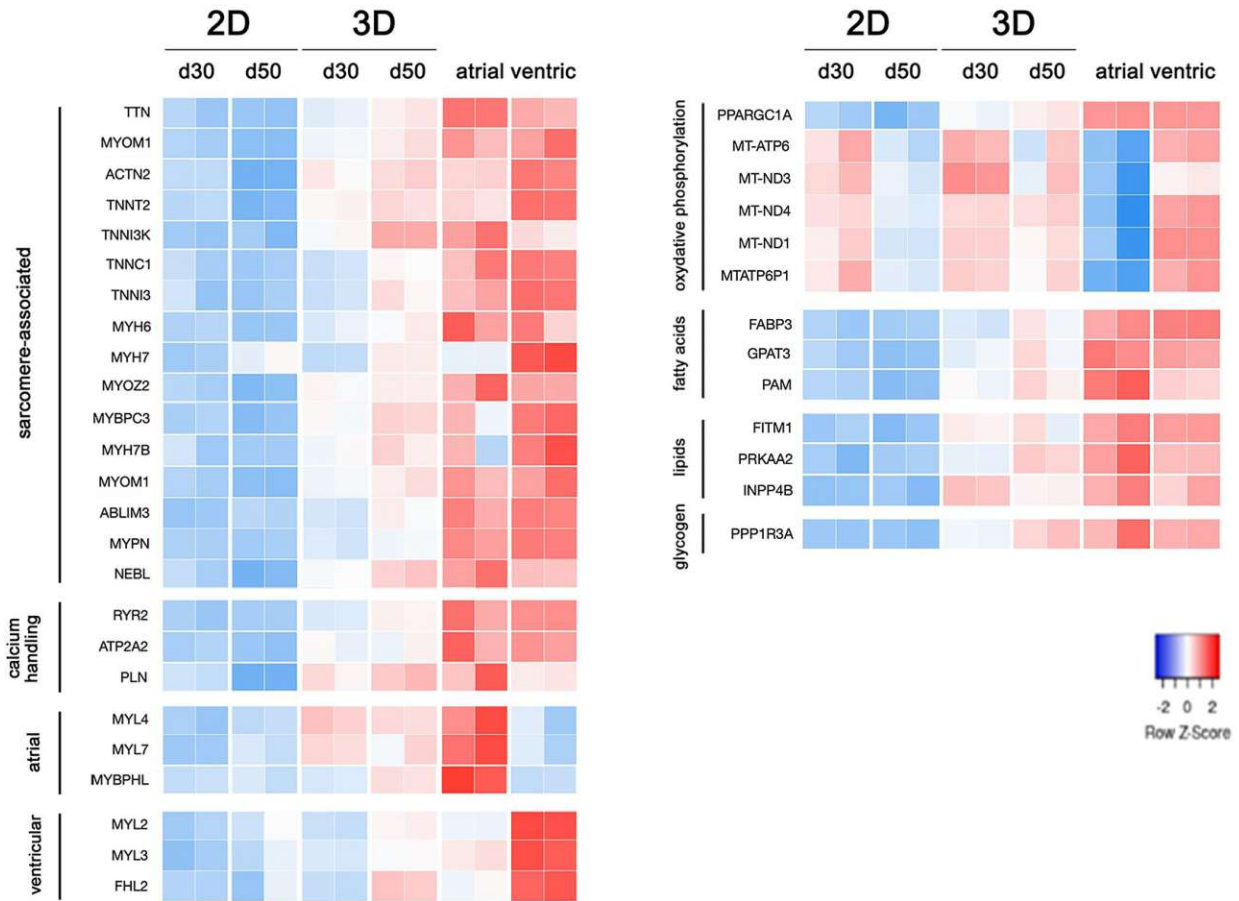


Figure 3. 24 3D long-term cultures show improved cardiac specification and cardiomyocyte maturation at transcriptional level than standard 2D cultures.

Heatmap representation of log₂fold changes in selected cardiac genes for the 3D hOCMTs and the 2D monolayers at the indicated time-points in comparison with available datasets for adult human atrial and ventricular tissues (p_{adj} < 0.05).

Finally, we compared the transcriptome of our 3D hOCMTs to Engineered Heart Tissue (EHT) [30], [407], a well-established model of 3D cardiac tissue obtained from hiPSCs. The analysis demonstrated that 3D long-term culture (day 50) prompted the expression of similar levels of genes encoding for sarcomere-associated proteins, which included *TTN*, *ACTN2*, troponins (*TNNT2*, *TNNI3K*, *TNNI3*), Myosin heavy chain (*MYH7*), calsequestrins (*CASQ2*) among many others (Figure 3.25).

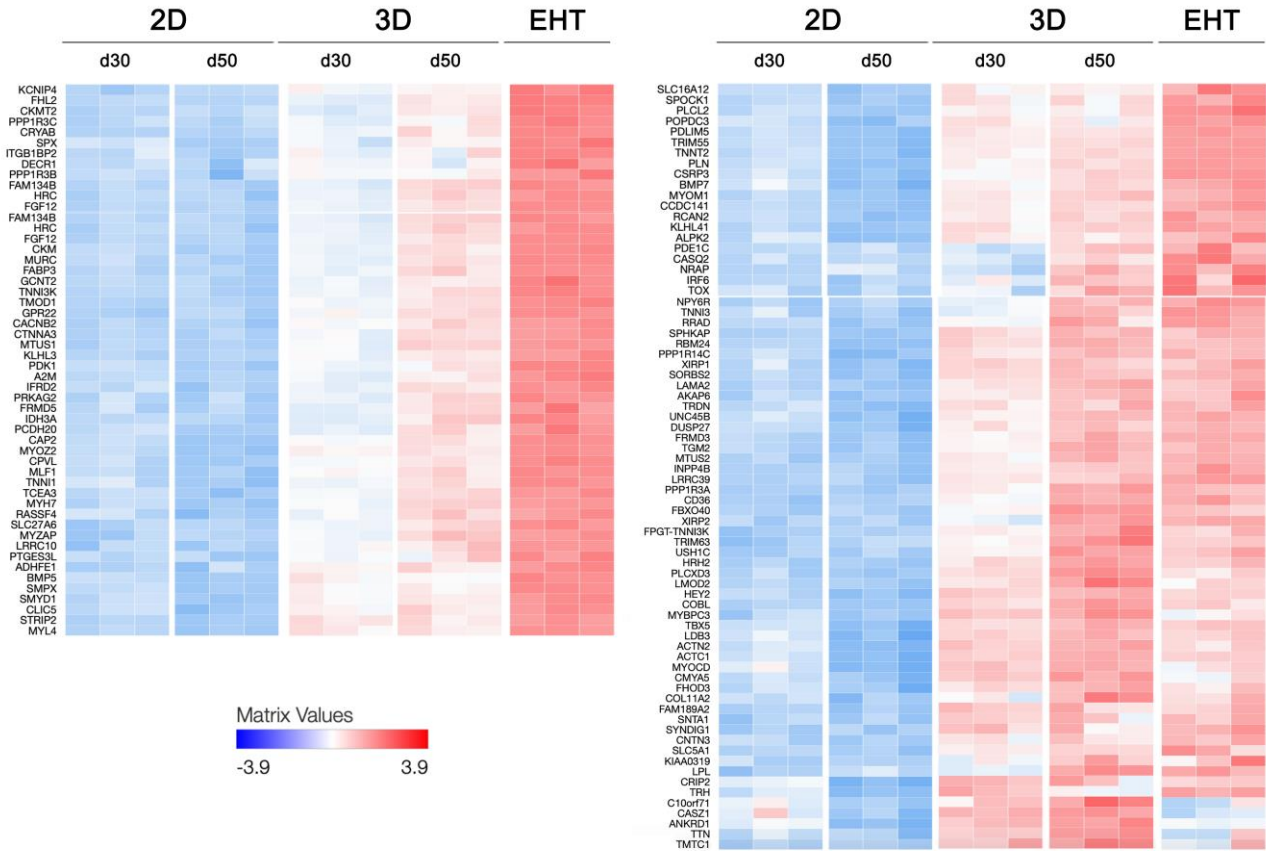


Figure 3. 25 3D hOCMT cultures show transcriptional similarities to in vitro engineered heart tissues (EHT) with respect to cardiac specification and cardiomyocyte maturation.

Heatmap representation of log₂fold changes in selected cardiac genes for the 3D hOCMTs and the 2D monolayers at the indicated time-points in comparison with available datasets for in vitro engineered heart tissues (EHT).

Overall, our transcriptomics analysis confirmed that the long-term 3D protocol set up induced hiPSCs cardiac specification and cardiomyocyte maturation at a metabolic, calcium handling and sarcomeric level. The maturation of 3D hOCMTs is strongly promoted by time in culture.

3.5 Long-term human iPSC-derived organotypic cardiac microtissues display enhanced metabolic activity

The transcriptomic analysis of 3D hOCMTs was further exploited to investigate their metabolic maturation as compared to the 2D monolayers.

The heart is characterized by very high and distinct metabolic demands, with adult cardiomyocytes relying on oxidative phosphorylation for ATP production. On the contrary, immature hiPSC-derived cardiomyocytes display continued reliance on glycolysis as the primary source of energy [163]. Although the healthy heart can oxidize several substrates from energy production, classic studies estimate that ATP production comes preferentially from fatty acid (FA) oxidation, accounting for around 70% of the total generation. The rest is provided by alternative substrates, including glucose, lactate and pyruvate [164].

Our 3D hOCMTs displayed higher expression of genes related to the FA β -oxidation, which has been previously associated with a more mature phenotype in hPSC-CMs (Figure 3.27) [414]. The expression of key regulator PPARA was - in fact - enhanced in the 3D culture. More directly into the lipid metabolism, the heart-type fatty acid binding protein (*FABP3*) and the lipoprotein lipase (*LPL*) displayed 4 times fold upregulation (Figure 3.27). The cytosolic fatty acyl-CoA synthase (*ACSL1*) catabolizing the long-chain acyl-CoA ester production, and the proteins required for their transfer into mitochondria (*CPT1A*, *CPT2*, *CRAT*, *SLC25A20*) were also found increased in the hOCMTs. Inside the mitochondria, most of the genes related to β -oxidation were found significantly upregulated as well, including the sequential acyl-CoA dehydrogenases (*ACDVL*, *ACDL*, *ACDM*, *ACDS*), which are highly expressed in the myocardium. The expression of several genes associated with peroxisomal FA intake and β -oxidation were also found upregulated.

Nevertheless, crucial genes related to glucose and pyruvate metabolism were also upregulated in the hOCMTs: this list included the glucose transporters *SLCA3* (GLUT3) and *SLCA4* (GLUT4), most of the enzymes associated with glycolysis, the proteins transporting the resulting pyruvate into the mitochondria (*MPC1*, *MPC2*), and its conversion into Acetyl-CoA (*PDHAI*, *DLAT*, *DLD*). Similarly, transcripts encoding for all the catabolic steps of the tricarboxylic acid cycle were more abundant in the 3D hOCMTs (Figure 3.26).

In accordance with the increased number of mitochondria (see Figures 3.16A, 3.17), this increase in mitochondrial metabolism was combined with an increase in the expression of genes associated to ATP synthesis-coupled electron transport. Most of the genes encoding

for the proteins composing the four electron transport protein complexes were found upregulated, as well as the vast majority of the subunits of the adenosine triphosphate (ATP) synthase itself (Figure 3.26, up). Several of the mitochondrial genes associated with the electron transport chain were likewise enriched in the hOCMTs, including NADH-ubiquinone oxidoreductase chain subunits (ND1, ND2, ND3, ND4, ND4L, ND5) and ATP synthase subunits (ATP6, ATP8).

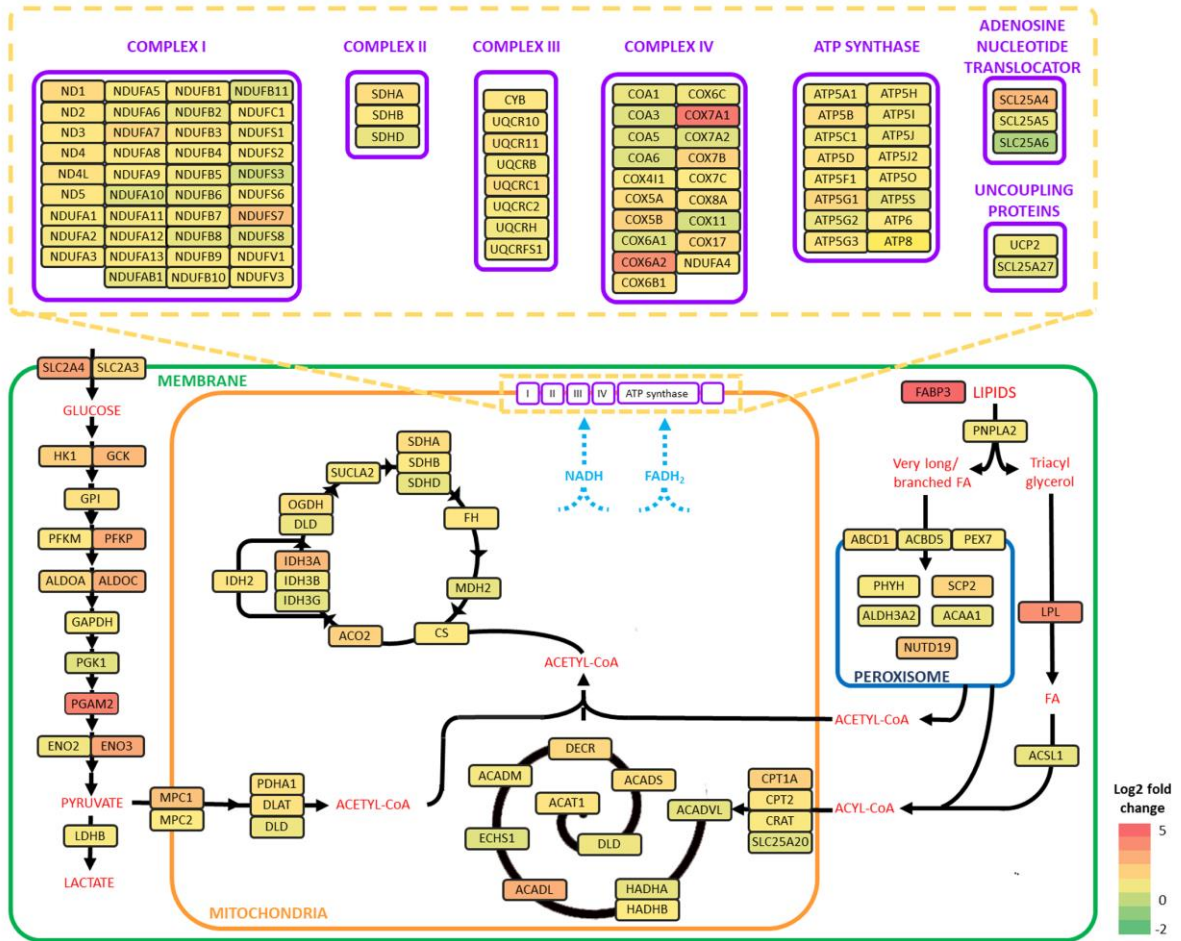


Figure 3. 26 hOCMTs display the upregulation of metabolic genes.

Diagram showing metabolic genes with significantly upregulated (in red) and downregulated (in green) genes between long-term 3D vs 2D monolayer cultures. (log2fold change; p.adj < 0.05).

In order to confirm that 3D long-term (over 50 days) culture induces hiPSC metabolic maturation, we performed real-time analyses of 2D monolayer and 3D microtissue cultures' energy metabolism using the Seahorse XFP Analyzer and Seahorse Mito Stress Test Kit. Results presented in Figure 3.27A indicate a highly energetic phenotype of 3D hOCMTs compared to the 2D cultures. The 3D cultures not only exhibited a significantly higher oxygen consumption rate (OCR) than the 2D cultures (111.83 ± 17.21 vs 55.43 ± 2.82 pmol/min/300 ng DNA - the last baseline measurement before Oligomycin injection) but also increased extracellular acidification rate (ECAR, 35.09 ± 4.60 vs 12.19 ± 1.24 mpH/min/300 ng DNA - the last baseline measurement before Oligomycin injection).

A detailed analysis of the Mito Stress Test data revealed a significantly higher basal mitochondrial respiration in the 3D cultures (94.38 ± 16.28 vs 40.22 ± 1.89 pmol/min/300 ng DNA, $p < 0.05$; Figure 3.28B). Interestingly, the 2D cultures showed a higher spare respiratory capacity than the 3D cultures (125.35 ± 15.52 vs 48.20 ± 10.18 pmol/min/300 ng DNA, $p < 0.01$; Figure 3.28B). Notably, despite a relatively high dissipation of the mitochondrial proton gradient in hOCMTs (proton leak, 37.37 ± 5.75 vs 8.02 ± 2.13 pmol/min/300 ng DNA, $p < 0.01$; Figure 3.28B), the 3D cultures produced significantly more ATP via mitochondrial respiration than their 2D counterparts (ATP production, 32.62 ± 7.08 vs 2.59 ± 0.95 pmol/min/300 ng DNA, $p < 0.01$; Figure 3.28B).

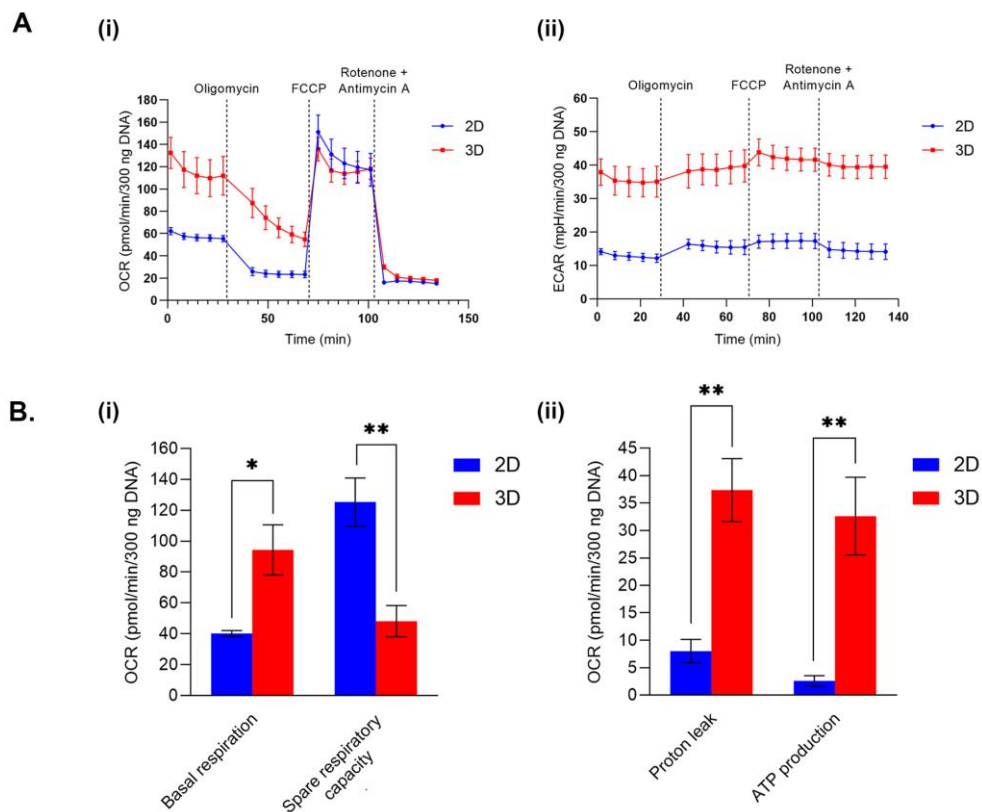


Figure 3. 27 3D long-term cultures promote changes in hOCMT metabolic activity.

A. Graphs for comparing the cellular energy metabolism of long-term 3D hOCMTs vs 2D monolayer cultures after day 50 using Seahorse XFp Analyzer and Seahorse Mito Stress Test Kit: (i) oxidative phosphorylation (oxygen consumption rate, OCR) and (ii) glycolytic flux (extracellular acidification rate, ECAR). (Mean \pm SEM obtained in four independent analyses. Total sample size: $n_{2D}=12$, $n_{3D}=9$) **B.** Bar graphs providing a detailed analysis of the oxygen consumption rate (OCR) Seahorse XFp Analyzer data presented in (A): (i) basal respiration and spare respiratory capacity, (ii) proton leak, ATP production. (Mean \pm SEM, $N=4$, $n_{2D}=12$, $n_{3D}=9$, unpaired Student's t-test – two-tailed)

In conclusion, our transcriptomics and Seahorse XF metabolic flux data suggest that hOCMTs showed an enhanced metabolic activity, which was associated with increased metabolic signatures related to FA oxidation, mitochondrial respiration and glycolysis.

3.6 Human iPSC-derived organotypic cardiac microtissues functionally respond to drugs in a dose dependent fashion in long-term culture

An essential feature of *bona fide* organoids is to replicate at least one specialized function of the modelled organ [58]–[60], which in the case of heart tissue can be assessed by the contractile activity of human cardiac organoids (hCOs). As previously indicated, once our 3D hOCMTs acquired spontaneous contractile activity early in culture (48h post aggregation), the contractility persisted for more than 100 days (Online Supplementary Video 2).

In order to test their physiological significance, 3D hOCMTs were exposed to clinically relevant doses of cardioactive drugs[415], [416] in long-term cultures (> day 50). In detail, isoproterenol and verapamil were used as positive and negative inotropes, respectively. Isoproterenol, a beta-adrenergic agonist, increases the contractile force and beating frequency [417], while verapamil, a calcium channel blocker, decreases the beating rate[418]. The hOCMTs were incubated with increasing drug doses (0.01 - 1 μ M) for 15-20 minutes and further monitored by live imaging using a confocal microscope.

The response to the treatment was evaluated and quantified based on the contraction (Figure 3.28A) and beating rate (Figure 3.28B) of the hOCMTs, analysed through the open-source software tool MUSCLEMOTION [362], [410]. The acquired data shows that increasing concentrations of isoproterenol resulted in enhanced contraction amplitude and beating rate, with the beating rate peak at 1 μ M. As expected, increasing concentrations of verapamil had the opposite effect, with the beating being completely hindered at 1 μ M drug dosage (Online Supplementary videos 3-8). These observations are in accordance with

those reported in previous studies in cardiac microtissues [419] and confirm that our constructs can functionally respond to cardioactive drugs in a dose dependent manner.

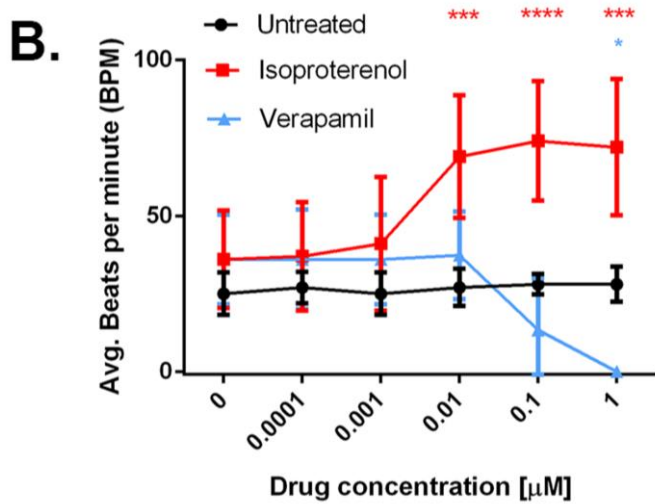
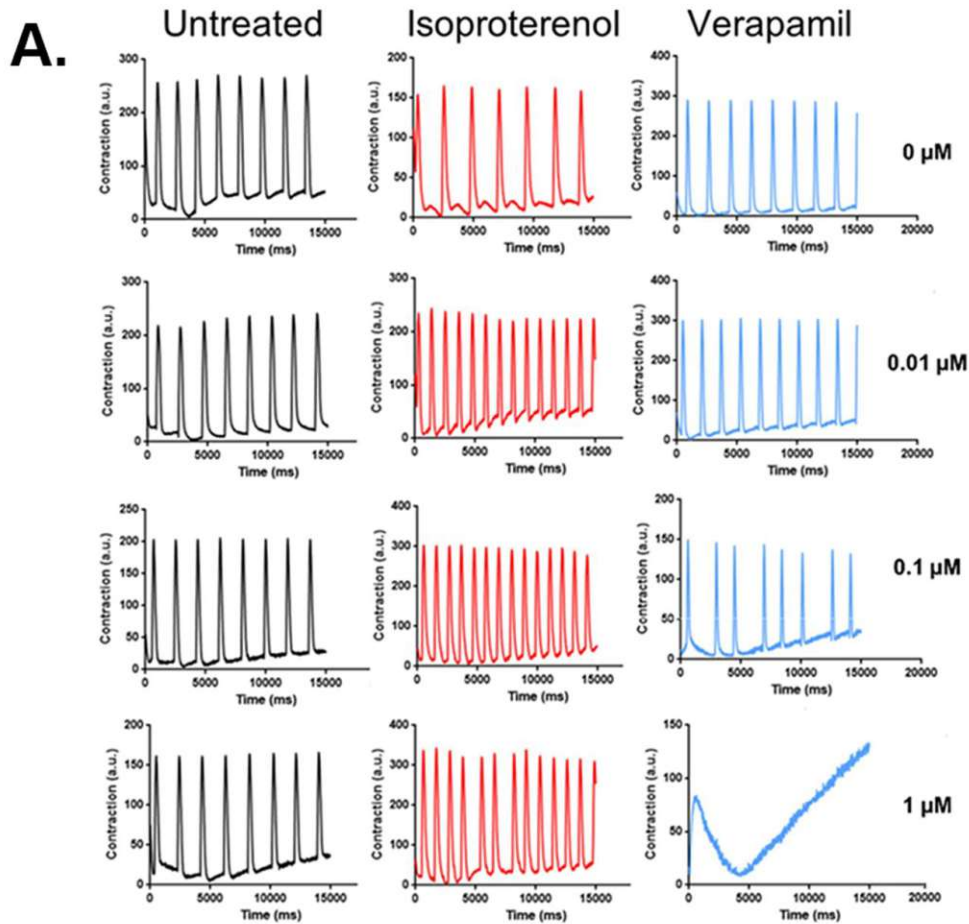


Figure 3. 28 Long-term 3D hOCMTs show functional response to cardioactive drugs in a dose and time dependent manner.

A. Representative contraction amplitude plots of long-term (>day 50) Long-term 3D hOCMTs in response to untreated vs increasing doses of Isoproterenol and Verapamil. **B.** Average beating rates of 3D long-term cardiac microtissues hOCMTs in response to increasing doses of Isoproterenol and Verapamil. (n=3, Mean \pm SD, Dunnett's multiple comparisons test)

Finally, we investigated the possibility of modelling drug-induced cardiotoxicity on our hiPSC-derived microtissues, by treating them with doxorubicin (Doxo), a well-known chemotherapeutic agent widely used in the treatment of several types of cancers [420]. The drug is - in fact - also known to have cardiotoxic and pro-fibrotic effects, thus able to cause or exacerbate heart failure *in vivo* [421]–[426].

The 3D hOCMTs were exposed to 0.1 $\mu\text{g}/\text{mL}$ and 1 $\mu\text{g}/\text{mL}$ of Doxo and their morphology and contractile activity was compared with untreated controls (n=6) for the next 6 following days. The culture medium was exchanged every 3 days and the cultures were monitored on a daily basis. Figure 3.29A shows that the morphology of the constructs gradually changed over the course of treatment, and with the occurrence of more irregular edges when exposed to higher Doxo doses. In addition, clear changes could also be observed in the beating profiles of the constructs treated with Doxo (Figure 3.29B, C, and Online Supplementary Videos 9-14).

We figured the changes in the morphology of the microtissues treated with the chemotherapeutics might be due to the induction of cell death by the drug. Therefore, after 6 days of Doxo treatment, we assessed the viability of the constructs with a luminescence-based assay. The results in Figure 3.29D and E revealed that the 3D hOCMTs treated with 1 $\mu\text{g}/\text{mL}$ Doxo were significantly less viable than both the control group and the group treated with lower drug concentration (0.1 $\mu\text{g}/\text{mL}$) (Average viability on day 6: 100 \pm 4.1% for ctrl, 86.4 \pm 9.3 for 0.1 $\mu\text{g}/\text{mL}$ Doxo, 28.3 \pm 6.6% for 1 $\mu\text{g}/\text{mL}$ Doxo, Mean \pm SD, $p < 0.0001$).

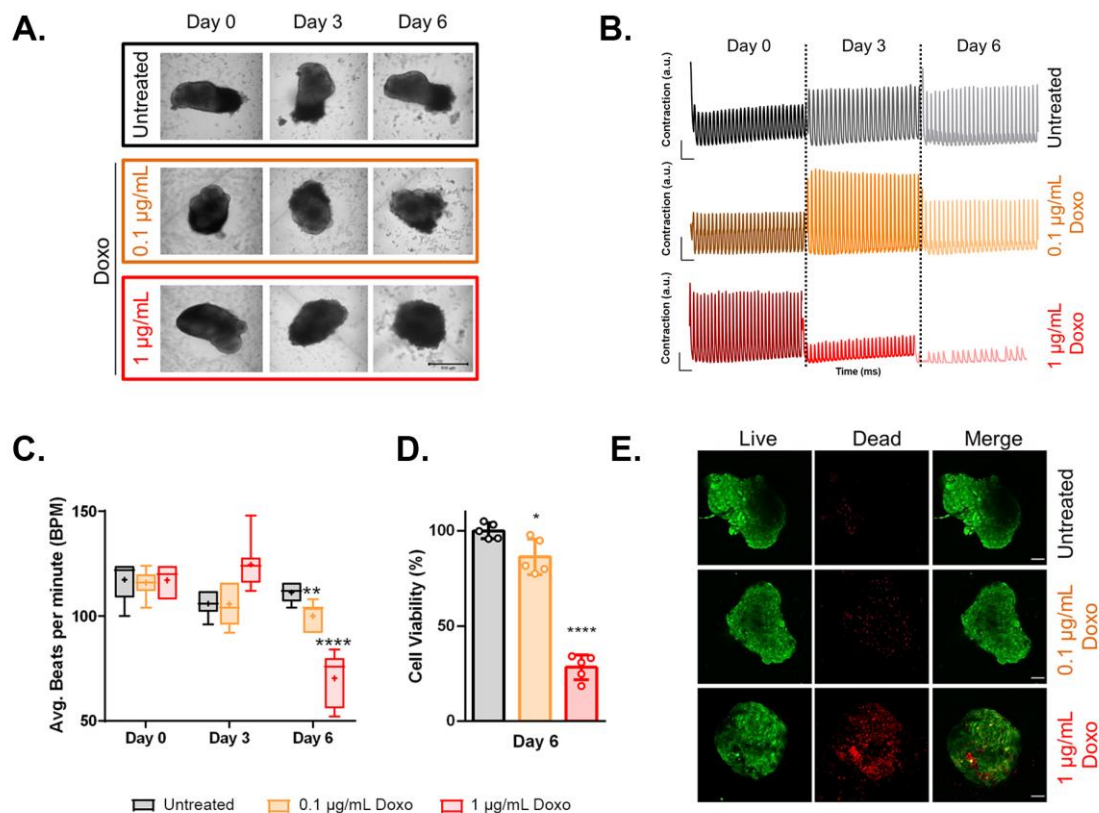


Figure 3. 29 Long-term 3D hOCMTs show functional response to cardiotoxic drugs in a dose and time dependent manner.

A. Morphology of 3D long-term (>day 50) Long-term 3D hOCMTs in response to untreated vs increasing doses of Doxorubicin (Doxo) over 6 days. (Scale bar = 500 μm). **B.** Representative contraction amplitude plots of Long-term 3D hOCMTs in response to untreated vs increasing doses of Doxo over 6 days ($t=15\text{s}$). **C.** Average beating rates of Long-term 3D hOCMTs in response untreated vs increasing doses of Doxo over 6 days. ($n=6$, Lines = Median \pm min/max, Dots = Mean value, Dunnett's multiple comparisons test) **D.** Luminescence-based quantification of cell viability Long-term 3D hOCMTs on day 6 of Doxo treatment normalized to untreated samples (untreated vs 0.1 $\mu\text{g/mL}$ vs 1 $\mu\text{g/mL}$) ($n=6$, Mean \pm SD, Tukey's multiple comparisons test). **E.** Representative cell viability of v on day 6 of Doxo treatment (untreated vs 0.1 $\mu\text{g/mL}$ vs 1 $\mu\text{g/mL}$) with Calcein/AM staining, green =live, red= dead. (Scale bar = 100 μm).

4 DISCUSSION

In this study, we have established a simple methodology to generate a 3D iPSC-derived human cardiac microtissue model – namely human organotypic cardiac microtissues (3D hOCMTs) – in scaffold-free conditions that could be cultured for extended time.

This study has shown that our long-term 3D organotypic cardiac microtissues resemble some key characteristics of the human heart, including: (1) spontaneous formation and 3D organization in the absence of an external scaffold; (2) long-term spontaneous beating without external stimuli; (3) having multiple cell types of the heart with a tendency to proto-self –organization into distinct cardiac structures; (4) ultrastructural organization and maturation of cardiomyocytes at sarcomere and mitochondria; (5) improved survival, cardiac specificity and maturation at transcriptional and metabolic levels; (6) functional response to cardioactive and cardiotoxic drugs in a dose- and time-dependent fashion. As our long-term cultured 3D cardiac microtissues satisfy the abovementioned characteristics, we propose that the hOCMTs could be confirmed as human cardiac organoids (hCOs).

Compared to standard 2D culture of iPSC-derived cardiomyocytes, 3D hOCMTs showed an enhanced survival rate. Notably, their cellular composition was shown to be more representative of the cellular heterogeneity of the native human heart, although their overall phenotype appeared to be close to foetal heart [419], [427].

Although the effects of long-term culture in promoting the maturation of PSC-derived cardiomyocytes is well established [272], [428], 2D culture remains challenging for extended culture periods, as the cardiomyocytes tend to delaminate from the traditional tissue culture plates [272], causing non-myocyte cell populations such as fibroblasts to take over and overgrow instead.

A significant advantage of our model is the lack of requirement of an external ECM scaffold like Matrigel or similar, as the microtissues self-organize on their own, and can survive for extended culture times in static culture conditions as they are. While there are other studies of scaffold-free microtissue models in literature, these usually require the differentiation of other stromal cells separately (such as epicardial or fibroblastic cells), followed by their manual assembly with cardiomyocytes [42], [63].

By exploiting the limited efficiency of the original 2D cardiac differentiation protocol by Lian et al [17], [18] via simply switching the culture dimensionality from 2D to 3D, we were able to generate long-term 3D hOCMTs where epicardial cells, fibroblasts, cardiac myocytes, and endothelial/endocardial cells co-emerge and show self-organization spontaneously in time, without the need to set up separate lineage differentiation cultures and manual assembly. Our histological analyses showed that the 2D-to-3D culture switch method yielded more complex results for extended culture times, and when the initial microtissue aggregation was performed around day 15 instead of day 7 of iPSC-derived cardiac differentiation. This could be because more cell types in addition to

cardiomyocytes are expected to emerge on towards day 15, and they can help better with the self-organization. Furthermore, the extended spontaneous beating of our hOCMTs was observed for more than 100 days. At the time of our manuscript preparation, a similar culture time was only reported by Silva et al. with their cardio-gut organoids. Of note, the aforementioned study reported the developmental co-emergence of gut tissue together with the cardiac tissue [72]. In our model, however, a distinct gut tissue was not observed after 50 days of culture according to our immunofluorescence analyses. During our manuscript revisions, another cardiac organoid study by Marini et al. has revealed a long-term culture up to 93 days from patient-derived iPSCs that recapitulated Duchene muscular dystrophy cardiomyopathy and disease progression phenotypes [368].

We have shown via histological analyses that our 3D hOCMTs manifest distinct populations of WT1-, TBX18-positive epicardial cells, TE-7-, SM22 α -positive fibroblast-like cells, NFAT2-positive endocardial cells along with distinct regions of cardiomyocytes. CD31-positive endothelial cells could also be detected, although at lower levels. The low number of CD31- positive cells might be explained by the fact that endothelial cells have different developmental origins in native human heart [429], and the lack of supplementation of our culture media with particularly endothelial-lineage favouring factors, like VEGF, during the study.

Another remarkable feature of the hOCMTs is the presence of cardiomyocytes featuring both atrial and ventricular cardiomyocyte subtype markers, as revealed by immunostaining for MYL2 and MYL7 markers. Although MYL7 is known to be observed on all cardiomyocyte subtypes during early development [158], some distinct cardiomyocytes that are only MYL7 positive, but not MYL2 positive could be identified, or vice versa, suggesting there could be a tendency of commitment to formation of different cardiomyocyte subtypes. A similar phenomenon of atrial/ventricular cardiomyocyte subtype distinction was also shown by Israeli and colleagues, which appeared to be losing their characteristics with long-term culture [71]. Meanwhile, our 3D hOCMTs has revealed higher cardiac-specific cellular heterogeneity and maturation in terms of histological, ultrastructural, and transcriptional-levels in long-term 3D cultures as compared to shorter culture times and standard 2D monolayer culture.

The ultrastructural maturity and complexity of our constructs could be confirmed by our TEM analyses over long culture times. Compared to earlier timepoints, on day 50 and 85, our hOCMTs displayed clearly aligned myofibers resulting in well-organized sarcomeres. These morphological adaptations are in line with the hallmarks of mature cardiac tissues [140], which were further supported by transcriptomic analyses. The 3D hOCMTs showed an increased expression of genes related to cardiac contraction and sarcomeric structures at transcriptional levels. The maturity of our long-term 3D hOCMTs could also be compared with Engineered Heart Tissues (EHTs), a well-recognized 3D model of cardiac tissue *in vitro*, where our day 50 3D constructs share similar transcriptional landscapes with EHTs.

In terms of contractility, immature cardiomyocytes have different calcium handling properties than their mature counterparts. While immature cardiomyocytes can rely on the calcium released at the cell periphery to initiate the contraction of sarcomeres, mature cardiomyocytes develop plasma membrane invaginations called “t-tubules” wrapped around the myofibrils in order to achieve faster and more efficient calcium release and re-uptake [142], [143]. The first polarization triggers the release of calcium stored in the sarcoplasmic reticulum by RYR2, which is then pumped back to the sarcoplasmic reticulum by SERCA2 (sarco/endoplasmic reticulum Ca^{2+} -ATPase). The ultrastructural analysis of hOCMTs by TEM confirmed the presence of t-tubules at extended culture time-points (> day 50). Additionally, our transcriptional analysis has shown the upregulation of some of the genes involved in t-tubule biogenesis (*JPH2*, *ACTN2*, *NEXN*) and sarcomeric calcium management (*RYR2*, *PLN*, *SERCA*), thus demonstrating long-term 3D culture leads to functional maturation of hOCMTs.

Additionally, cardiomyocytes also experience several metabolic changes during *in vivo* maturation in order to generate the required amount of ATP, notably by a switch from glycolytic to fatty acid oxidation [158],[159]. Our ultrastructural analyses can confirm this metabolic switch, showing that long-term hOCMTs acquired elongated mitochondria distributed around the contractile apparatus compared to shorter culture times. This outcome is further supported by the upregulation of genes related to electron transport chain-linked phosphorylation and FA β -oxidation in long-term 3D cultured hOCMTs, which was previously linked to a more mature phenotype in hiPSC-CMs [414]. Interestingly, the increase in electron transport chain activity is connected to cardiomyocyte differentiation and maturation not only by metabolic support, but also by generating calcium oscillations through complex III activity [430]. Recent studies have revealed alternative formulations that improve pluripotent stem cell-derived cardiomyocyte metabolic maturation, and push them closer to adult cardiomyocytes, which rely on oxidative phosphorylation for ATP production [163].

Metabolic flux analyses by using the Seahorse XF technology has shown that 3D hOCMTs are highly energetic compared to standard 2D cultures. The 3D hOCMTs consumed higher amounts of oxygen, in which a significant proportion of it was needed for producing mitochondrial ATP. The proton leak in the mitochondria of 3D hOCMTs might serve as a protective mechanism against mitochondrial damage by limiting the production of reactive oxygen species [431]. Surprisingly, the maximum respiration capacity induced by FCCP stimulation was similar for both 2D and 3D cultures, indicating that the mitochondria of 2D culture cells were also metabolically competent. However, their respiratory capacity was only partially used for mitochondrial ATP production under standard culture conditions. The extracellular acidification rate was also observed to be increased in the 3D cultures, which was consistent with our transcriptomics analyses showing an upregulation of metabolic gene expression, including glycolysis genes. Increased glycolysis might indicate individual metabolic adaptations of the different cell types in hOCMTs and not

just the cardiomyocytes, which could potentially be linked to differential oxygen availability inside hOCMTs. Overall, the Seahorse XF analyses reveal that cellular energy metabolism strongly differs in the 2D and 3D cultures, and the 3D hOCMTs relies on mitochondrial respiration significantly more to meet their energy needs.

Functional characterization of the hiPSC-derived 3D hOCMTs demonstrated that they were responsive to clinically relevant doses of cardioactive and cardiotoxic drugs. This is an important first step to consider the generation of patient-specific models of disease for drug testing applications.

As a proof-of-concept for modelling chemotherapy-induced cardiotoxicity, doxorubicin was chosen as a well-known chemotherapeutic agent known to cause heart failure as a side effect [421]–[426]. Meanwhile, the *in vitro* modelling of chemotherapy-induced cardiotoxicity in cardiac microtissues is still not well-established due to the limitations of reproducing the physiological cellular heterogeneity and cardiomyocyte maturity [69]. Furthermore, it is crucial to consider the effect of cell-cell interactions of cardiomyocyte vs other cardiac cell types - especially fibroblasts - and cell-ECM interactions [182]. Our hOCMT platform offers the advantages of long-term viability, cellular heterogeneity, and advanced maturity *in vitro*, making it a physiologically relevant alternative for future studies – in addition to the potential or personalized models via patient iPSC-derived microtissues. Further clinical parameters such as the cardio-fibrotic potential of doxorubicin treatment [424], [425], [432], the secretion of serum cardiac troponins and natriuretic peptides as clinically relevant markers of chemotherapy-induced cardiotoxicity [433] or simply the potential for personalized medicine could be possible by using our hiPSC-derived hOCMTs [434].

While promising, our model still has some limitations. In spite of showing features of structural and functional maturation in the 3D long-term culture model as compared to standard 2D monolayers, 3D hOCMTs still display more foetal characteristics than adult heart. For instance, the cardiomyocytes of our hOCMTs have $\sim 1.5 \mu\text{m}$ length of sarcomeres (similar to foetal mammalian hearts), while in adult hearts, this length is usually $2 \mu\text{m}$ [140]. To improve the maturity of our constructs, the adoption of additional stimuli (i.e.: additional growth factors, dynamic culture, mechanical conditioning and electrical stimulation) might be helpful, including leading to even earlier maturation times [144]. Additionally, although our 3D hOCMTs show hints of histological similarities to the heart tissue – such as cellular heterogeneity of cardiac cell types, and spontaneous re-organization of these multiple cell types at distinct regions – additional cues and optimization steps would be needed to improve the self-organization, and modelling different compartments of the heart (eg. chamber formation trabeculation, left/right ventricles, atria, aorta, outflow tract, vasculature...) following similar principles of embryonic human heart development. These improvements could additionally help to reduce batch-to-batch differences commonly observed in iPSC-derived organoid technologies [273]–[276]. The utilization of “organoid-on-a-chip”, mechanobiology and

similar bioengineering technologies could additionally help with the standardization, spatio-temporal patterning, scalability and real-time monitoring of cardiac organoid generation, culture, and functional applications [334], [435]–[439].

As for some technical limitations, the size, density, and spontaneous movement of the organoids has limited intact microtissue characterization with whole-mount and live 3D imaging with the confocal microscope due to significant light scattering. To overcome this, fixed tissues could be characterized by more advanced microscopy techniques such as with tissue clearing and light sheet microscopy. Further electrophysiological characterization by live calcium imaging was also challenging by conventional staining methods as the dye was not visible inside the core of the organoids. To overcome this, iPSC cell lines containing genetically encoded calcium reporters could be used [440], or further electrophysiological characterization can be performed with multi-electrode arrays (MEA) or patch-clamp experiments. Furthermore, if the organoid dissociation protocols could be optimized with improved viability, the true cellular heterogeneity could be assessed more precisely by single cell sequencing technologies.

In future studies, *in vitro* cardiotoxicity studies should also consider the importance of multi-organ interactions. Though drugs in their native chemistries may not always cause direct cardiac damage [441], their metabolic by-products might lead to cardiotoxicity *in vivo* due to systemic multi-organ interactions [366], [441]. Future pre-clinical studies could benefit from high throughput technologies [437], and microphysiological platforms that could model multi-organ interactions *in vitro* (eg. body-on-a-chip [54], [442], [443]). While more studies are required to see if *in vitro* models could fully rule out *in vivo* experiments – as systemic results are still required – they can already help reduce excessive animal experimentations by providing more accurate reflections of native human tissues faster.

5 CONCLUSION AND SCIENTIFIC VALUE

This doctoral dissertation sets at expanding the possibilities of *in vitro* microphysiological cardiovascular modelling, and to establish a methodology to generate a 3D iPSC-derived human cardiac microtissue model that could reflect the physiological complexity, cellular heterogeneity and maturity of a human heart, and demonstrate its functionality for translational research applications.

In this regard, we have established a simple procedure to generate such a physiologically relevant and miniaturized human cardiac model: human 3D human induced pluripotent stem cell-derived organotypic cardiac microtissues – or 3D hOCMTs.

With our model, we were able to satisfy several important criteria relevant for faithful modelling of the native human heart including (1) containing multiple cell types of the heart with some distinct self-organization, (2) long-term spontaneous beating without external stimuli, (3) ultrastructural, transcriptional and metabolic maturation of cardiomyocytes, (4) functional response to cardioactive and cardiotoxic drugs in a dose- and time-dependent fashion. Since our long-term cultured 3D cardiac microtissues satisfy the abovementioned characteristics, we propose that the hOCMTs could be considered as human cardiac organoids (hCOs).

Additionally, given that they (1) are human iPSC-derived, (2) can be formed without the need of any external scaffold and (3) can be maintained in extended culture times (more than 100 days), and (4) show signs of tissue maturation, 3D microtissues could be very practical and powerful *in vitro* platforms for translational research applications, such as personalized disease modelling and drug screening.

Furthermore, by using physiologically relevant human tissue models would help reducing animal experimentations by providing more accurate characteristics of native human tissues, potentially leading to more precise, more ethical and faster approval of drug candidates at pre-clinical stages. Indeed, on September 29, 2022, the U.S. Senate has passed the FDA Modernization Act 2.0, S.5002, without dissent [444]., which was then signed into law in late December 2022 as part of the Consolidated Appropriations Act. This means the existing regulations would be updated to allow drug developers to use human-relevant testing methods in order to replace animal experiments [445].

Future studies are now warranted that could further improve the complexity and maturity of 3D hOCMT constructs by further bioengineering, developmental biology and mechanobiology applications, with a focus on their ability to be used as pre-clinical drug screening and personalized cardiac disease modelling platforms.

6 BIBLIOGRAPHY

- [1] C. Abbafati *et al.*, ‘Global burden of 369 diseases and injuries in 204 countries and territories, 1990–2019: a systematic analysis for the Global Burden of Disease Study 2019’, *Lancet Lond. Engl.*, vol. 396, no. 10258, p. 1204, Oct. 2020, doi: 10.1016/S0140-6736(20)30925-9.
- [2] G. A. Roth *et al.*, ‘Global Burden of Cardiovascular Diseases and Risk Factors, 1990–2019: Update From the GBD 2019 Study’, *J. Am. Coll. Cardiol.*, vol. 76, no. 25, pp. 2982–3021, Dec. 2020, doi: 10.1016/j.jacc.2020.11.010.
- [3] S. Shi *et al.*, ‘Association of Cardiac Injury With Mortality in Hospitalized Patients With COVID-19 in Wuhan, China’, *JAMA Cardiol.*, vol. 5, no. 7, pp. 802–810, Jul. 2020, doi: 10.1001/JAMACARDIO.2020.0950.
- [4] B. J. R. Buckley, S. L. Harrison, E. Fazio-Eynullayeva, P. Underhill, D. A. Lane, and G. Y. H. Lip, ‘Prevalence and clinical outcomes of myocarditis and pericarditis in 718,365 COVID-19 patients’, *Eur. J. Clin. Invest.*, vol. 51, no. 11, Nov. 2021, doi: 10.1111/eci.13679.
- [5] Z. Al-Aly, Y. Xie, and B. Bowe, ‘High-dimensional characterization of post-acute sequelae of COVID-19’, *Nature*, vol. 594, no. 7862, pp. 259–264, Jun. 2021, doi: 10.1038/s41586-021-03553-9.
- [6] M. Chilazi, E. Y. Duffy, A. Thakkar, and E. D. Michos, ‘COVID and Cardiovascular Disease: What We Know in 2021’, *Curr. Atheroscler. Rep.*, vol. 23, no. 7, Jul. 2021, doi: 10.1007/S11883-021-00935-2.
- [7] M. O. Mohamed and A. Banerjee, ‘Long COVID and cardiovascular disease: a learning health system approach’, *Nat. Rev. Cardiol.*, vol. 19, no. 5, pp. 287–288, May 2022, doi: 10.1038/s41569-022-00697-7.
- [8] Y. Xie, E. Xu, B. Bowe, and Z. Al-Aly, ‘Long-term cardiovascular outcomes of COVID-19’, *Nat. Med.*, vol. 28, no. 3, pp. 583–590, Mar. 2022, doi: 10.1038/S41591-022-01689-3.
- [9] B. Seruga, A. Ocana, E. Amir, and I. F. Tannock, ‘Failures in Phase III: Causes and Consequences’, *Clin Cancer Res*, vol. 21, no. 20, pp. 4552–4560, Oct. 2015, doi: 10.1158/1078-0432.ccr-15-0124.
- [10] R. McNaughton, G. Huet, and S. Shakir, ‘An investigation into drug products withdrawn from the EU market between 2002 and 2011 for safety reasons and the evidence used to support the decision-making’, *BMJ Open*, vol. 4, no. 1, 2014, doi: 10.1136/BMJOPEN-2013-004221.
- [11] A. Y. Khakoo, N. R. Yurgin, P. R. Eisenberg, and G. C. Fonarow, ‘Overcoming Barriers to Development of Novel Therapies for Cardiovascular Disease: Insights

From the Oncology Drug Development Experience’, *JACC Basic Transl. Sci.*, vol. 4, no. 2, pp. 269–274, Apr. 2019, doi: 10.1016/J.JACBTS.2019.01.011.

- [12] S. Cho, C. Lee, M. A. Skylar-Scott, S. C. Heilshorn, and J. C. Wu, ‘Reconstructing the heart using iPSCs: Engineering strategies and applications’, *J. Mol. Cell. Cardiol.*, vol. 157, pp. 56–65, Aug. 2021, doi: 10.1016/j.yjmcc.2021.04.006.
- [13] J. Kim, B. K. Koo, and J. A. Knoblich, ‘Human organoids: model systems for human biology and medicine’, *Nat. Rev. Mol. Cell Biol.*, vol. 21, no. 10, pp. 571–584, Oct. 2020, doi: 10.1038/s41580-020-0259-3.
- [14] J. J. Marshall and J. O. Mason, ‘Mouse vs man: Organoid models of brain development & disease’, *Brain Res.*, vol. 1724, Dec. 2019, doi: 10.1016/J.BRAINRES.2019.146427.
- [15] S. B. Gorzalczany and A. G. Rodriguez Basso, ‘Strategies to apply 3Rs in preclinical testing’, *Pharmacol. Res. Perspect.*, vol. 9, no. 5, Oct. 2021, doi: 10.1002/prp2.863.
- [16] K. Takahashi *et al.*, ‘Induction of Pluripotent Stem Cells from Adult Human Fibroblasts by Defined Factors’, *Cell*, vol. 131, no. 5, pp. 861–872, Nov. 2007, doi: 10.1016/j.cell.2007.11.019.
- [17] X. Lian *et al.*, ‘Robust cardiomyocyte differentiation from human pluripotent stem cells via temporal modulation of canonical Wnt signaling’, *Proc. Natl. Acad. Sci. U. S. A.*, vol. 109, no. 27, pp. E1848–E1857, Jul. 2012, doi: 10.1073/pnas.1200250109.
- [18] X. Lian *et al.*, ‘Directed cardiomyocyte differentiation from human pluripotent stem cells by modulating Wnt/ β -catenin signaling under fully defined conditions.’, *Nat. Protoc.*, vol. 8, no. 1, pp. 162–175, Jan. 2013, doi: 10.1038/nprot.2012.150.
- [19] T. Sadahiro, S. Yamanaka, and M. Ieda, ‘Direct Cardiac Reprogramming: Progress and Challenges in Basic Biology and Clinical Applications’, *Circ. Res.*, vol. 116, no. 8, pp. 1378–1391, 2015, doi: 10.1161/CIRCRESAHA.116.305374.
- [20] P. W. Burridge *et al.*, ‘Chemically defined generation of human cardiomyocytes.’, *Nat. Methods*, vol. 11, no. 8, pp. 855–860, Jun. 2014, doi: 10.1038/nmeth.2999.
- [21] P. W. Burridge, S. Diecke, E. Matsa, A. Sharma, H. Wu, and J. C. Wu, ‘Modeling cardiovascular diseases with patient-specific human pluripotent stem cell-derived cardiomyocytes’, *Methods Mol. Biol.*, vol. 1353, pp. 119–130, 2014, doi: 10.1007/7651_2015_196.
- [22] P. W. Burridge *et al.*, ‘Human induced pluripotent stem cell-derived cardiomyocytes recapitulate the predilection of breast cancer patients to doxorubicin-induced cardiotoxicity’, *Nat. Med.*, vol. 22, no. 5, pp. 547–556, May 2016, doi: 10.1038/NM.4087.
- [23] A. Sharma, G. Li, K. Rajarajan, R. Hamaguchi, P. W. Burridge, and S. M. Wu, ‘Derivation of highly purified cardiomyocytes from human induced pluripotent stem

cells using small molecule-modulated differentiation and subsequent glucose starvation.’, *J. Vis. Exp. JoVE*, no. 97, p. e52628, Jan. 2015, doi: 10.3791/52628.

- [24] A. Sharma *et al.*, ‘Use of human induced pluripotent stem cell–derived cardiomyocytes to assess drug cardiotoxicity’, *Nat. Protoc.*, vol. 13, no. 12, pp. 3018–3041, Dec. 2018, doi: 10.1038/s41596-018-0076-8.
- [25] F. Lan *et al.*, ‘Abnormal calcium handling properties underlie familial hypertrophic cardiomyopathy pathology in patient-specific induced pluripotent stem cells.’, *Cell Stem Cell*, vol. 12, no. 1, pp. 101–113, Jan. 2013, doi: 10.1016/j.stem.2012.10.010.
- [26] A. Sharma *et al.*, ‘Human Induced Pluripotent Stem Cell–Derived Cardiomyocytes as an In Vitro Model for Coxsackievirus B3–Induced Myocarditis and Antiviral Drug Screening Platform’, *Circ. Res.*, vol. 115, no. 6, pp. 556–566, Aug. 2014, doi: 10.1161/CIRCRESAHA.115.303810.
- [27] A. M. Becker, M. Rubart, and L. J. Field, ‘Regenerating the Heart’, 2011, doi: 10.1007/978-1-61779-021-8.
- [28] E. R. Porrello and E. N. Olson, ‘A neonatal blueprint for cardiac regeneration.’, *Stem Cell Res.*, vol. 13, no. 3 Pt B, pp. 556–70, Nov. 2014, doi: 10.1016/j.scr.2014.06.003.
- [29] E. Cimetta, A. Godier-Furnémont, and G. Vunjak-Novakovic, ‘Bioengineering heart tissue for in vitro testing’, *Curr. Opin. Biotechnol.*, vol. 24, pp. 926–932, 2013, doi: 10.1016/j.copbio.2013.07.002.
- [30] G. Vunjak Novakovic, T. Eschenhagen, and C. Mummery, ‘Myocardial tissue engineering: In vitro models’, *Cold Spring Harb. Perspect. Med.*, vol. 4, no. 3, pp. 1–16, Mar. 2014, doi: 10.1101/CSHPERSPECT.A014076.
- [31] T.-S. Li *et al.*, ‘Cardiospheres recapitulate a niche-like microenvironment rich in stemness and cell-matrix interactions, rationalizing their enhanced functional potency for myocardial repair.’, *Stem Cells Dayt. Ohio*, vol. 28, no. 11, pp. 2088–98, Nov. 2010, doi: 10.1002/stem.532.
- [32] D. C. Nguyen *et al.*, ‘Microscale generation of cardiospheres promotes robust enrichment of cardiomyocytes derived from human pluripotent stem cells.’, *Stem Cell Rep.*, vol. 3, no. 2, pp. 260–8, Aug. 2014, doi: 10.1016/j.stemcr.2014.06.002.
- [33] D. J. Richards *et al.*, ‘Inspiration from heart development: Biomimetic development of functional human cardiac organoids’, *Biomaterials*, vol. 142, pp. 112–123, Oct. 2017, doi: 10.1016/j.biomaterials.2017.07.021.
- [34] W.-H. Zimmermann, ‘Tissue Engineering of a Differentiated Cardiac Muscle Construct’, *Circ. Res.*, vol. 90, no. 2, pp. 223–230, Dec. 2001, doi: 10.1161/hh0202.103644.

- [35] F. Weinberger, I. Mannhardt, and T. Eschenhagen, ‘Engineering Cardiac Muscle Tissue: A Maturing Field of Research’, *Circ. Res.*, vol. 120, no. 9, pp. 1487–1500, Apr. 2017, doi: 10.1161/CIRCRESAHA.117.310738.
- [36] W. Dhahri, R. Romagnuolo, and M. A. Laflamme, ‘Training heart tissue to mature’, *Nat. Biomed. Eng.*, vol. 2, no. 6, pp. 351–352, Jun. 2018, doi: 10.1038/s41551-018-0253-7.
- [37] M. N. Hirt, A. Hansen, and T. Eschenhagen, ‘Cardiac Tissue Engineering’, *Circ. Res.*, vol. 114, no. 2, 2014, Accessed: Aug. 22, 2017. [Online]. Available: <http://circres.ahajournals.org/content/114/2/354>
- [38] S. Schaaf *et al.*, ‘Human Engineered Heart Tissue as a Versatile Tool in Basic Research and Preclinical Toxicology’, *PLoS ONE*, vol. 6, no. 10, p. e26397, Oct. 2011, doi: 10.1371/journal.pone.0026397.
- [39] A. Mathur *et al.*, ‘Human iPSC-based cardiac microphysiological system for drug screening applications’, *Sci. Rep.*, vol. 5, no. 1, pp. 1–7, Mar. 2015, doi: 10.1038/srep08883.
- [40] Z. Ma *et al.*, ‘Self-organizing human cardiac microchambers mediated by geometric confinement’, *Nat. Commun.* 2015 61, vol. 6, no. 1, pp. 1–10, Jul. 2015, doi: 10.1038/ncomms8413.
- [41] E. Giacomelli *et al.*, ‘Three-dimensional cardiac microtissues composed of cardiomyocytes and endothelial cells co-differentiated from human pluripotent stem cells’, *Dev. Camb.*, vol. 144, no. 6, pp. 1008–1017, Mar. 2017, doi: 10.1242/DEV.143438.
- [42] E. Giacomelli *et al.*, ‘Human-iPSC-Derived Cardiac Stromal Cells Enhance Maturation in 3D Cardiac Microtissues and Reveal Non-cardiomyocyte Contributions to Heart Disease’, *Cell Stem Cell*, vol. 26, no. 6, pp. 862-879.e11, Jun. 2020, doi: 10.1016/j.stem.2020.05.004.
- [43] E. Giacomelli, L. Sala, D. W. van Oostwaard, and M. Bellin, ‘Cardiac microtissues from human pluripotent stem cells recapitulate the phenotype of long-QT syndrome’, *Biochem. Biophys. Res. Commun.*, vol. 572, pp. 118–124, Oct. 2021, doi: 10.1016/J.BBRC.2021.07.068.
- [44] Y. C. Tsan *et al.*, ‘Physiologic biomechanics enhance reproducible contractile development in a stem cell derived cardiac muscle platform’, *Nat. Commun.*, vol. 12, no. 1, pp. 1–16, Oct. 2021, doi: 10.1038/s41467-021-26496-1.
- [45] A. Grosberg, P. W. Alford, M. L. McCain, and K. K. Parker, ‘Ensembles of engineered cardiac tissues for physiological and pharmacological study: Heart on a chip’, *Lab Chip*, vol. 11, no. 24, pp. 4165–4173, Dec. 2011, doi: 10.1039/c1lc20557a.

- [46] J. Shim, A. Grosberg, J. C. Nawroth, K. K. Parker, and K. Bertoldi, ‘Modeling of cardiac muscle thin films: pre-stretch, passive and active behavior.’, *J. Biomech.*, vol. 45, no. 5, pp. 832–41, Mar. 2012, doi: 10.1016/j.jbiomech.2011.11.024.
- [47] G. Wang *et al.*, ‘Modeling the mitochondrial cardiomyopathy of Barth syndrome with induced pluripotent stem cell and heart-on-chip technologies’, *Nat. Med.*, vol. 20, no. 6, pp. 616–623, 2014, doi: 10.1038/NM.3545.
- [48] A. Marsano *et al.*, ‘Beating heart on a chip: a novel microfluidic platform to generate functional 3D cardiac microtissues’, *Lab Chip*, vol. 16, no. 3, pp. 599–610, Jan. 2016, doi: 10.1039/C5LC01356A.
- [49] G. S. Ugolini *et al.*, ‘On-chip assessment of human primary cardiac fibroblasts proliferative responses to uniaxial cyclic mechanical strain’, *Biotechnol. Bioeng.*, 2016, doi: 10.1002/bit.25847.
- [50] G. S. Ugolini, R. Visone, A. Redaelli, M. Moretti, and M. Rasponi, ‘Generating Multicompartmental 3D Biological Constructs Interfaced through Sequential Injections in Microfluidic Devices’, *Adv. Healthc. Mater.*, vol. 6, no. 10, 2017, doi: 10.1002/adhm.201601170.
- [51] P. Occhetta *et al.*, ‘A three-dimensional *in vitro* dynamic micro-tissue model of cardiac scar formation’, *Integr. Biol.*, vol. 10, no. 3, pp. 174–183, Mar. 2018, doi: 10.1039/C7IB00199A.
- [52] O. Schneider, L. Zeifang, S. Fuchs, C. Sailer, and P. Loskill, ‘User-Friendly and Parallelized Generation of Human Induced Pluripotent Stem Cell-Derived Microtissues in a Centrifugal Heart-on-a-Chip’, *Tissue Eng. - Part A*, vol. 25, no. 9–10, pp. 786–798, 2019, doi: 10.1089/ten.tea.2019.0002.
- [53] A. Khademhosseini *et al.*, ‘Microfluidic patterning for fabrication of contractile cardiac organoids.’, *Biomed. Microdevices*, vol. 9, no. 2, pp. 149–57, Apr. 2007, doi: 10.1007/s10544-006-9013-7.
- [54] A. Skardal *et al.*, ‘Multi-tissue interactions in an integrated three-tissue organ-on-a-chip platform’, *Sci. Rep.*, vol. 7, no. 1, p. 8837, Dec. 2017, doi: 10.1038/s41598-017-08879-x.
- [55] Y. S. Zhang *et al.*, ‘From cardiac tissue engineering to heart-on-a-chip: Beating challenges’, *Biomed. Mater. Bristol*, vol. 10, no. 3, Jun. 2015, doi: 10.1088/1748-6041/10/3/034006.
- [56] M. A. Lancaster and J. A. Knoblich, ‘Organogenesis in a dish: Modeling development and disease using organoid technologies’, *Science*, vol. 345, no. 6194, pp. 1247125–1247125, Jul. 2014, doi: 10.1126/SCIENCE.1247125.
- [57] H. Clevers, ‘Modeling Development and Disease with Organoids’, *Cell*, vol. 165, no. 7, pp. 1586–1597, Jun. 2016, doi: 10.1016/j.cell.2016.05.082.

- [58] M. A. Lancaster and M. Huch, ‘Disease modelling in human organoids’, *DMM Dis. Models Mech.*, vol. 12, no. 7, p. dmm039347, 2019, doi: 10.1242/dmm.039347.
- [59] Y. Sasai, ‘Next-generation regenerative medicine: organogenesis from stem cells in 3D culture’, *Cell Stem Cell*, vol. 12, no. 5, pp. 520–530, May 2013, doi: 10.1016/J.STEM.2013.04.009.
- [60] Y. Sasai, ‘Cytosystems dynamics in self-organization of tissue architecture’, *Nature*, vol. 493, no. 7432, pp. 318–326, Jan. 2013, doi: 10.1038/NATURE11859.
- [61] F. Schutgens and H. Clevers, ‘Human Organoids: Tools for Understanding Biology and Treating Diseases’, *Annu. Rev. Pathol. Mech. Dis.*, vol. 15, pp. 211–234, Jan. 2020, doi: 10.1146/annurev-pathmechdis-012419-032611.
- [62] C. Corrò, L. Novellademunt, and V. S. W. Li, ‘A brief history of organoids’, *Am. J. Physiol. - Cell Physiol.*, vol. 319, no. 1, pp. C151–C165, Jul. 2020, doi: 10.1152/AJPCELL.00120.2020/ASSET/IMAGES/LARGE/ZH00072087490002.JPG.
- [63] P. Hofbauer *et al.*, ‘Cardioids reveal self-organizing principles of human cardiogenesis’, *Cell*, vol. 184, no. 12, pp. 3299–3317.e22, Jun. 2021, doi: 10.1016/J.CELL.2021.04.034.
- [64] P. Andersen *et al.*, ‘Precardiac organoids form two heart fields via Bmp/Wnt signaling’, *Nat. Commun.*, vol. 9, no. 1, pp. 1–13, 2018, doi: 10.1038/S41467-018-05604-8.
- [65] J. Lee *et al.*, ‘In vitro generation of functional murine heart organoids via FGF4 and extracellular matrix’, *Nat. Commun.*, vol. 11, no. 1, 2020, doi: 10.1038/s41467-020-18031-5.
- [66] G. Rossi *et al.*, ‘Capturing Cardiogenesis in Gastruloids’, *Cell Stem Cell*, vol. 28, no. 2, pp. 230–240.e6, Feb. 2021, doi: 10.1016/j.stem.2020.10.013.
- [67] H. K. Voges, R. J. Mills, D. A. Elliott, R. G. Parton, E. R. Porrello, and J. E. Hudson, ‘Development of a human cardiac organoid injury model reveals innate regenerative potential’, *Dev. Camb.*, vol. 144, no. 6, pp. 1118–1127, 2017, doi: 10.1242/dev.143966.
- [68] R. J. Mills *et al.*, ‘Functional screening in human cardiac organoids reveals a metabolic mechanism for cardiomyocyte cell cycle arrest’, *Proc Natl Acad Sci USA*, vol. 114, no. 40, pp. E8372–E8381, Oct. 2017, doi: 10.1073/pnas.1707316114.
- [69] D. J. Richards *et al.*, ‘Human cardiac organoids for the modelling of myocardial infarction and drug cardiotoxicity’, *Nat. Biomed. Eng.*, vol. 4, no. 4, pp. 446–462, Apr. 2020, doi: 10.1038/S41551-020-0539-4.

- [70] L. Drakhlis *et al.*, ‘Human heart-forming organoids recapitulate early heart and foregut development’, *Nat. Biotechnol.*, vol. 39, no. 6, pp. 737–746, Jun. 2021, doi: 10.1038/S41587-021-00815-9.
- [71] Y. R. Lewis-Israeli *et al.*, ‘Self-assembling human heart organoids for the modeling of cardiac development and congenital heart disease’, *Nat. Commun.*, vol. 12, no. 1, Dec. 2021, doi: 10.1038/s41467-021-25329-5.
- [72] A. C. Silva *et al.*, ‘Co-emergence of cardiac and gut tissues promotes cardiomyocyte maturation within human iPSC-derived organoids.’, *Cell Stem Cell*, vol. 28, no. 12, pp. 2137-2152.e6, Dec. 2021, doi: 10.1016/j.stem.2021.11.007.
- [73] L. Drakhlis, S. B. Devadas, and R. Zweigerdt, ‘Generation of heart-forming organoids from human pluripotent stem cells’, *Nat. Protoc.*, vol. 16, no. 12, pp. 5652–5672, Dec. 2021, doi: 10.1038/S41596-021-00629-8.
- [74] X. Yang, L. Pabon, and C. E. Murry, ‘Engineering adolescence: maturation of human pluripotent stem cell-derived cardiomyocytes.’, *Circ. Res.*, vol. 114, no. 3, pp. 511–23, Jan. 2014, doi: 10.1161/CIRCRESAHA.114.300558.
- [75] S. A. Murphy, E. Z. Chen, L. Tung, K. R. Boheler, and C. Kwon, ‘Maturing heart muscle cells: Mechanisms and transcriptomic insights’, *Semin. Cell Dev. Biol.*, vol. 119, pp. 49–60, Nov. 2021, doi: 10.1016/J.SEMCDB.2021.04.019.
- [76] M. D. Tallquist and J. D. Molkentin, ‘Redefining the identity of cardiac fibroblasts’, *Nat. Rev. Cardiol.*, vol. 14, no. 8, Art. no. 8, Aug. 2017, doi: 10.1038/nrcardio.2017.57.
- [77] M. Xin, E. N. Olson, and R. Bassel-Duby, ‘Mending broken hearts: cardiac development as a basis for adult heart regeneration and repair.’, *Nat. Rev. Mol. Cell Biol.*, vol. 14, no. 8, pp. 529–41, Aug. 2013, doi: 10.1038/nrm3619.
- [78] F. H. Martini, J. L. Nath, and E. F. Bartholomew, *Fundamentals of Anatomy & Physiology*, 11th ed. Pearson Education Limited, 2018.
- [79] S. Li, D.-Z. Wang, Z. Wang, J. a Richardson, and E. N. Olson, ‘The serum response factor coactivator myocardin is required for vascular smooth muscle development.’, *Proc. Natl. Acad. Sci. U. S. A.*, vol. 100, pp. 9366–9370, 2003, doi: 10.1073/pnas.1233635100.
- [80] M. Günthel, P. Barnett, and V. M. Christoffels, ‘Development, Proliferation, and Growth of the Mammalian Heart’, *Mol. Ther.*, vol. 26, no. 7, pp. 1599–1609, Jul. 2018, doi: 10.1016/j.yymthe.2018.05.022.
- [81] H. D. Devalla and R. Passier, ‘Cardiac differentiation of pluripotent stem cells and implications for modeling the heart in health and disease’, *Sci. Transl. Med.*, vol. 10, no. 435, pp. 1–14, 2018, doi: 10.1126/scitranslmed.aah5457.

- [82] B. G. Bruneau, 'The developmental genetics of congenital heart disease', *Nature*, vol. 451, no. 7181, pp. 943–948, Feb. 2008, doi: 10.1038/nature06801.
- [83] L. Feulner, P. P. van Vliet, M. Puceat, and G. Andelfinger, 'Endocardial Regulation of Cardiac Development', *J. Cardiovasc. Dev. Dis.*, vol. 9, no. 5, Art. no. 5, May 2022, doi: 10.3390/jcdd9050122.
- [84] X. Qu, C. Harmelink, and H. S. Baldwin, 'Endocardial-Myocardial Interactions During Early Cardiac Differentiation and Trabeculation', *Front. Cardiovasc. Med.*, vol. 9, 2022, Accessed: Oct. 09, 2022. [Online]. Available: <https://www.frontiersin.org/articles/10.3389/fcvm.2022.857581>
- [85] L. A. Samsa, B. Yang, and J. Liu, 'Embryonic Cardiac Chamber Maturation: Trabeculation, Conduction and Cardiomyocyte Proliferation', *Am. J. Med. Genet. C Semin. Med. Genet.*, vol. 163, no. 3, pp. 157–168, Aug. 2013, doi: 10.1002/ajmg.c.31366.
- [86] J. Liu *et al.*, 'A dual role for ErbB2 signaling in cardiac trabeculation', *Dev. Camb. Engl.*, vol. 137, no. 22, pp. 3867–3875, Nov. 2010, doi: 10.1242/dev.053736.
- [87] W. T. J. Aanhaanen *et al.*, 'The Tbx2⁺ primary myocardium of the atrioventricular canal forms the atrioventricular node and the base of the left ventricle', *Circ. Res.*, vol. 104, no. 11, pp. 1267–1274, Jun. 2009, doi: 10.1161/CIRCRESAHA.108.192450.
- [88] R. G. Kelly, M. E. Buckingham, and A. F. Moorman, 'Heart Fields and Cardiac Morphogenesis', *Cold Spring Harb. Perspect. Med.*, vol. 4, no. 10, p. a015750, Jan. 2014, doi: 10.1101/cshperspect.a015750.
- [89] M. Sahara, F. Santoro, and K. R. Chien, 'Programming and reprogramming a human heart cell', *EMBO J.*, vol. 34, pp. 710–738, 2015, doi: 10.15252/embj.
- [90] M. J. Doyle, J. L. Lohr, C. S. Chapman, N. Koyano-Nakagawa, M. G. Garry, and D. J. Garry, 'Human Induced Pluripotent Stem Cell-Derived Cardiomyocytes as a Model for Heart Development and Congenital Heart Disease', *Stem Cell Rev. Rep.*, vol. 11, no. 5, pp. 710–727, Oct. 2015, doi: 10.1007/s12015-015-9596-6.
- [91] B. G. Bruneau, 'Signaling and Transcriptional Networks in Heart Development and Regeneration', *Cold Spring Harb. Perspect. Biol.*, vol. 5, no. 3, p. a008292, Mar. 2013, doi: 10.1101/cshperspect.a008292.
- [92] T. Brade, L. S. Pane, A. Moretti, K. R. Chien, and K.-L. Laugwitz, 'Embryonic Heart Progenitors and Cardiogenesis', *Cold Spring Harb. Perspect. Med.*, vol. 3, no. 10, p. a013847, Jan. 2013, doi: 10.1101/cshperspect.a013847.
- [93] J. J. H. Chong, E. Forte, and R. P. Harvey, 'Developmental origins and lineage descendants of endogenous adult cardiac progenitor cells', *Stem Cell Res.*, vol. 13, no. 3, Part B, pp. 592–614, Nov. 2014, doi: 10.1016/j.scr.2014.09.008.

- [94] M. Buckingham, S. Meilhac, and S. Zaffran, ‘Building the mammalian heart from two sources of myocardial cells’, *Nat. Rev. Genet.*, vol. 6, no. 11, pp. 826–835, Nov. 2005, doi: 10.1038/nrg1710.
- [95] J. Fujita, S. Tohyama, Y. Kishino, M. Okada, and Y. Morita, ‘Concise Review: Genetic and Epigenetic Regulation of Cardiac Differentiation from Human Pluripotent Stem Cells’, *STEM CELLS*, vol. 37, no. 8, pp. 992–1002, 2019, doi: 10.1002/stem.3027.
- [96] J. L. de la Pompa *et al.*, ‘Role of the NF-ATc transcription factor in morphogenesis of cardiac valves and septum’, *Nature*, vol. 392, no. 6672, pp. 182–186, Mar. 1998, doi: 10.1038/32419.
- [97] A. A. Mikryukov *et al.*, ‘BMP10 Signaling Promotes the Development of Endocardial Cells from Human Pluripotent Stem Cell-Derived Cardiovascular Progenitors’, *Cell Stem Cell*, vol. 28, no. 1, pp. 96-111.e7, Jan. 2021, doi: 10.1016/j.stem.2020.10.003.
- [98] B. van Wijk *et al.*, ‘Epicardium and myocardium separate from a common precursor pool by crosstalk between bone morphogenetic protein- and fibroblast growth factor-signaling pathways’, *Circ. Res.*, vol. 105, no. 5, pp. 431–441, Aug. 2009, doi: 10.1161/CIRCRESAHA.109.203083.
- [99] F. Kraus, B. Haenig, and A. Kispert, ‘Cloning and expression analysis of the mouse T-box gene *Tbx18*’, *Mech. Dev.*, vol. 100, no. 1, pp. 83–86, Jan. 2001, doi: 10.1016/S0925-4773(00)00494-9.
- [100] C.-L. Cai *et al.*, ‘A myocardial lineage derives from *Tbx18* epicardial cells’, *Nature*, vol. 454, no. 7200, p. 104, Jul. 2008, doi: 10.1038/nature06969.
- [101] B. Zhou *et al.*, ‘Epicardial progenitors contribute to the cardiomyocyte lineage in the developing heart’, *Nature*, vol. 454, no. 7200, pp. 109–113, Jul. 2008, doi: 10.1038/nature07060.
- [102] N. S. Asli, M. Xaymardan, and R. P. Harvey, ‘Epicardial Origin of Resident Mesenchymal Stem Cells in the Adult Mammalian Heart’, *J. Dev. Biol.*, vol. 2, no. 2, Art. no. 2, Jun. 2014, doi: 10.3390/jdb2020117.
- [103] M.-T. Zhao, N.-Y. Shao, and V. Garg, ‘Subtype-specific cardiomyocytes for precision medicine: Where are we now?’, *STEM CELLS*, vol. 38, no. 7, pp. 822–833, 2020, doi: 10.1002/stem.3178.
- [104] Y. Cui *et al.*, ‘Single-Cell Transcriptome Analysis Maps the Developmental Track of the Human Heart’, *Cell Rep.*, vol. 26, no. 7, pp. 1934-1950.e5, Feb. 2019, doi: 10.1016/j.celrep.2019.01.079.
- [105] C. E. Friedman *et al.*, ‘Single-Cell Transcriptomic Analysis of Cardiac Differentiation from Human PSCs Reveals HOPX-Dependent Cardiomyocyte

Maturation’, *Cell Stem Cell*, vol. 23, no. 4, pp. 586-598.e8, Oct. 2018, doi: 10.1016/j.stem.2018.09.009.

- [106] D. Yang *et al.*, ‘Modeling human multi-lineage heart field development with pluripotent stem cells’, *Cell Stem Cell*, vol. 29, no. 9, pp. 1382-1401.e8, Sep. 2022, doi: 10.1016/j.stem.2022.08.007.
- [107] K. Yamamoto *et al.*, ‘Fluid shear stress induces differentiation of Flk-1-positive embryonic stem cells into vascular endothelial cells in vitro.’, *Am. J. Physiol. Heart Circ. Physiol.*, vol. 288, no. 4, pp. H1915-24, Apr. 2005, doi: 10.1152/ajpheart.00956.2004.
- [108] M.-C. Tsai *et al.*, ‘Shear stress induces synthetic-to-contractile phenotypic modulation in smooth muscle cells via peroxisome proliferator-activated receptor alpha/delta activations by prostacyclin released by sheared endothelial cells.’, *Circ. Res.*, vol. 105, no. 5, pp. 471–80, Aug. 2009, doi: 10.1161/CIRCRESAHA.109.193656.
- [109] S. S. M. Rensen, P. a F. M. Doevendans, and G. J. J. M. van Eys, ‘Regulation and characteristics of vascular smooth muscle cell phenotypic diversity.’, *Neth. Heart J. Mon. J. Neth. Soc. Cardiol. Neth. Heart Found.*, vol. 15, no. 3, pp. 100–108, 2007, doi: 10.1007/BF03085963.
- [110] Y. Huang, X. Jia, K. Bai, X. Gong, and Y. Fan, ‘Effect of fluid shear stress on cardiomyogenic differentiation of rat bone marrow mesenchymal stem cells.’, *Arch. Med. Res.*, vol. 41, no. 7, pp. 497–505, Oct. 2010, doi: 10.1016/j.arcmed.2010.10.002.
- [111] Y. Huang *et al.*, ‘Effect of cyclic strain on cardiomyogenic differentiation of rat bone marrow derived mesenchymal stem cells.’, *PloS One*, vol. 7, no. 4, p. e34960, Jan. 2012, doi: 10.1371/journal.pone.0034960.
- [112] Y. Huang and Y. Fan, ‘Effect of Intermittent Fluid Shear Stress on Cardiomyogenic Differentiation of Rat Bone Marrow Mesenchymal Stem Cells’, *World Congr. Med. Phys. Biomed. Eng.*, pp. 1953–1956, 2013.
- [113] E. M. Redmond *et al.*, ‘Endothelial Cells Inhibit Flow-Induced Smooth Muscle Cell Migration : Role of Plasminogen Activator Inhibitor-1’, *Circulation*, vol. 103, no. 4, pp. 597–603, Jan. 2001, doi: 10.1161/01.CIR.103.4.597.
- [114] F. Colazzo *et al.*, ‘Shear stress and VEGF enhance endothelial differentiation of human adipose-derived stem cells.’, *Growth Factors Chur Switz.*, vol. 32, no. 5, pp. 139–49, Oct. 2014, doi: 10.3109/08977194.2014.945642.
- [115] E. C. James, E. Tomaskovic-Crook, and J. M. Crook, ‘Bioengineering Clinically Relevant Cardiomyocytes and Cardiac Tissues from Pluripotent Stem Cells’, *Int. J. Mol. Sci.*, vol. 22, no. 6, Art. no. 6, Jan. 2021, doi: 10.3390/ijms22063005.

- [116] A. R. Pinto *et al.*, ‘Revisiting Cardiac Cellular Composition’, *Circ. Res.*, vol. 118, no. 3, pp. 400–409, 2016, doi: 10.1161/CIRCRESAHA.115.307778.
- [117] S. Doll *et al.*, ‘Region and cell-type resolved quantitative proteomic map of the human heart’, *Nat. Commun.*, vol. 8, p. 1469, Nov. 2017, doi: 10.1038/s41467-017-01747-2.
- [118] M. Litviňuková *et al.*, ‘Cells of the adult human heart’, *Nature*, vol. 588, no. 7838, pp. 466–472, Dec. 2020, doi: 10.1038/S41586-020-2797-4.
- [119] J. Packer and C. Trapnell, ‘Single-Cell Multi-omics: An Engine for New Quantitative Models of Gene Regulation’, *Trends Genet.*, vol. 34, no. 9, pp. 653–665, Sep. 2018, doi: 10.1016/j.tig.2018.06.001.
- [120] ‘Heart Cell Atlas | Home’. <https://www.heartcellatlas.org/> (accessed Oct. 10, 2022).
- [121] G. W. Moore, G. M. Hutchins, B. H. Bulkley, J. S. Tseng, and P. F. Ki, ‘Constituents of the human ventricular myocardium: Connective tissue hyperplasia accompanying muscular hypertrophy’, *Am. Heart J.*, vol. 100, no. 5, pp. 610–616, Nov. 1980, doi: 10.1016/0002-8703(80)90224-0.
- [122] H. W. VLIEGEN, A. VAN DER LAARSE, C. J. CORNELISSE, and F. EULDERINK, ‘Myocardial changes in pressure overload-induced left ventricular hypertrophy: A study on tissue composition, polyploidization and multinucleation’, *Eur. Heart J.*, vol. 12, no. 4, pp. 488–494, Apr. 1991, doi: 10.1093/oxfordjournals.eurheartj.a059928.
- [123] O. Bergmann *et al.*, ‘Dynamics of Cell Generation and Turnover in the Human Heart’, *Cell*, vol. 161, no. 7, 2015, doi: 10.1016/j.cell.2015.05.026.
- [124] P. Zhou and W. T. Pu, ‘Recounting cardiac cellular composition’, *Circ. Res.*, vol. 118, no. 3, p. 368, 2016, doi: 10.1161/CIRCRESAHA.116.308139.
- [125] C. A. Henderson, C. G. Gomez, S. M. Novak, L. Mi-Mi, and C. C. Gregorio, ‘Overview of the Muscle Cytoskeleton’, *Compr. Physiol.*, vol. 7, no. 3, pp. 891–944, Jun. 2017, doi: 10.1002/cphy.c160033.
- [126] M. Gautel and K. Djinović-Carugo, ‘The sarcomeric cytoskeleton: from molecules to motion’, *J. Exp. Biol.*, vol. 219, no. 2, pp. 135–145, Jan. 2016, doi: 10.1242/jeb.124941.
- [127] R. Bassel-Duby and E. N. Olson, ‘Biochemistry of Development: Striated Muscle’, in *Encyclopedia of Biological Chemistry*, Elsevier, 2013, pp. 179–186. doi: 10.1016/B978-0-12-378630-2.00091-8.
- [128] Y. Guo and W. T. Pu, ‘Cardiomyocyte Maturation’, *Circ. Res.*, vol. 126, no. 8, pp. 1086–1106, Apr. 2020, doi: 10.1161/CIRCRESAHA.119.315862.

- [129] P. P. de Tombe, 'Cardiac myofilaments: mechanics and regulation', *J. Biomech.*, vol. 36, no. 5, pp. 721–730, May 2003, doi: 10.1016/S0021-9290(02)00450-5.
- [130] F. Z. Asumda and P. B. Chase, 'Nuclear cardiac troponin and tropomyosin are expressed early in cardiac differentiation of rat mesenchymal stem cells.', *Differ. Res. Biol. Divers.*, vol. 83, no. 3, pp. 106–15, Mar. 2012, doi: 10.1016/j.diff.2011.10.002.
- [131] T. Hong and R. M. Shaw, 'Cardiac T-Tubule Microanatomy and Function', *Physiol. Rev.*, vol. 97, no. 1, pp. 227–252, Jan. 2017, doi: 10.1152/physrev.00037.2015.
- [132] J. J. Smolich, 'Ultrastructural and functional features of the developing mammalian heart: a brief overview', *Reprod. Fertil. Dev.*, vol. 7, no. 3, pp. 451–461, 1995, doi: 10.1071/rd9950451.
- [133] P. S. Haddock *et al.*, 'Subcellular [Ca²⁺]_i Gradients During Excitation-Contraction Coupling in Newborn Rabbit Ventricular Myocytes', *Circ. Res.*, vol. 85, no. 5, pp. 415–427, Sep. 1999, doi: 10.1161/01.RES.85.5.415.
- [134] F. Brette and C. Orchard, 'T-Tubule Function in Mammalian Cardiac Myocytes', *Circ. Res.*, vol. 92, no. 11, pp. 1182–1192, Jun. 2003, doi: 10.1161/01.RES.0000074908.17214.FD.
- [135] M. Ibrahim, J. Gorelik, M. H. Yacoub, and C. M. Terracciano, 'The structure and function of cardiac t-tubules in health and disease', *Proc. R. Soc. B Biol. Sci.*, vol. 278, no. 1719, pp. 2714–2723, Sep. 2011, doi: 10.1098/rspb.2011.0624.
- [136] E. Page, 'Quantitative ultrastructural analysis in cardiac membrane physiology', *Am. J. Physiol.-Cell Physiol.*, vol. 235, no. 5, pp. C147–C158, Nov. 1978, doi: 10.1152/ajpcell.1978.235.5.C147.
- [137] J. M. Cordeiro, K. W. Spitzer, W. R. Giles, P. E. Ershler, M. B. Cannell, and J. H. B. Bridge, 'Location of the initiation site of calcium transients and sparks in rabbit heart Purkinje cells', *J. Physiol.*, vol. 531, no. 2, pp. 301–314, 2001, doi: 10.1111/j.1469-7793.2001.0301i.x.
- [138] J. S. Mitcheson, J. C. Hancox, and A. J. Levi, 'Action potentials, ion channel currents and transverse tubule density in adult rabbit ventricular myocytes maintained for 6 days in cell culture', *Pflüg. Arch.*, vol. 431, no. 6, pp. 814–827, Jun. 1996, doi: 10.1007/s004240050073.
- [139] P. Lipp, J. Hüser, L. Pott, and E. Niggli, 'Spatially non-uniform Ca²⁺ signals induced by the reduction of transverse tubules in citrate-loaded guinea-pig ventricular myocytes in culture.', *J. Physiol.*, vol. 497, no. 3, pp. 589–597, 1996, doi: 10.1113/jphysiol.1996.sp021792.

- [140] X. Yang, L. Pabon, and C. E. Murry, ‘Engineering adolescence: maturation of human pluripotent stem cell-derived cardiomyocytes.’, *Circ. Res.*, vol. 114, no. 3, pp. 511–523, Jan. 2014, doi: 10.1161/CIRCRESAHA.114.300558.
- [141] N. Anto Michel, S. Ljubojevic-Holzer, H. Bugger, and A. Zirlik, ‘Cellular Heterogeneity of the Heart’, *Front. Cardiovasc. Med.*, vol. 9, no. April, p. 918, Apr. 2022, doi: 10.3389/FCVM.2022.868466.
- [142] X. H. Zhang, H. Wei, T. Šarić, J. Hescheler, L. Cleemann, and M. Morad, ‘Regionally diverse mitochondrial calcium signaling regulates spontaneous pacing in developing cardiomyocytes’, *Cell Calcium*, vol. 57, no. 0, p. 321, May 2015, doi: 10.1016/J.CECA.2015.02.003.
- [143] E. Karbassi *et al.*, ‘Cardiomyocyte maturation: advances in knowledge and implications for regenerative medicine’, *Nat. Rev. Cardiol.*, vol. 17, no. 6, p. 341, Jun. 2020, doi: 10.1038/S41569-019-0331-X.
- [144] S. Marchianò, A. Bertero, and C. E. Murry, ‘Learn from Your Elders: Developmental Biology Lessons to Guide Maturation of Stem Cell-Derived Cardiomyocytes’, *Pediatr. Cardiol.*, vol. 40, no. 7, pp. 1367–1387, Oct. 2019, doi: 10.1007/s00246-019-02165-5.
- [145] P. J. Reiser, M. A. Portman, X.-H. Ning, and C. S. Moravec, ‘Human cardiac myosin heavy chain isoforms in fetal and failing adult atria and ventricles’, *Am. J. Physiol.-Heart Circ. Physiol.*, vol. 280, no. 4, pp. H1814–H1820, Apr. 2001, doi: 10.1152/ajpheart.2001.280.4.H1814.
- [146] A. Selewa *et al.*, ‘Systematic Comparison of High-throughput Single-Cell and Single-Nucleus Transcriptomes during Cardiomyocyte Differentiation’, *Sci. Rep.*, vol. 10, no. 1, Art. no. 1, Jan. 2020, doi: 10.1038/s41598-020-58327-6.
- [147] Y. Guo *et al.*, ‘Hierarchical and stage-specific regulation of murine cardiomyocyte maturation by serum response factor’, *Nat. Commun.*, vol. 9, no. 1, Art. no. 1, Sep. 2018, doi: 10.1038/s41467-018-06347-2.
- [148] S. W. Kubalak, W. C. Miller-Hance, T. X. O’Brien, E. Dyson, and K. R. Chien, ‘Chamber specification of atrial myosin light chain-2 expression precedes septation during murine cardiogenesis’, *J. Biol. Chem.*, vol. 269, no. 24, pp. 16961–16970, Jun. 1994, doi: 10.1016/S0021-9258(19)89483-8.
- [149] T. X. O’Brien, K. J. Lee, and K. R. Chien, ‘Positional specification of ventricular myosin light chain 2 expression in the primitive murine heart tube.’, *Proc. Natl. Acad. Sci.*, vol. 90, no. 11, pp. 5157–5161, Jun. 1993, doi: 10.1073/pnas.90.11.5157.
- [150] F. B. Bedada *et al.*, ‘Acquisition of a Quantitative, Stoichiometrically Conserved Ratiometric Marker of Maturation Status in Stem Cell-Derived Cardiac Myocytes’,

Stem Cell Rep., vol. 3, no. 4, pp. 594–605, Oct. 2014, doi: 10.1016/j.stemcr.2014.07.012.

- [151] S. Lahmers, Y. Wu, D. R. Call, S. Labeit, and H. Granzier, ‘Developmental Control of Titin Isoform Expression and Passive Stiffness in Fetal and Neonatal Myocardium’, *Circ. Res.*, vol. 94, no. 4, pp. 505–513, Mar. 2004, doi: 10.1161/01.RES.0000115522.52554.86.
- [152] C. J. Weeland, M. M. van den Hoogenhof, A. Beqqali, and E. E. Creemers, ‘Insights into alternative splicing of sarcomeric genes in the heart’, *J. Mol. Cell. Cardiol.*, vol. 81, pp. 107–113, Apr. 2015, doi: 10.1016/j.yjmcc.2015.02.008.
- [153] N. Kapoor, W. Liang, E. Marbán, and H. C. Cho, ‘Direct conversion of quiescent cardiomyocytes to pacemaker cells by expression of Tbx18.’, *Nat. Biotechnol.*, vol. 31, no. 1, pp. 54–62, Jan. 2013, doi: 10.1038/nbt.2465.
- [154] A. Mihic *et al.*, ‘The effect of cyclic stretch on maturation and 3D tissue formation of human embryonic stem cell-derived cardiomyocytes.’, *Biomaterials*, vol. 35, no. 9, pp. 2798–808, Mar. 2014, doi: 10.1016/j.biomaterials.2013.12.052.
- [155] G. D. Lopaschuk and J. S. Jaswal, ‘Energy metabolic phenotype of the cardiomyocyte during development, differentiation, and postnatal maturation.’, *J. Cardiovasc. Pharmacol.*, vol. 56, no. 2, pp. 130–40, Aug. 2010, doi: 10.1097/FJC.0b013e3181e74a14.
- [156] H.-D. Kim, C. H. Kim, B.-J. Rah, H.-I. Chung, and T.-S. Shim, ‘Quantitative study on the relation between structural and functional properties of the hearts from three different mammals’, *Anat. Rec.*, vol. 238, no. 2, pp. 199–206, 1994, doi: 10.1002/ar.1092380206.
- [157] J. Piquereau *et al.*, ‘Mitochondrial dynamics in the adult cardiomyocytes: which roles for a highly specialized cell?’, *Front. Physiol.*, vol. 4, p. 102, May 2013, doi: 10.3389/fphys.2013.00102.
- [158] Y. Guo and W. T. Pu, ‘Cardiomyocyte Maturation’, *Circ. Res.*, pp. 1086–1106, Apr. 2020, doi: 10.1161/CIRCRESAHA.119.315862.
- [159] J. Schaper, E. Meiser, and Stammeler, ‘Ultrastructural morphometric analysis of myocardium from dogs, rats, hamsters, mice, and from human hearts’, *Circ. Res.*, vol. 56, no. 3, pp. 377–391, 1985, doi: 10.1161/01.RES.56.3.377.
- [160] H. Uosaki *et al.*, ‘Transcriptional Landscape of Cardiomyocyte Maturation’, *Cell Rep.*, vol. 13, no. 8, pp. 1705–1716, Nov. 2015, doi: 10.1016/j.celrep.2015.10.032.
- [161] C. B. Sim *et al.*, ‘Dynamic changes in the cardiac methylome during postnatal development’, *FASEB J.*, vol. 29, no. 4, pp. 1329–1343, 2015, doi: 10.1096/fj.14-264093.

- [162] D. M. DeLaughter *et al.*, ‘Single-Cell Resolution of Temporal Gene Expression during Heart Development’, *Dev. Cell*, vol. 39, no. 4, pp. 480–490, Nov. 2016, doi: 10.1016/j.devcel.2016.10.001.
- [163] D. A. M. Feyen *et al.*, ‘Metabolic Maturation Media Improve Physiological Function of Human iPSC-Derived Cardiomyocytes’, *Cell Rep.*, vol. 32, no. 3, p. 107925, Jul. 2020, doi: 10.1016/J.CELREP.2020.107925/ATTACHMENT/84AE3F74-4D9C-43FD-8529-5FCDA4D596E7/MMC1.PDF.
- [164] V. Lionetti, W. C. Stanley, and F. A. Recchia, ‘Modulating fatty acid oxidation in heart failure’, *Cardiovasc. Res.*, vol. 90, no. 2, p. 202, May 2011, doi: 10.1093/CVR/CVR038.
- [165] B. Bhana *et al.*, ‘Influence of substrate stiffness on the phenotype of heart cells’, *Biotechnol. Bioeng.*, vol. 105, no. 6, pp. 1148–1160, 2010, doi: 10.1002/bit.22647.
- [166] V. Y. Brodsky, A. M. Arefyeva, I. G. Gvasava, D. S. Sarkisov, and N. W. Panova, ‘Polyploidy in cardiac myocytes of normal and hypertrophic human hearts; range of values’, *Virchows Arch.*, vol. 424, no. 4, pp. 429–435, May 1994, doi: 10.1007/BF00190566.
- [167] G. Olivetti *et al.*, ‘Aging, Cardiac Hypertrophy and Ischemic Cardiomyopathy Do Not Affect the Proportion of Mononucleated and Multinucleated Myocytes in the Human Heart’, *J. Mol. Cell. Cardiol.*, vol. 28, no. 7, pp. 1463–1477, Jul. 1996, doi: 10.1006/jmcc.1996.0137.
- [168] O. Bergmann *et al.*, ‘Dynamics of Cell Generation and Turnover in the Human Heart’, *Cell*, vol. 161, no. 7, pp. 1566–1575, Jun. 2015, doi: 10.1016/j.cell.2015.05.026.
- [169] D. Zhang *et al.*, ‘Mitochondrial Cardiomyopathy Caused by Elevated Reactive Oxygen Species and Impaired Cardiomyocyte Proliferation’, *Circ. Res.*, vol. 122, no. 1, pp. 74–87, Jan. 2018, doi: 10.1161/CIRCRESAHA.117.311349.
- [170] B. N. Puente *et al.*, ‘The oxygen-rich postnatal environment induces cardiomyocyte cell-cycle arrest through DNA damage response.’, *Cell*, vol. 157, no. 3, pp. 565–79, Apr. 2014, doi: 10.1016/j.cell.2014.03.032.
- [171] K. Bersell, S. Arab, B. Haring, and B. Kühn, ‘Neuregulin1/ErbB4 Signaling Induces Cardiomyocyte Proliferation and Repair of Heart Injury’, *Cell*, vol. 138, no. 2, pp. 257–270, Jul. 2009, doi: 10.1016/j.cell.2009.04.060.
- [172] T. Heallen *et al.*, ‘Hippo signaling impedes adult heart regeneration’, *Development*, vol. 140, no. 23, pp. 4683–4690, Dec. 2013, doi: 10.1242/dev.102798.
- [173] T. Heallen *et al.*, ‘Hippo Pathway Inhibits Wnt Signaling to Restrain Cardiomyocyte Proliferation and Heart Size’, *Science*, vol. 332, no. 6028, pp. 458–461, Apr. 2011, doi: 10.1126/science.1199010.

- [174] A. von Gise *et al.*, ‘YAP1, the nuclear target of Hippo signaling, stimulates heart growth through cardiomyocyte proliferation but not hypertrophy’, *Proc. Natl. Acad. Sci.*, vol. 109, no. 7, pp. 2394–2399, Feb. 2012, doi: 10.1073/pnas.1116136109.
- [175] D. Mosqueira *et al.*, ‘Hippo Pathway Effectors Control Cardiac Progenitor Cell Fate by Acting as Dynamic Sensors of Substrate Mechanics and Nanostructure’, *ACS Nano*, vol. 8, no. 3, pp. 2033–2047, Mar. 2014, doi: 10.1021/nn4058984.
- [176] F. Martino, A. R. Perestrelo, V. Vinarský, S. Pagliari, and G. Forte, ‘Cellular Mechanotransduction: From Tension to Function’, *Front. Physiol.*, vol. 9, 2018, Accessed: Nov. 07, 2022. [Online]. Available: <https://www.frontiersin.org/articles/10.3389/fphys.2018.00824>
- [177] G. Nardone *et al.*, ‘YAP regulates cell mechanics by controlling focal adhesion assembly’, *Nat. Commun.*, vol. 8, no. 1, Art. no. 1, May 2017, doi: 10.1038/ncomms15321.
- [178] M. Günthel, P. Barnett, and V. M. Christoffels, ‘Development, Proliferation, and Growth of the Mammalian Heart’, *Mol. Ther.*, vol. 26, no. 7, pp. 1599–1609, Jul. 2018, doi: 10.1016/j.yymthe.2018.05.022.
- [179] S. Liu and J. F. Martin, ‘The regulation and function of the Hippo pathway in heart regeneration’, *WIREs Dev. Biol.*, vol. 8, no. 1, Jan. 2019, doi: 10.1002/wdev.335.
- [180] J. Wang, S. Liu, T. Heallen, and J. F. Martin, ‘The Hippo pathway in the heart: pivotal roles in development, disease, and regeneration’, *Nat. Rev. Cardiol.*, vol. 15, no. 11, pp. 672–684, Nov. 2018, doi: 10.1038/s41569-018-0063-3.
- [181] A. A. Gibb, M. P. Lazaropoulos, and J. W. Elrod, ‘Myofibroblasts and Fibrosis’, *Circ. Res.*, vol. 127, no. 3, pp. 427–447, Jul. 2020, doi: 10.1161/CIRCRESAHA.120.316958.
- [182] A. R. Perestrelo *et al.*, ‘Multiscale Analysis of Extracellular Matrix Remodeling in the Failing Heart’, *Circ. Res.*, vol. 128, pp. 24–38, Jan. 2021, doi: 10.1161/CIRCRESAHA.120.317685.
- [183] C. Hall, K. Gehmlich, C. Denning, and D. Pavlovic, ‘Complex Relationship Between Cardiac Fibroblasts and Cardiomyocytes in Health and Disease’, *J. Am. Heart Assoc.*, vol. 10, no. 5, p. e019338, Mar. 2021, doi: 10.1161/JAHA.120.019338.
- [184] C. Humeres and N. G. Frangogiannis, ‘Fibroblasts in the Infarcted, Remodeling, and Failing Heart’, *JACC Basic Transl. Sci.*, vol. 4, no. 3, pp. 449–467, Jun. 2019, doi: 10.1016/j.jacbts.2019.02.006.
- [185] G. Gaudesius, M. Miragoli, S. P. Thomas, and S. Rohr, ‘Coupling of Cardiac Electrical Activity Over Extended Distances by Fibroblasts of Cardiac Origin’, *Circ.*

Res., vol. 93, no. 5, pp. 421–428, Sep. 2003, doi: 10.1161/01.RES.0000089258.40661.0C.

- [186] E. Kizana *et al.*, ‘Fibroblasts modulate cardiomyocyte excitability: implications for cardiac gene therapy’, *Gene Ther.*, vol. 13, no. 22, Art. no. 22, Nov. 2006, doi: 10.1038/sj.gt.3302813.
- [187] A. Hussain, G. Collins, D. Yip, and C. H. Cho, ‘Functional 3-D cardiac co-culture model using bioactive chitosan nanofiber scaffolds’, *Biotechnol. Bioeng.*, vol. 110, no. 2, pp. 637–647, 2013, doi: 10.1002/bit.24727.
- [188] P. Kohl and R. G. Gourdie, ‘Fibroblast–myocyte electrotonic coupling: Does it occur in native cardiac tissue?’, *J. Mol. Cell. Cardiol.*, vol. 70, pp. 37–46, May 2014, doi: 10.1016/j.yjmcc.2013.12.024.
- [189] M. Eghbali *et al.*, ‘Collagen chain mRNAs in isolated heart cells from young and adult rats’, *J. Mol. Cell. Cardiol.*, vol. 20, no. 3, pp. 267–276, Mar. 1988, doi: 10.1016/S0022-2828(88)80059-2.
- [190] W. Chen, W. Bian, Y. Zhou, and J. Zhang, ‘Cardiac Fibroblasts and Myocardial Regeneration’, *Front. Bioeng. Biotechnol.*, vol. 9, 2021, Accessed: Oct. 19, 2022. [Online]. Available: <https://www.frontiersin.org/articles/10.3389/fbioe.2021.599928>
- [191] N. R. Tucker *et al.*, ‘Transcriptional and Cellular Diversity of the Human Heart’, *Circulation*, vol. 142, no. 5, pp. 466–482, Aug. 2020, doi: 10.1161/CIRCULATIONAHA.119.045401.
- [192] L. Wang *et al.*, ‘Single-cell reconstruction of the adult human heart during heart failure and recovery reveals the cellular landscape underlying cardiac function’, *Nat. Cell Biol.*, vol. 22, no. 1, Art. no. 1, Jan. 2020, doi: 10.1038/s41556-019-0446-7.
- [193] C. K. Nagaraju *et al.*, ‘Myofibroblast Phenotype and Reversibility of Fibrosis in Patients With End-Stage Heart Failure’, *J. Am. Coll. Cardiol.*, vol. 73, no. 18, pp. 2267–2282, May 2019, doi: 10.1016/j.jacc.2019.02.049.
- [194] S. Sridhar, N. Vandersickel, and A. V. Panfilov, ‘Effect of myocyte-fibroblast coupling on the onset of pathological dynamics in a model of ventricular tissue’, *Sci. Rep.*, vol. 7, no. 1, Art. no. 1, Jan. 2017, doi: 10.1038/srep40985.
- [195] C. M. Braitsch, O. Kanisicak, J. H. van Berlo, J. D. Molkenin, and K. E. Yutzey, ‘Differential expression of embryonic epicardial progenitor markers and localization of cardiac fibrosis in adult ischemic injury and hypertensive heart disease’, *J. Mol. Cell. Cardiol.*, vol. 65, p. 10.1016/j.yjmcc.2013.10.005, Dec. 2013, doi: 10.1016/j.yjmcc.2013.10.005.
- [196] O. Kanisicak *et al.*, ‘Genetic lineage tracing defines myofibroblast origin and function in the injured heart’, *Nat. Commun.*, vol. 7, p. 12260, Jul. 2016, doi: 10.1038/ncomms12260.

- [197] C. L. Smith, S. T. Baek, C. Y. Sung, and M. D. Tallquist, ‘Epicardial-derived cell epithelial-to-mesenchymal transition and fate specification require PDGF receptor signaling’, *Circ. Res.*, vol. 108, no. 12, pp. e15-26, Jun. 2011, doi: 10.1161/CIRCRESAHA.110.235531.
- [198] A. Acharya *et al.*, ‘The bHLH transcription factor Tcf21 is required for lineage-specific EMT of cardiac fibroblast progenitors’, *Dev. Camb. Engl.*, vol. 139, no. 12, pp. 2139–2149, Jun. 2012, doi: 10.1242/dev.079970.
- [199] P. Kong, P. Christia, A. Saxena, Y. Su, and N. G. Frangogiannis, ‘Lack of specificity of fibroblast-specific protein 1 in cardiac remodeling and fibrosis’, *Am. J. Physiol.-Heart Circ. Physiol.*, vol. 305, no. 9, pp. H1363–H1372, Nov. 2013, doi: 10.1152/ajpheart.00395.2013.
- [200] M. E. Floy *et al.*, ‘Developmental lineage of human pluripotent stem cell-derived cardiac fibroblasts affects their functional phenotype’, *FASEB J.*, vol. 35, no. 9, p. e21799, 2021, doi: <https://doi.org/10.1096/fj.202100523R>.
- [201] T. Goodpaster, A. Legesse-Miller, M. R. Hameed, S. C. Aisner, J. Randolph-Habecker, and H. A. Collier, ‘An Immunohistochemical Method for Identifying Fibroblasts in Formalin-fixed, Paraffin-embedded Tissue’, *J. Histochem. Cytochem.*, vol. 56, no. 4, pp. 347–358, Apr. 2008, doi: 10.1369/jhc.7A7287.2007.
- [202] A. J. Whitehead, J. D. Hocker, B. Ren, and A. J. Engler, ‘Improved epicardial cardiac fibroblast generation from iPSCs’, *J. Mol. Cell. Cardiol.*, vol. 164, pp. 58–68, Mar. 2022, doi: 10.1016/j.yjmcc.2021.11.011.
- [203] J. Zhang *et al.*, ‘Functional cardiac fibroblasts derived from human pluripotent stem cells via second heart field progenitors’, *Nat. Commun.*, vol. 10, no. 1, Art. no. 1, May 2019, doi: 10.1038/s41467-019-09831-5.
- [204] M. J. Ivey and M. D. Tallquist, ‘Defining the Cardiac Fibroblast’, *Circ. J. Off. J. Jpn. Circ. Soc.*, vol. 80, no. 11, pp. 2269–2276, Oct. 2016, doi: 10.1253/circj.CJ-16-1003.
- [205] K. M. Herum, J. Choppe, A. Kumar, A. J. Engler, and A. D. McCulloch, ‘Mechanical regulation of cardiac fibroblast profibrotic phenotypes’, *Mol. Biol. Cell*, vol. 28, no. 14, pp. 1871–1882, Jul. 2017, doi: 10.1091/mbc.e17-01-0014.
- [206] Y. Ma, R. P. Iyer, M. Jung, M. P. Czubryt, and M. L. Lindsey, ‘Cardiac Fibroblast Activation Post-Myocardial Infarction: Current Knowledge Gaps’, *Trends Pharmacol. Sci.*, vol. 38, no. 5, pp. 448–458, May 2017, doi: 10.1016/j.tips.2017.03.001.
- [207] A. V. Shinde and N. G. Frangogiannis, ‘Fibroblasts in myocardial infarction: a role in inflammation and repair’, *J. Mol. Cell. Cardiol.*, vol. 70, pp. 74–82, May 2014, doi: 10.1016/j.yjmcc.2013.11.015.

- [208] C. K. Nagaraju *et al.*, ‘Myofibroblast modulation of cardiac myocyte structure and function’, *Sci. Rep.*, vol. 9, no. 1, Art. no. 1, Jun. 2019, doi: 10.1038/s41598-019-45078-2.
- [209] W. A. Border and N. A. Noble, ‘Interactions of Transforming Growth Factor- β and Angiotensin II in Renal Fibrosis’, *Hypertension*, vol. 31, no. 1, pp. 181–188, Jan. 1998, doi: 10.1161/01.HYP.31.1.181.
- [210] S. Rosenkranz, ‘TGF- β 1 and angiotensin networking in cardiac remodeling’, *Cardiovasc. Res.*, vol. 63, no. 3, pp. 423–432, Aug. 2004, doi: 10.1016/j.cardiores.2004.04.030.
- [211] H. Kawano *et al.*, ‘Angiotensin II Has Multiple Profibrotic Effects in Human Cardiac Fibroblasts’, *Circulation*, vol. 101, no. 10, pp. 1130–1137, Mar. 2000, doi: 10.1161/01.CIR.101.10.1130.
- [212] J. M. Schnee and W. A. Hsueh, ‘Angiotensin II, adhesion, and cardiac fibrosis’, *Cardiovasc. Res.*, vol. 46, no. 2, pp. 264–268, May 2000, doi: 10.1016/S0008-6363(00)00044-4.
- [213] H. Khalil *et al.*, ‘Fibroblast-specific TGF- β –Smad2/3 signaling underlies cardiac fibrosis’, *J. Clin. Invest.*, vol. 127, no. 10, pp. 3770–3783, Oct. 2017, doi: 10.1172/JCI94753.
- [214] V. Talman and H. Ruskoaho, ‘Cardiac fibrosis in myocardial infarction—from repair and remodeling to regeneration’, *Cell Tissue Res.*, vol. 365, no. 3, pp. 563–581, Sep. 2016, doi: 10.1007/s00441-016-2431-9.
- [215] D. T. Nguyen, N. Nagarajan, and P. Zorlutuna, ‘Effect of Substrate Stiffness on Mechanical Coupling and Force Propagation at the Infarct Boundary’, *Biophys. J.*, vol. 115, no. 10, pp. 1966–1980, Nov. 2018, doi: 10.1016/j.bpj.2018.08.050.
- [216] R. Emig *et al.*, ‘Human Atrial Fibroblast Adaptation to Heterogeneities in Substrate Stiffness’, *Front. Physiol.*, vol. 10, 2020, Accessed: Oct. 20, 2022. [Online]. Available: <https://www.frontiersin.org/articles/10.3389/fphys.2019.01526>
- [217] P. Kollmannsberger, C. M. Bidan, J. W. C. Dunlop, P. Fratzl, and V. Vogel, ‘Tensile forces drive a reversible fibroblast-to-myofibroblast transition during tissue growth in engineered clefts’, *Sci. Adv.*, vol. 4, no. 1, p. eaao4881, Jan. 2018, doi: 10.1126/sciadv.aao4881.
- [218] N. G. Frangogiannis, ‘Cardiac fibrosis: Cell biological mechanisms, molecular pathways and therapeutic opportunities’, *Mol. Aspects Med.*, vol. 65, pp. 70–99, Feb. 2019, doi: 10.1016/j.mam.2018.07.001.
- [219] P. C. H. Hsieh, M. E. Davis, L. K. Lisowski, and R. T. Lee, ‘Endothelial-Cardiomyocyte Interactions in Cardiac Development and Repair’, *Annu. Rev. Physiol.*, vol. 68, pp. 51–66, 2006, doi: 10.1146/annurev.physiol.68.040104.124629.

- [220] A. Colliva, L. Braga, M. Giacca, and S. Zacchigna, ‘Endothelial cell–cardiomyocyte crosstalk in heart development and disease’, *J. Physiol.*, vol. 598, no. 14, pp. 2923–2939, 2020, doi: 10.1113/JP276758.
- [221] A. Lother, S. Bergemann, L. Deng, M. Moser, C. Bode, and L. Hein, ‘Cardiac Endothelial Cell Transcriptome’, *Arterioscler. Thromb. Vasc. Biol.*, vol. 38, no. 3, pp. 566–574, Mar. 2018, doi: 10.1161/ATVBAHA.117.310549.
- [222] Y. Ishii, J. Langberg, K. Rosborough, and T. Mikawa, ‘Endothelial cell lineages of the heart’, *Cell Tissue Res.*, vol. 335, no. 1, pp. 67–73, Jan. 2009, doi: 10.1007/s00441-008-0663-z.
- [223] M. Wolfien *et al.*, ‘Single nuclei sequencing of entire mammalian hearts: strain-dependent cell-type composition and velocity’, *Cardiovasc. Res.*, vol. 116, no. 7, pp. 1249–1251, Jun. 2020, doi: 10.1093/cvr/cvaa054.
- [224] L. Zhuang, L. Lu, R. Zhang, K. Chen, and X. Yan, ‘Comprehensive Integration of Single-Cell Transcriptional Profiling Reveals the Heterogeneities of Non-cardiomyocytes in Healthy and Ischemic Hearts’, *Front. Cardiovasc. Med.*, vol. 7, 2020, Accessed: Oct. 29, 2022. [Online]. Available: <https://www.frontiersin.org/articles/10.3389/fcvm.2020.615161>
- [225] X. Shi *et al.*, ‘Integrative Analysis of Bulk and Single-Cell RNA Sequencing Data Reveals Cell Types Involved in Heart Failure’, *Front. Bioeng. Biotechnol.*, vol. 9, 2022, Accessed: Oct. 29, 2022. [Online]. Available: <https://www.frontiersin.org/articles/10.3389/fbioe.2021.779225>
- [226] E. Forte *et al.*, ‘Dynamic Interstitial Cell Response during Myocardial Infarction Predicts Resilience to Rupture in Genetically Diverse Mice’, *Cell Rep.*, vol. 30, no. 9, pp. 3149–3163.e6, Mar. 2020, doi: 10.1016/j.celrep.2020.02.008.
- [227] K. L. Du *et al.*, ‘Myocardin is a critical serum response factor cofactor in the transcriptional program regulating smooth muscle cell differentiation.’, *Mol. Cell. Biol.*, vol. 23, no. 7, pp. 2425–37, Apr. 2003.
- [228] X. Long, R. D. Bell, W. T. Gerthoffer, B. V. Zlokovic, and J. M. Miano, ‘Myocardin is sufficient for a smooth muscle-like contractile phenotype’, *Arterioscler. Thromb. Vasc. Biol.*, vol. 28, no. 8, pp. 1505–1510, 2008, doi: 10.1161/ATVBAHA.108.166066.
- [229] Z. Wang, D.-Z. Wang, G. C. T. Pipes, and E. N. Olson, ‘Myocardin is a master regulator of smooth muscle gene expression.’, *Proc. Natl. Acad. Sci. U. S. A.*, vol. 100, no. 12, pp. 7129–7134, 2003, doi: 10.1073/pnas.1232341100.
- [230] X. Guo and S.-Y. Chen, ‘Transforming growth factor- β and smooth muscle differentiation.’, *World J. Biol. Chem.*, vol. 3, no. 3, pp. 41–52, 2012, doi: 10.4331/wjbc.v3.i3.41.

- [231] C. P. Mack, ‘Signaling mechanisms that regulate smooth muscle cell differentiation.’, *Arterioscler. Thromb. Vasc. Biol.*, vol. 31, no. 7, pp. 1495–505, Jul. 2011, doi: 10.1161/ATVBAHA.110.221135.
- [232] S. Kajioka *et al.*, ‘Endogenous cardiac troponin T modulates Ca(2+)-mediated smooth muscle contraction.’, *Sci. Rep.*, vol. 2, p. 979, 2012, doi: 10.1038/srep00979.
- [233] J. A. Beamish, P. He, K. Kottke-Marchant, and R. E. Marchant, ‘Molecular regulation of contractile smooth muscle cell phenotype: implications for vascular tissue engineering.’, *Tissue Eng. Part B Rev.*, vol. 16, no. 5, pp. 467–91, Oct. 2010, doi: 10.1089/ten.TEB.2009.0630.
- [234] E. Tanai and S. Frantz, ‘Pathophysiology of Heart Failure’, *Compr. Physiol.*, vol. 6, no. 1, pp. 187–214, Dec. 2015, doi: 10.1002/cphy.c140055.
- [235] L. Lu, M. Liu, R. Sun, Y. Zheng, and P. Zhang, ‘Myocardial Infarction: Symptoms and Treatments’, *Cell Biochem. Biophys.*, vol. 72, no. 3, pp. 865–867, Jul. 2015, doi: 10.1007/s12013-015-0553-4.
- [236] K. Chan, A. Harper, H. Ashrafian, and A. Yavari, ‘Cardiomyopathies’, *Medicine (Baltimore)*, vol. 46, no. 10, 2018, Accessed: Nov. 12, 2022. [Online]. Available: <https://ora.ox.ac.uk/objects/uuid:5c0f5498-fc75-4547-bb02-bf67b22908b1>
- [237] E. Braunwald, ‘Cardiomyopathies: An Overview’, *Circ. Res.*, vol. 121, no. 7, pp. 711–721, Sep. 2017, doi: 10.1161/CIRCRESAHA.117.311812.
- [238] M. Cassani, S. Fernandes, J. Vrbsky, E. Ergir, F. Cavalieri, and G. Forte, ‘Combining Nanomaterials and Developmental Pathways to Design New Treatments for Cardiac Regeneration: The Pulsing Heart of Advanced Therapies’, *Front. Bioeng. Biotechnol.*, vol. 8, Apr. 2020, doi: 10.3389/FBIOE.2020.00323/PDF.
- [239] A. A. Alfares *et al.*, ‘Results of clinical genetic testing of 2,912 probands with hypertrophic cardiomyopathy: expanded panels offer limited additional sensitivity’, *Genet. Med. Off. J. Am. Coll. Med. Genet.*, vol. 17, no. 11, pp. 880–888, Nov. 2015, doi: 10.1038/gim.2014.205.
- [240] H. G. van Velzen *et al.*, ‘Outcomes of Contemporary Family Screening in Hypertrophic Cardiomyopathy’, *Circ. Genomic Precis. Med.*, vol. 11, no. 4, p. e001896, Apr. 2018, doi: 10.1161/CIRCGEN.117.001896.
- [241] F. Mazzarotto *et al.*, ‘Defining the diagnostic effectiveness of genes for inclusion in panels: the experience of two decades of genetic testing for hypertrophic cardiomyopathy at a single center’, *Genet. Med.*, vol. 21, no. 2, pp. 284–292, 2019, doi: 10.1038/s41436-018-0046-0.
- [242] L. R. Lopes *et al.*, ‘Novel genotype-phenotype associations demonstrated by high-throughput sequencing in patients with hypertrophic cardiomyopathy’, *Heart Br.*

Card. Soc., vol. 101, no. 4, pp. 294–301, Feb. 2015, doi: 10.1136/heartjnl-2014-306387.

- [243] R. E. Hershberger, D. J. Hedges, and A. Morales, ‘Dilated cardiomyopathy: the complexity of a diverse genetic architecture’, *Nat. Rev. Cardiol.*, vol. 10, no. 9, pp. 531–547, Sep. 2013, doi: 10.1038/nrcardio.2013.105.
- [244] T. J. Cahill, H. Ashrafian, and H. Watkins, ‘Genetic cardiomyopathies causing heart failure’, *Circ. Res.*, vol. 113, no. 6, pp. 660–675, Aug. 2013, doi: 10.1161/CIRCRESAHA.113.300282.
- [245] H. Watkins, H. Ashrafian, and C. Redwood, ‘Inherited cardiomyopathies’, *N. Engl. J. Med.*, vol. 364, no. 17, pp. 1643–1656, Apr. 2011, doi: 10.1056/NEJMra0902923.
- [246] H.-P. Schultheiss *et al.*, ‘Dilated cardiomyopathy’, *Nat. Rev. Dis. Primer*, vol. 5, no. 1, Art. no. 1, May 2019, doi: 10.1038/s41572-019-0084-1.
- [247] M. A. Burke, S. A. Cook, J. G. Seidman, and C. E. Seidman, ‘Clinical and Mechanistic Insights Into the Genetics of Cardiomyopathy’, *J. Am. Coll. Cardiol.*, vol. 68, no. 25, pp. 2871–2886, Dec. 2016, doi: 10.1016/j.jacc.2016.08.079.
- [248] S. Schafer *et al.*, ‘Titin-truncating variants affect heart function in disease cohorts and the general population’, *Nat. Genet.*, vol. 49, no. 1, pp. 46–53, Jan. 2017, doi: 10.1038/ng.3719.
- [249] M. Colegrave and M. Peckham, ‘Structural implications of β -cardiac myosin heavy chain mutations in human disease’, *Anat. Rec. Hoboken NJ 2007*, vol. 297, no. 9, pp. 1670–1680, Sep. 2014, doi: 10.1002/ar.22973.
- [250] J. England *et al.*, ‘Tropomyosin 1: Multiple roles in the developing heart and in the formation of congenital heart defects’, *J. Mol. Cell. Cardiol.*, vol. 106, pp. 1–13, May 2017, doi: 10.1016/j.yjmcc.2017.03.006.
- [251] R. E. Hershberger *et al.*, ‘Clinical and functional characterization of TNNT2 mutations identified in patients with dilated cardiomyopathy’, *Circ. Cardiovasc. Genet.*, vol. 2, no. 4, pp. 306–313, Aug. 2009, doi: 10.1161/CIRCGENETICS.108.846733.
- [252] Z. Xu *et al.*, ‘Genotype-phenotype relationship in patients with arrhythmogenic right ventricular cardiomyopathy caused by desmosomal gene mutations: A systematic review and meta-analysis’, *Sci. Rep.*, vol. 7, p. 41387, Jan. 2017, doi: 10.1038/srep41387.
- [253] E. Muchtar, L. A. Blauwet, and M. A. Gertz, ‘Restrictive Cardiomyopathy: Genetics, Pathogenesis, Clinical Manifestations, Diagnosis, and Therapy’, *Circ. Res.*, vol. 121, no. 7, pp. 819–837, Sep. 2017, doi: 10.1161/CIRCRESAHA.117.310982.

- [254] A. Pollack, A. R. Kontorovich, V. Fuster, and G. W. Dec, ‘Viral myocarditis--diagnosis, treatment options, and current controversies’, *Nat. Rev. Cardiol.*, vol. 12, no. 11, pp. 670–680, Nov. 2015, doi: 10.1038/nrcardio.2015.108.
- [255] V. Dhulipala, P. Bezwada, R. Gottimukkula, and J. Abboud, ‘Stress-Induced Cardiomyopathy: As a Diagnosis That Is Time Sensitive and Anticipative in Certain Individuals’, *Case Rep. Cardiol.*, vol. 2018, p. 5243419, Dec. 2018, doi: 10.1155/2018/5243419.
- [256] K. Takahashi and S. Yamanaka, ‘Induction of Pluripotent Stem Cells from Mouse Embryonic and Adult Fibroblast Cultures by Defined Factors’, *Cell*, vol. 126, no. 4, pp. 663–676, Aug. 2006, doi: 10.1016/j.cell.2006.07.024.
- [257] D. M. Lyra-Leite, Ó. Gutiérrez-Gutiérrez, M. Wang, Y. Zhou, L. Cyganek, and P. W. Burridge, ‘A review of protocols for human iPSC culture, cardiac differentiation, subtype-specification, maturation, and direct reprogramming’, *STAR Protoc.*, vol. 3, no. 3, p. 101560, Sep. 2022, doi: 10.1016/j.xpro.2022.101560.
- [258] C. A. B. Hey, K. B. Saltöková, H. C. Bisgaard, and L. B. Møller, ‘Comparison of two different culture conditions for derivation of early hiPSC’, *Cell Biol. Int.*, vol. 42, no. 11, pp. 1467–1473, Nov. 2018, doi: 10.1002/cbin.10966.
- [259] P. P. K. Ph.D, ‘What is Matrigel, why a shortage, & alternatives?’, *The Niche*, Mar. 01, 2022. <https://ipscell.com/2022/03/what-is-matrigel-why-a-shortage-alternatives/> (accessed Nov. 10, 2022).
- [260] N. Emre *et al.*, ‘The ROCK Inhibitor Y-27632 Improves Recovery of Human Embryonic Stem Cells after Fluorescence-Activated Cell Sorting with Multiple Cell Surface Markers’, *PLOS ONE*, vol. 5, no. 8, p. e12148, Aug. 2010, doi: 10.1371/journal.pone.0012148.
- [261] I. Kehat and D. Kenyagin-Karsenti, ‘Human embryonic stem cells can differentiate into myocytes with structural and functional properties of cardiomyocytes’, *J. Clin. Invest.*, vol. 108, no. 3, pp. 407–414, Aug. 2001, doi: 10.1172/JCI200112131.Introduction.
- [262] P. W. Burridge *et al.*, ‘Improved human embryonic stem cell embryoid body homogeneity and cardiomyocyte differentiation from a novel V-96 plate aggregation system highlights interline variability’, *Stem Cells Dayt. Ohio*, vol. 25, no. 4, pp. 929–938, Apr. 2007, doi: 10.1634/stemcells.2006-0598.
- [263] L. Yang *et al.*, ‘Human cardiovascular progenitor cells develop from a KDR+ embryonic-stem-cell-derived population.’, *Nature*, vol. 453, no. 7194, pp. 524–8, May 2008, doi: 10.1038/nature06894.
- [264] S. J. Kattman *et al.*, ‘Stage-Specific Optimization of Activin/Nodal and BMP Signaling Promotes Cardiac Differentiation of Mouse and Human Pluripotent Stem

Cell Lines’, *Cell Stem Cell*, vol. 8, no. 2, pp. 228–240, Feb. 2011, doi: 10.1016/j.stem.2010.12.008.

- [265] P. W. Burridge *et al.*, ‘A Universal System for Highly Efficient Cardiac Differentiation of Human Induced Pluripotent Stem Cells That Eliminates Interline Variability’, *PLOS ONE*, vol. 6, no. 4, p. e18293, Apr. 2011, doi: 10.1371/journal.pone.0018293.
- [266] E. Willems *et al.*, ‘Small-molecule inhibitors of the Wnt pathway potently promote cardiomyocytes from human embryonic stem cell-derived mesoderm’, *Circ. Res.*, vol. 109, no. 4, pp. 360–364, Aug. 2011, doi: 10.1161/CIRCRESAHA.111.249540.
- [267] M. A. Laflamme *et al.*, ‘Cardiomyocytes derived from human embryonic stem cells in pro-survival factors enhance function of infarcted rat hearts’, *Nat. Biotechnol.*, vol. 25, no. 9, Art. no. 9, Sep. 2007, doi: 10.1038/nbt1327.
- [268] X. Lian *et al.*, ‘Chemically defined, albumin-free human cardiomyocyte generation’, *Nat. Methods*, vol. 12, no. 7, Art. no. 7, Jul. 2015, doi: 10.1038/nmeth.3448.
- [269] Y. Lin *et al.*, ‘Heparin Promotes Cardiac Differentiation of Human Pluripotent Stem Cells in Chemically Defined Albumin-Free Medium, Enabling Consistent Manufacture of Cardiomyocytes’, *Stem Cells Transl. Med.*, vol. 6, no. 2, pp. 527–538, Feb. 2017, doi: 10.5966/sctm.2015-0428.
- [270] Y. Lin and J. Zou, ‘Differentiation of Cardiomyocytes from Human Pluripotent Stem Cells in Fully Chemically Defined Conditions’, *STAR Protoc.*, vol. 1, no. 1, p. 100015, Jun. 2020, doi: 10.1016/j.xpro.2020.100015.
- [271] X. Lian, J. Zhang, K. Zhu, T. J. Kamp, and S. P. Palecek, ‘Insulin inhibits cardiac mesoderm, not mesendoderm, formation during cardiac differentiation of human pluripotent stem cells and modulation of canonical Wnt signaling can rescue this inhibition’, *Stem Cells Dayt. Ohio*, vol. 31, no. 3, p. 447, Mar. 2013, doi: 10.1002/STEM.1289.
- [272] F. S. Pasqualini, A. P. Nesmith, R. E. Horton, S. P. Sheehy, and K. K. Parker, ‘Mechanotransduction and Metabolism in Cardiomyocyte Microdomains’, *BioMed Res. Int.*, vol. 2016, 2016, doi: 10.1155/2016/4081638.
- [273] S. M. Biendarra-Tiegs, F. J. Secreto, and T. J. Nelson, ‘Addressing Variability and Heterogeneity of Induced Pluripotent Stem Cell-Derived Cardiomyocytes’, *Adv. Exp. Med. Biol.*, vol. 1212, pp. 1–29, 2020, doi: 10.1007/5584_2019_350.
- [274] J. Yang, M. A. Argenziano, M. Burgos Angulo, A. Bertalovitz, M. N. Beidokhti, and T. V. McDonald, ‘Phenotypic Variability in iPSC-Induced Cardiomyocytes and Cardiac Fibroblasts Carrying Diverse LMNA Mutations’, *Front. Physiol.*, vol. 12, 2021, Accessed: Oct. 26, 2022. [Online]. Available: <https://www.frontiersin.org/articles/10.3389/fphys.2021.778982>

- [275] B. Williams *et al.*, ‘Prediction of Human Induced Pluripotent Stem Cell Cardiac Differentiation Outcome by Multifactorial Process Modeling’, *Front. Bioeng. Biotechnol.*, vol. 8, 2020, Accessed: Oct. 26, 2022. [Online]. Available: <https://www.frontiersin.org/articles/10.3389/fbioe.2020.00851>
- [276] I. Mannhardt *et al.*, ‘Comparison of 10 Control hPSC Lines for Drug Screening in an Engineered Heart Tissue Format’, *Stem Cell Rep.*, vol. 15, no. 4, pp. 983–998, Oct. 2020, doi: 10.1016/j.stemcr.2020.09.002.
- [277] S. D. Lundy, W.-Z. Zhu, M. Regnier, and M. A. Laflamme, ‘Structural and Functional Maturation of Cardiomyocytes Derived from Human Pluripotent Stem Cells’, *Stem Cells Dev.*, vol. 22, no. 14, pp. 1991–2002, Jul. 2013, doi: 10.1089/scd.2012.0490.
- [278] T. Kamakura *et al.*, ‘Ultrastructural Maturation of Human-Induced Pluripotent Stem Cell-Derived Cardiomyocytes in a Long-Term Culture’, *Circ. J.*, vol. 77, no. 5, pp. 1307–1314, 2013, doi: 10.1253/circj.CJ-12-0987.
- [279] K. K. Dunn *et al.*, ‘Coculture of Endothelial Cells with Human Pluripotent Stem Cell-Derived Cardiac Progenitors Reveals a Differentiation Stage-Specific Enhancement of Cardiomyocyte Maturation’, *Biotechnol. J.*, vol. 14, no. 8, p. 1800725, 2019, doi: 10.1002/biot.201800725.
- [280] M. Ieda *et al.*, ‘Cardiac Fibroblasts Regulate Myocardial Proliferation through β 1 Integrin Signaling’, *Dev. Cell*, vol. 16, no. 2, pp. 233–244, Feb. 2009, doi: 10.1016/j.devcel.2008.12.007.
- [281] T. K. Feaster *et al.*, ‘Matrigel Mattress: A Method for the Generation of Single Contracting Human-Induced Pluripotent Stem Cell-Derived Cardiomyocytes’, *Circ. Res.*, vol. 117, no. 12, pp. 995–1000, Dec. 2015, doi: 10.1161/CIRCRESAHA.115.307580.
- [282] T. J. Herron *et al.*, ‘Extracellular matrix-mediated maturation of human pluripotent stem cell-derived cardiac monolayer structure and electrophysiological function’, *Circ Arrhythm Electrophysiol*, vol. 9, no. 4, p. e003638, Apr. 2016, doi: 10.1161/circep.113.003638.
- [283] A. J. S. Ribeiro *et al.*, ‘Contractility of single cardiomyocytes differentiated from pluripotent stem cells depends on physiological shape and substrate stiffness.’, *Proc. Natl. Acad. Sci. U. S. A.*, vol. 112, no. 41, pp. 12705–10, Oct. 2015, doi: 10.1073/pnas.1508073112.
- [284] M. C. Ribeiro *et al.*, ‘Functional maturation of human pluripotent stem cell derived cardiomyocytes in vitro – Correlation between contraction force and electrophysiology’, *Biomaterials*, vol. 51, pp. 138–150, May 2015, doi: 10.1016/j.biomaterials.2015.01.067.

- [285] N. N. Chattergoon, G. D. Giraud, S. Louey, P. Stork, A. L. Fowden, and K. L. Thornburg, ‘Thyroid hormone drives fetal cardiomyocyte maturation’, *FASEB J.*, vol. 26, no. 1, pp. 397–408, Jan. 2012, doi: 10.1096/fj.10-179895.
- [286] X. Yang *et al.*, ‘Tri-iodo-L-thyronine promotes the maturation of human cardiomyocytes-derived from induced pluripotent stem cells’, *J. Mol. Cell. Cardiol.*, vol. 72, pp. 296–304, 2014, doi: 10.1016/j.yjmcc.2014.04.005.
- [287] S. S. Parikh *et al.*, ‘Thyroid and glucocorticoid hormones promote functional T-tubule development in human-induced pluripotent stem cell-derived cardiomyocytes’, *Circ. Res.*, vol. 121, no. 12, pp. 1323–1330, Dec. 2017, doi: 10.1161/circresaha.117.311920.
- [288] C. Jackman, H. Li, and N. Bursac, ‘Long-term contractile activity and thyroid hormone supplementation produce engineered rat myocardium with adult-like structure and function’, *Acta Biomater.*, vol. 78, pp. 98–110, Sep. 2018, doi: 10.1016/j.actbio.2018.08.003.
- [289] C. Correia *et al.*, ‘Distinct carbon sources affect structural and functional maturation of cardiomyocytes derived from human pluripotent stem cells’, *Sci. Rep.*, vol. 7, no. 1, Art. no. 1, Aug. 2017, doi: 10.1038/s41598-017-08713-4.
- [290] X. Yang *et al.*, ‘Fatty Acids Enhance the Maturation of Cardiomyocytes Derived from Human Pluripotent Stem Cells’, *Stem Cell Rep.*, vol. 13, no. 4, pp. 657–668, Oct. 2019, doi: 10.1016/j.stemcr.2019.08.013.
- [291] W. E. Knight, Y. Cao, P. Dillon, and K. Song, ‘A simple protocol to produce mature human-induced pluripotent stem cell-derived cardiomyocytes’, *STAR Protoc.*, vol. 2, no. 4, p. 100912, Dec. 2021, doi: 10.1016/j.xpro.2021.100912.
- [292] W. E. Knight *et al.*, ‘Maturation of Pluripotent Stem Cell-Derived Cardiomyocytes Enables Modeling of Human Hypertrophic Cardiomyopathy’, *Stem Cell Rep.*, vol. 16, no. 3, pp. 519–533, Mar. 2021, doi: 10.1016/j.stemcr.2021.01.018.
- [293] M. Snir *et al.*, ‘Assessment of the ultrastructural and proliferative properties of human embryonic stem cell-derived cardiomyocytes’, *Am. J. Physiol. Heart Circ. Physiol.*, vol. 285, no. 6, pp. H2355-2363, Dec. 2003, doi: 10.1152/ajpheart.00020.2003.
- [294] S. Pagliari *et al.*, ‘YAP–TEAD1 control of cytoskeleton dynamics and intracellular tension guides human pluripotent stem cell mesoderm specification’, *Cell Death Differ.* 2020 284, vol. 28, no. 4, pp. 1193–1207, Oct. 2020, doi: 10.1038/s41418-020-00643-5.
- [295] C. Mummery *et al.*, ‘Differentiation of human embryonic stem cells to cardiomyocytes: role of coculture with visceral endoderm-like cells’, *Circulation*,

vol. 107, no. 21, pp. 2733–2740, Jun. 2003, doi: 10.1161/01.CIR.0000068356.38592.68.

- [296] J. Cutts, M. Nikkhah, and D. A. Brafman, ‘Biomaterial Approaches for Stem Cell-Based Myocardial Tissue Engineering.’, *Biomark. Insights*, vol. 10, no. Suppl 1, pp. 77–90, Jan. 2015, doi: 10.4137/BMLS20313.
- [297] V. F. M. Segers and R. T. Lee, ‘Stem-cell therapy for cardiac disease.’, *Nature*, vol. 451, no. 7181, pp. 937–942, 2008, doi: 10.1038/nature06800.
- [298] M. a Laflamme and C. E. Murry, ‘Heart regeneration.’, *Nature*, vol. 473, no. 7347, pp. 326–335, 2011, doi: 10.1038/nature10147.
- [299] N. L. Tulloch *et al.*, ‘Growth of engineered human myocardium with mechanical loading and vascular coculture.’, *Circ. Res.*, vol. 109, no. 1, pp. 47–59, Jun. 2011, doi: 10.1161/CIRCRESAHA.110.237206.
- [300] S. Cho, C. Lee, M. A. Skylar-Scott, S. C. Heilshorn, and J. C. Wu, ‘Reconstructing the heart using iPSCs: Engineering strategies and applications’, *J. Mol. Cell. Cardiol.*, vol. 157, pp. 56–65, Aug. 2021, doi: 10.1016/J.YJMCC.2021.04.006.
- [301] T. Eschenhagen *et al.*, ‘Three-dimensional reconstitution of embryonic cardiomyocytes in a collagen matrix: a new heart muscle model system’, *FASEB J.*, vol. 11, no. 8, pp. 683–694, Jul. 1997, doi: 10.1096/FASEBJ.11.8.9240969.
- [302] W. H. Zimmermann *et al.*, ‘Tissue engineering of a differentiated cardiac muscle construct’, *Circ. Res.*, vol. 90, no. 2, pp. 223–230, Feb. 2002, doi: 10.1161/hh0202.103644.
- [303] W. H. Zimmermann *et al.*, ‘Engineered heart tissue grafts improve systolic and diastolic function in infarcted rat hearts’, *Nat. Med.*, vol. 12, no. 4, pp. 452–458, Apr. 2006, doi: 10.1038/nm1394.
- [304] A. Grosberg, P. W. Alford, M. L. McCain, and K. K. Parker, ‘Ensembles of engineered cardiac tissues for physiological and pharmacological study: heart on a chip.’, *Lab. Chip*, vol. 11, no. 24, pp. 4165–73, Dec. 2011, doi: 10.1039/c1lc20557a.
- [305] H. Sekine *et al.*, ‘Endothelial Cell Coculture Within Tissue-Engineered Cardiomyocyte Sheets Enhances Neovascularization and Improves Cardiac Function of Ischemic Hearts’, *Circulation*, vol. 118, no. 14_suppl_1, pp. S145–S152, Sep. 2008, doi: 10.1161/CIRCULATIONAHA.107.757286.
- [306] I. Mannhardt *et al.*, ‘Human Engineered Heart Tissue: Analysis of Contractile Force’, *Stem Cell Rep.*, vol. 7, no. 1, pp. 29–42, Jul. 2016, doi: 10.1016/j.stemcr.2016.04.011.
- [307] B. M. Ulmer *et al.*, ‘Contractile Work Contributes to Maturation of Energy Metabolism in hiPSC-Derived Cardiomyocytes’, *Stem Cell Rep.*, vol. 10, no. 3, pp. 834–847, Mar. 2018, doi: 10.1016/j.stemcr.2018.01.039.

- [308] S. Schaaf *et al.*, ‘Human engineered heart tissue as a versatile tool in basic research and preclinical toxicology’, *PLoS ONE*, vol. 6, no. 10, p. e26397, 2011, doi: 10.1371/JOURNAL.PONE.0026397.
- [309] M. Tiburcy *et al.*, ‘Defined Engineered Human Myocardium With Advanced Maturation for Applications in Heart Failure Modeling and Repair.’, *Circulation*, vol. 135, no. 19, pp. 1832–1847, May 2017, doi: 10.1161/CIRCULATIONAHA.116.024145.
- [310] W. J. de Lange *et al.*, ‘Human iPSC-engineered cardiac tissue platform faithfully models important cardiac physiology’, *Am. J. Physiol. - Heart Circ. Physiol.*, vol. 320, no. 4, pp. H1670–H1686, Apr. 2021, doi: 10.1152/AJPHEART.00941.2020.
- [311] K. Ronaldson-Bouchard *et al.*, ‘Engineering of human cardiac muscle electromechanically matured to an adult-like phenotype’, *Nat. Protoc.*, vol. 14, no. 10, Art. no. 10, Oct. 2019, doi: 10.1038/s41596-019-0189-8.
- [312] K. Ronaldson-Bouchard *et al.*, ‘Advanced maturation of human cardiac tissue grown from pluripotent stem cells’, *Nature*, vol. 556, no. 7700, Art. no. 7700, Apr. 2018, doi: 10.1038/s41586-018-0016-3.
- [313] S. S. Nunes *et al.*, ‘Biowire: a platform for maturation of human pluripotent stem cell–derived cardiomyocytes’, *Nat. Methods*, vol. 10, no. 8, pp. 781–787, Aug. 2013, doi: 10.1038/nmeth.2524.
- [314] N. Thavandiran, S. S. Nunes, Y. Xiao, and M. Radisic, ‘Topological and electrical control of cardiac differentiation and assembly’, *Stem Cell Res. Ther.*, vol. 4, no. 1, p. 14, 2013, doi: 10.1186/scrt162.
- [315] Y. Xiao *et al.*, ‘Microfabricated perfusable cardiac biowire: A platform that mimics native cardiac bundle’, *Lab. Chip*, vol. 14, no. 5, pp. 869–882, Mar. 2014, doi: 10.1039/c3lc51123e.
- [316] V. Y. Sidorov, P. C. Samson, T. N. Sidorova, J. M. Davidson, C. C. Lim, and J. P. Wikswo, ‘I-Wire Heart-on-a-Chip I: Three-dimensional cardiac tissue constructs for physiology and pharmacology’, *Acta Biomater.*, vol. 48, pp. 68–78, Jan. 2017, doi: 10.1016/j.actbio.2016.11.009.
- [317] I. Goldfracht *et al.*, ‘Generating ring-shaped engineered heart tissues from ventricular and atrial human pluripotent stem cell-derived cardiomyocytes’, *Nat. Commun.*, vol. 11, no. 1, p. 75, Jan. 2020, doi: 10.1038/s41467-019-13868-x.
- [318] M. Tiburcy, T. Meyer, N. Y. Liaw, and W.-H. Zimmermann, ‘Generation of Engineered Human Myocardium in a Multi-well Format’, *STAR Protoc.*, vol. 1, no. 1, p. 100032, Jun. 2020, doi: 10.1016/j.xpro.2020.100032.

- [319] R. A. Li *et al.*, ‘Bioengineering an electro-mechanically functional miniature ventricular heart chamber from human pluripotent stem cells’, *Biomaterials*, vol. 163, pp. 116–127, May 2018, doi: 10.1016/j.biomaterials.2018.02.024.
- [320] L. A. MacQueen *et al.*, ‘A tissue-engineered scale model of the heart ventricle’, *Nat. Biomed. Eng.*, vol. 2, no. 12, pp. 930–941, Dec. 2018, doi: 10.1038/s41551-018-0271-5.
- [321] A. Eder, I. Vollert, A. Hansen, and T. Eschenhagen, ‘Human engineered heart tissue as a model system for drug testing’, *Adv. Drug Deliv. Rev.*, vol. 96, pp. 214–224, Jan. 2016, doi: 10.1016/j.addr.2015.05.010.
- [322] N. Huebsch *et al.*, ‘Miniaturized iPS-Cell-Derived Cardiac Muscles for Physiologically Relevant Drug Response Analyses’, *Sci. Rep.*, vol. 6, pp. 1–12, Apr. 2016, doi: 10.1038/srep24726.
- [323] R. J. Mills *et al.*, ‘Drug Screening in Human PSC-Cardiac Organoids Identifies Proliferative Compounds Acting via the Mevalonate Pathway’, *Cell Stem Cell*, vol. 24, no. 6, pp. 895–907.e6, 2019, doi: 10.1016/j.stem.2019.03.009.
- [324] N. K. Inamdar and J. T. Borenstein, ‘Microfluidic cell culture models for tissue engineering’, *Curr. Opin. Biotechnol.*, vol. 22, no. 5, pp. 681–689, 2011, doi: 10.1016/j.copbio.2011.05.512.
- [325] A. van de Stolpe and J. den Toonder, ‘Workshop meeting report Organs on Chips: human disease models’, *Lab. Chip*, vol. 13, pp. 3449–3470, 2013, doi: 10.1039/c3lc50248a.
- [326] A. Khademhosseini, R. Langer, J. Borenstein, and J. P. Vacanti, ‘Microscale technologies for tissue engineering and biology.’, *Proc. Natl. Acad. Sci. U. S. A.*, vol. 103, no. 8, pp. 2480–7, Feb. 2006, doi: 10.1073/pnas.0507681102.
- [327] S. N. Bhatia and D. E. Ingber, ‘Microfluidic organs-on-chips.’, *Nat. Biotechnol.*, pp. 1–13, Aug. 2014, doi: 10.1038/nbt.2989.
- [328] A. Hasan *et al.*, ‘Microfluidic techniques for development of 3D vascularized tissue.’, *Biomaterials*, vol. 35, no. 26, pp. 7308–25, Aug. 2014, doi: 10.1016/j.biomaterials.2014.04.091.
- [329] A. Polini, L. Prodanov, N. S. Bhise, V. Manoharan, M. R. Dokmeci, and A. Khademhosseini, ‘Organs-on-a-chip: a new tool for drug discovery.’, *Expert Opin. Drug Discov.*, vol. 9, no. 4, pp. 335–52, Apr. 2014, doi: 10.1517/17460441.2014.886562.
- [330] P. Ertl, D. Sticker, V. Charwat, C. Kasper, and G. Lepperdinger, ‘Lab-on-a-chip technologies for stem cell analysis.’, *Trends Biotechnol.*, vol. 32, no. 5, pp. 245–53, May 2014, doi: 10.1016/j.tibtech.2014.03.004.

- [331] F. Kurth *et al.*, ‘Chapter 3 - Organs-on-a-chip engineering’, in *Organ-on-a-chip*, J. Hoeng, D. Bovard, and M. C. Peitsch, Eds. Academic Press, 2020, pp. 47–130. doi: 10.1016/B978-0-12-817202-5.00003-6.
- [332] J. H.-C. Wang and B. P. Thampatty, ‘An Introductory Review of Cell Mechanobiology’, *Biomech. Model. Mechanobiol.*, vol. 5, no. 1, pp. 1–16, 2006, doi: 10.1007/s10237-005-0012-z.
- [333] K. A. Jansen, D. M. Donato, H. E. Balcioglu, T. Schmidt, E. H. J. Danen, and G. H. Koenderink, ‘A guide to mechanobiology: Where biology and physics meet’, *Biochim. Biophys. Acta BBA - Mol. Cell Res.*, vol. 1853, no. 11, Part B, pp. 3043–3052, 2015, doi: <https://doi.org/10.1016/j.bbamcr.2015.05.007>.
- [334] E. Ergir, B. Bachmann, H. Redl, G. Forte, and P. Ertl, ‘Small Force, Big Impact: Next Generation Organ-on-a-Chip Systems Incorporating Biomechanical Cues’, *Front. Physiol.*, vol. 9, p. 1417, Oct. 2018, doi: 10.3389/fphys.2018.01417.
- [335] L. G. Griffith and M. A. Swartz, ‘Capturing complex 3D tissue physiology in vitro’, *Nat. Rev. Mol. Cell Biol.*, vol. 7, no. 3, pp. 211–224, 2006, doi: 10.1038/nrm1858.
- [336] J. L. Drury and D. J. Mooney, ‘Hydrogels for tissue engineering: scaffold design variables and applications’, *Biomaterials*, vol. 24, no. 24, pp. 4337–4351, Nov. 2003, doi: 10.1016/S0142-9612(03)00340-5.
- [337] G. Chen, T. Ushida, and T. Tateishi, ‘Scaffold design for tissue engineering’, *Macromol. Biosci.*, vol. 2, no. 2, pp. 67–77, 2002, doi: 10.1002/1616-5195(20020201)2:2<67::AID-MABI67>3.0.CO;2-F.
- [338] E. Fennema, N. Rivron, J. Rouwkema, C. van Blitterswijk, and J. de Boer, ‘Spheroid culture as a tool for creating 3D complex tissues.’, *Trends Biotechnol.*, vol. 31, no. 2, pp. 108–115, Feb. 2013, doi: 10.1016/j.tibtech.2012.12.003.
- [339] A. J. Engler, S. Sen, H. L. Sweeney, and D. E. Discher, ‘Matrix Elasticity Directs Stem Cell Lineage Specification’, *Cell*, vol. 126, no. 4, pp. 677–689, 2006, doi: 10.1016/j.cell.2006.06.044.
- [340] S. Kumar, ‘Cellular mechanotransduction: Stiffness does matter.’, *Nat. Mater.*, vol. 13, no. 10, pp. 918–20, Sep. 2014, doi: 10.1038/nmat4094.
- [341] M. Ahearne, ‘Introduction to cell-hydrogel mechanosensing’, *Interface Focus*, 2014, doi: 10.1098/rsfs.2013.0038.
- [342] M. Lovett, K. Lee, A. Edwards, and D. L. Kaplan, ‘Vascularization Strategies for Tissue Engineering’, *Tissue Eng. Part B Rev.*, vol. 15, no. 3, pp. 353–370, 2009, doi: 10.1089/ten.teb.2009.0085.
- [343] B. D. Riehl, J.-H. Park, I. K. Kwon, and J. Y. Lim, ‘Mechanical Stretching for Tissue Engineering: Two-Dimensional and Three-Dimensional Constructs’, *Tissue Eng. Part B Rev.*, 2012, doi: 10.1089/ten.teb.2011.0465.

- [344] M. Shachar, N. Benishti, and S. Cohen, 'Effects of mechanical stimulation induced by compression and medium perfusion on cardiac tissue engineering', *Biotechnol. Prog.*, vol. 28, no. 6, pp. 1551–1559, 2012, doi: 10.1002/btpr.1633.
- [345] A. Grosberg, P. W. Alford, M. L. McCain, and K. K. Parker, 'Ensembles of engineered cardiac tissues for physiological and pharmacological study: heart on a chip.', *Lab. Chip*, vol. 11, no. 24, pp. 4165–73, Dec. 2011, doi: 10.1039/c1lc20557a.
- [346] G. Wang *et al.*, 'Modeling the mitochondrial cardiomyopathy of Barth syndrome with induced pluripotent stem cell and heart-on-chip technologies.', *Nat. Med.*, vol. 20, no. 6, pp. 616–23, Jun. 2014, doi: 10.1038/nm.3545.
- [347] A. Marsano *et al.*, 'Beating heart on a chip: a novel microfluidic platform to generate functional 3D cardiac microtissues', *Lab Chip*, vol. 16, no. 3, pp. 599–610, 2016, doi: 10.1039/C5LC01356A.
- [348] P. Occhetta *et al.*, 'A three-dimensional *in vitro* dynamic micro-tissue model of cardiac scar formation', *Integr. Biol.*, vol. 10, no. 3, pp. 174–183, 2018, doi: 10.1039/C7IB00199A.
- [349] N. Huebsch *et al.*, 'Metabolically driven maturation of human-induced-pluripotent-stem-cell-derived cardiac microtissues on microfluidic chips', *Nat. Biomed. Eng.*, vol. 6, no. 4, Art. no. 4, Apr. 2022, doi: 10.1038/s41551-022-00884-4.
- [350] N. Huebsch *et al.*, 'Metabolically-Driven Maturation of hiPSC-Cell Derived Cardiac Chip'. bioRxiv, p. 485169, Nov. 14, 2020. doi: 10.1101/485169.
- [351] M. J. Kim, S. C. Lee, S. Pal, E. Han, and J. M. Song, 'High-content screening of drug-induced cardiotoxicity using quantitative single cell imaging cytometry on microfluidic device.', *Lab. Chip*, vol. 11, no. 1, pp. 104–14, Jan. 2011, doi: 10.1039/c0lc00110d.
- [352] S. R. Braam, L. Tertoolen, A. van de Stolpe, T. Meyer, R. Passier, and C. L. Mummery, 'Prediction of drug-induced cardiotoxicity using human embryonic stem cell-derived cardiomyocytes', *Stem Cell Res.*, vol. 4, no. 2, pp. 107–116, 2010, doi: 10.1016/j.scr.2009.11.004.
- [353] M. Moya, D. Tran, and S. C. George, 'An integrated *in vitro* model of perfused tumor and cardiac tissue.', *Stem Cell Res. Ther.*, vol. 4 Suppl 1, no. Suppl 1, p. S15, 2013, doi: 10.1186/scrt376.
- [354] J. Lee *et al.*, 'A Heart-Breast Cancer-on-a-Chip Platform for Disease Modeling and Monitoring of Cardiotoxicity Induced by Cancer Chemotherapy', *Small*, vol. 17, no. 15, pp. 1–17, 2021, doi: 10.1002/sml.202004258.
- [355] B. Nugraha, M. F. Buono, L. von Boehmer, S. P. Hoerstrup, and M. Y. Emmert, 'Human Cardiac Organoids for Disease Modeling', *Clin. Pharmacol. Ther.*, Nov. 2018, doi: 10.1002/cpt.1286.

- [356] S. C. van den Brink and A. van Oudenaarden, ‘3D gastruloids: a novel frontier in stem cell-based in vitro modeling of mammalian gastrulation’, *Trends Cell Biol.*, vol. 31, no. 9, pp. 747–759, Sep. 2021, doi: 10.1016/j.tcb.2021.06.007.
- [357] D. Thomas, V. A. de Jesus Perez, and N. Sayed, ‘An evidence appraisal of heart organoids in a dish and commensurability to human heart development in vivo’, *BMC Cardiovasc. Disord.*, vol. 22, no. 1, pp. 1–8, Dec. 2022, doi: 10.1186/S12872-022-02543-7/FIGURES/1.
- [358] G. Ramirez-Calderon, G. Colombo, C. A. Hernandez-Bautista, V. Astro, and A. Adamo, ‘Heart in a Dish: From Traditional 2D Differentiation Protocols to Cardiac Organoids’, *Front. Cell Dev. Biol.*, vol. 10, p. 245, Feb. 2022, doi: 10.3389/FCELL.2022.855966/BIBTEX.
- [359] C. R. Archer, R. Sargeant, J. Basak, J. Pilling, J. R. Barnes, and A. Pointon, ‘Characterization and validation of a human 3D cardiac microtissue for the assessment of changes in cardiac pathology’, *Sci. Rep.*, vol. 8, no. 1, pp. 1–15, Dec. 2018, doi: 10.1038/S41598-018-28393-Y.
- [360] P. Beauchamp *et al.*, ‘Development and Characterization of a Scaffold-Free 3D Spheroid Model of Induced Pluripotent Stem Cell-Derived Human Cardiomyocytes’, *Tissue Eng. Part C Methods*, vol. 21, no. 8, pp. 852–861, Aug. 2015, doi: 10.1089/ten.tec.2014.0376.
- [361] P. Beauchamp *et al.*, ‘3D Co-culture of hiPSC-Derived Cardiomyocytes With Cardiac Fibroblasts Improves Tissue-Like Features of Cardiac Spheroids’, *Front. Mol. Biosci.*, vol. 7, 2020, Accessed: Oct. 23, 2022. [Online]. Available: <https://www.frontiersin.org/articles/10.3389/fmolb.2020.00014>
- [362] L. Sala *et al.*, ‘Musclemotion: A versatile open software tool to quantify cardiomyocyte and cardiac muscle contraction in vitro and in vivo’, *Circ. Res.*, vol. 122, no. 3, pp. e5–e16, Feb. 2018, doi: 10.1161/CIRCRESAHA.117.312067.
- [363] Z. T. Olmsted and J. L. Paluh, ‘A combined human gastruloid model of cardiogenesis and neurogenesis’, *iScience*, vol. 25, no. 6, Jun. 2022, doi: 10.1016/j.isci.2022.104486.
- [364] Z. T. Olmsted, M. B. Paredes-Espinosa, and J. L. Paluh, ‘Generation of human elongating multi-lineage organized cardiac gastruloids’, *STAR Protoc.*, vol. 3, no. 4, p. 101898, Dec. 2022, doi: 10.1016/j.xpro.2022.101898.
- [365] P. Hoang, J. Wang, B. R. Conklin, K. E. Healy, and Z. Ma, ‘Generation of spatial-patterned early-developing cardiac organoids using human pluripotent stem cells’, *Nat. Protoc.*, vol. 13, no. 4, pp. 723–737, Apr. 2018, doi: 10.1038/nprot.2018.006.

- [366] P. Hoang *et al.*, ‘Engineering spatial-organized cardiac organoids for developmental toxicity testing’, *Stem Cell Rep.*, vol. 16, no. 5, pp. 1228–1244, 2021, doi: 10.1016/j.stemcr.2021.03.013.
- [367] E. Ergir *et al.*, ‘Generation and maturation of human iPSC-derived 3D organotypic cardiac microtissues in long-term culture’, *Sci. Rep.*, vol. 12, no. 1, Art. no. 1, Oct. 2022, doi: 10.1038/s41598-022-22225-w.
- [368] V. Marini *et al.*, ‘Long-term culture of patient-derived cardiac organoids recapitulated Duchenne muscular dystrophy cardiomyopathy and disease progression’, *Front. Cell Dev. Biol.*, vol. 10, no. August, pp. 1–23, 2022, doi: 10.3389/fcell.2022.878311.
- [369] C. Schmidt *et al.*, ‘Multi-chamber cardioids unravel human heart development and cardiac defects’. bioRxiv, p. 2022.07.14.499699, Jul. 16, 2022. doi: 10.1101/2022.07.14.499699.
- [370] S.-G. Lee *et al.*, ‘Generation of human iPSCs derived heart organoids structurally and functionally similar to heart’, *Biomaterials*, vol. 290, p. 121860, Nov. 2022, doi: 10.1016/j.biomaterials.2022.121860.
- [371] M. A. Branco, T. P. Dias, J. M. S. Cabral, P. Pinto-do-Ó, and M. M. Diogo, ‘Human multilineage pro-epicardium/foregut organoids support the development of an epicardium/myocardium organoid’, *Nat. Commun.*, vol. 13, p. 6981, Nov. 2022, doi: 10.1038/s41467-022-34730-7.
- [372] ‘Ncardia Home’. <https://www.ncardia.com> (accessed Feb. 10, 2023).
- [373] ‘Valo Health - FDA Collaborative Study in Human Cardiac Tissues...’, *Valo*, Dec. 14, 2022. <https://www.valohealth.com/press/valo-health-fda-collaborative-study-in-human-cardiac-tissues-demonstrates-potential-to-predict-clinical-efficacy-of-cardiac-tractility-modulation-devices-to-treat-heart-failure> (accessed Feb. 10, 2023).
- [374] ‘myriamed-the drug development accelerator - myriamed’. <https://www.myriamed.com/home> (accessed Feb. 10, 2023).
- [375] ‘Evotec and Medical Center Hamburg-Eppendorf Enter Partnership to Develop iPSC-Based Tissue Therapy for Heart Failure - Evotec’. <https://www.evotec.com/en/investor-relations/news/p/evotec-and-medical-center-hamburg-eppendorf-enter-partnership-to-develop-ipsc-based-tissue-therapy-for-heart-failure-6024> (accessed Feb. 10, 2023).
- [376] ‘HeartBeat.bio – REINVENTING CARDIAC DRUG DISCOVERY’. <https://heartbeat.bio/> (accessed Feb. 10, 2023).
- [377] ‘Home - Bi/ond’. <https://www.gobiond.com/> (accessed Feb. 10, 2023).
- [378] ‘uHeart’, *BiomimX*. <https://www.biomimx.com/uheart/> (accessed Feb. 10, 2023).

- [379] ‘Cardiac assay’, *4Dcell*. <https://www.4dcell.com/cell-culture-systems/gels/cardio-assay/> (accessed Feb. 10, 2023).
- [380] ‘Delivering Tomorrow’s Therapies Today’, *Medera Incorporation*. <https://www.medera.bio/> (accessed Feb. 10, 2023).
- [381] ‘Engineered Heart Tissue from iPSC-Cardiomyocytes | Propria’. <https://www.propriabio.com> (accessed Feb. 10, 2023).
- [382] ‘EHT - Engineered Heart Tissue’. <https://www.eht-technologies.com/> (accessed Feb. 10, 2023).
- [383] ‘About our brands: Cellartis’. <https://www.takarabio.com/about/our-brands/cellartis> (accessed Feb. 10, 2023).
- [384] ‘Cardiac Models’, *Curi Bio*. <https://www.curibio.com/cardiac-models> (accessed Feb. 10, 2023).
- [385] ‘River Biomedics – Closer to the heart’. <https://riverbiomedics.com/> (accessed Feb. 10, 2023).
- [386] J. Vrbský *et al.*, ‘Evidence for discrete modes of YAP1 signaling via mRNA splice isoforms in development and diseases’, *Genomics*, vol. 113, no. 3, pp. 1349–1365, May 2021, doi: 10.1016/J.YGENO.2021.03.009.
- [387] T. Smith, A. Heger, and I. Sudbery, ‘UMI-tools: modeling sequencing errors in Unique Molecular Identifiers to improve quantification accuracy’, *Genome Res.*, vol. 27, no. 3, pp. 491–499, Mar. 2017, doi: 10.1101/GR.209601.116.
- [388] H. Li, ‘seqtk: Toolkit for processing sequences in FASTA/Q formats’, *GitHub 767*, 2012. <https://github.com/lh3/seqtk/> (accessed Jan. 29, 2022).
- [389] S. Andrews, ‘FastQC A Quality Control tool for High Throughput Sequence Data’, [Online], 2010. <https://www.bioinformatics.babraham.ac.uk/projects/fastqc/> (accessed Jan. 29, 2022).
- [390] A. M. Bolger, M. Lohse, and B. Usadel, ‘Trimmomatic: a flexible trimmer for Illumina sequence data’, *Bioinformatics*, vol. 30, no. 15, p. 2114, Aug. 2014, doi: 10.1093/BIOINFORMATICS/BTU170.
- [391] A. Dobin *et al.*, ‘STAR: ultrafast universal RNA-seq aligner’, *Bioinformatics*, vol. 29, no. 1, p. 15, Jan. 2013, doi: 10.1093/BIOINFORMATICS/BTS635.
- [392] L. Wang, S. Wang, and W. Li, ‘RSeQC: quality control of RNA-seq experiments’, *Bioinformatics*, vol. 28, no. 16, pp. 2184–2185, Aug. 2012, doi: 10.1093/BIOINFORMATICS/BTS356.
- [393] . Broad Institute, ‘Picard Toolkit’, *GitHub Repository*, 2018. <https://broadinstitute.github.io/picard/> (accessed Jan. 29, 2022).

- [394] K. Okonechnikov, A. Conesa, and F. García-Alcalde, ‘Qualimap 2: advanced multi-sample quality control for high-throughput sequencing data’, *Bioinformatics*, vol. 32, no. 2, p. 292, Jan. 2016, doi: 10.1093/BIOINFORMATICS/BTV566.
- [395] J. Chu *et al.*, ‘BioBloom tools: fast, accurate and memory-efficient host species sequence screening using bloom filters’, *Bioinformatics*, vol. 30, no. 23, p. 3402, Dec. 2014, doi: 10.1093/BIOINFORMATICS/BTU558.
- [396] Y. Liao, G. K. Smyth, and W. Shi, ‘featureCounts: an efficient general purpose program for assigning sequence reads to genomic features’, *Bioinformatics*, vol. 30, no. 7, pp. 923–930, Apr. 2014, doi: 10.1093/BIOINFORMATICS/BTT656.
- [397] M. I. Love, W. Huber, and S. Anders, ‘Moderated estimation of fold change and dispersion for RNA-seq data with DESeq2’, *Genome Biol.*, vol. 15, no. 12, pp. 1–21, Dec. 2014, doi: 10.1186/S13059-014-0550-8/FIGURES/9.
- [398] R. Kolde, ‘Package “pheatmap”’, *R Package 1.7*, 2015. <https://cran.r-project.org/web/packages/pheatmap/index.html> (accessed Jan. 29, 2022).
- [399] H. Wickham, ‘ggplot2’, *Wiley Interdiscip. Rev. Comput. Stat.*, vol. 3, no. 2, pp. 180–185, Mar. 2011, doi: 10.1002/WICS.147.
- [400] A. Kassambara, ‘ggpubr: “ggplot2” based publication ready plots’, *R package version 0.1 7*, 2018. <https://rpkgs.datanovia.com/ggpubr/> (accessed Jan. 29, 2022).
- [401] E. Y. Chen *et al.*, ‘Enrichr: Interactive and collaborative HTML5 gene list enrichment analysis tool’, *BMC Bioinformatics*, vol. 14, Apr. 2013, doi: 10.1186/1471-2105-14-128.
- [402] M. V. Kuleshov *et al.*, ‘Enrichr: a comprehensive gene set enrichment analysis web server 2016 update’, *Nucleic Acids Res.*, vol. 44, no. W1, pp. W90–W97, Jul. 2016, doi: 10.1093/nar/gkw377.
- [403] Z. Xie *et al.*, ‘Gene Set Knowledge Discovery with Enrichr’, *Curr. Protoc.*, vol. 1, no. 3, p. e90, Mar. 2021, doi: 10.1002/CPZ1.90.
- [404] P. Shannon *et al.*, ‘Cytoscape: a software environment for integrated models of biomolecular interaction networks’, *Genome Res.*, vol. 13, no. 11, pp. 2498–2504, Nov. 2003, doi: 10.1101/GR.1239303.
- [405] ‘A novel approach for the diagnosis of dilated cardiomyopathy (DCM), ID 667310 - BioProject - NCBI’. <https://www.ncbi.nlm.nih.gov/bioproject/PRJNA667310> (accessed Dec. 09, 2021).
- [406] ‘RNA-seq of heart tissues from healthy individuals and DMD patients, ID 628736 - BioProject - NCBI’. <https://www.ncbi.nlm.nih.gov/bioproject/?term=PRJNA628736> (accessed Dec. 09, 2021).

- [407] ‘Physiological Calcium Combined with Electrical Pacing accelerates Maturation of Human Engineered Heart Tissue, ID 831794 - BioProject - NCBI’. <https://www.ncbi.nlm.nih.gov/bioproject/PRJNA831794> (accessed Jul. 12, 2022).
- [408] S. Shen *et al.*, ‘Physiological calcium combined with electrical pacing accelerates maturation of human engineered heart tissue’, *Stem Cell Rep.*, vol. 17, no. 9, pp. 2037–2049, Sep. 2022, doi: 10.1016/j.stemcr.2022.07.006.
- [409] D. Torre, A. Lachmann, and A. Ma’ayan, ‘BioJupies: Automated Generation of Interactive Notebooks for RNA-Seq Data Analysis in the Cloud’, *Cell Syst.*, vol. 7, no. 5, pp. 556-561.e3, Nov. 2018, doi: 10.1016/j.cels.2018.10.007.
- [410] B. J. van Meer, L. Sala, L. G. J. Tertoolen, G. L. Smith, F. L. Burton, and C. L. Mummery, ‘Quantification of Muscle Contraction In Vitro and In Vivo Using MUSCLEMOTION Software: From Stem Cell-Derived Cardiomyocytes to Zebrafish and Human Hearts’, *Curr. Protoc. Hum. Genet.*, vol. 99, no. 1, pp. 1–21, 2018, doi: 10.1002/cphg.67.
- [411] C. Zuppinger, ‘3D Cardiac Cell Culture: A Critical Review of Current Technologies and Applications’, *Front. Cardiovasc. Med.*, vol. 6, p. 87, Jun. 2019, doi: 10.3389/FCVM.2019.00087/BIBTEX.
- [412] A. R. Pinto *et al.*, ‘Revisiting Cardiac Cellular Composition’, *Circ. Res.*, vol. 118, no. 3, p. 400, 2016, doi: 10.1161/CIRCRESAHA.115.307778.
- [413] R. E. Ahmed, T. Anzai, N. Chanthra, and H. Uosaki, ‘A Brief Review of Current Maturation Methods for Human Induced Pluripotent Stem Cells-Derived Cardiomyocytes’, *Front. Cell Dev. Biol.*, vol. 8, p. 178, Mar. 2020, doi: 10.3389/fcell.2020.00178.
- [414] F. M. Drawnel *et al.*, ‘Disease modeling and phenotypic drug screening for diabetic cardiomyopathy using human induced pluripotent stem cells’, *Cell Rep.*, vol. 9, no. 3, pp. 810–820, 2014, doi: 10.1016/J.CELREP.2014.09.055.
- [415] L. Guo *et al.*, ‘Estimating the Risk of Drug-Induced Proarrhythmia Using Human Induced Pluripotent Stem Cell-Derived Cardiomyocytes’, *Toxicol. Sci.*, vol. 123, no. 1, pp. 281–289, Sep. 2011, doi: 10.1093/TOXSCI/KFR158.
- [416] I. Mannhardt *et al.*, ‘Human Engineered Heart Tissue: Analysis of Contractile Force’, *Stem Cell Rep.*, vol. 7, no. 1, pp. 29–42, Jul. 2016, doi: 10.1016/j.stemcr.2016.04.011.
- [417] G. Vandecasteele, T. Eschenhagen, H. Scholz, B. Stein, I. Verde, and R. Fischmeister, ‘Muscarinic and beta-adrenergic regulation of heart rate, force of contraction and calcium current is preserved in mice lacking endothelial nitric oxide synthase’, *Nat. Med.*, vol. 5, no. 3, pp. 331–334, 1999, doi: 10.1038/6553.

- [418] R. H. G. Schwinger, M. Böhm, and E. Erdmann, ‘Negative inotropic properties of isradipine, nifedipine, diltiazem, and verapamil in diseased human myocardial tissue’, *J. Cardiovasc. Pharmacol.*, vol. 15, no. 6, pp. 892–899, 1990, doi: 10.1097/00005344-199006000-00006.
- [419] N. Thavandiran *et al.*, ‘Functional arrays of human pluripotent stem cell-derived cardiac microtissues’, *Sci. Rep. 2020 101*, vol. 10, no. 1, pp. 1–13, Apr. 2020, doi: 10.1038/s41598-020-62955-3.
- [420] C. F. Thorn *et al.*, ‘Doxorubicin pathways: pharmacodynamics and adverse effects’, *Pharmacogenet. Genomics*, vol. 21, no. 7, p. 440, 2011, doi: 10.1097/FPC.0B013E32833FFB56.
- [421] Y. Octavia, C. G. Tocchetti, K. L. Gabrielson, S. Janssens, H. J. Crijns, and A. L. Moens, ‘Doxorubicin-induced cardiomyopathy: From molecular mechanisms to therapeutic strategies’, *J. Mol. Cell. Cardiol.*, vol. 52, no. 6, pp. 1213–1225, Jun. 2012, doi: 10.1016/J.YJMCC.2012.03.006.
- [422] G. Takemura and H. Fujiwara, ‘Doxorubicin-Induced Cardiomyopathy. From the Cardiotoxic Mechanisms to Management’, *Prog. Cardiovasc. Dis.*, vol. 49, no. 5, pp. 330–352, Mar. 2007, doi: 10.1016/J.PCAD.2006.10.002.
- [423] D. Silva, D. Santos, R. Coeli, and S. Goldenberg, ‘Doxorubicin-Induced Cardiotoxicity: From Mechanisms to Development of Efficient Therapy’, *Cardiotoxicity*, Nov. 2018, doi: 10.5772/INTECHOPEN.79588.
- [424] R. Tanaka *et al.*, ‘Reactive fibrosis precedes doxorubicin-induced heart failure through sterile inflammation’, *ESC Heart Fail.*, vol. 7, no. 2, pp. 588–603, Apr. 2020, doi: 10.1002/EHF2.12616.
- [425] S. P. Levick *et al.*, ‘Doxorubicin-Induced Myocardial Fibrosis Involves the Neurokinin-1 Receptor and Direct Effects on Cardiac Fibroblasts’, *Heart Lung Circ.*, vol. 28, no. 10, pp. 1598–1605, Oct. 2019, doi: 10.1016/J.HLC.2018.08.003.
- [426] R. L. Page *et al.*, ‘Drugs That May Cause or Exacerbate Heart Failure’, *Circulation*, vol. 134, no. 6, pp. e32–e69, Aug. 2016, doi: 10.1161/CIR.0000000000000426.
- [427] R. Gilsbach *et al.*, ‘Dynamic DNA methylation orchestrates cardiomyocyte development, maturation and disease’, *Nat. Commun.*, vol. 5, Oct. 2014, doi: 10.1038/NCOMMS6288.
- [428] T. Grancharova *et al.*, ‘A comprehensive analysis of gene expression changes in a high replicate and open-source dataset of differentiating hiPSC-derived cardiomyocytes’, *Sci. Rep. 2021 111*, vol. 11, no. 1, pp. 1–21, Aug. 2021, doi: 10.1038/s41598-021-94732-1.

- [429] S. M. Meilhac and M. E. Buckingham, ‘The deployment of cell lineages that form the mammalian heart’, *Nat. Rev. Cardiol.*, vol. 15, no. 11, pp. 705–724, Nov. 2018, doi: 10.1038/s41569-018-0086-9.
- [430] D. Spitkovsky *et al.*, ‘Activity of complex III of the mitochondrial electron transport chain is essential for early heart muscle cell differentiation’, *FASEB J.*, vol. 18, no. 11, pp. 1300–1302, Aug. 2004, doi: 10.1096/FJ.03-0520FJE.
- [431] S. Cadenas, ‘Mitochondrial uncoupling, ROS generation and cardioprotection’, *Biochim. Biophys. Acta BBA - Bioenerg.*, vol. 1859, no. 9, pp. 940–950, Sep. 2018, doi: 10.1016/J.BBABIO.2018.05.019.
- [432] P. G. Rodrigues *et al.*, ‘Early myocardial changes induced by doxorubicin in the nonfailing dilated ventricle’, *Am. J. Physiol. - Heart Circ. Physiol.*, vol. 316, no. 3, pp. H459–H475, 2019, doi: 10.1152/ajpheart.00401.2018.
- [433] A. Dolci, R. Dominici, D. Cardinale, M. T. Sandri, and M. Panteghini, ‘Biochemical markers for prediction of chemotherapy-induced cardiotoxicity systematic review of the literature and recommendations for use’, *Am. J. Clin. Pathol.*, vol. 130, no. 5, pp. 688–695, 2008, doi: 10.1309/AJCPB66LRIIVMQDR.
- [434] B. X. Ho, N. M. Q. Pek, and B. S. Soh, ‘Disease modeling using 3D organoids derived from human induced pluripotent stem cells’, *Int. J. Mol. Sci.*, vol. 19, no. 4, Apr. 2018, doi: 10.3390/ijms19040936.
- [435] M. Rothbauer *et al.*, ‘A Decade of Organs-on-a-Chip Emulating Human Physiology at the Microscale: A Critical Status Report on Progress in Toxicology and Pharmacology’, *Micromachines*, vol. 12, no. 5, Art. no. 5, May 2021, doi: 10.3390/mi12050470.
- [436] S. Spitz *et al.*, ‘Development of a multi-sensor integrated midbrain organoid-on-a-chip platform for studying Parkinson’s disease’. bioRxiv, p. 2022.08.19.504522, Aug. 22, 2022. doi: 10.1101/2022.08.19.504522.
- [437] C. Eilenberger *et al.*, ‘A Microfluidic Multisize Spheroid Array for Multiparametric Screening of Anticancer Drugs and Blood–Brain Barrier Transport Properties’, *Adv. Sci.*, vol. 8, no. 11, p. 2004856, Jun. 2021, doi: 10.1002/ADVS.202004856.
- [438] K. Achberger *et al.*, ‘Merging organoid and organ-on-a-chip technology to generate complex multi-layer tissue models in a human retina-on-a-chip platform’, *eLife*, vol. 8, Aug. 2019, doi: 10.7554/ELIFE.46188.
- [439] M. Hofer and M. P. Lutolf, ‘Engineering organoids’, *Nat. Rev. Mater.*, vol. 6, no. 5, Art. no. 5, May 2021, doi: 10.1038/s41578-021-00279-y.
- [440] N. Huebsch *et al.*, ‘Automated video-based analysis of contractility and calcium flux in human-induced pluripotent stem cell-derived cardiomyocytes cultured over

different spatial scales’, *Tissue Eng - Part C Methods*, vol. 21, no. 5, pp. 467–479, May 2015, doi: 10.1089/ten.tec.2014.0283.

- [441] T. Xu, L. Wu, M. Xia, A. Simeonov, and R. Huang, ‘Systematic Identification of Molecular Targets and Pathways Related to Human Organ Level Toxicity’, *Chem. Res. Toxicol.*, vol. 34, no. 2, pp. 412–421, Feb. 2021, doi: 10.1021/acs.chemrestox.0c00305.
- [442] C. Miranda *et al.*, ‘Towards Multi-Organoid Systems for Drug Screening Applications’, *Bioengineering*, vol. 5, no. 3, p. 49, Jun. 2018, doi: 10.3390/bioengineering5030049.
- [443] J. H. Sung *et al.*, ‘Using physiologically-based pharmacokinetic-guided “body-on-a-chip” systems to predict mammalian response to drug and chemical exposure’, *Exp. Biol. Med.*, vol. 239, no. 9, pp. 1225–1239, Sep. 2014, doi: 10.1177/1535370214529397.
- [444] ‘Passage of Senate Bill S. 5002, “FDA Modernization Act 2.0,” Relating to Animal Testing’. <https://www.cov.com/en/news-and-insights/insights/2022/10/passage-of-senate-bill-s-5002-fda-modernization-act-2-0-relating-to-animal-testing> (accessed Oct. 26, 2022).
- [445] M. Wadman, ‘FDA no longer has to require animal testing for new drugs’, *Science*, vol. 379, no. 6628, pp. 127–128, Jan. 2023, doi: 10.1126/science.adg6276.

7 LIST OF ONLINE SUPPLEMENTARY MATERIALS

Online supplementary material could be found at the online version of:

Ergir, E., Oliver-De La Cruz, J., Fernandes, S. *et al.* Generation and maturation of human iPSC-derived 3D organotypic cardiac microtissues in long-term culture. *Sci Rep* **12**, 17409 (2022). <https://doi.org/10.1038/s41598-022-22225-w>

7.1 List of Supplementary Videos

Supplementary video 1– Representative spontaneously beating long-term 3D hiPSC-derived organotypic cardiac microtissue (hOCMTs) under light microscope (Day 53). Scale bar = 100 μm

Supplementary video 2 – Representative spontaneously beating long-term 3D hOCMT under light microscope (Day 107). Scale bar = 100 μm

Supplementary videos (3-8) – Representative videos of beating long-term hOCMTs before (t=0) & after (t=1) maximum dose of cardioactive drugs on day 50; taken under transmitted light mode of confocal microscope (Scale bars = 200 μm):

3. Control hOCMT (t=0)
4. Control hOCMT (t=1)
5. hOCMT with 0 μM isoproterenol (t=0)
6. hOCMT with 1 μM isoproterenol (t=1)
7. hOCMT with 0 μM verapamil (t=0)
8. hOCMT with 1 μM verapamil (t=1)

Supplementary videos (9-14) – Representative videos of beating long-term hOCMTs (Day 53) before & after Doxorubicin (Doxo) treatment on day 0 and day 6 of the treatments; taken under transmitted light mode of confocal microscope (Scale bars = 200 μm):

9. Control hOCMT on day 0
10. hOCMT with 0.1 $\mu\text{g}/\text{mL}$ Doxo on day 0
11. hOCMT with 1 $\mu\text{g}/\text{mL}$ Doxo on day 0
12. Control hOCMT on day 6
13. hOCMT with 0.1 $\mu\text{g}/\text{mL}$ Doxo on day 6
14. hOCMT with 1 $\mu\text{g}/\text{mL}$ Doxo on day 6

7.2 List of Supplementary Datasets

Online supplementary material could be found at the online version of:

Ergir, E., Oliver-De La Cruz, J., Fernandes, S. *et al.* Generation and maturation of human iPSC-derived 3D organotypic cardiac microtissues in long-term culture. *Sci Rep* **12**, 17409 (2022). <https://doi.org/10.1038/s41598-022-22225-w>

Supplementary dataset 1 – log₂changes and p-values for the different comparisons

Supplementary dataset 2 – GO BP clustering analysis for the differentially regulated genes at the different comparisons

8 LIST OF ABBREVIATIONS

μg	micrograms
μm	micrometers
μM	micromolars
a.u.	Amplitude
ACTA2 / α -SMA	α -Smooth Muscle Actin 2 (α -SMA)
ACTN2	Sarcomeric α -Actinin 2
Anti – Hu	Anti – Human
APC	Allophycocyanin
ASCL2	Achaete-Scute Family BHLH Transcription Factor 2
ATP	Adenosine triphosphate
AV-CM	Atrioventricular nodal CMs
AVN	Atrioventricular node
BPM	Beats per minute
BSA	Bovine Serum Albumin
BV421	Brilliant Violet™ 421
Ca^{2+}	Calcium
Calcein- AM	Calcein acetoxymethyl ester
CF	Cardiac fibroblast
CHIR99021	Glycogen synthase kinase 3 (GSK3) inhibitor
CM	Cardiomyocyte
cSMC	Contractile Smooth Muscle Cell
CX43	Connexin 43 (Gap junction alpha-1; GJA1)
D	Day
DAPI	4',6-diamidino-2-phenylindole
DE	Differential expression
DMEM	Dulbecco's modified Eagle's medium
DMEM-HG	DMEM with High-Glucose
DMSO	Dimethyl sulfoxide

DNA	Deoxyribonucleic acid
Doxo	Doxorubicin
E8	Essential 8 Media
EC	Endothelial Cell
ECAR	Extracellular acidification rate
ECM	Extracellular matrix
EHT	Engineered heart tissue
ESC	Embryonic stem cell
EthD-1	Ethidium Homodimer-1
FACS	Fluorescence-activated cell sorting
FBS	Fetal Bovine Serum
FCCP	Carbonyl cyanide – <i>p</i> – trifluoromethoxyphenyl hydrazone
FDA	The United States Food and Drug Administration
FHF	First heart field
FITC	Fluorescein isothiocyanate
GATA4	GATA Binding Protein 4
GEO	Gene Expression Omnibus
GFP	Green Fluorescent Protein
GO	Gene Ontology
GSK3	Glycogen synthase kinase 3
h	hours
H&E	Haematoxylin & Eosin staining
hESC	Human embryonic stem cell
hiPSC	Human induced pluripotent stem cell
HoC	Heart-on-a-chip
hOCMT	Human organotypic cardiac microtissue
hPSC	Human pluripotent stem cell
IF	Immunofluorescence
Ins	Insulin
iPSC	Induced pluripotent stem cell

IWP	Inhibitor of Wnt production
KSR	Knockout Serum Replacement
LOC	Lab-on-a-chip
MESP1	Mesoderm Posterior BHLH Transcription Factor 1
min	minutes
mL	milliliters
mm	millimeters
mM	millimolars
ms	milliseconds
MT	Microtissue
MYH	Myosin Heavy Chain
MYL	Myosin Light Chain
NFAT2	Nuclear Factor of Activated T Cells 2
Nkx2.5	NK2 Homeobox 5
nm	nanometers
OCR	Oxygen consumption rate
OoC	Organ-on-a-chip
P/S or Pen/Strep	Penicillin/Streptomycin
PBS	Phosphate Buffered Saline
PDMS	Polydimethylsiloxane
PFA	Paraformaldehyde
PORCN	Protein-serine O-palmitoleoyltransferase “porcupine”
PSC	Pluripotent stem cell
RI	ROCK inhibitor
RNA	Ribonucleic acid
RNA-seq	RNA sequencing
ROCK	Rho-kinase inhibitor
rpm	revolutions per minute
RPMI	Roswell Park Memorial Institute Medium
s	seconds

SA-CM	Sinoatrial nodal CM (Pacemaker cell)
SAN	Sinoatrial node
SD	Standard deviation
SEM*	Scanning Electron Microscopy (<i>Introduction chapter</i>)
SEM	Standard error of mean (<i>Methods & Results chapters</i>)
SERCA2	Sarco/endoplasmic reticulum Ca ²⁺ -ATPase
SHF	Second heart field
SM22 α	Smooth Muscle Protein 22-Alpha (Transgelin; TAGLN)
SMC	Smooth Muscle Cell
SOX2	(Sex determining region Y)-box 2
sSMC	Synthetic Smooth Muscle Cell
ssRNA-seq	Single cell RNA-sequencing
T	Brachyury
t	timepoint
TBX18	T-Box Transcription Factor 18
TE-7	Anti-Fibroblasts antibody
TEM	Transmission Electron Microscopy
TGF- β	Transforming growth factor β
TNNI	Cardiac Troponin I
TNNT2	Cardiac Troponin T 2
TTN	Titin
TUNEL	Terminal deoxynucleotidyl transferase (TdT) dUTP Nick-End Labeling
WNT	Wingless/Integrated
WT1	Wilms tumor 1
YAP	Yes-associated protein

9 LIST OF FIGURES

Figure 1. 1 Classical approaches in cardiovascular tissue engineering	2
Figure 1. 2 Anatomy and cell types of the mammalian heart.	4
Figure 1. 3 Developmental timeline of mammalian cardiogenesis.	6
Figure 1. 4 Cardiac trabeculation and chamber maturation.	7
Figure 1. 5 Developmental origins of different cardiac cell types.....	8
Figure 1. 6 Regulation of heart development by transcriptional networks and signalling pathways.	9
Figure 1. 7 Regulation of cardiac subtype commitment in response to signalling pathways.	10
Figure 1. 8 Summary of mammalian cardiac commitment from embryonic development to mature heart.	11
Figure 1. 9 Cells of the adult human heart.....	12
Figure 1. 10 Cardiomyocyte ultrastructure.	14
Figure 1. 11 Ultrastructural differences in immature and mature CMs.....	15
Figure 1. 12 Hippo pathway during heart development and homeostasis.	19
Figure 1. 13 Cardiac fibroblast to myofibroblast conversion.	21
Figure 1. 14 Histopathology from healthy heart to cardiac fibrosis.	22
Figure 1. 15 Endothelial cell – cardiomyocyte crosstalk.....	23
Figure 1. 16 Characteristics of the smooth muscle cells.....	25
Figure 1. 17 The histopathology of common cardiomyopathies: HCM and DCM	28
Figure 1. 18 Characteristics of 2D hiPSC-derived CMs during culture timeline	31
Figure 1. 19 Different maturation approaches for hiPSC-CM cultures.....	33
Figure 1.20 Bioengineering approaches for cardiovascular tissue modelling	35
Figure 1.21 Heart-Dyno platform as a miniaturized EHT model.	38
Figure 1. 22 Basic design and operating steps of an exemplary organ-on-a-chip model ..	40
Figure 1. 23 Bridging the <i>in vitro</i> vs. <i>in vivo</i> gap on a "mechanobiology-on-chip" system	42
Figure 1. 24 Beating 3D “heart-on-a-chip” device featuring mechanical actuation.....	44
Figure 1. 25 Cardiac microtissue-chip used for metabolic maturation.....	45

Figure 1. 26 An example of cardio-breast cancer on-a-chip platform with integrated sensors.....	46
Figure 1. 27 Tri-cellular cardiac microtissues derived from pre-differentiated hiPSC-derived cell types	47
Figure 1. 28 Number of publications with keywords related to organoids and other cardiac tissue models on Pubmed between years 2011-2022.....	48
Figure 1. 29 Spheroids vs Organoids.....	49
Figure 1. 30 A brief history of human organoid models	49
Figure 1. 31 Capturing cardiogenesis in mammalian gastruloids.....	50
Figure 1. 32 Embryo-like Cardiac (Organoid) models vs native embryonic heart.....	51
Figure 1. 33 A schematic summary of 2D/3D methodologies to derive human cardiac organoids.....	53
Figure 1. 34 A schematic summary of developmental co-emergence of cardiac and gut tissues in long-term multilineage organoids.	55
Figure 3. 1 Schematic workflow for the generation and long-term culture of hiPSC derived cardiac microtissues.	77
Figure 3. 2 H&E staining on day 30 endpoint for microtissues made on day 7 vs. day 15 of differentiation.....	78
Figure 3. 3 H&E staining on day 50 endpoint for microtissues made on day 7 of differentiation (D7i).....	78
Figure 3. 4 H&E staining on day 50 endpoint for microtissues made on day 15 of differentiation (D15i).....	79
Figure 3. 5 Representative confocal images on day 30 and day 50 endpoints for D7i and D15i microtissue sections.	80
Figure 3. 6 Monitoring the spontaneous self-organization of hiPSC-derived cardiomyocytes within 3D microtissues over culture time	81
Figure 3. 7 Average diameter of 3D long-term cultured cardiac microtissues.....	81
Figure 3. 8 Cell viability of 3D long-term cultured microtissues with Calcein/AM staining on day 50.....	82
Figure 3. 9 TUNEL staining of human iPSC-derived microtissue (hOCMTs) cryosections.	83
Figure 3. 10 Ultrastructural analysis of the core of the microtissues.	84

Figure 3. 11 Long-term 3D cultures of hOCMTs results in the enrichment of the contractile cell population.....	85
Figure 3. 12 Long-term 3D cultures favour the enrichment of troponin T-positive cells.	86
Figure 3. 13 Long-term 3D culture of hOCMTs recapitulate es advanced cardiac morphology and cellular heterogeneity in vitro showing markers for cardiomyocyte, epicardial and fibroblast cell types.	89
Figure 3. 14 Long-term 3D culture of hOCMTs recapitulates advanced cardiac morphology and cellular heterogeneity in vitro showing markers for endocardial, endothelial, and cardiomyocyte subtypes.....	91
Figure 3. 15 Long-term hOCMTs show no evidence of gut tissue emergence.	92
Figure 3. 16 Ultrastructural analysis of 3D hOCMTs indicates enhanced maturation in 3D environment over time.	94
Figure 3. 17 Ultrastructural analysis of long-term hOCMTs indicates enhanced cardiomyocyte and metabolic maturation in 3D environment over time.	94
Figure 3. 18 DE analysis for 3D long-term cultures vs standard 2D monolayer cultures on day 30 and 50 timepoints	95
Figure 3. 19 GO biological process categories for the top 20 differentially regulated genes between 3D hOCMTs vs standard 2D monolayer cultures.	96
Figure 3. 20 3D long term culture determines an enrichment in the expression of cardiomyocyte-specific genes.....	97
Figure 3. 21 3D culture induces improved cardiac specification and cardiomyocyte maturation.	99
Figure 3. 22 Cluster analysis of the upregulated genes reveals an interconnected network of genes involved in heart contraction and sarcomeric organization.	100
Figure 3. 23 Cluster analysis of the upregulated genes hints at a network of genes involved in cardiomyocyte metabolism.	101
Figure 3. 24 3D long-term cultures show improved cardiac specification and cardiomyocyte maturation at transcriptional level than standard 2D cultures.....	102
Figure 3. 25 3D hOCMT cultures show transcriptional similarities to in vitro engineered heart tissues (EHT) with respect to cardiac specification and cardiomyocyte maturation.	103
Figure 3. 26 hOCMTs display the upregulation of metabolic genes.	105
Figure 3. 27 3D long-term cultures promote changes in hOCMT metabolic activity.	107
Figure 3. 28 Long-term 3D hOCMTs show functional response to cardioactive drugs in a dose and time dependent manner.	109

Figure 3. 29 Long-term 3D hOCMTs show functional response to cardiotoxic drugs in a dose and time dependent manner.110

10 LIST OF TABLES

Table 1. 1 Major Hallmarks of CM Maturation.....19

Table 1. 2 Various differentiation protocols to generate hPSC-derived CMs32

Table 1. 3 Comprehensive overview of cardiac microtissue, gastruloid and organoid models.....56

Table 1. 4 Non-exhaustive list of start-ups and companies focusing on *in vitro* cardiac models.....63

Table 2. 1 List of antibodies used for immunofluorescence experiments69

Table 2. 2 List of antibodies used for flow cytometry experiments.70

11 Curriculum Vitae as of April 2023

Ece Ergir, M.Sc.

Tissue Engineer | *Joint PhD candidate at TU Wien, Vienna, AUSTRIA & FNUSA-ICRC, Brno, CZECHIA* |

e-mail: eceergir2@gmail.com | *LinkedIn:* www.linkedin.com/in/ece-ergir-802029234

OVERVIEW

Tissue engineer with 5+ years of experience in pluripotent stem cells, 2D/3D cell culture, organoids, *in vitro* cardiovascular biology and organ-on-a-chip applications. Passionate about alternatives to animals for translational medicine and industrial applications following the 3R principles. Interested in bridging the gap between academia & industry, and science outreach to non-experts and general public.

EDUCATION

VIENNA UNIVERSITY OF TECHNOLOGY (TU Wien), Vienna, AUSTRIA

Doctor of Technical Sciences in Technical Chemistry (PhD/Dr. Tech.), Expected 2023

“Generation and Characterization of Human Organotypic Cardiac Microtissues for Translational Medicine” | *Joint dissertation with TU Wien, Vienna, AUSTRIA & FNUSA-ICRC, Brno, CZECHIA* | *Co-supervisors: Prof. Peter Ertl (TU Wien) & Dr. Giancarlo Forte (FNUSA-ICRC)* | *FEMTECH fellowship (Austria)* | *GPA: 1.14/1.00 (Austrian Grading System)*

UNIVERSITY OF APPLIED SCIENCES (FH) TECHNIKUM WIEN, Vienna, AUSTRIA

Master of Science in Tissue Engineering and Regenerative Medicine (M.Sc.), Awarded 2016

“Enrichment of Cardiac and Smooth Muscle Cells for the Establishment of a Microfluidic – based Heart Model” | *Co-supervisors: DI Dr. Carina Huber-Gries (FH Technikum Wien) & Prof. Peter Ertl (TU Wien)*

BILKENT UNIVERSITY, Ankara, TURKEY

Bachelor of Science in Molecular Biology and Genetics (B. Sc.), High Honor, Awarded 2008

Full Scholarship | High Honor Student | BilGent (Bilkent MBG Club) | GPA: 3.61/4.00 (Top 10%)

SCHOLARSHIPS & AWARDS

- 2022 Roche Travel Award for attending EuroOoCs meeting 2022, Grenoble (turned down due to being unable to attend in-person)
- 2019 Falling Walls Czech Republic- Audience Award
- 2016 FEMTECH Fellowship -Austria
- 2009 Awarded “Bourse du Gouvernement Français” for M2 studies
- 2008 Awarded full scholarship for one-year special studentship at Bilkent University
- 2008 Graduated from Bilkent University with High Honour degree (CGPA: 3.61/4.00 at first 10% of students)
- 2005 Awarded Full Scholarship for undergraduate studies at Bilkent University.
- 2004 Awarded Bilingual Diploma from International Baccalaureate Organization (IBO)

RESEARCH & WORK EXPERIENCE

PhD Student / Junior Researcher (FNUSA-ICRC, Brno, CZ)

2017 - 2023

“Generation and characterization of organotypic 3D cardiac microtissues / cardiac organoids.”

- Established new methodologies for the generation, characterization, and applications for long-term 3D cardiac microtissue / organoid methodologies derived from human induced pluripotent stem cells (hiPSCs).
- Conducted literature search, designed and performed experiments, analysed data, and reported results.
- Experienced in 2D/3D cell culture techniques, human induced pluripotent stem cells (hiPSCs), cardiac differentiation, RNA isolation, RT-qPCR, immunofluorescence, confocal microscopy, flow cytometry, basic bulk RNA-sequencing analysis.
- Drafted and finalized 3 peer-reviewed manuscripts.
- Supervised two first-year Ph.D. candidates.
- Scientific presentations & poster proceedings in various conferences.
- Visiting scientist at University of Melbourne, Australia. (November – December 2018).
- Student member of TERMIS (Tissue Engineering and Regenerative Medicine International Society).
- Student member of EUROoCS (European Organ-on-Chip Society).
- Audience Award Winner for Falling Walls Lab, CZ. (2019)
- Event & Social Media Manager at Pint of Science Austria. (2020 – Present)
- Short science communication video about PhD project for European Researchers' Night Intersections 2021: https://youtu.be/iDvQ_UhFyKs

PhD Candidate (Vienna University of Technology, Vienna, AT)

2016 - 2023

- Joint dissertation in progress on microphysiological cardiac tissue modelling between FNUSA-ICRC and TU Wien, co-supervised by Prof. Peter Ertl (TU Wien) and Dr. Giancarlo Forte (FNUSA-ICRC).
- Microfabrication of PDMS-based devices.
- FEMTECH Fellowship at LBI-Trauma Vienna (2016-2017)

M.Sc. Fellow / Junior Researcher (FH Technikum Wien, Vienna, AT)

2015 -2016

- Thesis on “Enrichment of cardiac and smooth muscle cells for the Establishment of a Microfluidic – based Heart Model” co-supervised by DI Dr. Carina Huber-Gries (FH Technikum Wien) & Prof. Peter Ertl (TU Wien).
- Conducted literature search, wrote SOPs, designed and performed experiments, analysed data, and reported results.
- Experienced in mouse embryonic stem cell culture & differentiation, cardiac differentiation, RT-qPCR, immunofluorescence, confocal microscopy, PDMS-based device microfabrication, microfluidic cell culture.
- Supervision of first-year tissue engineering M.Sc. students in project lab.
- Scientific presentations & poster proceedings in various conferences.

Research Associate (Vienna General Hospital (AKH), Vienna, AT) 2012 -2014

- Lab management & researcher at Department of Molecular Neurooncology, Department of Pediatrics at Okay Saydam Lab. “Characterization of circulating extracellular microvesicles in brain tumors”
- Serum isolation / biobanking from brain tumor patients, mammalian cell culture, RNA& Protein isolation, SDS-PAGE, Western Blotting, grant proposal writing.

Research Associate (Max Perutz Laboratories, Vienna, AT) 2011 -2012

- RNA biology at Renée Schroeder Lab.

Master 2 Recherche (Institut Albert Bonniot, Grenoble, FR) 2009 -2010

- RNAi & Epigenetics at André Verdel Lab.
- Yeast cell biology (*S. pombe*), gene silencing, RNA isolation, RT-qPCR

LIST OF PUBLICATIONS

- **Ergir, E.**, Oliver-De La Cruz, J., Fernandes, S. *et al.* Generation and maturation of human iPSC-derived 3D organotypic cardiac microtissues in long-term culture. *Sci Rep* **12**, 17409 (2022). <https://doi.org/10.1038/s41598-022-22225-w> (Original Research Article)
- Cassani M., Fernandes S., Vrbsky J., **Ergir E.**, Cavalieri F., Forte G. (2020) "Combining Nanomaterials and Developmental Pathways to Design New Treatments for Cardiac Regeneration: The Pulsing Heart of Advanced Therapies" *Frontiers in Bioengineering and Biotechnology*, **8**, 323. <https://doi.org/10.3389/fbioe.2020.00323> (Review Article)
- **Ergir, E.**, Bachmann, B., Redl, H., Forte, G., & Ertl, P. (2018). "Small Force, Big Impact: Next Generation Organ-on-a-Chip Systems Incorporating Biomechanical Cues." *Frontiers in Physiology*, **9**, 1417. <https://doi.org/10.3389/fphys.2018.01417> (Mini-review article).

ABSTRACTS and PRESENTATIONS

- **Ergir.E.**, “Generation and Characterization of Human iPSC-derived Cardiac Organoids for Translational Medicine”. TERMIS-EU Chapter 2022, Krakow, PL. *Oral presentation*
- **Ergir.E.**, et al. “Generation and Characterization of Human iPSC-derived Cardiac Organoids for Personalized Medicine” Biomania Student Scientific Meeting 2022, Brno, CZ, *Poster presentation.*
- **Ergir.E.**, et al. “Generation and Characterization of Organotypic Cardiac Microtissues for Personalized Medicine” TERMIS World Congress 2021, Maastricht, NL (Virtual Meeting) *Poster presentation.*
- **Ergir.E.**, et al. "Generation and Characterization of Cardiac Microtissues for Establishing a Heart Organoid-on-a-Chip Model" Conference: European Organ on a Chip Society Meeting 2021 (Virtual meeting.) *Poster presentation.*
- **Ergir.E.**, “Generation and Characterization of Organotypic Cardiac Microtissues for Translational Research” TERMIS-EU Workshop 2021, Brno, CZ (Virtual Meeting) *Rapid fire presentation.*
- **Ergir.E.**, et al. “Microphysiological Cardiac Spheroids in Translational Medicine” Conference: European Organ on a Chip Society Meeting 2020 (Virtual meeting). *Poster presentation.*
- **Ergir.E.**, et al. “Microphysiological Cardiac Spheroids in Health and Disease” Conference: European Organ on a Chip Society Meeting 2019, Graz, AT. *Poster presentation.*
- Purtscher M., **Ergir E.**, Monforte-Vila X., Huber-Gries C. “Establishment of an *in vitro* heart tissue model for pre-clinical screening of therapeutic agents using microfluidic technology.” Dechema 3D Cell Culture (2016), Freiburg, DE. *Poster presentation*
- Purtscher M., **Ergir E.**, Szwarc D., Huber-Gries C. (2016). “Microfluidic-based heart tissue model for directed development of cardiac-specific cell types.” Conference: Select Bio Organ-on-a-Chip Europe 2016, Cambridge, UK. *Poster presentation.*
- Purtscher M., **Ergir E.**, Szwarc D., Monforte-Vila X., Rünzler D., Huber-Gries C. “A microfluidic-based easy-to-use cardiac tissue model for drug screening applications” (2016), *Poster presentation.*
- **Ergir E.**, Perazza D., Todeschini L., Lambert E., Yoshida M., Verdel A . (2010). “A new actor in heterochromatin formation in *S. pombe*?” Conference: 6th Course of Epigenetics, Institut Curie, Paris, France. *Poster presentation.*

SKILLS AND INTERESTS

- **Wet-lab:**

Cell culture: Mammalian cell culture, (2D/3D), human induced pluripotent stem cell (iPSC) culture and differentiation techniques, murine stem cell culture and differentiation techniques (Embryonic Stem Cells & Cardiovascular Progenitor Cells), formation of embryoid and cardiac bodies, generation and handling of 3D microtissues & organoids, immunofluorescence staining, live and fixed cell imaging, confocal microscopy, flow cytometry

Molecular Biology: PCR, RT-qPCR, DNA & RNA isolation, bulk RNA-sequencing differential expression analysis (basic).

Microfluidics: Fabrication of miniaturized systems based on PDMS (polydimethylsiloxane), Cell culture handling within microfluidic setups.

- **Computational:** Microsoft Office (Word, Excel, Powerpoint), ImageJ, FlowJo, GraphPad Prism, Adobe Photoshop, AutoCAD, R & Python Languages (beginner, self-learner)
- **Languages:** Turkish (Native), English (C2), German (B1), French (A1), Czech (A1)
- **Other:** Drawing scientific cartoons, Science communication, VBC Mol Biol Orchestra (2011-2013), Piano

Vienna, April 2023



Signature

12 APPENDIX A: Additional Data and Clarifications

12.1 Excerpts from point-by-point responses to reviewers

Explanation for Fig 3.6 – 3.7 : High diameter distribution in microtissues of Day 42. The significance of the difference between D30 and D42 is doubtful.

In order to clarify the diameter distribution and the significance, we have included Table RA1-A displaying the raw measurement data from the center diameter of 6 independent microtissues calculated via ImageJ (where representative microtissue images were shown on the manuscript), and Tables RA1-B and C for the statistics used to generate Figure 3.7 in the manuscript via GraphPad Prism. The diameter variance of the microtissues is stated as: “The diameter of the microtissues reached up to 0.9 ± 0.04 mm on day 21 and 1 ± 0.09 mm on day 42 [...]”

The high diameter distribution could be attributed to batch to batch variances of individual iPSC-derived microtissues in long term culture. Despite the variance, the one-way ANOVA test between D30 and D42 was shown as significant, with adjusted p value being 0.0294 ($p < 0.05 = *$), as highlighted in Table RA1-B (please see below). Please notice the main scope of this analysis is mainly to highlight that the microtissues can reach up to 1 mm in long-term culture without any ECM supplementation.

A.

Diameter (μm), n=6		
D21	D30	D42
920.952	954.054	832.06
929.807	903.919	1000.198
928.452	930.058	926.991
944.888	829.642	1066.1
1025.052	799.686	1053.116
942.4	831.008	1045.163

B.

Ordinary one-way ANOVA

Number of families	1							
Number of comparisons per family	3							
Alpha	0.05							
Tukey's multiple comparisons test	Mean Diff.	95.00% CI of diff.	Significant?	Summary	Adjusted P Value			
D21 vs. D30	73.86	-27.84 to 175.6	No	ns	0.1768	A-B		
D21 vs. D42	-38.68	-140.4 to 63.03	No	ns	0.5954	A-C		
D30 vs. D42	-112.5	-214.3 to -10.84	Yes	*	0.0294	B-C		
Test details	Mean 1	Mean 2	Mean Diff.	SE of diff.	n1	n2	q	DF
D21 vs. D30	948.6	874.7	73.86	39.16	6	6	2.67	15
D21 vs. D42	948.6	987.3	-38.68	39.16	6	6	1.4	15
D30 vs. D42	874.7	987.3	-112.5	39.16	6	6	4.07	15

C.

	D21	D30	D42
Number of values	6	6	6
Minimum	921	799.7	832.1
Maximum	1025	954.1	1066
Range	104.1	154.4	234
Mean	948.6	874.7	987.3
Std. Deviation	38.52	62.9	91.42
Std. Error of Mean	15.73	25.68	37.32

Tables RA -1 –

- A. Raw measurement data from the center diameter of 6 independent microtissues generated via ImageJ in μm .
- B. One-way ANOVA analysis results of the diameter measurements, where Tukey's multiple comparisons test was used. (adjusted p-val $< 0.05 = *$)
- C. Descriptive statistics for the diameters on table RA1- A.

Explanation for Figure 3.14: Staining for CD31 remained poor. The size of the Day50 microtissues is very different in all three panels– at A is a too small one, at B is too big while at C is a middle.

Figures 3.13 and .14 are organized as to display the whole organoid cryosection in the top image and a detail in the bottom for each combination of antibodies. The position of the magnified detail is highlighted by a square in the top image. The rather different size of the microtissues in the panels can be explained by the position of the section within the construct. We are convinced the reader will be able to catch all the information on the size of the microtissues from Figure 3 and Table RA1.

Regarding the staining for CD31 in Figure 4 the signal was validated by using appropriate negative and positive controls, including human umbilical vein endothelial cells (HUVEC) and human iPSC-derived cardiac fibroblasts (iPSC-CFs) (Figure RA1). The antibody signal is acquired by confocal microscope and displays a very specific and discrete distribution in given areas of the microtissues. The presence of a limited number of CD31-positive cells is acknowledged in our flow cytometry results in Figures 3.11 and 3.12: “While a very limited number of CD31-positive cells was observed in any of the 2D culture timepoints, a significant increase in cells expressing the endothelial marker CD31 occurred during 3D culture (3D day 50: 12.78 ± 2.71 % vs 2D day 50: 4.07 ± 2.76 % in, $p < 0.001$).” Meanwhile on Day 50 3D microtissues, TNNT2-positive cardiomyocyte population is 83.27 ± 9.45 % and CD90-positive cell population is 23.38 ± 7.35 % as shown in Figure 2B. We have also already discussed the low number of CD31-positive cells in the Discussion section in the original manuscript: “The low number of CD31-positive cells might be explained by the fact that in native human heart endothelial cells have different developmental origins (*), and we did not supplement our culture media with endothelial-lineage favouring factors, like VEGF, during our study.”

(*) S. M. Meilhac and M. E. Buckingham, “The deployment of cell lineages that form the mammalian heart,” *Nat. Rev. Cardiol.*, vol. 15, no. 11, pp. 705–724, Nov. 2018.

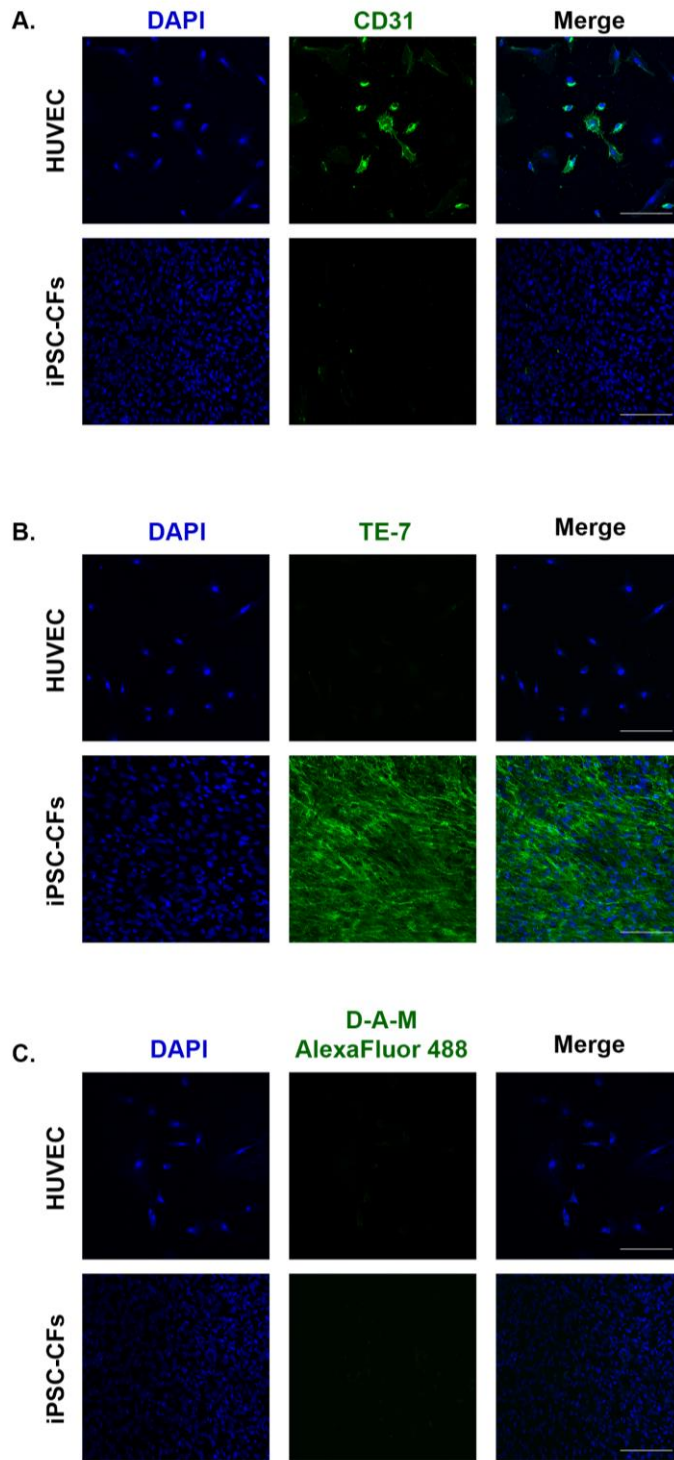


Figure RA1 – Control immunostaining for the antibody specificity of **A.** endothelial (primary: mouse anti-CD31, secondary: Donkey-anti-mouse Alexa Fluor 488; green), and **B.** fibroblast (primary: mouse anti-TE-7, secondary: Donkey-anti-mouse Alexa Fluor 488; green) markers on HUVEC and iPSC-CFs. **C.** Secondary antibody-only staining as negative control (Donkey-anti-mouse Alexa Fluor 488). Counterstaining was performed with DAPI (blue). Scale bars = 200µm

What changes have taken place in the beating of organoids during long-term culture?

As for the beating rate change of the microtissues in time, day 15 of the original protocol from Lian and colleagues is the timepoint where we generate our 3D microtissues, by enzymatic dissociation from the 2D cultures, followed by seeding 150,000 cells/well to round bottom ultra-low attachment plates with maintenance medium containing Rock inhibitor. Possibly due to the harsh nature of this dissociation and re-aggregation protocol, we could observe no beating until some microtissue and cell-cell contact is re-established, and stabilized again. Spontaneous microtissue formation without any ECM-supplementation occurs within 24-48 hours, and after the removal of Rock inhibitor from the medium, the beating gradually resumes again (could take up to 5-7 days since microtissue aggregation) in the following days, and stabilizes for an extended culture time. Please see [Supplementary videos 1 and 2](#) to see beating examples on day 50+ and day 100+ microtissues.

Although not included in the manuscript, we have analysed some beating microtissues at day 23 and day 57 timepoints to be able to answer the reviewer. Please see Figure RA2 below:

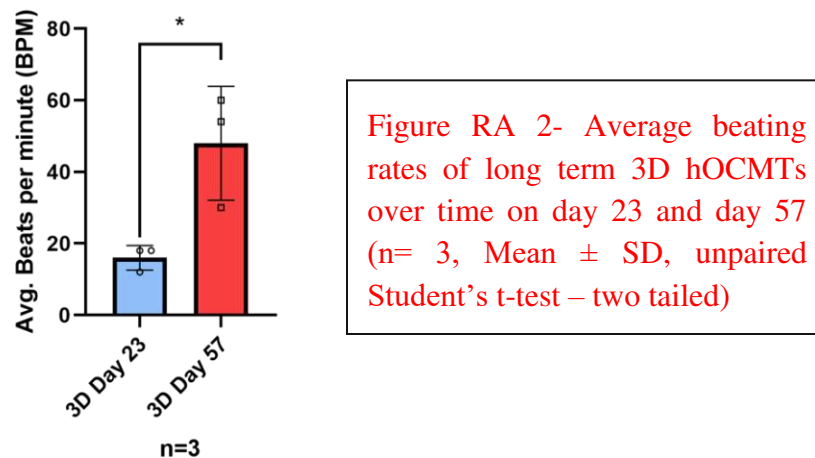


Figure RA 2- Average beating rates of long term 3D hOCMTs over time on day 23 and day 57 (n= 3, Mean ± SD, unpaired Student's t-test – two tailed)

Here a beating change between day 23 and day 57 timepoints could be observed (16 ± 3.46 bpm for day 23 vs 48 ± 15.57 bpm for day 57, mean ± SD, $p < 0.05$). Nevertheless, the value at day 23 could be affected by the experimental conditions, meaning that the microtissue might still be recovering from the dissociation at day 15. More characterization would be required to see the effect of cardiomyocyte number vs. beating rate on microtissues.

As for the request for electrophysiology studies of the microtissues, this is a very challenging request which we could not complete at this stage. Considering the short time proposed for the revision and the expertise needed to fulfil this request, a longer time would be needed to find expert collaborators and set up the appropriate experiment.

13 APPENDIX B: First attempt at hCO-on-Chip



«Orthogonal» interstitial fluid flow influences pre-vascular network formation

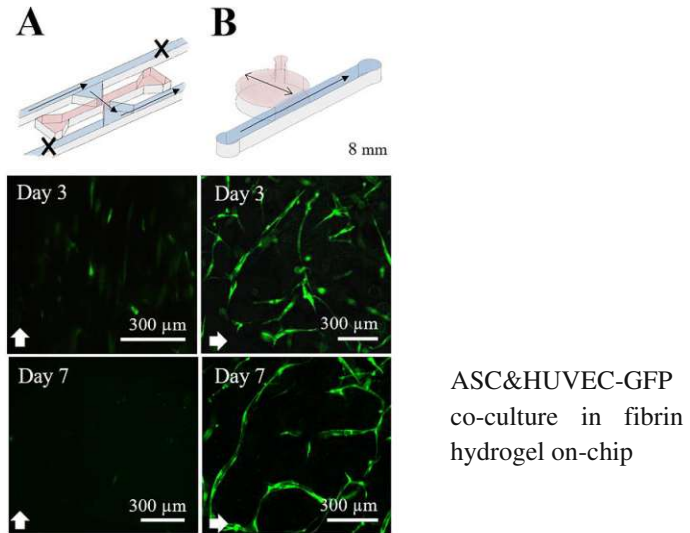
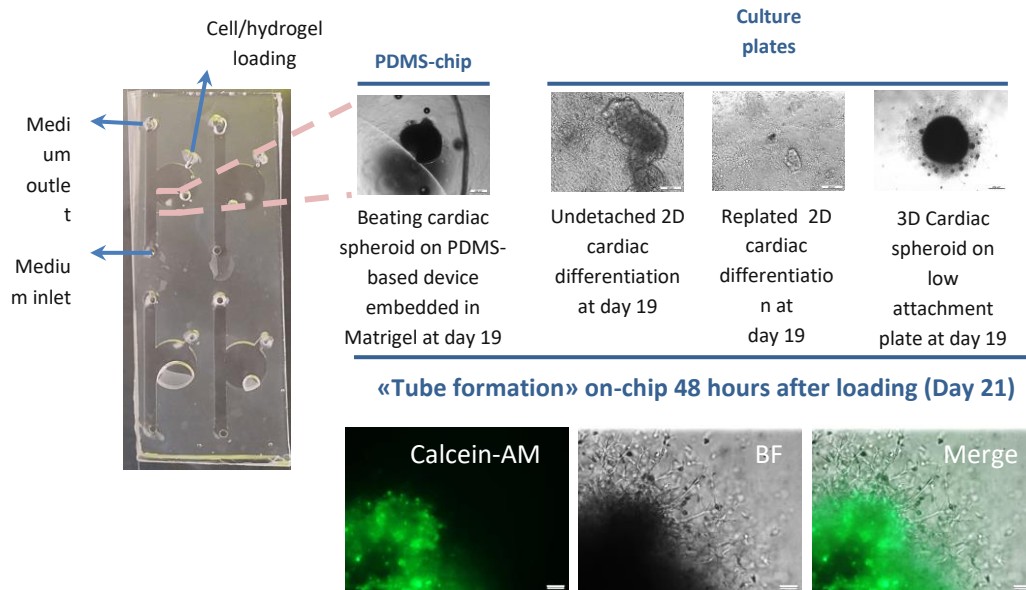


FIG. 4. Influence of direct compared to orthogonal interstitial fluid flow on pre-vascular network formation.

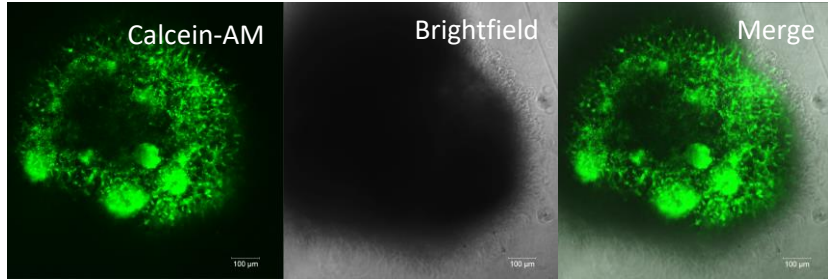
(Bachmann et al, 2018) *

Translation to Static Miniaturized Setup with Hydrogel

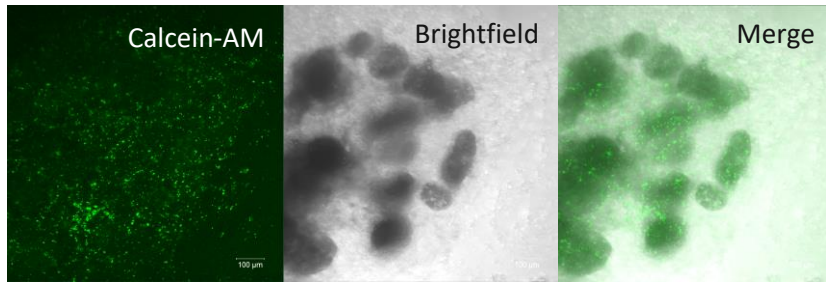


*Bachmann B, Spitz S, Rothbauer M, et al. Engineering of three-dimensional pre-vascular networks within fibrin hydrogel constructs by microfluidic control over reciprocal cell signaling. *Biomicrofluidics*. 2018 Jun 20;12(4):042216. doi: 10.1063/1.5027054. PMID: 29983840; PMCID: PMC6010359.

48 hours after chip seeding (D20)

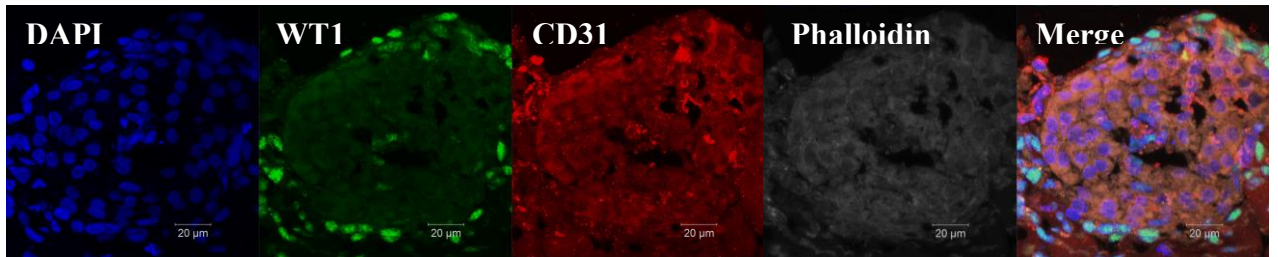
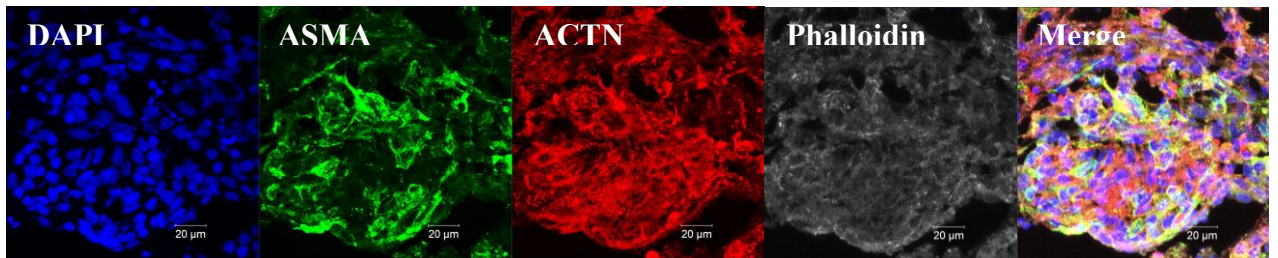


D50 on chip



Beware of cell spreading in classical Matrigel for long term culture

Differentiation «on-chip» (Day 50)



ACTN2: Cardiomyocytes, ACTA2: Smooth muscle, CD31: Endothelial, WT1: Epicardial marker

Despite cell spreading, cellular heterogeneity is preserved in long-term on-chip static culture with maintained beating.

14 APPENDIX C: Original Publications During Dissertation

- **Ergir, E.**, Oliver-De La Cruz, J., Fernandes, S. *et al.* (2022). "Generation and maturation of human iPSC-derived 3D organotypic cardiac microtissues in long-term culture." *Sci Rep* **12**, 17409. <https://doi.org/10.1038/s41598-022-22225-w> (Original Research Article)
- **Ergir, E.**, Bachmann, B., Redl, H., Forte, G., & Ertl, P. (2018). "Small Force, Big Impact: Next Generation Organ-on-a-Chip Systems Incorporating Biomechanical Cues." *Frontiers in Physiology*, *9*, 1417. <https://doi.org/10.3389/fphys.2018.01417> (Mini-review article).
- Cassani M., Fernandes S., Vrbsky J., **Ergir E.**, Cavalieri F., Forte G. (2020) "Combining Nanomaterials and Developmental Pathways to Design New Treatments for Cardiac Regeneration: The Pulsing Heart of Advanced Therapies" *Frontiers in Bioengineering and Biotechnology*, *8*, 323. <https://doi.org/10.3389/fbioe.2020.00323> (Review Article)

Manuscript I

Parts of this dissertation, including figures and tables, have been reproduced, with or without modifications, based on my original manuscript (Ergir et al., 2022) licensed for reuse under Creative Commons Attribution 4.0 International License. To view a copy of this licence, visit <http://creativecommons.org/licenses/by/4.0/>.

Generation and Maturation of Human iPSC-derived 3D Organotypic Cardiac Microtissues in Long-Term Culture

Sci Rep 12, 17409 (2022). <https://doi.org/10.1038/s41598-022-22225-w>

Ece Ergir^{1,2}, Jorge Oliver-De La Cruz¹, Soraia Fernandes¹, Marco Cassani¹, Francesco Niro^{1,3}, Daniel Pereira-Sousa^{1,3}, Jan Vrbský¹, Vladimír Vinarský¹, Ana Rubina Perestrelo¹, Doriana Debellis⁴, Natália Vadovičová³, Stjepan Uldrijan³, Francesca Cavalieri^{5,6}, Stefania Pagliari¹, Heinz Redl^{7,8}, Peter Ertl^{2,8}, and Giancarlo Forte^{1,9}

1 Center for Translational Medicine (CTM), St. Anne's University Hospital, International Clinical Research Centre (FNUSA-ICRC), CZ-62500, Brno, Czech Republic

2 Faculty of Technical Chemistry, Institute of Applied Synthetic Chemistry & Institute of Chemical Technologies and Analytics, Vienna University of Technology, AT-1040, Vienna, Austria

3 Faculty of Medicine, Department of Biomedical Sciences, Masaryk University, CZ-62500, Brno, Czech Republic.

4 Electron Microscopy Facility, Fondazione Istituto Italiano Di Tecnologia, Via Morego 30, IT-16163, Genova, Italy

5 Department of Chemical Engineering, The University of Melbourne, Parkville, Victoria 3010, Australia;

6 Dipartimento di Scienze e Tecnologie Chimiche, Università degli Studi di Roma Tor Vergata, via della Ricerca Scientifica 1, 00133, Rome, Italy

7 Ludwig Boltzmann Institute for Experimental and Clinical Traumatology, AUVA Research Center, AT-1200, Vienna, Austria

8 Austrian Cluster for Tissue Regeneration, AT-1200, Vienna, Austria

9 Department of Biomaterials Science, Institute of Dentistry, University of Turku, FI-20014, Turku, Finland

E.E. conceptualized the study, designed and performed the experiments, analysed the data and drafted the manuscript. J.O.D.L.C., S.F., M.C., V.V., A.R.P. and S.P. provided essential information and techniques, and assisted in designing, planning, carrying out and interpreting experiments. F.N. and D.P.S. performed experiments and analysed the data. J.V. and J.O.D.L.C. assisted with bioinformatics analysis. M.C. and D.D. performed the TEM analysis. N.V. and S.U. performed the Seahorse XF experiments and metabolic data analysis. F.C. and H.R. assisted in funding acquisition and manuscript revision. P.E. provided study supervision and manuscript revision. G.F. provided study supervision, funding acquisition, paper conceptualization and manuscript finalization. All authors contributed in interpretation, and presentation of data as well as manuscript editing. All authors reviewed and approved the final version. Figure 1a and 7a were drawn by J.O.D.L.C.

We acknowledge the CF Genomics of CEITEC supported by the NCMG research infrastructure (LM2018132 funded by MEYS CR) Bioinformatics for their support with obtaining scientific data presented in this study.



OPEN

Generation and maturation of human iPSC-derived 3D organotypic cardiac microtissues in long-term culture

Ece Ergir^{1,2}, Jorge Oliver-De La Cruz¹, Soraia Fernandes¹, Marco Cassani¹, Francesco Niro^{1,3}, Daniel Pereira-Sousa^{1,3}, Jan Vrbský¹, Vladimír Vinarský¹, Ana Rubina Perestrelo¹, Doriana Debellis⁴, Natália Vadovičová³, Stjepan Uldrijan⁵, Francesca Cavalieri^{5,6}, Stefania Pagliari¹, Heinz Redl^{7,8}, Peter Ertl^{2,8} & Giancarlo Forte^{1,9,✉}

Cardiovascular diseases remain the leading cause of death worldwide; hence there is an increasing focus on developing physiologically relevant in vitro cardiovascular tissue models suitable for studying personalized medicine and pre-clinical tests. Despite recent advances, models that reproduce both tissue complexity and maturation are still limited. We have established a scaffold-free protocol to generate multicellular, beating human cardiac microtissues in vitro from hiPSCs—namely human organotypic cardiac microtissues (hOCMTs)—that show some degree of self-organization and can be cultured for long term. This is achieved by the differentiation of hiPSC in 2D monolayer culture towards cardiovascular lineage, followed by further aggregation on low-attachment culture dishes in 3D. The generated hOCMTs contain multiple cell types that physiologically compose the heart and beat without external stimuli for more than 100 days. We have shown that 3D hOCMTs display improved cardiac specification, survival and metabolic maturation as compared to standard monolayer cardiac differentiation. We also confirmed the functionality of hOCMTs by their response to cardioactive drugs in long-term culture. Furthermore, we demonstrated that they could be used to study chemotherapy-induced cardiotoxicity. Due to showing a tendency for self-organization, cellular heterogeneity, and functionality in our 3D microtissues over extended culture time, we could also confirm these constructs as human cardiac organoids (hCOs). This study could help to develop more physiologically-relevant cardiac tissue models, and represent a powerful platform for future translational research in cardiovascular biology.

Cardiovascular diseases (CVD) remain the leading cause of death worldwide^{1–4}, and developing new therapies is still a major challenge, since a significant number of drug candidates fail to pass clinical trials, or are withdrawn from the market due to adverse side effects^{5–7}. In order to approve safer and more effective therapies, there is an increasing demand to develop faithful models of human heart tissue for pre-clinical research⁷. While recent technologies provide some insight into how human CVDs can be modelled in vitro, a comprehensive overview of the complexity of the human heart remains elusive due to the limited cellular heterogeneity, physiological complexity, or maturity of the constructs produced⁸. Furthermore, animal models may not always faithfully reflect the unique features of human biology and disease, and could give rise to ethical concerns^{9–11}.

¹Center for Translational Medicine (CTM), International Clinical Research Centre (FNUSA-ICRC), St. Anne's University Hospital, Studentská 812/6, 62500 Brno, Czech Republic. ²Faculty of Technical Chemistry, Institute of Applied Synthetic Chemistry and Institute of Chemical Technologies and Analytics, Vienna University of Technology, 1040 Vienna, Austria. ³Faculty of Medicine, Department of Biomedical Sciences, Masaryk University, 62500 Brno, Czech Republic. ⁴Electron Microscopy Facility, Fondazione Istituto Italiano Di Tecnologia, Via Morego 30, 16163 Genoa, Italy. ⁵Department of Chemical Engineering, The University of Melbourne, Parkville, VIC 3010, Australia. ⁶Dipartimento di Scienze e Tecnologie Chimiche, Università degli Studi di Roma Tor Vergata, via della Ricerca Scientifica 1, 00133 Rome, Italy. ⁷Ludwig Boltzmann Institute for Experimental and Clinical Traumatology, AUVA Research Center, 1200 Vienna, Austria. ⁸Austrian Cluster for Tissue Regeneration, 1200 Vienna, Austria. ⁹Department of Biomaterials Science, Institute of Dentistry, University of Turku, 20014 Turku, Finland. ✉email: giancarlo.forte@fnusa.cz

Induced pluripotent stem cell (iPSC) technology has revolutionized the differentiation and derivation of cardiomyocytes for personalized disease modelling and drug testing^{8,12–20}. However, when cultured in 2D as models for development, disease and toxicology^{18,21,22}, cardiomyocytes do not reflect the 3D complexity of the native tissue, where the geometry, the presence of different cell types and their interaction with the extracellular matrix (ECM) play a crucial role.

Early 3D cardiac tissue models called “cardiospheres” were developed by culturing human heart tissue biopsies, or by mixing non-isogenic populations of cardiomyocytes, non-myocytes and biocompatible hydrogels^{23–25}; however, such microtissues generally have limited culture continuity, self-organization and fail to capture the heterogeneity characteristic of organotypic models. Recently, cardiac tissue engineering technologies have enabled the development of more physiologically-relevant tissue models, which entail a higher degree of complexity, organization and dynamics^{26–29}, such as engineered heart tissues (EHTs)^{27,30,31}, isogenic cardiac microtissues^{24,32–37}, and organs-on-a-chip^{38–48}.

Organoids, defined as 3D miniaturized versions of an organ, are emerging as promising tools showing realistic micro-anatomy, and organ specific function^{9,49–51}. In order to be considered as an “organoid”, an *in vitro* model must fulfil specific requirements, including: (1) 3D multicellular composition with organ-specific cell types, (2) self-organization and histological resemblance to the tissue of origin and (3) recapitulation of at least one specialized biological function similar to the organ being modelled^{51–53}.

Well-established organoids have been already generated for the brain, kidneys, intestines, guts, lungs and many other organs^{9,54}, while organoid models of the heart have only started to emerge in the last couple of years^{55,56}. Notably, early mammalian cardiac organoids showing spontaneous self-organization with distinct atrium- and ventricle- like regions were generated from mouse pluripotent stem cells (PSCs)^{57,58}, or as a part of gastruloids⁵⁹. Shortly afterwards, human PSC-derived cardiac organoid models were described^{56,60–65}, which were developed with different approaches varying from assembling different cardiac cell types⁶², followed by other self-organized models more faithful to cardiac-specific development^{56,63–66}.

Recently reported human cardiac organoids include single chamber models—namely the left ventricle in the case of “cardioids”⁵⁶—, relying on an external ECM scaffold, such as Matrigel^{61,63}, display chamber-like structures^{56,64}, featuring the co-emergence of gut tissue together with atrial- and ventricular-like regions^{63,65}. While being extremely informative, most of these models are generated by short-term culture, while long-term culture could help them acquire a more mature phenotype, a feature which is usually desirable for more physiologically relevant *in vitro* tissue models^{67,68}.

Here, we aimed to establish a simple protocol to generate induced pluripotent stem cell (iPSC)-based human 3D cardiac microtissues that could be generated in scaffold-free conditions, cultured for extended periods, featuring multiple cell types of the human heart with spontaneous proto-tissue organization, preserve coordinated contractile activity for several months, and functionally responsive to cardioactive drugs—which are hereby referred as 3D human organotypic cardiac microtissues (hOCMTs). By combining RNA-sequencing, ultrastructural and metabolic analyses, we demonstrated that dimensionality and time in culture are crucial mediators of survival, differentiation, collective organization and maturation of hOCMTs. Finally, we confirmed our human organotypic cardiac microtissues (hOCMTs) qualify as 3D human cardiac organoids (hCOs), hence as an *in vitro* heart model, by proving their response to cardioactive and cardiotoxic drugs in long-term culture.

Results

2D-to-3D culture switch promotes spontaneous cardiac microtissue formation in scaffold-free conditions and proto-tissue organization in long-term culture. Since the 2D monolayer differentiation of induced pluripotent stem cell (iPSC)-derived cardiomyocytes is well established in the literature, and long-term cultures of iPSC-derived cardiomyocyte monolayers naturally tend to delaminate into beating clusters⁶⁹, we first performed human iPSC (hereafter hiPSC) differentiation in a 2D system and tested whether they could be used to generate 3D cardiac aggregates in the absence of any external ECM scaffold.

Cardiac differentiation was induced in confluent 2D hiPSC monolayers by sequential modulation of the WNT pathway with small molecules, in the absence of insulin⁷⁰ as previously described by Lian et al.^{13,14}. First, mesoderm specification was achieved by transient WNT activation through chemical inhibition of GSK3, followed by cardiac mesoderm differentiation through the inhibition of the WNT palmitoleoyltransferase PORCN^{13,14} (Fig. 1A). When beating cell clusters were observed (day 7), insulin supplement was added to the media, since it was needed for cell survival after early contractile cardiomyocytes emerged during differentiation⁷⁰. On day 15 of differentiation, the monolayer was dissociated into single cells and seeded on round-bottom ultra-low attachment plates in order to induce the spontaneous formation of aggregates in the presence of ROCK inhibitor (Fig. 1A). Throughout the study, we used 2D monolayer cultures as controls.

One day after switching the culture from 2 to 3D, we observed under the light microscope a tendency for the spontaneous formation of 3D microtissues without the need for any ECM scaffold, which started to show spontaneous beating behaviour upon removing the ROCK inhibitor after 48 h. To monitor this spontaneous cellular organization, we repeated the experiment to generate microtissues from hiPSC expressing GFP-tagged cardiac troponin I (TNNI1) reporter. As expected, we observed the emergence of GFP-expressing contractile cardiomyocytes together with non-GFP-tagged non-myocyte cells within the microtissues. With time in culture from day 21 to day 42, the GFP-tagged contractile cardiomyocytes and non-myocytes gradually and spontaneously rearranged within the microtissues from a random distribution to more discrete regions (Fig. 1B, Supplementary Fig. 1A). The diameter of the microtissues reached up to 0.9 ± 0.04 mm on day 21 and 1 ± 0.09 mm on day 42, in the absence of any external ECM supplementation (Fig. 1C, Supplementary Video 1 for day 53). The microtissues went on displaying spontaneous contractile activity in long-term culture and until at least day 100 (Supplementary Video 2 for day 107).

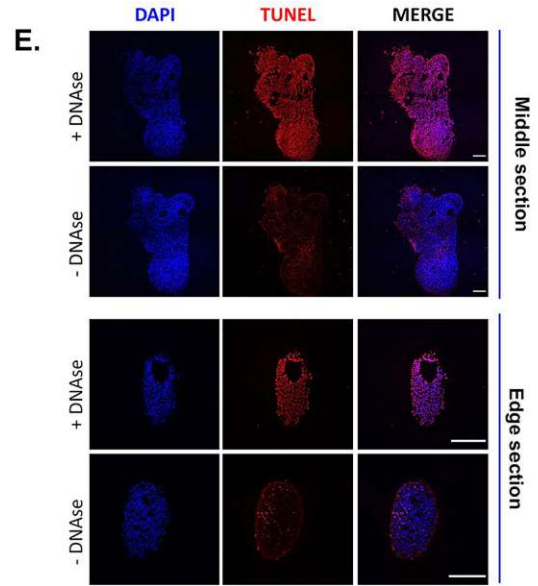
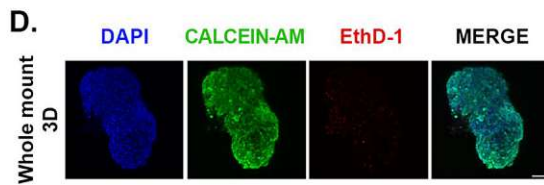
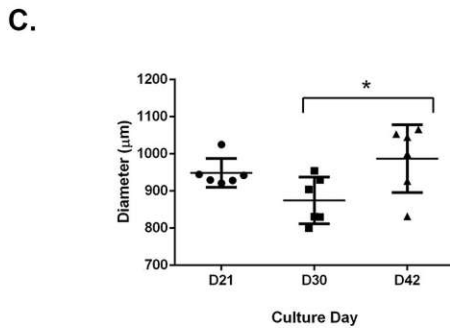
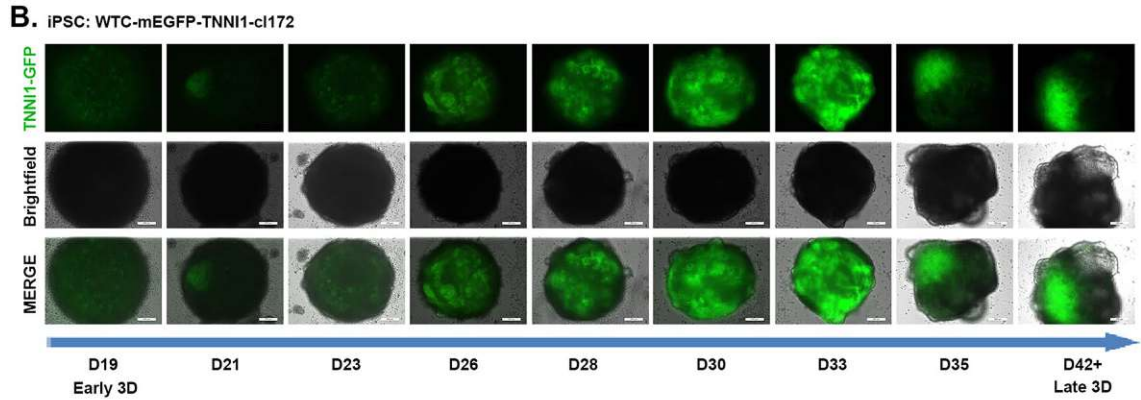
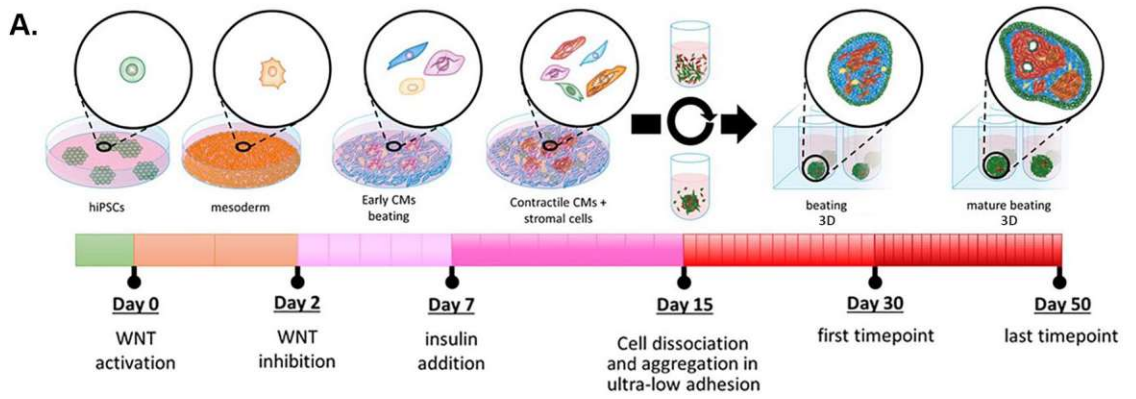


Figure 1. Long-term human cardiac microtissues can be spontaneously generated by scaffold-free conditions in 3D. **(A)** Schematic workflow for the generation and long-term culture of hiPSC derived cardiac microtissues. Warm colours represent cardiomyocyte lineages, while the rest of the colours represent non-myocytes. **(B)** Monitoring spontaneous self-organization of hiPSC-derived cardiomyocytes within 3D microtissues expressing GFP-tagged Cardiac Troponin I reporter over culture time (scale bar = 200 μ m). **(C)** Average diameter of 3D long-term cultured cardiac microtissues over time (n = 6, Mean \pm SD, Tukey's multiple comparisons test). **(D)** Cell viability of 3D long-term cultured microtissues with Calcein/AM staining on day 50, green = live, red = dead, blue = DAPI counterstain (Scale bar = 200 μ m). **(E)** TUNEL staining (red) depicting apoptotic cells on day 50 3D long-term cultured microtissue cryosections, and positive controls with DNase I treatment (edge and center). Nuclei were counterstained with DAPI (blue) (scale bar = 200 μ m).

This observation suggested that modifying a well-established 2D protocol^{13,14} into our 3D differentiation protocol could give rise to scaffold-free contractile cardiac microtissues that contain not only cardiomyocytes (GFP-tagged), but also other non-myocyte cell populations (non-GFP tagged), which collectively showed a tendency to be spontaneously redistributed in extended culture times.

A common drawback of 3D cultures is the possibility of apoptotic/necrotic core formation due to poor oxygen and nutrient diffusion towards the core of the construct⁷¹. In order to rule out that this occurs in our extended 3D cultures (day 50), we performed whole mount cell viability assay and despite some physiological levels of dead cells throughout the microtissues, we demonstrated no accumulation of non-viable cells was visible at the core of the constructs (Fig. 1D). Moreover, we complemented this analysis by performing Terminal deoxynucleotidyl transferase (TdT) dUTP Nick-End Labeling (TUNEL) assay, which detects the presence of apoptotic cells, on cryosections obtained from the edge and the core of the 3D tissues. Here we noticed no accumulation of apoptotic cells at either position in the 3D microtissues (Fig. 1E and Supplementary Fig. 1B). Finally, we confirmed the absence of a necrotic/apoptotic core by ultrastructural analysis of the core of the microtissue by transmission electron microscopy (TEM) (Supplementary Fig. 1C).

Due to the presence of intrinsic and spontaneous signs of proto-self-organization, cellular heterogeneity, and functional beating in our 3D microtissues over extended culture time, we will hereafter refer to these constructs as human organotypic cardiac microtissues (hOCMTs).

2D-to-3D culture switch prompts the formation of human iPSC-derived organotypic cardiac microtissues composed of multiple heart cell types. One of the key features of *bona fide* organoids is the presence of different cell types typical of the given organ, as well as their ability to self-organize in microstructures similar to the organ being modelled^{51–53}.

To assess the cellular heterogeneity of our 3D hOCMTs, we quantified the presence of the three most represented cell populations in the human heart over time^{72,73}—cardiomyocytes, fibroblasts and endothelial cells—by flow cytometry at given time-points (day 15, day 30 and day 50, Fig. 2A,B). On day 15 of differentiation (i.e. the first time-point of microtissue aggregation), the flow cytometry analysis of cardiac troponin T2 (TNNT2)-positive population indicated the differentiation into cardiomyocytes in 2D ($54.14 \pm 9.08\%$) in addition to a distinct population of CD90-positive non-myocytes ($28.87 \pm 13.04\%$). The flow cytometry analysis demonstrated that 3D extended culture was associated with a significant increase in the percentage of TNNT2-positive cardiomyocytes as compared to 2D culture (3D day 50: $83.27 \pm 9.45\%$ vs 2D day 50: $27.23 \pm 15.86\%$, $p < 0.0001$) (Fig. 2B). On the contrary, 2D culture was shown to favour the overgrowth of CD90-positive cells (2D day 50: $52.97 \pm 13.44\%$ vs 3D day 50: $23.38 \pm 7.35\%$, $p < 0.001$) (Fig. 2B). While a very limited number of CD31-positive cells was observed in any of the 2D culture timepoints, a significant increase in cells expressing the endothelial marker CD31 occurred during 3D culture (3D day 50: $12.78 \pm 2.71\%$ vs 2D day 50: $4.07 \pm 2.76\%$ in, $p < 0.001$) (Fig. 2B).

These results indicate that 2D-to-3D culture switch promotes the generation of heterogeneous microtissues and favours the survival of the cardiomyocyte population in extended culture.

To explore the cellular heterogeneity and the spatial distribution of different cell subsets in our 3D hOCMTs in more detail, cryosections were performed at day 50 of culture and stained to detect the presence of cells expressing markers specific of the different populations in the human heart⁷³ (Figs. 3, 4).

Confocal imaging showed that cells located at the periphery of the construct stained positive for markers of epicardial cells Wilms tumor protein 1 (WT1) and TBX18, in addition to epicardial/fibroblast markers TE-7 and SM22a (Tagln), which suggested the presence of these cells primarily forming an outermost layer (Fig. 3A–D). The center of the construct—instead—stained positive for cardiac troponin T2 (TNNT2) and sarcomeric α -actinin (ACTN2), thus describing the formation of a discrete cluster of cardiomyocytes. This result further confirmed the tendency of contractile cells to re-locate to the core of the construct within time in 3D culture that we noticed by using GFP-tagged cardiac troponin I (TNNI1) reporter hiPSC line (see Fig. 1B). Discrete areas could also be stained with endocardial cell markers NFAT2 and endothelial cell marker CD31 (Fig. 4A,B).

Next, we stained for ventricular (MYL2) or atrial (MYL7) Myosin Light Chain isoforms, as specific markers of atrial and ventricular cardiomyocytes or contractile cells at different stages of maturation⁷⁴. Here we could identify two distinct pools of cardiomyocytes that stained either positive for MYL7 only, or co-stained positive MYL2 and MYL7 (Fig. 4C). This result hinted at the possibility that either differentially specified cardiomyocytes or contractile cells at different stages of maturation co-existed with the contractile core of the 3D constructs.

In recent reports, the formation of 3D cardiac organoids was associated with the developmental co-emergence of elements of endoderm and mesoderm tissues resembling the development of the heart and gut in the embryo^{63,65}. We thus stained for markers of embryonic (SOX2) or adult gut tissue (ASCL2) together with markers of undifferentiated cells (MESP1, Brachyury) and detected no such cells in day 50 3D constructs (Supplementary Fig. 2A,B).

Furthermore, for cardiac morphogenesis (GATA4), Sarcoplasmic/Endoplasmic Reticulum Calcium ATPase 2 (SERCA2), smooth muscle/fibroblastic cells (α -SMA), and gap junction proteins (Connexin 43, or Cx43) were also observed within the microstructures (Supplementary Fig. 2C).

Altogether, these results confirmed that iPSC-derived 3D hOCMTs favours the survival of cardiomyocytes and contain multiple cell types of the human heart organized in distinct domains.

Human iPSC-derived organotypic cardiac microtissues display ultrastructural organization and maturation in long-term culture. A key feature of the adult heart is the existence of a highly recognizable three-dimensional ultrastructure due to the periodical repetition of the functional units of the contractile apparatus, the sarcomere. The length and the alignment of the sarcomeres, together with the interspacing of

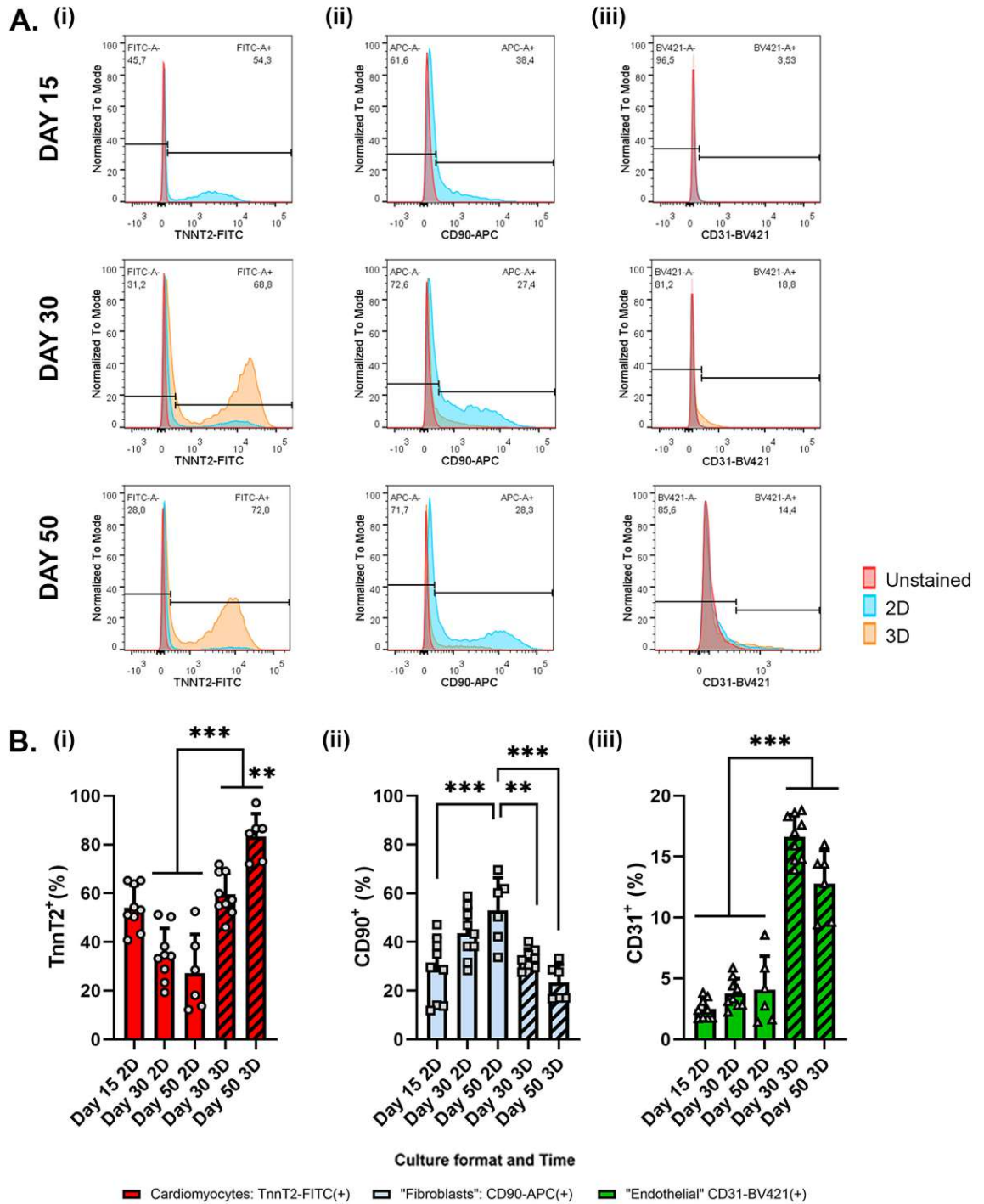


Figure 2. Long-term 3D cultures of hOCMTs contain multiple cardiac cell populations. (A) Representative flow cytometry histograms for analysis of cardiac cell types on day 15, day 30 and day 50, with a comparison of 2D and 3D cultures. (i) Cardiomycytes (TNNT2-FITC), (ii) "Fibroblasts" (CD90-APC), (iii) Endothelial cells (CD31-BV421). Red group represents unstained cells, blue group represents 2D cultures, and orange group represents 3D long-term cultured microtissues, and the gating with the black line depicts the percentage of populations for 3D long-term cultured microtissues. (B) Composite average of cardiac cell populations from all flow cytometry experiments: (i) Cardiomycytes (TNNT2-FITC⁺ %), (ii) "Fibroblasts" (CD90-APC⁺ %), (iii) Endothelial cells (CD31-BV421⁺ %), on day 15, day 30 and day 50, with a comparison of 2D and 3D cultures. The percentage indicates the positive cells versus total cells (mean ± SD obtained in three independent analyses, n = 9 per condition, Tukey's multiple comparisons test).

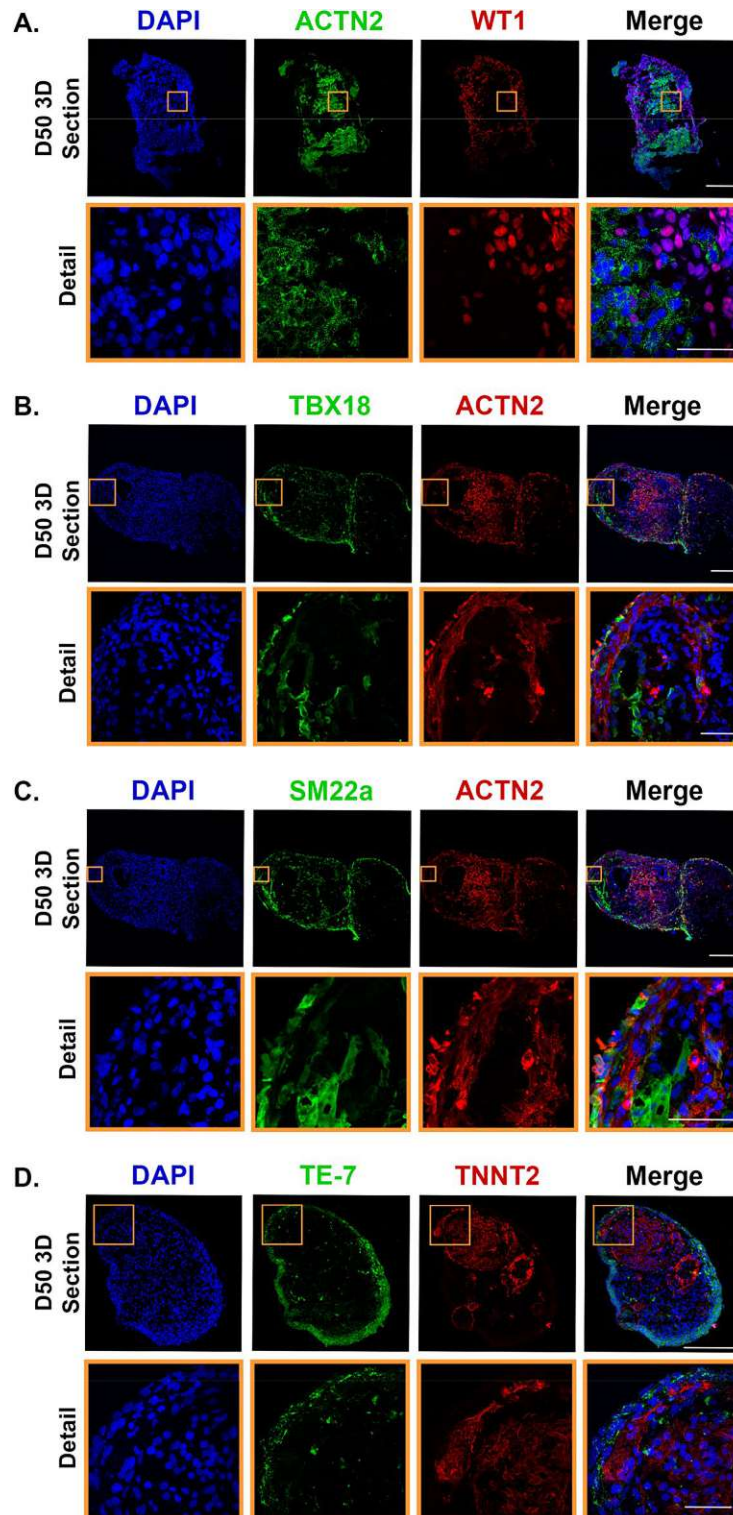


Figure 3. Long-term 3D culture of hOCMTs recapitulates advanced cardiac morphology and cellular heterogeneity in vitro showing markers for cardiomyocyte, epicardial and fibroblast cell types. Immunofluorescence analysis showing the representative co-specification of multiple cell type markers in 3D long-term cultured hOCMT sections on day 50 including cardiomyocytes ([A–D] ACTN2 in green or red, TNNT2 in red), epicardial cells ([A] WT1 in red, [B] TBX18 in green, [C] SM22a in green), epicardial/fibroblastic and smooth muscle cells ([C] SM22a in green), “fibroblasts” ([D] TE-7 in green). Nuclei were counterstained with DAPI (blue). Full 3D hOCMTs scale bar = 200 μ m, Detail scale bar = 50 μ m.

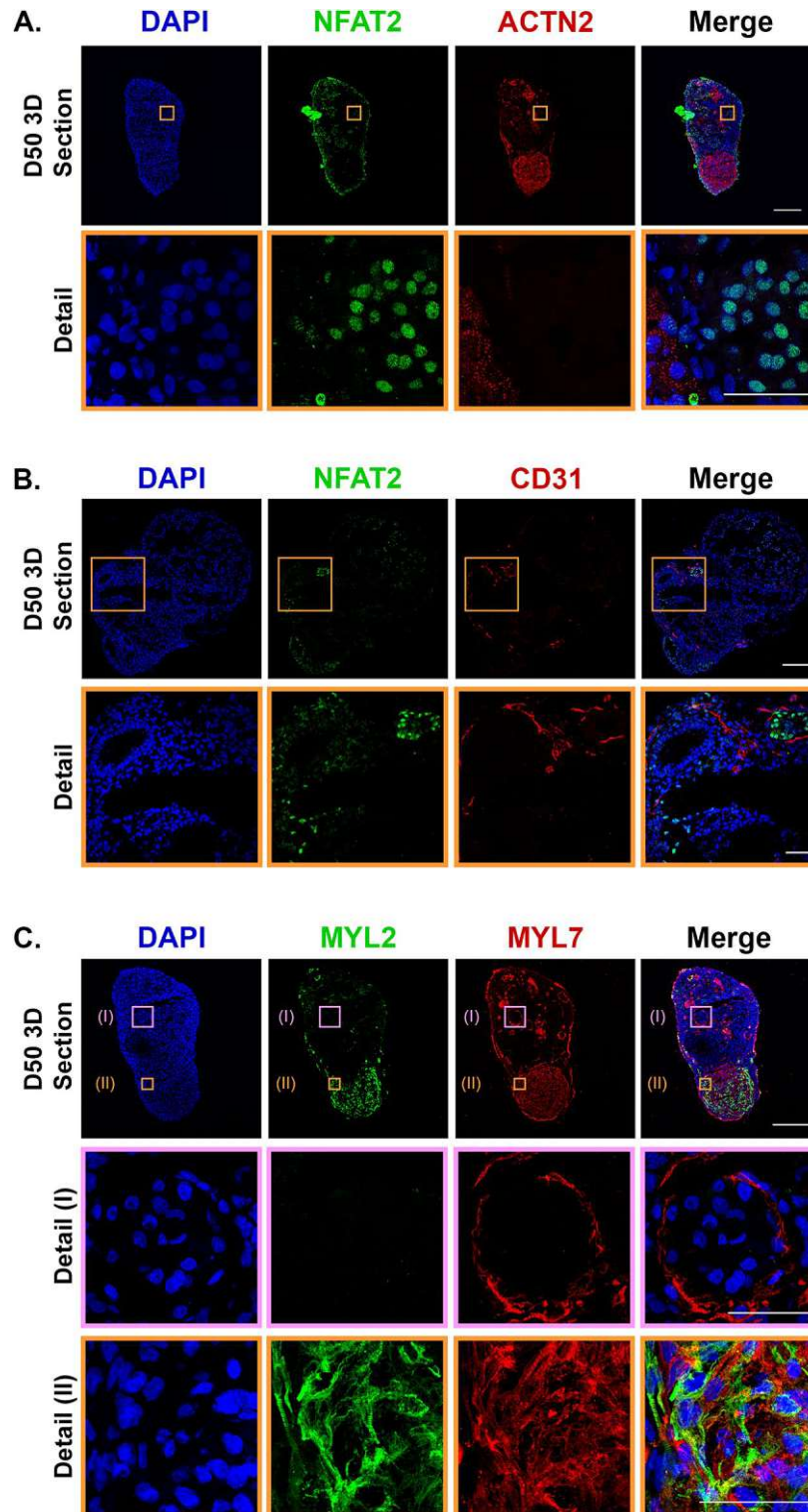


Figure 4. Long-term 3D culture of hOCMTs recapitulates advanced cardiac morphology and cellular heterogeneity in vitro showing markers for endocardial, endothelial, and cardiomyocyte subtypes. Immunofluorescence analysis showing the representative co-specification of multiple cell type markers in 3D hiPSCs-derived cardiac microtissue/hOCMT sections on day 50 including endocardial ([A,B] NFAT2 in green), endothelial cells ([B] CD31 in red), pan-cardiomyocytes ([A] ACTN2 in red), atrial ([C] MYL7 in green) and ventricular ([C] MYL2 in red) cardiomyocyte subtypes. Nuclei were counterstained with DAPI (blue). Full 3D hOCMTs scale bar = 200 μ m, Close-up scale bar = 50 μ m.

myosin-actin myofilaments and the abundance and shape of mitochondria, are considered representative of the maturity of the contractile tissue.

We analysed the ultrastructure of the contractile core of hOCMTs and assessed how it developed with time in culture by transmission electron microscopy (TEM). TEM analysis clarified that the prototypical contractile apparatus was hardly recognizable in hOCMTs cultured for 21 days, while highly organized sarcomeres with distinct z-disks and evenly distributed myofilaments could be detected in those cultured for 50 days (Fig. 5A,B).

The same analysis also demonstrated that longer culture times (day 85) led to the assembly of t-tubules close to the regularly spaced myofibrils, together with the appearance of packed and elongated mitochondria (Fig. 5F and Supplementary Fig. 3). The presence of t-tubules, extensions of the sarcolemma interspersed around the contractile apparatus to maximize the efficiency of calcium exchange, is only found in mature cardiac muscle and was not reported for standard 2D monolayer cultures⁷⁵. We found the sarcomere length to be approximately 1.5 μm (Fig. 5C,D). This value did not change at later time-points (day 85) and is consistent with the values described for young mammalian cardiomyocytes⁶⁷. Meanwhile, Z-band was found to increase slightly in width, but not significantly, with time in culture (700 ± 250 nm on day 85 vs. 450 ± 100 nm on day 50, $p < 0.0001$) as to get closer to the values typical of adult heart⁶⁷ (Fig. 5E–G).

Furthermore, TEM also demonstrated a higher amount of mitochondria and glycogen accumulation at later time-points (day 50 and 85) compared to day 21 (Supplementary Fig. 3), which suggests a metabolic shift to advanced maturation of cardiomyocytes⁶⁷. All these features indicate hOCMTs undergo structural and metabolic maturation⁶⁷ when cultured for long time in 3D.

3D long-term culture induces human iPSC-derived organotypic cardiac microtissue maturation. Contractile cell maturation can be monitored by tracking the evolution of the expression of specific genes encoding for contractile proteins. Hence, we set at investigating the transcriptional landscape of hOCMTs in order to assess the impact of time and dimensionality on the maturation of the contractile cells.

To this end, we performed bulk RNA-sequencing and differential expression analysis (DE analysis) on day 30 and 50 of the 3D culture and compared them to 2D monolayer cultures harvested at the same time-points (GEO: GSE209997), adult heart tissues and Engineered Heart Tissues (EHTs) obtained from previously published datasets (NCBI Bioproject accession numbers: PRJNA667310⁷⁶ and PRJNA628736⁷⁷ for adult heart, and PRJNA831794⁷⁸ for EHTs [alias GEO: GSE201437]).

A total of 2975 genes were found to be significantly and differentially regulated in 3D microtissues compared to monolayer cultures at day 30. This number increased to 6437 at day 50 (Fig. 6A and Supplementary Dataset 1, 2), possibly indicating a bigger divergence between 2 and 3D cultures over time.

The functional annotation at both time-points revealed that the genes differentially regulated 3D hOCMTs had a fingerprint for cardiogenesis, which included the categories of myofibril assembly and sarcomeric organization, muscle contraction and cardiac tissue morphogenesis (Fig. 6B). As an example, the top 20 deregulated genes at day 50 between 3D and monolayer cultures included genes which are well known to be involved in cardiac muscle maturation and function, namely cardiac muscle α -actin (*ACTC1*), sarcomeric α -actinin (*ACTN2*), phospholamban (*PLN*) and myosin heavy chain 7 (*MYH7*) (Fig. 6C). On the contrary, 2D cultures showed an increased expression in ECM-related genes, most likely as a result of the predominance of cardiac fibroblast population in monolayer culture (Fig. 6B,C and Supplementary Fig. 4).

Clustering analysis of the genes upregulated in 3D hOCMTs compared to 2D monolayer cultures at day 50 showed a highly interconnected network of genes involved in heart contraction and sarcomeric organization, which included important structural proteins of the contractile apparatus such as *ACTC1*, *ACTN2*, troponins (*TNNT2*, *TNNC1*, *TNNI1*, *TNNI3*), myosin heavy (*MYH6*, *MYH7*) and light (*MYL2*, *MYL3*) chains, dystrophin (*DMD*), titin (*TTN*), obscurin (*OBSCN*) and myozenin 2 (*MYOZ2*), among many others (Fig. 6D).

In good agreement with the presence of t-tubules in 3D hOCMTs and their drift towards a more mature intracellular Ca^{2+} -dependent contraction, we detected the enhanced expression of the SERCA Ca-ATPase 2 (*AT2A2*) and its inhibitor phospholamban (*PLN*), triadin (*TRDN*), ryanodine receptors (*RYR2* and the Purkinje's cell specific *RYR3*), calsequestrins (*CASQ1*, *CASQ2*), as well as genes related to cardio-renal homeostasis angiotensinogen, atrial natriuretic peptide and corin (*AGT*, *NPPA*, *CORIN*). Interestingly, in accordance with the marked increase in the number of mitochondria observed in the TEM images (see Fig. 5A, Supplementary Fig. 3), day 50 3D hOCMTs showed an upregulation in the network of genes associated with mitochondrial ATP synthesis coupled electron transport, including several NADH:ubiquinone oxidoreductase and Cytochrome c oxidase subunits (Fig. 6D).

Since long-term 3D cultures seemed to be able to promote the maturation of hOCMTs, we set at comparing the transcriptomic landscape of our in vitro constructs with available datasets obtained from adult atrial and ventricular heart tissues^{76,77} (Fig. 6E).

Sample clustering showed that day 50 3D hOCMTs were closer to adult heart at transcriptional level, with the most similar levels being associated with the expression of several sarcomere-associated genes, including *TTN*, *ACTN2*, troponins (*TNNT2*, *TNNI3K*, *TTNC1*, *TNNI3*) and Myosin heavy chains (*MYH6*, *MYH7*, *MYH7B*), as well as important components of the calcium handling apparatus (*RYR2*, *ATP2A2*, *PLN*). Consistent with our immunostaining results, day 50 3D microtissues displayed both atrial (*MYL4*, *MYL7*, *MYBHL*) and ventricular (*MYL2*, *MYL3*, *FHL2*) chamber markers (Fig. 6E). In accordance with the increased number of mitochondria (see Fig. 5A, Supplementary Fig. 4), and the upregulation of mitochondrial ATP-synthesis related transcript (Fig. 6D), the comparison of day 50 hOCMTs also showed similar clusters on metabolic genes to adult heart, such as oxidative phosphorylation (*PPPARGC1A*, *MT-ATP6*), fatty acid metabolism (*FABP3*, *GPAT3*, *PAM*), lipid metabolism (*FITM1*, *PRKAA2*, *INPP4B*), and glycogen metabolism (*PPP1R3A*).

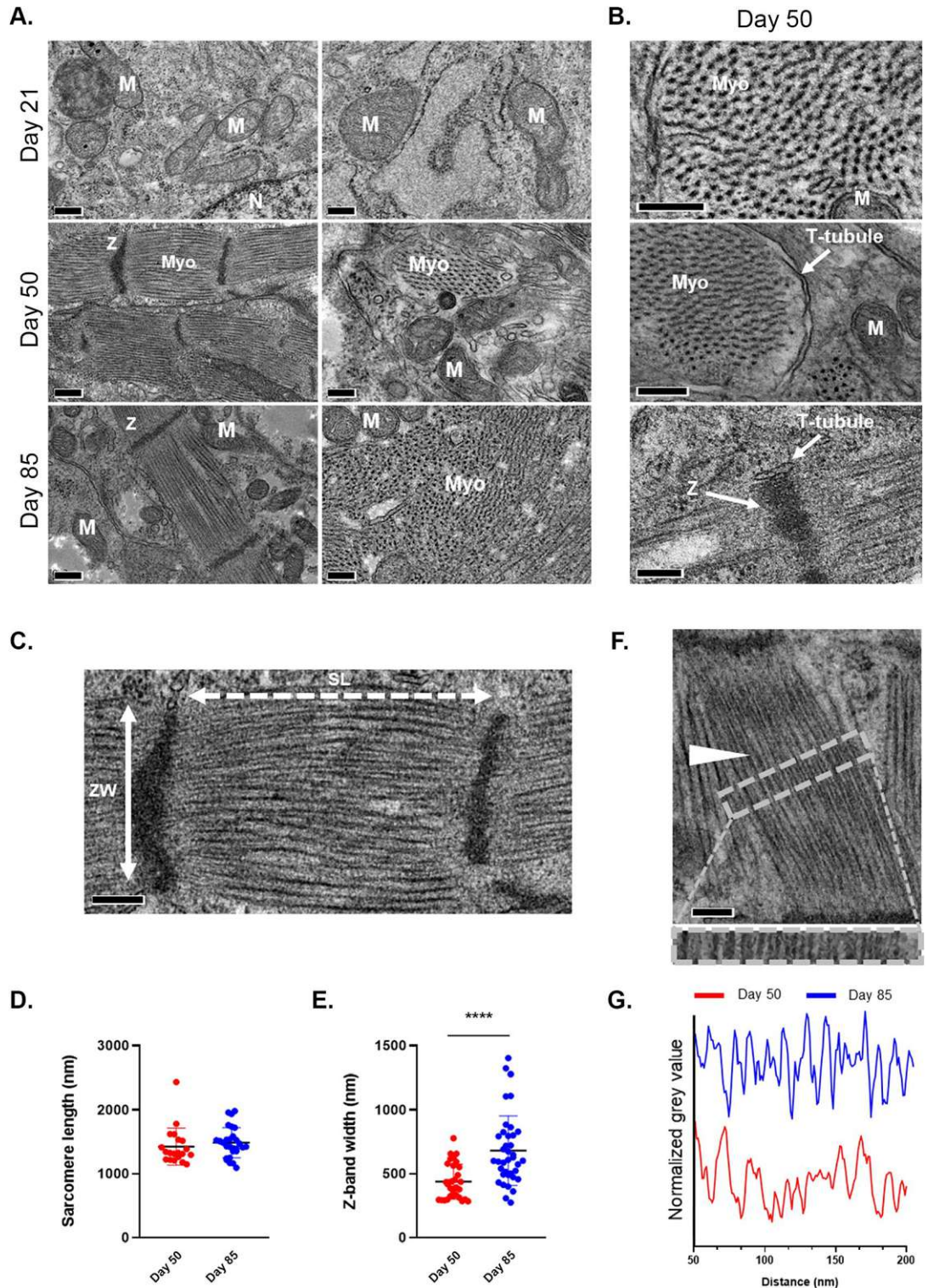


Figure 5. Ultrastructural analysis of 3D hOCMTs indicates enhanced maturation in 3D environment over time. (A) TEM images of 3D hOCMTs showing increasing ultrastructural organization over time, from day 21 to day 85: Cardiomyocyte myofibers (Myo), Mitochondria (M) Z-band (Z), T-tubules. Scale bars = 200 nm. (B) Close-up images on day 50. Scale bars = 200 nm. (C) Representative micrograph showing sarcomere length (SL; white dotted two-headed arrow) and z-band width (ZW; cross sectional length; white solid two-headed arrow) with the corresponding sarcomere length (D); day 50, 1400 ± 300 nm; day 85, 1500 ± 200 nm; N > 20, Mean ± SD)- and z-band width (E); day 50, 450 ± 100 nm; day 85 700 ± 250 nm; N > 30, Mean ± SD). Scale bar = 200 nm. (F) Micrograph showing myofiber organization (white arrow) with their relative organization as defined by the plot profile intensity on day 50 vs day 85 (G) of the area indicated by the grey dashed box of (F). Scale bar = 200 nm.

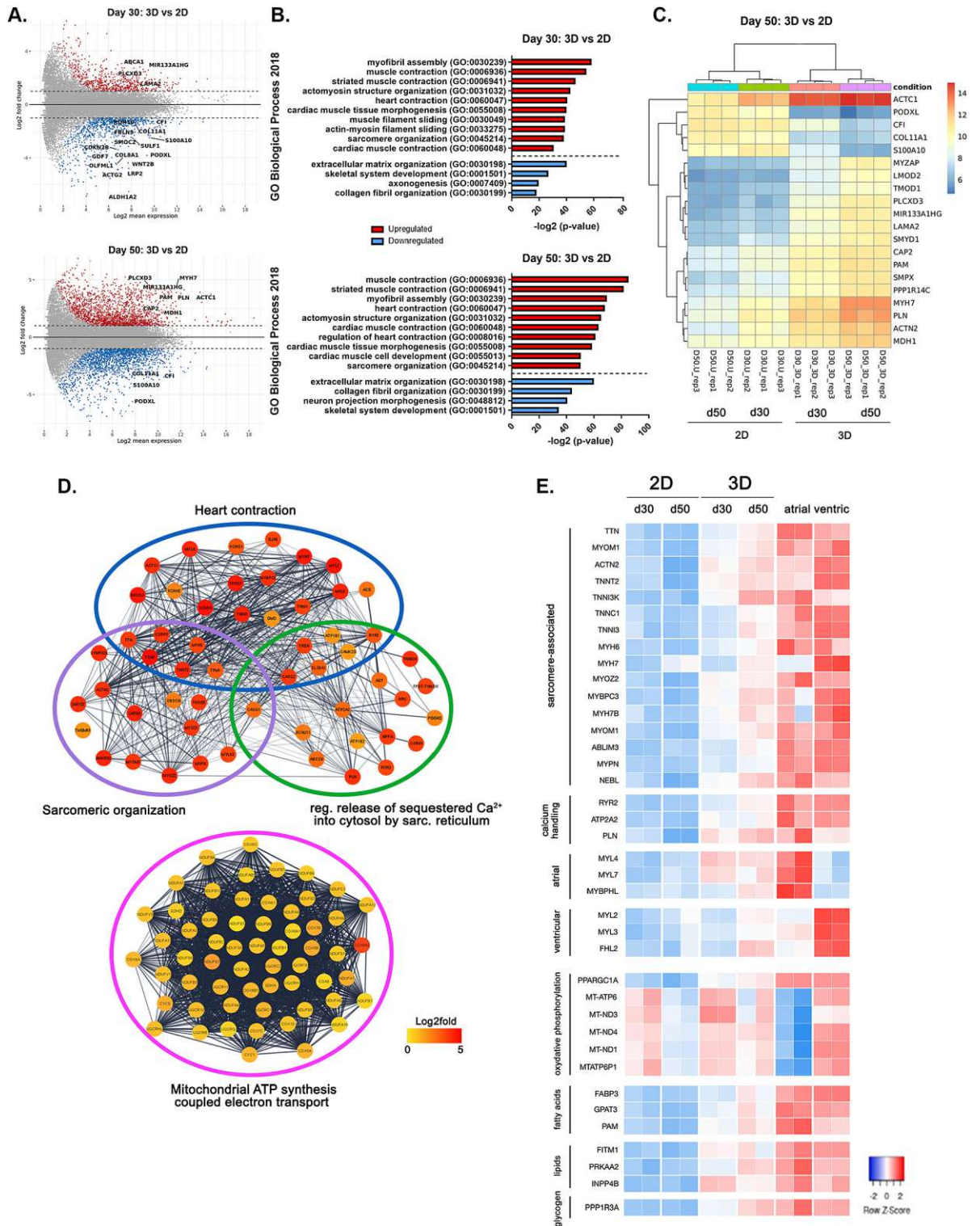


Figure 6. 3D long-term cultures induce improved cardiac specification and cardiomyocyte maturation at transcriptional level. (A) MA plot of the differentially regulated genes between 2D monolayer and 3D hOCMTs at day 30 (up) and day 50 (down) (\log_2 mean, $p_{\text{adj}} < 0.05$). (B) Graph representing the $-\log_2$ value adjusted p-value of significantly upregulated (red) or downregulated (blue) GO Biological process categories when comparing 3D hOCMTs and 2D monolayers at day 30 (up) and day 50 (down) ($p_{\text{adj}} < 0.05$). (C) Heatmap representing the \log_2 fold change for the top 20 differentially regulated genes between 2D monolayer and 3D hOCMTs at day 50 ($p_{\text{adj}} < 0.05$). (D) STRING network of the upregulated genes at day 50 hOCMTs as compared to monolayer cultures for the indicated GO biological processes categories by Cytoscape (Kappa score = 0.3). \log_2 fold change for the nodes (genes) is represented using a color-coded scale. (E) Heatmap encoding for \log_2 fold changes in selected cardiac genes for the 3D hOCMTs and the 2D monolayers at both time-points in comparison with available datasets for adult human atrial and ventricular tissues ($p_{\text{adj}} < 0.05$).

Finally, we compared the transcriptome of our 3D hOCMTs to Engineered Heart Tissue (EHT)^{31,78}, a well-established model of 3D cardiac tissue obtained from hiPSCs. The analysis demonstrated that 3D long-term culture (day 50) prompted the expression of similar levels of genes encoding for sarcomere-associated proteins, which included *TTN*, *ACTN2*, troponins (*TNNT2*, *TNNI3K*, *TNNI3*), Myosin heavy chain (*MYH7*), calsequestrins (*CASQ2*) among many others (Supplementary Fig. 5).

Overall, transcriptomics analysis confirmed that our long-term 3D protocol induced hiPSCs cardiac specification and cardiomyocyte maturation at a metabolic, calcium handling and sarcomeric level. The maturation of 3D hOCMTs is strongly promoted by time in culture.

Long-term human iPSC-derived organotypic cardiac microtissues display enhanced metabolic activity. The transcriptomic analysis of 3D hOCMTs was further exploited to investigate their metabolic maturation as compared to the 2D monolayers.

The heart is characterized by very high and distinct metabolic demands, with adult cardiomyocytes relying on oxidative phosphorylation for ATP production. On the contrary, immature hiPSC-derived cardiomyocytes display continued reliance on glycolysis as the primary source of energy⁷⁹. Although the healthy heart can oxidize several substrates from energy production, classic studies estimate that ATP production comes preferentially from fatty acid (FA) oxidation, accounting for around 70% of the total generation. The rest is provided by alternative substrates, including glucose, lactate and pyruvate⁸⁰.

Our 3D hOCMTs displayed higher expression of genes related to the FA β -oxidation, which has been previously associated with a more mature phenotype in hPSC-CMs (Fig. 7A)⁸¹. The expression of key regulator PPARA was—in fact—enhanced in the 3D culture. More directly into the lipid metabolism, the heart-type fatty acid binding protein (*FABP3*) and the lipoprotein lipase (*LPL*) displayed 4 times fold upregulation (Fig. 7A). The cytosolic fatty acyl-CoA synthase (*ACSL1*) catabolizing the long-chain acyl-CoA ester production, and the proteins required for their transfer into mitochondria (*CPT1A*, *CPT2*, *CRAT*, *SLC25A20*) were also found increased in the hOCMTs. Inside the mitochondria, most of the genes related to β -oxidation were found significantly upregulated as well, including the sequential acyl-CoA dehydrogenases (*ACDVL*, *ACDL*, *ACDM*, *ACDS*), which are highly expressed in the myocardium. The expression of several genes associated with peroxisomal FA intake and β -oxidation were also found upregulated.

Nevertheless, crucial genes related to glucose and pyruvate metabolism were also upregulated in the hOCMTs: this list included the glucose transporters *SLCA3* (GLUT3) and *SLCA4* (GLUT4), most of the enzymes associated with glycolysis, the proteins transporting the resulting pyruvate into the mitochondria (*MPC1*, *MPC2*), and its conversion into Acetyl-CoA (*PDHA1*, *DLAT*, *DLDD*). Similarly, transcripts encoding for all the catabolic steps of the tricarboxylic acid cycle were more abundant in the 3D hOCMTs (Fig. 7A).

In accordance with the increased number of mitochondria (see Fig. 5A, Supplementary Fig. 3), this increase in mitochondrial metabolism was combined with an increase in the expression of genes associated to ATP synthesis-coupled electron transport. Most of the genes encoding for the proteins composing the four electron transport protein complexes were found upregulated, as well as the vast majority of the subunits of the adenosine triphosphate (ATP) synthase itself (Fig. 7A, up). Several of the mitochondrial genes associated with the electron transport chain were likewise enriched in the hOCMTs, including NADH-ubiquinone oxidoreductase chain subunits (ND1, ND2, ND3, ND4, ND4L, ND5) and ATP synthase subunits (ATP6, ATP8).

In order to confirm that 3D long-term (over 50 days) culture induces hiPSC metabolic maturation, we performed real-time analyses of 2D monolayer and 3D microtissue cultures' energy metabolism using the Seahorse XFp Analyzer and Seahorse Mito Stress Test Kit. Results presented in Fig. 7B indicate a highly energetic phenotype of 3D hOCMTs compared to the 2D cultures. The 3D cultures not only exhibited a significantly higher oxygen consumption rate (OCR) than the 2D cultures (111.83 ± 17.21 vs 55.43 ± 2.82 pmol/min/300 ng DNA—the last baseline measurement before Oligomycin injection) but also increased extracellular acidification rate (ECAR, 35.09 ± 4.60 vs 12.19 ± 1.24 mpH/min/300 ng DNA—the last baseline measurement before Oligomycin injection).

A detailed analysis of the Mito Stress Test data revealed a significantly higher basal mitochondrial respiration in the 3D cultures (94.38 ± 16.28 vs 40.22 ± 1.89 pmol/min/300 ng DNA, $p < 0.05$; Fig. 7C). Interestingly, the 2D cultures showed a higher spare respiratory capacity than the 3D cultures (125.35 ± 15.52 vs 48.20 ± 10.18 pmol/min/300 ng DNA, $p < 0.01$; Fig. 7C). Notably, despite a relatively high dissipation of the mitochondrial proton gradient in hOCMTs (proton leak, 37.37 ± 5.75 vs 8.02 ± 2.13 pmol/min/300 ng DNA, $p < 0.01$; Fig. 7C), the 3D cultures produced significantly more ATP via mitochondrial respiration than their 2D counterparts (ATP production, 32.62 ± 7.08 vs 2.59 ± 0.95 pmol/min/300 ng DNA, $p < 0.01$; Fig. 7C).

Our transcriptomics and Seahorse XF metabolic flux data suggest that hOCMTs showed an enhanced metabolic activity, which was associated with increased metabolic signatures related to FA oxidation, mitochondrial respiration and glycolysis.

Human iPSC-derived organotypic cardiac microtissues functionally respond to drugs in a dose dependent fashion in long-term culture. An essential feature of *bona fide* organoids is to replicate at least one specialized function of the modelled organ^{51–53}, which in the case of heart tissue can be assessed by the contractile activity of human cardiac organoids (hCOs). As previously indicated, once our 3D hOCMTs acquired spontaneous contractile activity early in culture (48 h post aggregation), the contractility persisted for more than 100 days (Supplementary Video 2).

In order to test their physiological significance, 3D hOCMTs were exposed to clinically relevant doses of cardioactive drugs^{82,83} in long-term cultures (> day 50). In detail, isoproterenol and verapamil were used as positive and negative inotropes, respectively. Isoproterenol, a beta-adrenergic agonist, increases the contractile force and beating frequency⁸⁴, while verapamil, a calcium channel blocker, decreases the beating rate⁸⁵. The hOCMTs

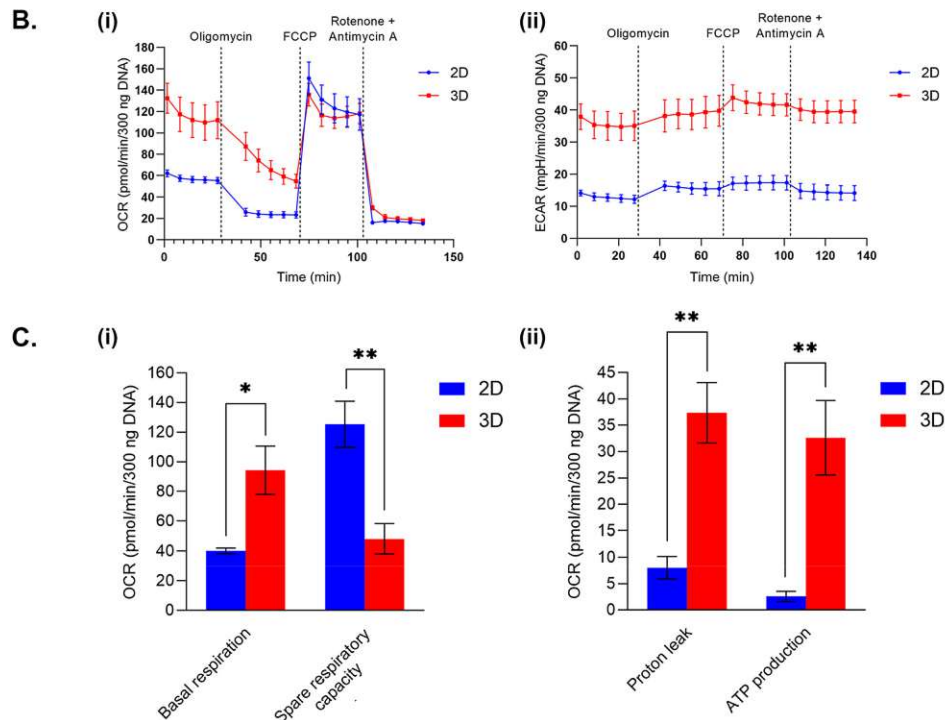
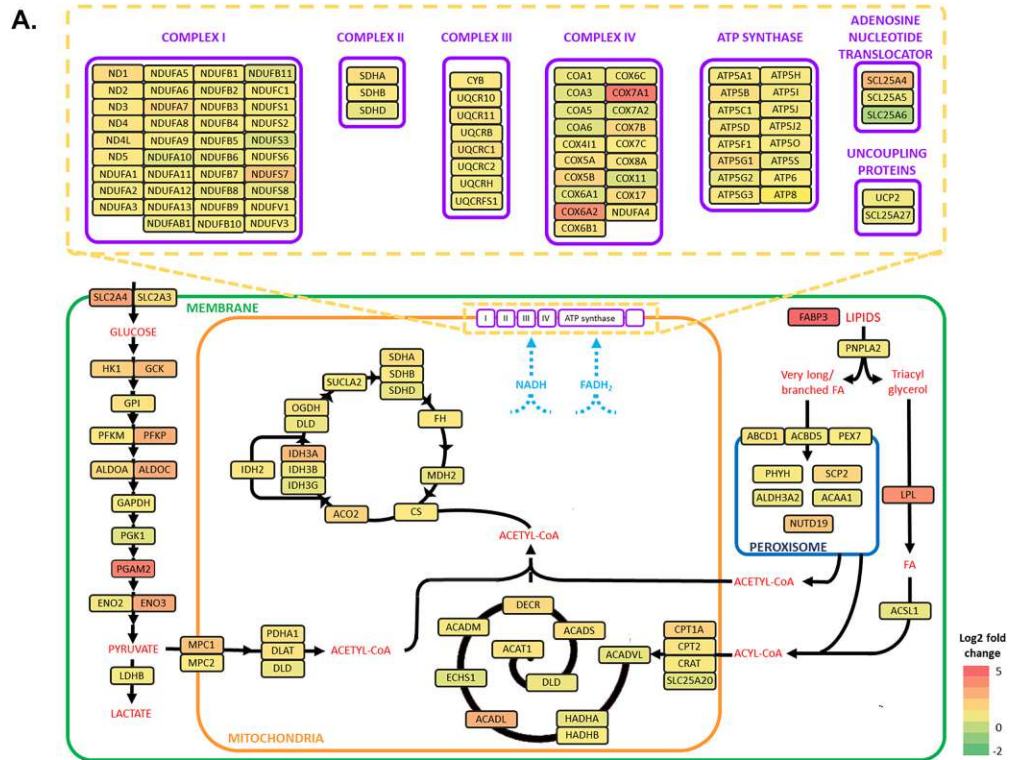


Figure 7. 3D long-term cultures promote changes in metabolic activity towards maturation. **(A)** Diagram showing metabolic genes with significantly upregulated (in red) and downregulated (in green) genes between long-term 3D hOCMTs vs 2D monolayer cultures (log₂fold change; p_{adj} < 0.05). **(B)** Graphs for comparing the cellular energy metabolism of long-term 3D hOCMTs vs 2D monolayer cultures after day 50 using Seahorse XFP Analyzer and Seahorse Mito Stress Test Kit: (i) oxidative phosphorylation (oxygen consumption rate, OCR) and (ii) glycolytic flux (extracellular acidification rate, ECAR) (Mean ± SEM obtained in four independent analyses. Total sample size: n_{2D} = 12, n_{3D} = 9). **(C)** Bar graphs providing a detailed analysis of the oxygen consumption rate (OCR) Seahorse XFP Analyzer data presented in **(B)**: (i) basal respiration and spare respiratory capacity, (ii) proton leak, ATP production (Mean ± SEM, N = 4, n_{2D} = 12, n_{3D} = 9, unpaired Student's *t* test—two-tailed).

Die approbierte gedruckte Originalversion dieser Dissertation ist an der TU Wien Bibliothek verfügbar. The approved original version of this doctoral thesis is available in print at TU Wien Bibliothek.



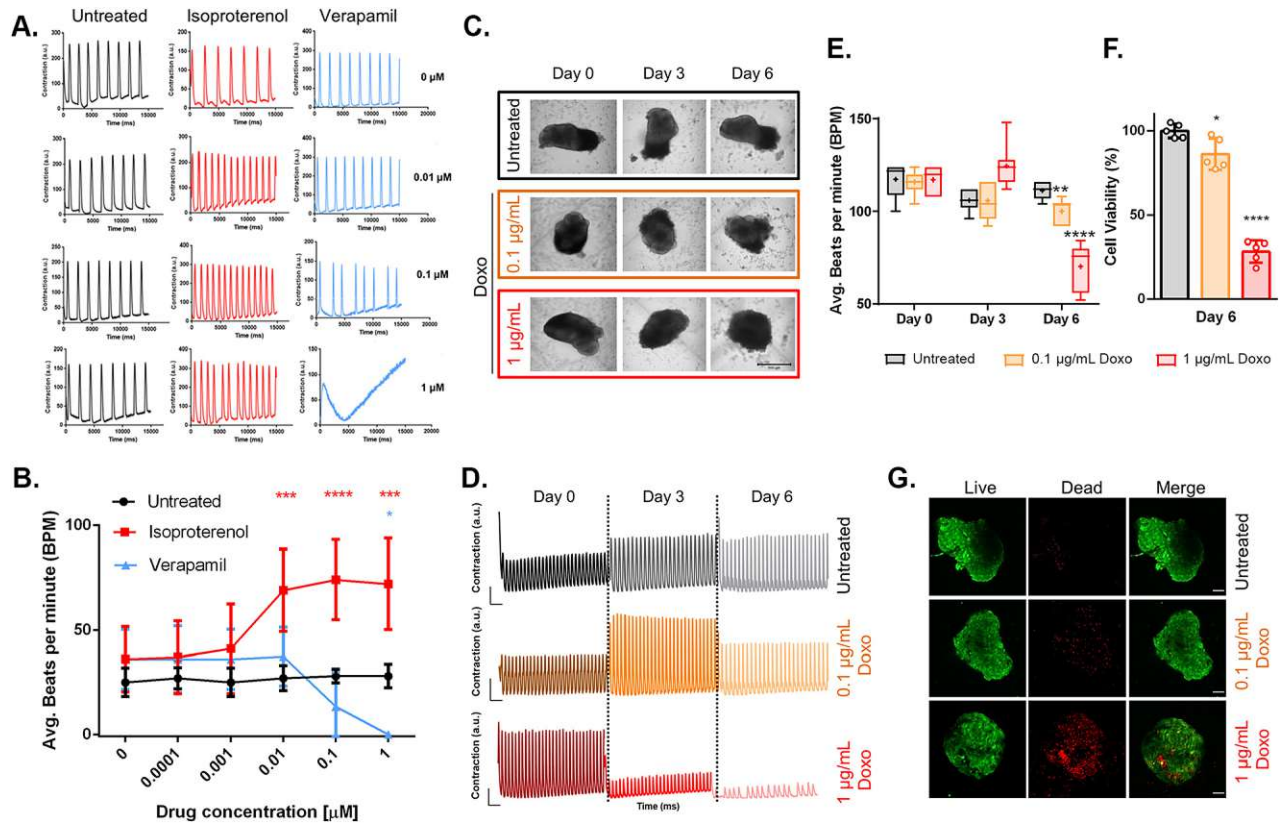


Figure 8. Long-term 3D hOCMTs show functional response to cardioactive and cardiotoxic drugs in a dose and time dependent manner. (A) Representative contraction amplitude plots of long-term (> day 50) Long-term 3D hOCMTs in response to untreated vs increasing doses of Isoproterenol and Verapamil. (B) Average beating rates of 3D long-term cardiac microtissues hOCMTs in response to increasing doses of Isoproterenol and Verapamil ($n = 3$, Mean \pm SD, Dunnett's multiple comparisons test). (C) Morphology of 3D long-term (> day 50) Long-term 3D hOCMTs in response to untreated vs increasing doses of Doxorubicin (Doxo) over 6 days (scale bar = 500 μm). (D) Representative contraction amplitude plots of Long-term 3D hOCMTs in response to untreated vs increasing doses of Doxo over 6 days ($t = 15$ s). (E) Average beating rates of Long-term 3D hOCMTs in response untreated vs increasing doses of Doxo over 6 days ($n = 6$, Lines = Median \pm min/max, Dots = Mean value, Dunnett's multiple comparisons test). (F) Luminescence-based quantification of cell viability Long-term 3D hOCMTs on day 6 of Doxo treatment normalized to untreated samples (untreated vs 0.1 $\mu\text{g}/\text{mL}$ vs 1 $\mu\text{g}/\text{mL}$) ($n = 6$, Mean \pm SD, Tukey's multiple comparisons test). (G) Representative cell viability of v on day 6 of Doxo treatment (untreated vs 0.1 $\mu\text{g}/\text{mL}$ vs 1 $\mu\text{g}/\text{mL}$) with Calcein/AM staining, green = live, red = dead (Scale bar = 100 μm).

were incubated with increasing drug doses (0.01–1 μM) for 15–20 min and further monitored by live imaging using a confocal microscope.

The response to the treatment was evaluated and quantified based on the contraction (Fig. 8A) and beating rate (Fig. 8B) of the hOCMTs, analysed through the open-source software tool MUSCLEMOTION^{86,87}. The acquired data shows that increasing concentrations of isoproterenol resulted in enhanced contraction amplitude and beating rate, with the beating rate peak at 1 μM . As expected, increasing concentrations of verapamil had the opposite effect, with the beating being completely hindered at 1 μM drug dosage (Supplementary Videos 3–8). These observations are in accordance with those reported in previous studies in cardiac microtissues⁸⁸ and confirm that our constructs can functionally respond to cardioactive drugs in a dose dependent manner.

Finally, we investigated the possibility of modelling drug-induced cardiotoxicity on our hiPSC-derived microtissues, by treating them with doxorubicin (Doxo), a well-known chemotherapeutic agent widely used in the treatment of several types of cancers⁸⁹. The drug is—in fact—also known to have cardiotoxic and pro-fibrotic effects, thus able to cause or exacerbate heart failure in vivo^{90–95}.

The 3D hOCMTs were exposed to 0.1 $\mu\text{g}/\text{mL}$ and 1 $\mu\text{g}/\text{mL}$ of Doxo and their morphology and contractile activity was compared with untreated controls ($n = 6$) for the next 6 following days. The culture medium was exchanged every 3 days and the cultures were monitored on a daily basis. Figure 8C shows that the morphology of the constructs gradually changed over the course of treatment, and with the occurrence of more irregular edges when exposed to higher Doxo doses. In addition, clear changes could also be observed in the beating profiles of the constructs treated with Doxo (Fig. 8D,E, and Supplementary Videos 9–14).

We figured the changes in the morphology of the microtissues treated with the chemotherapeutics might be due to the induction of cell death by the drug. Therefore, after 6 days of Doxo treatment, we assessed the viability

of the constructs with a luminescence-based assay. The results in Fig. 8E,G revealed that the 3D hOCMTs treated with 1 $\mu\text{g}/\text{mL}$ Doxo were significantly less viable than both the control group and the group treated with lower drug concentration (0.1 $\mu\text{g}/\text{mL}$) (Average viability on day 6: $100 \pm 4.1\%$ for ctrl, 86.4 ± 9.3 for 0.1 $\mu\text{g}/\text{mL}$ Doxo, $28.3 \pm 6.6\%$ for 1 $\mu\text{g}/\text{mL}$ Doxo, Mean \pm SD, $p < 0.0001$).

Discussion

In this study we present a simple method to generate 3D iPSC-derived human cardiac microtissues in the absence of an external scaffold that could be cultured for extended periods.

Our study has demonstrated that long-term cultured 3D cardiac microtissues reveal some characteristics resembling native human heart, such as: (1) spontaneous 3D organization in scaffold-free conditions; (2) presence of multiple cell types of the heart with a tendency to re-organize into distinct and discrete structures; (3) ultrastructural organization and maturation of cardiac muscle sarcomeres and mitochondria; (4) improved survival, cardiac specificity and maturation at transcriptional and metabolic levels; (5) long-term functional beating in the absence of external stimuli; (6) functional response to cardioactive and cardiotoxic drugs in a dose- and time-dependent fashion. Given that long-term cultured 3D cardiac microtissues possess the abovementioned characteristics, we propose that the hOCMTs can be defined as human cardiac organoids (hCOs).

When compared to standard 2D cardiomyocytes culture, 3D hOCMTs showed an enhanced survival rate. More importantly, their cellular composition appeared to be more representative of the physiological conditions in the heart, although their overall phenotype appeared to be close to foetal heart^{88,96}.

While the effects of long-term culture in promoting the maturation of PSC-derived cardiomyocytes is well established^{69,97}, 2D culture is usually challenging in the long run, as the cardiomyocytes tend to delaminate from the traditional tissue culture plates⁶⁹, leaving non-myocyte cell populations such as fibroblasts to overgrow.

One of the greatest advantages of our model is that there is no need for an external scaffold as the microtissues self-organize and survive for a long time in static culture conditions. Other models have been developed in the absence of an external ECM, however they usually require the differentiation of other stromal cells (such as epicardial or fibroblastic cells) separately, followed by their assembly with cardiac myocytes^{35,56}.

On the contrary, by exploiting the limited efficiency of the original 2D cardiac differentiation protocol by Lian et al.^{13,14} and simply switching the dimensionality from 2 to 3D, we have generated long-term 3D hOCMTs in which epicardial cells, fibroblasts, and endocardial cells emerge spontaneously together with cardiomyocytes, without the need to set up separate lineage differentiation protocols and further assembly. In addition, the spontaneous beating of our hOCMTs was observed for more than 100 days as, to this date, only reported by Silva et al. as well. The latter paper, though, reported that the developmental co-emergence of gut also occurred together with the heart tissue⁶⁵.

In our model, a distinct gut tissue was not observed after 50 days of culture through immunofluorescence analysis. Histological analysis of the hOCMTs has shown distinct populations of WT1-, TBX18-positive epicardial cells, TE-7-, SM22 α -positive fibroblast-like cells, NFAT2-positive endocardial cells along with a distinct core of cardiomyocytes. CD31-positive endothelial cells could also be detected. The low number of CD31-positive cells might be explained by the fact that in native human heart endothelial cells have different developmental origins⁹⁸, and we did not supplement our culture media with endothelial-lineage favouring factors, like VEGF, during our study.

Another interesting feature of the hOCMTs is the occurrence of cardiomyocytes expressing both atrial and ventricular markers, as identified by confocal imaging of MYL2 and MYL7. Although MYL7 is known to be observed on all cardiomyocyte subtypes during development⁷⁴, we could identify cardiomyocytes that are MYL7 positive, but not MYL2 positive, or vice versa, suggesting there could be a tendency of commitment to formation of different cardiomyocyte subtypes. Despite significant differences, a similar phenomenon of atrial/ventricular cardiomyocyte subtype distinction was also shown by Israeli and colleagues, which appeared to be blunted with long-term culture⁶⁴. Instead, the herein reported hOCMTs revealed higher cardiac-specific cellular heterogeneity and maturation in terms of histological, ultrastructural, and transcriptional-levels in long-term 3D cultures compared to shorter culture times and standard 2D monolayer culture.

The maturity and complexity of our construct could be shown at the ultrastructural level by our TEM analysis over long culture times. On day 50 and 85, our hOCMTs displayed clearly aligned myofibers resulting in well-organized sarcomeres, as compared to earlier time points. These morphological adaptations, which are hallmarks of mature cardiac tissues⁶⁷, were further supported by transcriptomics analysis, where hOCMTs showed an increased expression of genes related to cardiac contraction and sarcomeric structures. The maturity of our long-term 3D hOCMTs could also be demonstrated by comparison with Engineered Heart Tissues (EHTs), a well-recognized 3D model of cardiac tissue in vitro, by showing our 3D constructs share with EHTs a similar transcriptional landscape.

The calcium handling properties of immature cardiomyocytes diverge from their mature counterpart. While immature cardiomyocytes can rely on the calcium released at the cell periphery to initiate sarcomere contraction, mature cardiomyocytes develop plasma membrane invaginations (t-tubules) which are wrapped around the myofibrils as to make the process of calcium release and re-uptake faster and more efficient^{99,100}. The first polarization triggers the release of calcium stored in the sarcoplasmic reticulum by RYR2, which is pumped back to the sarcoplasmic reticulum by SERCA2 (sarco/endoplasmic reticulum Ca^{2+} -ATPase). The analysis of hOCMTs confirmed the presence of t-tubules at the longer time-points (> day 50), the upregulation of some of the genes involved in their biogenesis (*JPH2*, *ACTN2*, *NEXN*) and sarcomeric calcium management (*RYR2*, *PLN*, *SERCA*), hence demonstrating long-term 3D culture determines functional maturation of hOCMTs.

Furthermore, cardiomyocytes also experience several metabolic adaptations during in vivo maturation in order to generate the required amount of ATP^{74,101}. Our ultrastructural results are compatible with this metabolic

switch, showing that hOCMTs acquired elongated mitochondria distributed around the contractile apparatus with time in culture. This idea is further reinforced by the upregulation of genes related to electron transport chain-linked phosphorylation and FA β -oxidation in long-term 3D cultured hOCMTs, which has been previously linked to a more mature phenotype in hPSC-CMs⁸¹. Interestingly, the increase in electron transport chain activity has been linked to the cardiomyocyte differentiation and maturation not only through metabolic support, but also by generating calcium oscillations through complex III activity¹⁰². Recent protocols have been devised that improve pluripotent stem cell-derived cardiomyocyte metabolic maturation, and push them closer to adult cardiomyocytes, which rely on oxidative phosphorylation for ATP production⁷⁹.

Our analyses of cell energy metabolism using the Seahorse XF technology revealed hOCMTs as highly energetic compared to the 2D cultures. The 3D hOCMTs consumed much more oxygen, a significant proportion of which was used for mitochondrial ATP production. The proton leak in the mitochondria of hOCMTs might serve as a protective mechanism against mitochondrial damage by limiting reactive oxygen species production¹⁰³. The surprisingly similar levels of maximal respiration in the 3D and 2D cultures induced by FCCP stimulation indicated that the mitochondria of 2D culture cells were also metabolically competent and possessed a high respiratory capacity. However, their respiratory capacity was only partially used for mitochondrial ATP production under standard culture conditions. We also observed an increased extracellular acidification rate in the 3D cultures that nicely correlated with the results of transcriptomics analyses showing a general upregulation of metabolic gene expression, including glycolysis genes. This increase in glycolysis might reflect individual metabolic adaptations of various cell types and subpopulations in hOCMTs and could potentially be linked to differential oxygen availability inside hOCMTs. Together, our Seahorse XF analyses showed that cellular energy metabolism strongly differs in the 2D and 3D cultures, and the 3D hOCMTs relied significantly more on mitochondrial respiration to satisfy their energy needs.

Functional analysis of the 3D hOCMTs proved that they were responsive to clinically relevant doses of cardioactive and cardiotoxic drugs. This is the first step required to consider the generation of patient-specific models of disease for drug testing.

As for modelling chemotherapy-induced cardiotoxicity, while doxorubicin is a well-established chemotherapeutic known to cause heart failure as a side effect^{90–95}, the *in vitro* modelling in cardiac microtissues is still not well-established due to the limitations so far encountered in reproducing the physiological cellular heterogeneity, and cardiomyocyte maturity⁶². Furthermore, it is crucial to consider the influence of cell–cell interactions of cardiomyocyte vs non-myocytes—especially fibroblasts—and cell–ECM interactions¹⁰⁴. Our hOCMT platform offers the advantages of long-term viability, cellular heterogeneity and advanced maturity *in vitro*, rendering it a physiologically relevant alternative for future studies. For instance, further clinical parameters such as the cardio-fibrotic potential of doxorubicin treatment^{93,94,105}, the secretion of cardiac troponins and natriuretic peptides as clinically relevant markers of chemotherapy-induced cardiotoxicity¹⁰⁶ or simply the potential for personalized medicine could be exploited by using this iPSC-derived hOCMT¹⁰⁷.

Although promising, our study shows some limitations. Despite the structural and functional maturation in the long-term culture model as compared to traditional monolayers, hOCMTs still display features of the foetal rather than the adult heart. For example, myocytes of our hOCMTs have $\sim 1.5 \mu\text{m}$ length of sarcomeres (as in foetal mammalian hearts), whereas in adult hearts, this length is usually $2 \mu\text{m}$ ⁶⁷. We believe the adoption of additional stimuli (i.e.: dynamic culture, mechanical conditioning and electrical stimulation) might in the future help further improve the model here described¹⁰⁸. Furthermore, despite showing hints of histological similarities to the heart tissue, cellular heterogeneity of cardiac cell types, and spontaneous re-organization of these multiple cell types at distinct regions, additional cues would be needed to establish true self-organization following the same principles of embryonic human heart development.

In a longer perspective, *in vitro* cardiotoxicity studies should not underestimate the importance of multi-organ interactions. While drugs in their native chemistries may not always result in direct cardiac damage¹⁰⁹, their metabolic by-products might cause cardiotoxicity *in vivo*^{109,110}.

In conclusion, we have established a simple procedure to prepare human induced pluripotent stem cell-derived organotypic cardiac microtissues. We propose that hOCMTs could be considered as cardiac organoids, for their ability to recapitulate different key features of the human heart, and display improved maturation and functionality in long-term culture, thus enhancing the potential of *in vitro* platforms to be used in translational research applications.

Methods

Stem cell culture and maintenance. The human iPSC cell line DF 19-9-7 T (iPS, karyotype: 46, XY) was purchased from WiCell (Madison, WI, USA), and the Troponin I1 reporter iPSC line (TNNI1-iPS) was purchased from Coriell Institute (Cat. no. AICS-0037-172, Camden, New Jersey, USA). All iPSC cells were cultured and maintained in feeder-free conditions as previously described^{111,112} on Growth Factor Reduced Matrigel[®]-coated plates, (1:100 in DMEM/F12, Corning) in complete Essential 8[™] Medium (E8, Thermo Fisher Scientific) containing penicillin/streptomycin (P/S) (0.5%, VWR), incubated at 37 °C, 5% CO₂.

hiPSC-derived monolayer cardiac differentiation and maintenance. Cardiac differentiation from hiPSCs was performed following the Wnt signalling modulation protocol by Lian et al.^{13,14}, with slight modifications as previously described¹¹¹. Briefly, prior to cardiovascular differentiation, hiPSCs were dissociated into single cells (TrypLE Select, Thermo Fisher Scientific) and re-seeded onto 12-well Matrigel-coated plates with 2.0×10^5 cells/cm², with complete Essential 8 medium including Y27632 Rock Inhibitor (RI) (1:4000 dilution from 10 μM stock, 2.5 μM final, Selleck chemicals, Houston, TX, USA). The next day, the medium was replaced with complete Essential 8 medium without RI, and the medium exchange was performed daily until the cells

reached 100% confluency. On day 0, to start mesoderm differentiation, the medium was changed with RPMI 1640 with L-Glutamine (Biosera) media supplemented with P/S, B-27™ supplement minus insulin (1×, Thermo Fisher Scientific) and CHIR99021 (8 μM, Sigma-Aldrich). On day 2, the medium was exchanged with RPMI 1640 + B-27 minus insulin (RPMI + B27-Ins), supplemented with IWP-2 (5 μM, Selleck chemicals). On day 4, the medium was replaced with RPMI + B27-Ins, and medium exchange was performed every 2 days until the cells started beating (usually on day 7, but may depend on the iPSC line). Once beating clusters started to emerge, the medium was replaced with RPMI 1640 + B-27™ supplement (RPMI + B27 + Ins) (1×, Thermo Fisher Scientific), and medium exchange was performed every 2–3 days until day 15 of differentiation. From day 15 on, the cells were used either for generation of 3D hOCMTs or were continued to be cultured as 2D monolayers as controls, with medium exchange every 3–4 days until the end of experiments.

hiPSC-derived 3D organotypic cardiac microtissue (hOCMT) generation and maintenance. On day 15 of monolayer cardiac differentiation, cells were dissociated by putting 0.5 mL StemPro™ Accutase™ (Gibco) per well, and incubating in room temperature or in 37 °C incubator for 10–20 min with occasional mechanical pipetting, until the cells were visually dissociated. After sufficient dissociation, Accutase™ was stopped by putting 3 mL RPMI 1640 with 20% Knockout Serum Replacement (Gibco) per well, and the cells were pelleted by centrifugation at 150×g for 3 min. The resulting pellet was resuspended with RPMI/B27 + Ins + P/S + RI (1:2000 dilution from 10 μM stock, 5 μM final), counted by LUNA™ cell counter (Logos), and seeded 150,000 cells/well in 96-well round bottom ultra-low attachment plates (Corning Costar 7007) at a volume of 150 μL/well. The plates were then centrifuged at 200×g for 5 min and incubated at 37 °C, 5% CO₂. As 2D control, either 200,000 cells per well were seeded in Matrigel-coated 96-well tissue culture plates at a volume of 200 μL/well, or 1.5 × 10⁶ cells were seeded on Matrigel-coated 24-well tissue culture plates in 1 mL volume per well, or left undetached in 12-well plates. After 48 h, medium was replaced with RPMI/B27 + Ins without RI from hOCMTs and 2D-controls that were re-seeded. From this point on, medium was changed partially every 2–3 days with RPMI/B27 + Ins + P/S until day 30, then every 3–4 days at least until day 50, or longer.

Cell viability with Calcein AM/EthD-1 staining. 3D hOCMT viability was assessed with LIVE/DEAD™ Viability/Cytotoxicity Kit, for mammalian cells (Thermo Fisher Scientific), according to manufacturer's instructions, and confocal imaging was performed with Zeiss LSM 780 confocal microscope.

Terminal deoxynucleotidyl transferase (TdT) dUTP nick-end labeling (TUNEL) assay. The presence of 3D hOCMT apoptotic/necrotic core was assessed on hOCMT cryosections with Click-iT Plus TUNEL Assay Kit with Alexa Fluor 647 fluorophore (Thermo Fisher Scientific) according to manufacturer's instructions. Positive control of cell death was performed by DNase I treatment according to manufacturer's instructions (Thermo Fisher Scientific, Cat. no. 18068015). Confocal imaging was performed with Zeiss LSM 780 confocal microscope.

Immunofluorescence (IF). 3D hOCMT fixation, cryosectioning, and immunostaining was modified from Perestrello et al.¹⁰⁴. Briefly, 3D hOCMTs were collected with low binding pipette tips, and fixed in 4% PFA (Santa Cruz Biotechnology) supplemented with 0.03% eosin (Sigma Aldrich) for 2 h at room temperature, followed by washing with 1×PBS (Lonza), and embedding in 30% sucrose solution at 4 °C until they sink at the bottom (~2 days). The hOCMTs were then embedded in OCT solution (Leica), frozen in cassettes embedded in isopentane (VWR) cooled with dry ice, and were stored in –80 °C until further processing. The frozen hOCMTs were cryosectioned by cryotome (Leica CM1950) onto Menzel Gläser, SuperFrost™ Plus slides (Thermo Fisher Scientific) at 10 μM thickness.

For IF analysis, the hOCMT sections were washed with PBS for 2 × 5 min at RT, followed by permeabilization with 0.2% Triton X-100 (Sigma Aldrich) for 5 min. Blocking was done by 2.5% bovine serum albumin (BSA) (Biowest) in PBS at room temperature. Primary antibodies were incubated overnight at 4 °C (SI—Supplementary Table 1). The next day, the samples were washed with PBS, followed by appropriate Alexa-conjugated secondary antibodies (SI—Supplementary Table 1). Counterstaining was done by DAPI (Roche), and hOCMT slides were mounted with Mowiol™ 4-88 (Sigma Aldrich). Confocal imaging was performed with Zeiss LSM 780 confocal microscope.

Further histological procedures can be found in Supplementary Methods.

Microscopy and image analysis. Confocal imaging was performed with Zeiss LSM 780 confocal microscope. Light microscopy imaging was performed with Leica DM IL LED inverted microscope, and fluorescence images were collected with Leica DMI4000 B inverted fluorescence microscope. Image analysis was performed with ImageJ (v1.53o).

3D hOCMT dissociation. For flow cytometry and RNA isolation, hOCMTs were collected in Eppendorf tubes with low binding pipettes on day 30 and 50, and dissociated with MACS Multi Tissue Dissociation Kit 3 (Miltenyi Biotec, Cat. no. 130-110-204) according to manufacturer's instructions. As controls, 2D monolayer cultures were directly dissociated on the plates with the same kit.

Flow cytometry. Flow cytometry analyses on 3D hOCMTs and 2D controls were performed on day 15 (for 2D), day 30 (for 2D and 3D) and day 50 (for 2D and 3D) timepoints as described previously^{104,112} with modifications. Briefly, on each timepoint, samples were dissociated with MACS Multi Tissue Dissociation Kit

3, washed with FACS buffer (99.4% PBS + 0.1% UltraPure™ 0.5 M EDTA pH 8.0 by Invitrogen™ + 0.5% FBS by Sigma Aldrich [Cat. no. F9665-500ML]) and surface marker staining with CD90-APC (Exbio; 1:10 dilution in FACS buffer) and CD31-BV421 (Biolegend; 1:10 dilution in FACS buffer) antibodies was performed together with corresponding unstained controls for 30 min on ice. Afterwards, sample fixation and permeabilization was performed with Intracellular Fixation and Permeabilization Buffer Set (eBiosciences) per manufacturer's instructions, followed by intracellular marker staining with TNNT2-FITC (Miltenyi Biotec; 1:50 dilution in 1× Permeabilization Buffer) antibody together with corresponding unstained controls for 30 min in room temperature. Sample acquisition was performed by using BD FACSCanto II (Becton, Dickinson and Company, Franklin Lakes, NJ, USA), and cell populations were analysed with FlowJo v.10 (Tree Star) (see SI—Supplementary Table 1 for detailed antibody information).

Transmission electron microscopy (TEM) sample preparation and analysis. 3D hOCMTs were transferred to new well-plates with low binding pipettes, and washed 2× with PBS. Fixation was done by 1.5% PFA + 1.5% glutaraldehyde (Sigma Aldrich) diluted in RPMI 1640 culture media for 1 h, then washed with 0.1 M cacodylate buffer (pH 7.4) (Sigma Aldrich) for 3 times 5 min each, and incubated overnight at 4 °C in cacodylate buffer with glutaraldehyde. The next day, samples were rewashed 3 times with cacodylate buffer, and incubated at 4 °C in cacodylate buffer until sending the samples, protected from light. The 3D hOCMTs were post-fixed for 1.5 h with 1% osmium tetroxide in 0.1 M cacodylate buffer and washed for 3 times with 0.1 M cacodylate buffer, 10 min each, then stained with 1% uranyl acetate in milli-Q water overnight at 4 °C, followed by washing in milli-Q water. The samples were then dehydrated in an ascending EtOH series using solutions of 70%, 90%, 96% and 3 times 100% for 10 min each, incubated in propylene oxide (PO) 3 times for 20 min before incubation in a mixture of PO and Epon resin overnight, and incubated in pure Epon for 2 h and embedded by polymerizing Epon at 68 °C for 48 h. Ultra-thin sections of 70 nm were cut using a Leica Ultracut EM UC 6 Cryo-ultramicrotome. TEM images were collected with a JEOL JEM 1011 electron microscope and recorded with a 2 Mp charge coupled device camera (Gatan Orius).

RNA isolation, bulk RNA-sequencing and DE analysis. For RNA isolation, 3D hOCMTs and 2D controls were dissociated by using MACS Multi Tissue Dissociation Kit 3 on day 30 and day 50. After cell dissociation, RNA was extracted with High Pure RNA Isolation Kit (Roche) according to manufacturer's instructions, and quantified with Nanodrop 2000 Spectrophotometer (Thermo Fisher Scientific). Quality control for RNA integrity number (RIN) was also determined with Agilent 2100 Bioanalyzer.

Bulk RNA-sequencing and DE analysis procedures are further described in Supplementary Methods.

Data were deposited in the NCBI Gene Expression Omnibus repository with the GEO ID GSE209997.

Gene ontology (GO) enrichment analysis for biological processes was performed with EnrichR web-tool^{113–115}. Clustering analysis of upregulated genes was done with Cytoscape¹¹⁶.

RNA-seq data from this study were also compared to adult human heart RNA-seq data (from BioProjects PRJNA667310⁷⁶ and PRJNA628736⁷⁷), and EHT RNA-seq data (from BioProject PRJNA831794⁷⁸) obtained from the NCBI BioProject database (<https://www.ncbi.nlm.nih.gov/bioproject/>) (Accession numbers: SRR12771050, SRR12771052, SRR11620685, SRR11620686, SRR18911472, SRR18911473, SRR18911476, SRR18911477) by using Biojupies web-tool¹¹⁷.

Metabolic flux analysis. Mitochondrial respiration of 3D hOCMTs and 2D controls was assessed using Seahorse XFp Analyzer (Agilent) with Seahorse XFp Cell Mito Stress Test Kit (Agilent). On the Day 50 time-point, 8-well XFp Cell Culture Miniplates (Agilent) were coated with Matrigel (1:20 dilution), and both 3D hOCMTs (one centered 3D hOCMT per well) and 2D controls (dissociated with MACS Multi-tissue dissociation kit 3 and seeded at 200,000 cells/well) were plated. The miniplates were cultured for 48 h in RPMI/B27 + Ins + P/S + RI (1:2000 dilution from 10 μM stock, 5 μM final) media to allow stabilization, and for the next 24 h in RPMI/B27 + Ins + P/S media. For 3D hOCMTs, only beating samples located at the center of the well were included in the subsequent statistical analysis.

One hour before measurement, RPMI/B27 + Ins + P/S media was replaced with Seahorse XF RPMI Medium pH 7.4 (Agilent) supplemented with 10 mM glucose, 2 mM glutamine, and 1 mM pyruvate (Agilent). Metabolic inhibitors were diluted in the supplemented XF Medium, loaded into the injection ports of the hydrated Seahorse XFp Sensor Cartridge (Agilent), and injected at specified time points to the wells as follows: Oligomycin (3 μM), FCCP (4 μM), and Rotenone/Antimycin A (2 μM). The Mito Stress Test was performed according to the manufacturer's instructions and included five measurements for basal consumption and five measurements after every drug injection. An extra five-minute waiting step was included after the Oligomycin injection.

After the measurement, both 3D hOCMTs and 2D controls were dissociated with MACS MultiTissue Dissociation Kit 3 (Miltenyi Biotec), and lysed for 2 h at 60 °C (10 mM Tris, 1 mM EDTA, 50 mM KCl, 2 mM MgCl₂, 200 μg/mL Proteinase K as described previously by Giacomelli et al.³⁵). Metabolic data were normalized by measuring the DNA content of each sample with a Quant-iT™ PicoGreen™ dsDNA Assay Kit (Thermo Fisher Scientific) according to the manufacturer's protocol. Wave software (Agilent), Microsoft Excel, and Prism 9 (GraphPad Software) were used for data analysis.

Drug treatments. Isoproterenol hydrochloride (Sigma Aldrich) was dissolved in dimethyl sulfoxide (DMSO) (Sigma Aldrich), and Verapamil hydrochloride (Sigma Aldrich) in methanol (VWR) to prepare 1 M stock solutions. Each drug solution was 10-fold serially diluted in RPMI/B27 + Ins media to make final concentrations between 0.0001–1 μM. As untreated controls, complete RPMI/B27 + Ins media supplemented with DMSO or methanol were used. For data collection, the 3D hOCMTs with drug-supplemented media were incu-

bated for 10 min at 37 °C, 5% CO₂ each time the drug concentration changed, followed by live imaging with video acquisition per condition with Zeiss LSM 780 confocal microscope. Chemotherapy-induced cardiotoxicity was evaluated in 3D hOCMTs treated with RPMI/B27 + Ins supplemented with doxorubicin (Doxo) (Sigma Aldrich), at 0.1 µg/mL and 1 µg/mL concentrations, or plain RPMI/B27 + Ins as control for 6 days. Growth medium was exchanged every 3 days, and 3D hOCMT morphology and beating were monitored daily by live video recording with Zeiss LSM 780 confocal microscope for 6 days. On day 6 of drug treatment, the 3D hOCMTs were collected for evaluating viability.

Live video acquisition and contraction analysis. To evaluate the contractile function of 3D hOCMTs, live image sequences were acquired with Zeiss LSM 780 Confocal microscope using transmitted light mode (37 °C, 5% CO₂), as equivalent to 60 fps for 15 s; where the image sequences were later turned into .avi files with ImageJ. The beating rates were counted and calculated manually from the video analysis, and representative contraction graphs were derived with the open-source video analysis software MUSCLEMOTION^{86,87} per providers' instructions.

Luminescence-based cell viability assay. 3D hOCMTs viability after 6 days of Doxo treatment was assessed by CellTiter-Glo[®] Luminescent Cell Viability Assay Kit (Promega) according to manufacturer's instructions. After the 3D hOCMTs were dissociated by the assay treatment, the samples were transferred to a clear-bottom 96-well white assay plate (Corning Costar 3610) and cell viability was quantified with Centro LB 960 Microplate Luminometer (Berthold Technologies).

Statistics. Data are expressed as mean ± SD or mean ± SEM where applicable, unless otherwise stated. Statistical analyses were performed using Microsoft Excel 2010 and GraphPad Prism 8.0.2 unless otherwise stated, using one-way ANOVA (with Tukey's multiple comparisons test), two-way ANOVA (with Dunnett's multiple comparisons test), or unpaired Student's *t* test (two-tailed) where $p < 0.05$ was considered to be significantly different as denoted with asterisks [$*p \leq 0.05$, $**p \leq 0.01$, $***p \leq 0.001$, $****p \leq 0.0001$]. Sample sizes of independent experiments, statistical methods used and the significance were described in the figure legends wherever applicable.

Data availability

The RNA-sequencing data obtained and presented in this study were generated at CF Genomics of CEITEC, and is available in the NCBI GEO public repository with accession no. GSE209997 (<https://www.ncbi.nlm.nih.gov/geo/query/acc.cgi?acc=GSE209997>). The data that support the findings of this study are available from the corresponding author upon reasonable request.

Received: 3 March 2022; Accepted: 11 October 2022

Published online: 18 October 2022

References

1. Abbafati, C. *et al.* Global burden of 369 diseases and injuries in 204 countries and territories, 1990–2019: A systematic analysis for the Global Burden of Disease Study 2019. *Lancet (London, England)* **396**(10258), 1204 (2020).
2. Namara, K. M., Alzubaidi, H. & Jackson, J. K. Cardiovascular disease as a leading cause of death: How are pharmacists getting involved?. *Integr. Pharm. Res. Pract.* **8**, 1 (2019).
3. Roth, G. A. *et al.* Global burden of cardiovascular diseases and risk factors, 1990–2019: Update from the GBD 2019 study. *J. Am. Coll. Cardiol.* **76**(25), 2982–3021 (2020).
4. Heidenreich, P. A. *et al.* Forecasting the impact of heart failure in the United States a policy statement from the American Heart Association. *Circ. Heart Fail.* **6**(3), 606–619 (2013).
5. Seruga, B., Ocana, A., Amir, E. & Tannock, I. F. Failures in phase III: Causes and consequences. *Clin. Cancer Res.* **21**(20), 4552–4560 (2015).
6. McNaughton, R., Huet, G. & Shakir, S. An investigation into drug products withdrawn from the EU market between 2002 and 2011 for safety reasons and the evidence used to support the decision-making. *BMJ Open* **4**(1), e004221 (2014).
7. Khakoo, A. Y., Yurgin, N. R., Eisenberg, P. R. & Fonarow, G. C. Overcoming barriers to development of novel therapies for cardiovascular disease: Insights from the oncology drug development experience. *JACC Basic Transl. Sci.* **4**(2), 269–274 (2019).
8. Cho, S., Lee, C., Skylar-Scott, M. A., Heilshorn, S. C. & Wu, J. C. Reconstructing the heart using iPSCs: Engineering strategies and applications. *J. Mol. Cell. Cardiol.* **157**, 56–65 (2021).
9. Kim, J., Koo, B. K. & Knoblich, J. A. Human organoids: Model systems for human biology and medicine. *Nat. Rev. Mol. Cell Biol.* **21**(10), 571–584 (2020).
10. Marshall, J. J. & Mason, J. O. Mouse vs man: Organoid models of brain development and disease. *Brain Res.* **1724**, 146427 (2019).
11. Gorzalczany, S. B. & Rodriguez Basso, A. G. Strategies to apply 3Rs in preclinical testing. *Pharmacol. Res. Perspect.* **9**(5), e00863 (2021).
12. Takahashi, K. *et al.* Induction of pluripotent stem cells from adult human fibroblasts by defined factors. *Cell* **131**(5), 861–872 (2007).
13. Lian, X. *et al.* Robust cardiomyocyte differentiation from human pluripotent stem cells via temporal modulation of canonical Wnt signaling. *Proc. Natl. Acad. Sci. U.S.A.* **109**(27), E1848–E1857 (2012).
14. Lian, X. *et al.* Directed cardiomyocyte differentiation from human pluripotent stem cells by modulating Wnt/ β -catenin signaling under fully defined conditions. *Nat. Protoc.* **8**(1), 162–175 (2013).
15. Sadahiro, T., Yamanaka, S. & Ieda, M. Direct cardiac reprogramming: Progress and challenges in basic biology and clinical applications. *Circ. Res.* **116**(8), 1378–1391 (2015).
16. BurrIDGE, P. W. *et al.* Chemically defined generation of human cardiomyocytes. *Nat. Methods* **11**(8), 855–860 (2014).
17. BurrIDGE, P. W. *et al.* Modeling cardiovascular diseases with patient-specific human pluripotent stem cell-derived cardiomyocytes. *Methods Mol. Biol.* **1353**, 119–130 (2014).
18. BurrIDGE, P. W. *et al.* Human induced pluripotent stem cell-derived cardiomyocytes recapitulate the predilection of breast cancer patients to doxorubicin-induced cardiotoxicity. *Nat. Med.* **22**(5), 547–556 (2016).

19. Sharma, A. *et al.* Derivation of highly purified cardiomyocytes from human induced pluripotent stem cells using small molecule-modulated differentiation and subsequent glucose starvation. *J. Vis. Exp.* **97**, e52628 (2015).
20. Sharma, A. *et al.* Use of human induced pluripotent stem cell-derived cardiomyocytes to assess drug cardiotoxicity. *Nat. Protoc.* **13**(12), 3018–3041 (2018).
21. Lan, F. *et al.* Abnormal calcium handling properties underlie familial hypertrophic cardiomyopathy pathology in patient-specific induced pluripotent stem cells. *Cell Stem Cell* **12**(1), 101–113 (2013).
22. Sharma, A. *et al.* Human induced pluripotent stem cell-derived cardiomyocytes as an in vitro model for coxsackievirus B3-induced myocarditis and antiviral drug screening platform. *Circ. Res.* **115**(6), 556–566 (2014).
23. Li, T.-S. *et al.* Cardiospheres recapitulate a niche-like microenvironment rich in stemness and cell-matrix interactions, rationalizing their enhanced functional potency for myocardial repair. *Stem Cells* **28**(11), 2088–2098 (2010).
24. Nguyen, D. C. *et al.* Microscale generation of cardiospheres promotes robust enrichment of cardiomyocytes derived from human pluripotent stem cells. *Stem Cell Rep.* **3**(2), 260–268 (2014).
25. Richards, D. J. *et al.* Inspiration from heart development: Biomimetic development of functional human cardiac organoids. *Biomaterials* **142**, 112–123 (2017).
26. Zimmermann, W.-H. Tissue engineering of a differentiated cardiac muscle construct. *Circ. Res.* **90**(2), 223–230 (2001).
27. Weinberger, F., Mannhardt, I. & Eschenhagen, T. Engineering cardiac muscle tissue: A maturing field of research. *Circ. Res.* **120**(9), 1487–1500 (2017).
28. Dhahri, W., Romagnuolo, R. & Laflamme, M. A. Training heart tissue to mature. *Nat. Biomed. Eng.* **2**(6), 351–352 (2018).
29. Hirt, M. N., Hansen, A. & Eschenhagen, T. Cardiac tissue engineering. *Circ. Res.* **114**(2), 354–367 (2014).
30. Schaaf, S. *et al.* Human engineered heart tissue as a versatile tool in basic research and preclinical toxicology. *PLoS One* **6**(10), e26397 (2011).
31. Vunjak Novakovic, G., Eschenhagen, T. & Mummery, C. Myocardial tissue engineering: In vitro models. *Cold Spring Harb. Perspect. Med.* **4**(3), a014076 (2014).
32. Mathur, A. *et al.* Human iPSC-based cardiac microphysiological system for drug screening applications. *Sci. Rep.* **5**(1), 1–7 (2015).
33. Ma, Z. *et al.* Self-organizing human cardiac microchambers mediated by geometric confinement. *Nat. Commun.* **6**, 7413 (2015).
34. Giacomelli, E. *et al.* Three-dimensional cardiac microtissues composed of cardiomyocytes and endothelial cells co-differentiated from human pluripotent stem cells. *Development* **144**(6), 1008–1017 (2017).
35. Giacomelli, E. *et al.* Human-iPSC-derived cardiac stromal cells enhance maturation in 3D cardiac microtissues and reveal non-cardiomyocyte contributions to heart disease. *Cell Stem Cell* **26**(6), 862–879.e11 (2020).
36. Giacomelli, E., Sala, L., van Oostwaard, D. W. & Bellin, M. Cardiac microtissues from human pluripotent stem cells recapitulate the phenotype of long-QT syndrome. *Biochem. Biophys. Res. Commun.* **572**, 118–124 (2021).
37. Tsan, Y. C. *et al.* Physiologic biomechanics enhance reproducible contractile development in a stem cell derived cardiac muscle platform. *Nat. Commun.* **12**(1), 1–16 (2021).
38. Grosberg, A., Alford, P. W., McCain, M. L. & Parker, K. K. Ensembles of engineered cardiac tissues for physiological and pharmacological study: Heart on a chip. *Lab Chip* **11**(24), 4165–4173 (2011).
39. Shim, J., Grosberg, A., Nawroth, J. C., Parker, K. K. & Bertoldi, K. Modeling of cardiac muscle thin films: Pre-stretch, passive and active behavior. *J. Biomech.* **45**(5), 832–841 (2012).
40. Wang, G. *et al.* Modeling the mitochondrial cardiomyopathy of Barth syndrome with induced pluripotent stem cell and heart-on-chip technologies. *Nat. Med.* **20**(6), 616–623 (2014).
41. Marsano, A. *et al.* Beating heart on a chip: A novel microfluidic platform to generate functional 3D cardiac microtissues. *Lab Chip* **16**(3), 599–610 (2016).
42. Ugolini, G. S. *et al.* On-chip assessment of human primary cardiac fibroblasts proliferative responses to uniaxial cyclic mechanical strain. *Biotechnol. Bioeng.* **113**, 859–869 (2016).
43. Ugolini, G. S., Visone, R., Redaelli, A., Moretti, M. & Rasponi, M. Generating multicompartmental 3D biological constructs interfaced through sequential injections in microfluidic devices. *Adv. Healthc. Mater.* <https://doi.org/10.1002/adhm.201601170> (2017).
44. Occhetta, P. *et al.* A three-dimensional in vitro dynamic micro-tissue model of cardiac scar formation. *Integr. Biol.* **10**(3), 174–183 (2018).
45. Schneider, O., Zeifang, L., Fuchs, S., Sailer, C. & Loskill, P. User-friendly and parallelized generation of human induced pluripotent stem cell-derived microtissues in a centrifugal heart-on-a-chip. *Tissue Eng. Part A* **25**(9–10), 786–798 (2019).
46. Khademhosseini, A. *et al.* Microfluidic patterning for fabrication of contractile cardiac organoids. *Biomed. Microdevices* **9**(2), 149–157 (2007).
47. Skardal, A. *et al.* Multi-tissue interactions in an integrated three-tissue organ-on-a-chip platform. *Sci. Rep.* **7**(1), 8837 (2017).
48. Zhang, Y. S. *et al.* From cardiac tissue engineering to heart-on-a-chip: Beating challenges. *Biomed. Mater.* **10**(3), 034006 (2015).
49. Lancaster, M. A. & Knoblich, J. A. Organogenesis in a dish: Modeling development and disease using organoid technologies. *Science* **345**(6194), 1247125 (2014).
50. Clevers, H. Modeling development and disease with organoids. *Cell* **165**(7), 1586–1597 (2016).
51. Lancaster, M. A. & Huch, M. Disease modelling in human organoids. *DMM Dis. Model. Mech.* **12**(7), dmm039347 (2019).
52. Sasai, Y. Next-generation regenerative medicine: Organogenesis from stem cells in 3D culture. *Cell Stem Cell* **12**(5), 520–530 (2013).
53. Sasai, Y. Cytosystems dynamics in self-organization of tissue architecture. *Nature* **493**(7432), 318–326 (2013).
54. Schutgens, F. & Clevers, H. Human organoids: Tools for understanding biology and treating diseases. *Annu. Rev. Pathol. Mech. Dis.* **15**, 211–234 (2020).
55. Corrò, C., Novellasedemunt, L. & Li, V. S. W. A brief history of organoids. *Am. J. Physiol. Cell Physiol.* **319**(1), C151–C165 (2020).
56. Hofbauer, P. *et al.* Cardiods reveal self-organizing principles of human cardiogenesis. *Cell* **184**(12), 3299–3317.e22 (2021).
57. Andersen, P. *et al.* Precardiac organoids form two heart fields via Bmp/Wnt signaling. *Nat. Commun.* **9**(1), 1–13 (2018).
58. Lee, J. *et al.* In vitro generation of functional murine heart organoids via FGF4 and extracellular matrix. *Nat. Commun.* **11**(1), 4283 (2020).
59. Rossi, G. *et al.* Capturing cardiogenesis in gastruloids. *Cell Stem Cell* **28**(2), 230–240.e6 (2021).
60. Voges, H. K. *et al.* Development of a human cardiac organoid injury model reveals innate regenerative potential. *Development* **144**(6), 1118–1127 (2017).
61. Mills, R. J. *et al.* Functional screening in human cardiac organoids reveals a metabolic mechanism for cardiomyocyte cell cycle arrest. *Proc. Natl Acad. Sci. U.S.A.* **114**(40), E8372–E8381 (2017).
62. Richards, D. J. *et al.* Human cardiac organoids for the modelling of myocardial infarction and drug cardiotoxicity. *Nat. Biomed. Eng.* **4**(4), 446–462 (2020).
63. Drakhlis, L. *et al.* Human heart-forming organoids recapitulate early heart and foregut development. *Nat. Biotechnol.* **39**(6), 737–746 (2021).
64. Lewis-Israeli, Y. R. *et al.* Self-assembling human heart organoids for the modeling of cardiac development and congenital heart disease. *Nat. Commun.* **12**(1), 5142 (2021).

65. Silva, A. C. *et al.* Co-emergence of cardiac and gut tissues promotes cardiomyocyte maturation within human iPSC-derived organoids. *Cell Stem Cell* **28**(12), 2137–2152.e6 (2021).
66. Drakhlis, L., Devadas, S. B. & Zweigerdt, R. Generation of heart-forming organoids from human pluripotent stem cells. *Nat. Protoc.* **16**(12), 5652–5672 (2021).
67. Yang, X., Pabon, L. & Murry, C. E. Engineering adolescence: Maturation of human pluripotent stem cell-derived cardiomyocytes. *Circ. Res.* **114**(3), 511–523 (2014).
68. Murphy, S. A., Chen, E. Z., Tung, L., Boheler, K. R. & Kwon, C. Maturing heart muscle cells: Mechanisms and transcriptomic insights. *Semin. Cell Dev. Biol.* **119**, 49–60 (2021).
69. Pasqualini, F. S., Nesmith, A. P., Horton, R. E., Sheehy, S. P. & Parker, K. K. Mechanotransduction and metabolism in cardiomyocyte microdomains. *Biomed Res. Int.* **2016**, 4081638 (2016).
70. Lian, X., Zhang, J., Zhu, K., Kamp, T. J. & Palecek, S. P. Insulin inhibits cardiac mesoderm, not mesendoderm, formation during cardiac differentiation of human pluripotent stem cells and modulation of canonical Wnt signaling can rescue this inhibition. *Stem Cells* **31**(3), 447 (2013).
71. Zuppinger, C. 3D cardiac cell culture: A critical review of current technologies and applications. *Front. Cardiovasc. Med.* **6**, 87 (2019).
72. Pinto, A. R. *et al.* Revisiting cardiac cellular composition. *Circ. Res.* **118**(3), 400 (2016).
73. Litviňuková, M. *et al.* Cells of the adult human heart. *Nature* **588**(7838), 466–472 (2020).
74. Guo, Y. & Pu, W. T. Cardiomyocyte maturation. *Circ. Res.* **126**, 1086–1106 (2020).
75. Ahmed, R. E., Anzai, T., Chanthra, N. & Uosaki, H. A brief review of current maturation methods for human induced pluripotent stem cells-derived cardiomyocytes. *Front. Cell Dev. Biol.* **8**, 178 (2020).
76. A novel approach for the diagnosis of dilated cardiomyopathy (DCM), ID 667310—BioProject—NCBI [Online]. <https://www.ncbi.nlm.nih.gov/bioproject/PRJNA667310>. Accessed 09 Dec 2021.
77. RNA-seq of heart tissues from healthy individuals and DMD patients, ID 628736—BioProject—NCBI [Online]. <https://www.ncbi.nlm.nih.gov/bioproject/?term=PRJNA628736>. Accessed 09 Dec 2021.
78. Physiological calcium combined with electrical pacing accelerates maturation of human engineered heart tissue, ID 831794—BioProject—NCBI [Online]. <https://www.ncbi.nlm.nih.gov/bioproject/PRJNA831794>. Accessed 12 Jul 2022.
79. Feyen, D. A. M. *et al.* Metabolic maturation media improve physiological function of human iPSC-derived cardiomyocytes. *Cell Rep.* **32**(3), 107925 (2020).
80. Lionetti, V., Stanley, W. C. & Recchia, F. A. Modulating fatty acid oxidation in heart failure. *Cardiovasc. Res.* **90**(2), 202 (2011).
81. Drawnel, F. M. *et al.* Disease modeling and phenotypic drug screening for diabetic cardiomyopathy using human induced pluripotent stem cells. *Cell Rep.* **9**(3), 810–820 (2014).
82. Guo, L. *et al.* Estimating the risk of drug-induced proarrhythmia using human induced pluripotent stem cell-derived cardiomyocytes. *Toxicol. Sci.* **123**(1), 281–289 (2011).
83. Mannhardt, I. *et al.* Human engineered heart tissue: Analysis of contractile force. *Stem Cell Rep.* **7**(1), 29–42 (2016).
84. Vandecasteele, G. *et al.* Muscarinic and beta-adrenergic regulation of heart rate, force of contraction and calcium current is preserved in mice lacking endothelial nitric oxide synthase. *Nat. Med.* **5**(3), 331–334 (1999).
85. Schwinger, R. H. G., Böhm, M. & Erdmann, E. Negative inotropic properties of isradipine, nifedipine, diltiazem, and verapamil in diseased human myocardial tissue. *J. Cardiovasc. Pharmacol.* **15**(6), 892–899 (1990).
86. Sala, L. *et al.* Musclemotion: A versatile open software tool to quantify cardiomyocyte and cardiac muscle contraction in vitro and in vivo. *Circ. Res.* **122**(3), e5–e16 (2018).
87. van Meer, B. J. *et al.* Quantification of muscle contraction in vitro and in vivo using MUSCLEMOTION software: From stem cell-derived cardiomyocytes to zebrafish and human hearts. *Curr. Protoc. Hum. Genet.* **99**(1), 1–21 (2018).
88. Thavandiran, N. *et al.* Functional arrays of human pluripotent stem cell-derived cardiac microtissues. *Sci. Rep.* **10**(1), 1–13 (2020).
89. Thorn, C. F. *et al.* Doxorubicin pathways: Pharmacodynamics and adverse effects. *Pharmacogenet. Genom.* **21**(7), 440 (2011).
90. Octavia, Y. *et al.* Doxorubicin-induced cardiomyopathy: From molecular mechanisms to therapeutic strategies. *J. Mol. Cell. Cardiol.* **52**(6), 1213–1225 (2012).
91. Takemura, G. & Fujiwara, H. Doxorubicin-induced cardiomyopathy. From the cardiotoxic mechanisms to management. *Prog. Cardiovasc. Dis.* **49**(5), 330–352 (2007).
92. Silva, D., Santos, D., Coeli, R. & Goldenberg, S. Doxorubicin-induced cardiotoxicity: From mechanisms to development of efficient therapy. *Cardiotoxicity*. (ed. Tan, W.) 3–24. (IntechOpen, 2018) <https://doi.org/10.5772/intechopen.79588> (2018).
93. Tanaka, R. *et al.* Reactive fibrosis precedes doxorubicin-induced heart failure through sterile inflammation. *ESC Heart Fail.* **7**(2), 588–603 (2020).
94. Levick, S. P. *et al.* Doxorubicin-induced myocardial fibrosis involves the neurokinin-1 receptor and direct effects on cardiac fibroblasts. *Heart Lung Circ.* **28**(10), 1598–1605 (2019).
95. Page, R. L. *et al.* Drugs that may cause or exacerbate heart failure. *Circulation* **134**(6), e32–e69 (2016).
96. Gilsbach, R. *et al.* Dynamic DNA methylation orchestrates cardiomyocyte development, maturation and disease. *Nat. Commun.* **5**, 5288 (2014).
97. Grancharova, T. *et al.* A comprehensive analysis of gene expression changes in a high replicate and open-source dataset of differentiating hiPSC-derived cardiomyocytes. *Sci. Rep.* **11**(1), 1–21 (2021).
98. Meilhac, S. M. & Buckingham, M. E. The deployment of cell lineages that form the mammalian heart. *Nat. Rev. Cardiol.* **15**(11), 705–724 (2018).
99. Zhang, X. H. *et al.* Regionally diverse mitochondrial calcium signaling regulates spontaneous pacing in developing cardiomyocytes. *Cell Calcium* **57**, 321 (2015).
100. Karbassi, E. *et al.* Cardiomyocyte maturation: Advances in knowledge and implications for regenerative medicine. *Nat. Rev. Cardiol.* **17**(6), 341 (2020).
101. Schaper, J., Meiser, E. & Stammler, G. Ultrastructural morphometric analysis of myocardium from dogs, rats, hamsters, mice, and from human hearts. *Circ. Res.* **56**(3), 377–391 (1985).
102. Spitkovsky, D. *et al.* Activity of complex III of the mitochondrial electron transport chain is essential for early heart muscle cell differentiation. *FASEB J.* **18**(11), 1300–1302 (2004).
103. Cadenas, S. Mitochondrial uncoupling, ROS generation and cardioprotection. *Biochim. Biophys. Acta Bioenerg.* **1859**(9), 940–950 (2018).
104. Perestrelo, A. R. *et al.* Multiscale analysis of extracellular matrix remodeling in the failing heart. *Circ. Res.* **128**, 24–38 (2021).
105. Rodrigues, P. G. *et al.* Early myocardial changes induced by doxorubicin in the nonfailing dilated ventricle. *Am. J. Physiol. Heart Circ. Physiol.* **316**(3), H459–H475 (2019).
106. Dolci, A., Dominici, R., Cardinale, D., Sandri, M. T. & Panteghini, M. Biochemical markers for prediction of chemotherapy-induced cardiotoxicity systematic review of the literature and recommendations for use. *Am. J. Clin. Pathol.* **130**(5), 688–695 (2008).
107. Ho, B. X., Pek, N. M. Q. & Soh, B. S. Disease modeling using 3D organoids derived from human induced pluripotent stem cells. *Int. J. Mol. Sci.* **19**, 936 (2018).

108. Marchianò, S., Bertero, A. & Murry, C. E. Learn from your elders: Developmental biology lessons to guide maturation of stem cell-derived cardiomyocytes. *Pediatr. Cardiol.* **40**(7), 1367–1387 (2019).
109. Xu, T., Wu, L., Xia, M., Simeonov, A. & Huang, R. Systematic identification of molecular targets and pathways related to human organ level toxicity. *Chem. Res. Toxicol.* **34**(2), 412–421 (2021).
110. Hoang, P. *et al.* Engineering spatial-organized cardiac organoids for developmental toxicity testing. *Stem Cell Rep.* **16**(5), 1228–1244 (2021).
111. Pagliari, S. *et al.* YAP–TEAD1 control of cytoskeleton dynamics and intracellular tension guides human pluripotent stem cell mesoderm specification. *Cell Death Differ.* **28**(4), 1193–1207 (2020).
112. Vrbský, J. *et al.* Evidence for discrete modes of YAP1 signaling via mRNA splice isoforms in development and diseases. *Genomics* **113**(3), 1349–1365 (2021).
113. Chen, E. Y. *et al.* Enrichr: Interactive and collaborative HTML5 gene list enrichment analysis tool. *BMC Bioinform.* **14**, 128 (2013).
114. Kuleshov, M. V. *et al.* Enrichr: A comprehensive gene set enrichment analysis web server 2016 update. *Nucleic Acids Res.* **44**(W1), W90–W97 (2016).
115. Xie, Z. *et al.* Gene set knowledge discovery with Enrichr. *Curr. Protoc.* **1**(3), e90 (2021).
116. Shannon, P. *et al.* Cytoscape: A software environment for integrated models of biomolecular interaction networks. *Genome Res.* **13**(11), 2498–2504 (2003).
117. Torre, D., Lachmann, A. & Maayan, A. BioJupies: Automated generation of interactive notebooks for RNA-Seq data analysis in the cloud. *Cell Syst.* **7**(5), 556–561.e3 (2018).

Acknowledgements

We thank Václav Hejret, Boris Tichý, Jana Vašíčková, and Jana Bartoňová for scientific advice and technical assistance. We acknowledge the CF Genomics of CEITEC supported by the NCMG research infrastructure (LM2018132 funded by MEYS CR) Bioinformatics for their support with obtaining scientific data presented in this paper. We are grateful to Ivana Andrejčinová, Marco de Zuani and Jan Frič for the NFAT2 and ASCL1 antibodies. We also thank Romana Vlčková, Hana Duřová, and Helena Ďuríková for their support on continuation of the study. Ece Ergir, Giancarlo Forte, Stefania Pagliari and Vladimír Vinarský were supported by the European Regional Development Fund—Project ENOCH (No. CZ.02.1.01/0.0/0.0/16_019/0000868). Jorge Oliver-De La Cruz and Soraia Fernandes were supported by the European Social Fund and European Regional Development Fund-Project MAGNET (CZ.02.1.01/0.0/0.0/15_003/0000492). Marco Cassani, an iCARE-2 fellow, has received funding from Fondazione per la Ricerca sul Cancro (AIRC) and the European Union's Horizon 2020 research and innovation programme under the Marie Skłodowska-Curie Grant Agreement No. 800924. Francesco Niro and Daniel Pereira-Sousa were supported by the European Union's Horizon 2020 Research and Innovation Program under grant agreement No. 860715 (SINERGIA).

Author contributions

E.E. conceptualized the study, designed and performed the experiments, analysed the data and drafted the manuscript. J.O.D.L.C., S.F., M.C., V.V., A.R.P. and S.P. provided essential information and techniques, and assisted in designing, planning, carrying out and interpreting experiments. F.N. and D.P.S. performed experiments and analysed the data. J.V. and J.O.D.L.C. assisted with bioinformatics analysis. M.C. and D.D. performed the TEM analysis. N.V. and S.U. performed the Seahorse XF experiments and metabolic data analysis. F.C. and H.R. assisted in funding acquisition and manuscript revision. P.E. provided study supervision and manuscript revision. G.F. provided study supervision, funding acquisition, paper conceptualization and manuscript finalization. All authors contributed in interpretation, and presentation of data as well as manuscript editing. All authors reviewed and approved the final version.

Competing interests

The authors declare no competing interests.


Additional information

Supplementary Information The online version contains supplementary material available at <https://doi.org/10.1038/s41598-022-22225-w>.

Correspondence and requests for materials should be addressed to G.F.

Reprints and permissions information is available at www.nature.com/reprints.

Publisher's note Springer Nature remains neutral with regard to jurisdictional claims in published maps and institutional affiliations.

 **Open Access** This article is licensed under a Creative Commons Attribution 4.0 International License, which permits use, sharing, adaptation, distribution and reproduction in any medium or format, as long as you give appropriate credit to the original author(s) and the source, provide a link to the Creative Commons licence, and indicate if changes were made. The images or other third party material in this article are included in the article's Creative Commons licence, unless indicated otherwise in a credit line to the material. If material is not included in the article's Creative Commons licence and your intended use is not permitted by statutory regulation or exceeds the permitted use, you will need to obtain permission directly from the copyright holder. To view a copy of this licence, visit <http://creativecommons.org/licenses/by/4.0/>.

© The Author(s) 2022

SUPPLEMENTARY INFORMATION

Generation and Maturation of Human iPSC-derived 3D Organotypic Cardiac Microtissues in Long-Term Culture

Ece Ergir^{1,2}, Jorge Oliver-De La Cruz¹, Soraia Fernandes¹, Marco Cassani¹, Francesco Niro^{1,3}, Daniel Pereira-Sousa^{1,3}, Jan Vrbský¹, Vladimír Vinarský¹, Ana Rubina Perestrelo¹, Doriana Debellis⁴, Natália Vadovičová³, Stjepan Uldrijan³, Francesca Cavalieri^{5,6}, Stefania Pagliari¹, Heinz Redl^{7,8}, Peter Ertl^{2,8}, and Giancarlo Forte^{1,9}

¹ Center for Translational Medicine (CTM), St. Anne's University Hospital, International Clinical Research Centre (FNUSA-ICRC), CZ-62500, Brno, Czech Republic

² Faculty of Technical Chemistry, Institute of Applied Synthetic Chemistry & Institute of Chemical Technologies and Analytics, Vienna University of Technology, AT-1040, Vienna, Austria

³ Faculty of Medicine, Department of Biomedical Sciences, Masaryk University, CZ-62500, Brno, Czech Republic.

⁴ Electron Microscopy Facility, Fondazione Istituto Italiano Di Tecnologia, Via Morego 30, IT-16163, Genova, Italy

⁵ Department of Chemical Engineering, The University of Melbourne, Parkville, Victoria 3010, Australia;

⁶ Dipartimento di Scienze e Tecnologie Chimiche, Università degli Studi di Roma Tor Vergata, via della Ricerca Scientifica 1, 00133, Rome, Italy

⁷ Ludwig Boltzmann Institute for Experimental and Clinical Traumatology, AUVA Research Center, AT-1200, Vienna, Austria

⁸ Austrian Cluster for Tissue Regeneration, AT-1200, Vienna, Austria

⁹ Department of Biomaterials Science, Institute of Dentistry, University of Turku, FI-20014, Turku, Finland

Corresponding author:

Giancarlo Forte, PhD
Center for Translational Medicine (CTM)
International Clinical Research Center (ICRC)
St. Anne's University Hospital
Studentska 6, Brno
Czech Republic, 62500
Tel: +420-543185449
giancarlo.forte@fnusa.cz

Supplementary Figures

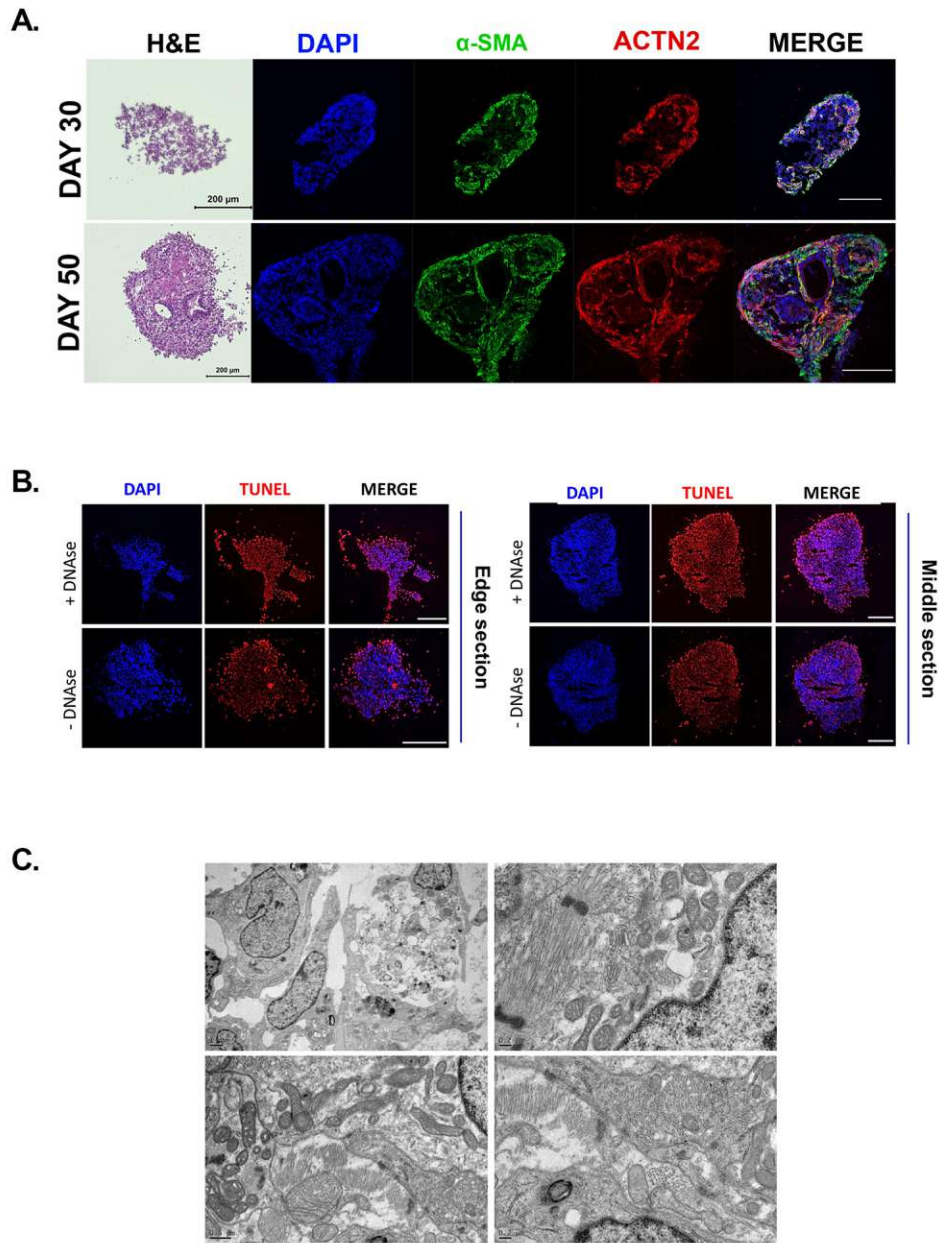


Figure SI-1 - 3D hOCMTs recapitulate advanced morphology and cellular heterogeneity in longer culture times

- A.** H&E staining and immunofluorescence analysis showing the increasing histological complexity of 3D hOCMT sections on day 30 vs day 50. Markers for cardiomyocytes (ACTN2 - red), smooth muscle/fibroblastic cells (α -SMA - green), shown, counterstained with DAPI (blue). Scale bars = 200 μ m
- B.** TUNEL staining (red) on day 30 3D hOCMT cryosections, with DAPI counterstain (blue) (edge and center sections) Scale bar = 200 μ m
- C.** TEM images of day 50 hOCMTs ultrastructural organization, depicting viable and necrotic areas. Scale bars: top left = 1 μ m, top right = 0.2 μ m, bottom left = 0.5 μ m, bottom right = 0.2 μ m.

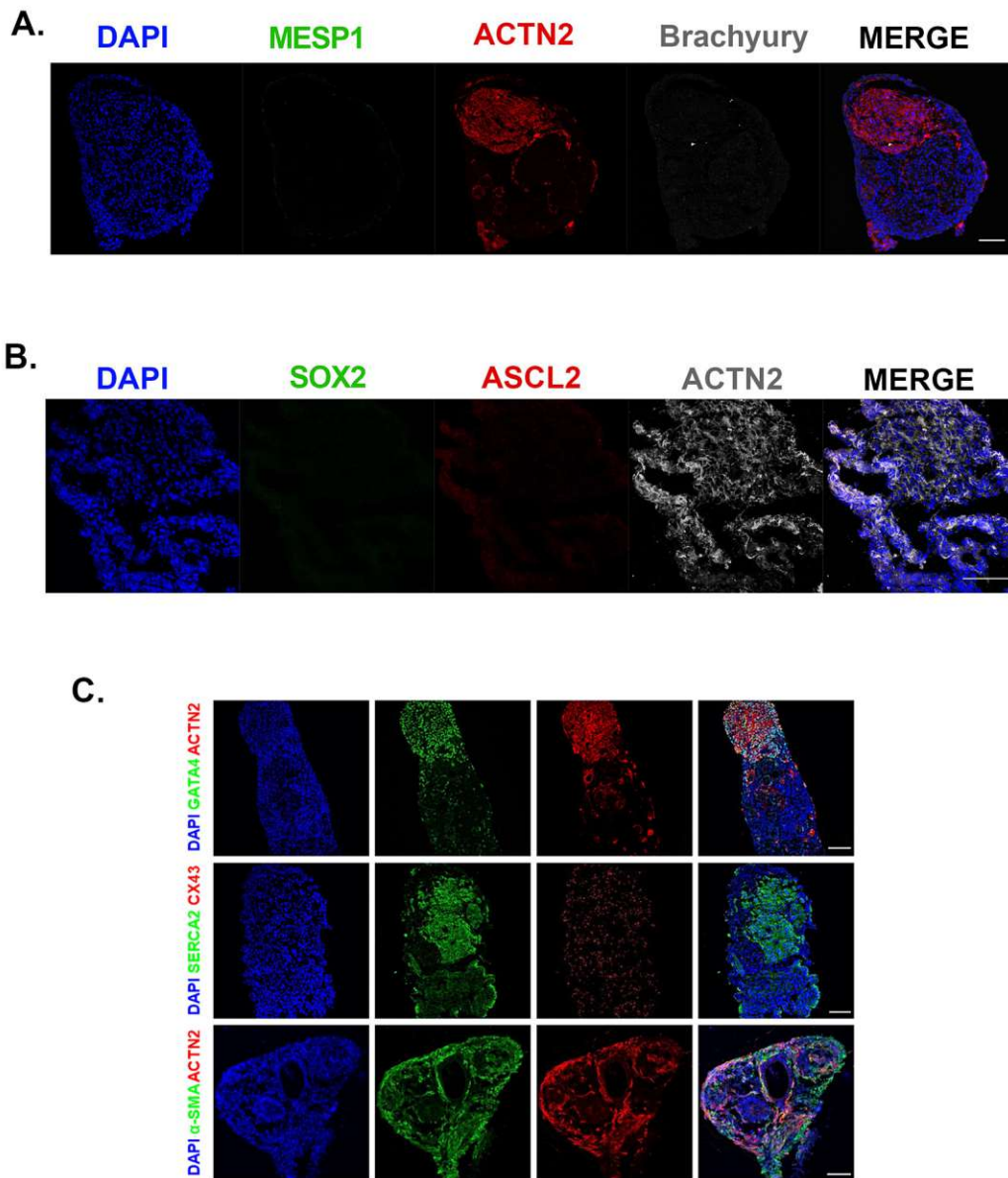


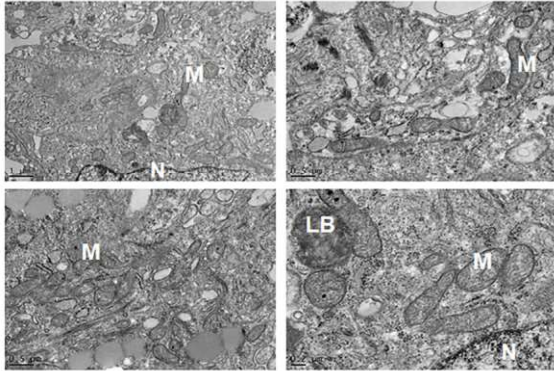
Figure SI-2 – Long-term hOCMTs show cardiovascular cellular heterogeneity and do not show markers for undifferentiated cells or co-emergence of gut tissue

A. IF staining of hOCMT sections for undifferentiated cell markers including MESP1 (green) and Brachyury (grey), compared to differentiated cardiomyocytes (ACTN2 - red) on day 50. Counterstaining with DAPI (blue). Scale bar = 100 μ m

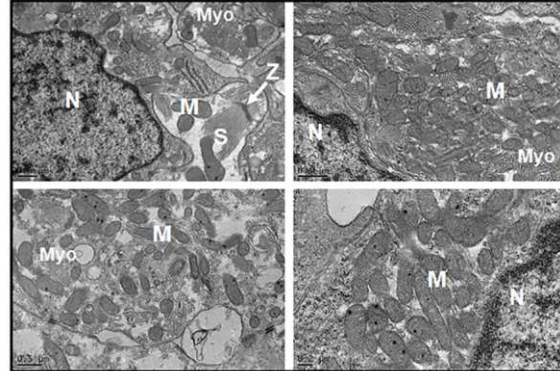
B. IF staining of hOCMT sections for undifferentiated cell & embryonic gut (SOX2 - green), and adult gut (ASCL2 - red) tissue markers, compared to differentiated cardiomyocytes (ACTN2 - grey) on day 50. Counterstaining with DAPI (blue). Scale bar = 100 μ m

C. IF staining of hOCMT sections for cardiomyocytes (ACTN2 - red), cardiac morphogenesis (GATA4 -green), calcium ATPase (SERCA2 - green), gap junction proteins (CX43- red), and smooth muscle/fibroblastic cells (α -SMA - green). Counterstaining with DAPI (blue). Scale bar = 100 μ m

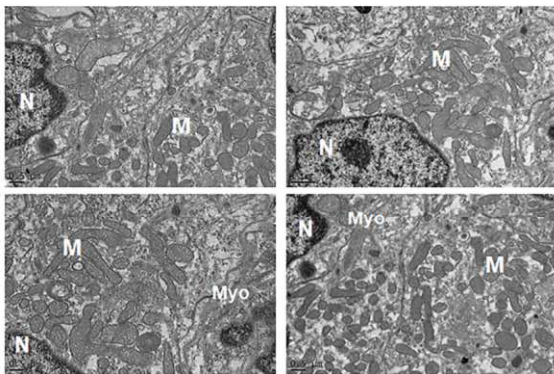
DAY 21



DAY 50



DAY 85



DAY 50

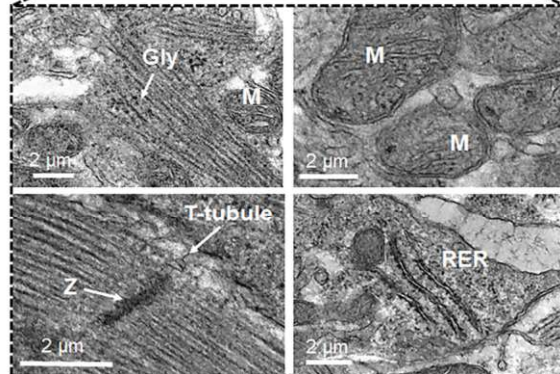


Figure SI-3 – Ultrastructural analysis of long-term hOCMTs indicates enhanced cardiomyocyte and metabolic maturation in 3D environment over time

TEM images of hOCMTs increasing ultrastructural organization and structural & metabolic maturity over time, from day 21 to day 85: Depicted: Cardiomyocyte myofibers (Myo), Sarcomeres (S), Mitochondria (M) Z-band (Z), T-tubules, Nuclei (N), Rough endoplasmic reticulum (RER), Glycogen granules (Gly), Lamellar bodies (LB). Scale bars are 1 μm and 0.5 μm for day 21, 0.5 μm for day 85, 0.5 μm for day 50 and 2 μm for magnified images of day 50.

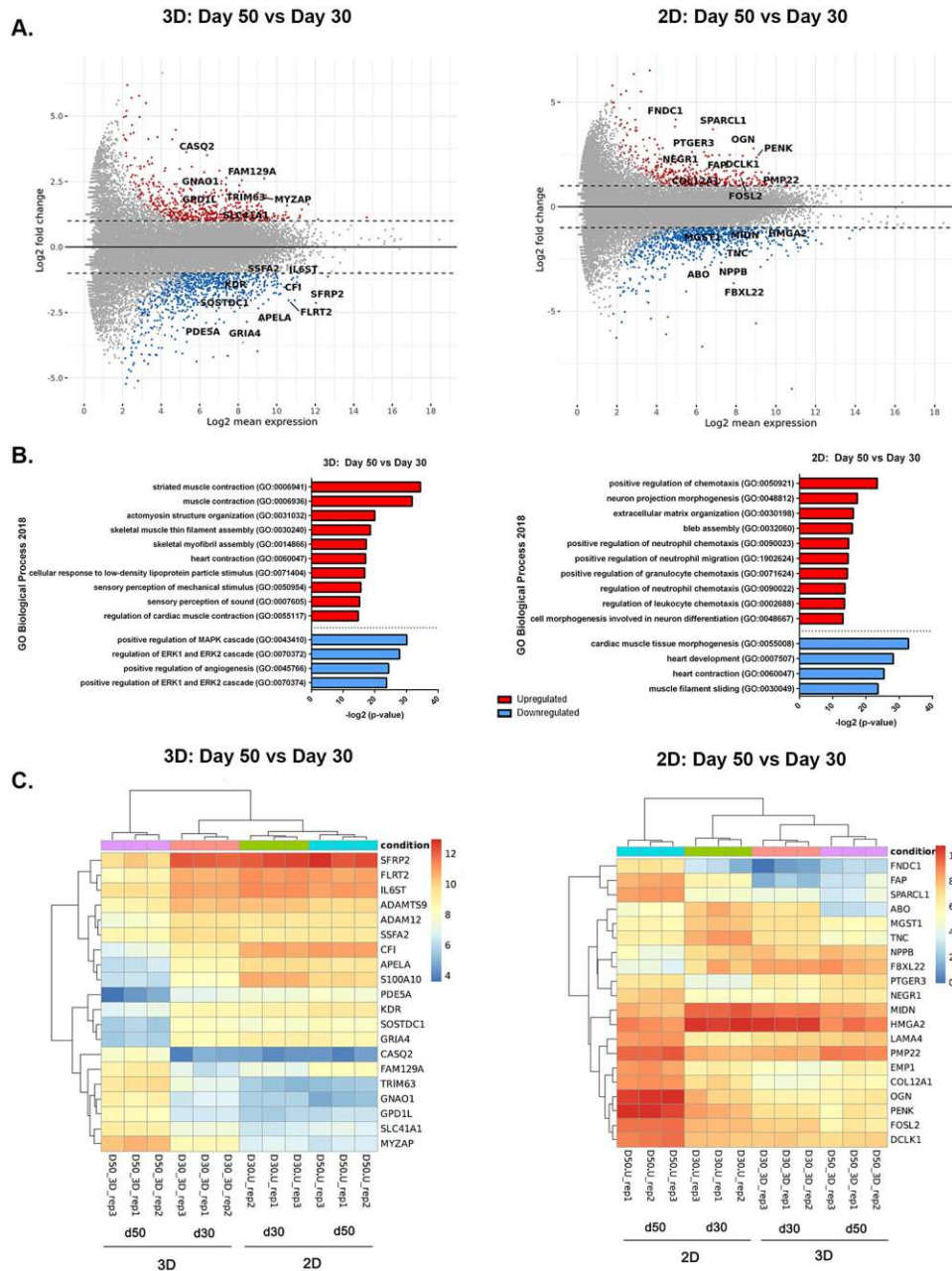


Figure SI-4 – 3D hOCMT cultures induce improved cardiac specification and cardiomyocyte maturation at a transcriptomic level with respect to culture dimensionality and time

A. MA plot of the differentially regulated genes between day 30 and day 50 for 3D hOCMTs (left) and 2D monolayer culture (right) (\log_2 mean, $p_{adj} < 0.05$)

B. Graph representing the $-\log_2$ adjusted p-value of significantly upregulated (red) or downregulated (blue) GO Biological process categories when comparing between day 30 and day 50 of culture for 3D hOCMTs (left) and 2D monolayer culture (right) ($p_{adj} < 0.05$)

C. Heatmap representing the \log_2 fold change for the top 20 differentially regulated genes between day 30 and day 50 of culture for 3D hOCMTs (left) and 2D monolayer culture (right) ($p_{adj} < 0.05$)

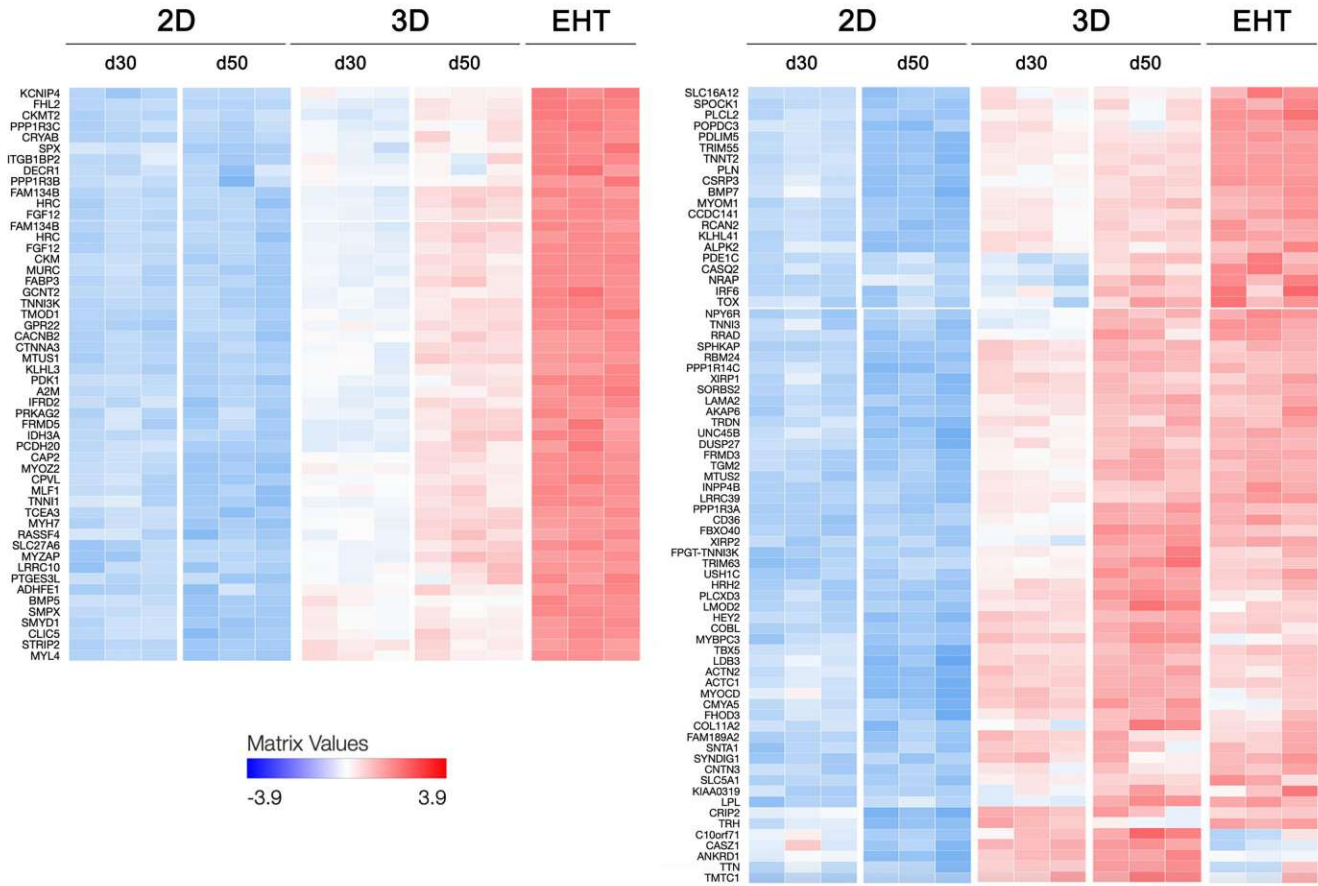


Figure SI-5 – 3D hOCMT cultures show transcriptional similarities to in vitro engineered heart tissues (EHT) with respect to cardiac specification and cardiomyocyte maturation

Heatmap encoding for log₂fold changes in selected cardiac genes for the 3D hOCMTs and the 2D monolayers at both time-points in comparison with available datasets for in vitro engineered heart tissues (EHT).

Supplementary Methods

Histology and Immunofluorescence (IF)

After organoid fixation and cryosectioning, to assess the overall histology, the sections were stained with hematoxylin and eosin (H&E) (Sigma Aldrich), and imaged under slide scanner Zeiss Axio Scan Z1 microscope using the bright-field mode.

In addition to 3D hCO cryosections, 2D monolayer cultures were used as controls. As 2D monolayer controls were grown adherently on Matrigel-coated plates, for the IF procedure, the samples were fixed with 4% PFA for 15 minutes, and rest of the IF procedures were performed as previously described in the main text. The resulting samples were stored in PBS with 0.01% Sodium Azide (VWR) at 4°C, and protected from light until confocal image analysis.

See Supplementary table 1 for full list of antibodies used in the study.

RNA-sequencing and Differential Expression analysis (DE analysis)

Sequencing library preparation

500 nanograms of total RNA per sample was used as an input for library preparation using QuantSeq FWD 3'mRNA Library Prep Kit (Lexogen). Briefly, RNA was transcribed into cDNA using oligodT primer (FS1) at half volume compared to the manufacturer's instructions to minimize the off-target products. Following the first strand synthesis, RNA removal and second strand synthesis were performed using the UMI Second Strand Synthesis Mix (USS) containing Unique Molecular Identifiers (UMIs) that allow detection and removal of PCR duplicates. Finally, sequencing libraries were created by PCR with i5 Unique Dual Indexing Add-on Kit for Illumina (Lexogen). The quality and quantity of libraries was determined using Fragment Analyzer by DNF-474 High Sensitivity NGS Fragment Analysis Kit (Agilent Technologies) and QuantiFluor dsDNA System (Promega). Final library pool was sequenced on Illumina NextSeq 500 with 75 bp single-ends, producing about 10 million reads per library.

Data analysis

High-throughput RNA-Seq data were prepared using Lexogen QuantSeq 3' mRNA-Seq Library Prep Kit FWD for Illumina with polyA selection and sequenced on Illumina NextSeq 500 sequencer (run length 1x75 nt). Bcl files were converted to Fastq format using bcl2fastq v. 2.20.0.422 Illumina software for basecalling. 6-nt long UMIs were extracted and subsequently used for deduplication of aligned reads by UMI-tools v. 1.1.1 [1]. As a next step 6-nt long barcode sequence related to Lexogen QuantSeq Library Prep Kit were trimmed using seqtk 1.3-r106 [2]. Quality check of raw single-end fastq reads was carried out by FastQC v0.11.9 [3]. The adapters and quality trimming of raw fastq reads was performed using Trimmomatic v0.36 [4] with settings CROP:250 LEADING:3 TRAILING:3 SLIDINGWINDOW:4:5 MINLEN:35 and adaptor sequence ILLUMINACLIP:AGATCGGAAGAGCACACGTCT. Trimmed RNA-Seq reads were mapped against the human genome (hg38) and Ensembl GRCh38 v.94 annotation using STAR v2.7.3a [5] as splice-aware short read aligner and default parameters except --outFilterMismatchNoverLmax 0.1 and --twopassMode Basic. Quality control after alignment concerning the number and percentage of uniquely and multi-mapped reads, rRNA contamination, mapped regions, read coverage distribution, strand specificity, gene biotypes and PCR duplication was performed using several tools namely RSeQC v2.6.2 [6], Picard toolkit v2.18.27 [7] and Qualimap v.2.2.2 [8] and BioBloom tools v 2.3.4-6-g433f [9].

The differential gene expression analysis was calculated based on the gene counts produced using featureCounts tool v1.6.3 [10] with settings -s 2 -T 10 -F GTF -Q 0 -d 1 -D 25000 and using Bioconductor package DESeq2 v1.20.0 [11]. Data generated by DESeq2 with independent filtering were selected for the differential gene expression analysis to avoid potential false positive results. Genes were considered as differentially expressed based on a cut-off of adjusted p-value ≤ 0.05 and $\log_2(\text{fold-change}) \geq 1$ or ≤ -1 . Clustered heatmaps were generated from selected top differentially regulated genes using R package pheatmap v1.0.10 [12]. Volcano plots were produced using ggplot v3.3.3 package [13] and MA plots were generated using ggpupr v0.4.0 package [14].

See Supplementary dataset 1 for \log_2 changes and p-values for the different comparisons, and Supplementary dataset 2 for GO BP clustering analysis for the differentially regulated genes at the different comparisons.

IMMUNOFLUORESCENCE				
<i>IF- Primary Antibodies</i>				
Name	Host species	Dilution	Company	Catalog no
Anti- α -SMA (ACTA2)	Rabbit	1:500	Abcam	ab5694
Anti-ACTN2 (sarcomeric α -actinin)	Mouse	1:800	Sigma Aldrich	A7811
Anti-ASCL2	Sheep	1:50	Thermo Fisher Scientific	PA5-47852
Anti-Brachyury (T)	Goat	1:50	R&D Systems	967332
Anti-CD31 (PECAM-1)	Mouse	1:100	Biologend	303102
Anti-CX43 (Connexin 43, GJA1)	Rabbit	1:400	Sigma Aldrich	C6219-100UL
Anti-GATA4	Rabbit	1:400	Cell signalling	36966S
Anti-MESP1	Rabbit	1:200	Abcam	ab129387
Anti-MYL2 (α -MLC2, MLC2v)	Rabbit	1:200	Abcam	ab79935
Anti-MYL7 (MLC2a)	Mouse	1:200	Santa Cruz	sc-365255
Anti-NFAT2 (NFATc1)	Rabbit	1:100	Cell Signalling	8032S
Anti-SERCA2 (ATP2A2)	Mouse	1:100	Novus Biologicals	NB300-581
Anti-SM22a (Transgelin, TAGLN)	Rabbit	1:500	Abcam	ab14106
Anti-SOX2	Rabbit	1:400	Cell Signalling	3579
Anti-TE - 7	Mouse	1:100	Sigma Aldrich	CBL271
Anti-TBX18	Rabbit	1:200	Thermo Fisher Scientific	PA5-101921
Anti-TNNT2	Mouse	1:200	Thermo Fisher Scientific	MA5-12960
Anti-TNNT2	Rabbit	1:3000	Sigma Aldrich	HPA015774
Anti-WT1	Rabbit	1:200	Cell Signalling	83535
<i>IF- Secondary Antibodies</i>				
Name	Dilution	Company	Catalog no	
Alexa Fluor 488 Donkey anti-Rabbit IgG (H+L)	1:500	Thermo Fisher Scientific	A-21206	
Alexa Fluor 488 Donkey anti-Mouse IgG (H+L)	1:500	Thermo Fisher Scientific	A-21202	
Alexa Fluor 555 Donkey anti-Rabbit IgG (H+L)	1:500	Thermo Fisher Scientific	A-31572	
Alexa Fluor 555 Donkey anti- Mouse IgG (H+L)	1:500	Thermo Fisher Scientific	A-31570	
Alexa Fluor 546 Donkey anti-Sheep IgG (H+L)	1:500	Thermo Fisher Scientific	A-21098	
Alexa Fluor 647 Donkey anti-Goat IgG (H+L)	1:500	Thermo Fisher Scientific	A-21447	
Alexa Fluor 647 Goat anti-Mouse IgG (H+L)	1:500	Thermo Fisher Scientific	A-21235	
FLOW CYTOMETRY				
Name	Dilution	Company	Catalog no	
Anti Cardiac Troponin T-FITC Clone REA400 (REAFinity™)	1:50	Miltenyi Biotec	130-119-575	
Anti-Hu CD90 APC	1:10	Exbio	1A-652-T100	
Anti-Hu CD31 BV421	1:10	Biologend	303123	

Supplementary Table 1. List of antibodies used in the study.

List of Supplementary Videos

Supplementary video 1 – Representative spontaneously beating long-term 3D hiPSC-derived organotypic cardiac microtissue (hOCMTs) under light microscope (Day 53). Scale bar = 100 μ m

Supplementary video 2 – Representative spontaneously beating long-term 3D hOCMT under light microscope (Day 107). Scale bar = 100 μ m

Supplementary videos (3-8) – Representative videos of beating long-term hOCMTs before ($t=0$) & after ($t=1$) maximum dose of cardioactive drugs on day 50; taken under transmitted light mode of confocal microscope (Scale bars = 200 μ m):

3. Control hOCMT ($t=0$)
4. Control hOCMT ($t=1$)
5. hOCMT with 0 μ M isoproterenol ($t=0$)
6. hOCMT with 1 μ M isoproterenol ($t=1$)
7. hOCMT with 0 μ M verapamil ($t=0$)
8. hOCMT with 1 μ M verapamil ($t=1$)

Supplementary videos (9-14) – Representative videos of beating long-term hOCMTs (Day 53) before & after Doxorubicin (Doxo) treatment on day 0 and day 6 of the treatments; taken under transmitted light mode of confocal microscope (Scale bars = 200 μ m):

9. Control hOCMT on day 0
10. hOCMT with 0.1 μ g/mL Doxo on day 0
11. hOCMT with 1 μ g/mL Doxo on day 0
12. Control hOCMT on day 6
13. hOCMT with 0.1 μ g/mL Doxo on day 6
14. hOCMT with 1 μ g/mL Doxo on day 6

List of Supplementary Datasets

Supplementary dataset 1 – log₂changes and p-values for the different comparisons

Supplementary dataset 2 – GO BP clustering analysis for the differentially regulated genes at the different comparisons

Supplementary References

- [1] T. Smith, A. Heger, and I. Sudbery, “UMI-tools: modeling sequencing errors in Unique Molecular Identifiers to improve quantification accuracy,” *Genome Res.*, vol. 27, no. 3, pp. 491–499, Mar. 2017.
- [2] H. Li, “seqtk: Toolkit for processing sequences in FASTA/Q formats,” *GitHub* 767, 2012. [Online]. Available: <https://github.com/lh3/seqtk/>. [Accessed: 29-Jan-2022].
- [3] S. Andrews, “FastQC A Quality Control tool for High Throughput Sequence Data,” [Online], 2010. [Online]. Available: <https://www.bioinformatics.babraham.ac.uk/projects/fastqc/>. [Accessed: 29-Jan-2022].
- [4] A. M. Bolger, M. Lohse, and B. Usadel, “Trimmomatic: a flexible trimmer for Illumina sequence data,” *Bioinformatics*, vol. 30, no. 15, p. 2114, Aug. 2014.
- [5] A. Dobin *et al.*, “STAR: ultrafast universal RNA-seq aligner,” *Bioinformatics*, vol. 29, no. 1, p. 15, Jan. 2013.
- [6] L. Wang, S. Wang, and W. Li, “RSeQC: quality control of RNA-seq experiments,” *Bioinformatics*, vol. 28, no. 16, pp. 2184–2185, Aug. 2012.
- [7] “Picard Toolkit.” 2018. Broad Institute, GitHub Repository. 2018. [Online]. Available: <https://broadinstitute.github.io/picard/>. [Accessed: 29-Jan-2022].
- [8] K. Okonechnikov, A. Conesa, and F. García-Alcalde, “Qualimap 2: advanced multi-sample quality control for high-throughput sequencing data,” *Bioinformatics*, vol. 32, no. 2, p. 292, Jan. 2016.
- [9] J. Chu *et al.*, “BioBloom tools: fast, accurate and memory-efficient host species sequence screening using bloom filters,” *Bioinformatics*, vol. 30, no. 23, p. 3402, Dec. 2014.
- [10] Y. Liao, G. K. Smyth, and W. Shi, “featureCounts: an efficient general purpose program for assigning sequence reads to genomic features,” *Bioinformatics*, vol. 30, no. 7, pp. 923–930, Apr. 2014.
- [11] M. I. Love, W. Huber, and S. Anders, “Moderated estimation of fold change and dispersion for RNA-seq data with DESeq2,” *Genome Biol.*, vol. 15, no. 12, pp. 1–21, Dec. 2014.
- [12] R. Kolde, “Package ‘pheatmap,’” *R Package* 1.7, 2015. [Online]. Available: <https://cran.r-project.org/web/packages/pheatmap/index.html>. [Accessed: 29-Jan-2022].
- [13] H. Wickham, “ggplot2,” *Wiley Interdiscip. Rev. Comput. Stat.*, vol. 3, no. 2, pp. 180–185, Mar. 2011.
- [14] A. Kassambara, “ggpubr: ‘ggplot2’ based publication ready plots,” *R package version 0.1 7*, 2018. [Online]. Available: <https://rpkgs.datanovia.com/ggpubr/>. [Accessed: 29-Jan-2022].

Manuscript II

Parts of this dissertation, including figures and tables, have been reproduced, with or without modifications, based on my original published mini-review article (Ergir et al., 2018) licensed for reuse under Creative Commons Attribution 4.0 International License. To view a copy of this licence, visit <http://creativecommons.org/licenses/by/4.0/>.

MINI REVIEW article
Front. Physiol., 09 October 2018
Sec. Integrative Physiology
<https://doi.org/10.3389/fphys.2018.01417>

Small Force, Big Impact: Next Generation Organ-on-a-Chip Systems Incorporating Biomechanical Cues

Ece Ergir^{1,2†}, Barbara Bachmann^{2,3,4,5†}, Heinz Redl^{3,4,5}, Giancarlo Forte^{1,6,7} and Peter Ertl^{2,4,5}

- 1 Center for Translational Medicine, International Clinical Research Center, St. Anne's University Hospital, Brno, Czechia,
- 2 Faculty of Technical Chemistry, Institute of Applied Synthetic Chemistry and Institute of Chemical Technologies and Analytics, Vienna University of Technology, Vienna, Austria
- 3 AUVA Research Centre, Ludwig Boltzmann Institute for Experimental and Clinical Traumatology, Vienna, Austria
- 4 Austrian Cluster for Tissue Regeneration, Vienna, Austria
- 5 Kompetenzzentrum für MechanoBiologie (INTERREG V-A Austria – Czech Republic Programme, ATCZ133), Vienna, Austria
- 6 Competence Center for Mechanobiology (INTERREG V-A Austria – Czech Republic Programme, ATCZ133), Brno, Czechia
- 7 Department of Biomaterials Science, Institute of Dentistry, University of Turku, Turku, Finland

† These authors have contributed equally to this work

EE and BB conceived the general structure of the review, revised the existing literature, and drafted the manuscript. HR, GF, and PE revised the text and contributed to the final manuscript. Figure 1 was drawn by EE.



Small Force, Big Impact: Next Generation Organ-on-a-Chip Systems Incorporating Biomechanical Cues

Ece Ergir^{1,2†}, Barbara Bachmann^{2,3,4,5†}, Heinz Redl^{3,4,5}, Giancarlo Forte^{1,6,7*} and Peter Ertl^{2,4,5*}

¹ Center for Translational Medicine, International Clinical Research Center, St. Anne's University Hospital, Brno, Czechia,

² Faculty of Technical Chemistry, Institute of Applied Synthetic Chemistry and Institute of Chemical Technologies

and Analytics, Vienna University of Technology, Vienna, Austria, ³ AUVA Research Centre, Ludwig Boltzmann Institute

for Experimental and Clinical Traumatology, Vienna, Austria, ⁴ Austrian Cluster for Tissue Regeneration, Vienna, Austria,

⁵ Kompetenzzentrum für MechanoBiologie (INTERREG V-A Austria – Czech Republic Programme, ATCZ133), Vienna,

Austria, ⁶ Competence Center for Mechanobiology (INTERREG V-A Austria – Czech Republic Programme, ATCZ133), Brno,

Czechia, ⁷ Department of Biomaterials Science, Institute of Dentistry, University of Turku, Turku, Finland

OPEN ACCESS

Edited by:

Leonardo Alexandre

Peyré-Tartaruga,

Universidade Federal do Rio Grande do Sul (UFRGS), Brazil

Reviewed by:

Khashayar Khoshmanesh,

RMIT University, Australia

Irena Levitan,

University of Illinois at Chicago,

United States

T. Alexander Quinn,

Dalhousie University, Canada

*Correspondence:

Giancarlo Forte

giancarlo.forte@fnusa.cz

Peter Ertl

peter.ertl@tuwien.ac.at

[†]These authors have contributed equally to this work

Specialty section:

This article was submitted to

Integrative Physiology,

a section of the journal

Frontiers in Physiology

Received: 01 April 2018

Accepted: 18 September 2018

Published: 09 October 2018

Citation:

Ergir E, Bachmann B, Redl H,

Forte G and Ertl P (2018) Small Force,

Big Impact: Next Generation

Organ-on-a-Chip Systems

Incorporating Biomechanical Cues.

Front. Physiol. 9:1417.

doi: 10.3389/fphys.2018.01417

Mechanobiology-on-a-chip is a growing field focusing on how mechanical inputs modulate physico-chemical output in microphysiological systems. It is well known that biomechanical cues trigger a variety of molecular events and adjustment of mechanical forces is therefore essential for mimicking *in vivo* physiologies in organ-on-a-chip technology. Biomechanical inputs in organ-on-a-chip systems can range from variations in extracellular matrix type and stiffness and applied shear stresses to active stretch/strain or compression forces using integrated flexible membranes. The main advantages of these organ-on-a-chip systems are therefore (a) the control over spatiotemporal organization of *in vivo*-like tissue architectures, (b) the ability to precisely control the amount, duration and intensity of the biomechanical stimuli, and (c) the capability of monitoring in real time the effects of applied mechanical forces on cell, tissue and organ functions. Consequently, over the last decade a variety of microfluidic devices have been introduced to recreate physiological microenvironments that also account for the influence of physical forces on biological functions. In this review we present recent advances in mechanobiological lab-on-a-chip systems and report on lessons learned from these current mechanobiological models. Additionally, future developments needed to engineer next-generation physiological and pathological organ-on-a-chip models are discussed.

Keywords: microfluidics, mechanobiology, organ-on-a-chip, lab-on-a-chip, *in vitro* organ models, mechanical cell actuation

INTRODUCTION

Conventional mammalian cell culture systems are predominantly based on two-dimensional (2D) monolayer cultures to study cellular mechanisms in pharmaceutical research, toxicology and biomedicine. Even though 2D cell culture models are routinely used, they fail to recapitulate the spatiotemporal dynamics that cells encounter *in vivo*. The discrepancy between *in vitro*

monolayers and native tissue structures leads in many cases to altered phenotype, cell morphology and behavior, thus rendering results from 2D cell-based assays questionable (Baker and Chen, 2012). To overcome the drawbacks associated with 2D monocultures, recent cell cultivation setups aim to re-engineer the physiological cellular microenvironment of native tissues. This can be accomplished by moving toward three-dimensional (3D) culture systems through cultivating cells in hydrogels, scaffolds or aggregates (Chen et al., 2002; Drury and Mooney, 2003; Griffith and Swartz, 2006; Fennema et al., 2013). The implementation of 3D cell culture systems by itself allows for indirect mechanical stimulation by controlling the rigidity and stiffness of the extracellular matrix, which has shown to modulate cellular responses (Engler et al., 2006; Kumar, 2014). Additionally, 3D-tissue models can be further subjected to dynamic mechanical stimuli including fluid flow, stretch/strain and compression. The application of indirect and/or direct mechanical stimuli in tissue cultures has become a rapidly growing research field that is commonly known as mechanobiology (Eyckmans et al., 2011). It is important to highlight that almost every tissue of a human body is subjected to either constant or temporary mechanical stimuli. This means that the application of mechanobiological forces represents a vital step toward the establishment of physiological microenvironments *in vitro* (Wang and Thampatty, 2006; Jansen et al., 2015). To date a variety of mechanobiological forces, shown in **Figure 1A**, have been employed in 2D and 3D *in vitro* cultures including (a) matrix stiffness that mimic the respective Young's moduli of native tissue, (b) fluid flow in vascular systems and interstitial tissue, (c) stretch/strain mechanisms in the lung, heart and gastrointestinal tract as well as (d) compression in the musculoskeletal system (Lovett et al., 2009; Riehl et al., 2012; Shachar et al., 2012; Ahearne, 2014). These mechanobiological systems demonstrated improved cell-to-cell and cell-to-matrix interactions resulting in significant progress in recapitulating physiological microenvironments *in vitro*. Although these tissue models led to substantial advances in understanding mechanobiology on a macroscale, common tissue engineering-based approaches require sizeable amounts of cells as well as reagents but lack precise control over location and amount of the stimulus. A commonly accepted solution in fostering our understanding of biomechanical effects is taking the tissue to the microscale. This can be accomplished by mimicking cellular microenvironments in microfluidic devices, which not only offer a decrease in cell numbers and consumables but also allow precise control over spatio-temporal stiffness and growth factor gradients as well as mechanical stimulus type, amount and location (Huh et al., 2011; Bhatia and Ingber, 2014; Rothbauer et al., 2015; van Duinen et al., 2015). In other words, microdevices can be used to investigate contractility, cell confinement and micropatterning, all of which are crucial in gaining deeper insights into mechanobiological phenomena. Moreover, microfluidic chips are compatible with high resolution microscopy for cell observation and also allow the integration of actuators and sensors, which provides the opportunity to trigger and monitor cellular behavior *in situ*. Overall this review focuses on emerging physiologically relevant

micro-tissue models in mechanobiology-on-a-chip setups in both culture environments since 2012, shortly summarized in **Table 1**.

MICROFLUIDIC MECHANOBIOLOGY IN MONOLAYERS AND BARRIER MODELS

Shear Stress

Microfluidic devices with their laminar flow regimes have widely been used to expose cells to fluid flow induced shear stress. This has led to substantial improvements in understanding the mechanobiological effect of shear stress variations on endothelial cells in vascular models but also in osteocyte, cardiomyocyte and epithelial cell biology. In particular, fluid flow plays a major role in vascular biology as the endothelial cell lining layer inside blood vessels is constantly exposed to pulsatile blood flow (Baratchi et al., 2017). Subjecting endothelial cells to physiological unidirectional or disturbed shear stress patterns has been shown to significantly alter cell morphology and phenotype. For example, it has been shown that shear stress influences nanoparticle uptake of endothelial cells where higher flow rates led to reduced uptake. Using an *in vitro* as well as *in silico* approach, Charwat et al. (2018) found that clathrin-mediated uptake of nanoparticles is drastically reduced when exceeding shear forces of 1.8 dyn/cm², implying an important role of shear stress when investigating *in vitro* nanoparticle uptake. Another study, published by Griep et al. (2013), successfully recreated the smallest unit of the blood brain barrier using immortalized brain endothelial cells to study barrier integrity in the presence of physiological shear force. While unidirectional shear stress plays an important role in assessing healthy vessel physiology, microfluidic devices can also be utilized to create bi- and multidirectional flow patterns for mimicking endothelial pathology. Such disturbed flow patterns allow for flow type-dependent gene expression profiling of endothelial cells (Zheng et al., 2017) as well as observation of leucocyte – endothelial cell interactions (Venugopal Menon et al., 2018) and the role of glucose uptake in endothelial dysfunction (Patibandla et al., 2014) for modeling inflammation and hyperglycemia in atherosclerosis. The effect of shear stress on endothelial cells and microfluidic technologies have recently been extensively reviewed elsewhere (Smith and Gerecht, 2014; Haase and Kamm, 2017; Kim et al., 2017). Furthermore, microfluidic devices have also been used outside of endothelial research to record phenotypic transformations of aortic valve interstitial cells during applied shear stress and to monitor morphological changes of osteocytes during application of flow. Additionally, Middleton et al. (2017a) showed that in the presence of shear stress, cell to cell interactions of osteocytes co-cultured with osteoclast are enhanced, leading to the improved mechanical response of bone cells. A more detailed review on monitoring cell-cell interaction using microfluidic devices was recently published by Rothbauer et al. (2017). Altogether, microfluidic devices are an important tool to study shear stress, but while the effects on endothelial cells have been studied extensively, other cell types

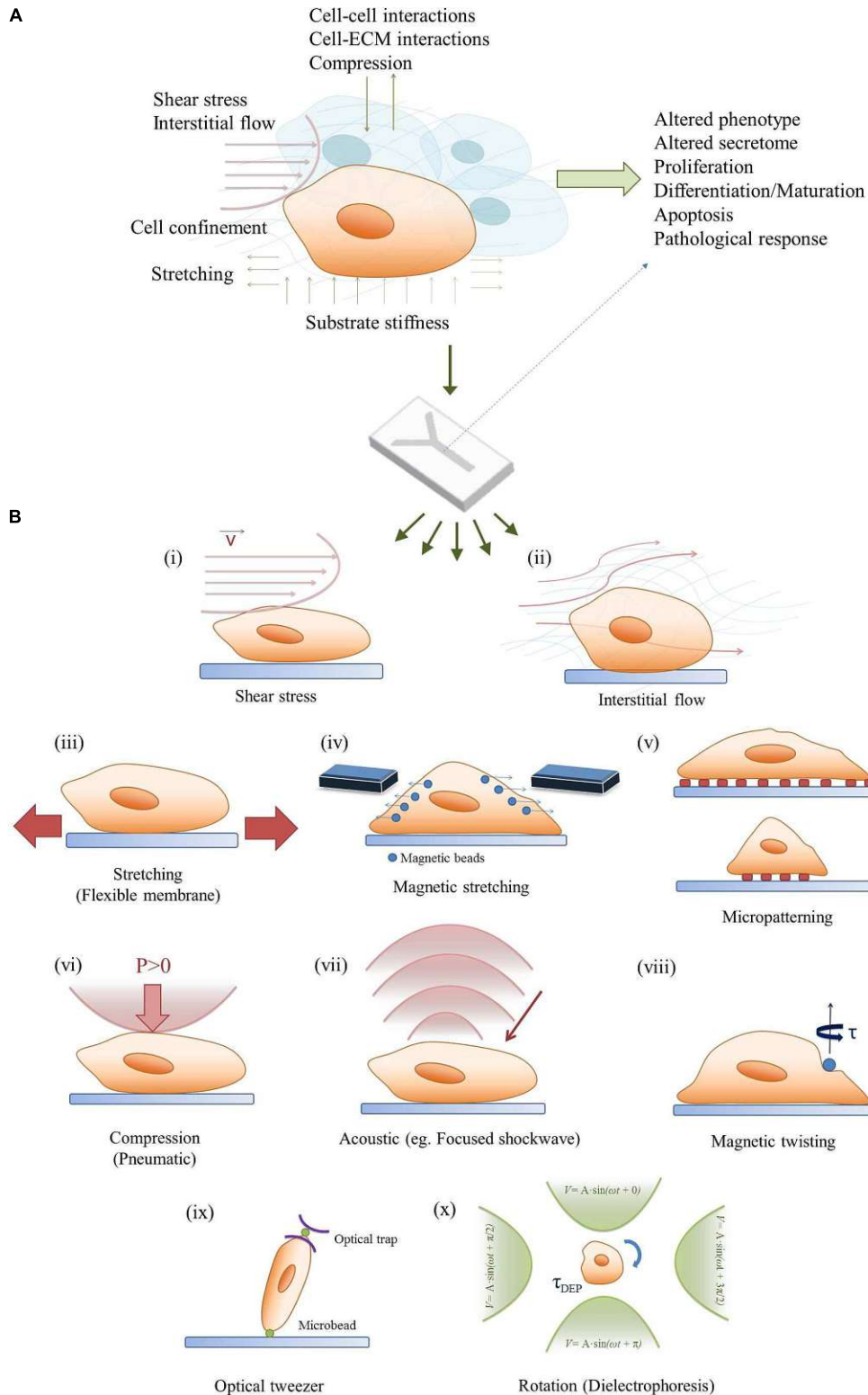


FIGURE 1 | Bridging the *in vivo/in vitro* gap in mechanobiology. **(A)** A combination of mechanobiological cues in the microenvironment can regulate cell signaling and phenotype as well as physiological and pathological tissue response. **(B)** A simplified demonstration of a mechanobiology-on-a-chip, and potential on-chip stimulation strategies for microfluidic 2D/3D cell cultures: (i) Shear stress, (ii) Interstitial flow, (iii) Stretching, (iv) Magnetic stimulation, (v) Micropatterning, (vi) Compression, (vii) Acoustic stimulation, (viii) Magnetic twisting, (ix) Optical tweezers, and (x) Rotation (dielectrophoresis).

Die approbierte gedruckte Originalversion dieser Dissertation ist an der TU Wien Bibliothek verfügbar. The approved original version of this doctoral thesis is available in print at TU Wien Bibliothek.

TABLE 1 | Summary on recent reports on mechanobiological approaches for cell manipulation in microfluidic devices.

Biomechanical stimulus	Organ culture	Cell type	Environment	Reference
Interstitial flow	Vasculature	Primary	3D	Hsu et al., 2013; Jeon et al., 2014; Kim S. et al., 2016
Interstitial flow	Brain	Primary	3D	Park et al., 2015; Wang et al., 2018
Interstitial flow	Liver	Primary	3D	Lee et al., 2013
Substrate stiffness	–	Cell line	2D	García et al., 2015
Electromechanical	–	Primary	2D	Pavesi et al., 2015
Shear stress	Vasculature	Primary	2D	Charwat et al., 2018
Shear stress	–	Cell line	2D	Soffe et al., 2017
Shear stress	Blood brain barrier	Cell line	2D	Griep et al., 2013
Shear stress	Aortic valve	Primary	2D	Wang et al., 2017
Shear stress	Blood brain barrier	Primary	2D/3D	Brown et al., 2015
Shear stress	Blood brain barrier	Cell line	2D/3D	Sellgren et al., 2015
Shear stress	Extravasation	Primary	3D	Jeon et al., 2015
Shear stress	Vasculature	Primary	3D	Kim et al., 2013
Shear stress	Bone	Cell line	2D	Middleton et al., 2017a,b
Shear stress	Bone	Primary	3D	Altmann et al., 2014
Shear stress	Vasculature	Primary	2D	Zheng et al., 2017
Shear stress	Vasculature	Primary	2D	Venugopal Menon et al., 2018
Shear stress	Vasculature	Primary	2D	Patibandla et al., 2014
Stretching	Lung	Primary and cell line	2D	Huh et al., 2010, 2012; Benam et al., 2016; Hassell et al., 2017; Jain et al., 2018
Stretching	Gut	Primary and cell line	2D	Kim H.J. et al., 2016; Villenave et al., 2017
Stretching	Heart	Primary	2D	Ugolini et al., 2016, 2017
Stretching	Muscle	Primary and cell line	2D	Michielin et al., 2015
Stretching	Vasculature	Primary	2D	Zhou and Niklason, 2012
Stretching	–	Primary	3D	Liu et al., 2016
Stretching	Heart	Primary	3D	Marsano et al., 2016; Occhetta et al., 2018
Stretching	–	Cell line	3D	Li et al., 2016
Stretching	–	–	2D/3D	Gizzi et al., 2017
Stretching	Artery	Primary	2D	van Engeland et al., 2018
Compression	Bone	Primary	2D	Park et al., 2012
Compression	Vasculature	Primary	2D	Sticker et al., 2017

The dashes (–) identify studies with devices without a defined target organ, tissue or cell culture.

and different co-culture models would certainly benefit from further research.

Stretching

In contrast to shear-dependent mechanobiological effects, microfluidic devices have recently come into focus for their ability to engineer miniaturized functional barrier units. Different from the aforementioned models where cells are grown in monolayer in microchannels, these systems aim to recreate the smallest possible unit of an organ by mimicking the barrier between two monolayers. An overview of such a microfluidic device including the respective cell actuation can be found in **Figure 1B**. The cells are cultivated back-to-back on cyclically stretched flexible membranes emulating organotypic movements. With the most famous example still being the Lung-on-a-Chip published by Huh et al. (2010), a number of similar systems have since been used to investigate a variety of different barrier models. For example, using the same microdevice containing a flexible membrane that is stretched by applying vacuum to two air channels on either side of the cultivation chamber, different pathological scenarios have been

recapitulated, including pulmonary edema (Huh et al., 2012), small-airway inflammation (Benam et al., 2016), orthotopic lung cancer extravasation, growth and therapy (Hassell et al., 2017) and intravascular thrombosis assessment (Jain et al., 2018). A similar device has also been used to mimic bacterial overgrowth, inflammatory bowel disease (Kim H.J. et al., 2016) and virus infection (Villenave et al., 2017) in a gut-on-a-chip system and to study the effect of cyclic strain on proliferation and adaptive responses of cardiac fibroblasts (Ugolini et al., 2016, 2017) and to study endothelial cell and smooth muscle cell signaling under hemodynamic loading (van Engeland et al., 2018). A different design approach to exert stretch/strain forces in microfluidic cell cultures employ pressurized air to deflect a membrane on which cells are cultured. Cyclic mechanical actuation of a myoblast cell line and primary myoblasts using such a device is demonstrated in a muscular dystrophy model (Michielin et al., 2015) and to recreate the cyclic strain of blood vessels (Zhou and Niklason, 2012). While most examples in the literature focus on uniaxial stretching, a computationally informed, vacuum-actuated multi-axial microfluidic chip device has recently been developed that allows programmable actuation

along different directions (Gizzi et al., 2017), further advancing the opportunities for mechanobiological on-chip investigations from the broadly used uniaxial strain barrier model devices.

Compression and Other Novel Methods

A relatively new approach for mechanobiological stimulation in microfluidic devices is cellular compression. Even though this has been shown to stimulate the osteogenic differentiation of stem cells (Park et al., 2012) and used to investigate wound healing (Sticker et al., 2017), further studies need to be conducted to improve our understanding of compression-based biomechanical stimuli. Other methods to incorporate mechanobiological signals in microchips exploit the fact that microfluidics is ideally suited to create and monitor spatiotemporal gradients. For example, Soffe et al. (2017) showed that human embryonic kidney cells respond to shear stress gradients using trapezoid microchannel geometries, while García et al. (2015) investigated the effects of substrate stiffness gradients on cell behavior (Soffe et al., 2017). A sophisticated approach is reported by Pavesi et al. (2015): cells were subjected to multiple mechanical stimuli by adding the possibility of simultaneous electrical stimulation. The dual-stimulation strategy led to morphological and phenotypical cellular changes as well as altered cytoskeletal fiber orientation in mesenchymal stem cells. Nonetheless, while all the mentioned studies report an increase in physiological behavior of the cultured cells upon the exposure to mechanobiological cues, recreating of physiological microenvironment in a two-dimensional cultivation setup remains challenging.

MICROFLUIDIC MECHANOBIOLOGY IN THE THIRD DIMENSION

Even though the above described microfluidic 2D models seem suitable for recreating lining layers and barrier models, they still do not resemble physiological tissue architecture since most cells reside in a three-dimensional tissue matrix in their native environment. Hence, the third dimension remains an important issue that needs to be considered when aiming to re-engineer organ models *in vitro*. It is important to note that the physiological tissue microenvironment is composed of a variety of complex physical properties ranging from cell-cell interactions to the extracellular matrix composition and biomechanical stimuli such as dynamic stretching and compression. This biological complexity, to date, poses a significant challenge, since only a limited number of studies incorporating 3D mechanobiology on microfluidic chips have been reported.

Interstitial Flow

Additional to utilizing microfluidic devices in endothelial biology for investigating the effect of shear stress on monolayers, microchips are routinely used to determine the effects of interstitial flow on 3D vasculo- and angiogenesis. One approach involves the combination of vasculature with fluid flow where endothelial cells are co-cultured with supporting mural cells in hydrogels to generate blood vessels via vasculogenesis or

angiogenesis. Hsu et al. (2013) developed a microfluidic device that is based on a resistive circuit concept to create an array of vascularized microtissue chambers. Interstitial fluid flow in the physiological range of 0.5 to 10 $\mu\text{m/s}$ showed enhanced vessel-like structure formation corroborating similar studies from Jeon et al. (2014) for blood angiogenesis and from Kim S. et al. (2016) for lymphangiogenesis (Hsu et al., 2013). A more detailed review of recent advances in on-chip vascularization was recently published by Haase and Kamm (2017). However, microfluidics not only provides the perfect tool for exploring the importance of interstitial flow in endothelial cell biology but also for bone and brain organ-on-a-chip devices. In a recent study by Altmann et al. (2014), the morphogenesis of 3D cultured human primary alveolar bone osteoblasts under static and microfluidic growth conditions was compared. The cells were allowed to form aggregates in 300 μm cavities with fibronectin coating in poly (methyl methacrylate)-based chips and exposed to perfusion of 15, 30, and 60 $\mu\text{l/min}$ flow rates. It was found that fluid flow lead to more distinct morphogenesis and more bone-specific gene expression and extracellular matrix formation after 7 days of culture. Additionally, Park et al. (2015) reported the design of a microfluidic chip-based 3D neurospheroid culture consisting in concave microwell arrays in which interstitial flow was generated by an osmotic micropump system. The results of the study showed that when neurospheroids are cultured under flow conditions, larger and more complex neural networks were formed compared to static culture. In a more recent 3D brain model, human induced pluripotent stem cell derived organoids were integrated into a microdevice using three-dimensional Matrigel. The on-chip cultured organoids showed improved neural differentiation and cortical organization under perfusion culture as well as enhanced expression of cortical layer markers, thus demonstrating the importance of 3D culture and mechanical fluid flow in enhancing brain organogenesis (Wang et al., 2018). Furthermore, Brown et al. (2015) created a complex physiologically relevant blood-brain-barrier model based on a back-to-back culture of endothelial cells that mimic blood vasculature with a co-culture of astrocytes, pericytes and hydrogel-embedded neurons that showed improved tight-junction formation under fluid flow conditions. These examples show that interstitial flow plays a crucial role for recreating physiological microenvironments and call for further research including a variety of other organ models.

Stretching and Compression in 3D

Other than the sophisticated stretch/strain devices for monolayer barrier models, compression and stretching of 3D microfluidic organ models is still in its infancy. One of the first applications involve a 3D cell construct that is exposed to cyclic mechanical strain to develop a beating heart-on-a-chip (Marsano et al., 2016). In this study, human induced pluripotent stem cell-derived cardiomyocytes were embedded in a fibrin gel prior to injection into the microdevices, and subsequently exposed to mechanical stimulation using a deformable PDMS (Polydimethylsiloxane) membrane (10% uniaxial strain, 1 Hz frequency). Interestingly, the mechanically stimulated constructs showed similar gene

expression levels of cardiac markers when compared to non-actuated controls. However, the mechanical stimulus resulted in decreased expression of MYH6 (a marker for less developed phenotype), thus indicating superior cardiac maturity compared to static conditions. Furthermore, elongated cardiac-like morphology was observed in the mechanically stimulated constructs. Recently, the same group employed a similar concept to propose a model of cardiac fibrosis by applying cyclic mechanical stretch to cardiac fibroblasts embedded in a 3D fibrin hydrogel. By exploiting this strategy, the authors claim to be able to mimic some of the key steps of cardiac fibrosis onset in a timely fashion: early fibroblast proliferation, their phenotype switch into myofibroblasts, extracellular matrix deposition and its final stiffening (Occhetta et al., 2018). An alternative microfluidic device containing deformable membranes was developed to investigate differentiation associated matrix production using a real-time stiffness sensor. The authors showed that mesenchymal stromal cells embedded in hydrogels and subjected to dynamic mechanical stimulation undergo myofibroblast differentiation and synthesize collagen, leading to gel stiffening (Liu et al., 2016). In another study, 3D responses of cells were quantified in the presence of extreme strain within 3D hydrogel matrices. Here, micro-magnetically actuated synthetic tissue cultures were developed and consisted of a polyethylene glycol dimethacrylate hydrogel layer containing iron microspheres, and a stiffness tunable gelatin methacryloyl hydrogel containing a population of fibroblasts. Using this magnetic field focusing device, strain-dependent proliferation, spreading, polarization, differentiation, and matrix adhesion was studied (Li et al., 2016). Although the system can be used to readily adjust mechanical strain within 3D hydrogel cell cultures, some limitations remain concerning extracellular matrix porosity and non-fibrous matrices not being representative of the cell environment in a real tissue. **Table 1** lists currently available technologies according to applied stimuli, organ culture and cell type using microfluidic 2D as well as 3D cell culture systems.

CONCLUDING REMARKS AND FURTHER PERSPECTIVES

The combination of microfabrication-based technologies with complex biology has enabled the development of advanced *in vitro* models capable of culturing and analyzing cell and tissue constructs under physiologically relevant conditions (Ertl, 2015; Rothbauer et al., 2015, 2017). While microfluidic models for 2D mechanical stimulation involving stretch and strain has been widely investigated, the application of physiologically relevant axial strain in 3D cell culture systems is still

in its infancy. To date only few microdevices have been developed that are capable of recreating mechanobiological relevant three-dimensional cellular microenvironments. Current mechanobiology-on-a-chip advances are hindered by both technological shortcomings and the limited reliability of current *in vitro* 3D cell culture systems. One possible solution to improve fabrication speed, precision, material selection, and (bio)compatibility could be stereolithography, which already enables (a) additive manufacturing of microchannels down to 300 μm and (b) the integration of pneumatic valves for automated cell handling and manipulation of complex biological structures on chip. Next generation microfluidic devices will need to contain computer-controlled valves and micropumps for fluid-mechanical stimulation of cells (Rogers et al., 2015; Chen et al., 2016) and integrated actuators to reliably regulate and modify mechanical forces on tissue constructs. Furthermore, future microfluidic devices will need to address current limitations in microdevice operation to minimize the need for bulky off-chip equipment such as pumps, heaters, microscope, gas-supply, and connectors. While the incorporation of micropumps and -valves or alternative approaches for on-chip fluid handling have already been demonstrated in state-of-the-art devices (Sung et al., 2010; Kim et al., 2012; Hasenberg et al., 2015), integrated sensing solutions that replace off-chip detection methods are still scarce. The integration of micro- and nanosensors will ultimately enable the investigation of dynamic cellular responses to any imaginable physical, chemical and biological stimuli, thus providing detailed information on tissue behavior down to the molecular level. In conclusion, given the complexity of *in vivo* biological architectures of tissues and organs, next generation mechanobiology-on-a-chip systems will need to significantly increase the similarity of *in vitro* 3D biologically inspired constructs using highly integrated, fully automated and miniaturized cell analysis systems.

AUTHOR CONTRIBUTIONS

EE and BB conceived the general structure of the review, revised the existing literature, and drafted the manuscript. HR, GF, and PE revised the text and contributed to the final manuscript.

FUNDING

This work was funded by the European Union's INTERREG V-A AT-CZ program (ATCZ133), the European Social Fund and European Regional Development Fund–Project MAGNET (No. CZ.02.1.01/0.0/0.0/15_003/0000492).

REFERENCES

- Ahearne, M. (2014). Introduction to cell-hydrogel mechanosensing. *Interface Focus* 4:20130038. doi: 10.1098/rsfs.2013.0038
- Altmann, B., Löchner, A., Swain, M., Kohal, R. J., Giselbrecht, S., Gottwald, E., et al. (2014). Differences in morphogenesis of 3D cultured

primary human osteoblasts under static and microfluidic growth conditions. *Biomaterials* 35, 3208–3219. doi: 10.1016/j.biomaterials.2013.12.088

- Baker, B. M., and Chen, C. S. (2012). Deconstructing the third dimension – how 3D culture microenvironments alter cellular cues. *J. Cell Sci.* 125, 3015–3024. doi: 10.1242/jcs.079509

- Baratchi, S., Khoshmanesh, K., Woodman, O. L., Potocnik, S., Peter, K., and McIntyre, P. (2017). Molecular sensors of blood flow in endothelial cells. *Trends Mol. Med.* 23, 850–868. doi: 10.1016/j.molmed.2017.07.007
- Benam, K. H., Villenave, R., Lucchesi, C., Varone, A., Hubeau, C., Lee, H.-H., et al. (2016). SL Small airway-on-a-chip enables analysis of human lung inflammation and drug responses *in vitro*. *Nat. Methods* 13, 151–157. doi: 10.1038/nmeth.3697
- Bhatia, S. N., and Ingber, D. E. (2014). Microfluidic organs-on-chips. *Nat. Biotechnol.* 32, 760–772. doi: 10.1038/nbt.2989
- Brown, J. A., Pensabene, V., Markov, D. A., Allwardt, V., Diana Neely, M., Shi, M., et al. (2015). Recreating blood-brain barrier physiology and structure on chip: a novel neurovascular microfluidic bioreactor. *Biomicrofluidics* 9:054124. doi: 10.1063/1.4934713
- Charwat, V., Olmos Calvo, I., Rothbauer, M., Kratz, S. R. A., Jungreuthmayer, C., Zanghellini, J., et al. (2018). Combinatorial In Vitro and in silico approach to describe shear-force dependent uptake of nanoparticles in microfluidic vascular models. *Anal. Chem.* 90, 3651–3655. doi: 10.1021/acs.analchem.7b04788
- Chen, C., Mehl, B. T., Munshi, A. S., Townsend, A. D., Spence, D. M., and Martin, R. S. (2016). 3D-printed microfluidic devices: fabrication, advantages and limitations—a mini review. *Anal. Methods* 8, 6005–6012. doi: 10.1039/C6AY01671E
- Chen, G., Ushida, T., and Tateishi, T. (2002). Scaffold design for tissue engineering. *Macromol. Biosci.* 2, 67–77.
- Drury, J. L., and Mooney, D. J. (2003). Hydrogels for tissue engineering: scaffold design variables and applications. *Biomaterials* 24, 4337–4351. doi: 10.1016/S0142-9612(03)00340-5
- Engler, A. J., Sen, S., Sweeney, H. L., and Discher, D. E. (2006). Matrix elasticity directs stem cell lineage specification. *Cell* 126, 677–689. doi: 10.1016/j.cell.2006.06.044
- Ertl, P. (2015). Recent advances of biologically inspired 3D microfluidic hydrogel cell culture systems. *Cell Biol. Cell Metab.* 2:005. doi: 10.24966/CBCM-1943/100005
- Eyckmans, J., Boudou, T., Yu, X., and Chen, C. S. (2011). A hitchhiker's guide to mechanobiology. *Dev. Cell* 21, 35–47. doi: 10.1016/j.devcel.2011.06.015
- Fennema, E., Rivron, N., Rouwkema, J., van Blitterswijk, C., and de Boer, J. (2013). Spheroid culture as a tool for creating 3D complex tissues. *Trends Biotechnol.* 31, 108–115. doi: 10.1016/j.tibtech.2012.12.003
- García, S., Sunyer, R., Olivares, A., Noailly, J., Atencia, J., and Trepas, X. (2015). Generation of stable orthogonal gradients of chemical concentration and substrate stiffness in a microfluidic device. *Lab Chip* 15:12. doi: 10.1039/C5LC00140D
- Gizzi, A., Giannitelli, S. M., Trombetta, M., Cherubini, C., Filippi, S., De Ninno, A., et al. (2017). Computationally informed design of a multi-axial actuated microfluidic chip device. *Sci. Rep.* 7:5489. doi: 10.1038/s41598-017-05237-9
- Griep, L. M., Wolbers, F., De Wagenaar, B., Ter Braak, P. M., Weksler, B. B., Romero, I. A., et al. (2013). BBB on CHIP: microfluidic platform to mechanically and biochemically modulate blood-brain barrier function. *Biomed. Microdev.* 15, 145–150. doi: 10.1007/s10544-012-9699-7
- Griffith, L. G., and Swartz, M. A. (2006). Capturing complex 3D tissue physiology in vitro. *Nat. Rev. Mol. Cell Biol.* 7, 211–224. doi: 10.1038/nrm1858
- Haase, K., and Kamm, R. D. (2017). Advances in on-chip vascularization. *Regen. Med.* 12, 285–302. doi: 10.2217/rme-2016-0152
- Hasenberg, T., Mühleder, S., Dotzler, A., Bauer, S., Labuda, K., Holnthoner, W., et al. (2015). Emulating human microcapillaries in a multi-organ-chip platform. *J. Biotechnol.* 216, 1–10. doi: 10.1016/j.jbiotec.2015.09.038
- Hassell, B. A., Goyal, G., Lee, E., Sontheimer-Phelps, A., Levy, O., Chen, C. S., et al. (2017). Human organ chip models recapitulate orthotopic lung cancer growth, therapeutic responses, and tumor dormancy in Vitro. *Cell Rep.* 21, 508–516. doi: 10.1016/j.celrep.2017.09.043
- Hsu, Y.-H., Moya, M. L., Hughes, C. C. W., George, S. C., and Lee, A. P. (2013). A microfluidic platform for generating large-scale nearly identical human microphysiological vascularized tissue arrays. *Lab Chip* 13, 2990–2998. doi: 10.1039/c3lc50424g
- Huh, D., Hamilton, G. A., and Ingber, D. E. (2011). From 3D cell culture to organs-on-chips. *Trends Cell Biol.* 21, 745–754. doi: 10.1016/j.tcb.2011.09.005
- Huh, D., Leslie, D. C., Matthews, B. D., Fraser, J. P., Jurek, S., Hamilton, G. A., et al. (2012). A human disease model of drug toxicity-induced pulmonary edema in a lung-on-a-chip microdevice. *Sci. Transl. Med.* 4:159ra147. doi: 10.1126/scitranslmed.3004249
- Huh, D., Matthews, B. D., Mammoto, A., Montoya-Zavala, M., Hsin, H. Y., and Ingber, D. E. (2010). Reconstituting organ-level lung functions on a chip. *Science* 328, 1662–1668. doi: 10.1126/science.1188302
- Jain, A., Barrile, R., van der Meer, A. D., Mammoto, A., Mammoto, T., De Ceunynck, K., et al. (2018). Primary human lung alveolus-on-a-chip model of intravascular thrombosis for assessment of therapeutics. *Clin. Pharmacol. Ther.* 103, 332–340. doi: 10.1002/cpt.742
- Jansen, K. A., Donato, D. M., Balcioglu, H. E., Schmidt, T., Danen, E. H. J., and Koenderink, G. H. (2015). A guide to mechanobiology: where biology and physics meet. *Biochim. Biophys. Acta Mol. Cell Res.* 1853, 3043–3052. doi: 10.1016/j.bbamcr.2015.05.007
- Jeon, J. S., Bersini, S., Gilardi, M., Dubini, G., Charest, J. L., Moretti, M., et al. (2015). Human 3D vascularized organotypic microfluidic assays to study breast cancer cell extravasation. *Proc. Natl. Acad. Sci. U.S.A.* 112, 214–219. doi: 10.1073/pnas.1417115112
- Jeon, J. S., Bersini, S., Whisler, J. A., Chen, M. B., Dubini, G., Charest, J. L., et al. (2014). Generation of 3D functional microvascular networks with mural cell-differentiated human mesenchymal stem cells in microfluidic vasculogenesis systems. *Integr. Biol.* 6, 555–563. doi: 10.1039/c3ib40267c
- Kim, H. J., Li, H., Collins, J. J., and Ingber, D. E. (2016). Contributions of microbiome and mechanical deformation to intestinal bacterial overgrowth and inflammation in a human gut-on-a-chip. *Proc. Natl. Acad. Sci. U.S.A.* 113, E7–E15. doi: 10.1073/pnas.1522193112
- Kim, S., Chung, M., and Jeon, N. L. (2016). Three-dimensional biomimetic model to reconstitute sprouting lymphangiogenesis in vitro. *Biomaterials* 78, 115–128. doi: 10.1016/j.biomaterials.2015.11.019
- Kim, J., Kang, M., Jensen, E. C., and Mathies, R. A. (2012). Lifting gate polydimethylsiloxane microvalves and pumps for microfluidic control. *Anal. Chem.* 84, 2067–2071. doi: 10.1021/ac202934x
- Kim, S., Kim, W., Lim, S., and Jeon, J. (2017). Vasculature-On-A-Chip for In vitro disease models. *Bioengineering* 4:E8. doi: 10.3390/bioengineering4010008
- Kim, S., Lee, H., Chung, M., and Jeon, N. L. (2013). Engineering of functional, perfusable 3D microvascular networks on a chip. *Lab Chip* 13:1489. doi: 10.1039/c3lc41320a
- Kumar, S. (2014). Cellular mechanotransduction: stiffness does matter. *Nat. Mater.* 13, 918–920. doi: 10.1038/nmat4094
- Lee, S.-A., No, D. Y., Kang, E., Ju, J., Kim, D.-S., and Lee, S.-H. (2013). Spheroid-based three-dimensional liver-on-a-chip to investigate hepatocyte-hepatic stellate cell interactions and flow effects. *Lab Chip* 13:3529. doi: 10.1039/c3lc50197c
- Li, Y., Huang, G., Li, M., Wang, L., Elson, E. L., Jian Lu, T., et al. (2016). An approach to quantifying 3D responses of cells to extreme strain. *Sci. Rep.* 6:19550. doi: 10.1038/srep19550
- Liu, H., Simmons, C. A., and Sun, Y. (2016). A microfabricated platform with on-chip strain sensing and hydrogel arrays for 3D mechanical stimulation of cells. *Proc. IEEE Int. Conf. Micro Electro Mech. Syst.* 4, 267–270. doi: 10.1109/MEMSYS.2016.7421611
- Lovett, M., Lee, K., Edwards, A., and Kaplan, D. L. (2009). Vascularization strategies for tissue engineering. *Tissue Eng. Part B Rev.* 15, 353–370. doi: 10.1089/ten.teb.2009.0085
- Marsano, A., Conficconi, C., Lemme, M., Occhetta, P., Gaudiello, E., Votta, E., et al. (2016). Beating heart on a chip: a novel microfluidic platform to generate functional 3D cardiac microtissues. *Lab Chip* 16, 599–610. doi: 10.1039/C5LC01356A
- Michielin, F., Serena, E., Pavan, P., and Elvassore, N. (2015). Microfluidic-assisted cyclic mechanical stimulation affects cellular membrane integrity in a human muscular dystrophy in vitro model. *RSC Adv.* 5, 98429–98439. doi: 10.1039/C5RA16957G
- Middleton, K., Al-Dujaili, S., Mei, X., Günther, A., and You, L. (2017a). Microfluidic co-culture platform for investigating osteocyte-osteoclast signalling during fluid shear stress mechanostimulation. *J. Biomech.* 59, 35–42. doi: 10.1016/j.jbiomech.2017.05.012
- Middleton, K., Kondiboyina, A., Borrett, M., Cui, Y., Mei, X., and You, L. (2017b). Microfluidics approach to investigate the role of dynamic similitude in osteocyte mechanobiology. *J. Orthop. Res.* 36, 663–671. doi: 10.1002/jor.23773

- Occhetta, P., Isu, G., Lemme, M., Conficconi, C., Oertle, P., R az, C., et al. (2018). A three-dimensional in vitro dynamic micro-tissue model of cardiac scar formation. *Integr. Biol.* 10, 174–183. doi: 10.1039/C7IB00199A
- Park, J., Lee, B. K., Jeong, G. S., Hyun, J. K., Lee, C. J., and Lee, S.-H. (2015). Three-dimensional brain-on-a-chip with an interstitial level of flow and its application as an in vitro model of Alzheimer's disease. *Lab Chip* 15, 141–150. doi: 10.1039/C4LC00962B
- Park, S.-H., Sim, W. Y., Min, B.-H., Yang, S. S., Khademhosseini, A., and Kaplan, D. L. (2012). Chip-based comparison of the osteogenesis of human bone marrow- and adipose tissue-derived mesenchymal stem cells under mechanical stimulation. *PLoS One* 7:e46689. doi: 10.1371/journal.pone.0046689
- Patibandla, P. K., Rogers, A. J., Giridharan, G. A., Pallero, M. A., Murphy-Ullrich, J. E., and Sethu, P. (2014). Hyperglycemic arterial disturbed flow niche as an in vitro model of atherosclerosis. *Anal. Chem.* 86, 10948–10954. doi: 10.1021/ac503294p
- Pavesi, A., Adriani, G., Rasponi, M., Zervantonakis, I. K., Fiore, G. B., and Kamm, R. D. (2015). Controlled electromechanical cell stimulation on-a-chip. *Sci. Rep.* 5:11800. doi: 10.1038/srep11800
- Riehl, B. D., Park, J.-H., Kwon, I. K., and Lim, J. Y. (2012). Mechanical stretching for tissue engineering: two-dimensional and three-dimensional constructs. *Tissue Eng. Part B Rev.* 18, 288–300. doi: 10.1089/ten.teb.2011.0465
- Rogers, C. I., Qaderi, K., Woolley, A. T., and Nordin, G. P. (2015). 3D printed microfluidic devices with integrated valves. *Biomicrofluidics* 9:16501. doi: 10.1063/1.4905840
- Rothbauer, M., Wartmann, D., Charwat, V., and Ertl, P. (2015). Recent advances and future applications of microfluidic live-cell microarrays. *Biotechnol. Adv.* 33(Pt 1), 948–961. doi: 10.1016/j.biotechadv.2015.06.006
- Rothbauer, M., Zirath, H., and Ertl, P. (2017). Recent advances in microfluidic technologies for cell-to-cell interaction studies. *Lab Chip* 10:1. doi: 10.1039/C7LC00815E
- Sellgren, K. L., Hawkins, B. T., and Grego, S. (2015). An optically transparent membrane supports shear stress studies in a three-dimensional microfluidic neurovascular unit model. An optically transparent membrane supports shear stress studies in a three-dimensional microfluidic neurovascular unit model. *Biomicrofluidics* 9:061102. doi: 10.1063/1.4935594
- Shachar, M., Benishti, N., and Cohen, S. (2012). Effects of mechanical stimulation induced by compression and medium perfusion on cardiac tissue engineering. *Biotechnol. Prog.* 28, 1551–1559. doi: 10.1002/btpr.1633
- Smith, Q., and Gerecht, S. (2014). Going with the flow: microfluidic platforms in vascular tissue engineering. *Curr. Opin. Chem. Eng.* 3, 42–50. doi: 10.1016/j.coche.2013.11.001
- Soffe, R., Baratchi, S., Nasabi, M., Tang, S. Y., Boes, A., McIntyre, P., et al. (2017). Lateral trapezoid microfluidic platform for investigating mechanotransduction of cells to spatial shear stress gradients. *Sensors Actuat. B Chem.* 251, 963–975. doi: 10.1016/j.snb.2017.05.145
- Sticker, D., Lechner, S., Jungreuthmayer, C., Zanghellini, J., and Ertl, P. (2017). Microfluidic migration and wound healing assay based on mechanically induced injuries of defined and highly reproducible areas. *Anal. Chem.* 89, 2326–2333. doi: 10.1021/acs.analchem.6b03886
- Sung, J. H., Kam, C., and Shuler, M. L. (2010). A microfluidic device for a pharmacokinetic-pharmacodynamic (PK-PD) model on a chip. *Lab Chip* 10, 446–455. doi: 10.1039/B917763A
- Ugolini, G. S., Pavesi, A., Rasponi, M., Fiore, G. B., Kamm, R., and Soncini, M. (2017). Human cardiac fibroblasts adaptive responses to controlled combined mechanical strain and oxygen changes in vitro. *eLife* 6:e22847. doi: 10.7554/eLife.22847
- Ugolini, G. S., Rasponi, M., Pavesi, A., Santoro, R., Kamm, R., Fiore, G. B., et al. (2016). On-chip assessment of human primary cardiac fibroblasts proliferative responses to uniaxial cyclic mechanical strain. *Biotechnol. Bioeng.* 113, 859–869. doi: 10.1002/bit.25847
- van Duinen, V., Trietsch, S. J., Joore, J., Vulto, P., and Hankemeier, T. (2015). Microfluidic 3D cell culture: from tools to tissue models. *Curr. Opin. Biotechnol.* 35, 118–126. doi: 10.1016/j.copbio.2015.05.002
- van Engeland, N. C. A., Pollet, A. M. A. O., den Toonder, J. M. J., Bouten, C. V. C., Stassen, O. M. J. A., and Sahlgren, C. M. (2018). A biomimetic microfluidic model to study signalling between endothelial and vascular smooth muscle cells under hemodynamic conditions. *Lab Chip* 18, 1607–1620. doi: 10.1039/c8lc00286j
- Venugopal Menon, N., Tay, H. M., Pang, K. T., Dalan, R., Wong, S. C., Wang, X., et al. (2018). A tunable microfluidic 3D stenosis model to study leukocyte-endothelial interactions in atherosclerosis. *APL Bioeng.* 2:16103. doi: 10.1063/1.4993762
- Villeneuve, R., Wales, S. Q., Hamkins-Indik, T., Papafragkou, E., Weaver, J. C., Ferrante, T. C., et al. (2017). Human gut-on-a-chip supports polarized infection of coxsackie B1 virus in vitro. *PLoS One* 12:e0169412. doi: 10.1371/journal.pone.0169412
- Wang, J. H.-C., and Thampatty, B. P. (2006). An introductory review of cell mechanobiology. *Biomech. Model. Mechanobiol.* 5, 1–16. doi: 10.1007/s10237-005-0012-z
- Wang, X., Lee, J., Ali, M., Kim, J., and Lacerda, C. M. R. (2017). Phenotype transformation of aortic valve interstitial cells due to applied shear stresses within a microfluidic chip. *Ann. Biomed. Eng.* 45, 2269–2280. doi: 10.1007/s10439-017-1871-z
- Wang, Y., Wang, L., Guo, Y., Zhu, Y., and Qin, J. (2018). Engineering stem cell-derived 3D brain organoids in a perfusable organ-on-a-chip system. *RSC Adv.* 8, 1677–1685. doi: 10.1039/C7RA11714K
- Zheng, C., Zhang, X., Li, C., Pang, Y., and Huang, Y. (2017). Microfluidic device for studying controllable hydrodynamic flow induced cellular responses. *Anal. Chem.* 89, 3710–3715. doi: 10.1021/acs.analchem.7b00013
- Zhou, J., and Niklason, L. E. (2012). Microfluidic artificial “vessels” for dynamic mechanical stimulation of mesenchymal stem cells. *Integr. Biol.* 4, 1487–1497. doi: 10.1039/c2ib00171c

Conflict of Interest Statement: The authors declare that the research was conducted in the absence of any commercial or financial relationships that could be construed as a potential conflict of interest.

Copyright © 2018 Ergir, Bachmann, Redl, Forte and Ertl. This is an open-access article distributed under the terms of the Creative Commons Attribution License (CC BY). The use, distribution or reproduction in other forums is permitted, provided the original author(s) and the copyright owner(s) are credited and that the original publication in this journal is cited, in accordance with accepted academic practice. No use, distribution or reproduction is permitted which does not comply with these terms.

Manuscript III

Parts of this dissertation, including figures and tables, have been reproduced, with or without modifications, based on my contribution to the original published review article (Cassani et al., 2020)) licensed for reuse under Creative Commons Attribution 4.0 International License. To view a copy of this licence, visit <http://creativecommons.org/licenses/by/4.0/>.

REVIEW article

Front. Bioeng. Biotechnol., 24 April 2020

Sec. Biomaterials

<https://doi.org/10.3389/fbioe.2020.00323>

Combining Nanomaterials and Developmental Pathways to Design New Treatments for Cardiac Regeneration: The Pulsing Heart of Advanced Therapies

Marco Cassani¹, Soraia Fernandes¹, Jan Vrbsky¹, Ece Ergir^{1,2}, Francesca Cavalieri^{3,4} and Giancarlo Forte¹

1 International Clinical Research Center, St Anne's University Hospital, Brno, Czechia

2 Faculty of Technical Chemistry, Institute of Applied Synthetic Chemistry and Institute of Chemical Technologies and Analytics, Vienna University of Technology, Vienna, Austria

3 School of Science, RMIT University, Melbourne, VIC, Australia

4 Dipartimento di Scienze e Tecnologie Chimiche, Università di Roma "Tor Vergata", Via Della Ricerca Scientifica, Rome, Italy

MC proposed the subject and conceived the general structure of the review. MC and SF revised the existing literature regarding nanomedicine and the use of nanoparticles for cardiac regeneration. JV revised the literature on miRNAs involved in cardiac development and repair. EE revised the literature on cardiac diseases biology. MC and SF wrote the manuscript. FC and GF revised the text and contributed to the writing, discussion and conclusions.



Combining Nanomaterials and Developmental Pathways to Design New Treatments for Cardiac Regeneration: The Pulsing Heart of Advanced Therapies

Marco Cassani¹, Soraia Fernandes¹, Jan Vrbsky¹, Ece Ergir^{1,2}, Francesca Cavalieri^{3,4} and Giancarlo Forte^{1*}

OPEN ACCESS

Edited by:

Valeria Chiono,
Politecnico di Torino, Italy

Reviewed by:

Daniele Catalucci,
Institute for Genetic and Biomedical
Research (IRGB), Italy
Susanna Sartori,
Politecnico di Torino, Italy
Jochen Salber,
Surgical Clinic, University Hospital
Bochum GmbH, Germany

*Correspondence:

Giancarlo Forte
giancarlo.forte@fnusa.cz

Specialty section:

This article was submitted to
Biomaterials,
a section of the journal
Frontiers in Bioengineering and
Biotechnology

Received: 21 October 2019

Accepted: 24 March 2020

Published: 24 April 2020

Citation:

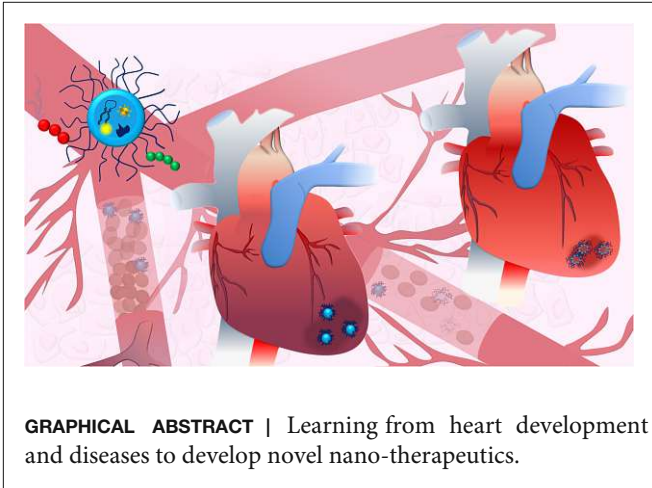
Cassani M, Fernandes S,
Vrbsky J, Ergir E, Cavalieri F and
Forte G (2020) Combining
Nanomaterials and Developmental
Pathways to Design New Treatments
for Cardiac Regeneration: The Pulsing
Heart of Advanced Therapies.
Front. Bioeng. Biotechnol. 8:323.
doi: 10.3389/fbioe.2020.00323

¹ International Clinical Research Center, St Anne's University Hospital, Brno, Czechia, ² Faculty of Technical Chemistry, Institute of Applied Synthetic Chemistry and Institute of Chemical Technologies and Analytics, Vienna University of Technology, Vienna, Austria, ³ School of Science, RMIT University, Melbourne, VIC, Australia, ⁴ Dipartimento di Scienze e Tecnologie Chimiche, Università di Roma "Tor Vergata", Via Della Ricerca Scientifica, Rome, Italy

The research for heart therapies is challenged by the limited intrinsic regenerative capacity of the adult heart. Moreover, it has been hampered by the poor results obtained by tissue engineering and regenerative medicine attempts at generating functional beating constructs able to integrate with the host tissue. For this reason, organ transplantation remains the elective treatment for end-stage heart failure, while novel strategies aiming to promote cardiac regeneration or repair lag behind. The recent discovery that adult cardiomyocytes can be ectopically induced to enter the cell cycle and proliferate by a combination of microRNAs and cardioprotective drugs, like anti-oxidant, anti-inflammatory, anti-coagulants and anti-platelets agents, fueled the quest for new strategies suited to foster cardiac repair. While proposing a revolutionary approach for heart regeneration, these studies raised serious issues regarding the efficient controlled delivery of the therapeutic cargo, as well as its timely removal or metabolic inactivation from the site of action. Especially, there is need for innovative treatment because of evidence of severe side effects caused by pleiotropic drugs. Biocompatible nanoparticles possess unique physico-chemical properties that have been extensively exploited for overcoming the limitations of standard medical therapies. Researchers have put great efforts into the optimization of the nanoparticles synthesis and functionalization, to control their interactions with the biological milieu and use as a viable alternative to traditional approaches. Nanoparticles can be used for diagnosis and deliver therapies in a personalized and targeted fashion. Regarding the treatment of cardiovascular diseases, nanoparticles-based strategies have provided very promising outcomes, in preclinical studies, during the last years. Efficient encapsulation of a large variety of cargos, specific release at the desired site and improvement of cardiac

function are some of the main achievements reached so far by nanoparticle-based treatments in animal models. This work offers an overview on the recent nanomedical applications for cardiac regeneration and highlights how the versatility of nanomaterials can be combined with the newest molecular biology discoveries to advance cardiac regeneration therapies.

Keywords: nanoparticles, cardiac regeneration, cardiomyopathy, targeted delivery, Hippo pathway, YAP



INTRODUCTION

For the last decades, cardiologists and researchers in the field have been fascinated by the idea of treating cardiomyopathies by inducing adult cardiomyocytes (CMs) to proliferate and generate new contractile force (Hashmi and Ahmad, 2019). The regenerative potential of mammalian heart is an age-dependent process and is already limited in newborns (Porrello et al., 2011b). After a few studies reported the limited potential of CMs to regenerate in human hearts during physiological aging and after injury (Bergmann et al., 2009; Senyo et al., 2013), a consensus was recently reached that their capacity is insufficient to restore heart function in case of injury (Eschenhagen et al., 2017). Also, cardiac muscle regenerative potential remains elusive due to the poor understanding of the biology of resident progenitor cells (Tzahor and Poss, 2017).

When damage occurs, rather than producing new functional muscle mass, the human heart is prone to protect its integrity by depositing a non-compliant scar, while inducing cardiomyocyte hypertrophy. Consequently, these two processes lead to the insurgence of arrhythmias and eventually to heart failure (HF). Therefore, overcoming this limitation would revolutionize the good clinical practice by finding a measure to counteract HF (Foglia and Poss, 2016).

To date, several clinical trials have been proposed to test cardiac repair stimulation in adults. However, no satisfactory outcomes were achieved (Banerjee et al., 2018), mainly due to either the poor understanding of resident cardiac progenitor (CPCs) biology in adult heart or by the lack of appropriate

delivery tools (Smith et al., 2014; Vicinanza et al., 2017; Cianflone et al., 2018; Marino et al., 2019).

The proposed therapies entailed the transplantation of CPCs or the application of human induced pluripotent stem cells (hiPSCs), mainly delivered through cell injections (Bartunek et al., 2017; Butler et al., 2017), cell-matrix inoculation (Traverse et al., 2019; U.S. National Library of Medicine, 2019a), cell sheets (Miyagawa et al., 2017) and cell patches (Dolan et al., 2019). Despite the amount of work done in this direction, the lack of robust pre-clinical mechanistic studies remains the main hurdle for the failure of cardiac treatment (Menasché, 2018).

In this context, the design of nanoparticles (NPs) targeting the contractile component of the heart may offer interesting solutions to overcome the limitations of current therapeutics, by selective modulation of developmental pathways in cardiac cells. Currently, nanoparticles properties can be tuned and designed opportunely for different medical applications, thus offering the possibility for loading and delivering different kinds of cargos, according to the desired therapy. In this work, the current state-of-the-art of NP-based system for cardiac therapy and their therapeutic cargos such as microRNAs (miRNAs), cardioprotective drugs or growth factors is reported and critically discussed.

In conclusion, we point at Hippo pathway, a recently discovered intracellular axis being involved in fetal heart growth and cardiomyocyte proliferation (von Gise et al., 2012; Heallen et al., 2013), as a promising target for nanoparticle-based therapies.

THE BIOLOGY OF CARDIOMYOPATHIES

Heart failure is either determined by a primary cardiac event, such as in myocardial infarction (MI), or is chronically reached over a long time in non-ischemic cardiomyopathies (Tanai and Frantz, 2015). The treatment options for MI range from anti-inflammatory, anti-coagulants and analgesic drugs to angioplasty, coronary bypass or electronic implants, up to heart transplantation in the most severe cases (Lu et al., 2015). However, if the ischemic event persists for prolonged period, the damage to the heart muscle can be irreversible, and cardiac remodeling, achieved by myocardial fibrosis, results in impaired cardiac function (Briceno et al., 2016). Non-ischemic cardiomyopathies refer, instead, to muscle diseases affecting heart size, shape and structure, that eventually reduce the pumping function of the organ (Chan et al., 2018). They – in fact –

proceed to heart blood pump dysfunction, followed by the consequent remodeling of cardiac structures and eventually heart failure (Vikhorev and Vikhoreva, 2018). Based on structural and functional heart changes, several types of cardiomyopathies, having a non-ischemic basis, can be identified. Among them, hypertrophic (HCM), dilated (DCM), restrictive (RC), and arrhythmogenic right ventricular (ARVC) cardiomyopathies are inheritable, and caused by mutations in a single gene (Braunwald, 2017).

HCM is caused by single mutations on different specific genes encoding for proteins from the cardiac sarcomere and it is transmitted as a dominant trait (Alfares et al., 2015). Thus, direct relatives of affected people have 50% probability of acquiring the disease. Nevertheless, due to its incomplete penetrance at very young ages, diagnosis of the disease might be delayed till adulthood (Velzen et al., 2018). HCM is characterized by an inappropriate left ventricular hypertrophy (LVH) developed in the absence of pressure overload or infiltration, and, generally, it results in asymmetric septal hypertrophy, but any LVH pattern can be associated with the disease (Mazzarotto et al., 2019). Similarly, gene mutations can result in very distinct LVH patterns in terms of myocardial fibrosis and susceptibility to arrhythmias. Several genes that bear pathogenic mutations causing HCM have been identified. Among them, the combined cardiac myosin binding protein-C (MYBPC3) and b-myosin heavy chain (MYH7) account for up to 50% of the clinically recognized HCM cases (Lopes et al., 2015). Histologically, HCM is defined by interstitial fibrosis, myocyte enlargement and microstructure disarray (Figure 1, middle panel).

DCM is the most common cardiomyopathy and a leading cause of heart failure, transplantation and death (Hershberger et al., 2013). It is caused by the pathological dilation of the left ventricle, followed by progressive contractile failure. It is histologically characterized by cardiomyocyte hypertrophy, loss of myofibrils, and interstitial fibrosis (Figure 1, right panel) (Cahill et al., 2013). DCM is a progressive disease that can originate from various factors (acquired or inherited) such as ischemia, infection, autoimmune disease, collagen vascular disease, toxins and drugs, nutritional deficiency, and genetic disease (Watkins et al., 2011; Schultheiss et al., 2019). Although patients with DCM may be initially asymptomatic, progressive heart failure or arrhythmia are often responsible for sudden death cases. DCM has a diverse array of familial or sporadic genetic causes, where mutations can be found in sarcomeric proteins and other structural protein genes (Burke et al., 2016). Mutations in the titin gene (*TTN*) are the most common causes of pathogenicity (~25–27.6% of familial and 11.6–18% of sporadic cases) (Schafer et al., 2016). Other frequent mutations affect *MYH7* (Colegrave and Peckham, 2014), tropomyosin $\alpha 1$ chain (*TPM1*) (England et al., 2017), and the genes of cardiac troponins (*TNNT2*) (Hershberger et al., 2009).

ARVC is characterized by a progressive replacement of right ventricular myocardium by fibro-fatty tissue leading to ventricular arrhythmias and sudden cardiac death (Xu et al., 2017). Pathogenic mutations in 13 genes have been identified for patients with ARVC with genes encoding the cardiac desmosome accounting for more than 50% of the cases (Xu et al., 2017).

The later include plakoglobin (JUP), plakophilin-2 (PKP2), desmoplakin (DSP), desmoglein-2 (DSG2), and desmocollin-2 (DSC2) (Xu et al., 2017).

Analogously to DCM, RC – the least common of the cardiomyopathies – may result from acquired or inherited predispositions. The most significant inherited mutations include *TNNT2*, troponin I (*TNNI3*), α -actin (*ACTC*), and *MYH7* (Mughtar et al., 2017). RC results in increased myocardial stiffness that ultimately leads to impaired ventricular filling (Mughtar et al., 2017). Usually RC is manifested from infiltrative processes, i.e., sarcoidosis, hemochromatosis and amyloidosis, for which tailored interventions and precise diagnosis are required to reveal the disease cause (Mughtar et al., 2017).

Other acquired disorders such as stress-induced and myocarditis cardiomyopathies have been identified. The first one is defined, according to the World Health Organization (WHO) classification of cardiomyopathies, as an inflammatory disease often resulting from viral infections (Pollack et al., 2015). Clinically it is manifested by acute heart failure, ventricular arrhythmias or cardiogenic shock, being associated with significant rates of morbidity and death (Pollack et al., 2015).

Stress or Takotsubo cardiomyopathy is a reversible disorder associated with transient left ventricular dysfunction and affects predominantly post-menopausal women (Nef et al., 2010). It mimics a myocardial infarction but in the absence of coronary artery occlusion and it is manifested by systolic apical ballooning (Dhulipala et al., 2018).

Currently available treatments for cardiomyopathies are mainly focused on the mitigation of the most severe symptoms instead of solving the pathology and in most cases the only resolutive intervention is the heart transplantation (U.S. Department of Health & Human Services).

Conversely, cardiac regeneration therapy looks for the complete remission of the disease to improve the patient's life quality, aiming to re-establish the lost heart functionality by stimulating the activity of cardiomyocytes.

NOVEL THERAPEUTIC APPROACHES TO TREAT CARDIOMYOPATHIES

Over the years, different kinds of therapies have been used to repair or regenerate the damaged heart. These include: (1) cell-based therapies (Behfar et al., 2014; Madonna et al., 2016); (2) direct reprogramming of resident cardiac fibroblasts into contractile cells (Fu et al., 2015; Engel and Ardehali, 2018); (3) endogenous cardiomyocyte proliferation induction *via* modulation of cardiomyocyte cell cycle regulators, e.g., the Hippo signaling pathway (Mohamed et al., 2018); (4) gene therapy *via* adeno associated viruses (AAVs) (Chamberlain et al., 2017). Since most of these approaches have been exploited when using nanoparticles for cardiac repair, we will briefly introduce them in the following paragraphs.

Cell-Based Therapies

Cell-based therapies envision the transplantation of cells to restore cardiac function. Implanted cells need to be able to

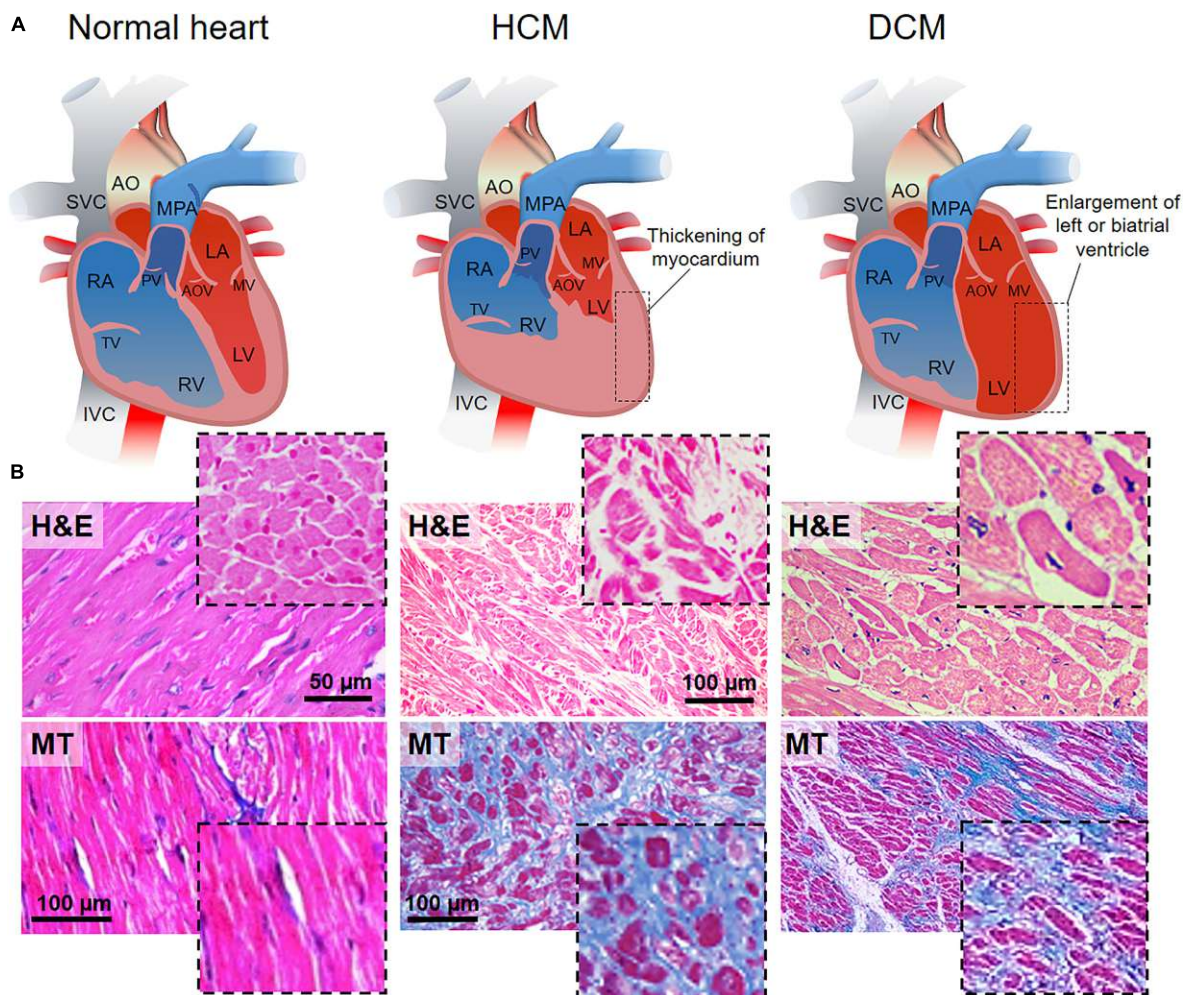


FIGURE 1 | HCM and DCM as the most common cardiomyopathies. **(A)** Schematic representations of the anatomy of normal (left), hypertrophic (hypertrophic cardiomyopathy, HCM, middle) and dilated (dilated cardiomyopathy, DCM, right) heart. HCM is characterized by left ventricle thickening, while DCM is defined by the dilation of the left ventricle. AO, aorta; SVC, superior vena cava; MPA, main pulmonary artery; RA, right atrium; RV, right ventricle; TV, tricuspid valve; PV, pulmonary valve; LA, left atrium; LV, left ventricle; MV, mitral valve; AOV, aortic valve; IVC, inferior vena cava. **(B)** Hematoxylin-eosin (H&E, top) staining in longitudinal and transversal (inset) sections of the cardiac muscle. Normal heart shows the organized and parallel alignment of cardiomyocytes (dashed black line) with preserved cell body and sarcomeric structures. Disorganized cellular structures are highlighted in HCM and DCM sections. Nuclei appear in violet, cytoplasm in pink. Masson's trichrome (MT, bottom) staining in longitudinal and transversal (inset) sections of cardiac muscle. The homogeneity, the continuity and organization of the healthy tissue (pink) is perturbed by the accumulation of fibrotic non-contractile tissue (blue) in HCM and DCM hearts. Missing scale bars were not provided in the original article. H&E healthy: Reprinted and adapted from Marian and Braunwald (2017) under the terms of the Creative Commons Attribution License. MT healthy: Reprinted and adapted from Wang et al. (2014) under the terms of the Creative Commons Attribution License. H&E HCM: Reprinted and adapted from Jain et al. (2017) under the terms of the Creative Commons Attribution License. MT HCM: Reprinted and adapted from: Guo et al. (2017) under the terms of the Creative Commons Attribution License. H&E DCM: Jain et al. (2017) under the terms of the Creative Commons Attribution License. MT DCM: Reprinted and adapted from: Mitrut et al. (2018) under the terms of the Creative Commons Attribution License.

engraft and differentiate into functional cardiomyocytes *in vivo* (Sanganalmath and Bolli, 2013). Several types of cells including skeletal myoblasts (Gavira et al., 2010), bone marrow-derived cells and mesenchymal stem cells (MSCs), cardiac progenitors and pluripotent stem cells [i.e., human embryonic (hESCs) and human induced pluripotent (hiPSCs) stem cells], have been proposed as suitable candidates for cardiac cell therapies (Psaltis et al., 2010; Müller et al., 2018). Despite the promising *in vitro* results and the beneficial short-term outcomes in *in vivo* tests, controversial evidence regarding long term side effects,

like arrhythmias or possible tumor growth due to ineffective differentiation, together with inconsistencies in the reported cell engraftment rate and differentiation, have impaired the translation of such approaches into clinics (Rikhtegar et al., 2019). Nevertheless, different clinical trials featuring the delivery of cells, deemed to be beneficial to the heart, are currently undergoing. Most of these studies are based on the direct injection of different preparations of bone marrow-derived cells and are either in the recruitment phase – with estimated completion dates on May 2020 (NCT02032004) and March 2030 (NCT02503280) (Borow

et al., 2019; U.S. National Library of Medicine, 2019b, 2020a) – or with completion dates expected on June 2021 (NCT02438306), January 2023 (NCT02408432) and July 2023 (NCT02962661) (Raval et al., 2018; U.S. National Library of Medicine, 2019c,d). The outcomes of these clinical trials are likely to clarify the potentiality of cell-based therapy and mark the future direction for the application of this technique in cardiac regeneration.

Direct Reprogramming of Resident Cardiac Fibroblasts

Recently, the possibility that cardiomyocytes can be generated by direct cardiac reprogramming of non-contractile cells has gained momentum (Isomi et al., 2019). This approach consists in converting fully differentiated fibroblasts into cardiomyocytes. It combines the beneficial potential of increasing the contractile workforce of the heart with the reduction of the scar tissue formation (Ieda et al., 2010). The protocols currently in use utilize the forced expression of cardiac-specific transcription factors (e.g., GATA4, HAND2, MEF2C, TBX5) (Song et al., 2012) and relevant cardiac miRNAs to hijack the genetic program of non-contractile cells (Jayawardena et al., 2012). Several studies, both *in vitro* and *in vivo*, have reported the use of different combinations of transcription factors, miRNAs or chemical compounds to engineer mouse or human cardiac fibroblasts into cardiomyocyte-like cells, proving functional improvements in MI models (Nam et al., 2013; Wada et al., 2013; Cao et al., 2016). However, problems like inadequate reprogramming efficiency, uncertainty of the molecular mechanisms involved, and the heterogeneous population of induced cardiomyocyte-like cells still need to be addressed before the clinical application of this methodology can be foreseen (Engel and Ardehali, 2018). More details on the use of transcription factors used in cardiac repair have been reported in the literature (Hashimoto et al., 2018).

In the following paragraph, we will describe the role of miRNAs, growth factors and other cardioprotective drugs, in connection with their use as cargos in nanoparticle-driven cardiac regeneration.

Endogenous Cardiomyocytes Proliferation Induction miRNA Regulation

Because of their regulatory role in cell fate, miRNAs are considered interesting molecular tools and new potent drugs for a number of diseases (Raso and Dirckx, 2017). miRNAs are small endogenous non-coding RNAs (~23 nucleotides) that play gene-regulatory roles in plants and animals by directing the post-transcriptional repression of protein-coding mRNAs (Bartel, 2009). Over the last two decades, different cardiac miRNAs have been described. Here we refer to heart-specific microRNAs known together as myomiRs (myo = muscle + miR = microRNA), such as mir-128, miR-19a/19b, and other miRNAs with known effects on the heart. They were recently found to play a role in pivotal cell functions involved in cardiac regeneration, i.e., proliferation,

reprogramming and differentiation (Huang et al., 2018; Gao et al., 2019).

Additionally, high throughput screening analysis recently performed by different laboratories identified a handful of miRNAs (Table 1) able to induce cardiomyocyte proliferation and stimulate cardiac regeneration in mice and rats (Giacca and Zacchigna, 2015). Following on these studies, miRNAs have also been found to be involved in the cardiac regulation of Hippo pathway, an evolutionarily conserved signaling pathway known for its role in proliferation and apoptosis control during organ development (Meng et al., 2016). This pathway and its impact on cardiac regeneration are described later in this review.

Growth Factors

Biologically active compounds (i.e., growth factors, cytokines) that act at different levels of regulatory processes can be exploited for cardiac repair. They can, for example, (1) activate resident progenitors to attract and differentiate them at the injury site, (2) induce cardiomyocyte dedifferentiation and proliferation, or (3) induce circulating progenitor cells to trigger neovascularization (Hastings et al., 2015). Unfortunately, growth factors and cytokine have usually pleiotropic effects and very short half-life *in vivo*.

A number of growth factors has been recently conjugated to nanoparticles for a controlled delivery at the heart (Table 2). Vascular endothelial growth factor (VEGF) and fibroblast growth factor (FGF) are among the most potent regulators of neo-vascularization and their efficacy has been tested in pre-clinical applications for improving cardiac function after heart failure (Unger et al., 2000; Simons et al., 2002; Henry et al., 2003). However, neither of them has been yet successfully used in clinical practice (U.S. National Library of Medicine, 2020c; Taimeh et al., 2013), due to their pleiotropic effects and limited half-life *in vivo* (Epstein et al., 2001; Henry et al., 2001).

Furthermore, insulin-like growth factor I (IGF-1) regulates contractility, metabolism, hypertrophy, autophagy, senescence, and apoptosis in the heart and its deficiency in humans and animal models has been associated with an elevated risk of cardiovascular disorders (Troncoso et al., 2014). More specifically, low levels of circulating IGF have been related to the development of heart diseases in patients diagnosed with ischemic heart (Juul et al., 2002). These evidences on the roles of IGF-1 explain the interest on developing new IGF-1-based treatments for heart repair.

Noteworthy, two drugs have been approved by food and drug administration (FDA) for the treatment of IGF1 deficiency: mecasermin (Increlex) and mecasermin rinfabate (IPLEX1) (Table 2; Troncoso et al., 2014). Nevertheless, the safety of chronic systemic IGF-1 therapy is still open to debate due to the possibility of severe adverse effects such as cancer risk (Troncoso et al., 2014). In order to solve these problems, scientists have selectively overexpressed IGF-1 in the heart, revealing that IGF-1 in cardiomyocytes protects the heart from oxidative stress and promotes functional recovery after MI (Troncoso et al., 2014).

Despite the promising evidence supporting the use of growth factors for cardiac therapy, the development of delivery strategies

TABLE 1 | Cardiac function associated miRNAs with references to heart human orthologs.

MyomiRs gene family	Stem-loop sequence (human orthologs)	Mature sequence (human orthologs)	Heart linked function	Cardiac pathology associated function	
mir-1	hsa-mir-1-1 hsa-mir-1-2	hsa-miR-1-3p hsa-miR-1-3p	Regulators of cardiac muscle growth and differentiation (Zhao et al., 2005, 2007; Liu et al., 2007, 2008; Callis et al., 2009; Sluijter et al., 2010).	Depletion induces myocyte hyperplasia (Zhao et al., 2007)	
mir-133	hsa-mir-133a	hsa-miR-133a-3p			Reduced in patients with hypertrophic cardiomyopathy (Carè et al., 2007)
mir-208	hsa-mir-208a hsa-mir-208b	hsa-miR-208a-3p hsa-miR-208b-3p			Possible cardio protective effect of miR-208 inhibition in heart failure patients (Kakimoto et al., 2016)
mir-499	hsa-mir-499a	hsa-miR-499a-5p	Enhancement of fibroblast survival, interstitial fibrosis and consequent myocyte hypertrophy (Thum et al., 2008)	N.A.	
mir-21	hsa-mir-21-5p	N.A.		N.A.	
mir-15	hsa-mir-15a	hsa-miR-15a-5p	Persistence of CM mitosis beyond the normal development window of cell cycle arrest and prolonged cellular proliferation of mouse CMs (Porrello et al., 2011a; Botting et al., 2012)	N.A.	
mir-497	hsa-mir-497	hsa-miR-497-5p			
mir-126	hsa-mir-126	hsa-miR-126-5p hsa-miR-126-3p			Embryonic heart development (Fish et al., 2008)
mir-128	hsa-mir-128-1	hsa-miR-128-1-5p	Regulator of cell cycle-related genes (Huang et al., 2018)	Deletion promotes cardiac regeneration in adults by activating CM proliferation (Huang et al., 2018)	
mir-19	hsa-mir-19a hsa-mir-19b	hsa-miR-19a-5p hsa-miR-19b-1-5p	Cardiac protection-mediated expression induced in heart failure (Gao et al., 2019)	Enhancement of cardiomyocytes proliferation in response to cardiac injury (Gao et al., 2019)	
mir-138	hsa-mir-138-1 hsa-mir-138-2	hsa-miR-138-5p hsa-miR-138-5p	Required to establish appropriate chamber-specific gene expression pattern, contributes to CM maturation in zebrafish (Morton et al., 2008)	N.A.	
mir-143	hsa-mir-143	hsa-miR-143-3p	Chamber morphogenesis, heartbeat (Miyasaka et al., 2011)	N.A.	
mir-195	hsa-mir-195	hsa-miR-195-5p	Ventricular hypertrophy-regulated miRNA (van Rooij et al., 2006)	N.A.	
mir-218	hsa-mir-218-1	hsa-miR-218-5p	Heart patterning during embryonic development (Chiavacci et al., 2012)	N.A.	
mir-302	hsa-mir-302a Has	hsa-miR-302a-3p hsa	Heart specific miRNA found in human tissue screening (Lee et al., 2008; Tian et al., 2015)	N.A.	
mir-367	hsa-mir-367	hsa-miR-367-5p hsa-miR-367-3p			
mir-486	hsa-mir-486-1	hsa-miR-486-5p	Embryonic heart development via PI3K/Akt signaling (Small et al., 2010)	N.A.	

(Continued)

TABLE 1 | Continued

MyomiRs gene family	Stem-loop sequence (human orthologs)	Mature sequence (human orthologs)	Heart linked function	Cardiac pathology associated function
mir-25 (mir-92a family)	hsa-mir-25	hsa-miR-25-3p	N.A.	Inhibition improves cardiac contractility in the failing human heart by boosting intracellular calcium handling (Wahlquist et al., 2014) Inhibition of miR-25 in mouse reactivates Hand2 that is crucial for embryonic heart development (Dirkx et al., 2013)
	hsa-mir-92a	hsa-miR-92a-3p	N.A.	Reduces endothelial inflammation and promotes angiogenesis and functional recovery in ischemic myocardium (Bonauer et al., 2009; Loyer et al., 2014)
mir-34	hsa-mir-34a	hsa-miR-34a-5p	N.A.	Anti-apoptotic and telomere protective effect after MI in mice (Boon et al., 2013)
mir-199/mir-590	hsa-mir-199a-1 hsa-mir-590	hsa-miR-199a-3p hsa-miR-590-5p hsa-miR-590-3p	N.A.	Upregulation in rodent heart upon myocardial infarction re-induces mitosis that helps to preserve cardiac function (Eulalio et al., 2012)

N.A., not assessed.

able to increase the biocompatibility, the circulation time and the release efficiency of these molecules at the injured site must be considered before foreseeing their clinical translation (Rebouças et al., 2016).

Selective Regulation of Hippo Pathway to Promote Adult Cardiomyocyte Proliferation

The Yes-associated protein one (YAP) is the core downstream effector of Hippo pathway. The role of Hippo signaling pathway will be discussed further in the present section. For a more detailed review in cellular mechanobiology, see the review from Martino et al. (2018). The activation of the Hippo pathway results in YAP phosphorylation at Ser127 by upstream LATS kinases (LATS1/2 in human) (Varelas, 2014), which further leads to cytoplasmic sequestration of YAP according to ubiquitin-mediated protein degradation. Conversely, repression of Hippo kinases induces YAP reactivation and accumulation in the nucleus (Boopathy and Hong, 2019) (content **Box 1**). In the adult organism, YAP is involved in numerous key biological processes where it acts either as repressor or activator in combination with context-specific transcription factors (**Figure 2A**). From the analysis of almost four hundred direct protein interactors of YAP, it is clear that many biological effects remain unexplored (thebiogrid.org, 2019). Among the most studied functions YAP exerts are stemness maintenance and tumorigenesis (Chen et al., 2019), cell mechanic control via focal adhesions (Nardone et al., 2017) and the regulation of organ size (Watt et al., 2015). The Hippo–YAP pathway regulates heart growth during prenatal life and is considered important for adult heart homeostasis (**Figure 2B**; Wang et al., 2018). Noteworthy, overexpression of

YAP was proven to be sufficient for stimulating proliferation of post-natal rat cardiomyocytes (von Gise et al., 2012). In particular, inducible YAP overexpression in rat embryos and new-born individuals caused an increase in cardiomyocyte proliferation leading to hyperplasia and 20% gain in heart weight in 10 days. This happened due to the increase in cell number, whereas cell size remained unchanged.

Similarly, blocking the Hippo pathway upstream components MST1/2, LATS2 or SAV1 (WW45) enhanced cardiomyocytes proliferation during heart development (Heallen et al., 2013). Odashima et al. (2007) reported the occurrence of several “pro-regenerative” effects able to inhibit the development of heart failure after myocardial infarction in transgenic mice overexpressing MST1 dominant negative (resulting in downregulation of endogenous MST1 and subsequent YAP upregulation). These effects promoted the reduction of contractile cell apoptosis, intensification of proinflammatory cytokines, inhibition of cardiac dilation, and attenuation of cardiac dysfunction without inhibiting compensatory hypertrophy.

Although progresses in myocardial regeneration in Hippo-deficient heart was reported by Tao et al. (2016), restoration of overall cardiac function by tuning Hippo-pathway components seems to be a more complex task, which requires additional research and validation. In fact, Ikeda et al. (2019) described that long term activation of YAP facilitates the progression of heart failure, in response to pressure overload, in transgenic mice model lacking WW45 Hippo component. Despite homozygous knockout of WW45 (WW45cKO) in

TABLE 2 | Drugs and small molecules as cardioprotective agents in nanomedicine applications.

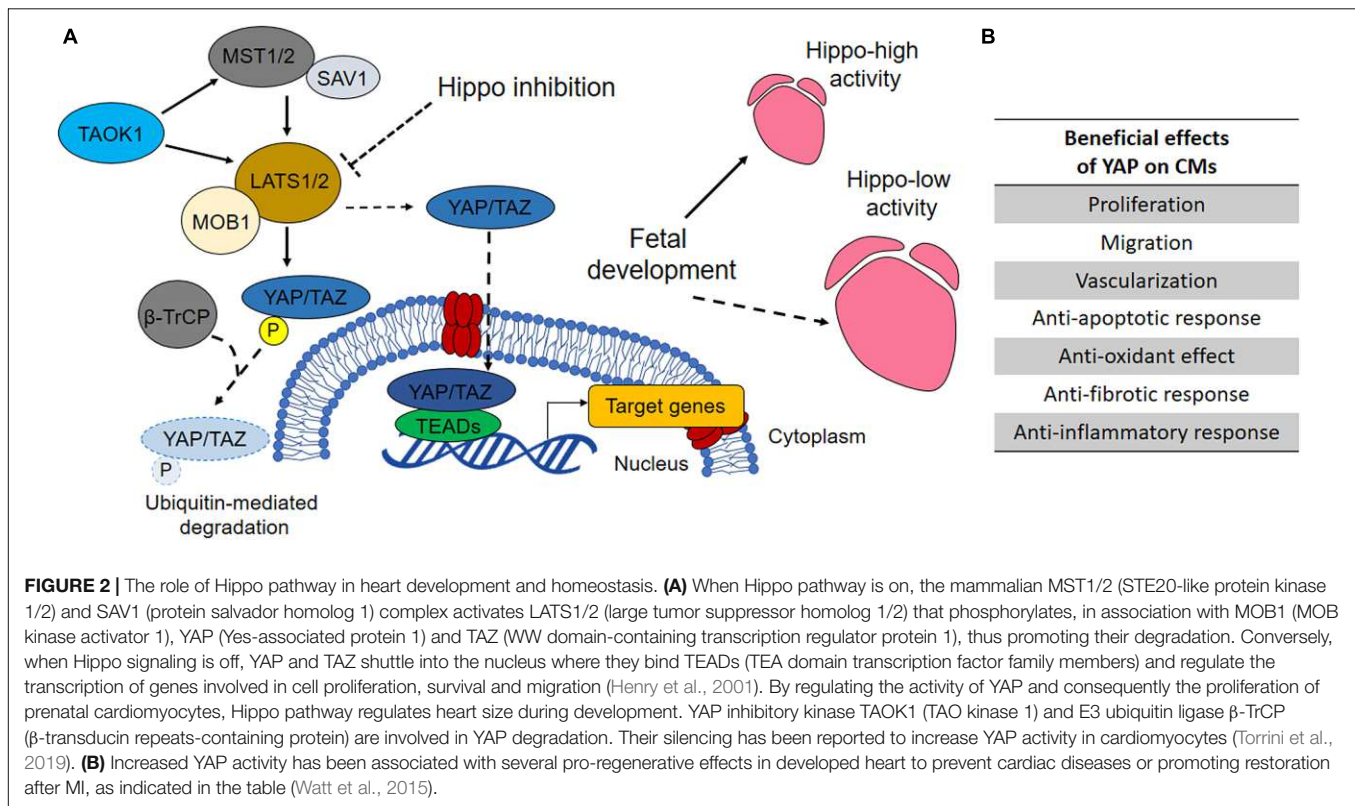
Molecule	class	Properties	Heart repair properties	Clinical trial	References
Simvastatin	Statin	Reduces LDL-C levels	Reduced cardiovascular morbidity and mortality in high risk patients	Heart failure	Heart Protection Study Collaborative and Group, 2002; Feringa et al., 2006; Cannon et al., 2015
VEGF	Growth factor	Promoting neovascularization	Enhanced angiogenesis	Ischemic heart disease and other cardiac conditions	Henry et al., 2001, 2003; U.S. National Library of Medicine, 2020c; Epstein et al., 2001; Taimeh et al., 2013
IGF-1	Growth factor	Regulates contractility, metabolism, hypertrophy, autophagy, senescence, and apoptosis in the heart.	IGF-1 in cardiomyocytes protects the heart from oxidative stress and promotes functional recovery after MI.	FDA approved drugs: Increlex1 and IPLEX1	Troncoso et al., 2014
AMO-1	Anti-miRNA oligonucleotide	Inhibition of miR-1	Reduce apoptosis of cardiomyocytes	N.A.	Xue et al., 2018
CoPP	Anti-oxidant	Suppresses the inflammatory activity of macrophages by induction of heme oxygenase-1 (HO-1) expression	Reduces adverse heart remodeling by controlling the inflammatory activity of macrophages	N.A.	Bulbake et al., 2017
SB431542	Inhibitor	TGF β inhibitor	Reduces fibrosis, decreases hypertrophy and improves cardiac function.	N.A.	Ferreira et al., 2018
CHIR99021	Inhibitor	GSK3 inhibitor	Upregulates Wnt signaling resulting in significant increase of mature cardiomyocyte proliferation.	N.A.	U.S. National Library of Medicine, 2020c
Berberine	Alkaloid	Anti-inflammatory, anti-microbial, anti-diharreal, anti-oxidative, vasorelaxant, cholesterol lowering	Reduces rate of MI	Study showed to improve survival of CHF patients when given oral or intraperitoneal	Zeng et al., 2003; Allijn et al., 2017

LDL-C, low density lipoprotein-C; CHF, congestive heart failure; Increlex1, mecasermin, a human recombinant IGF-1 analog; IPLEX1, mecasermin rinfabate, a binary protein complex of human recombinant IGF-1 and human recombinant IGBP-3; IGBP-3, insulin-like growth factor binding protein-3; HO-1, heme oxygenase-1; TGF β , transforming growth factor β ; GSK3, glycogen synthase kinase-3. N.A., not assessed.

BOX 1 | Hippo pathway overview.

Like every tissue of the human body, the heart tissue is subjected to either constant or temporary mechanical stimuli. The cell-extracellular matrix (ECM) interactions dynamically remodel the mechanical properties of the myocardium, and actively respond to extrinsic mechanical cues. **Hippo pathway** is a mechanosensitive signaling pathway transducing external mechanical stimuli into biochemical responses. The pathway functions as a negative regulator of the effectors YAP/TAZ, two paralogs acting as transcriptional co-activators. Here are the main components of Hippo pathway and their role in brief:

- YAP: Yes-associated protein. The effector of the pathway. It acts as a transcriptional co-activator (Boopathy and Hong, 2019);
- TAZ (WWTR1): WW domain-containing transcription regulator protein 1. Together with YAP, is the effector of the pathway. It acts as a transcriptional co-activator (Boopathy and Hong, 2019);
- LATS1/2: Large Tumor Suppressor Kinase 1. It is a serine/threonine protein kinase directly phosphorylating YAP/TAZ. The phosphorylation inhibits YAP/TAZ translocation to the nucleus (Tang et al., 2019);
- MOB1: MOB Kinase Activator 1A. It functions as a co-factor of LATS1/2 (Kulaberoglu et al., 2017);
- MST1/2 (STK3/4): Mammalian STE20-Like Protein Kinase 2. It acts upstream of LATS1/2 (Qin et al., 2013);
- SAV1 (WW45): Salvador Family WW Domain Containing Protein 1. It forms a heterodimer with MST1/2 (Bae et al., 2017);
- TAOK1: TAO kinase 1. It is a serine/threonine protein kinase acting upstream of MST1/2 (Plouffe et al., 2016);
- B-TrCP: Beta-Transducin Repeat Containing E3 Ubiquitin Protein Ligase (Fuchs et al., 2004);
- TEAD: transcription factor family forming an active transcriptional complex in association with YAP/TAZ (Boopathy and Hong, 2019).



mice exhibited greater cardiomyocytes cell cycle re-entry, adverse effects such as interstitial fibrosis, partial increase of infiltrating inflammatory cells and reduction in contractility were also observed.

Considering the very different effects Hippo pathway has on the contractile and structural components of the heart, pros and cons of targeting such a pathway in the whole organ need to be balanced. Also, the crosstalk with other regulatory pathways such as WNT/ β -catenin signaling should be considered (Wang et al., 2018). In fact, β -catenin heterozygous mutation (the major effector of WNT pathway) in SAV1 KO mice was able to normalize the proliferation rate of ventricular cardiomyocytes and myocardial thickness, thus confirming the crucial role of WNT pathway in cardiac overgrowth induced by Hippo inactivation (Heallen et al., 2011).

Regarding cardiomyocyte homeostasis, the group of Mauro Giacca lately demonstrated that some miRNAs work in a network that preside over cardiomyocyte homeostasis by converging in the activation of nuclear translocation of YAP (Torrini et al., 2019). In particular, the authors proved that miR-199a-3p, miR-302d, miR-373, miR-590-3p, and miR-1825 can target the TAOK1 and β -TrCP (content **Box 1**), thus driving E3 ubiquitin ligase-mediated YAP degradation.

These results highlight the crucial role of Hippo pathway in cardiomyocyte homeostasis and the possible cardiac therapy horizons emerging from the regulation of YAP activity in the contractile figures of the heart.

Adeno-Associated Viruses (AAVs) for Targeted Gene Therapy

Another methodology proposed to treat the failing heart relies on the use of engineered viruses as vectors for transfection, given their natural ability to deliver nucleic acids into replicating host cells (Chen et al., 2017). In this direction, the intra-cardiac administration of miRNA-199a through adeno-associated viral vectors restored contractility and increased pig muscle mass by sustaining cardiomyocyte proliferation and de-differentiation (Gabisonia et al., 2019). Nevertheless, the long-term uncontrolled expression of the miRNA resulted in arrhythmia events which led the animals to premature death, most likely due to the proliferation of poorly differentiated cardiac cells.

AAV technology is being used in clinics for several applications. A quick look at the website www.clinicaltrials.gov returns three clinical studies employing AAVs aiming to improve the function of the failing heart in patients with HF with reduced ejection fraction (HFrEF). The studies (CUPID and MYDICAR) relied on the intracoronary or the anterograde epicardial coronary artery infusion delivery of AAV1-encoding sarcoplasmic reticulum Ca^{2+} -ATPase (SERCA2a). Although encouraging, with favorable safety profile in terms of immunogenic responses and arrhythmias, the efficacy of the CUPID trial was not confirmed by the larger CUPID 2 study (Penny and Hammond, 2017).

As a general consideration, the use of AAVs still faces important limitations. In particular, several issues remain

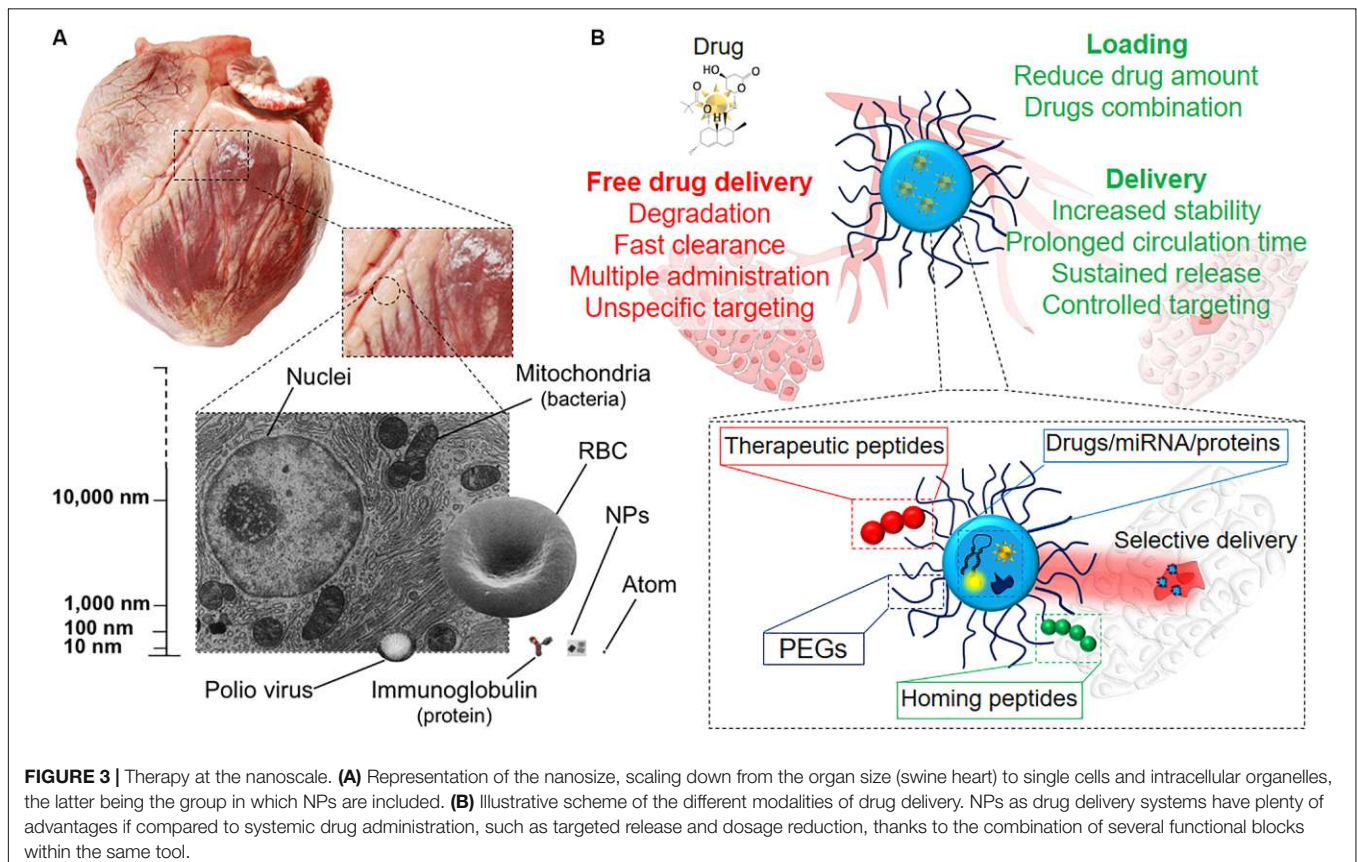
unsolved, such as (1) long manufacturing processes and scalability; (2) strictly defined cDNA packaging capacity (~5 kb) that dramatically limits the number of genes that can be carried; (3) the demanding screening of AAV variants suitable for the specific aim; (4) pre-existing immunological sensitivity along with the insurgence of immune response after repeated administrations (Chamberlain et al., 2017).

As an alternative to the use of AAVs, NPs, which can be “custom-made” by using different nano-constructs carrying therapeutic/regenerative drugs/miRNAs, have been proposed, thus opening the way to the application of nanomedicine in the cardiac regeneration field (Amezcuca et al., 2016).

NANOPARTICLES DESIGN FOR CARDIAC REGENERATION

Generally, the term *nanomedicine* is applied to a number of innovative therapeutic approaches entailing the use of precisely bioengineered nanostructured materials (Figure 3A), with at least one dimension in the 1–100 nm range (Zhang et al., 2008). However, a broader definition is now accepted for structures above the 100 nm, such as sub-micrometer and nanostructured microparticles, which are commonly regarded as nanomaterials and used for nanomedical applications (Boverhof et al., 2015). Nanomedicine can be defined as the application of nanotechnology to medicine for diagnosis and therapy

(Pelaz et al., 2017). It aims to minimize the side effects of therapeutic drugs while increasing their selective accumulation, thus enhancing the efficacy of the treatment in clinics (Davis et al., 2008). Conventional therapies are – in fact – often associated with tremendous side effects due to the intrinsic toxicity of the drugs, their broad spectrum of activity and the poor control over delivery (Jabir et al., 2012). Due to their tunable properties that potentially allow any kind of application, NPs can overwhelm the design limitations associated with AAVs described above. To date, various types of NPs have been loaded with miRNAs and drugs and used to vehiculate therapeutic agents *via* different administration routes, providing several advantages when compared to the standard therapies (Figure 3B). Remarkably, a major limitation in the therapeutic use of miRNAs is their fast clearance and rapid degradation in blood circulation and cellular cytoplasm mainly by ribonucleases, resulting in a short half-life (Sioud, 2005). Furthermore, these molecules cannot freely penetrate into the cell efficiently (Zhang et al., 2007). Extracellular miRNAs are physiologically carried inside the cell by membrane-derived vesicles, lipoprotein and ribonucleoprotein complexes (Boon and Vickers, 2013). Among these systems, exosomes are the main effectors of miRNA carriage and exosome miRNA-loaded release has been found to be involved in intercellular communications (Valadi et al., 2007). Therefore, the use of engineered miRNA nanocarriers represents a nature-inspired approach overcoming the previously described limitations. Several NP-based systems



for miRNA delivery were so far developed, as recently reviewed in (Lee et al., 2019).

Along with the miRNA delivery, the use of bioengineered nanocarriers can enhance the circulation time, biodistribution and bioavailability of different drugs and proteins, as well as protecting them from degradation and inactivation (Patra et al., 2018). Indeed, many of the drugs currently available are lipophilic and their systemic administration is challenged by their scarce aqueous solubility, with consequent poor delivery and therapeutic efficiency (Kalepu and Nekkanti, 2015). Consequently, the encapsulation of these molecules inside amphiphilic systems may enhance their efficacy and promote their long lasting and sustained release at the desired site (Din et al., 2017).

Protein therapy offers higher specificity, greater activity, and less toxicity compared to standard drugs. However, the maintenance of their structural complexity and activity, which are crucial for achieving high therapeutic performances, can be challenged by (1) their enzymatic degradation/inactivation, (2) their short circulation half-lives and (3) their poor membrane permeability (Yu et al., 2016). Therefore, the use of nanoparticles may also protect therapeutic proteins from proteolysis while improving their delivery efficiency and sustaining their release at the target site (Zhao et al., 2016).

As a result, the use of nanotechnology to deliver cardioprotective drugs and assist the prolonged release of growth factors has arisen in the last years as a promising tool to restore compromised heart function, as it will be discussed below. Different administration routes, based on the physico-chemical properties of the drug/nanoparticle, on the predicted effect and desired target have been pursued for obtaining an optimal delivery of NPs to treat cardiomyopathies. Intravascular, including intra-cardiac (i.c.) and intravenous (i.v.) injection, and extravascular like inhalation (Figure 4A) are the most common administration routes used for this purpose. They all provide different advantages, and intrinsic disadvantages (Figure 4B; Dib et al., 2011; Yildirimer et al., 2011; Chenthamara et al., 2019), for the treatment of several pathological conditions, such as compromised vascularization, fibrosis and inflammation, while attempting to improve cardiac functionality (Figure 4C). However, despite the encouraging premises, the use of NP-based system for direct cardiac repair is still lagging at the preclinical stage.

In the next chapter we will provide an overview of the state-of-the-art in the field of nanomedicine for cardiac regeneration, and revise the main properties of the NPs – and their cargos – used to this aim (Table 3).

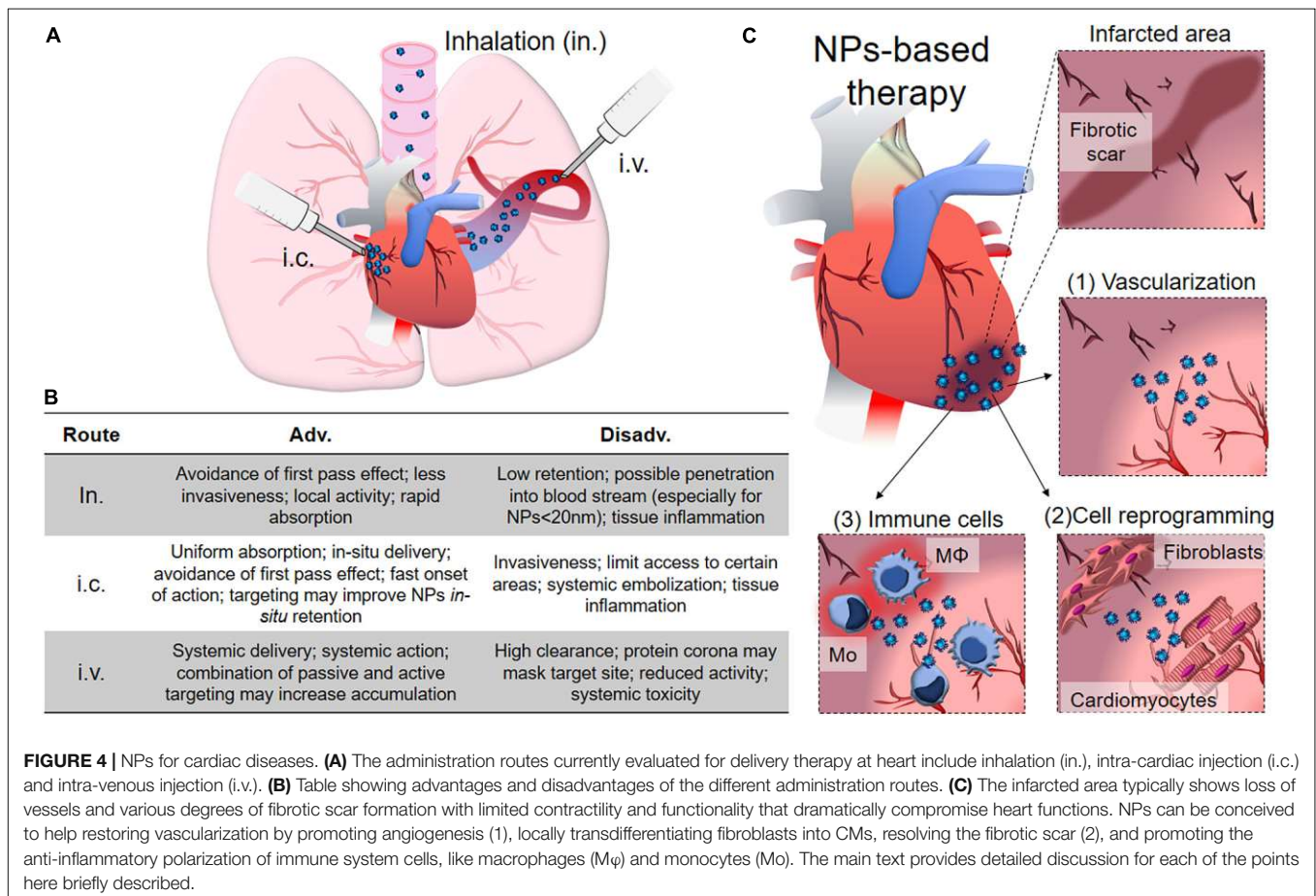


TABLE 3 | NPs for cardiac regeneration.

NPs type	Composition	Cargo	Hydrodynamic size and surface charge	Targeting moiety	Application	Stage of research	References
Polymeric	DSPE-PEG-NH ₂ , DSPE-PEG-Maleimide, PBFT	miR-199a	110 nm, ~15–20 mV	TAT	Targeted miR-199a delivery for reducing scar size while maximizing muscle and vessel restoration and promote CMs proliferation.	<i>In vivo</i> : Rat MI model	Yang et al., 2019
	PEG-DGL	AMO-1	~200 nm, ~4 mV	AT1	Targeted delivery of miR-1 inhibitor (AMO-1) to attenuate cardiomyocytes apoptosis.	<i>In vivo</i> : C57BL/6 mice MI model	Xue et al., 2018
	HA-sulfate	miR-21	130 nm, -10 mV	N.A.	Delivery of miRNA-21 to cardiac macrophages after MI for inducing their modulation toward an anti-inflammatory, reparative state.	<i>In vivo</i> : C57BL/6 mice MI model	Bejerano et al., 2018
	PLGA	Simvastatin	~160 nm, -4 mV (referred in a different work for similar NPs)	N.A.	Local recruitment of statin-PLGA-NPs-loaded AdSCs to the infarcted site and gradual release of the drug to improve neovascularization and cardiac regeneration.	<i>In vivo</i> : BALB/c nu/nu mice	Katsuki et al., 2014; Yokoyama et al., 2019
	PLGA	VEGF	113 nm, -55 mV	N.A.	Local release of reduced dosage of VEGF to favor angiogenesis and reduce risks associated with higher dosage therapy.	<i>In vivo</i> : NOD/SCID MI mice	Oduk et al., 2018
	AcDXSp	SB431542 CHIR99021	~350 nm, ~10 mV	ANP	pH-triggered delivery of combined poorly water-soluble small drug molecules for promoting cardiac regeneration.	<i>In vitro</i> : primary cardiac cells isolated from neonatal rats	Ferreira et al., 2018
Liposomes	DSPE-PEG-Maleimide, PCPDTBT	N.A.	~50 nm	CPP	Photoacoustic imaging (PAI)	<i>In vivo</i> : NOD/SCID mice	Qin et al., 2018
	HSPC, cholesterol, DSPE-PEG-OH, DSPE-PEG- Maleimide	VEGF	180 nm, N.A.	Anti-P-selectin	Targeted delivery of VEGF to the infarcted site to enhance vascularization.	<i>In vivo</i> : rat MI model	Scott et al., 2009
	DSPE-PEG-carboxy, HSPC, cholesterol	N.A.	142 nm, N.A.	AT1	Targeted delivery of NPs (48% accumulation in 24 h) to the left ventricle after MI.	<i>In vivo</i> : C57BL/6 mice MI model	Dvir et al., 2011
	PS, PC, cholesterol	N.A.	1.2 μm, -98 mV	PS	Apoptotic cell-like treatment for reducing inflammation at infarcted heart and promoting angiogenesis.	<i>In vivo</i> : Balb/c mice MI model	Harel-Adar et al., 2011

(Continued)

TABLE 3 | Continued

NPs type	Composition		Cargo	Hydrodynamic size and surface charge	Targeting moiety	Application	Stage of research	References
Liposomes	PMPs		CoPP	100 nm, -2.25 mV	N.A.	Promote biomimicked platelet like proteoliposomes interaction with monocytes, which serve as vehicle for enhanced liposome accumulation at the injured area for local release of therapeutic cargo.	<i>In vivo</i> : BALB/c mice	Cheng et al., 2016
	DPPC, DSPE-PEG-OH, cholesterol		Berberine	110 nm, N.A.	N.A.	EPR effect for liposome accumulation and local release of berberine after macrophage uptake, reducing inflammatory damage.	<i>In vivo</i> : C57BL/6 mice MI model	Allijn et al., 2017
Inorganic	Core	Shell						
	SiO ₂	IRIS3-APTS	N.A.	50 nm, -25 mV	N.A.	Promoting hMSCs engraftment	<i>Ex vivo</i> : Wistar rat infarcted hearts	Popara et al., 2018
	Ca ₂ (PO ₄) ₂	Citrate	Hemagglutinin or mimetic peptide	~200 nm, ~31 mV	N.A.	Accumulation of nanoparticles at the myocardium via inhalation for local therapy aiming to restore heart contractility.	<i>In vivo</i> : Landrace pigs	Miragoli et al., 2018
	Fe _{x-1} O _x /SiO ₂	SiO ₂	N.A.	60 nm, N.A.	N.A.	Magnetic nanoparticles internalization on endothelial cells for their guidance to the ischemic heart resulting in improved remodeling and cardiac function.	<i>In vivo</i> : rat MI model	Zhang et al., 2019
	Fe ₂ O ₃	DMSA, APTs, Glu	N.A.	10/35 nm, -43.1/28.9/-2.1 mV	N.A.	Cardioprotective activity via inhibition of intracellular ROS and decrease of peroxidation injury.	<i>In vivo</i> : Sprague-Dawley rats and Guinea pigs	Xiong et al., 2015
Au	PEG-SH, OPSS-PEG-SVA	N.A.	80 nm, N.A.	CNA35	Myocardial scar detection with CT imaging	<i>In vivo</i> : Sprague-Dawley rat MI model	Kee and Danila, 2018	

TAT, transactivator of transcription peptide; AT1, angiotensin II type 1 ligand; ANP, atrial natriuretic peptide; CPP, cell-penetrating peptide; AMO-1, Anti-miRNA-oligonucleotide; VEGF, vascular endothelial growth factor; TGFβ inhi, transforming growth factor β inhibitor; GSK3 inhi, glycogen synthase 3 inhibitor; DSPE-PEG, 1,2-distearoylphosphatidyl-ethanolamine-PEG; PBFT, poly(9,9-dioctylfluorene-alt-benzothiadiazole); PEG-DGL, pegylated dendrigraft poly-L-lysine; HA-sulfate, Hyaluronan sulfate; PLGA, Poly lactic-co-glycolic acid; AcDXSp, spermine-acetalated dextran; PCPDTBT, Poly [2, 6- (4,4-bis- (2- ethylhexyl) – 4H -cyclopenta [2,1-b;3,4-b'] dithiophene) –alt -4,7 (2,1,3 – benzothiadiazole)]; AT1, angiotensin II type 1 ligand; CoPP, cobalt protoporphyrin IX; D-PE-PEG, 1,2-distearoylphosphatidyl-ethanolamine-PEG; HSPC, L-α-phosphatidylcholine; PS, phosphatidyl serine; MPs, platelet membrane proteins; IRIS3-APTS, aminopropyltriethoxysilane derivative of IRIS3 cyanine; DMSA, dimercaptosuccinic acid: PEG-SH, PEG-thiol; OPSS-PEG-SVA, orthopyridyl disulfide-polyethylene glycol-succinimidyl valerate; CNA35, collagen binding adhesion protein 35. N.A, not assessed.

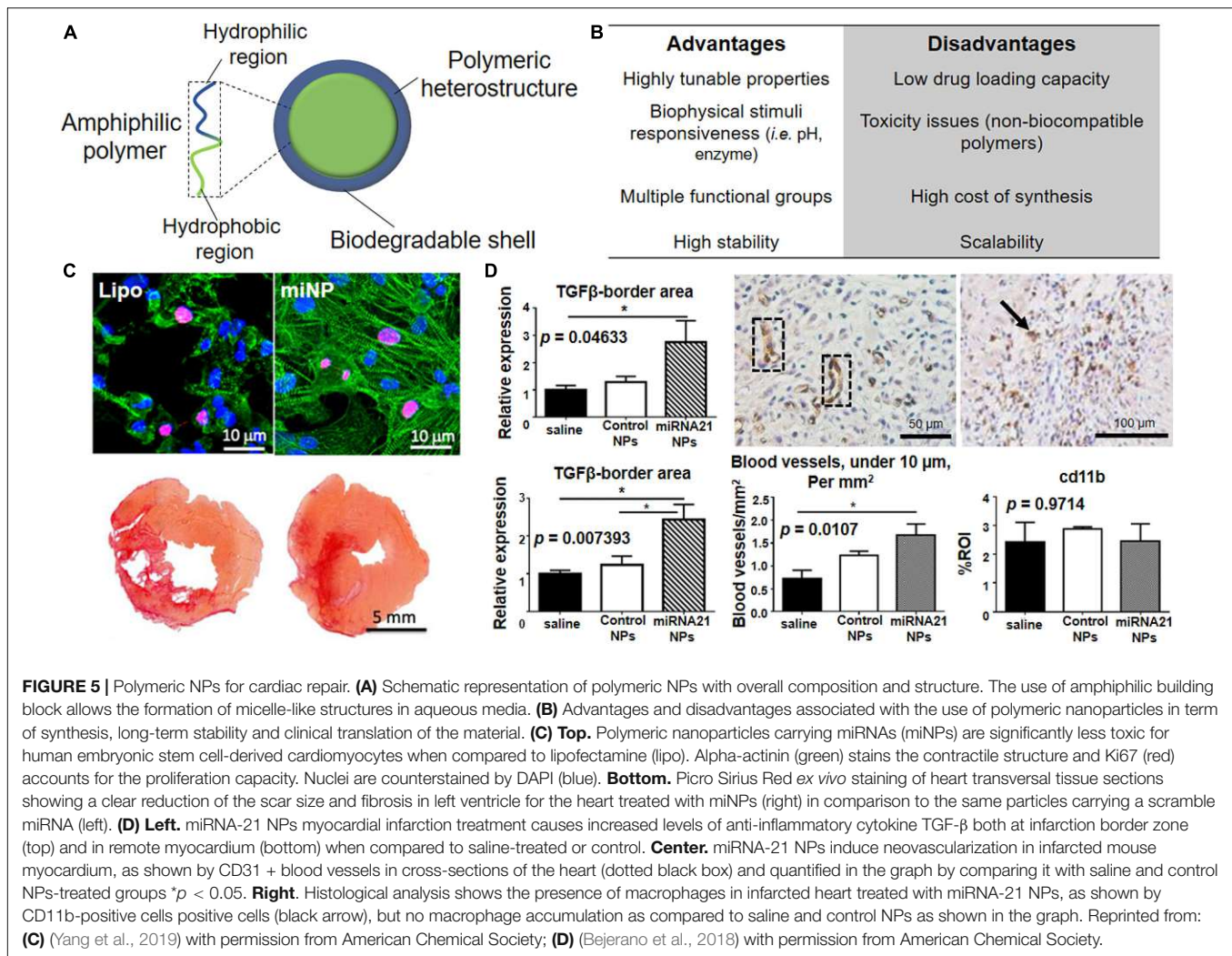


FIGURE 5 | Polymeric NPs for cardiac repair. **(A)** Schematic representation of polymeric NPs with overall composition and structure. The use of amphiphilic building block allows the formation of micelle-like structures in aqueous media. **(B)** Advantages and disadvantages associated with the use of polymeric nanoparticles in terms of synthesis, long-term stability and clinical translation of the material. **(C) Top.** Polymeric nanoparticles carrying miRNAs (miNPs) are significantly less toxic for human embryonic stem cell-derived cardiomyocytes when compared to lipofectamine (lipo). Alpha-actinin (green) stains the contractile structure and Ki67 (red) accounts for the proliferation capacity. Nuclei are counterstained by DAPI (blue). **Bottom.** Picro Sirius Red *ex vivo* staining of heart transversal tissue sections showing a clear reduction of the scar size and fibrosis in left ventricle for the heart treated with miNPs (right) in comparison to the same particles carrying a scramble miRNA (left). **(D) Left.** miRNA-21 NPs myocardial infarction treatment causes increased levels of anti-inflammatory cytokine TGF- β both at infarction border zone (top) and in remote myocardium (bottom) when compared to saline-treated or control. **Center.** miRNA-21 NPs induce neovascularization in infarcted mouse myocardium, as shown by CD31 + blood vessels in cross-sections of the heart (dotted black box) and quantified in the graph by comparing it with saline and control NPs-treated groups * $p < 0.05$. **Right.** Histological analysis shows the presence of macrophages in infarcted heart treated with miRNA-21 NPs, as shown by CD11b-positive cells (black arrow), but no macrophage accumulation as compared to saline and control NPs as shown in the graph. Reprinted from: **(C)** (Yang et al., 2019) with permission from American Chemical Society; **(D)** (Bejano et al., 2018) with permission from American Chemical Society.

POLYMERIC NANOPARTICLES

Polymeric NPs have recently caught attention by virtue of their versatility and higher tunable properties, which make them extremely interesting tools for controlled drug encapsulation and release (Figures 5A,B). Indeed, their physico-chemical properties (i.e., surface charge, surface functionalities, hydrophobicity) can be finely tuned for accommodating nucleic acids, drugs and proteins to promote their efficient release inside the cells (Patil and Panyam, 2009; Fortuni et al., 2019). This large class of NP-based systems include amphiphilic micelles, vesicles, dendrimers and polymersomes possessing unique structures and properties, which can be efficiently adjusted during synthesis for hosting different kinds of cargos (Chandarana et al., 2018). Most of the designed polymeric NPs propose new synthetic copolymers able to combine different functionalities such as targeting and selective cargo delivery systems (El-Say and El-Sawy, 2017). Moreover, given the emerging use of miRNAs for cardiac regeneration, it is not surprising that many studies developed polymeric NPs as miRNA carriers, alone or in combination with targeting moieties or therapeutic drugs (see Table 2).

Recently, Yang and colleagues have reported the use of polymeric NPs composed by a combination of poly(9,9-dioctylfluorene-*alt*-benzothiadiazole) (PBFT) and 1,2-distearoylphosphatidyl-ethanolamine-PEG-amino (DSPE-PEG-NH₂), for the conjugation with miRNA molecules, or DSPE-PEG-maleimide for the binding of transcription activator of transcription (TAT) peptide, in order to deliver therapeutic miRNA to the infarcted myocardium (Figure 5C) (Yang et al., 2019). The polymeric matrix provided by these miRNA NPs (miNPs) protects miR-199a against enzymatic degradation and facilitates the functionalization with TAT for improved cell uptake. *In vitro* experiments, performed by using hESC-derived cardiac cells, revealed that the miNPs are less cytotoxic than commercially available lipocomplexes, while exhibiting comparable transfection efficiency, both in normoxia and hypoxia. Interestingly, miNPs were shown to selectively trigger the proliferation of both hESC-derived cardiomyocytes and endothelial cells, but not human cardiac fibroblasts (hCFs). This strategy was able to reduce scar size and maximize muscle and vessel restoration, giving good results *in vivo* when miNPs were injected into mice beating hearts in

combination with an injectable hydrogel. Indeed, cardiac function of the neo-vascularized myocardium was restored for over 3 months, indicating the long-term therapeutic effects of this treatment.

In another study the authors pursued targeted delivery of NPs carrying a miRNA inhibitor instead of a therapeutic miRNA. In detail, Xue et al. (2018) developed a pegylated dendrigraft poly-L-lysine (PEG-DGL) dendrimer functionalized with an early myocardium targeting peptide (AT1) and an antisense oligonucleotide able to inhibit miR-1 (AMO-1) (AT1-PEG-DGL-AMO-1). *In vivo* results showed that the nanovector was able to target the infarcted mouse heart within 30–60 min after a single i.v. injection and significantly reduced the infarcted area. The inhibition of miR-1 successfully attenuated cardiomyocytes apoptosis, thus reducing cell death and promoting cardiac repair.

Other than targeting directly cardiomyocytes, immune system cells can be programmed to enhance cardiac repair. The myocardium is – in fact – the site of massive immune cell infiltration during the acute phase of the infarction. In this context, co-assembled miR-21, Ca²⁺ and hyaluronan-sulfate NPs (HASCa²⁺-miRNA) were used to target macrophages in the heart (Figure 5D) (Bejano et al., 2018). After i.v. injection, NPs promoted the switch of macrophages from the pro-inflammatory to the reparative phenotype, thus promoting angiogenesis while reducing fibrosis and cell apoptosis. However, the poor understanding of the mechanism by which the interaction between NPs and macrophages occurs remains the major obstacle to the translation of this appealing procedure.

By using a different approach, Yokoyama et al. (2019) combined nanomaterials and stem cell therapy. The capacity of adipose-derived stem cell (ADSCs) for promoting neovascularization and inhibiting cell death after MI was exploited. The authors reported that simvastatin-conjugated PLGA NPs loaded *in vitro* on ADSCs induce spontaneous recovery of infarcted myocardium and increase vascularity. Indeed, statin-PLGA-NPs-loaded ADSCs were shown to be recruited to the ischemic myocardium to locally release the payload. This combined approach is bound to increase the cardiac regeneration potential of a very limited number of cells (10,000 cells per mouse), since the effect would be amplified by statin gradual release. This research work interestingly pointed out the therapeutic benefits emerging from the combination of NP-based and cell-based therapies for treating cardiac diseases.

Additionally, Oduk et al. (2018) described the use of PLGA NPs VEGF-loaded to restore the vascularization at the infarcted heart. The particles were able to continuously release VEGF for at least 31 days after injection in a mice model of MI, with improvements in cardiovascular system being still detected 4 weeks after the treatment. Noteworthy, the controlled release of the growth factor, due to the continuous biodegradation of PLGA matrix, effectively increased the delivery of VEGF at the target site, while reducing its systemic side effects.

In the context of cell reprogramming, spermine-modified acetylated dextran (AcDXSp) nanoparticles have been designed to encapsulate poorly water-soluble drugs (SB431542 – transforming growth factor β (TGF β) inhibitor – and CHIR99021

– Glycogen synthase kinase-3 (GSK3) inhibitor) used to reprogram fibroblasts (Ferreira et al., 2018). These NPs were also tagged with a targeting peptide (atrial natriuretic peptide, ANP) specific for cardiac fibroblasts. The authors claimed the dual targeting and therapeutic effect might be exploited to circumvent the limitations of local injection. Nevertheless, *in vivo* experiments to prove this theory were not carried out so far.

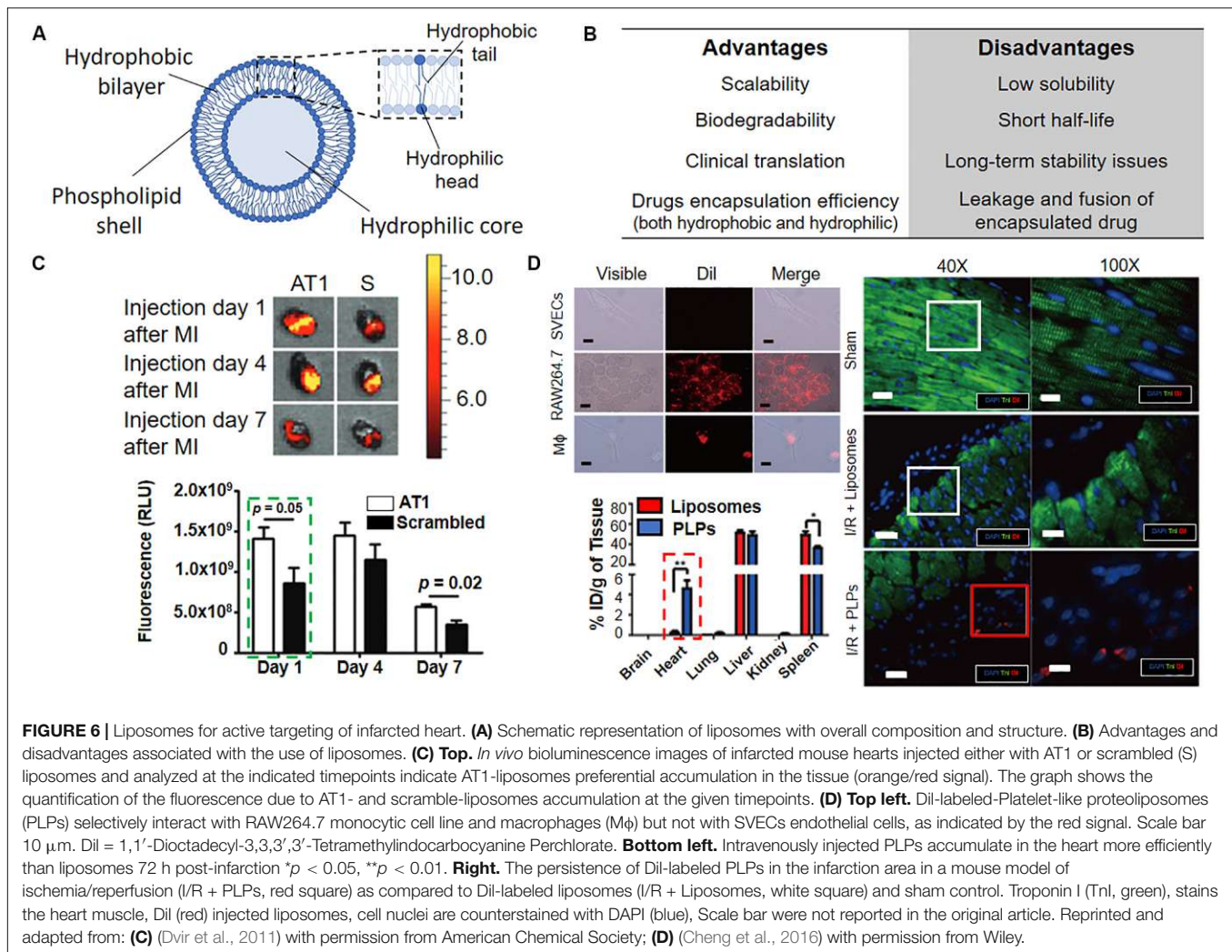
Along with the efforts spent for developing therapeutic nanomaterials, NPs can also be designed as diagnostic tools allowing for superior performance in imaging cardiomyocytes in the failing heart or to monitor the progress of therapeutic protocols. Among the diagnostic techniques available at present, photoacoustic imaging (PAI) is a non-invasive diagnostic tool which provides high sensitivity and helps overcoming the limited depth penetration and spatial resolution of the conventional optical imaging (Wang and Hu, 2012). In order to increase the image contrast when using this technique, nanoparticles have been successfully employed as contrast agent material (Calcagno et al., 2019).

Qin et al. (2018) recently reported the use of NPs composed by a semiconductor polymeric contrast agent (PCPDTBT) encapsulated in a FDA approved lipid-based copolymer (DSPE-PEG-Maleimide). NPs functionalized with cell-penetrating peptide (CPP) were able to target and label hECSs-derived cardiomyocytes (hECS-CM). This labeling technique was suitable for cell detection using PAI both *ex vivo* and *in vivo*. In the latter case, the resolution obtained was as low as 2,000 injected cells, twenty-five times lower than what can be achieved with fluorescent imaging. Photoacoustic imaging was also successfully applied to monitor hECS-CMs transplantation in living mouse heart. Although being able to detect NPs-labeled cells, PAI sensitivity was lower for imaging the host myocardium, as recognized by the same authors. Nevertheless, this strategy holds great promises for monitoring cardiac regenerative processes and for live imaging of heart in the future. However, its application in monitoring cardiac disease and cardiac regeneration is still poorly investigated.

Despite the invaluable properties of polymeric NPs, their toxicity and biodegradability have to be carefully considered during their design. The use of non-biodegradable polymers has been associated with chronic toxicity and, as general warning, the long-term toxicity of these materials is still largely unknown (Banik et al., 2016). Consequently, the use of well-know and established biocompatible polymers is instead more likely to facilitate and improve the clinical translation of polymeric NPs (Ferrari et al., 2018).

LIPOSOMES

Another type of widely studied carrier for drug delivery/transfection applications is represented by liposomes (Figures 6A,B). Liposomes are artificial vesicles of phospholipids and cholesterol mixture, able to encapsulate drugs, proteins/peptides, and DNA (Akbarzadeh et al., 2013). Although they may face long-term stability issues in blood circulation, liposomes are extremely interesting for their cost-effective and



scalable synthesis. These features have favored their clinical development (Doxil was the first FDA-approved nanodrug) as compared to other kinds of NPs (Sercombe et al., 2015). One of the first examples of liposomes applied to cardiomyopathy treatment was represented by anti-P-selectin-conjugated liposomes containing VEGF, as reported by Scott et al. (2009). The authors attempted to enhance neovascularization in a rat model of myocardial infarction. Targeted delivery through P-selectin antibody, overexpressed at the infarcted inflammatory site, promoted the selective and efficient delivery of VEGF, thus enhancing the fractional shortening and systolic function, with a 21% increase in anatomical vessels and 74% increase in perfused vessels in MI area. Conversely, systemic administration of VEGF resulted in no significant improvement in cardiac function.

In another study, PEGylated liposomes containing a targeting ligand against angiotensin II type 1 (AT1), a receptor which is widely expressed in infarcted heart were reported (Figure 6C; Dvir et al., 2011). *In vivo* experiments have confirmed particles accumulation in the left ventricle after MI (48% within 24 h post-i.v. injection), thus revealing a specific delivery at injured myocardium. No detail on the functional therapeutic cardiac

regeneration potential of the nanovector was given, as the main rationale of the authors was to demonstrate the targeting efficiency of NPs at the heart after MI. Nevertheless, this study provides crucial information for understanding the accumulation of NP-based system at the diseased heart, as discussed below.

The use of liposomes for targeting the immune system cells, which regulates the inflammatory response at the infarcted heart, has also been studied. Targeting the immune system cells at the site of inflammation can be indeed an alternative and effective solution for increasing the targeting and delivery of NP-based therapy, due to the natural tendency of the innate components to recognize and internalize external materials administered in the body such as nanoparticles (Fadeel, 2019). The group of Cohen S. reported the use of phosphatidylserine (PS)-presenting liposomes, mimicking the anti-inflammatory effects of apoptotic cells (Harel-Adar et al., 2011). The uptake of PS-liposome induced the secretion by macrophages of high levels of anti-inflammatory cytokines (i.e., TGFβ and interleukin 10, IL-10) both *in vitro* and *in vivo*. The i.v. injection in a rat model of acute MI promoted angiogenesis, while preserving small scars and preventing ventricular dilatation and remodeling.

More recently, an alternative approach was presented by Cheng and collaborators (**Figure 6D**; Cheng et al., 2016). The authors developed biomimicking platelet-like proteoliposomes able to interact with monocytes. This methodology foresees the interaction between the immune system cells and platelet membrane proteins (PMPs) for promoting the accumulation of liposomes at the injured heart, where monocytes are recruited. Proteoliposomes were loaded with therapeutic cobalt protoporphyrin IX (CoPP), a compound able to suppress the inflammatory activity of macrophages and were “dragged” by the monocytes to the infarcted zone. This system showed promising results *in vivo* when compared to systemic administration of free CoPP. However, the randomization of the surface coating may jeopardize the reproducibility of this synthetic technique, as raw material, i.e., the PMPs derived from different samples or batches, could give different results in term of composition and biophysical features of the final particles. Moreover, the poor understanding of the interaction with monocytes, which can reduce the effective control over this mechanism, makes the clinical translation of proteoliposomes unlikely.

Furthermore, the group of Schifflers have developed a liposomal carrier for berberine delivery, a natural product which is known for its anti-inflammatory, anti-oxidative and cardio-protective functions (Allijn et al., 2017). In its free form, berberine is poorly soluble in aqueous medium and have a short half-life time in circulation. The liposomes encapsulated with the drug tested *in vivo* in C57BL/6J mice showed to preserve the cardiac function by 64% at day 28 post-MI, in comparison to control liposomes and free drug. Liposomes administered I.V. targeted the inflammatory site and release the drug after macrophage uptake, reducing both inflammatory damage and systemic adverse effects. This study appears particularly promising because of the reproducible synthesis of the liposome formulation and for its effective targeting and long-term stability.

So far, liposomes have been the most tested NP-based system in clinical trials, encountering several cases of successful clinical translation, and many liposome formulations are currently available on the market for several therapies (Bulbake et al., 2017). However, their application in heart diseases therapy is still limited and needs further investigation.

INORGANIC NANOPARTICLES

Inorganic NPs are known for exhibiting appealing physical properties that can be potentially exploited for simultaneous diagnosis and therapy (i.e. theranostic) of several pathologies (**Figures 7A,B**; Giner-Casares et al., 2016). They are generally composed by an inorganic core surrounded by an organic/inorganic shell, which aim to increase the biocompatibility of the system and the interactions of the NP with the biological environment (Conde et al., 2014). Recently, Popara et al. (2018) showed that SiO₂-NPs passively interacted with human MSCs (hMSCs) mediating important molecular processes (**Figure 7C**; Popara et al., 2018). More

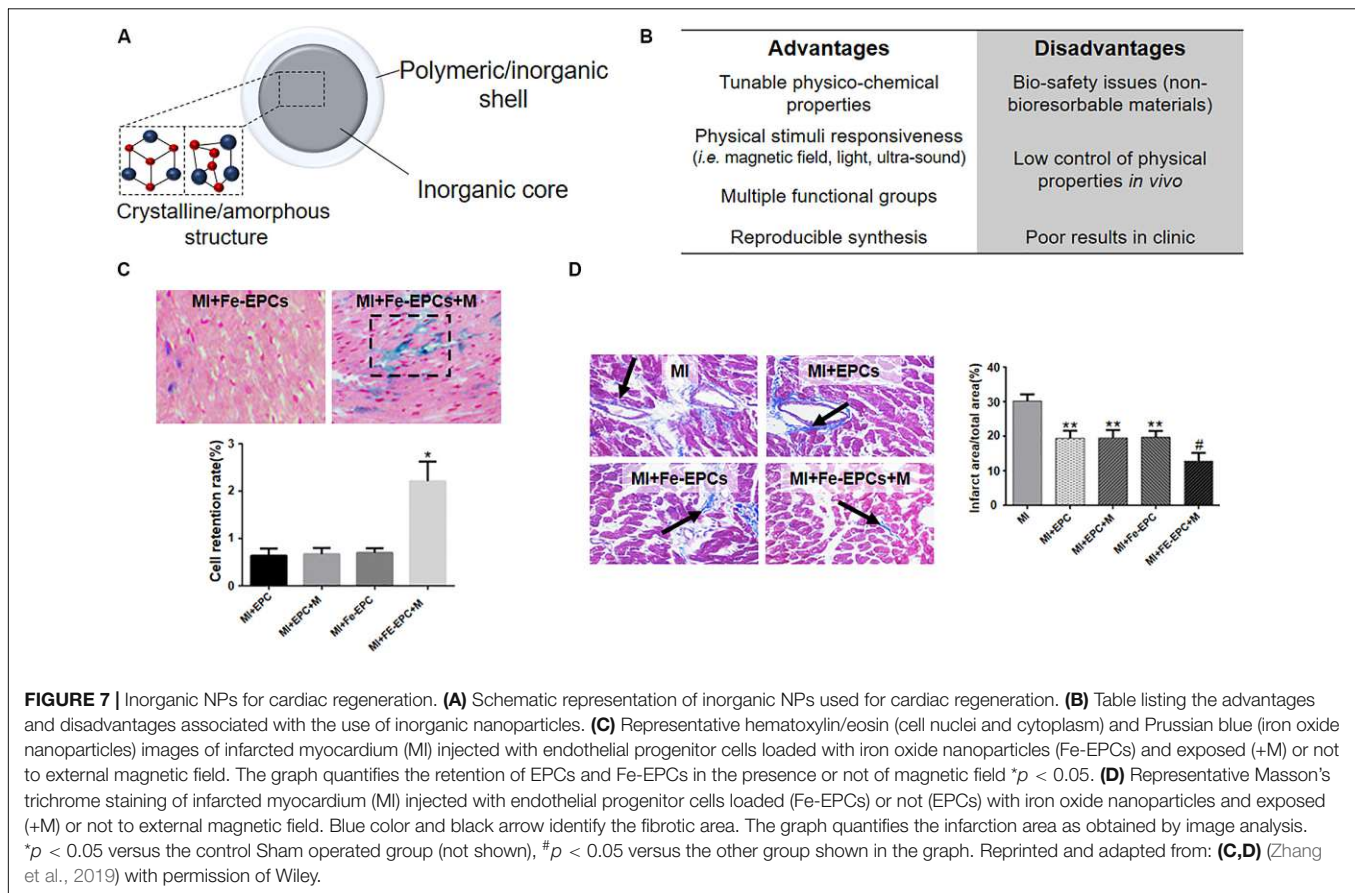
specifically, the internalization of the SiO₂-NPs affected focal adhesions by promoting cell adhesive phenotype both *in vitro* and *ex vivo* upon injection in the infarcted rat heart. In addition, NPs internalization contributed to cell cross-talk between transplanted cells and the host, which is essential for an effective engraftment and tissue regeneration. However, the transient inhibition of lysosomal function by SiO₂-NPs was reported, pointing out the need for a thorough evaluation of NPs long-term toxicity and possible side effects due to their sustained intracellular accumulation (Croissant et al., 2017).

Biodegradable inorganic particles have been also proposed to improve myocardial function after heart failure (Miragoli et al., 2018). Miragoli and co-workers demonstrated that biodegradable negatively charged calcium phosphate NPs (CaP-NPs) accumulated at the myocardium 60 min after inhalation in a mice model. The NPs functionalized with a non-penetrating mimetic peptide (NPs-MP) were shown to cross the alveolar-capillary barrier in the lung and translocate to the myocardium where the loaded peptide can be release for therapy. Despite the great potential, there are still some limitations to the use of such therapy. One above all, the mechanisms through which the NPs cross alveolar-capillary barrier are still unclear and unlikely to be accepted for clinical translation.

Interestingly, also the exploitation of hybrid materials, i.e., NPs composed by different inorganic core-shell structures, have been reported. Zhang et al. (2019) described the use of silica-coated magnetic nanoparticles for labeling endothelial progenitor cells (EPCs) for their magnetic guidance at the ischemic heart (**Figure 7D**), since EPCs are the most used cells for cell therapy after MI due to their mobilization, homing, and angiogenic effects (Zhang et al., 2019). In this study the authors showed the increased retention of EPCs at the infarcted border zone and the consequent attenuation of myocardial apoptosis associated to improved remodeling and cardiac function. Nevertheless, the evidenced improvements only lasted for a very limited term, claiming for the necessity of multiple administrations of the NP-cell system and possibly limiting the advantages obtainable with a NP-based therapy in comparison with other treatments.

Iron oxide nanoparticles have also been investigated as cardioprotective agents, as shown by Xiong et al. (2015). The authors demonstrated the potential of maghemite NPs for protecting the heart from ischemic damage both *in vivo* and *in vitro*. More specifically, Fe₂O₃ NPs coated with dimercaptosuccinic acid (DMSA) were demonstrated to efficiently inhibit calcium influx, which is responsible for the reactive oxygen species (ROS) production, therefore decreasing the peroxidation injury of membrane lipids. In addition, these NPs were able to increase the level of S-nitrosothiols and then to participate in nitric oxide (NO)-mediated protection against ischemia and reperfusion injury. However, the mechanisms which regulate the crosstalk between ROS, NO and calcium influx pathways and NPs remain unknown and possible long-term side effects of this activity has not been elucidated.

Diagnostic tools were also developed using inorganic nanoparticles. In particular, gold nanoparticles have been demonstrated to be promising tools for computed tomography (CT), an X-ray-based image diagnostic technique able to



exploit the differences in the absorption from different human tissues in order to produce images of body structures and tissues (Xi et al., 2012). In this context, Kee and Danila (2018) reported the use of gold nanoparticles coated with collagen-binding adhesion protein 35 (CNA35) for CT imaging of infarcted heart at molecular level. Thanks to their ability to target collagen I, abundant at myocardial scar, CNA35-Au NPs were able to enhance the signal from the infarcted site at 6 h after injection. Conversely, no detectable enhancement was noted when non-functionalized AuNPs was injected into rats with or without MI or CNA35-AuNPs in control rats without MI. These results highlighted the preferable use of gold nanoparticles as contrast agents compare to iodinated agents in terms of functionalization and blood circulation time, which ultimately could improve the *in vivo* targeting and detection of infarcted heart. However, some issues such as the relatively high amount of nanoparticles required and the inefficiency to enhance the contrast of the entire infarcted area may wane the application of Au NPs for CT-imaging, as stated by the same authors.

Currently, several clinical trials using inorganic nanoparticles are under investigation for applications in cardiovascular diseases (U.S. National Library of Medicine, 2020b). However, with regard to MI, only magnetic resonance imaging (MRI) applications were assessed, mainly *via* Ferumoxytol – a ultrasmall superparamagnetic iron oxide nanoparticles

(USPIO) formulation – and all of them were discontinued or did not provide acceptable outcomes (U.S. National Library of Medicine, 2013, 2014a,b). Indeed, as far as we know, the overall application of this kind of nanoparticles for MRI did not obtained the expected results and Ferumoxytol is now only used as iron replacement therapy for deficiency anemia in adult patient with chronic kidney diseases (Bobo et al., 2016).

Consequently, despite the long-dated use of inorganic nanoparticles in nanomedical applications, relatively few examples were reported for cardiac regeneration purposes and efficient clinical translation is still missing.

NANOMEDICINE IN CARDIAC REGENERATION: WHERE ARE WE HEADING TO?

Multi-therapies aiming to combine the regeneration potential of undifferentiated cells, the *in situ* reprogramming of cardiac fibroblasts and the simultaneous release of drugs appear promising, especially when fueled by the potential of cell-based therapies. Indeed, the use of different smart nanomaterials in combination with other technologies may lead to the development of advanced therapeutic strategies, which may strengthen the applicability of nanomedicine in the treatment of cardiac diseases.

As an example, hiPSC-derived cardiomyocytes (hiPSC-CMs) were recently combined with injectable nanostructured hydrogels loaded with erythropoietin (EPO), resulting in reduced cell death and increased remodeling post-MI (Chow et al., 2017). Also, injectable biomaterials have been used as stand-alone scaffolds for promoting endogenous repair or delivering therapeutics such as cells, growth factors or small molecules.

In this context, Nguyen et al. (2015) used matrix metalloproteinase (MMP)-responsive hydrogels that displayed the ability to be retained at the infarcted site upon enzymatically triggered bio-transformation, thus being potentially suitable for the sustained delivery of therapeutic molecules. Another recently developed strategy called *THEREPI* relies on the use of a biocompatible patch, which is placed epicardially at the border zone of the infarcted heart to achieve the sustained delivery of drugs, macromolecules and possibly cells for cardiac therapy (Whyte et al., 2018). Ideally, *THEREPI* can be efficiently used for the *in situ* administration of therapeutic nanoparticles, thus increasing their retention at the diseased site and improving cargo delivery.

In the case of ischemic cardiomyopathies, improved cargo delivery can be potentially obtained by relying on the enhanced permeability and retention effect (EPR). Similar to the blood vessels originated during tumor development, also those formed at the initial stages after MI are typically aberrant, marked by capillary sprouting, excessive vessels branching, abnormal levels of endothelial cell proliferation, distorted and enlarged vessels, resulting in weak and leaky vasculature (Paulis et al., 2012; Lundy et al., 2016). For those reasons, EPR phenomenon has been exploited for promoting the targeting of NPs at the diseased area, limiting their accumulation in healthy tissues (Golombek et al., 2018). However, while EPR occurring at tumor sites has shown poorly reproducible results, thus jeopardizing the applicability of NPs to cancer therapy (Danhier, 2016), the same phenomenon has been proven to be stable and reproducible following MI in the heart (Weis, 2008). Although mature fibrotic scar is known to be poorly vascularized (van der Meel et al., 2017) the exploitation of EPR phenomenon in the heart, soon after infarction, appears as a promising approach to be translated to the clinics in future for MI treatment (Kalyane et al., 2019).

Besides the pursue of innovative materials and strategies for enhancing therapeutics delivery, the investigation of new pathways involved in cardiac homeostasis is of utmost importance, due to the possibility to target their components for ultimately improving therapeutic outcomes, hence delaying or reversing cardiac dysfunction. In particular, the modulation of cardiac metabolism, gene expression, pharmacological therapy and miRNA-mediated regulatory network represent new and appealing opportunities for the treatment of cardiovascular diseases (Rochette et al., 2015).

In this direction, Hippo pathway has emerged as a possible switch in cardiomyocyte proliferation (Torrini et al., 2019), being tightly connected to the onset and progression of cardiomyopathies (Clippinger et al., 2019), as explained above. Its specific manipulation in the contractile figures of the heart may become a novel therapeutic option for treating cardiac diseases. Nevertheless, to the best of our knowledge, the only

NP-based formulation for targeting YAP is at present represented by siRNA-lipid nanoparticles for silencing the protein expression in hepatocellular carcinoma cells and promote tumor regression (Fitamant et al., 2015). Therefore, research for developing NPs able to modulate the YAP activity in cardiomyocytes is at its infancy and may revolutionize the treatment of cardiac diseases and the applicability of NPs in the near future.

Furthermore, it is worth to highlight the potential held by gene editing in the restoration of cardiac function. The discovery that the clustered regularly interspaced short palindromic repeats (CRISPR)/CRISPR-associated (Cas) system could be used to introduce sequence-specific dsDNA cleavage in human cells has revolutionized the research worldwide (Jinek et al., 2012). CRISPR is involved in bacteria and archaea's adaptive immune system against viruses and their engineering for biological applications has enabled their application in different areas of investigations (Doudna and Charpentier, 2014). Nanomedicine-related sciences are of course included in this development and different systems have been engineered for carrying CRISPR/CAS9 machinery components and guide the genetic reprogramming inside the cells, based on lipid and inorganic nanoparticles (Lee et al., 2017; Liu et al., 2019). Therefore, although the exploitation of this technique in nanomedicine applied to cardiac regeneration can be attractive in the case of genetically-determined cardiomyopathies, technical challenges connected to its specificity must be considered. Indeed, while few studies have already shown that cardiomyocytes can be edited in the post-natal murine heart by CRISPR/Cas9 system components, the efficiency and safety of this strategy is still far from being characterized (Carroll and Olson, 2017). Moreover, the carriage of multiple components (Cas9 ribonucleoprotein, donor DNA and guide RNA) required for this therapy need complex nanoparticle-based systems, hardly scalable and possibly expensive.

Finally, in developing new therapies it is important to consider more practically physiological-like tissue models, not only for a more effective *in vitro* to *in vivo* transition of pharmacological studies, but also for disease modeling and studying the potential toxicity of nanomaterials. Traditional pre-clinical screenings are either made with monolayer cells on top of two dimensional (2D) and often rigid substrates, or in animal models which may not always reflect the human physiology precisely. Instead, a promising strategy to overcome these limitations involves utilizing organ-on-a-chip technologies, where recent microfluidic advances are combined with complex three-dimensional (3D) cell biology that provides organ-like physiology and pathophysiological cellular and tissue level responses (Ergir et al., 2018; Rothbauer et al., 2019).

CONCLUSION

Despite any progresses based on healthier life styles, cardiovascular diseases remain the major cause of death globally, according to the WHO (World Health Organization, 2019). Therefore, the development of new therapies to induce cardiac protection and repair are required to help reducing

undesirable drugs' side effects and ultimately improving the life quality of the patient.

In this scenario, material scientists need to exploit the physico-chemical properties of nanomaterials to develop suitable nanotools for smart delivery, targeting proteins and pathways involved in cardiomyocytes protection, differentiation and/or proliferation. Notwithstanding the great progresses made in the direction of a clearer comprehension of the nanoparticles behavior in biological environments, major challenges remain (Heath, 2015). The bioavailability, accumulation at the desired site and efficient release of the therapeutic cargo are just a small part of the challenges nanodrugs must face once administered to the body.

The poor understanding of the biological barriers, the misinterpretation of drug delivery concepts, the cost-effectiveness, manufacturing, scaling up, and regulatory issues have affected the clinical translation of nanomedicine so far, as well as its application for cardiac regeneration purposes (van der Meel et al., 2017).

Different NP-based systems were developed aiming to restore heart function. However, it is still difficult to deduct general guidelines describing the type of material, the class of drugs, the targeting strategies that may be more promising for the given purpose. The successes liposomes obtained in clinical outcomes and in different applications, make them suitable candidates for the treatment of cardiac diseases. However, it is undeniable that polymeric materials display higher tunable properties combined to superior capability of accommodating cargos.

Therefore, nanotechnologists, together with cell/molecular biologists and clinicians, have the duty of finding a

common ground with pharmaceutical companies in order to bring potential therapeutic nanomedical devices for cardiac regeneration closer to their clinical translation.

AUTHOR CONTRIBUTIONS

MC proposed the subject and conceived the general structure of the review. MC and SF revised the existing literature regarding nanomedicine and the use of nanoparticles for cardiac regeneration. JV revised the literature on miRNAs involved in cardiac development and repair. EE revised the literature on cardiac diseases biology. MC and SF wrote the manuscript. FC and GF revised the text and contributed to the discussion and conclusion.

FUNDING

The work was supported by the European Regional Development Fund-Project MAGNET (No. CZ.02.1.01/0.0/0.0/15_003/0000492) and by the European Union Horizon 2020 Research and Innovation Programme under the Marie Skłodowska-Curie grant agreement no. 690901.

ACKNOWLEDGMENTS

We would like to thank Mrs. Romana Vlckova, Helena Durikova, Sabina Gomelska, Hana Zpevakova, Jana Vasickova, and Jana Bartonova for continuous support.

REFERENCES

- Akbarzadeh, A., Rezaei-Sadabady, R., Davaran, S., Joo, S. W., Zarghami, N., Hanifehpour, Y., et al. (2013). Liposome: classification, preparation, and applications. *Nanoscale Res. Lett.* 8:102.
- Alfares, A. A., Kelly, M. A., McDermott, G., Funke, B. H., Lebo, M. S., Baxter, S. B., et al. (2015). Results of clinical genetic testing of 2,912 probands with hypertrophic cardiomyopathy: expanded panels offer limited additional sensitivity. *Genet. Med.* 17:880. doi: 10.1038/gim.2014.205
- Allijn, I. E., Czarny, B. M. S., Wang, X., Chong, S. Y., Weiler, M., da Silva, A. E., et al. (2017). Liposome encapsulated berberine treatment attenuates cardiac dysfunction after myocardial infarction. *J. Control. Release* 247, 127–133. doi: 10.1016/j.jconrel.2016.12.042
- Amezcuca, R., Shirolkar, A., Frazee, C., and Stout, D. A. (2016). Nanomaterials for cardiac myocyte tissue engineering. *Nanomaterials (Basel)* 6:133. doi: 10.3390/nano6070133
- Bae, S. J., Ni, L., Osinski, A., Tomchick, D. R., Brautigam, C. A., and Luo, X. (2017). SAV1 promotes Hippo kinase activation through antagonizing the PP2A phosphatase STRIPAK. *Elife* 6:e30278.
- Banerjee, M. N., Bolli, R., and Hare, J. M. (2018). Clinical studies of cell therapy in cardiovascular medicine recent developments and future directions. *Circ. Res.* 123, 266–287. doi: 10.1161/circresaha.118.311217
- Banik, B. L., Fattahi, P., and Brown, J. L. (2016). Polymeric nanoparticles: the future of nanomedicine. *Wiley Interdiscipl. Rev. Nanomed. Nanobiotechnol.* 8, 271–299. doi: 10.1002/wnan.1364
- Bartel, D. P. (2009). MicroRNAs: target recognition and regulatory functions. *Cell* 136, 215–233. doi: 10.1016/j.cell.2009.01.002
- Bartunek, J., Terzic, A., Davison, B. A., Filipatos, G. S., Radovanovic, S., Beleslin, B., et al. (2017). Cardiopoietic cell therapy for advanced ischaemic heart

- failure: results at 39 weeks of the prospective, randomized, double blind, sham-controlled CHART-1 clinical trial. *Eur. Heart J.* 38, 648–660.
- Behfar, A., Crespo-Diaz, R., Terzic, A., and Gersh, B. J. (2014). Cell therapy for cardiac repair—lessons from clinical trials. *Nat. Rev. Cardiol.* 11, 232–246. doi: 10.1038/nrcardio.2014.9
- Bejerano, T., Etzion, S., Elyagon, S., Etzion, Y., and Cohen, S. (2018). Nanoparticle delivery of miRNA-21 mimic to cardiac macrophages improves myocardial remodeling after myocardial infarction. *Nano Lett.* 18, 5885–5891. doi: 10.1021/acs.nanolett.8b02578
- Bergmann, O., Bhardwaj, R. D., Bernard, S., Zdunek, S., Barnabé-Heider, F., Walsh, S., et al. (2009). Evidence for cardiomyocyte renewal in humans. *Science* 324, 98–102. doi: 10.1126/science.1164680
- Bobo, D., Robinson, K. J., Islam, J., Thurecht, K. J., and Corrie, S. R. (2016). Nanoparticle-based medicines: a review of FDA-approved materials and clinical trials to date. *Pharm. Res.* 33, 2373–2387. doi: 10.1007/s11095-016-1958-5
- Bonauer, A., Carmona, G., Iwasaki, M., Mione, M., Koyanagi, M., Fischer, A., et al. (2009). MicroRNA-92a controls angiogenesis and functional recovery of ischemic tissues in mice. *Science* 324, 1710–1713. doi: 10.1126/science.1174381
- Boon, R. A., Iekushi, K., Lechner, S., Seeger, T., Fischer, A., Heydt, S., et al. (2013). MicroRNA-34a regulates cardiac ageing and function. *Nature* 495:107. doi: 10.1038/nature11919
- Boon, R. A., and Vickers, K. C. (2013). Intercellular transport of microRNAs. *Arterioscler. Thrombos. Vasc. Biol.* 33, 186–192. doi: 10.1161/atvbaha.112.300139
- Boopathy, G. T. K., and Hong, W. (2019). Role of hippo pathway-YAP/TAZ signaling in angiogenesis. *Front. Cell Dev. Biol.* 7:49. doi: 10.3389/fcell.2019.00049
- Borow, K. M., Yaroshinsky, A., Greenberg, B., and Perin, E. C. (2019). Phase 3 DREAM-HF trial of mesenchymal precursor cells in chronic heart failure. *Circ. Res.* 125, 265–281. doi: 10.1161/circresaha.119.314951

- Botting, K., Wang, K., Padhee, M., McMillen, I., Summers-Pearce, B., Rattanaraj, L., et al. (2012). Early origins of heart disease: low birth weight and determinants of cardiomyocyte endowment. *Clin. Exp. Pharmacol. Physiol.* 39, 814–823. doi: 10.1111/j.1440-1681.2011.05649.x
- Boverhof, D. R., Bramante, C. M., Butala, J. H., Clancy, S. F., Lafranconi, M., West, J., et al. (2015). Comparative assessment of nanomaterial definitions and safety evaluation considerations. *Regul. Toxicol. Pharmacol.* 73, 137–150. doi: 10.1016/j.yrtph.2015.06.001
- Braunwald, E. (2017). Cardiomyopathies. *Circ. Res.* 121, 711–721.
- Briceno, N., Schuster, A., Lumley, M., and Perera, D. (2016). Ischaemic cardiomyopathy: pathophysiology, assessment and the role of revascularisation. *Heart* 102, 397–406. doi: 10.1136/heartjnl-2015-308037
- Bulbake, U., Doppalapudi, S., Kommineni, N., and Khan, W. (2017). Liposomal formulations in clinical use: an updated review. *Pharmaceutics* 9:12. doi: 10.3390/pharmaceutics9020012
- Burke, M. A., Cook, S. A., Seidman, J. G., and Seidman, C. E. (2016). Clinical and mechanistic insights into the genetics of cardiomyopathy. *J. Am. Coll. Cardiol.* 68, 2871–2886. doi: 10.1016/j.jacc.2016.08.079
- Butler, J., Epstein, S. E., Greene, S. J., Quyyumi, A. A., Sikora, S., Kim, R. J., et al. (2017). Intravenous allogeneic mesenchymal stem cells for nonischemic cardiomyopathy safety and efficacy results of a phase II-A randomized trial. *Circ. Res.* 120, 332–340. doi: 10.1161/circresaha.116.309717
- Cahill, T. J., Ashrafian, H., and Watkins, H. (2013). Genetic cardiomyopathies causing heart failure. *ESC Heart Fail* 113, 660–675. doi: 10.1161/circresaha.113.300282
- Calcagno, V., Vecchione, R., Quagliarello, V., Marzola, P., Busato, A., Giustetto, P., et al. (2019). Oil core-PEG shell nanocarriers for in vivo MRI imaging. *Adv. Healthc. Mater.* 8:1801313. doi: 10.1002/adhm.201801313
- Callis, T. E., Pandya, K., Seok, H. Y., Tang, R.-H., Tatsuguchi, M., Huang, Z.-P., et al. (2009). MicroRNA-208a is a regulator of cardiac hypertrophy and conduction in mice. *J. Clin. Investig.* 119, 2772–2786. doi: 10.1172/jci36154
- Cannon, C. P., Blazing, M. A., Giugliano, R. P., McCagg, A., White, J. A., Theroux, P., et al. (2015). Ezetimibe added to statin therapy after acute coronary syndromes. *N. Engl. J. Med.* 372, 2387–2397.
- Cao, N., Huang, Y., Zheng, J., Spencer, C. I., Zhang, Y., Fu, J.-D., et al. (2016). Conversion of human fibroblasts into functional cardiomyocytes by small molecules. *Science* 352, 1216–1220. doi: 10.1126/science.aaf1502
- Carè, A., Catalucci, D., Felicetti, F., Bonci, D., Addario, A., Gallo, P., et al. (2007). MicroRNA-133 controls cardiac hypertrophy. *Nat. Med.* 13, 613–618.
- Carroll, K. J., and Olson, E. N. (2017). Considerations for cardiac CRISPR. *Circ. Res.* 121, 1111–1112. doi: 10.1161/circresaha.117.311974
- Chamberlain, K., Riyad, J. M., and Weber, T. (2017). Cardiac gene therapy with adeno-associated virus-based vectors. *Curr. Opin. Cardiol.* 32, 275–282.
- Chan, K., Harper, A. R., Ashrafian, H., and Yavari, A. (2018). Cardiomyopathies. *Medicine* 46, 606–617.
- Chandarana, M., Curtis, A., and Hoskins, C. J. A. N. (2018). The use of nanotechnology in cardiovascular disease. *Nanomedicine* 8, 1607–1619. doi: 10.1007/s13204-018-0856-z
- Chen, C., Seeger, T., Termglinchan, V., and Karakikes, I. (2017). Recent advances in cardiac gene therapy strategies targeting advanced heart failure. *Continu. Cardiol. Educ.* 3, 163–169. doi: 10.1002/cce2.68
- Chen, Y.-A., Lu, C.-Y., Cheng, T.-Y., Pan, S.-H., Chen, H.-F., and Chang, N.-S. (2019). WW domain-containing proteins YAP and TAZ in the hippo pathway as key regulators in stemness maintenance, tissue homeostasis, and tumorigenesis. *Front. Oncol.* 9:60. doi: 10.3389/fonc.2019.00060
- Cheng, B., Toh, E. K. W., Chen, K.-H., Chang, Y.-C., Hu, C.-M. J., Wu, H.-C., et al. (2016). Biomimicking platelet-monocyte interactions as a novel targeting strategy for heart healing. *Adv. Healthc. Mater.* 5, 2686–2697. doi: 10.1002/adhm.201600724
- Chenthamara, D., Subramaniam, S., Ramakrishnan, S. G., Krishnaswamy, S., Essa, M. M., Lin, F.-H., et al. (2019). Therapeutic efficacy of nanoparticles and routes of administration. *Biomater. Res.* 23:20.
- Chiavacci, E., Dolfi, L., Verduci, L., Meghini, F., Gestri, G., Evangelista, A. M. M., et al. (2012). MicroRNA 218 mediates the effects of Tbx5a over-expression on zebrafish heart development. *PLoS ONE* 7:e50536. doi: 10.1371/journal.pone.0050536
- Chow, A., Stuckey, D. J., Kidher, E., Rocco, M., Jabbar, R. J., Mansfield, C. A., et al. (2017). Human induced pluripotent stem cell-derived cardiomyocyte encapsulating bioactive hydrogels improve rat heart function post myocardial infarction. *Stem Cell Rep.* 9, 1415–1422. doi: 10.1016/j.stemcr.2017.09.003
- Cianflone, E., Aquila, I., Scalise, M., Marotta, P., Torella, M., Nadal-Ginard, B., et al. (2018). Molecular basis of functional myogenic specification of Bona Fide multipotent adult cardiac stem cells. *Cell Cycle* 17, 927–946. doi: 10.1080/15384101.2018.1464852
- Clippinger, S. R., Cloonan, P. E., Greenberg, L., Ernst, M., Stump, W. T., and Greenberg, M. J. (2019). Disrupted mechanobiology links the molecular and cellular phenotypes in familial dilated cardiomyopathy. *Proc. Natl. Acad. Sci. U.S.A.* 116, 17831–17840. doi: 10.1073/pnas.1910962116
- Colegrave, M., and Peckham, M. (2014). Structural implications of β -cardiac myosin heavy chain mutations in human disease. *Anatom. Rec.* 297, 1670–1680. doi: 10.1002/ar.22973
- Conde, J., Dias, J. T., Grz  , V., Moros, M., Baptista, P. V., and de la Fuente, J. M. (2014). Revisiting 30 years of biofunctionalization and surface chemistry of inorganic nanoparticles for nanomedicine. *Front. Chem.* 2:48. doi: 10.3389/fchem.2014.00048
- Croissant, J. G., Fatieiev, Y., and Khashab, N. M. (2017). Degradability and clearance of silicon, organosilica, silsesquioxane, silica mixed oxide, and mesoporous silica nanoparticles. *Adv. Mater.* 29:1604634. doi: 10.1002/adma.201604634
- Danhier, F. (2016). To exploit the tumor microenvironment: since the EPR effect fails in the clinic, what is the future of nanomedicine? *J. Control. Release* 244, 108–121. doi: 10.1016/j.jconrel.2016.11.015
- Davis, M. E., Chen, Z. G., and Shin, D. M. (2008). Nanoparticle therapeutics: an emerging treatment modality for cancer. *Nat. Rev. Drug Discov.* 7, 771–782. doi: 10.1038/nrd2614
- Dhulipala, V., Bezwada, P., Gottimukkula, R., and Abboud, J. (2018). Stress-induced cardiomyopathy: as a diagnosis that is time sensitive and anticipative in certain individuals. *Case Rep. Cardiol.* 2018:4.
- Dib, N., Khawaja, H., Varner, S., McCarthy, M., and Campbell, A. (2011). Cell therapy for cardiovascular disease: a comparison of methods of delivery. *J. Cardiovasc. Transl. Res.* 4, 177–181. doi: 10.1007/s12265-010-9253-z
- Din, F. U., Aman, W., Ullah, I., Qureshi, O. S., Mustapha, O., Shafique, S., et al. (2017). Effective use of nanocarriers as drug delivery systems for the treatment of selected tumors. *Int. J. Nanomed.* 12, 7291–7309. doi: 10.2147/ijn.s146315
- Dirkx, E., Gladka, M. M., Philippen, L. E., Armand, A.-S., Kinet, V., Leptidis, S., et al. (2013). Nfat and miR-25 cooperate to reactivate the transcription factor Hand2 in heart failure. *Nat. Cell Biol.* 15:1282. doi: 10.1038/ncb2866
- Dolan, E. B., Hofmann, B., de Vaal, M. H., Bellavia, G., Straino, S., Kovarova, L., et al. (2019). A bioresorbable biomaterial carrier and passive stabilization device to improve heart function post-myocardial infarction. *Mater. Sci. Eng. C* 103, 109751. doi: 10.1016/j.msec.2019.109751
- Doudna, J. A., and Charpentier, E. (2014). The new frontier of genome engineering with CRISPR-Cas9. *Science* 346:1258096. doi: 10.1126/science.1258096
- Dvir, T., Bauer, M., Schroeder, A., Tsui, J. H., Anderson, D. G., Langer, R., et al. (2011). Nanoparticles targeting the infarcted heart. *Nano Lett.* 11, 4411–4414. doi: 10.1021/nl2025882
- El-Say, K. M., and El-Sawy, H. S. (2017). Polymeric nanoparticles: promising platform for drug delivery. *Int. J. Pharm.* 528, 675–691. doi: 10.1016/j.ijpharm.2017.06.052
- Engel, J. L., and Ardehali, R. (2018). Direct cardiac reprogramming: progress and promise. *Stem Cells Int.* 2018:10.
- England, J., Granados-Riveron, J., Polo-Parada, L., Kuriakose, D., Moore, C., Brook, J. D., et al. (2017). Tropomyosin 1: multiple roles in the developing heart and in the formation of congenital heart defects. *J. Mol. Cell Cardiol.* 106, 1–13. doi: 10.1016/j.yjmcc.2017.03.006
- Epstein, S. E., Kornowski, R., Fuchs, S., and Dvorak, H. F. (2001). Angiogenesis therapy: amidst the hype, the neglected potential for serious side effects. *Circulation* 104, 115–119. doi: 10.1161/01.cir.104.1.115
- Ergir, E., Bachmann, B., Redl, H., Forte, G., and Ertl, P. (2018). Small Force, big impact: next generation organ-on-a-chip systems incorporating biomechanical cues. *Front. Physiol.* 9:1417. doi: 10.3389/fphys.2018.01417
- Eschenhagen, T., Bolli, R., Braun, T., Field, L. J., Fleischmann, B. K., Fris  n, J., et al. (2017). Cardiomyocyte regeneration. *Cells* 136, 680–686.

- Eulalio, A., Mano, M., Ferro, M. D., Zentilin, L., Sinagra, G., Zacchigna, S., et al. (2012). Functional screening identifies miRNAs inducing cardiac regeneration. *Nature* 492:376. doi: 10.1038/nature11739
- Fadeel, B. (2019). Hide and seek: nanomaterial interactions with the immune system. *Front. Immunol.* 10:133. doi: 10.3389/fimmu.2019.00133
- Feringa, H. H. H., van Waning, V. H., Bax, J. J., Elhendy, A., Boersma, E., Schouten, O., et al. (2006). Cardioprotective medication is associated with improved survival in patients with peripheral arterial disease. *J. Am. College Cardiol.* 47, 1182–1187. doi: 10.1016/j.jacc.2005.09.074
- Ferrari, R., Sponchioni, M., Morbidelli, M., and Moscatelli, D. (2018). Polymer nanoparticles for the intravenous delivery of anticancer drugs: the checkpoints on the road from the synthesis to clinical translation. *Nanoscale* 10, 22701–22719. doi: 10.1039/c8nr05933k
- Ferreira, M. P. A., Talman, V., Torrieri, G., Liu, D., Marques, G., Moslova, K., et al. (2018). Dual-drug delivery using dextran-functionalized nanoparticles targeting cardiac fibroblasts for cellular reprogramming. *Adv. Funct. Mater.* 28:1705134. doi: 10.1002/adfm.201705134
- Fish, J. E., Santoro, M. M., Morton, S. U., Yu, S., Yeh, R.-F., Wythe, J. D., et al. (2008). miR-126 regulates angiogenic signaling and vascular integrity. *Dev. Cell* 15, 272–284. doi: 10.1016/j.devcel.2008.07.008
- Fitamant, J., Kottakis, F., Benhamouche, S., Tian, H. S., Chuvin, N., Parachoniak, C. A., et al. (2015). YAP inhibition restores hepatocyte differentiation in advanced HCC, leading to tumor regression. *Cell Rep.* 10, 1692–1707. doi: 10.1016/j.celrep.2015.02.027
- Foglia, M. J., and Poss, K. D. (2016). Building and re-building the heart by cardiomyocyte proliferation. *Development* 143, 729–740. doi: 10.1242/dev.132910
- Fortuni, B., Inose, T., Ricci, M., Fujita, Y., Van Zundert, I., Masuhara, A., et al. (2019). Polymeric engineering of nanoparticles for highly efficient multifunctional drug delivery systems. *Sci. Rep.* 9:2666.
- Fu, Y., Huang, C., Xu, X., Gu, H., Ye, Y., Jiang, C., et al. (2015). Direct reprogramming of mouse fibroblasts into cardiomyocytes with chemical cocktails. *Cell Res.* 25, 1013–1024. doi: 10.1038/cr.2015.99
- Fuchs, S. Y., Spiegelman, V. S., and Suresh Kumar, K. G. (2004). The many faces of β -TrCP E3 ubiquitin ligases: reflections in the magic mirror of cancer. *Oncogene* 23, 2028–2036. doi: 10.1038/sj.onc.1207389
- Gabisonia, K., Prosdocimo, G., Aquaro, G. D., Carlucci, L., Zentilin, L., Secco, I., et al. (2019). MicroRNA therapy stimulates uncontrolled cardiac repair after myocardial infarction in pigs. *Nature* 569, 418–422. doi: 10.1038/s41586-019-1191-6
- Gao, F., Kataoka, M., Liu, N., Liang, T., Huang, Z.-P., Gu, F., et al. (2019). Therapeutic role of miR-19a/19b in cardiac regeneration and protection from myocardial infarction. *Nat. Commun.* 10:1802.
- Gavira, J. J., Nasarre, E., Abizanda, G., Perez-Ilzarbe, M., de Martino-Rodriguez, A., de Jalon, J. A. G., et al. (2010). Repeated implantation of skeletal myoblast in a swine model of chronic myocardial infarction. *Eur. Heart J.* 31, 1013–1021. doi: 10.1093/eurheartj/ehp342
- Giacca, M., and Zacchigna, S. (2015). Harnessing the microRNA pathway for cardiac regeneration. *J. Mol. Cell Cardiol.* 89, 68–74. doi: 10.1016/j.yjmcc.2015.09.017
- Giner-Casares, J. J., Henriksen-Lacey, M., Coronado-Puchau, M., and Liz-Marzán, L. M. (2016). Inorganic nanoparticles for biomedicine: where materials scientists meet medical research. *Mater. Today* 19, 19–28. doi: 10.1016/j.mattod.2015.07.004
- Golombek, S. K., May, J.-N., Theek, B., Appold, L., Drude, N., Kiessling, F., et al. (2018). Tumor targeting via EPR: strategies to enhance patient responses. *Adv. Drug Deliv. Rev.* 130, 17–38. doi: 10.1016/j.addr.2018.07.007
- Guo, X., Fan, C., Tian, L., Liu, Y., Wang, H., Zhao, S., et al. (2017). The clinical features, outcomes and genetic characteristics of hypertrophic cardiomyopathy patients with severe right ventricular hypertrophy. *PLoS One.* 12:e0174118. doi: 10.1371/journal.pone.0174118
- Harel-Adar, T., Mordechai, T. B., Amsalem, Y., Feinberg, M. S., Leor, J., and Cohen, S. (2011). Modulation of cardiac macrophages by phosphatidylserine-presenting liposomes improves infarct repair. *Proc. Natl. Acad. Sci. U.S.A.* 108, 1827–1832. doi: 10.1073/pnas.1015623108
- Hashimoto, H., Olson, E. N., and Bassel-Duby, R. (2018). Therapeutic approaches for cardiac regeneration and repair. *Nat. Rev. Cardiol.* 15, 585–600. doi: 10.1038/s41569-018-0036-6
- Hashmi, S., and Ahmad, H. R. (2019). Molecular switch model for cardiomyocyte proliferation. *Cell Regen. (Lond.)* 8, 12–20. doi: 10.1016/j.cr.2018.11.002
- Hastings, C. L., Roche, E. T., Ruiz-Hernandez, E., Schenke-Layland, K., Walsh, C. J., and Duffy, G. P. (2015). Drug and cell delivery for cardiac regeneration. *Adv. Drug Deliv. Rev.* 84, 85–106. doi: 10.1016/j.addr.2014.08.006
- Heallen, T., Morikawa, Y., Leach, J., Tao, G., Willerson, J. T., Johnson, R. L., et al. (2013). Hippo signaling impedes adult heart regeneration. *Development* 140, 4683–4690. doi: 10.1242/dev.102798
- Heallen, T., Zhang, M., Wang, J., Bonilla-Claudio, M., Klysik, E., Johnson, R. L., et al. (2011). Hippo pathway inhibits wnt signaling to restrain cardiomyocyte proliferation and heart size. *Science* 332, 458–461. doi: 10.1126/science.1199010
- Heart Protection Study Collaborative and Group. (2002). MRC/BHF heart protection study of cholesterol lowering with simvastatin in 20 536 high-risk individuals: a randomised placebocontrolled trial. *Lancet* 360, 7–22. doi: 10.1016/s0140-6736(02)09327-3
- Heath, J. R. (2015). Nanotechnologies for biomedical science and translational medicine. *Proc. Natl. Acad. Sci. U.S.A.* 112, 14436–14443. doi: 10.1073/pnas.1515202112
- Henry, T. D., Annex, B. H., McKendall, G. R., Azrin, M. A., Lopez, J. J., Giordano, F. J., et al. (2003). The VIVA trial. *Circulation* 107, 1359–1365.
- Henry, T. D., Rocha-Singh, K., Isner, J. M., Kereiakes, D. J., Giordano, F. J., Simons, M., et al. (2001). Intracoronary administration of recombinant human vascular endothelial growth factor to patients with coronary artery disease. *Am. Heart J.* 142, 872–880. doi: 10.1067/mhj.2001.118471
- Hershberger, R. E., Hedges, D. J., and Morales, A. (2013). Dilated cardiomyopathy: the complexity of a diverse genetic architecture. *Nat. Rev. Cardiol.* 10, 531–547. doi: 10.1038/nrcardio.2013.105
- Hershberger, R. E., Pinto, J. R., Parks, S. B., Kushner, J. D., Li, D., Ludwigsen, S., et al. (2009). Clinical and functional characterization of TNNT2 mutations identified in patients with dilated cardiomyopathy. *Circulation* 120, 306–313. doi: 10.1161/circgenetics.108.846733
- Huang, W., Feng, Y., Liang, J., Yu, H., Wang, C., Wang, B., et al. (2018). Loss of microRNA-128 promotes cardiomyocyte proliferation and heart regeneration. *Nat. Commun.* 9:700.
- Ieda, M., Fu, J.-D., Delgado-Olguin, P., Vedantham, V., Hayashi, Y., Bruneau, B. G., et al. (2010). Direct reprogramming of fibroblasts into functional cardiomyocytes by defined factors. *Cell* 142, 375–386. doi: 10.1016/j.cell.2010.07.002
- Ikedo, S., Mizushima, W., Sciarretta, S., Abdellatif, M., Zhai, P., Mukai, R., et al. (2019). Hippo deficiency leads to cardiac dysfunction accompanied by cardiomyocyte dedifferentiation during pressure overload. *Circ. Res.* 124, 292–305. doi: 10.1161/circresaha.118.314048
- Isomi, M., Sadahiro, T., and Ieda, M. (2019). Progress and challenge of cardiac regeneration to treat heart failure. *J. Cardiol.* 73, 97–101. doi: 10.1016/j.jjcc.2018.10.002
- Jabir, N. R., Tabrez, S., Ashraf, G. M., Shakil, S., Damanhoury, G. A., and Kamal, M. A. (2012). Nanotechnology-based approaches in anticancer research. *Int. J. Nanomed.* 7, 4391–4408.
- Jain, P., Arava, S., Seth, S., Lalwani, S., and Ray, R. (2017). Histological and morphometric analysis of dilated cardiomyopathy with special reference to collagen IV expression. *Ind. J. Pathol. Microbiol.* 60, 481–486.
- Jayawardena, T. M., Egemnazarov, B., Finch, E. A., Zhang, L., Payne, J. A., Pandya, K., et al. (2012). MicroRNA-mediated in vitro and in vivo direct reprogramming of cardiac fibroblasts to cardiomyocytes. *Circ. Res.* 110, 1465–1473. doi: 10.1161/circresaha.112.269035
- Jinek, M., Chylinski, K., Fonfara, I., Hauer, M., Doudna, J. A., and Charpentier, E. (2012). A programmable dual-RNA-guided DNA endonuclease in adaptive bacterial immunity. *Science* 337, 816–821. doi: 10.1126/science.1225829
- Juul, A., Scheike, T., Davidsen, M., Gyllenberg, J., and Jørgensen, T. (2002). Low serum insulin-like growth factor I is associated with increased risk of ischemic heart disease. *Circulation* 106, 939–944. doi: 10.1161/01.cir.0000027563.44593.cc
- Kakimoto, Y., Tanaka, M., Kamiguchi, H., Hayashi, H., Ochiai, E., and Osawa, M. (2016). MicroRNA deep sequencing reveals chamber-specific miR-208 family

- expression patterns in the human heart. *Int. J. Cardiol.* 211, 43–48. doi: 10.1016/j.ijcard.2016.02.145
- Kalepu, S., and Nekkanti, V. (2015). Insoluble drug delivery strategies: review of recent advances and business prospects. *Acta Pharm. Sin. B* 5, 442–453. doi: 10.1016/j.apsb.2015.07.003
- Kalyane, D., Raval, N., Maheshwari, R., Tambe, V., Kalia, K., and Tekade, R. K. (2019). Employment of enhanced permeability and retention effect (EPR): nanoparticle-based precision tools for targeting of therapeutic and diagnostic agent in cancer. *Mater. Sci. Eng. C* 98, 1252–1276. doi: 10.1016/j.msec.2019.01.066
- Katsuki, S., Matoba, T., Nakashiro, S., Sato, K., Koga J-i, Nakano, K., et al. (2014). Nanoparticle-mediated delivery of pitavastatin inhibits atherosclerotic plaque destabilization/rupture in mice by regulating the recruitment of inflammatory monocytes. *Circulation* 129, 896–906. doi: 10.1161/circulationaha.113.002870
- Kee, P. H., and Danila, D. (2018). CT imaging of myocardial scar burden with CNA35-conjugated gold nanoparticles. *Nanomedicine* 14, 1941–1947. doi: 10.1016/j.nano.2018.06.003
- Kulaberoglu, Y., Lin, K., Holder, M., Gai, Z., Gomez, M., Assefa Shifa, B., et al. (2017). Stable MOB1 interaction with Hippo/MST is not essential for development and tissue growth control. *Nat. Commun.* 8:695.
- Lee, E. J., Baek, M., Gusev, Y., Brackett, D. J., Nuovo, G. J., and Schmittgen, T. D. (2008). Systematic evaluation of microRNA processing patterns in tissues, cell lines, and tumors. *RNA* 14, 35–42. doi: 10.1261/rna.804508
- Lee, K., Conboy, M., Park, H. M., Jiang, F., Kim, H. J., Dewitt, M. A., et al. (2017). Nanoparticle delivery of Cas9 ribonucleoprotein and donor DNA in vivo induces homology-directed DNA repair. *Nat. Biomed. Eng.* 1, 889–901. doi: 10.1038/s41551-017-0137-2
- Lee, S. W. L., Paoletti, C., Campisi, M., Osaki, T., Adriani, G., Kamm, R. D., et al. (2019). MicroRNA delivery through nanoparticles. *J. Control. Release* 313, 80–95. doi: 10.1016/j.jconrel.2019.10.007
- Liu, J., Chang, J., Jiang, Y., Meng, X., Sun, T., Mao, L., et al. (2019). Fast and efficient CRISPR/Cas9 genome editing in vivo enabled by bio-reducible lipid and messenger RNA nanoparticles. *Adv. Mater.* 31:1902575. doi: 10.1002/adma.201902575
- Liu, N., Bezprozvannaya, S., Williams, A. H., Qi, X., Richardson, J. A., Bassel-Duby, R., et al. (2008). microRNA-133a regulates cardiomyocyte proliferation and suppresses smooth muscle gene expression in the heart. *Genes Dev.* 22, 3242–3254. doi: 10.1101/gad.1738708
- Liu, N., Williams, A. H., Kim, Y., McAnally, J., Bezprozvannaya, S., Sutherland, L. B., et al. (2007). An intragenic MEF2-dependent enhancer directs muscle-specific expression of microRNAs 1 and 133. *Proc. Natl. Acad. Sci. U.S.A.* 104, 20844–20849. doi: 10.1073/pnas.0710558105
- Lopes, L. R., Syrris, P., Guttmann, O. P., O'Mahony, C., Tang, H. C., Dalageorgou, C., et al. (2015). Novel genotype-phenotype associations demonstrated by high-throughput sequencing in patients with hypertrophic cardiomyopathy. *Heart* 101, 294–301. doi: 10.1136/heartjnl-2014-306387
- Loyer, X., Potteaux, S., Vion, A.-C., Guérin, C. L., Boulkroun, S., Rautou, P.-E., et al. (2014). Inhibition of MicroRNA-92a prevents endothelial dysfunction and atherosclerosis in mice. *Circ. Res.* 114, 434–443. doi: 10.1161/circresaha.114.302213
- Lu, L., Liu, M., Sun, R., Zheng, Y., and Zhang, P. J. C. B. (2015). Biophysics. *Myocardial Infarct.* 72, 865–867.
- Lundy, D. J., Chen, K.-H., Toh, E. K. W., and Hsieh, P. C. H. (2016). Distribution of systemically administered nanoparticles reveals a size-dependent effect immediately following cardiac ischaemia-reperfusion injury. *Sci. Rep.* 6: 25613.
- Madonna, R., Van Laake, L. W., Davidson, S. M., Engel, F. B., Hausenloy, D. J., Lecour, S., et al. (2016). Position paper of the European society of cardiology working group cellular biology of the heart: cell-based therapies for myocardial repair and regeneration in ischemic heart disease and heart failure. *Eur. Heart J.* 37, 1789–1798. doi: 10.1093/eurheartj/ehw113
- Marian, A. J., and Braunwald, E. (2017). Hypertrophic cardiomyopathy: genetics, pathogenesis, clinical manifestations, diagnosis, and therapy. *Circ. Res.* 121, 749–770. doi: 10.1161/circresaha.117.311059
- Marino, F., Scalise, M., Cianflone, E., Mancuso, T., Aquila, I., Agosti, V., et al. (2019). Role of c-kit in myocardial regeneration and aging. *Front. Endocrinol. (Lausanne)* 10:371. doi: 10.3389/fendo.2019.00371
- Martino, F., Perestrelo, A. R., Vinarski, V., Pagliari, S., and Forte, G. (2018). Cellular mechanotransduction: from tension to function. *Front. Physiol.* 9:824. doi: 10.3389/fphys.2018.00824
- Mazzarotto, F., Girolami, F., Boschi, B., Barlocco, F., Tomberli, A., Baldini, K., et al. (2019). Defining the diagnostic effectiveness of genes for inclusion in panels: the experience of two decades of genetic testing for hypertrophic cardiomyopathy at a single center. *Genet. Med.* 21, 284–292. doi: 10.1038/s41436-018-0046-0
- Menasché, P. (2018). Cell therapy trials for heart regeneration — lessons learned and future directions. *Nat. Rev. Cardiol.* 15, 659–671. doi: 10.1038/s41569-018-0013-0
- Meng, Z., Moroishi, T., and Guan, K.-L. (2016). Mechanisms of hippo pathway regulation. *Genes Dev.* 30, 1–17. doi: 10.1101/gad.274027.115
- Miragoli, M., Ceriotti, P., Iafisco, M., Vacchiano, M., Salvarani, N., Alogna, A., et al. (2018). Inhalation of peptide-loaded nanoparticles improves heart failure. *Sci. Transl. Med.* 10:eaan6205. doi: 10.1126/scitranslmed.aan6205
- Mitrut, R., Stepan, A. E., and Pirici, D. (2018). Histopathological aspects of the myocardium in dilated cardiomyopathy. *Curr. Health Sci. J.* 44, 243–249. doi: 10.12865/CHSJ.44.03.07
- Miyagawa, S., Domaie, K., Yoshikawa, Y., Fukushima, S., Nakamura, T., Saito, A., et al. (2017). Phase I clinical trial of autologous stem cell-sheet transplantation therapy for treating cardiomyopathy. *J. Am. Heart Assoc.* 6:e003918.
- Miyasaka, K. Y., Kida, Y. S., Banjo, T., Ueki, Y., Nagayama, K., Matsumoto, T., et al. (2011). Heartbeat regulates cardiogenesis by suppressing retinoic acid signaling via expression of miR-143. *Mech. Dev.* 128, 18–28. doi: 10.1016/j.mod.2010.09.002
- Mohamed, T. M. A., Ang, Y. S., Radzinsky, E., Zhou, P., Huang, Y., Elfenbein, A., et al. (2018). Regulation of cell cycle to stimulate adult cardiomyocyte proliferation and cardiac regeneration. *Cell* 173, 104–116.
- Morton, S. U., Scherz, P. J., Cordes, K. R., Ivey, K. N., Stainier, D. Y. R., and Srivastava, D. (2008). microRNA-138 modulates cardiac patterning during embryonic development. *Proc. Natl. Acad. Sci. U.S.A.* 105, 17830–17835. doi: 10.1073/pnas.0804673105
- Muchtar, E., Blauwet, L. A., and Gertz, M. A. (2017). Restrictive cardiomyopathy: genetics, pathogenesis, clinical manifestations, diagnosis, and therapy. *Circ. Res.* 121, 819–837. doi: 10.1161/circresaha.117.310982
- Müller, P., Lemcke, H., and David, R. (2018). Stem cell therapy in heart diseases – Cell types, mechanisms and improvement strategies. *Cell. Physiol. Biochem.* 48, 2607–2655. doi: 10.1159/000492704
- Nam, Y.-J., Song, K., Luo, X., Daniel, E., Lambeth, K., West, K., et al. (2013). Reprogramming of human fibroblasts toward a cardiac fate. *Proc. Natl. Acad. Sci. U.S.A.* 110, 5588–5593. doi: 10.1073/pnas.1301019110
- Nardone, G., Oliver-De, La Cruz, J., Vrbsky, J., Martini, C., Pribyl, J., et al. (2017). YAP regulates cell mechanics by controlling focal adhesion assembly. *Nat. Commun.* 8:15321.
- Nef, H. M., Möllmann, H., Akashi, Y. J., and Hamm, C. W. (2010). Mechanisms of stress (Takotsubo) cardiomyopathy. *Nat. Rev. Cardiol.* 7, 187–193.
- Nguyen, M. M., Carlini, A. S., Chien, M.-P., Sonnenberg, S., Luo, C., Braden, R. L., et al. (2015). Enzyme-responsive nanoparticles for targeted accumulation and prolonged retention in heart tissue after myocardial infarction. *Adv. Mater.* 27, 5547–5552. doi: 10.1002/adma.201502003
- Odashima, M., Usui, S., Takagi, H., Hong, C., Liu, J., Yokota, M., et al. (2007). Inhibition of endogenous Mst1 prevents apoptosis and cardiac dysfunction without affecting cardiac hypertrophy after myocardial infarction. *Circ. Res.* 100, 1344–1352. doi: 10.1161/01.res.0000265846.23485.7a
- Oduk, Y., Zhu, W., Kannappan, R., Zhao, M., Borovjagin, A. V., Oparil, S., et al. (2018). VEGF nanoparticles repair the heart after myocardial infarction. *Am. J. Physiol. Heart Circ. Physiol.* 314, H278–H284.
- Patil, Y., and Panyam, J. (2009). Polymeric nanoparticles for siRNA delivery and gene silencing. *Int. J. Pharm.* 367, 195–203. doi: 10.1016/j.ijpharm.2008.09.039
- Patra, J. K., Das, G., Fraceto, L. F., Campos, E. V. R., Rodriguez-Torres, MdP, et al. (2018). Nano based drug delivery systems: recent developments and future prospects. *J. Nanobiotechnol.* 16:71.

- Paulis, L. E., Geelen, T., Kuhlmann, M. T., Coolen, B. F., Schäfers, M., Nicolay, K., et al. (2012). Distribution of lipid-based nanoparticles to infarcted myocardium with potential application for MRI-monitored drug delivery. *J. Controll. Release* 162, 276–285. doi: 10.1016/j.jconrel.2012.06.035
- Pelaz, B., Alexiou, C., Alvarez-Puebla, R. A., Alves, F., Andrews, A. M., Ashraf, S., et al. (2017). Diverse applications of nanomedicine. *ACS Nano* 11, 2313–2381.
- Penny, W. F., and Hammond, H. K. (2017). Randomized clinical trials of gene transfer for heart failure with reduced ejection fraction. *Hum. Gene Ther.* 28, 378–384. doi: 10.1089/hum.2016.166
- Plouffe, S. W., Meng, Z., Lin, K. C., Lin, B., Hong, A. W., Chun, J. V., et al. (2016). Characterization of hippo pathway components by gene inactivation. *Mol. Cell* 64, 993–1008. doi: 10.1016/j.molcel.2016.10.034
- Pollack, A., Kontorovich, A. R., Fuster, V., and Dec, G. W. (2015). Viral myocarditis—diagnosis, treatment options, and current controversies. *Nat. Rev. Cardiol.* 12, 670–680. doi: 10.1038/nrcardio.2015.108
- Popara, J., Accomasso, L., Vitale, E., Gallina, C., Roggio, D., Iannuzzi, A., et al. (2018). Silica nanoparticles actively engage with mesenchymal stem cells in improving acute functional cardiac integration. *Nanomedicine* 13, 1121–1138. doi: 10.2217/nnm-2017-0309
- Porrello, E. R., Johnson, B. A., Aurora, A. B., Simpson, E., Nam, Y.-J., Matkovich, S. J., et al. (2011a). miR-15 Family regulates postnatal mitotic arrest of cardiomyocytes. *Circ. Res.* 109, 670–679. doi: 10.1161/circresaha.111.248880
- Porrello, E. R., Mahmoud, A. I., Simpson, E., Hill, J. A., Richardson, J. A., Olson, E. N., et al. (2011b). Transient regenerative potential of the neonatal mouse heart. *Science* 331, 1078–1080. doi: 10.1126/science.1200708
- Psaltis, P. J., Carbone, A., Nelson, A. J., Lau, D. H., Jantzen, T., Manavis, J., et al. (2010). Reparative effects of allogeneic mesenchymal precursor cells delivered transcendocardially in experimental nonischemic cardiomyopathy. *JACC* 3, 974–983. doi: 10.1016/j.jcin.2010.05.016
- Qin, F., Tian, J., Zhou, D., and Chen, L. (2013). Mst1 and Mst2 kinases: regulations and diseases. *Cell Biosci.* 3:31. doi: 10.1186/2045-3701-3-31
- Qin, X., Chen, H., Yang, H., Wu, H., Zhao, X., Wang, H., et al. (2018). Photoacoustic imaging of embryonic stem cell-derived cardiomyocytes in living hearts with ultrasensitive semiconducting polymer nanoparticles. *Adv. Funct. Mater.* 28:1704939. doi: 10.1002/adfm.201704939
- Raso, A., and Dirxk, E. (2017). Cardiac regenerative medicine: at the crossroad of microRNA function and biotechnology. *Non-coding RNA Res.* 2, 27–37. doi: 10.1016/j.ncrna.2017.03.001
- Raval, A. N., Cook, T. D., Duckers, H. J., Johnston, P. V., Traverse, J. H., Abraham, W. T., et al. (2018). The CardiAMP heart failure trial: a randomized controlled pivotal trial of high-dose autologous bone marrow mononuclear cells using the CardiAMP cell therapy system in patients with post-myocardial infarction heart failure: trial rationale and study design. *Am. Heart J.* 201, 141–148. doi: 10.1016/j.ahj.2018.03.016
- Rebouças, JdS, Santos-Magalhães, N. S., and Formiga, F. R. (2016). Cardiac regeneration using growth factors: advances and challenges. *Arq. Bras. Cardiol.* 107, 271–275.
- Rikhtegar, R., Pezeshkian, M., Dolati, S., Safaie, N., Afrasiabi Rad, A., Mahdipour, M., et al. (2019). Stem cells as therapy for heart disease: iPSCs, ESCs, CSCs, and skeletal myoblasts. *Biomed. Pharmacother.* 109, 304–313. doi: 10.1016/j.biopha.2018.10.065
- Rochette, L., Zeller, M., Cottin, Y., and Vergely, C. (2015). Growth and differentiation factor 11 (GDF11): functions in the regulation of erythropoiesis and cardiac regeneration. *Pharmacol. Therapeut.* 156, 26–33. doi: 10.1016/j.pharmthera.2015.10.006
- Rothbauer, M., Rosser, J. M., Zirath, H., and Ertl, P. (2019). Tomorrow today: organ-on-a-chip advances towards clinically relevant pharmaceutical and medical in vitro models. *Curr. Opin. Biotechnol.* 55, 81–86. doi: 10.1016/j.copbio.2018.08.009
- Sanganalmath, S. K., and Bolli, R. (2013). Cell therapy for heart failure. *Curr. Cardiol. Rev.* 113, 810–834.
- Schafer, S., de Marvao, A., Adams, E., Fiedler, L. R., Ng, B., Khin, E., et al. (2016). Titin-truncating variants affect heart function in disease cohorts and the general population. *Nat. Genet.* 49:46. doi: 10.1038/ng.3719
- Schultheiss, H.-P., Fairweather, D., Caforio, A. L. P., Escher, F., Hershberger, R. E., Lipshultz, S. E., et al. (2019). Dilated cardiomyopathy. *Nat. Rev. Dis. Primers* 5:32.
- Scott, R. C., Rosano, J. M., Ivanov, Z., Wang, B., Chong, P. L.-G., Issekutz, A. C., et al. (2009). Targeting VEGF-encapsulated immunoliposomes to MI heart improves vascularity and cardiac function. *FASEB J.* 23, 3361–3367. doi: 10.1096/fj.08-127373
- Senyo, S. E., Steinhauser, M. L., Pizzimenti, C. L., Yang, V. K., Cai, L., Wang, M., et al. (2013). Mammalian heart renewal by pre-existing cardiomyocytes. *Nature* 493, 433–436. doi: 10.1038/nature11682
- Sercombe, L., Veerati, T., Moheimani, F., Wu, S. Y., Sood, A. K., and Hua, S. (2015). Advances and challenges of liposome assisted drug delivery. *Front. Pharmacol.* 6:286. doi: 10.3389/fphar.2015.00286
- Simons, M., Annex, B. H., Laham, R. J., Kleiman, N., Henry, T., Dauerman, H., et al. (2002). Pharmacological treatment of coronary artery disease with recombinant fibroblast growth factor-2. 105, 788–793. doi: 10.1161/hc0802.104407
- Sioud, M. (2005). On the delivery of small interfering RNAs into mammalian cells. *Expert Opin. Drug Deliv.* 2, 639–651. doi: 10.1517/17425247.2.4.639
- Sluijter, J. P. G., Mil, A. V., Vliet, P. V., and Metz, C. H. G., (2010). MicroRNA-1 and -499 regulate differentiation and proliferation in human-derived cardiomyocyte progenitor cells. *Arteriosclerosis Thrombosis Vasc. Biol.* 30, 859–868. doi: 10.1161/atvbaha.109.197434
- Small, E. M., O'Rourke, J. R., Moresi, V., Sutherland, L. B., McAnally, J., Gerard, R. D., et al. (2010). Regulation of PI3-kinase/Akt signaling by muscle-enriched microRNA-486. *Proc. Natl. Acad. Sci. U.S.A.* 107, 4218–4223. doi: 10.1073/pnas.1000300107
- Smith, A. J., Lewis, F. C., Aquila, I., Waring, C. D., Nocera, A., Agosti, V., et al. (2014). Isolation and characterization of resident endogenous c-Kit+ cardiac stem cells from the adult mouse and rat heart. *Nat. Protoc.* 9, 1662–1681. doi: 10.1038/nprot.2014.113
- Song, K., Nam, Y.-J., Luo, X., Qi, X., Tan, W., Huang, G. N., et al. (2012). Heart repair by reprogramming non-myocytes with cardiac transcription factors. *Nature* 485, 599–604. doi: 10.1038/nature11139
- Taimel, Z., Loughran, J., Birks, E. J., and Bolli, R. (2013). Vascular endothelial growth factor in heart failure. *Nat. Rev. Cardiol.* 10, 519–530.
- Tanai, E., and Frantz, S. (2015). Pathophysiology of heart failure. *Compr. Physiol.* 6, 187–214.
- Tang, F., Gao, R., Jeevan-Raj, B., Wyss, C. B., Kalathur, R. K. R., Piscuoglu, S., et al. (2019). LATS1 but not LATS2 represses autophagy by a kinase-independent scaffold function. *Nat. Commun.* 10:5755.
- Tao, G., Kahr, P. C., Morikawa, Y., Zhang, M., Rahmani, M., Heallen, T. R., et al. (2016). Pitx2 promotes heart repair by activating the antioxidant response after cardiac injury. *Nature* 534:119. doi: 10.1038/nature17959
- thebiogrid.org. (2019). Available from: <https://thebiogrid.org/115684>.
- Thum, T., Gross, C., Fiedler, J., Fischer, T., Kissler, S., Bussen, M., et al. (2008). MicroRNA-21 contributes to myocardial disease by stimulating MAP kinase signalling in fibroblasts. *Nature* 456, 980–984. doi: 10.1038/nature07511
- Tian, Y., Liu, Y., Wang, T., Zhou, N., Kong, J., Chen, L., et al. (2015). A microRNA-Hippo pathway that promotes cardiomyocyte proliferation and cardiac regeneration in mice. *Sci. Transl. Med.* 7, ra38–ra38.
- Torrini, C., Cubero, R. J., Dirxk, E., Braga, L., Ali, H., Prosdócimo, G., et al. (2019). Common regulatory pathways mediate activity of microRNAs inducing cardiomyocyte proliferation. *Cell Rep.* 27, 2759–2771.e5. doi: 10.1016/j.celrep.2019.05.005
- Traverse, J. H., Henry, T. D., Dib, N., Patel, A. N., Pepine, C., Schaer, G. L., et al. (2019). First-in-man study of a cardiac extracellular matrix hydrogel in early and late myocardial infarction patients. *JACC* 4, 659–669. doi: 10.1016/j.jacbt.2019.07.012
- Troncoso, R., Ibarra, C., Vicencio, J. M., Jaimovich, E., and Lavandero, S. (2014). New insights into IGF-1 signaling in the heart. *Trends Endocrinol. Metabol.* 25, 128–137. doi: 10.1016/j.tem.2013.12.002
- Tzahor, E., and Poss, K. D. (2017). Cardiac regeneration strategies: staying young at heart. *Science* 356, 1035–1039. doi: 10.1126/science.aam5894

- U.S. Department of Health & Human Services (2013). *Health Topic: Cardiomyopathy*. Available online at: <https://www.nlm.nih.gov/health-topics/cardiomyopathy>
- U.S. National Library of Medicine (2013). *IRON Nanoparticle Enhanced MRI in the Assessment of Myocardial infarction (IRNMAN)*. Available online at: [ClinicalTrials.govUNLom](https://clinicaltrials.gov/ct2/show/study/NCT01901111)
- U.S. National Library of Medicine (2014a). *Ferumoxylol for Magnetic Resonance Imaging of Myocardial Infarction*. Available online at: [ClinicalTrials.govUNLom](https://clinicaltrials.gov/ct2/show/study/NCT01901111)
- U.S. National Library of Medicine (2014b). *Inflammatory Cell Trafficking After Myocardial Infarction*. Available online at: [ClinicalTrials.govUNLom](https://clinicaltrials.gov/ct2/show/study/NCT01901111)
- U.S. National Library of Medicine (2019a). *A Study of VentiGel in Post-MI Patient*. Available online at: [ClinicalTrials.govUNLom](https://clinicaltrials.gov/ct2/show/study/NCT01901111)
- U.S. National Library of Medicine (2019b). *The Transendocardial Autologous Cells (hMSC) or (hMSC) and (hCSC) in Ischemic Heart Failure Trial (TAC-HFT-II)*. Available online at: [ClinicalTrials.govUNLom](https://clinicaltrials.gov/ct2/show/study/NCT01901111)
- U.S. National Library of Medicine (2019c). *Bone Marrow Derived Mesenchymal Stem Cells in Improving Heart Function in Patients With Heart Failure Caused by Anthracyclines*. Available online at: [ClinicalTrials.govUNLom](https://clinicaltrials.gov/ct2/show/study/NCT01901111)
- U.S. National Library of Medicine (2019d). *CardiAMP™ Heart Failure Trial*. Available online at: [ClinicalTrials.govUNLom](https://clinicaltrials.gov/ct2/show/study/NCT01901111)
- U.S. National Library of Medicine (2020a). *Efficacy and Safety of Allogeneic Mesenchymal Precursor Cells (Rexlemestocel-L) for the Treatment of Heart Failure (DREAM HF-1)*. Available online at: [ClinicalTrials.govUNLom](https://clinicaltrials.gov/ct2/show/study/NCT01901111)
- U.S. National Library of Medicine (2020b). *Nanoparticles in Heart Diseases: Overview on the Existing Clinical Trials*. Available online at: <https://clinicaltrials.gov/ct2/results?term=nanoparticles&cond=Heart+Diseases&draw=2&rank=7#rowId6>. [ClinicalTrials.govUNLom](https://clinicaltrials.gov/ct2/results?term=nanoparticles&cond=Heart+Diseases&draw=2&rank=7#rowId6)
- U.S. National Library of Medicine (2020c). *VEGF in Heart Diseases: Overview on the Existing Clinical Trials*. Available online at: <https://clinicaltrials.gov/ct2/results?cond=heart&term=VEGF>. [ClinicalTrials.govUNLom](https://clinicaltrials.gov/ct2/results?cond=heart&term=VEGF)
- Unger, E. F., Goncalves, L., Epstein, S. E., Chew, E. Y., Trapnell, C. B., Cannon, R. O. III, et al. (2000). Effects of a single intracoronary injection of basic fibroblast growth factor in stable angina pectoris. *Am. J. Cardiol.* 85, 1414–1419. doi: 10.1016/s0002-9149(00)00787-6
- Valadi, H., Ekström, K., Bossios, A., Sjöstrand, M., Lee, J. J., and Lötvall, J. O. (2007). Exosome-mediated transfer of mRNAs and microRNAs is a novel mechanism of genetic exchange between cells. *Nat. Cell Biol.* 9, 654–659. doi: 10.1038/ncb1596
- van der Meel, R., Lammers, T., and Hennink, W. E. (2017). Cancer nanomedicines: oversold or underappreciated? *Expert Opin. Drug Deliv.* 14, 1–5. doi: 10.1080/17425247.2017.1262346
- van Rooij, E., Sutherland, L. B., Liu, N., Williams, A. H., McAnally, J., Gerard, R. D., et al. (2006). A signature pattern of stress-responsive microRNAs that can evoke cardiac hypertrophy and heart failure. *Proc. Natl. Acad. Sci. U.S.A.* 103, 18255–18260. doi: 10.1073/pnas.0608791103
- Varelas, X. (2014). The Hippo pathway effectors TAZ and YAP in development, homeostasis and disease. *Development* 141, 1614–1626. doi: 10.1242/dev.102376
- Velzen, HGv, Schinkel, A. F. L., Baart, S. J., Oldenburg, R. A., Frohn-Mulder, I. M. E., et al. (2018). Outcomes of contemporary family screening in hypertrophic cardiomyopathy. *Circulation* 11:e001896.
- Vicinanza, C., Aquila, I., Scalise, M., Cristiano, F., Marino, F., Cianflone, E., et al. (2017). Adult cardiac stem cells are multipotent and robustly myogenic: c-kit expression is necessary but not sufficient for their identification. *Cell Death Differ.* 24, 2101–2116. doi: 10.1038/cdd.2017.130
- Vikhorev, P. G., and Vikhoreva, N. N. (2018). Cardiomyopathies and related changes in contractility of human heart muscle. *Int. J. Mol. Sci.* 19:E2234.
- von Gise, A., Lin, Z., Schlegelmilch, K., Honor, L. B., Pan, G. M., Buck, J. N., et al. (2012). YAP1, the nuclear target of Hippo signaling, stimulates heart growth through cardiomyocyte proliferation but not hypertrophy. *Proc. Natl. Acad. Sci. U.S.A.* 109, 2394–2399. doi: 10.1073/pnas.1116136109
- Wada, R., Muraoka, N., Inagawa, K., Yamakawa, H., Miyamoto, K., Sadahiro, T., et al. (2013). Induction of human cardiomyocyte-like cells from fibroblasts by defined factors. *Proc. Natl. Acad. Sci. U.S.A.* 110, 12667–12672.
- Wahlquist, C., Jeong, D., Rojas-Muñoz, A., Kho, C., Lee, A., Mitsuyama, S., et al. (2014). Inhibition of miR-25 improves cardiac contractility in the failing heart. *Nature* 508:531. doi: 10.1038/nature13073
- Wang, H. P., Zhang, W. H., Wang, X. F., Zhu, J., Zheng, Y. Q., Xia, Q., et al. (2014). Exposure to AT1 receptor autoantibodies during pregnancy increases susceptibility of the maternal heart to postpartum ischemia-reperfusion injury in rats. *Int. J. Mol. Sci.* 15, 11495–11509. doi: 10.3390/ijms150711495
- Wang, J., Liu, S., Heallen, T., and Martin, J. F. (2018). The Hippo pathway in the heart: pivotal roles in development, disease, and regeneration. *Nat. Rev. Cardiol.* 15, 672–684. doi: 10.1038/s41569-018-0063-3
- Wang, L. V., and Hu, S. (2012). Photoacoustic tomography: in vivo imaging from organelles to organs. *Science* 335, 1458–1462. doi: 10.1126/science.1216210
- Watkins, H., Ashrafian, H., and Redwood, C. (2011). Inherited cardiomyopathies. *Circ. J.* 364, 1643–1656.
- Watt, K. I., Turner, B. J., Hagg, A., Zhang, X., Davey, J. R., Qian, H., et al. (2015). The Hippo pathway effector YAP is a critical regulator of skeletal muscle fibre size. *Nat. Commun.* 6:6048.
- Weis, S. M. (2008). Vascular permeability in cardiovascular disease and cancer. *Curr. Opin. Hematol.* 15, 243–249. doi: 10.1097/moh.0b013e3282f97d86
- Whyte, W., Roche, E. T., Varela, C. E., Mendez, K., Islam, S., O'Neill, H., et al. (2018). Sustained release of targeted cardiac therapy with a replenishable implanted epicardial reservoir. *Nat. Biomed. Eng.* 2, 416–428. doi: 10.1038/s41551-018-0247-5
- World Health Organization (2019). *Cardiovascular Diseases (CVDs)*. Available online at: <https://www.who.int/news-room/fact-sheets/detail/cardiovascular-diseases>.
- Xi, D., Dong, S., Meng, X., Lu, Q., Meng, L., and Ye, J. (2012). Gold nanoparticles as computerized tomography (CT) contrast agents. *RSC Adv.* 2, 12515–12524.
- Xiong, F., Wang, H., Feng, Y., Li, Y., Hua, X., Pang, X., et al. (2015). Cardioprotective activity of iron oxide nanoparticles. *Sci. Rep.* 5: 8579.
- Xu, Z., Zhu, W., Wang, C., Huang, L., Zhou, Q., Hu, J., et al. (2017). Genotype-phenotype relationship in patients with arrhythmogenic right ventricular cardiomyopathy caused by desmosomal gene mutations: a systematic review and meta-analysis. *Sci. Rep.* 7:41387.
- Xue, X., Shi, X., Dong, H., You, S., Cao, H., Wang, K., et al. (2018). Delivery of microRNA-1 inhibitor by dendrimer-based nanovector: an early targeting therapy for myocardial infarction in mice. *Nanomedicine* 14, 619–631. doi: 10.1016/j.nano.2017.12.004
- Yang, H., Qin, X., Wang, H., Zhao, X., Liu, Y., Wo, H.-T., et al. (2019). An in vivo miRNA delivery system for restoring infarcted myocardium. *ACS Nano* 13, 9880–9894. doi: 10.1021/acsnano.9b03343
- Yildirim, L., Thanh, N. T. K., Loizidou, M., and Seifalian, A. M. (2011). Toxicology and clinical potential of nanoparticles. *Nano Today* 6, 585–607. doi: 10.1016/j.nantod.2011.10.001
- Yokoyama, R., Ii, M., Masuda, M., Tabata, Y., Hoshiga, M., Ishizaka, N., et al. (2019). Cardiac regeneration by statin-polymer nanoparticle-loaded adipose-derived stem cell therapy in myocardial infarction. *Stem Cells Transl. Med.* 8, 1055–1067. doi: 10.1002/sctm.18-0244
- Yu, M., Wu, J., Shi, J., and Farokhzad, O. C. (2016). Nanotechnology for protein delivery: overview and perspectives. *J. Control. Release* 240, 24–37. doi: 10.1016/j.jconrel.2015.10.012
- Zeng, X.-H., Zeng, X.-J., and Li, Y.-Y. (2003). Efficacy and safety of berberine for congestive heart failure secondary to ischemic or idiopathic dilated cardiomyopathy. *Am. J. Cardiol.* 92, 173–176. doi: 10.1016/s0002-9149(03)00533-2
- Zhang, B.-F., Jiang, H., Chen, J., Hu, Q., Yang, S., and Liu, X.-P. (2019). Silica-coated magnetic nanoparticles labeled endothelial progenitor cells alleviate ischemic myocardial injury and improve long-term cardiac function with magnetic field guidance in rats with myocardial infarction. *J. Cell. Physiol.* 234, 18544–18559. doi: 10.1002/jcp.28492
- Zhang, L., Gu, F., Chan, J., Wang, A., Langer, R., and Farokhzad, O. (2008). Nanoparticles in medicine: therapeutic applications and developments. *Clin. Pharmacol. Ther.* 83, 761–769. doi: 10.1038/sj.clpt.6100400
- Zhang, S., Zhao, B., Jiang, H., Wang, B., and Ma, B. (2007). Cationic lipids and polymers mediated vectors for delivery of siRNA. *J. Control. Release* 123, 1–10. doi: 10.1016/j.jconrel.2007.07.016

- Zhao, H., Lin, Z. Y., Yildirim, L., Dhinakar, A., Zhao, X., and Wu, J. (2016). Polymer-based nanoparticles for protein delivery: design, strategies and applications. *J. Mater. Chem. B* 4, 4060–4071. doi: 10.1039/c6tb00308g
- Zhao, Y., Ransom, J. F., Li, A., Vedantham, V., von Drehle, M., Muth, A. N., et al. (2007). Dysregulation of cardiogenesis, cardiac conduction, and cell cycle in mice lacking miRNA-1-2. *Cell* 129, 303–317. doi: 10.1016/j.cell.2007.03.030
- Zhao, Y., Samal, E., and Srivastava, D. (2005). Serum response factor regulates a muscle-specific microRNA that targets Hand2 during cardiogenesis. *Nature* 436, 214–220. doi: 10.1038/nature03817

Conflict of Interest: The authors declare that the research was conducted in the absence of any commercial or financial relationships that could be construed as a potential conflict of interest.

Copyright © 2020 Cassani, Fernandes, Vrbsky, Ergir, Cavalieri and Forte. This is an open-access article distributed under the terms of the Creative Commons Attribution License (CC BY). The use, distribution or reproduction in other forums is permitted, provided the original author(s) and the copyright owner(s) are credited and that the original publication in this journal is cited, in accordance with accepted academic practice. No use, distribution or reproduction is permitted which does not comply with these terms.